XII Advanced Research Workshop on High Energy Spin Physics

(DSPIN-07)

Proceedings

Joint Institute for Nuclear Research

XII Advanced Research Workshop on High Energy Spin Physics

(DSPIN-07)

Dubna, September 3–7, 2007

Proceedings

Edited by *A.V. Efremov* and *S.V. Goloskokov*

Dubna 2008

УДК [539.12.01 + 539.12 ... 14 + 539.12 ... 162.8](063)
ББК [22.382.1 + 22.382.2 + 22.382.3] я 431
A20

XII Advanced Research Workshop on High Energy Spin Physics
(DSPIN-07): Proceedins. —Dubna: JINR, 2007. —454 p. A20
ISBN 5-9530-003-6

The collection includes contributions presented to the XII Advanced Research Workshop on High Energy Spin Physics (ARW DSPIN-07), (Dubna, September 3–7, 2007) on different theoretical, experimental and technical aspects of this branch of physics. Dedicated to the 80th anniversary of the birth of L.I. Lapidus (1927–1986), initiator of this series of workshops.

Sponsored by:
Joint Institute for Nuclear research,
International Committee for Spin Physics Symposia,
Russian Foundation for Basic Research.

The contributions are reproduced from the originals presented by the Organizing Committee.

XII Рабочее совещание по физике спина при высоких энергиях
(DSPIN-07): Труды совещания — Дубна: ОИЯИ, 2007. — 454 с.
ISBN 5-9530-003-6

Сборник докладов представленных на Рабочее совещание по физике спина при высоких энергиях (Дубна, 3–7 сентября 2007 г.) по теоретическим, экспериментальным и техническим аспектам этой области физики. Посвещается 80-летию со дня рождения Л.И. Лапидуса – инициатора этой серии совещаний.

УДК [539.12.01 + 539.12 ... 14 + 539.12 ... 162.8](063)
ББК [22.382.1 + 22.382.2 + 22.382.3] я 431
ISBN 5-9530-003-6

Contents

WELCOME ADDRESS
by JINR Vice-Director R. Lednicky

Dear Colleagues,
Ladies and Gentlemen,

On behalf of the Directorate of Joint Institute for Nuclear Research it is a pleasure to welcome you at the 12-th International Workshop on High Energy Spin Physics.

This workshop is devoted to the 80-th anniversary of the birth of Lev Lapidus who organized in Dubna the first Workshop of this series already 26 years ago, in 1981. Starting in the middle of fifties, Professor Lev Lapidus contributed significantly to the development of High Energy Spin Physics for about three decades. The well known examples of his achievements are the prediction of the analyzing power in the Coulomb-Nuclear Interference region and the first approach to the sum rule for the nucleon magnetic moment. Besides his own research, he supported spin activities in many laboratories and helped a lot to very fruitful and extensive participation of physicists from former USSR and from Eastern Europe in the important international projects devoted to this difficult field of physics.

I think there is no need to stress the importance of the spin phenomena for deeper understanding of particle physics. There will be opportunity to hear about the achievements, the goals and the yet unresolved problems at this Workshop. The JINR laboratories are largely involved in this important field of physics including both theoretical and experimental studies. The latter are carried out with unique polarized beams at JINR Nuclotron as well as in the outside experiments within collaborations HERMES, COMPASS and STAR.

You probably know that there are plans to built up here in Dubna the ion collider (so called project NICA) which will cover the energy range up to center-of-mass nucleon-nucleon energy of about 10 GeV. Besides the search for the mixed phase, there are foreseen experiments with polarized beams. I would like to stress that JINR directorate is very much interested in the assistance and recommendations of the international spin community in preparation of the ambitious and competitive program of polarization studies on this new facility. It is important that this program would be attractive and realized within a wide international collaboration.

Besides JINR, this Workshop is supported by Russian Foundation for Basic Research and by the International Committee of Spin Physics Symposia. In particular, thanks to this support there are many young scientists from Russia and other JINR Member States participating in the Workshop.

I would like to thank the Workshop organizers for their not easy work and express my hope that you will benefit from the traditional friendly and fruitful atmosphere of this meeting.

I wish you a productive work and a pleasant stay here in Dubna.

Thank you for the attention.

THEORY OF SPIN PHYSICS

SINGLE SPIN EFFECTS IN COLLISIONS OF HADRONS AND HEAVY IONS AT HIGH ENERGY

V.V. Abramov†

Institute for High Energy Physics, 142281 Protvino, Moscow region, Russia
† E-mail: Victor.Abramov@ihep.ru

Abstract

Experimental data on transverse single-spin asymmetry, hyperon polarization and vector meson alignment in h+h, h+A and A+A-collisions have been analyzed. A new mechanism for the origin of single spin effects is proposed, which takes into account the interaction of massive constituent quarks via their chromomagnetic moment with an effective inhomogeneous chromomagnetic field of strings, produced after the initial color exchange. Quark spin precession in the color field is taken into account, which can be the reason for an oscillation of the single spin observables as a function of Feynman x_F and its energy dependence. The model predictions are compared with the experimental data, in particular with the heavy ion collision data. The data are consistent with a large negative anomalous chromomagnetic moment of the constituent quarks which is predicted in the instanton model.

It is assumed in the model, that each quark or antiquark, which is not a constituent of the observed hadron C in the reaction $A\uparrow + B \to C + X$ contributes, with some probability, to the effective color field, which acts on the hadron C quarks. As is shown in [1], a string arises between the receding quark and antiquark, which has a longitudinal chromoelectric field $\mathbf{E^a}$ and a circular chromomagnetic field $\mathbf{B^a}$. The field $\mathbf{B^a}$ spreads around the string like an ordinary magnetic field surrounds a conductor with a current:

$$B_{\varphi}^{(2)} = -2\alpha_s r/\rho^3 exp(-r^2/\rho^2), \tag{1}$$

where r is a distance from the string axis, $\rho = 1.25R_c = 2.08$ GeV^{-1}, and R_c is the confinement radius, the index (2) in $B_{\varphi}^{(2)}$ means a color, and φ is the azimuthal angle.

This inhomogeneous field $\mathbf{B^a}$ acts on a color magnetic moment $\mu = sgq_s/2M_Q$ of the quark Q, where $q_s = \sqrt{4\pi\alpha_s}$ is the color coupling constant, g is the color gyromagnetic number, M_Q is the constituent quark (valon) mass. The Stern-Gerlach-like force given by

$$f_x = \mu_x \partial B_x^a/\partial x + \mu_y \partial B_y^a/\partial x, \tag{2}$$

can be the reason of the large single spin asymmetry (SSA) [2].

We assume a Larmore precession [3] of the mean quark spin ξ in the color field $\mathbf{B^a}$, which depends on the quark energy E_Q:

$$d\xi/dt = a[\xi \mathbf{B^a}], \tag{3}$$

$$a = q_s(g - 2 + 2M_Q/E_Q)/2M_Q. \tag{4}$$

A large negative value of the anomalous quark chromomagnetic moment $\mu_a = (g-2)/2$ is predicted in the framework of the instanton model: $\mu_a = -0.744$ (Diakonov, [4]).

At high quark energies $E_Q \gg 2M_Q/|g-2|$ the quark spin precession frequency $\Omega_s = aB$ is almost energy independent due to the high $|g-2|$ value and the energy-dependent term in (4) can be considered as a correction and estimated experimentally.

The Stern-Gerlach-like force (2) produces an additional transverse momentum:

$$\delta p_x \approx \frac{gv[1-\cos(kS)]}{2\rho kS(g-2+2M_Q/E_Q)}, \tag{5}$$

where $kS = aB/v$ is the precession angle, $dS = vdt$, v is the quark velocity, and S is a quark path length in the string field. We assume that $kS = \omega_A x_A$ in the hadron A fragmentation region, or $kS = \omega_B x_B$ in the hadron B fragmentation region, where ω_A and ω_B are dimensionless values and the scaling variables are defined as $x_A = (x_R + x_F)/2$ and $x_B = (x_R - x_F)/2$.

The analyzing power is related with the additional p_T by eq. (6), (M.Ryskin, [2]):

$$A_N \approx \delta p_x \partial/\partial p_T \ln(d^3\sigma/d^3p). \tag{6}$$

The final expression for the SSA or hadron polarization in pp, pA or AA collisions is:

$$A_N = C(\sqrt{s})V(E_{cm})F(p_T,A)[G(\omega_A y_A) - \sigma(\theta^{cm})G(\omega_B y_B)]; \tag{7}$$

$$G(\omega \cdot y) = [1-\cos(\omega \cdot y)]/(\omega \cdot y); \tag{8}$$

$$\sigma(\theta^{cm}) = \xi \sin\theta^{cm} + \varepsilon \ ; \quad F(p_T,A) = 1 - \exp[-(p_T/p_T^{min})^3](1-\eta \ln A) \ ; \tag{9}$$

$$y_A = x_A - (E_0/\sqrt{s} + f_A)[1+\cos\theta^{cm}] + a_0[1-\cos\theta^{cm}]; \tag{10}$$

$$y_B = x_B - (E_0/\sqrt{s} + f_B)[1-\cos\theta^{cm}] + a_0[1+\cos\theta^{cm}]; \tag{11}$$

$$C(\sqrt{s}) = C_0/(1-E_R/\sqrt{s}). \tag{12}$$

The Heaviside step function $V(E_{cm}) \approx \pm\Theta(E_{cm} - E_{cm}^{min})$ takes into account the threshold behavior of the SSA as a function of hadron C c.m. energy [5]. The eqs. (7) - (12) describe not only the SSA, but also the hyperon polarization in the unpolarized hadron collisions. The model has 8 phenomenological parameters in the case of identical particle collision ($\omega_A = \omega_B$, $f_A = f_B$, $\varepsilon = 1$, $\xi = 0$) and 12 parameters in a general case.

Due to the quark spin precession (3)-(4) the effective value of E_0 is given by

$$E_0 \approx 2M_Q[1 + \frac{2}{2-g}], \tag{13}$$

where it is assumed that the constituent quark mass for u- and d-quarks is the same: $M_U = M_D = 0.35$ GeV. The relation (13) and the estimated values of the $E_0 = 1.640 \pm 0.040$ GeV (π^+) and $E_0 = 2.02 \pm 0.21$ GeV (π^-) allow to extract the quark anomalous chromo-magnetic moment for u- and d-quarks: $\mu_a^U = -0.74 \pm 0.03(stat)$ and $\mu_a^D = -0.53^{+0.10}_{-0.07}(stat)$. These values of μ_a are compatible with the instanton model prediction [4].

The hyperon polarization arises due to the Stern-Gerlach-like forces, which separate the spin up and down quark states by adding a transverse momentum to the left or to the right in the scattering plane. The eq. (7) predicts an oscillation of A_N or P_N with the frequency ω_A (ω_B) as a function of y_A (y_B) and its energy dependence, eq. (12).

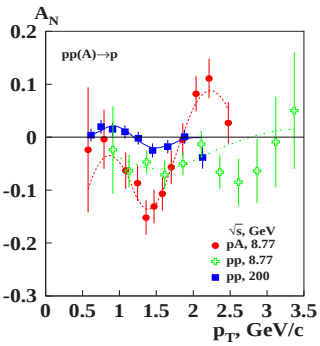

Figure 1: The analyzing power vs p_T for the reaction $p\uparrow + p(A) \to p + X$.

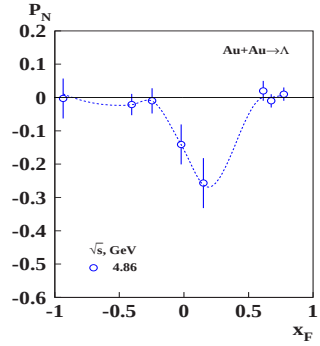

Figure 2: The transverse polarization vs x_F for the reaction $Au + Au \to \Lambda\uparrow + X$.

The following figures show examples of the oscillation of the SSA or hadron polarization in a wide range of energies and other kinematical variables. The curves in the figures show the fit result using the model function (7) discussed above. A direct evidence of the proton A_N oscillation as a function of p_T (Fig. 1) is obtained in the FODS-2 (IHEP) experiment using the 40 GeV/c polarized proton beam [6]. Recently the A_N oscillation with a smaller magnitude was observed in the BRAHMS (BNL) experiment at $\sqrt{s} = 200$ GeV [7]. The frequency ω_A is -10.7 ± 1.0 for $\sqrt{s} = 8.77$ GeV and -64 ± 14 for $\sqrt{s} = 200$ GeV. The rise of the ω_A is expected in the model due to additional sea quarks-spectators produced at high energy.

The transverse Λ polarization in Au+Au-collisions is measured at $\sqrt{s} = 4.86$ GeV (Fig. 2) [8]. The fit gives positive $\omega_A = +18.61 \pm 0.54$, as expected in the model. Recently

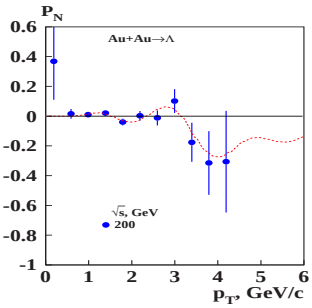

Figure 3: The global Λ polarization vs p_T for reaction $Au + Au \to \Lambda\uparrow + X$.

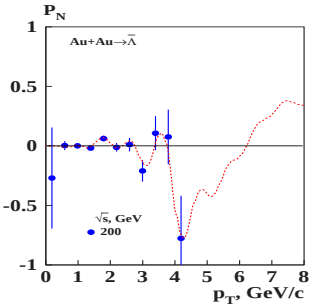

Figure 4: The global $\bar{\Lambda}$ polarization vs p_T for reaction $Au + Au \to \bar{\Lambda}\uparrow + X$.

very interesting data on the global hyperon polarization in Au+Au collisions were reported by the STAR experiment [19]. These data show examples of polarization oscillation with negative and very high frequency ω_A. This is exactly what is expected in the model due many spectator quarks $N_Q \propto A^{1/3} \exp(-w/\sqrt{s})$, whose number is proportional to the number of nucleons inside the tube of a transverse radius about the confinement radius, where $w = 236 \pm 16$ GeV. At high reaction energy many new spectator quarks and antiquarks are produced by each nucleon that increases the field B. The Λ-hyperon data fit gives $\omega_A = -374 \pm 51$ for 200 GeV (Fig. 3) and $\omega_A = -58 \pm 38$ for 62 GeV. The $\bar{\Lambda}$-hyperon data fit gives $\omega_A = -648 \pm 46$ and $\omega_A = -359 \pm 15$ for 200 GeV (Fig. 4) and 62 GeV, respectively.

The quark counting rule (QCR, Fig. 5) is designed to explain the dependence of the ω_A frequency on hadron quantum numbers, reaction energy and a projectile atomic weight. The quark counting rule for the ω_A assumes that each projectile spectator quark

contribute to the quark precession frequency with a weight $\nu = \lambda$ and each antiquark with a unity weight. For the target quarks or antiquarks an additional factor $-\tau$ should be used. The factor $R_Q = (M_S/M_Q)\mu_a^Q/\mu_a^S$ takes into account the fact that the ω_A is proportional to $(g-2)_Q/M_Q$. The model QCR parameters are obtained from a global fit of 26 reactions: $\omega_0 = -3.23\pm0.30$; $\lambda = -0.106\pm0.018$; $\tau = -0.016\pm0.027$; $R_U = 1.60\pm0.24$; $R_D = 1.95 \pm 0.41$; $R_S = 1$; $R_C = 0.78 \pm 0.29$.

Conclusion: A new mechanism is proposed which explains the origin of the transverse single spin asymmetries and the hyperon polarization. The origin of the single spin effects can be related with the Stern-Gerlach-like forces between chromomagnetic moment of the massive constituent quark and the effective color field created by the quarks-spectators.

The A_N and P_N oscillation due to the quark spin precession in the effective color field is predicted and confirmed for proton, Λ, $\bar{\Lambda}$, J/ψ, $K^{*-}(892)$, Ξ^0 and Ξ^- production in the inclusive reactions. The polarization oscillation is the main signature of the model.

The estimated color anomalous magnetic moment is -0.74 ± 0.03 and $-0.53^{+0.10}_{-0.07}$ for u and d quark, respectively, in agreement with the instanton model prediction $\mu_a = -0.744$.

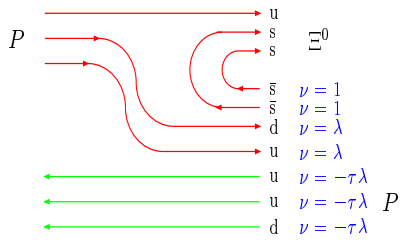

$pp \to \Xi^0 + X$ *production quark diagram.*

Color flux tube counting.

$\omega_\Xi^{pp} = \omega_0 R_S[2 + 2\lambda - 3\tau\lambda] = -5.77 \pm 0.57,$
$\omega_{exp} = -5.415 \pm 0.80$

Figure 5. Quark counting for the reaction $pp \to \Xi^0\uparrow + X$.

Acknowledgments: We are grateful to R.Bellwied, J.C.Dunlop and I.Selyuzhenkov for useful discussions and access to the E896 and STAR preliminary data.

References

[1] A.B. Migdal and S.B. Khokhlachev, *JETP Lett.* **41**, 194 (1985).
[2] M.G. Ryskin, *Sov. J. Nucl. Phys.* **48**, 708 (1988).
[3] V. Bargmann, L. Michel and V. Telegdy, *Phys. Rev. Lett.* **2**, 435 (1959).
[4] D. Diakonov, *Prog.Part.Nucl.Phys.* **51**, 173 (2003). e-Print Archive: hep-ph/0212026
[5] V.V. Abramov, *Yad.Fiz.* **70**, 2153, (2007).
[6] V.V. Abramov et al., *Yad.Fiz.* **70**, 1561 (2007).
[7] J. H. Lee and F. Videbaek for the BRAHMS Collaboration "Single Spin Asymmetries of Identified Hadrons in Polarized p+p at $\sqrt{s} = 62$ GeV and 200 GeV". Presented at The 17th International Spin Physics Symposium (SPIN2006), in Kyoto, Japan, Oct. 2-7, 2006. Published in AIP Conf.Proc. **915**, 533, (2007).
[8] R.Bellwied for the E896 collaboration, *Nucl.Phys.* **A698**, 499 (2002).
[9] B.I.Abelev at al., *Phys. Rev.* **C 76**, 024915 (2007).

Discussion

Q. (S.Belostotsky, PNPI, St.Petersburg) How many free parameters are involved in your model? Have you fitted them to the data?

A. There are 12 phenomenological parameters in the model in a general case. The number of parameters is reduced to 8 in the case of identical particle collision due to an additional symmetry of the model equations. The model parameters were fitted to the data.

TRANSVERSE Λ^0 POLARIZATION IN INCLUSIVE PHOTOPRODUCTION: QUARK RECOMBINATION MODEL

I. I. Alikhanov[1†] and O. Grebenyuk[2]

(1) *Saint Petersburg State University, Saint Petersburg, 198904, Russia*
(2) *Petersburg Nuclear Physics Institute, Gatchina, 188350, Russia*
† *E-mail: ialspbu@mail.ru*

Abstract

The transverse polarization of Λ^0 hyperons in inclusive photoproduction at $x_F > 0$ is tackled within the framework of the quark recombination model, which has been successfully applied to the polarization of different hyperons in a variety of unpolarized hadron-hadron reactions. The results are compared with recent experimental data of HERMES.

The problem of the Λ^0 polarization in hadron-hadron reactions at high energies remains still vital even in spite of the thirty years have passed since it was discovered [1]. Being produced in pN collisions at 300 GeV proton beam energy, the Λ^0 hyperons were found to be highly polarized while neither the beam nor the Beryllium target possessed any initial polarization. This phenomenon turned out to be quite surprising for the widely spread belief that spin flip processes would not take any significant place at such high energies as the helicity is conserved in the limit of massless quarks. Certainly, it has induced much attention to be focused as well on studies of the polarization experimentally, using a variety of projectiles and targets at different kinematic regimes, as on its theoretical explanations (see, e.g., [2–4] and the references therein).

We present here calculations of the transverse Λ^0 polarization in inclusive photoproduction at the current fragmentation ($x_F > 0$) carried out in the framework of the quark recombination model (QRM) [5]. The model has been shown to be successful in describing the polarizations of different hyperons in a variety of high energy hadron-hadron reactions. Let us briefly recall some key ingredients of QRM. Following the original notations, we will also abbreviate the collision $H_iN \to H_fX$ (e.g., $K^-N \to \Lambda X$) as $H_i \to H_f$ ($K^- \to \Lambda$).

The quantity proportional to the reaction probability of the transition $H_i \to H_f$ in the projectile infinite momentum frame (IMF) is written as

$$|\langle M_f|S|M_i\rangle|^2 = \sum_{s_k,\mu_k} G^{M_f}_{4s_4\mu_4}(r_4) \otimes G^{M_f}_{3s_3\mu_3}(r_3) \otimes |M(r_k;s_k,\mu_k)|^2 \otimes G^{M_i}_{2s_2\mu_2}(r_2) \otimes G^{M_i}_{1s_1\mu_1}(r_1) \otimes \Delta^3 \otimes \Delta^4, \quad (1)$$

where M_i and M_f are the spin projections of the hadrons H_i and H_f on the z axis, which is defined by the vector $[\,\mathbf{p}_{H_i} \times \mathbf{p}_{H_f}]$, here $\mathbf{p}_{H_i}$ and $\mathbf{p}_{H_f}$ are the momentum vectors of H_i and H_f; the x axis is chosen to be parallel to $\mathbf{p}_{H_i}$; $r_k = (x_k, y_k, z_k)$ are the momentum fractions carried by the partons with respect to the three independent directions (x, y, z); $G^{M_{i,f}}_{ks_k\mu_k}$ are the parton distribution functions, the index k denotes all the partons (k=1,2,3,4); the summations are performed over the parton spins

s_k and their z components μ_k; Δ^3 and Δ^4 are the delta-functions providing energy-momentum conservation; $|M(r_k;s_k,\mu_k)|^2$ is the squared amplitude of a parton-parton scattering subprocess; the sign $\otimes$ denotes the convolution in Bjorken r_k-space defined as $a \otimes b = \int \left[\prod_{m=1}^{4} dx_m dy_m dz_m/x_m\right] ab\ (r_k)$. For details of the calculations see [6].

The QRM can be straightforwardly extended to the Λ^0 photoproduction at $x_F > 0$ [7] provided one regards the photon as a hadron in the sense of its well known quark degrees of freedom [8]. A corresponding diagram is shown in Fig. 1. To produce the final Λ^0, a quark q with the quantum numbers (r_1,s_1,μ_1) coming directly from the photon recombines with an appropriate diquark (qq) of the proton with the numbers (r_2,s_2,μ_2). Unlike a hadron-hadron reaction (say $p \to \Lambda$), which is mostly contributed by a single dominant subprocess ($(ud)_0$+s), the situation for the $\gamma \to \Lambda^0$ transition can be fairly expected to be rather rich. The most probable scenarios we have assumed for this case are presented in Fig. 2, the pictures (a), (b) and (c) concern the recombinations of quarks with scalar diquarks (scalar case), u+$(ds)_0$, d+$(us)_0$ and s+$(ud)_0$, respectively, while the (d) and (e) refer to the recombinations of quarks with vector diquarks, u+$(ds)_1$ and d+$(us)_1$ (vector case).

One can find the following formula for the polarization [7]

$$P = \frac{\sum\limits_{i,j,k}\sum\limits_{l} R_l J_D^{lijk}}{\sum\limits_{i,j,k}\sum\limits_{l} J_I^{lijk}}, \tag{2}$$

where R_l are free parameters, so that the corresponding sum runs over the scalar ($l = 0$) and vector ($l = 1$) cases,

$$J_{D(I)}^{lijk} = G_\Lambda^2 \otimes \sigma_{D(I)}^l \otimes f_{(q_i q_j)_l}^p \otimes f_{q_k}^\gamma \otimes \Delta^3 \otimes \Delta^4. \tag{3}$$

Here, G_Λ is the light cone wave function of Λ^0; σ_D^l is the spin dependent term appearing due to the interference between the leading and next-to-leading amplitudes; σ_I^l is the quantity proportional to the total probability; $f_{(q_i q_j)_l}^p$ is the momentum distribution function of the $(q_i q_j)_l$ diquark in the proton (see Fig. 3); $f_{q_k}^\gamma$ is the structure function of the photon (see Fig 3). The sum over i, j, k is rather symbolic and includes only the appropriate combinations of quarks and diquarks to form the final Λ^0 (see Fig. 2). Explicit expressions for $\sigma_{D(I)}^l$ as well as the parameter values were taken from Ref. [5].

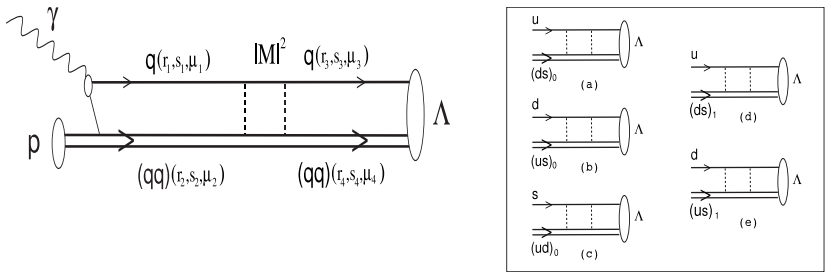

1. **2.**

Figure 1. A diagram corresponding to the Λ^0 photoproduction in the QRM.
Figure 2. Subprocesses of the Λ^0 photoproduction in the QRM.

The calculated p_T dependence of the polarization in the range 0.1 GeV $\leq p_T \leq$ 1.0 GeV in comparison with the HERMES measurements on the Λ^0 polarization in quasi-real photoproduction [10] is shown in Fig. 4.

In Fig. 5, we demonstrated the calculations of the x_F dependence in comparison with the HERMES data. However, we should make at this point a few comments. For some peculiarities of the HERMES experiment, the data are collected not as the traditional x_F dependence but as the dependence on $\zeta = (E_\Lambda + p_{L\Lambda})/(E_b + p_{Lb})$ averaged over p_T (E_b and p_{Lb} are the energy and longitudinal momentum of the beam particle). Unlike x_F, the variable ζ is, thus, just an approximate measure of whether the hyperons were produced in the current or target fragmentation regions. Hence there is some ambiguity in the correlation between x_F and ζ, which causes an arbitrariness in the comparison of the HERMES data with results expressed in terms of x_F. Additionally, the intermediate quasi-real photons of HERMES were not, certainly, monoenergetic, though this problem could be omitted by exploiting the fact that the polarization is incident particle energy independent.

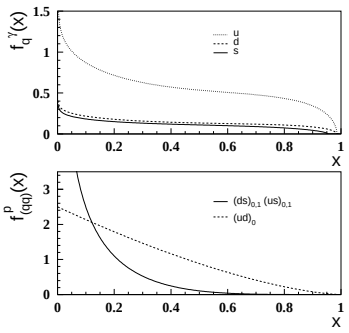

Figure 3. Upper: the photon structure function [8]. Lower: the diquark distribution functions of the proton [9].

To make the comparison with the experiment more correct, we have also averaged the calculated x_F dependence of the polarization over a typical p_T distribution of Λ^0 hyperons produced at HERMES [11]. We show thus obtained results in the lower panel of Fig. 5 in comparison with the experimental ζ dependence of the Λ^0 polarization. We used only the HERMES events at $\zeta > 0.25$ because they more adequately relate to the $x_F > 0$ region. One can see that the calculations sufficiently reproduce the experiment. Similar calculations have been carried out in [12].

We thank Professor A. Efremov and the Organizing Committee for inviting us to present the report at this Workshop, for the financial support I.A. and warm hospitality. We would also like to acknowledge K. Suzuki for providing useful information on the quark recombination model.

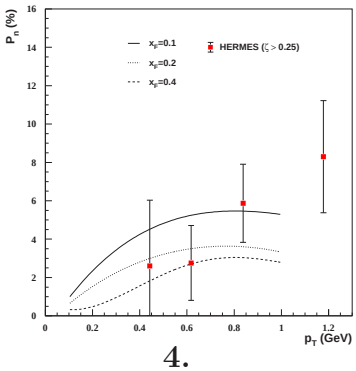

4.

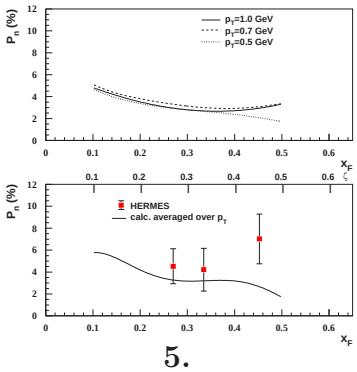

5.

Figure 4. The calculated Λ^0 polarization versus p_T in comparison with the HERMES data [10] taken at $\zeta > 0.25$ (solid points).

Figure 5. Upper: the calculated Λ^0 polarization versus x_F. Lower: the calculated Λ^0 polarization versus x_F after averaging over p_T in comparison with the HERMES data.

References

[1] G. Bunce *et al.*, Phys. Rev. Lett. **36**, 1113 (1976).

[2] A. D. Panagiotou, Int. J. Mod. Phys. A **5**, 1197 (1990).

[3] J. Soffer, hep-ph/9911373.

[4] S. M. Troshin, N. E. Tyurin, hep-ph/0201267.

[5] Y. Yamamoto, K.-I. Kubo and H. Toki, Prog. Theor. Phys. **98**, 95 (1997).

[6] I. Alikhanov and O. Grebenyuk, arXiv:0706.4364.

[7] N. Nakajima, K. Suzuki, H. Toki and K.-I. Kubo, hep-ph/9906451.

[8] M. Glück, E. Reya and A. Vogt, Phys. Rev. D **45**, 3986 (1992).

[9] S. Ekelin and S. Fredrikson, Phys. Lett. B **162**, 373 (1985).

[10] HERMES Collaboration, A. Airapetian *et al.*, arXiv:0704.3133.

[11] HERMES Collaboration, S. Belostotski, O. Grebenyuk and Yu. Naryshkin, Acta Phys. Polon. B **33**, 3785 (2002).

[12] K.-I. Kubo, K. Suzuki, hep-ph/0505179.

POSITIVITY DOMAINS FOR PAIRS OR TRIPLES OF SPIN OBSERVABLES

X. Artru[1†], J.M. Richard[2] and J. Soffer[3]

(1) *Institut de Physique Nucléaire de Lyon, Université de Lyon, CNRS- IN2P3 and Université Lyon 1, 69622 Villeurbanne, France*
(2) *Laboratoire de Physique Subatomique et Cosmologie, CNRS-IN2P3, Université Joseph Fourier and INPG, 38026 Grenoble, France*
(3) *Physics Department, Temple University Barton Hall, 1900 N. 13th Street, Philadelphia, PA 19122 -6082, USA*
† *E-mail: x.artru@ipnl.in2p3.fr*

Abstract

Positivity restrains the allowed domains for pairs or triples of spin observables in polarised reactions. Various domain shapes in $\frac{1}{2}+\frac{1}{2} \to \frac{1}{2}+\frac{1}{2}$ reactions are displayed. Some methods to determine these domains are mentioned and a new one based on the anticommutation between two observables is presented.

1 The spin observables

We consider the polarised 2×2 reaction

$$A + B \to C + D\,, \tag{1}$$

where A, B, C and D are spin one-half particles. An example is

$$\bar{\mathrm{p}}\mathrm{p} \to \overline{\Lambda}\Lambda. \tag{2}$$

The fully polarised differential cross section of (1) can be expressed as

$$\frac{d\sigma}{d\Omega} = I_0\ F\left(\boldsymbol{S}_A, \boldsymbol{S}_B, \check{\boldsymbol{S}}_C, \check{\boldsymbol{S}}_D\right)\,, \tag{3}$$

where F contains the spin dependence. $\boldsymbol{S}_A$ and $\boldsymbol{S}_B$ are the polarisation vectors of the initial particles ($|\boldsymbol{S}| \leq 1$). $\check{\boldsymbol{S}}_C$ and $\check{\boldsymbol{S}}_D$ are pure polarisations ($|\check{\boldsymbol{S}}| = 1$) *accepted* by an ideal spin-filtering detector. They must be distinguished from the *emitted* polarisations $\boldsymbol{S}_C$ and $\boldsymbol{S}_D$ of the final particles. The latter ones depend on the polarisations of the incoming particles, e.g.,

$$\boldsymbol{S}_C = \nabla_{\check{\boldsymbol{S}}_C} F\left(\boldsymbol{S}_A, \boldsymbol{S}_B, \check{\boldsymbol{S}}_C, \check{\boldsymbol{S}}_D = 0\right) \,/\, F\left(\boldsymbol{S}_A, \boldsymbol{S}_B, \check{\boldsymbol{S}}_C = 0, \check{\boldsymbol{S}}_D = 0\right) \tag{4}$$

F is given in terms of the *Cartesian reaction parameters* [3] by

$$F\left(\boldsymbol{S}_A, \boldsymbol{S}_B, \check{\boldsymbol{S}}_C, \check{\boldsymbol{S}}_D\right) = C_{\lambda\mu\nu\tau}\ S_A^\lambda\, S_B^\mu\, \check{S}_C^\nu\, \check{S}_D^\tau\,. \tag{5}$$

In the right-hand side the $\boldsymbol{S}$'s are promoted to four-vectors with $S^0 = 1$. The indices λ, μ, ν, τ, run from 0 to 3, whereas latin indices i, j, k, l, take the values 1, 2, 3, or x, y, z. A summation is understood over each repeated index. S^x, S^y, S^z are measured in a triad of unit vectors $\{\hat{\boldsymbol{x}}, \hat{\boldsymbol{y}}, \hat{\boldsymbol{z}}\}$ which may differ from one particle to the other. A standard choice is to take $\hat{\boldsymbol{z}}$ along the particle momentum and $\hat{\boldsymbol{y}}$ common to all particles and normal to the scattering plane. For example, $C_{0000} \equiv 1$, $C_{xy00} \equiv A_{xy}$ is an initial double-spin asymmetry, C_{000y} is the spontaneous polarisation of particle D along $\hat{\boldsymbol{y}}$, $C_{0y0y} \equiv D_{yy}$ is a spin transmission coefficient from B to D and $C_{00xy} \equiv C_{xy}$ is a final spin correlation.

The Cartesian reaction parameters are given by

$$C_{\lambda\mu\nu\tau} = \mathrm{Tr}\{\, \mathcal{M}\, [\sigma_\lambda(\mathcal{A}) \otimes \sigma_\mu(\mathcal{B})]\, \mathcal{M}^\dagger\, [\sigma_\nu(\mathcal{C}) \otimes \sigma_\tau(\mathcal{D})]\,\} \;/\; \mathrm{Tr}\{\, \mathcal{M}\, \mathcal{M}^\dagger\,\}\,, \tag{6}$$

which will be symbolically abbreviated as a sort of expectation value:

$$(\lambda\mu|\nu\tau) \equiv C_{\lambda\mu\nu\tau} = \langle \sigma_\lambda(A)\, \sigma_\mu(B)\, \sigma_\nu(C)\, \sigma_\tau(D) \rangle\ , \tag{7}$$

with $\sigma_0 = \mathbb{1} \equiv \begin{pmatrix} 1 & 0 \\ 0 & 1 \end{pmatrix}$.

2 The positivity constraints

The cross section (2) is positive for arbitrary *independent* polarisations of the external particles, that is to say

$$F\left(\boldsymbol{S}_A, \boldsymbol{S}_B, \check{\boldsymbol{S}}_C, \check{\boldsymbol{S}}_D\right) \leq 1 \quad \text{for} \quad \boldsymbol{S}_A,\ \boldsymbol{S}_B,\ \check{\boldsymbol{S}}_C,\ \check{\boldsymbol{S}}_D \in \text{unit ball } |\boldsymbol{S}| \leq 1\,. \tag{8}$$

However there are positivity conditions which are stronger than (14). The full positivity condition can be obtained from the positivity of the *cross section matrix* R defined by

$$\begin{aligned} \langle c, d|\mathcal{M}|\dashv, \lfloor\rangle\, \langle \dashv', \lfloor'|\mathcal{M}^\dagger|\rfloor', \lceil'\rangle &= \langle a', b'; c', d'|R|a, b\,; c, d\rangle \\ &= \langle a', b'; c, d|\tilde{R}|a, b\,; c', d'\rangle \end{aligned} \tag{9}$$

in terms of the helicity or transversity amplitudes $\langle c, d|\mathcal{M}|\dashv, \lfloor\rangle$. $\tilde{R}$ is the partial transpose R, the transposition $R \to \tilde{R}$ bearing on the final particles[1]. All spin observables of reaction (1) can be encoded in R or $\tilde{R}$. The diagonal elements of R or $\tilde{R}$ are the fully polarised cross sections when the particles are in the basic spin states. By construction, R (but not necessarily $\tilde{R}$) is *semi-positive definite*, that is to say $\langle\Psi|R|\Psi\rangle \geq 0$ for any Ψ.

Equations (2), (4) and (5) can be rewritten as:

$$\begin{aligned} \frac{d\sigma}{d\Omega}\,(\rho_A, \rho_B, \check{\rho}_C, \check{\rho}_D) &= \mathrm{Tr}\{\tilde{R}\, [\rho_A \otimes \rho_B \otimes \check{\rho}_C \otimes \check{\rho}_D]\}\ , \\ C_{\lambda\mu\nu\tau} &= \mathrm{Tr}\{\tilde{R}\, [\sigma_\lambda(A) \otimes \sigma_\mu(B) \otimes \sigma_\nu(C) \otimes \sigma_\tau(D)]\} \,/\, \mathrm{Tr}\,\tilde{R}\ , \\ &= \mathrm{Tr}\{R\, \left[\sigma_\lambda(A) \otimes \sigma_\mu(B) \otimes \sigma^t_\nu(C) \otimes \sigma^t_\tau(D)\right]\} \,/\, \mathrm{Tr}\, R\ , \end{aligned} \tag{10}$$

[1] Alternatively, keeping the same $\tilde{R}$, one may define R as the full transpose of that given by (9). Then the partial transposition between $\tilde{R}$ and R would bear on the initial particles. This choice was done in Ref. [5], where R is called "grand density matrix".

with $\rho = \frac{1}{2}(\mathbb{1} + \boldsymbol{S}\cdot\sigma)$, $\check{\rho} = \frac{1}{2}(\mathbb{1} + \check{\boldsymbol{S}}\cdot\sigma)$. The last two equations of (18) can be inverted as

$$\begin{aligned} \tilde{R}_1 \equiv (2^4/\operatorname{Tr}\tilde{R})\ \tilde{R} &= C_{\lambda\mu\nu\tau}\ \sigma_\lambda(A)\otimes\sigma_\mu(B)\otimes\sigma_\nu(C)\otimes\sigma_\tau(D)\ , \\ \text{or}\quad R_1 \equiv (2^4/\operatorname{Tr}R)\ R &= C_{\lambda\mu\nu\tau}\ \sigma_\lambda(A)\otimes\sigma_\mu(B)\otimes\sigma^t_\nu(C)\otimes\sigma^t_\tau(D)\ . \end{aligned} \tag{11}$$

The matrix $\tilde{R}_1$ is normalized to have the same trace as the unit matrix and is directly obtained from F replacing the S^μ's by σ^μ's.

3 Various domains for pairs of observables

For one observable, for example $\mathcal{O} = C_{0\mu0\nu} \equiv \langle\sigma_\mu(B)\,\sigma_\nu(D)\rangle$ we have the trivial positivity condition $\mathcal{O} \in [-1,+1]$. For a *pair* $\{\mathcal{O}_1,\mathcal{O}_2\}$ of such observables we have therefore $\{\mathcal{O}_1,\mathcal{O}_2\} \in [-1,+1]^2$. However, in many cases the allowed domain is more restricted than the square. An empirical but systematic method [2, 3] to find the domain simply consists of generating random, fictitious helicity or transversity amplitudes, computing the observables and plotting the results the one against the other. Once the contours revealed, it is an algebraic exercise to demonstrate rigorously the corresponding inequalities. Table 1 summarises the shapes of the domains for the sixteen independent observables of the reaction (2). These domains are either the full square $[-1,+1]^2$ or the unit disk or a triangle.

Table 1: Domain allowed for pairs of observables: the entire square (□), the unit disk (◯), the triangle $|2\mathcal{O}_1| \le \mathcal{O}_2 + 1$ (▽), or $|2\mathcal{O}_2| \le \mathcal{O}_1 + 1$ (◁), where $\mathcal{O}_1$ is horizontal and $\mathcal{O}_2$ vertical. The symbol ⊗indicates that the pair of observables is constrained in the unit disk, but the corresponding operators do not anticommute.

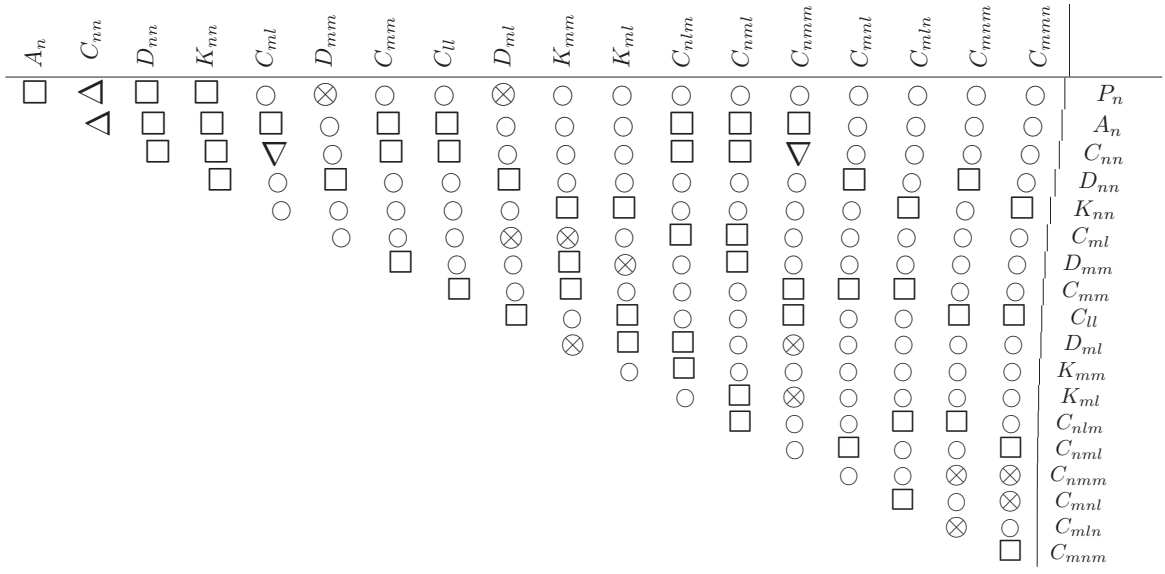

3.1 Anticommutation method

Disk-shaped domains are, in many cases, straightforward results of anticommutation of the observables of the pair. From the last equation of (18), one can consider the observables

as expectation values of operators. Since each σ_μ^2 is equal to the identity, we have $\mathcal{O}^2 = \mathbb{1}$. Furthermore two such operators $\mathcal{O}$ and $\mathcal{O}'$ differing by at least one index (λ, μ, ν or τ) either commute or anticommute.

For pairs of anticommuting observables, disk domains result from the following theorem:

$$\text{If } \mathcal{O}^2 = \mathcal{O}'^2 = \mathbb{1} \text{ and } \mathcal{O} \text{ and } \mathcal{O}' \text{ are anticommuting, then } \langle\mathcal{O}\rangle^2 + \langle\mathcal{O}'\rangle^2 \leq \mathbb{1} \ . \qquad (12)$$

Proof: set $x = \sqrt{\langle\mathcal{O}\rangle^2 + \langle\mathcal{O}'\rangle^2}$, $\langle\mathcal{O}\rangle = ax$, $\langle\mathcal{O}'\rangle = bx$. Then $a^2+b^2 = 1$ and $\langle a\mathcal{O}+b\mathcal{O}'\rangle = x$. From $\mathcal{O}^2 = \mathcal{O}'^2 = \mathbb{1}$ and $\mathcal{O}\mathcal{O}' + \mathcal{O}'\mathcal{O} = 0$ one gets $(a\mathcal{O} + b\mathcal{O}')^2 = \mathbb{1}$ which means that $a\mathcal{O} + b\mathcal{O}'$ has eigenvalues ± 1. Its expectation value x has to be within these eigenvalues, therefore $x^2 \leq 1$.

Note that a disk can occur even if the observables commute, for instance if, due to some symmetry, $\mathcal{O}_2$ has the same expectation value as another operator $\mathcal{O}_2'$ which anticommutes with $\mathcal{O}_1$ and $\mathcal{O}_3$. Examples of this situation are indicated by crossed circles of Table 1.

4 Various domains for triples of observables

The empirical and anticommutation methods generalize straightforwardly to triple of observables. Figure 1 shows the boundary of the domains that we have identified for the observables of the reaction (2): the unit sphere, a pyramid, an upside-down tent, a cone, a cylinder, the intersection of two orthogonal cylinders or a double cone which is slightly smaller than this intersection, a combination of the disk, square and triangle projections delimiting a volume similar to a "coffee filter", the intersection of three orthogonal cylinders (larger than the unit sphere!), a tetrahedron, the intersection of two cylinders and two planes, an octahedron, or figures deduced by mirror symmetry.

Can the domain of a triple be the whole cube? Suppose now that for instance 3 observables $\mathcal{O}_1$, $\mathcal{O}_2$, and $\mathcal{O}_3$, each of which has $+1$ and -1 as extreme eigenvalues, are commuting and that no symmetry relates a pair of them to a non-commuting pair. Does it means that their joint positivity domain $\mathcal{D}\{\mathcal{O}_1, \mathcal{O}_2, \mathcal{O}_3\}$ is the whole cube? A partial negative answer is the following: If the reaction depend on N independent amplitudes, $\mathcal{D}\{\mathcal{O}_1, \mathcal{O}_2, \mathcal{O}_3\}$ can reach at most N corners of the cube [2]. The domains shown in Figure 1 are those of the reaction (2), which has $N = 6$ and indeed none of them reaches more than 6 corners, this number being obtained for the domain (i). More generally, if $N < 8$, all triple observables are restricted in domains smaller than the cube.

5 Outlook

We have seen that the positivity restricts the pairs or triples of observables to subdomains of the square or the cube, some of which having non-trivial shapes. Here we have presented only two methods for determining these domains. Other methods use the Cauchy-Schwarz inequality or the positivity of the subdeterminants of R whose diagonal elements are on the diagonal of R. For exclusive reactions, R is of rank one, therefore all diagonal 2×2 subdeterminants vanish. This links the observables by a large number of quadratic identities, from which inequalities can be obtained straightforwardly. We must tell, however,

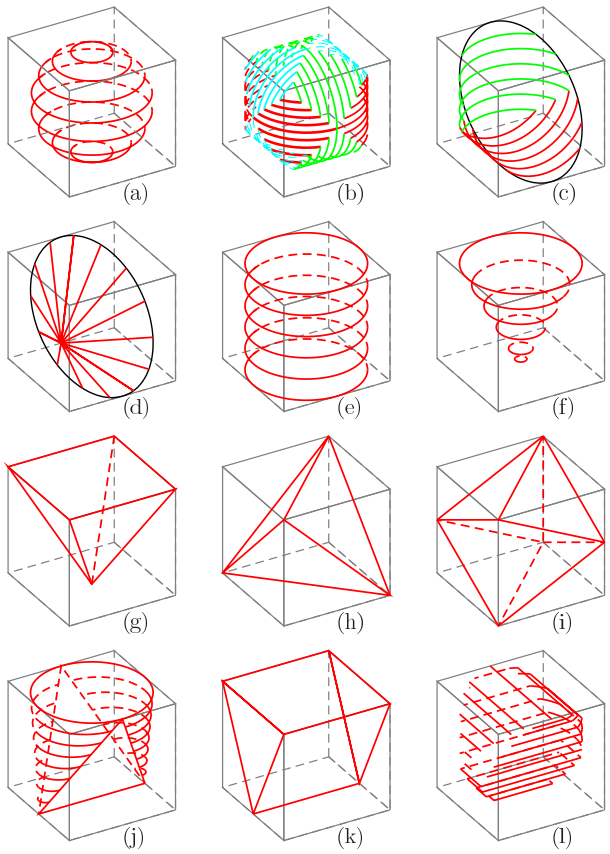

Figure 1: Some allowed domains encountered in simulating randomly three observables: the unit sphere (a), the intersection of three orthogonal cylinders of unit radius (b), the intersection of two cylinders (c), or a slightly smaller double cone (d), a cylinder (e), a cone (f), a pyramid (g), a tetrahedron (h), an octahedron (i), a "coffee filter" (j), an inverted tent (k), and the intersection of two cylinders and a dihedral (l). For clarity, part of the limiting surface is sometimes removed. Some figures transformed by parity with respect to the centre of the cube or by interchange of the axes are also obtained.

that inequalities expressing the positivity of R define joint domains for many observables and it is sometimes a straightforward but lenghty task to obtain the projected domain for two or three observables.

We thank M. Elchikh and O.V. Teryaev for help, useful discussions and comments.

References

[1] C. Bourrely, J. Soffer and E. Leader, Phys. Rept. **59** (1980) 95.

[2] J.M. Richard, Phys. Lett. B **369** (1996) 035205.

[3] M. Elchikh and J.M. Richard, Phys. Rev. C **61** (2000) 358.

[4] X. Artru, M. Elchikh, J.M. Richard, J. Soffer and O. V. Teryaev, submitted to Phys. Reports.

[5] X. Artru and J.M. Richard, Phys. Part. Nucl. **35** (2004) S126, Proc. Dubna Spin Workshop.

CLASSICAL AND QUANTUM CONSTRAINTS IN SPIN PHYSICS

X. Artru

Institut de Physique Nucléaire de Lyon, Université de Lyon,
CNRS- IN2P3 and Université Lyon 1, 69622 Villeurbanne, France
E-mail: x.artru@ipnl.in2p3.fr

Abstract

Constraints on spin observables coming from discrete symmetries such as P, C, T and identical particles may be divided in two types: 1) classical ones, which insure the invariance of the cross sections under the symmetry operation; 2) non-classical ones, which can only be obtained at the level of amplitudes. Similarly, positivity constraints can be divided into classical and non-classical constraints. The former insure the positivity of the cross section for arbitrary individual polarisations of the external particles, the latter extend this requirement to the case of entangled external spins. The domain of classical positivity is shown to be dual to the domain of separability.

1 The spin observables

We consider the polarised 2×2 reaction

$$A + B \to C + D\,, \tag{1}$$

where A, B, C and D are spin one-half particles. Let us recall some of the formalism presented in [1, 2]. The fully polarised differential cross section of (1) reads

$$\frac{d\sigma}{d\Omega} = I_0\ F\left(\boldsymbol{S}_A, \boldsymbol{S}_B, \check{\boldsymbol{S}}_C, \check{\boldsymbol{S}}_D\right)\,, \tag{2}$$

where F contains the spin dependence. $\boldsymbol{S}_A$ and $\boldsymbol{S}_B$ are the polarisation vectors of the initial particles ($|\boldsymbol{S}| \leq 1$). $\check{\boldsymbol{S}}_C$ and $\check{\boldsymbol{S}}_D$ are pure polarisations ($|\check{\boldsymbol{S}}| = 1$) *accepted* by an ideal spin-filtering detector. They must be distinguished from the *emitted* polarisations $\boldsymbol{S}_C$ and $\boldsymbol{S}_D$ of the final particles. These ones depend on the polarisations of the incoming particles, e.g.,

$$\boldsymbol{S}_C = \nabla_{\check{\boldsymbol{S}}_C} F(\boldsymbol{S}_A, \boldsymbol{S}_B, \check{\boldsymbol{S}}_C, \check{\boldsymbol{S}}_D = 0) \,/\, F(\boldsymbol{S}_A, \boldsymbol{S}_B, \check{\boldsymbol{S}}_C = 0, \check{\boldsymbol{S}}_D = 0) \tag{3}$$

F is given in terms of the *Cartesian reaction parameters* [3] by

$$F\left(\boldsymbol{S}_A, \boldsymbol{S}_B, \check{\boldsymbol{S}}_C, \check{\boldsymbol{S}}_D\right) = C_{\lambda\mu\nu\tau}\ S_A^\lambda\, S_B^\mu\, \check{S}_C^\nu\, \check{S}_D^\tau\,. \tag{4}$$

In the right-hand side the $\boldsymbol{S}$'s are promoted to four-vectors with $S^0 = 1$. The indices λ, μ, ν, τ, run from 0 to 3, whereas latin indices i, j, k, l, take the values 1, 2, 3, or x, y, z. A summation is understood over each repeated index. S^x, S^y, S^z are measured

in a triad of unit vectors $\{\hat{\boldsymbol{x}}, \hat{\boldsymbol{y}}, \hat{\boldsymbol{z}}\}$ which may differ from one particle to the other. A standard choice is to take $\hat{\boldsymbol{z}}$ along the particle momentum and $\hat{\boldsymbol{y}}$ common to all particles and normal to the scattering plane. Conversely we have

$$C_{\lambda\mu\nu\tau} = \mathrm{Tr}\{\, \mathcal{M}\, [\sigma_\lambda(\mathcal{A}) \otimes \sigma_\mu(\mathcal{B})]\, \mathcal{M}^\dagger\, [\sigma_\nu(\mathcal{C}) \otimes \sigma_\tau(\mathcal{D})]\,\} \;/\; \mathrm{Tr}\{\, \mathcal{M}\, \mathcal{M}^\dagger\,\}\,, \tag{5}$$

which will be symbolically abbreviated as a sort of expectation value:

$$(\lambda\mu|\nu\tau) \equiv C_{\lambda\mu\nu\tau} = \langle \sigma_\lambda(A)\, \sigma_\mu(B)\, \sigma_\nu(C)\, \sigma_\tau(D) \rangle\ , \tag{6}$$

with $\sigma_0 = \mathbb{1} \equiv \begin{pmatrix} 1 & 0 \\ 0 & 1 \end{pmatrix}$.

3. Classical and quantum constraints for parity

The scattering plane is a symmetry plane for the reaction (1), which is therefore symmetric under under the mirror reflection

$$\Pi = P\, \exp(-i\pi \boldsymbol{J}_y)\ . \tag{7}$$

If parity is conserved the matrix amplitude $\mathcal{M}$ of $A + B \to C + D$ fulfils:

$$\mathcal{M} = (\Pi_C \otimes \Pi_D)^{-1}\, \mathcal{M}\, (\Pi_A \otimes \Pi_B)\ . \tag{8}$$

For one fermion, $\Pi = -i\eta\, \sigma_y$, where η is the intrinsic parity of the fermion. Applying this equation to both $\mathcal{M}$ and $\mathcal{M}^\dagger$ in (5) one obtains the *classical parity rule*

$$\langle \sigma_\lambda(A)\, \sigma_\mu(B)\, \sigma_\nu(C) \sigma_\tau(D)\, \rangle = \left\langle \sigma^\Pi_\lambda(A)\, \sigma^\Pi_\mu(B)\, \sigma^\Pi_\nu(C)\, \sigma^\Pi_\tau(D) \right\rangle\ , \tag{9}$$

where $\mathcal{O}^\Pi$ denotes the reflected operator $\Pi\ \mathcal{O}\ \Pi^{-1}$. For the Pauli matrices, the reflection reads

$$(\sigma_0,\, \sigma_x,\, \sigma_y,\, \sigma_z) \to (\sigma_0,\, -\sigma_x,\, \sigma_u,\, \sigma_z)\ . \tag{10}$$

The multi-spin observable $O_{\lambda\mu\nu\tau} = O_\lambda(A) \otimes O_\mu(B) \otimes O_\nu(C) \otimes O_\tau(D)$ is Π-odd if it contains an odd number of Π-odd Pauli matrices, otherwise it is Π-even. The "classical" rule reads:

If parity is conserved, all Π*-odd observables vanish.*

For instance, $(z0|y0) = 0$, but $(00|y0) \neq 0$. This rule roughly reduces by a factor 2 the number of observables. It does not depend on the intrinsic parity of the particles. It just expresses a classical requirement of reflection symmetry at the level of polarised *cross sections*.

Applying (8) only to $\mathcal{M}$ or to $\mathcal{M}^\dagger$ in (5) one obtains the *non-classical* parity constraint

$$\left\langle \sigma^\lambda_A\, \sigma^\mu_B\, \sigma^\nu_C\, \sigma^\tau_D \right\rangle = \left\langle \left(\Pi_A\, \sigma^\lambda_A\right)\ \left(\Pi_B\, \sigma^\mu_B\right)\ \left(\sigma^\nu_C\, \Pi^{-1}_C\right)\ \left(\sigma^\tau_D\, \Pi^{-1}_D\right) \right\rangle\ , \tag{11}$$

with $\Pi = -i\eta\, \sigma_y$. For the $\frac{1}{2}^+$ baryons one can choose $\eta = i$ so that $\Pi = \Pi^{-1} = \sigma_y$ and

$$\Pi\ (\, \sigma_0,\ \sigma_x,\ \sigma_y,\ \sigma_z\,) = (\sigma_y,\ -i\sigma_z,\ \sigma_0,\ i\,\sigma_x\,)\ . \tag{12}$$

For a pseudoscalar meson, $\Pi = -1$. For example in $\pi + N \to K + \Lambda$ on gets

$$(y|y) = (0|0)\,, \quad (0|y) = (y|0)\,. \tag{13}$$

Clearly the first of these constraints, which relates a polarised cross section to an unpolarised one, cannot be obtained by classical parity arguments. The non-classical parity constraints in the case of spin one-half particles are known as the *Bohr identities* [4]. Non-classical parity rules depend on the intrinsic parities. They yield linear identities between the Π-even observables and reduce the number of independent correlation parameters roughly by another factor 2. For instance, in π^0 decay, the classical parity rule tells that the linear polarisations of the two gamma's are either parallel or orthogonal (not, e.g. at $\pi/4$). The analogue of (11) for photons selects the orthogonal solution.

The subdivision in constraints of the (9) and (11) types, both for parity and time-reversal, has already been made in literature (see Appendix 3.D. of [3]). Here we point out the "classical" versus "non-classical" or "quantum" characters of these two types. Inclusive reactions have only "classical" parity constraints, since the intrinsic parity of the undetected particles can take both signatures.

Similar divisions in classical versus non-classical constraints can be made for other symmetries like charge conjugation, time reversal and permutation of identical particles.

4. Classical positivity constraints

The cross section (2) has to be positive for arbitrary *independent* polarisations of the external particles, that is to say

$$F\left(\boldsymbol{S}_A, \boldsymbol{S}_B, \check{\boldsymbol{S}}_C, \check{\boldsymbol{S}}_D\right) \leq 1 \quad \text{for} \quad \boldsymbol{S}_A,\ \boldsymbol{S}_B,\ \check{\boldsymbol{S}}_C,\ \check{\boldsymbol{S}}_D \in \text{unit ball } |\boldsymbol{S}| \leq 1\,. \tag{14}$$

An equivalent condition is that the polarisation of, for instance, outgoing particle C for given $\boldsymbol{S}_A$, $\boldsymbol{S}_B$, and imposed $\check{\boldsymbol{S}}_D$,

$$\boldsymbol{S}_C(\boldsymbol{S}_A, \boldsymbol{S}_B, \check{\boldsymbol{S}}_D) = \nabla_{\check{\boldsymbol{S}}_C} F(\boldsymbol{S}_A, \boldsymbol{S}_B, \check{\boldsymbol{S}}_C, \check{\boldsymbol{S}}_D) \,/\, F(\boldsymbol{S}_A, \boldsymbol{S}_B, \check{\boldsymbol{S}}_C = 0, \check{\boldsymbol{S}}_D) \tag{15}$$

lies in the unit ball $|\boldsymbol{S}_C| \leq 1$ for any $\boldsymbol{S}_A$, $\boldsymbol{S}_B$ and $\check{\boldsymbol{S}}_D$. For instance in $\pi + N \to K + \Lambda$ the inequalities

$$(C_{0x} \pm C_{zx})^2 + (C_{0y} \pm C_{zy})^2 + (C_{0z} \pm C_{zz})^2 \leq (C_{00} \pm C_{z0})^2 \tag{16}$$

insure that the Λ polarisation does not exceed 1 when the nucleon polarisation is longitudinal.

The condition (14) defines a convex *classical positivity domain* $\mathcal{C}$ in the space of the Cartesian reaction parameters. As we shall see, it is a necessary but *not sufficient* positivity condition.

5. Quantum positivity constraints

All spin observables of reaction (1) can be encoded in the *cross section matrix* R, or its partial transpose $\tilde{R}$, defined by

$$\begin{aligned} \langle c, d|\mathcal{M}|\dashv, \rfloor\rangle \, \langle \dashv', \lfloor'|\mathcal{M}^\dagger|\rfloor', \lceil'\rangle &= \langle a', b'; c', d'|R|a, b\,; c, d\rangle \\ &= \langle a', b'; c, d|\tilde{R}|a, b\,; c', d'\rangle\,. \end{aligned} \tag{17}$$

The transposition linking $\tilde{R}$ to R bears on the final particles. The diagonal elements of R or $\tilde{R}$ are the fully polarised cross sections when the particles are in the basic spin

states. By construction, R (but not necessarily $\tilde{R}$) is *semi-positive definite*, that is to say $\langle\Psi|R|\Psi\rangle \geq 0$ for any Ψ.

Equations (2), (4) and (5) can be rewritten as:

$$\begin{aligned} \frac{d\sigma}{d\Omega}\,(\rho_A,\rho_B,\check{\rho}_C,\check{\rho}_D) &= \mathrm{Tr}\{\tilde{R}\,[\rho_A\otimes\rho_B\otimes\check{\rho}_C\otimes\check{\rho}_D]\}\,, \\ C_{\lambda\mu\nu\tau} &= \mathrm{Tr}\{\tilde{R}\,[\sigma_\lambda(A)\otimes\sigma_\mu(B)\otimes\sigma_\nu(C)\otimes\sigma_\tau(D)]\}\,/\,\mathrm{Tr}\,\tilde{R}\,, \end{aligned} \tag{18}$$

with $\rho=\frac{1}{2}(\mathbb{1}+\boldsymbol{S}\cdot\sigma)$, $\check{\rho}=\frac{1}{2}(\mathbb{1}+\check{\boldsymbol{S}}\cdot\sigma)$. The last equation of (18) can be inverted as

$$\begin{aligned} \tilde{R}_1\equiv(2^4/\,\mathrm{Tr}\,\tilde{R})\;\;\tilde{R} &= C_{\lambda\mu\nu\tau}\;\sigma_\lambda(A)\otimes\sigma_\mu(B)\otimes\sigma_\nu(C)\otimes\sigma_\tau(D)\,, \\ \text{or}\quad R_1\equiv(2^4/(\mathrm{Tr}\,R)\;\;R &= C_{\lambda\mu\nu\tau}\;\sigma_\lambda(A)\otimes\sigma_\mu(B)\otimes\sigma^t_\nu(C)\otimes\sigma^t_\tau(D)\,. \end{aligned} \tag{19}$$

The matrix $\tilde{R}_1$ is normalised to have the same trace as the unit matrix and is directly obtained from F replacing the S^μ's by σ^μ's. It allows to calculate the cross section for *entangled* initial states, replacing $\rho_A\otimes\rho_B$ by ρ_{A+B} in (18), as well as the joint density matrix of C and D:

$$\rho_{C+D}=\mathrm{Tr}_{A,B}\{\,\tilde{R}\,[\rho_A\otimes\rho_B]\,\}/\,\mathrm{Tr}\{\tilde{R}\,[\rho_A\otimes\rho_B]\,\}\,. \tag{20}$$

The single polarisation of particle C can then be obtained by $\rho_C=\mathrm{Tr}_D\{\rho_{C+D}\}$, in place of (3).

The semi-positivity of R leads to *quantum positivity* constraints on the Cartesian reaction parameters which are stronger than the classical ones. Suppose, for instance, that

$$F(\boldsymbol{S}_A,\boldsymbol{S}_B,0,0)=1+c\,\boldsymbol{S}_A\cdot\boldsymbol{S}_B\,. \tag{21}$$

The initially polarised cross section is then

$$\frac{d\sigma}{d\Omega}\,(\rho_{A+B})=\mathrm{Tr}\{\tilde{R}\;\,[\rho_{A+B}\otimes\mathbb{1}_{\mathbb{C}+\mathbb{D}}]\,\}\propto\mathrm{Tr}\{(\mathbb{1}+\mathbb{c}\,\sigma_{\mathbb{A}}\cdot\sigma_{\mathbb{B}})\,\rho_{\mathbb{A}+\mathbb{B}}\,\}\,, \tag{22}$$

where $\sigma_A\cdot\sigma_B\equiv\sum_{i=1}^3\sigma_A^i\otimes\sigma_B^i$. For uncorrelated $\boldsymbol{S}_A$ and $\boldsymbol{S}_B$ one has $d\sigma/d\Omega\propto 1+c\,\boldsymbol{S}_A\cdot\boldsymbol{S}_B\geq 0$, therefore classical positivity is fulfilled for $c\in[-1,+1]$. However, if A and B form a singlet spin state, of density matrix $\rho_{A+B}=\frac{1}{4}\,(\mathbb{1}-\sigma_{\mathbb{A}}\cdot\sigma_{\mathbb{B}})$, then $d\sigma/d\Omega$ is positive only for $c\in[-1,+1/3]$.

The occurrence of a negative cross section for $c>1/3$ comes from the non-positivity of $\mathbb{1}+\sigma_{\mathbb{A}}\cdot\sigma_{\mathbb{B}}$, therefore of R. This non-positivity was revealed by an entangled initial state (the spin singlet state). This example shows that positivity has to be tested not only with factorised (or separable states), but also with entangled ones.

Similarly, a final spin correlation of the form $F(0,0,\check{\boldsymbol{S}}_C,\check{\boldsymbol{S}}_D)=1+c\,\check{\boldsymbol{S}}_C\cdot\check{\boldsymbol{S}}_D$ is classically allowed for $c\in[-1,+1]$, but quantum-mechanically for $c\in[-1,+1/3]$ only. As a check rule, "quantum mechanics does not allow fully parallel spins". These examples have a crossed symmetric counterpart: a spin transmission between A and C of the form

$$F(\boldsymbol{S}_A,0,\check{\boldsymbol{S}}_C,0)=1+c\,\boldsymbol{S}_A\cdot\check{\boldsymbol{S}}_C \tag{23}$$

is classically allowed for $c\in[-1,+1]$, but quantum-mechanically for $c\in[-1/3,+1]$ only. For $c<-1/3$ the cross section matrix is non-positive and this can be revealed by an

"entangled state in the t-channel". The corresponding check rule is "quantum mechanics does not allow full spin reversal". The lesson of these examples is that positivity has to be tested with classical and *entangled* states in the *direct* and *crossed* channels.

An example of non-classical positivity constraint is the the Soffer inequality [6]:

$$2\delta q(x) \leq q(x) + \Delta q(x)$$

between the quark helicity- and transversity distributions $\Delta q(x)$ and $\delta q(x)$.

6. Domains of quantum positivity, classical positivity and separability

As we have seen one can distinguish a *classical positivity domain* which is larger than the true or *quantum* positivity domain. To have a more precise idea about the differences between these two domains, let us study the constraints on the initial spin observables only. For this purpose we introduce the matrix

$$\eta_{A+B} = \mathrm{Tr}_{C,D}\left[R/(\mathrm{Tr}\, R)\right] \tag{24}$$

obtained by taking the partial trace over the final particles and renormalising to unit trace. Like R, η_{A+B} has to be (semi-)positive. The initially polarised cross section reads

$$\frac{d\sigma}{d\Omega}\left(\rho_{A+B}\right) = \mathrm{Tr}\{\eta_{A+B}\ \rho_{A+B}\}\ , \tag{25}$$

Classical positivity requires $\mathrm{Tr}\{\eta_{A+B}\ (\rho_A \otimes \rho_B)\} \geq 0$ for any individual density matrices ρ_A and ρ_B. More generally

$$\mathrm{Tr}\{\eta_{A+B}\,\rho_{A+B}\} \geq 0 \quad \text{for any } \textit{separable } \rho_{A+B}\,, \tag{26}$$

whereas quantum positivity requires

$$\mathrm{Tr}\{\eta_{A+B}\,\rho_{A+B}\} \geq 0 \quad \text{for any separable } \textit{or entangled } \rho_{A+B}\,. \tag{27}$$

One can say that the classical positivity domain $\mathcal{C}$ is *dual* to the separability domain $\mathcal{S}$ in the sense that $\mathrm{Tr}\{\eta\,\rho\} \geq 0$ for any pair $\{\eta \in \mathcal{C}\,, \rho \in \mathcal{S}\}$. As for the quantum positivity domain $\mathcal{D}$, it is dual to itself. We have

$$\mathcal{S} \subset\ \mathcal{D}\ \subset \mathcal{C}\,, \tag{28}$$

these three domains being convex.

Let us take the traceless part $\rho_\perp = \rho - \mathbb{1}/\mathbb{N}$ of ρ, where $N = \mathrm{Tr}(\mathbb{1})$ is the dimension of the $A+B$ spin space, and introduce the Euclidian scalar product $\boldsymbol{\eta}_\perp \cdot \boldsymbol{\rho}_\perp = \mathrm{Tr}(\eta_\perp \rho_\perp)$ where $\boldsymbol{\rho}_\perp$ is considered as a N^2-1 dimensional vector. The duality between $\mathcal{C}$ and $\mathcal{S}$ can be expressed as

$$\boldsymbol{\rho}_\perp \cdot \boldsymbol{\eta}_\perp \geq -1/N\,, \quad \rho \in \mathcal{C}\,,\ \eta \in \mathcal{S}\,. \tag{29}$$

Figure 1 schematises the properties (28) and (29) in the $\boldsymbol{\rho}_\perp$ space. Equation (29) means that the boundaries $\partial\mathcal{C}$ and $\partial\mathcal{S}$ of the two domains are *polar reciprocal* of each other: when $\boldsymbol{\eta}_\perp$ moves on $\partial\mathcal{S}$, the reciprocal plane in $\boldsymbol{\rho}_\perp$ space defined by $\boldsymbol{\rho}_\perp.\boldsymbol{\eta}_\perp = -1/N$ envelops $\partial\mathcal{C}$, as shown in Fig. 1. Also shown in this figure is the symmetry between $\mathcal{D}$ and the domain $\mathcal{D}^{\sqrt{\sqcup}}$ where the partial transform ρ^{pt}_{A+B} of ρ_{A+B} is positive, the transposition concerning

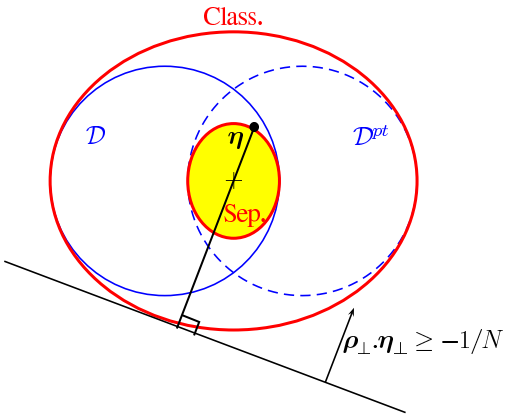

Figure 1: Schematic shapes of the classical positivity domain in the $\rho_\perp$ space. ($\mathcal{C} \equiv \mathcal{C}\updownarrow\dashv\int\int.$), the separability domain ($\mathcal{S} \equiv \mathcal{S}\rceil\ \sqrt{\ }.$) and the true positivity domain $\mathcal{D}$. The dashed contour indicates the domain $\mathcal{D}^{\sqrt{\sqcup}}$ where the partial transform is positive. A matrix η of the boundary $\partial\mathcal{S}$ is represented together with its reciprocal polar line $\boldsymbol{\rho}_\perp \cdot \boldsymbol{\eta}_\perp = 1/N$, which is tangent to $\partial\mathcal{C}$.

either A or B. Indeed separability [7,8] and classical positivity are preserved under partial transposition and we have

$$\mathcal{S} \subset \mathcal{D}^{\sqrt{\sqcup}} \subset \mathcal{C}\,. \tag{30}$$

The duality between $\mathcal{C}$ and $\mathcal{S}$ may still be visible with a subset of observables. For instance, for a two-fermion system of density matrix $\rho_{A+B} = \frac{1}{4}\, C_{\mu\nu}\, \sigma_\mu(A) \otimes \sigma_\nu(B)$, the classical positivity domain of the triple $\{C_{xx}\,, C_{yy}\,, C_{zz}\}$ is the whole cube $[-1, +1]^3$, the quantum positivity domain is the tetrahedron defined by

$$C_{xx} - C_{yy} - C_{zz} \leq 1 \quad \text{and circular permutations,} \quad C_{xx} + C_{yy} + C_{zz} \leq 1\,, \tag{31}$$

and the separability domain, an octahedron, is the intersection of the tetrahedron with its mirror figure. One can see on Fig. 2 the polar reciprocity (edge $\leftrightarrow$ edge) and (summit $\leftrightarrow$ face) between the cube and the octahedron. Related results are found in [9].

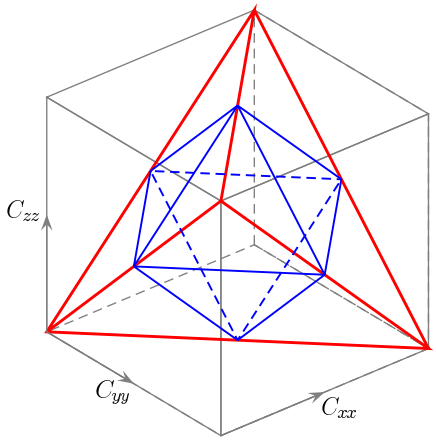

Figure 2: Classical positivity domain (cube), true positivity domain (tetrahedron) and separability domain (octahedron) for the triple $\{C_{xx}\,, C_{yy}\,, C_{zz}\}$ of observables.

7. Outlook

We have qualified as *classical* the symmetry and positivity constraints which can be derived by classical arguments concerning the polarised cross sections for separate polarisations of the external particles. Working at the level of amplitudes, or of the cross section matrix, one obtains quantum constraints which in many cases are stronger than

the classical ones, therefore called non-classical. The number of non-classical constraints is expected to decrease when only part of the external particles are polarised or analysed, and in fact, there is no non-classical parity constraint for inclusive reactions. The weakening of non-classical constraints when part of the information is lost or discarded has some similarity with decoherence. Nevertheless some non-classical positivity constraints, for instance the Soffer inequality, still remain in the inclusive case.

A duality has been established between the domains of separability $\mathcal{S}$ and classical positivity $\mathcal{C}$. In the space of the traceless components $\boldsymbol{\rho}_\perp$, the boundary $\partial\mathcal{S}$ and $\partial\mathcal{C}$ of these domains are polar reciprocal of each other. The boundary of $\mathcal{C}$ can be determined by algebraic equations using (14). This may offer a method for the long-standing problem of determining $\mathcal{S}$.

Acknowledgements The author thanks M. Elchikh, O.V. Teryaev, J.M. Richard and J. Soffer for help, useful discussions and comments.

References

[1] X. Artru, J.M. Richard and J. Soffer, submitted to this Proceedings.

[2] X. Artru, M. Elchikh, J.M. Richard, J. Soffer and O. V. Teryaev, submitted to Phys. Reports.

[3] C. Bourrely, J. Soffer and E. Leader, Phys. Rept. **59** (1980) 95.

[4] A. Bohr, Nucl. Phys. **10** (1959) 486.

[5] X. Artru and J.M. Richard, Phys. Part. Nucl. **35** (2004) S126, Proc. Dubna Spin Workshop.

[6] J. Soffer, Phys. Rev. Lett. **74** (1995) 1292.

[7] A. Peres, Phys. Rev. Lett. **77** (1996) 1413.

[8] M. Horodecki, P. Horodecki and R. Horodecki, Phys. Lett. A **233** (1996) 1.

[9] R. A. Bertlmann, H. Narnhofer and W. Thirring, Phys. Rev. A **66** (2002) 032319.

SPIN STRUCTURE OF NUCLEON AND ANTI-HYPERON POLARIZATION IN HIGH ENERGY PP COLLISION WITH POLARIZED BEAM

Ye Chen

Department of Physics, Shandong University, Jinan, Shandong 250100, China

Abstract

We study the longitudinal polarization of anti-hyperons in polarized high energy pp collisions at large transverse momenta. Using the Monte-Carlo event generator PYTHIA, we make a detailed analysis of the different contributions to the anti-hyperons in the final states. We calculate the anti-hyperon polarization using the different parameterizations of polarized parton densities and models for polarized fragmentation functions. We found out that the polarization of $\bar{\Lambda}$ and $\bar{\Xi}$ are quite sensitive to the polarization of the anti-strange sea of the nucleon while the polarization of $\bar{\Sigma}^-$ and $\bar{\Sigma}^+$ show sensitivities to the light sea quarks' polarized distribution. Our results show that, by measuring the polarization of those anti-hyperons, we should be able to obtain useful information on the anti-sea polarization of nucleon.

Hyperon polarization provides us a useful tool in studying the spin structure of nucleon and the spin effects in fragmentation. The following two reasons lead us to study the anti-hyperons' polarization: [1]

(I) HERMES did flavor decomposition of the sea quark helicity distribution in the nucleon. They found that the polarization of the strangeness quark consists with zero [2]. It is different from the earlier results derived from the inclusive DIS data. Studying the polarization of anti-hyperon in pp collision may help us to know more about the sea quarks' polarization in the nucleon.

(II) COMPASS's data indicate a difference between Λ and $\bar{\Lambda}$'s polarization in polarized DIS [3]. So further study on the polarization of anti-hyperon via other processes is necessary. The spin program at RHIC is also an ideal place to measure the anti-hyperon polarization for its high luminosity and high polarized beams.

This talk summarizes our recent studies on the longitudinal polarization of inclusive anti-hyperons $\bar{\Lambda}$, $\bar{\Sigma}^-$, $\bar{\Sigma}^+$, $\bar{\Xi}^0$ and $\bar{\Xi}^+$ at large transverse momenta in singly longitudinally polarized pp collision [1].

We consider the inclusive production of high p_T anti-hyperons ($\bar{H}$) in pp collisions with one of the beams longitudinally polarized. The longitudinal polarization of $\bar{H}$ is defined as,

$$P_{\bar{H}} \equiv \frac{d\sigma(p_+p \to \bar{H}_+X) - d\sigma(p_+p \to \bar{H}_-X)}{d\sigma(p_+p \to \bar{H}_+X) + d\sigma(p_+p \to \bar{H}_-X)} = \frac{d\Delta\sigma(\boldsymbol{p}p \to \bar{H}X)}{d\sigma(pp \to \bar{H}X)}, \tag{1}$$

where $\Delta\sigma$ and σ are the polarized and unpolarized inclusive production cross section respectively. At high p_T region, the factorization theorem works. In that case, the cross section of the final anti-hyperons can be written as a convolution integral of the three

parts,

$$\frac{d\Delta\sigma}{d\eta}(\boldsymbol{p}p \to \bar{H}X) = \int_{p_T^{min}} dp_T \sum_{abcd} \int dx_a dx_b \Delta f_a(x_a) f_b(x_b) D_L^{\boldsymbol{a}b\to\boldsymbol{c}d} \frac{d\hat{\sigma}}{d\hat{t}}(ab \to cd) \Delta D_c^{\bar{H}}(z), \quad (2)$$

where $\Delta f_a(x_a)$ and $f_b(x_b)$ are the polarized and unpolarized parton distribution functions in the protons, with x_a and x_b the momentum fractions carried by partons a and b. $D^{\boldsymbol{a}b\to\boldsymbol{c}d}$ is the spin transfer factor in the elementary hard scattering process $\boldsymbol{a}b \to \boldsymbol{c}d$. It can be calculated by pQCD and at leading order it is a function of the four momenta of the partons a–d. $\Delta D_c^{\bar{H}}(z)$ is the polarized fragmentation function of $\bar{H}$. The $\bar{H}$ transverse momentum is integrated above p_T^{min}; the summation concerns all elementary hard scattering processes.

The factors in Eq. (2) with less certainty are the polarized parton distribution function and the polarized fragmentation function. There are several parameterizations for the polarized parton distribution functions $\Delta f(x)$. However, large differences exist in different sets particularly for the anti-sea quarks' distributions.

And for the polarized fragmentation function, the anti-hyperons' production can be sorted into two classes according to their fragmentation originality. One is the polarized fragmentation function for the directly produced anti-hyperon; the other is the polarized fragmentation function for the anti-hyperon which is decayed from a heavier one. For the decayed anti-hyperon, the polarized fragmentation function can be written as,

$$\Delta D_c^{\bar{H}}(z; \text{decay}) = \sum_{\mathrm{j}} \int \mathrm{dz'} \mathrm{t}^{\mathrm{D}}_{\bar{\mathrm{H}},\bar{\mathrm{H}}_{\mathrm{j}}} \mathrm{K}_{\bar{\mathrm{H}},\bar{\mathrm{H}}_{\mathrm{j}}}(\mathrm{z},\mathrm{z'}) \Delta \mathrm{D}_{\mathrm{c}}^{\bar{\mathrm{H}}_{\mathrm{j}}}(\mathrm{z'}, \text{direct}). \quad (3)$$

$t^D_{\bar{H},\bar{H}_j}$ is the spin transfer factor in decay process. $K_{\bar{H},\bar{H}_j}(z,z')$ is the probability of producing an $\bar{H}$ with a fractional momentum z in decay of $\bar{H}_j$ with z'. The unknown part is thus the polarized fragmentation for directly produced anti-hyperon $\Delta D_c^{\bar{H}_j}(z', \text{direct})$. It cannot be calculated by pQCD and we have to model it [4].

The directly produced anti-hyperons were further divided into two classes. Class A is the anti-hyperon which contains the fragmenting quark with flavor f; class B is the anti-hyperon that does not contain the fragmenting quark. For class B, the polarized fragmentation function is approximately equal to zero, and therefore the polarized fragmentation function for directly produced anti-hyperon is only that of class A. It can be written as $\Delta D_f^{\bar{H}(A)}(z) = t^F_{\bar{H},f} D_f^{\bar{H}(A)}(z)$. Two pictures called SU(6) picture and DIS picture are adopted when calculating the spin transfer factor $t^F_{\bar{H},f}$ [4]. We also evaluate the fractional contributions to final anti-hyperons for different flavor compositions by a Monte-Carlo event generator PYTHIA [5].

With the calculation method we mentioned above, we can finally get the polarization of different anti-hyperons. We use different parameterizations for the polarized parton distributions and use the SU(6) and DIS pictures for spin transfer in fragmentation. Fig. 1 shows the polarization for transverse momenta $p_T > 8\,\mathrm{GeV}$ range versus pseudo-rapidity η. The parameterizations set GRSV2000 [6] for polarized parton distributions are taken. The main characteristics of the results are [1]:

(I)the size of the polarization increases in the forward direction with respect to the polarized proton beam and can be as large as 10% ($\bar{\Xi}^0$, $\bar{\Xi}^+$) at $\eta = 2$.

(II)the differences between the $\bar{H}$ polarization obtained for different parameterizations of the polarized parton distribution functions are generally larger than the differences between the results for different models for the spin transfer in fragmentation.

(III)the $\bar{\Xi}^0$ and $\bar{\Xi}^+$ polarization are similar to each other because of the dominance of $\bar{s}$-fragmentation; they are somewhat larger than the $\bar{\Lambda}$ polarization because of the smaller decay contributions and their sensitivity to $\Delta\bar{s}$ is thus more direct.

(IV)the results for $\bar{\Sigma}^-$ and $\bar{\Sigma}^+$ for the GRSV2000 valence distributions differ in sign because of the sign difference in $\Delta\bar{u}(x)$ and $\Delta\bar{d}(x)$, and in size and shape because of flavor-symmetry breaking in the unpolarized and this polarized parton distribution scenario.

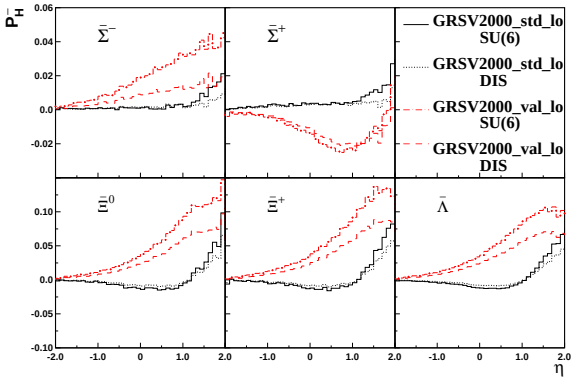

Fig. 1 Longitudinal polarization for anti-hyperons with transverse momentum $p_T \geq 8$ GeV/c in pp collisions at $\sqrt{s} = 200$ GeV with one longitudinally polarized beam versus pseudo-rapidity η. Positive η is taken along the direction of the polarized beam.

In summary, we have evaluated the longitudinal polarization of the $\bar{\Sigma}^-$, $\bar{\Sigma}^+$, $\bar{\Xi}^0$, and $\bar{\Xi}^+$ anti-hyperons in singly longitudinally polarized pp collision. The results show sensitivity to the anti-sea quarks' polarization in the nucleon. In particular, the $\bar{\Xi}^0$ and $\bar{\Xi}^+$ polarization are sensitive to strange anti-quark's polarization $\Delta\bar{s}(x)$ and the $\bar{\Sigma}^-$ and $\bar{\Sigma}^+$ polarization are sensitive to the light sea quarks' polarization. Precision measurements at the RHIC polarized pp-collider should be able to provide more information on the sea quarks' polarization in the nucleon.

Acknowledgments: The speaker would like to thank the organizer to provide such a nice chance to present the talk. Also many thanks to the collaborators Z. T. Liang, E. Sichtermann, Q. H. Xu and S. S. Zhou. This work was supported in part by the National Science Foundation of China (NSFC) with grant No. 10175037 and No. 10405016.

References

[1] Q. H. Xu, Z. T. Liang and E. Sichtermann, Phys. Rev. **D73**, 077503 (2006); Y. Chen, Z. T. Liang, E. Sichtermann, Q. H. Xu and S. S. Zhou, arXiv:0707.0534[hep-ph].

[2] A. Airapetian *et al.* [HERMES Collaboration], Phys. Rev. **D71**, 012003 (2005).

[3] M. G. Sapozhnikov, [COMPASS Collaboration], hep-ex/0503009 and hep-ex/0602002; also V. Yu. Alexakhin, [COMPASS Collaboration], hep-ex/0502014.

[4] C. Boros and Z. T. Liang, Phys. Rev. **D57**, 4491 (1998); C. X. Liu and Z. T. Liang, Phys. Rev. **D62**, 094001 (2000); Q. H. Xu, C. X. Liu and Z. T. Liang, Phys. Rev. **D65**, 114008 (2002); H. Dong, J. Zhou and Z. T. Liang, Phys. Rev. **D72**, 033006 (2005).

[5] T. Sjöstrand, S. Mrenna, P. Skands, **JHEP 0605**, 026 (2006); B. Andersson, G. Gustafson, G. Ingelman and T. Sjöstrand, Phys. Rep. **97**, 31 (1983).

[6] M. Glück, E. Reya, M. Stratmann and W. Vogelsang, Phys. Rev. **D63**, 094005 (2001); Phys. Rev. **D53**, 4775 (1996).

Discussion

Q. (O.Teryaev, JINR) Have you fitted the anti-hyperons' production in high p_T region when you do the Monte Carlo calculations using PYTHIA for unpolarized pp collision?

A. It is right that the production rates, in particular the contributions from different sub-processes, play a very important role in the calculations of the polarization in reactions using polarized beams. That is in fact why we have, unlike many of the authors in the studies of the similar problems, used PYTHIA to calculate them for the following reasons:

- High p_T jet cross section can be calculated using pQCD and PYTHIA provides a good fit in particular in pp collisions.
- PYTHIA provides a good fit to the ratios of different types of hadrons in a jet in e.g. e^+e^- annihilation.

Considering the universality of the hadronization mechanism, we think that this means that the generator can provide us a good fit to hadron production in high p_T jet in unpolarized pp reactions. Since there is no published data for high p_T anti-hyperon production available yet, we think PYTHIA provides us one of the best choice to make such estimations. That is why we used it in our calculations.

Q. (M. Sapozhnikov, JINR) Is the sensitivity to $\Delta\bar{s}$ large enough to be measured at RHIC?

A. We have estimated the precision with which $\bar{H}$ polarization measurements could be made at RHIC. For an analyzed integrated luminosity of $\mathcal{L} \simeq 300$ pb^{-1} and a proton beam polarization of $P \simeq 70\%$, we anticipate that e.g. $P_{\bar{\Xi}}$ could be measured to within $\sim$0.02 uncertainty. See ref. [1] for details.

GAUGE INVARIANCE AND RENORMALIZATION-GROUP EFFECTS IN TRANSVERSE-MOMENTUM DEPENDENT PARTON DISTRIBUTION FUNCTIONS

I. O. Cherednikov[1,2⋆], N. G. Stefanis[2†]

(1) *Bogoliubov Laboratory of Theoretical Physics, JINR, 141980 Dubna, Russia*
(2) *Institut für Theoretische Physik II, Ruhr-Universität Bochum, D-44780 Bochum, Germany*
⋆ *E-mail: igor.cherednikov@tp2.ruhr-uni-bochum.de*
† *E-mail: stefanis@tp2.ruhr-uni-bochum.de*

Abstract

A range of issues pertaining to the use of Wilson lines in integrated and transverse-momentum dependent (TMD) parton distribution functions (PDF) is discussed. The relation between gauge invariance and the renormalization properties of the Wilson-line integrals is given particular attention. Using an anomalous-dimensions based analysis in the light-cone gauge, a generalized definition of the TMD PDFs is proposed, which employs a cusped Wilson line, and contains an intrinsic "Coulomb-like" phase.

Introduction. Various calculations in the last few years have addressed TMD PDFs, among others those in which a previously overlooked transverse gauge link was proposed [1–3]. The sustained interest in integrated and unintegrated (TMD) PDFs lies in the fact that they encapsulate the nonperturbative quark dynamics of confinement and hence in their potential use in phenomenological applications to be compared with experimental data. But while integrated PDFs can be defined in a gauge-invariant way that is compatible with factorization theorems, the definition of TMD PDFs faces serious problems related to specific light-cone divergences (see, e.g., [4, 5]). These so-called rapidity divergences [6] are related to lightlike Wilson lines (or the use of the light-cone gauge $A^+ = 0$) [7, 8] and cannot be cured by ordinary ultraviolet (UV) renormalization alone. In addition, in order to recover the result found in the Feynman gauge, the advanced boundary condition has to be adopted to make the transverse gauge link reduce to unity [2].

The basic statement of the presented work [9] is this: In order to define an unintegrated PDF that preserves gauge invariance under the proviso of collinear factorization and multiplicative renormalizability, we shift our attention from the Wilson lines to their anomalous dimensions within the $\overline{\rm MS}$ scheme. We will provide concrete arguments that the appropriate contour which goes through light-cone infinity is a cusped one. To compensate the associated anomalous dimension, we introduce into the definition of the TMD PDF a soft counter term (in the sense of Collins and Hautmann [10–12]) which generates the same anomalous dimension but with opposite sign. Hence, the total TMD PDF expression has the same one-loop anomalous dimension as the one that would involve a straight lightlike line between the quark operators. Note, however, that such a gauge contour cannot be adopted because the gluons originating from this would not be collinear with the struck quark and hence they would cause a mismatch in the gluon rapidities.

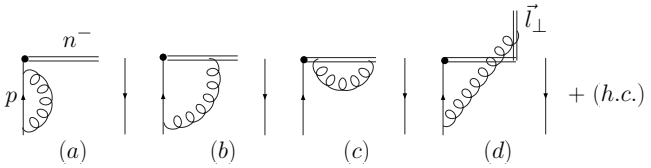

Figure 1: One-loop gluon contributions to the UV-divergences of the TMD PDF. Double lines denote gauge links. Diagrams (b) and (c) are absent in the light-cone gauge.

To substantiate our arguments, we write the standard expression for the TMD PDF [6] for a quark-to-quark distribution, supplemented by a transverse gauge link [2]:

$$f_{q/q}(x,\boldsymbol{k}_\perp) = \frac{1}{2}\int \frac{d\xi^- d^2\xi_\perp}{2\pi(2\pi)^2} \mathrm{e}^{-ik^+\xi^- + i\mathbf{k}_\perp\cdot\xi_\perp} \left\langle q(p)|\bar\psi(\xi^-,\xi_\perp)[\xi^-,\boldsymbol{\xi}_\perp;\infty^-,\boldsymbol{\xi}_\perp]^\dagger \right. \\ \times [\infty^-,\boldsymbol{\xi}_\perp;\infty^-,\boldsymbol{\infty}_\perp]^\dagger \gamma^+ [\infty^-,\boldsymbol{\infty}_\perp;\infty^-,\mathbf{0}_\perp][\infty^-,\mathbf{0}_\perp;0^-,\mathbf{0}_\perp] \\ \left. \times \psi(0^-,\mathbf{0}_\perp)|q(p)\right\rangle \ |_{\xi^+=0} \ , \tag{1}$$

where the gauge links are defined according to

$$[\infty^-,\boldsymbol{z}_\perp;z^-,\boldsymbol{z}_\perp] \equiv \mathcal{P}\mathrm{e}^{ig\int_0^\infty d\tau \ n_\mu \hat A^\mu(z+n\tau)} \ , \ [\infty^-,\boldsymbol{\infty}_\perp;\infty^-,\boldsymbol{\xi}_\perp] \equiv \mathcal{P}\mathrm{e}^{ig\int_0^\infty d\tau \ l_i \hat A_i(\boldsymbol{\xi}_\perp + l_i\tau)} \tag{2}$$

with analogous expressions for the other gauge links and where $\boldsymbol{l_i}$ represents an arbitrary vector in the transverse direction and $\mathcal{P}$ denotes path ordering.

Within the Collins-Soper approach [6] ($n^2 \neq 0$), the anomalous dimension of $f_{q/q}(x,k_\perp)$ is [13]

$$\gamma_{\rm CS} = \frac{1}{2}\ \mu\frac{d}{d\mu}\ \ln Z_f(\mu,\alpha_s;\epsilon) = \frac{3}{4}\frac{\alpha_s}{\pi}C_{\rm F} + O(\alpha_s^2) = \gamma_{\rm smooth} \ , \tag{3}$$

where Z_f is the renormalization constant of $f_{q/q}(x,k_\perp)$ in the $\overline{\rm MS}$ scheme. Recall that all smooth contours off the light cone in the transverse direction give rise to the same anomalous dimension due to the endpoints of the so-called connector insertion [14].

Figure 1 shows the one-loop diagrams, contributing to $f_{q/q}(x,\boldsymbol{k}_\perp)$ in the light-cone (LC) gauge $(A\cdot n^-) = 0,\ (n^-)^2 = 0$. The poles $1/q^+$ of the gluon propagator

$$D^{\rm LC}_{\mu\nu}(q) = \frac{1}{q^2}\Big(g_{\mu\nu} - \frac{q_\mu n^-_\nu + q_\nu n^-_\mu}{[q^+]}\Big) \ , \tag{4}$$

are regularized by $1/[q^+] = 1/(q^+ \pm i\Delta)$, where Δ is small but finite.

In addition to the standard UV renormalization terms, one has UV divergent contributions from diagrams (a) and (d) stemming from the p^+-dependent term in

$$\Sigma^{\rm UV}_{\rm LC}(\alpha_s,\epsilon) = \frac{\alpha_s}{\pi}C_{\rm F}2\ \left[\frac{1}{\epsilon}\left(\frac{3}{4} + \ln\frac{\Delta}{p^+}\right) - \gamma_E + \ln 4\pi\right] . \tag{5}$$

Noting that the contribution associated with the transverse gauge link at infinity (diagram Fig. 1(d)) exactly cancels against the term entailed by the adopted pole prescription in the gluon propagator, we find for the corresponding anomalous dimension

$$\gamma_{\rm LC} = \frac{\alpha_s}{\pi}C_{\rm F}\left(\frac{3}{4} + \ln\frac{\Delta}{p^+}\right) = \gamma_{\rm smooth} - \delta\gamma \ . \tag{6}$$

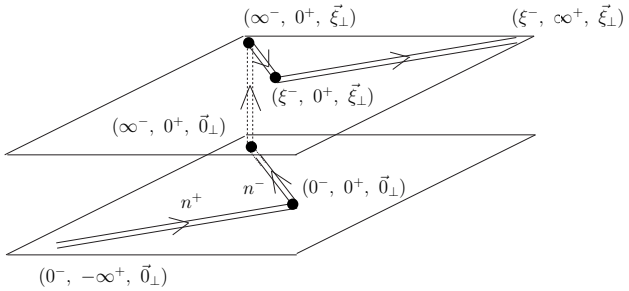

Figure 2: The integration contour associated with the additional soft counter term.

Here $\delta\gamma$ is the term induced by the additional divergence that has to be compensated by a suitable redefinition of the TMD PDF. It is important to realize that $p^+ = (p{\cdot}n^-) \sim \cosh\chi$ defines an angle χ between the direction of the quark momentum p_μ and the lightlike vector n^- with $\ln p^+ \to \chi,\ \chi \to \infty$. Hence, the "defect" of the anomalous dimension, $\delta\gamma$, can be identified with the well-known cusp anomalous dimension [15]

$$\gamma_{\rm cusp}(\alpha_s,\chi) = \frac{\alpha_s}{\pi} C_{\rm F}\ (\chi\coth\chi - 1)\ ,\ \ \frac{d}{d\ln p^+}\ \delta\gamma = \lim_{\chi\to\infty}\frac{d}{d\chi}\gamma_{\rm cusp}(\alpha_s,\chi) = \frac{\alpha_s}{\pi}C_{\rm F}\ . \tag{7}$$

Applying renormalization techniques for contour-dependent composite operators [16, 15, 17] in order to treat angle-dependent singularities, we introduce a compensatory soft term

$$R \equiv \Phi(p^+,n^-|0)\Phi^\dagger(p^+,n^-|\xi),\ \ \Phi(p^+,n^-|\xi) = \left\langle 0 \left| \mathcal{P}\exp\left[ig\int_{\Gamma_{\rm cusp}} d\zeta^\mu\ t^a A^a_\mu(\xi+\zeta)\right]\right| 0\right\rangle \tag{8}$$

and evaluate it along the *cusped* integration contour $\Gamma_{\rm cusp}$, illustrated in Fig. 2, which is defined by (n^-_μ is the minus light-cone vector)

$$\Gamma_{\rm cusp}:\ \ \zeta_\mu = \{[p^+_\mu s\ ,\ -\infty < s < 0]\ \cup\ [n^-_\mu s'\ ,\ 0 < s' < \infty]\ \cup\ [\boldsymbol{l}_\perp\tau,\ \ 0 < \tau < \infty]\}\,. \tag{9}$$

The one-loop gluon virtual corrections contributing to the UV divergences of R are given by

$$\Sigma_R^{\rm UV} = -\frac{\alpha_s}{\pi}C_{\rm F}\ 2\left(\frac{1}{\epsilon}\ \ln\frac{\Delta}{p^+} - \gamma_E + \ln 4\pi\right)\ . \tag{10}$$

This expression is equal, but with opposite sign, to the unwanted term in the UV singularity, related to the cusped contour, calculated before. This result enables us to redefine the conventional TMD PDF as follows:

$$\begin{aligned} f^{\rm mod}_{q/q}(x,\boldsymbol{k}_\perp\!\not\ni \frac{1}{2}\int\frac{d\xi^- d^2\xi_\perp}{2\pi(2\pi)^2}{\rm e}^{-ik^+\xi^- + i\mathbf{k}_\perp\cdot\xi_\perp}\ \big\langle q(p)|\bar\psi(\xi^-,\xi_\perp)[\xi^-,\boldsymbol{\xi}_\perp;\infty^-,\boldsymbol{\xi}_\perp;]^\dagger \\ \times\ [\infty^-,\boldsymbol{\xi}_\perp;\infty^-,\boldsymbol{\infty}_\perp;]^\dagger\gamma^+[\infty^-,\boldsymbol{\infty}_\perp;\infty^-,\mathbf{0}_\perp][\infty^-,\mathbf{0}_\perp;0^-,\mathbf{0}_\perp] \\ \times\ \psi(0^-,\mathbf{0}_\perp)|q(p)\big\rangle\ \cdot\left[\Phi(p^+,n^-|0^-,\mathbf{0}_\perp)\Phi^\dagger(p^+,n^-|\xi^-,\boldsymbol{\xi}_\perp)\right]\ , \end{aligned} \tag{11}$$

The renormalization of $f^{\rm mod}_{\rm ren}(x,\boldsymbol{k}_\perp) = Z^{\rm mod}_f(\alpha_s,\epsilon)f^{\rm mod}(x,\boldsymbol{k}_\perp,\epsilon)$ yields the renormalization constant

$$Z^{\rm mod}_f = 1 + \frac{\alpha_s}{4\pi}C_{\rm F}\ \frac{2}{\epsilon}\left(-3 - 4\ln\frac{\Delta}{p^+} + 4\ln\frac{\Delta}{p^+}\right) = 1 - \frac{3\alpha_s}{4\pi}C_{\rm F}\ \frac{2}{\epsilon}\,. \tag{12}$$

which in turn provides the anomalous dimension

$$\gamma_f^{\rm mod} = \frac{1}{2}\mu\frac{d}{d\mu}\ln Z_f^{\rm mod}(\mu,\alpha_s,\epsilon) = \frac{3}{4}\frac{\alpha_s}{\pi}C_{\rm F} + O(\alpha_s^2) = \gamma_{\rm smooth}\,. \tag{13}$$

To conclude, the soft counter term can be considered [9] as that part of the TMD PDF which accumulates the residual effects of the primordial separation of two oppositely color-charged particles, created at light-cone infinity and being unrelated to the existence of external color sources, thus corresponding to an "intrinsic Coulomb phase" that keeps track of the full gauge history of the colored quarks [18, 19].

I.O.C. is supported by the Alexander von Humboldt Foundation. This work was supported in part by the Deutsche Forschungsgemeinschaft under grant 436 RUS 113/881/0, Russian Federation President's grant 1450-2003-2, and the Heisenberg–Landau Program 2007.

References

[1] X. d. Ji and F. Yuan, Phys. Lett. B **543**, 66 (2002)
[2] A.V. Belitsky, X. Ji, and F. Yuan, Nucl. Phys. B **656**, 165 (2003).
[3] D. Boer, P.J. Mulders, and F. Pijlman, Nucl. Phys. **B667**, 201 (2003).
[4] A.V. Belitsky and A.V. Radyushkin, Phys. Rept. **418**, 1 (2005).
[5] J.C. Collins, Acta Phys. Pol. B **34**, 3103 (2003).
[6] J.C. Collins and D.E. Soper, Nucl. Phys. **B193**, 381 (1981); **B213**, 545 (E) (1983).
[7] J.C. Collins, Phys. Lett. B **536**, 43 (2002).
[8] J.C. Collins, T.C. Rogers, and A.M. Stasto, arXiv:0708.2833 [hep-ph].
[9] I. O. Cherednikov and N. G. Stefanis, arXiv:0710.1955 [hep-ph].
[10] J.C. Collins and F. Hautmann, Phys. Lett. B **472**, 129 (2000).
[11] J.C. Collins and A. Metz, Phys. Rev. Lett. **93**, 252001 (2004).
[12] F. Hautmann, arXiv:hep-ph/0702196.
[13] X. Ji, J. Ma, and F. Yuan, Phys. Rev. D **71**, 034005 (2005).
[14] N.G. Stefanis, Nuovo Cim. A **83**, 205 (1984).
[15] G.P. Korchemsky and A.V. Radyushkin, Nucl. Phys. B **283**, 342 (1987).
[16] A. M. Polyakov, Nucl. Phys. B **164**, 171 (1980).
[17] N.S. Craigie and H. Dorn, Nucl. Phys. B **185**, 204 (1981).
[18] R. Jakob and N. G. Stefanis, Annals Phys. **210**, 112 (1991).
[19] S. Mandelstam, Annals Phys. **19**, 1 (1962).

RELATIVISTIC TRANSFORMATION OF POLARIZATION VECTOR AND ITS PRACTICAL APPLICATIONS

V.A. Chetvertkova[1], S. B. Nurushev[2]

(1) *Lomonosov's Moscow State University, Moscow,Russia*
(2) *Institute for High Energy Physics, Protvino, Russia*
† *E-mail: tche@rambler.ru, nurushev@ihep.ru, sbnurushev@mail.ru*

Abstract

Two subjects are mainly discussed: first one is relevant to the Lorentz transformation of the polarization vector for particle with non zero mass. The relation connecting the angle between proton polarization and its momentum in Laboratory system with the one in Λ rest frame was derived and it differs form the formula given by O. Overseth. The second subject is to study the possibility of producing the polarized proton (antiproton) beam through hyperon (antihyperon) decay using the internal production target in the accelerators/colliders. Rough estimates of the polarized beam parameters are made for U70 and LHC. The conclusion: there is a possibility to obtain the polarized beam on the internal production target of the same quality as on the external target but avoiding several problems peculiar to the external production target scheme.

1. Introduction. The acceleration of the polarized proton beam is very complicated and expensive technic. Though theoretically it is possible to accelerate the polarized protons in the LHC [1] and U-70 [2], it's doubtful, that it will be done in the nearest future. In such situation was decided to analyze more simple method proposed by O. Overseth in 1969 [3]: producing the proton (antiproton) polarized beam through hyperon (antihyperon) decay [3, 4].

The paper is organized in the following way: Section 1 describes relativistic transformation of polarization vector. Next section is devoted to the review of the polarized beams obtained by using the external production target (EPT) and the estimation of the polarized beam parameters produced on the internal production target (IPT) at U70 and LHC.

2. Lorentz transformations of the polarization vector. The goal of the following transformations is to find the relation between ε and θ_{cm} (for notations see Fig.1).

Since for tagging the proton polarization in Λ-decay it's necessary to know the angle ε between proton polarization and its momentum in lab. system Overseth gave the following formula (without derivation):

$$\tan\varepsilon = \frac{\sin\theta_{cm}}{\gamma_0(\cos\theta_{cm} + \beta_0/\beta_f)}\,. \tag{1}$$

Here θ_{cm} is the proton emission angle in c.m.s. (Λ rest frame) and since the proton polarization aligned along its momentum in c.m.s (in case of Λ-decay), this angle presents

also the polarization angle in c.m.s., though in general case we introduce the additional angle η. β_0, γ_0 are velocity and Lorentz factor of proton in c.m.s. respectively, $\beta_f{=}v_\Lambda/c$ is the Λ-velocity in lab. system. In order to check this relation, the following formulae [7] could be used:

$$\boldsymbol{s} = \boldsymbol{s'} + \boldsymbol{\beta}\gamma(\frac{\gamma}{\gamma+1}\boldsymbol{\beta}\cdot\boldsymbol{s'} + \boldsymbol{s'_0}), s_0 = \gamma(s'_0 + \boldsymbol{\beta}\cdot\boldsymbol{s'}), \tag{2}$$

where primed symbols stand for spin in moving system with velocity β. The polarization and spin of the proton in lab. frame could be found by using the formulae (2) twice: firstly, to find these vectors in c.m.s and then to find them in lab. frame. The final formula for $\angle\varepsilon$ is obtained using the relation $\tan\varepsilon = \frac{[\vec{s_l}\times\vec{p_l}]_y}{(\vec{s_l}\cdot\vec{p_l})}$, in numerator y-component of vector product is taken. The final formula for $\angle\varepsilon$ looks like

$$\tan\varepsilon = \frac{\beta_f \sin\theta_{cm}}{\gamma_f\gamma_0^2(\beta_0 + \beta_f\cos\theta_{cm})(1 + \beta_f\beta_0\cos\theta_{cm})}, \tag{3}$$

here β_f and γ_f are relevant to Λ particle in lab. system.

The main difference with the Overseth's formula is the presence of γ_f factor in the denominator of formula (4) which means that if the energy is increasing the polarization and momentum vectors become collinear.

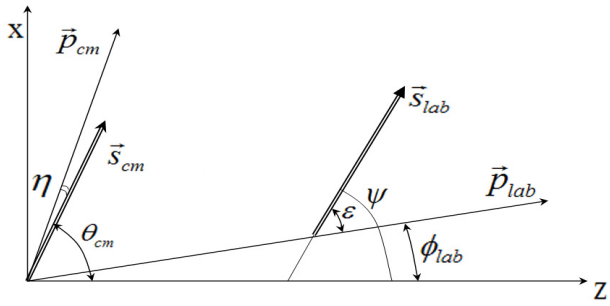

Figure 1. Notations of the angles in Λ-rest frame and Laboratory frame. Double line arrows mean polarization vector, single line arrows label momentum. Z-axis is Λ direction in lab. system.

3. Production of the polarized proton beam on the EPT and IPT. Polarized protons with equal polarizations produced in Λ-decay come from the same point of the plane of the virtual source, this means there is a correlation between the average particle polarization and its horizontal (or vertical) position at the intermediate focus [5].

This idea was used in E581/704 Experiment at FNAL [5]. Similar scheme was used in the experiment FODS at U-70 [6]. The parameters of these two polarized proton beams produced at the EPTs are presented in Table I.

The goal of using the IPT is to obtain the polarized beam with the same or better parameters like on the EPT and to get the possibility of running several experiments simultaneously.

The sketch of such IPT-scheme for U-70 is shown on Fig.2. The circulating proton beam of 70 GeV/c strikes the IPT. The thickness of IPT (carbon) was taken 0,7 μm in order to keep the beam life-time at the level of 2 sec. After IPT the charged particles are bent away by the accelerator's field and neutral particles go straightforward through the Λ-collimator(brass). Then there is the decay region (about 9 m) which is assumed to be out of reach of accelerator's magnetic field. In this region the polarized protons are produced through Λ-decay. The decay protons are captured by bending magnet. The collimator of special form inserted in bending magnet selects the vertically polarized decay protons and deflect them to the momentum collimator. Then they reach the standard beam

channel. The bending magnet and momentum collimator should furnish the momentum selection with precision much better than 20% in order to separate the forward and backward protons in the Λ-rest frame which have the opposite but equal polarizations. The properties of the polarized proton beam are shown in Table I.

Table I. Polarized proton beam parameters produced on the EPT and IPT.

Parameters	External target		Internal target
	TeVatron (Be, 30cm)	U-70 (Al, 30cm)	U-70 (C, 0.7 μm)
Luminosity at production target,$cm^{-2}s^{-1}$	$6.3 \cdot 10^{34}$	$3.6 \cdot 10^{36}$	$3.2 \cdot 10^{36}$
Intensity of the polarized beam for polarization > 35%,(duty-factor) p/sec	$5 \cdot 10^4$	$3.7 \cdot 10^6$	$2.8 \cdot 10^6$
Polarized beam momentum, GeV/c	200	40	50
Momentum band, %	± 10	± 4.5	± 10
Average beam polarization,%	40 ± 2%	40 ± 2%	¿ 35%
Beam profile at final focus, X, Y mm (max)	±15,±15	±10.6,±8.1	±4,±4
Beam divergence, X', Y' mrad (max)	±0.8,±0.6	±6.5,±6.0	± 2, ±2

Polarized proton beam could be obtained at LHC using the same idea. The circulating proton beam of 4 TeV/c strikes the IPT located in front of the dipole 1, D1 (Fig.3). The forward produced neutral particles pass D1 straightforward and hyperons decay in the region of 33 m. Then the decay charged particles are captured by dipole 2 (D2) and go straight to the external beam channel. The estimations of beam parameters are made for two types of IPTs in order to get different beam life-time (Table II).

Table II. The main parameter of LHC and its polarized beams from the EPT and IPT.

Parameters	External target (C, 30cm)	Internal target	
		Gas target (H_2)	Carbon target
Luminosity at production target,$cm^{-2}s^{-1}$	$1.1 \cdot 10^{39}$	$1.1 \cdot 10^{35}$	$2.7 \cdot 10^{37}$
Intensity, p/sec	$3.23 \cdot 10^{14}$	$3.23 \cdot 10^{14}$	$3.23 \cdot 10^{14}$
Polarized beam momentum, GeV/c	3765	3765	3765
Momentum band, %	±5	±5	±5.7
Average beam polarization,%	32	32	32
Beam life-time	-	22 hrs	34.5 sec
Number of polarized protons, *pol.*p/sec	$5.7 \cdot 10^8$	$6 \cdot 10^6$	$6.6 \cdot 10^9$
Number of polarized anti-protons, *pol.*$\bar{p}$/sec	$5.7 \cdot 10^6$	$6 \cdot 10^4$	$6.6 \cdot 10^7$

There are several advantages of using very thin IPT: 1) The multiple Coulomb scattering angle will be small. 2) The absorption of the produced Λ by the production target would be negligible. 3) Possibility of producing simultaneously several polarized beam lines. 4) The IPT can operate simultaneously with slow extracted proton beam. For LHC we do not know several beam parameters. Nevertheless LHC might

be the source of high energy polarized antiproton beam of highest energy at present.

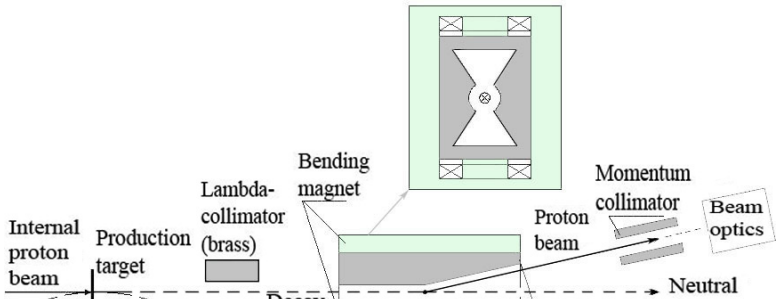

Figure 2. Sketch of obtaining the polarized proton beam from Internal Target (IT) at U-70 (top view). Insertion: the front view of the bending magnet and internal special collima-

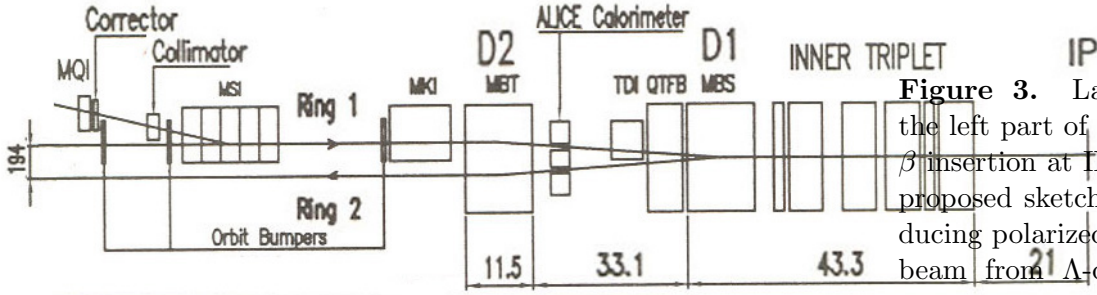

Figure 3. Layout of the left part of the low-β insertion at IP2. The proposed sketch of producing polarized proton beam from Λ-decay is presented.

Acknowledgements. We would like to express our thanks for useful discussions and practical help to professors A. Efremov, M. Ryskin, J. Soffer, X. Artru and doctors E. Troyanov, V. Zapolsky.

References

[1] S.Y. Lee, Prospects for Polarization at RHIC and SSC, AIP Conference Proc. **V.223**, 30.

[2] Yu. M. Shatunov, Proposal for Polarized Protons Acceleration At U-70, XI Advanced Research Workshop on High Energy Spin Physics, Dubna, September 27 - October 1, 2005.

[3] O.E. Overseth, Polarized Protons at the 200-GeV Accelerator. National Accelerator Laboratory,1969 Summer Study Report, **SS-118 2250**, vol. 1, pp 19-25.

[4] O.E. Overseth and J. Sandweiss, A polarized proton beam from decay, National Accelerator Laboratory, 1969 Summer Study Report, **SS-120 2250**, vol. 1, pp 28.

[5] D. Grosnick et al., Nuc. Instr. Meth. **A290(1990) 269**.

[6] Galyaev N.A. et al. IHEP Polarized Proton Beam,IHEP Preprint **92-159**, Protvino 1992, p.11, figs. 5, refs.:16

[7] R. Hagedorn, Relativistic kinematics, W.A. Benjamin, 1963, New York-Amsterdam, p.9.

ABOUT $s-\bar{s}$, $\Delta s-\Delta\bar{s}$ AND $D_d^{K^+-K^-}$ IN $K^\pm$ PRODUCTION IN SIDIS

E. Christova[1†] and E. Leader[2]

(1) *Institute for Nuclear research and Nuclear Energy, Bulgarian Academy of Sciences, Sofia*
(2) *Imperial College, London*
† *E-mail: echristo@inrne.bas.bg*

Abstract

We consider semi-inclusive unpolarized DIS for the production of charged Kaons and the different possibilities, both in LO and NLO, to test the conventionally used assumptions $s-\bar{s}=0$, $\Delta s-\Delta\bar{s}=0$ and $D_d^{K^+-K^-}=0$. The considered tests have the advantage that they do not require any knowledge of the fragmentation functions.

1. Introduction

Inclusive deep inelastic scattering (DIS) gives information about the parton densities (PD) $q+\bar{q}$ and $\Delta q+\Delta\bar{q}$. Analogously, $e^+e^-\to hX$ gives information about the fragmentation functions (FF) $D_q^{h+\bar{h}}$. However, the new generation of semi-inclusive DIS (SIDIS) experiments performed with increasing precision and variety during the last years, present a new powerful instrument to reveal in more details the spin and flavour structure of the nucleon. However, as data is still not enough and not precise enough, it has become conventional to make certain reasonable sounding assumptions in analyzing the data. The usually made assumptions are:

$$s(x)=\bar{s}(x),\quad \Delta s(x)=\Delta\bar{s}(x),\quad D_d^{K^+}(z)=D_d^{K^-}(z). \tag{1}$$

In this paper we discuss to what extent these assumptions can be justified and tested experimentally, in both, LO and NLO in QCD. We suggest possible tests for the reliability of the leading order (LO) treatment of the considered processes. The considered tests do not require any knowledge of the (FFs). In more details these results are published in [1].

2. Positivity constraints

Here we discuss what we can learn about the strange quark densities from positivity conditions. If s_+ ($\bar{s}_+$) and s_- ($\bar{s}_-$) denote the $s(\bar{s})$-quarks with helicities along and opposite the helicity of the nucleon, the unpolarized and polarized parton densities are defined as follows:

$$s=s_++s_-,\quad \bar{s}=\bar{s}_++\bar{s}_-,\quad \Delta s=s_+-s_-,\quad \Delta\bar{s}=\bar{s}_+-\bar{s}_-. \tag{2}$$

Then from $s_\pm\geq 0$ and $\bar{s}_\pm\geq 0$ the following positivity constraints follow:

$$|s-\bar{s}|\leq s+\bar{s},\quad |\Delta s\pm\Delta\bar{s}|\leq s+\bar{s}. \tag{3}$$

i.e. all parton densities are constrained only by $s+\bar{s}$, our knowledge of the sum $\Delta s+\Delta\bar{s}$ does not put any additional limits. Note that $s-\bar{s} \lesseqgtr 0$ and $\Delta s \pm \Delta\bar{s} \lesseqgtr 0$.

From experiment, it is known with a good accuracy that $s+\bar{s}$ is different from zero only for small $x \lesssim 0.4$. Then (3) implies that only in this same interval, $x \lesssim 0.4$, the combinations $s-\bar{s}$ and $\Delta s \pm \Delta\bar{s}$ can be different from zero. Also, as $\int_0^1 dx(s-\bar{s})=0$, it follows that $(s-\bar{s})$ changes sign in $x=[0,0.4]$.

3. SIDIS $e+N \to e+K^{\pm}+X$

Further we shall work with the difference cross sections in SIDIS. As shown in [2], the general expression for $K^{\pm}$ production in SIDIS is:

$$\tilde{\sigma}_p^{K^+-K^-}(x,z) = \frac{1}{9}\left[4u_V \otimes D_u + d_V \otimes D_d + (s-\bar{s}) \otimes D_s\right]^{K^+-K^-} \otimes \hat{\sigma}_{qq}(\gamma q \to qX) \quad (4)$$

$$\tilde{\sigma}_n^{K^+-K^-}(x,z) = \frac{1}{9}\left[4d_V \otimes D_u + u_V \otimes D_d + (s-\bar{s}) \otimes D_s\right]^{K^+-K^-} \otimes \hat{\sigma}_{qq}(\gamma q \to qX). \quad (5)$$

Here $D_q^{K^+-K^-} \equiv D_q^{K^+} - D_q^{K^-}$, $\hat{\sigma}_{qq}$ is the perturbatively calculable, hard partonic cross section $q\gamma^* \to q+X$:

$$\hat{\sigma}_{qq} = \hat{\sigma}_{qq}^{(0)} + \frac{\alpha_s}{2\pi}\hat{\sigma}_{qq}^{(1)}\,, \quad (6)$$

normalized so that the LO contribution is $\hat{\sigma}_{qq}^{(0)}=1$. For simplicity, we use $\tilde{\sigma}_N^{K^{\pm}}$ and $\tilde{\sigma}_N^{DIS}$ in which common kinematic factors have been removed [3].

As shown in [3], the advantage of the difference cross sections is that all terms in $\sigma_N^{K^+-K^-}$ are non-singlets both in PD and FF. This implies that 1) gluons do not enter – neither $g(x)$ nor $D_g^h(z)$ – and 2) their Q^2-evolution is rather simple.

As $D_s^{K^+-K^-}$ is a favoured transition and thus expected to be big, eqs. (4) and (5) show that $\sigma_N^{K^+-K^-}$ are sensitive to the combination $(s-\bar{s})$ which we are interested in. Up to now all analyses of data assume $s=\bar{s}$.

4. $s-\bar{s}$ and $D_d^{K^+-K^-}$, LO

We consider $(\tilde{\sigma}_p+\tilde{\sigma}_n)^{K^+-K^-}$ and $(\tilde{\sigma}_p-\tilde{\sigma}_n)^{K^+-K^-}$. In LO we have:

$$\tilde{\sigma}_d^{K^+-K^-} = (\tilde{\sigma}_p+\tilde{\sigma}_n)^{K^+-K^-} = \frac{1}{9}[(u_V+d_V)\,(4D_u+D_d)^{K^+-K^-} + 2(s-\bar{s})D_s^{K^+-K^-}] \quad (7)$$

$$(\tilde{\sigma}_p-\tilde{\sigma}_n)^{K^+-K^-} = \frac{1}{9}[(u_V-d_V)\,(4D_u-D_d)^{K^+-K^-}] \quad (8)$$

We define the following measurable quantities:

$$R_+(x,z) = \frac{\sigma_d^{K^+}-\sigma_d^{K^-}}{u_V+d_V} = (4D_u+D_d)(z)\left[1+\frac{(s-\bar{s})}{2(u_V+d_V)}\left(\frac{D_s}{D_u}\right)^{K^+-K^-}(z)\right] \quad (9)$$

and

$$R_-(x,z) = \frac{(\sigma_p-\sigma_n)^{K^+-K^-}}{u_V-d_V} = (4\,D_u-D_d)^{K^+-K^-}(z) \quad (10)$$

Note that the x-dependence in (9) is induced solely by the difference $s-\bar{s}$, while in R_- there is no x-dependence in LO. This result is independent of the FF. Then examining the x-dependence of $R_\pm(x,z_0)$ at some z_0, we can deduce the following:

1) if in some x-interval $R_+(x,z_0)$ is independent on x then, we can conclude that $(s-\bar{s})=0$ in this x-interval. Recall that since $D_s^{K^+-K^-}$ is a favoured transition $(D_s/D_u)^{K^+-K^-}>1$.

2) if $R_-(x,z_0)$ is also independent of x , then this suggests that the LO approximation is reasonable.

3) if $R_+(x,z_0)$ and $R_-(x,z_0)$ are *both* independent of x, and if in addition, $R_+(x,z_0)=R_-(x,z_0)$, then both $s-\bar{s}=0$ in the considered x-interval *and* $D_d^{K^+-K^-}(z_0)=0$.

4) if $R_+(x,z_0)$ and $R_-(x,z_0)$ are *both* independent of x, but they are *not* equal, $R_+(x,z_0)\neq R_-(x,z_0)$, we conclude that $s-\bar{s}=0$ in the considered x-interval, *but* $D_d^{K^+-K^-}(z_0)\neq 0$.

The above results 1) – 4) are independent of our knowledge of the FFs.

5) if $D_d^{K^\pm}$ are known at some z_0, limits on $s-\bar{s}$ can be obtained. We have:

$$\left|\frac{(s-\bar{s})}{2(u_V+d_V)}\left(\frac{D_s}{D_u}\right)^{K^+-K^-}(z_0)\right|\leq\frac{\delta r_+}{|r_+|} \tag{11}$$

where $\delta r_+/r_+$ is the precision of the measurement: $R_+(x,z_0)=r_+(z_0)\pm\delta r_+(z_0)$.

6) if $R_-(x,z)$ is not a function of z only, then NLO corrections are needed, which we consider below.

The above tests for $s-\bar{s}=0$ and $D_d^{K^+-K^-}=0$ can be spoilt either by $s-\bar{s}\neq 0$ and/or $D_d^{K^+-K^-}\neq 0$, or by NLO corrections, which are both complementary in size. That's why it is important to formulate tests sensitive to $s-\bar{s}=0$ and/or $D_d^{K^+-K^-}=0$ solely, i.e. to consider NLO.

5. $s-\bar{s}$ and $D_d^{K^+-K^-}$, NLO

If an NLO treatment is necessary it is still possible to reach some conclusions, though less detailed than in the LO case. We now have:

$$\tilde{\sigma}_d^{K^+-K^-}=\frac{1}{9}\left[(u_V+d_V)\otimes(4D_u+D_d)^{K^+-K^-}+2(s-\bar{s})\otimes D_s^{K^+-K^-}\right]\otimes(1+\alpha_s\,C_{qq}) \tag{12}$$

$$(\tilde{\sigma}_p-\tilde{\sigma}_n)^{K^+-K^-}=\frac{1}{9}(u_V-d_V)\otimes(1+\alpha_s\,C_{qq})\otimes(4D_u-D_d)^{K^+-K^-} \tag{13}$$

If instead of using (12) and (13), we succeed to obtain an acceptable fit for the x and z-dependence of both $p-n$ and $p+n$ data with the same fragmentation function $D(z)$:

$$(\tilde{\sigma}_p-\tilde{\sigma}_n)^{K^+-K^-}\approx\frac{4}{9}(u_V-d_V)\;\otimes\;(1+\alpha_s\,\mathcal{C}_{qq})\otimes\;D(z), \tag{14}$$

$$(\tilde{\sigma}_p+\tilde{\sigma}_n)^{K^+-K^-}\approx\frac{4}{9}(u_V+d_V)\;\otimes\;(1+\alpha_s\,\mathcal{C}_{qq})\otimes\;D(z). \tag{15}$$

than we can conclude that both $s-\bar{s}\approx 0$ *and* $D_d^{K^+-K^-}\approx 0$, and that $D(z)=D_u^{K^+-K^-}$.

Note that for all above tests, both in LO and NLO approximation, we don't require a knowledge of $D_q^{K^+-K^-}$.

6. $\Delta s - \Delta\bar{s}$ in $K^{\pm}$ production in SIDIS

Recently the COMPASS collaboration measured [4] the difference asymmetry in SIDIS with longitudinally polarized muons and protons:

$$A_d^{h-\bar{h}} = \frac{\Delta\tilde{\sigma}^{h-\bar{h}}}{\tilde{\sigma}^{h-\bar{h}}}. \tag{16}$$

and singled out the polarized valence quarks. Here we draw attention that if the same asymmetry is measured with final Kaons, information on $\Delta s - \Delta\bar{s}$ can be obtained:

$$A_d^{K^+-K^-}(x,z) \simeq \frac{\Delta u_V + \Delta d_V}{u_V + d_V}\left\{1+\left(\frac{\Delta s - \Delta\bar{s}}{\Delta u_V + \Delta d_V} - \frac{s-\bar{s}}{u_V+d_V}\right)\left(\frac{D_s}{2D_u}\right)^{K^+-K^-}\right\} \tag{17}$$

The z-dependence of $A_d^{K^+-K^-}$ is present only if $\Delta s - \Delta\bar{s}$ and/or $s-\bar{s}$ are non-zero. Thus, studying the z-dependence of $A_d^{K^+-K^-}$ one can obtain information about $\Delta s - \Delta\bar{s} \simeq 0$, suppose we already have the information about $s - \bar{s} \simeq 0$, as discussed above.

At the end a few remarks on the measurability of the discussed asymmetries. In general, these are difference asymmetries and high precision measurements are required. In addition, the data should be presented in bins in both x and z. Quite recently such binning was done in [14] for the very precise data of the HERMES collaboration on $K^{\pm}$-production in SIDIS on proton and deuterium. These results show that for $0,350 \leq z \leq 0,450$ and for $0,450 \leq z \leq 0,600$ in the x-interval $0,023 \leq x \leq 0,300$ the accuracy of the data allows to form the differences $(\sigma_d)^{K^+-K^-}$ and $(\sigma_p - \sigma_n)^{K^+-K^-}$ with errors not bigger than 7-13% and 10-15% respectively. Then one can form the ratios R_+ and R_- with these precisions and perform the above tests.

Acknowledgments
When this work was finished we understood about [6], where similar questions were treated. This work was supported by a JINR(Dubna)-Bulgaria Collaborative Grant.

References

[1] E. Leader and E. Christova, Eur.Phys.J. C **51**, 825 (2007).
[2] E. Christova and E. Leader, Proc. of XI-th workshop on high energy physics, Dubna-SPIN-2005, AIP Conference Proc. **V.570**, 541
[3] E. Leader and E. Christova, Nucl. Phys. B **607**, 369 (2001)
[4] A. Korzenev, arXiv:0704.3600(hep-ex)
[5] A. Hillenbrand, Measurement and Simulation of the Fragmentation Process at HERMES, Ph.D. theses, DESY-2005
[6] C. Bourrely, J. Soffer and F. Buccella, Phys. Lett. B**648** 39 (2007)

Discussion

Q. (J.Soffer, Temple Univ., Philadelphia) I would like to call your attention to the knowledge we have on strange quark distribution from neutrino DIS (CCFR and NuTeV). See on recent paper in polarized PDF (PLB648 39 2007).

A. OK. Thank you.

ON PRODUCTION OF POLARIZED VECTOR MESONS

A.E. Dorokhov[1†],

Joint Institute for Nuclear Research, Bogoliubov Laboratory of Theoretical Physics, 114980, Moscow region, Dubna, Russia

† *E-mail: dorokhov@theor.jinr.ru*

Abstract

Based on the model of instanton vacuum the nonperturbative photon and ρ meson light-cone distributions are constructed. We discuss the transverse size dependence of the photon light-cone wave function and investigate effects of nonperturbative input in electroproduction of longitudinally polarized ρ meson.

1 Introduction

Investigations of hard exclusive processes are essential for our understanding of the internal quark-gluon dynamics of hadrons. Theoretically, such studies are based on the assumption of factorization of dynamics at long and short distances. The short-distance physics is well elaborated by perturbative methods of QCD and depends on particular hard subprocesses. The long-distance dynamics is essentially nonperturbative and within the factorization formalism becomes parametrized in terms of hadronic *distribution amplitudes* (DAs). These nonperturbative quantities are universal and are defined as vacuum-to-hadron matrix elements of particular nonlocal light-cone quark or quark-gluon operators. The evolution of DAs at sufficiently large virtuality q^2 is controlled by the renormalization scale dependence of the quark bilinear operators within the QCD perturbation theory. For leading-order DAs this dependence is governed by QCD evolution equations. When the normalization scale goes to infinity the DAs reach an ultraviolet fixed point and are uniquely determined by perturbative QCD. However, the derivation of the DAs themselves at an initial scale μ_0^2 from first principles is a nonperturbative problem and remains a serious challenge.

Here we present the results [1] of study of the ρ-meson and photon DAs in the leading and higher twists at a low-momentum renormalization scale in the gauged non-local chiral quark model [2–5] based on the instanton picture of QCD vacuum. The important application of these results is the diffractive production of ρ-meson. The amplitude of this process is represented as a convolution of the hard subprocess and the ρ-meson and photon light-cone wave functions.

2 Definitions and notations

The distribution amplitudes of the mesons or the photon are defined via the matrix elements of quark-antiquark bilinear operators taken between the vacuum and the hadronic state $|h(q)\rangle$ of momentum q. It is assumed that the quark and antiquark are separated by the distance $2z$ and the light-like limit $z^2 \to 0$ is taken at a fixed scalar product $q \cdot z$.

We use the light-cone expansion of the matrix elements in order to define the DAs [1] (only leading twist terms are presented)

$$\frac{\langle 0|\overline{q}(z)\sigma_{\mu\nu}[z,-z]q(-z)|\gamma^{\lambda}(q)\rangle}{\langle 0\,|\overline{q}q|\,0\rangle} = ie_q\chi_{\rm m}f^t_{\perp\gamma}\left(q^2\right)\left(e^{(\lambda)}_{\mu}q_{\nu}-q_{\mu}e^{(\lambda)}_{\nu}\right)\int_0^1 dxe^{i\xi q\cdot z}\phi_{\perp\gamma}(x,q^2), \tag{1}$$

$$\langle 0|\overline{q}(z)\gamma_{\mu}[z,-z]q(-z)|\gamma^{\lambda}(q)\rangle = e_qf_{3\gamma}f^v_{\|\gamma}\left(q^2\right)q_{\mu}\frac{e^{(\lambda)}\cdot z}{q\cdot z}\int_0^1 dxe^{i\xi q\cdot z}\phi_{\|\gamma}(x,q^2), \tag{2}$$

where $\chi_{\rm m}$ is the magnetic susceptibility of the quark condensate $\langle 0\,|\overline{q}q|\,0\rangle$, and $f_{3\gamma}$ is related to the first moment of the magnetic susceptibility. The symbol $[-z,z]$ in the matrix elements denotes the path-ordered gauge link (Wilson line) for the gluon fields between the points $-z$ and z. The integration variable x corresponds to the momentum fraction carried by the quark and $\xi = 2x-1$ for the short-hand notation. For a real photon, due to condition $e^{(\lambda)}\cdot z = 0$, the structure corresponding to $\phi_{\|\gamma}$ decouples. The DAs $\phi_{\perp\rho}(x)$ and $\phi_{\|\rho}(x)$ for the ρ-meson state $|\rho^{\lambda}(q)\rangle$ are defined in analogy with photon case (1) and (2) with mass-shell condition $q^2 = -M_{\rho}^2$.

3 The distribution amplitudes within nonlocal chiral quark model

The results of calculations of the ρ-meson and photon DAs in the leading twist within the gauged non-local chiral quark model based on the instanton picture of QCD vacuum are are shown in Figs. 1-3. The DAs are scale dependent quantities. The above results correspond to the low momentum scale μ_0 typical for the instanton model, which is estimated as $\mu_0 = 530$ MeV [7], and need to be evolved to higher momenta scale in order to compare with experimentally available information. The distribution amplitudes of the real photon calculated in the chiral limit may be cast in a closed form

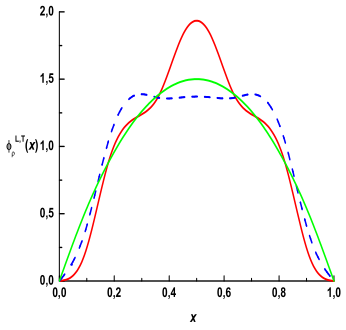

Figure 1: ρ-meson twist-2 distribution amplitudes: transverse (solid line) and longitudinal (dashed) projections. The third line is distribution amplitude at asymptotic scale.

$$\phi_{\perp\gamma}\left(x,q^2=0\right) = \frac{1}{|\langle\bar{q}q\rangle|\,\chi_{\rm m}}\frac{N_c}{4\pi^2}\left[\Theta(\overline{x}x)\int_0^{\infty}du\frac{M\left(u\right)}{D\left(u\right)}\right.$$
$$\left.-\int_0^{\infty}du\int_{-\infty}^{\infty}\frac{d\lambda}{2\pi}\frac{M_+M_-}{D_+D_-}M^{(1)}\left(u_+,u_-\right)\right] \tag{3}$$

$$\phi_{\|\gamma}\left(x,q^2=0\right) = \Theta(\overline{x}x), \tag{4}$$

where the notations $(\overline{x}=1-x)$ are introduced

$$u_+ = u-i\lambda x, \quad u_- = u+i\lambda\overline{x}, \quad M_{\pm} = M\left(u_{\pm}\right),$$
$$D(u) = u+M^2(u), \quad D_{\pm} = D\left(u_{\pm}\right),$$

[1] Our definitions of the photon and ρ-meson DAs follow closely the works of Braun, Ball and coauthors [6].

with the dynamical momentum dependent quark mass $M(p)$ related to the nonlocal properties of the QCD vacuum [8]. The parameters entering normalization coefficients are given by $\langle 0\,|\overline{q}q|\,0\rangle^{\rm inst}\Big|_{\rm 1GeV} = -(0.24\ {\rm GeV})^3$, $\quad \chi_{\rm m}^{\rm inst}\big|_{\rm 1GeV} = 2.73 \quad {\rm GeV}^{-2}$.

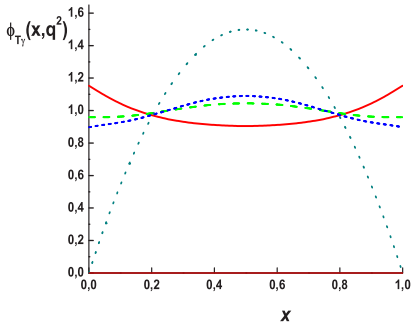

Figure 2: Dependence of the twist-2 tensor component of the photon DA on transverse momentum squared ($q^2 = 0.25$ GeV^2 solid line, $q^2 = 0$ GeV^2 dashed line, $q^2 = -0.09$ GeV^2 short-dashed line, asymptotic DA - dotted line) given at the quark model scale.

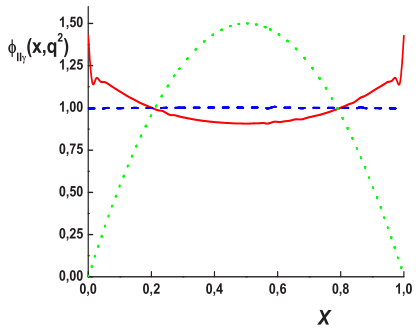

Figure 3: Same as Fig. 2 for the twist-2 vector component of the photon DA.

4 Discussion

In perturbative approach to the photon light-cone wave function one has the result [9] written in mixed coordinate-momentum representation as

$$\phi_{\perp,\|\gamma}^{\rm p.t.}\left(x,r_\perp\right) \sim K_0\left(\varepsilon r_\perp\right), \qquad \varepsilon_{\rm p.t.}^2 = m_q^2 + x\left(1-x\right)Q^2, \tag{5}$$

where m_q is the current quark mass, $r_\perp \sim \varepsilon^{-1}$ is the transverse distance. This result leads to the problem of the large transverse size of the asymmetric quark-antiquark configuration, when x or $1-x$ is small

$$r_\perp \sim \varepsilon_{\rm p.t.}^{-1} \approx m_q^{-1} >> R_{\rm hadron}, \quad \text{when} \quad x \to 0. \tag{6}$$

At the same time, in the nonperturbative approach one gets [1]

$$\phi_{\perp,\|\gamma}\left(x,r_\perp\right) \sim \frac{m_\rho\left(Q^2+m_\rho^2\right)\left(1+\varepsilon r_\perp\right)}{\varepsilon^3} e^{-\varepsilon r_\perp}, \qquad \varepsilon_{\rm p.t.}^2 = m_\rho^2 + x\left(1-x\right)Q^2, \tag{7}$$

where m_ρ is the ρ-meson mass, and thus the problem of "dangerous" configurations is solved.

Differential cross section for ρ_L^0 production is given by [10]

$$\left.\frac{d\sigma}{dt}\right|_{t=0}\left(\gamma^* N \to \rho^0 N\right) = \frac{1}{Q^6} 8\pi^4 \alpha_{\rm em}\alpha_{\rm s}\left(Q^2\right) f_\rho^2 \eta_\rho^2 \left[xG\left(x,Q^2\right)\right]^2, \tag{8}$$

where f_ρ is the $\rho \to e^+e^-$ decay constant, $G(x,Q^2)$ is the gluon distribution in the nucleon, and

$$\eta_\rho = \frac{1}{2}\frac{\int dx\phi_{\|\rho}(x)/[x(1-x)]}{\int dx\phi_{\|\rho}(x)} \tag{9}$$

is the inverse moment of the ρ_L^0 meson DA, controling the leading twist contribution to the leptoproduction amplitude. For asymptotic DA $\sim x(1-x)$ one has $\eta_\rho^{\rm As} = 3$. Phenomenolgy leads to $\eta_\rho^{\rm Exp} = 3.5-4$. By using nonperturbative DA [1] we get $\eta_\rho^{\rm NP} = 3.3-3.5$ in consistency with experimental value.

5 Conclusion

The instanton model of QCD vacuum is realistic tool to get nonperturbative properties of hadrons in terms of parameters characterizing the vacuum. All hadron DAs are suppressed at the boundary of kinematical interval in x variable due to localized wave function of hadrons. At the same time the photon DAs are not zero at edge points since the photon is not bound state object and has no own form factor. As was shown in [1], by applying the QCD evolution, the photon DAs become immediately zero at the edge points of x-interval. Nevertheless, the memory of the initial condition is that the leading twist photon DAs are always wider than asymptotic distribution.

Acknowledgements

The author thanks organizers for very fruitful meeting and Scientific School grant 4476.2006.2 and the JINR Heisenberg-Landau program for partial support.

References

[1] A. E. Dorokhov, W. Broniowski, and E. Ruiz Arriola, Phys. Rev. **D74**, 054023 (2006).

[2] A. E. Dorokhov and L. Tomio, Phys. Rev. **D62**, 014016 (2000).

[3] I. V. Anikin, A. E. Dorokhov, and L. Tomio, Phys. Part. Nucl. **31**, 509 (2000).

[4] A. E. Dorokhov and W. Broniowski, Eur. Phys. J. **C32**, 79 (2003).

[5] A. E. Dorokhov, Phys. Rev. **D70**, 094011 (2004).

[6] P. Ball, V. M. Braun, Y. Koike, and K. Tanaka, Nucl. Phys. **B529**, 323 (1998).

[7] A. E. Dorokhov, Eur. Phys. J. **C42**, 309 (2005).

[8] A. E. Dorokhov, S. V. Esaibegian and S. V. Mikhailov, Phys. Rev. D **56** (1997) 4062.

[9] N.N. Nikolaev and B.G. Zakharov, Z. Phys. C **49**, 607 (1991).

[10] S.J. Brodsky, L. Frankfurt, J.F. Gunion, A.H. Mueller and M. Strikman, Phys. Rev. **D50**, 3134 (1994).

SIVERS AND COLLINS SINGLE SPIN ASYMMETRIES

A. V. Efremov[1†], K. Goeke[2] and P. Schweitzer[2]

(1) *Joint Institute for Nuclear Research, Dubna, 141980 Russia*
(2) *Institut für Theoretische Physik II, Ruhr-Universität Bochum, Germany*
† *E-mail: efremov@theor.jinr.ru*

Abstract

The Sivers and Collins asymmetries are the most prominent Single Spin Asymmetries (SSA) in Semi-Inclusive Deeply Inelastic Scattering (SIDIS) with transverse target polarization. In this talk we present our understanding of these phenomena.

1 Introduction

SSAs in hard reactions have a long history dating back to the 1970s when significant polarizations of Λ-hyperons in collisions of unpolarized hadrons were observed [1], and to the early 1990s when large asymmetries in $p^\uparrow p \to \pi X$ or $p^\uparrow \bar{p} \to \pi X$ were found at Protvino [2] and FNAL [3]. No fully consistent and satisfactory unifying approach to the theoretical description of these observations has been found so far — see the review [4].

Interestingly, the most recently observed SSA and azimuthal phenomena, namely those in SIDIS and e^+e^- annihilations seem better under control. This is in particular the case for the transverse target SSA observed at HERMES and COMPASS [23, 24, 7] and the azimuthal correlations in hadron production in e^+e^- annihilations observed at BELLE [7]. On the basis of a generalized factorization approach in which transverse parton momenta are taken into account [26] these "leading twist" asymmetries can be explained [16, 17] in terms of the Sivers [11, 15, 14, 15] or Collins effect [6]. The former describes, loosely speaking, the distribution of unpolarized partons in a transversely polarized proton, the latter describes a left-right asymmetry in fragmentation of transversely polarized partons into unpolarized hadrons. In the transverse target SSA these effects can be distinguished by the different azimuthal angle distribution of the produced hadrons: Sivers effect $\propto \sin(\phi - \phi_S)$, while Collins effect $\propto \sin(\phi + \phi_S)$, where ϕ and ϕ_S denote respectively the azimuthal angles of the produced hadron and the target polarization vector with respect to the axis defined by the hard virtual photon [16]. Both effects have been subject to intensive phenomenological studies in hadron-hadron-collisions [35] and in SIDIS [18]- [26]. In this talk our understanding of these phenomena is presented.

For the longitudinal target SSA in SIDIS, which were observed first [27, 28] but are dominated by subleading-twist effects [29, 30], the situation is less clear and their description (*presuming* factorization holds) is more involved.

2 Sivers effect

The Sivers effect [11] was originally suggested to explain the large SSAs in $p^\uparrow p \to \pi X$ (and $\bar{p}^\uparrow p \to \pi X$) observed at FNAL [3] and confirmed at higher energies by RHIC [5]. It is due a correlation between (the transverse component of) the nucleon spin $\mathbf{S}_\mathrm{T}$ and

intrinsic transverse parton momenta $\mathbf{p}_{\rm T}$ in the nucleon, and decribed by the Sivers function $f_{1T}^{\perp}(x, \mathbf{p}_T^2)$ whose precise definition in QCD was worked out only recently [14, 15].

2.1 Sivers effect in SIDIS. The azimuthal SSA measured by HERMES & COMPASS in the SIDIS process $lp^{\uparrow} \to l'hX$ (see Fig. 1) is defined as

$$\frac{N^{\uparrow} - N^{\downarrow}}{N^{\uparrow} + N^{\downarrow}} \propto \underbrace{\sin(\phi - \phi_S)\, A_{UT}^{\sin(\phi-\phi_S)}}_{\text{Sivers}} + \underbrace{\sin(\phi + \phi_S)\, A_{UT}^{\sin(\phi+\phi_S)}}_{\text{Collins effect}} \quad \text{and} \tag{1}$$

where $N^{\uparrow(\downarrow)}$ are the event counts for the respective transverse target polarization. We assume the distributions of transverse parton and hadron momenta in distribution (DF) and fragmentation function (FF) to be Gaussian with corresponding averaged transverse momenta, $p_{\rm Siv}^2$ and $K_{D_1}^2$, taken x- or z- and flavour-independent. The Sivers SSA as measured in [23, 24] is then given by [21]

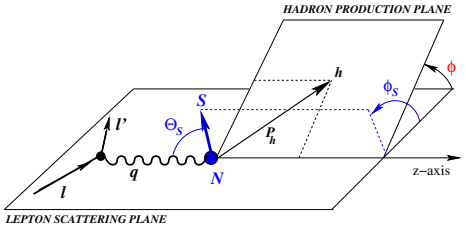

Figure 1: Kinematics of the SIDIS process $lN \to l'hX$.

$$A_{UT}^{\sin(\phi-\phi_S)} = (-2)\, \frac{a_{\rm G} \sum_a e_a^2\, x f_{1T}^{\perp(1)a}(x)\, D_1^a(z)}{\sum_a e_a^2\, x f_1^a(x)\, D_1^a(z)} \quad \text{with} \quad a_{\rm G} = \frac{\sqrt{\pi}}{2} \frac{M_N}{\sqrt{p_{\rm Siv}^2 + K_{D_1}^2/z^2}} \tag{2}$$

and $f_{1T}^{\perp(1)a}(x) \equiv \int {\rm d}^2\mathbf{p}_T \frac{\mathbf{p}_T^2}{2M_N^2} f_{1T}^{\perp a}(x, \mathbf{p}_T^2)$. In the limit a large number of colours N_c one has

$$f_{1T}^{\perp u}(x, \mathbf{p}_T^2) = -f_{1T}^{\perp d}(x, \mathbf{p}_T^2) \quad \text{modulo } 1/N_c \text{ corrections}, \tag{3}$$

and analog for antiquarks for x of the order $xN_c = \mathcal{O}(N_c^0)$ [32]. In the following effects of antiquarks and heavier flavours are neglected. It was shown [21] that the large-N_c relation (3) describes the HERMES data [23] by the following 2-parameter Ansatz and best fit

$$x f_{1T\,\rm SIDIS}^{\perp(1)u}(x) = -x f_{1T\,\rm SIDIS}^{\perp(1)d}(x) \overset{\text{Ansatz}}{=} A\, x^b\, (1-x)^5 \overset{\text{fit}}{=} -0.17 x^{0.66} (1-x)^5\,. \tag{4}$$

Fig. 2a shows the fit and its 1-σ uncertainty due to the statistical error of the data [23]. Fig. 2b shows that this fit very well describes the x-dependence of the HERMES data [23].

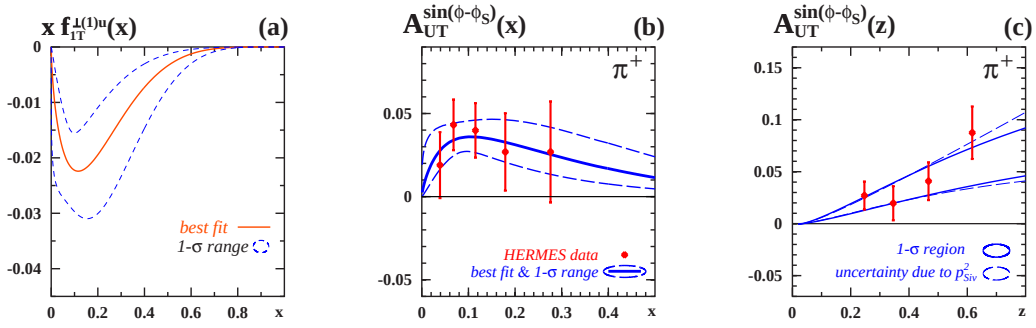

Figure 2: **a.** The u-quark Sivers function vs. x at a scale of 2.5 GeV^2, as obtained from the HERMES data [23]. Shown are the best fit and its 1-σ uncertainty. **b.** and **c.** The azimuthal SSA $A_{UT}^{\sin(\phi_h-\phi_S)}$ as function of x and z for positive pions as obtained from the fit (4) in comparison to the data [23].

Fig. 2c finally shows the equally good description of the z-dependence of the data [23] that were not included in the fit, and serves here as a cross check for the Gauss Ansatz.

We have explicitly checked that effects due to Sivers $\bar{u}$- and $\bar{d}$-distributions cannot be resolved within the error bars of the data [23] (however, see Sec. 4). We also checked that $1/N_c$-corrections are within the error bars of the data [23]. For that we assumed that the flavour singlet Sivers distribution is suppressed by exactly a factor of $1/N_c$ with respect to the flavour non-singlet combination according to Eq. (3). That is, with $N_c = 3$,

$$\left|(f_{1T}^{\perp(1)u} + f_{1T}^{\perp(1)d})(x)\right| \stackrel{!}{=} \pm \frac{1}{N_c}(f_{1T}^{\perp(1)u} - f_{1T}^{\perp(1)d})(x)\,, \tag{5}$$

where we use $f_{1T}^{\perp(1)q}(x)$ from (4) on the right-hand-side.

On an isoscalar target, such as deuteron, the entire effect is due to $1/N_c$-corrections. Assuming that charged hadrons at COMPASS are mainly pions, the rough estimate (5) of $1/N_c$-corrections yields results compatible with the COMPASS data [24], see Fig. 3.

Thus, the large-N_c approach works, because the precision of the first data [23,24] is comparable to the theoretical accuracy of the large-N_c relation (3). Our results are in agreement with other studies [22, 19, 22].

We conclude that the HERMES and COMPASS data [23, 24] are compatible with the large-N_c prediction (3) for the Sivers function [32]. Remarkably, the sign of the extracted Sivers function in Eq. (4) agrees with the physical picture discussed in [33].

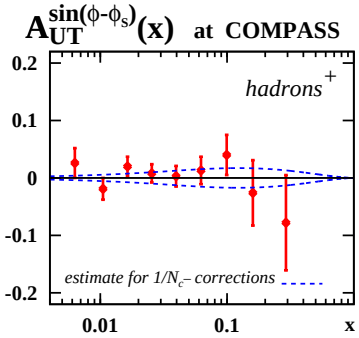

Figure 3: The Sivers SSA for positive hadrons from deuteron. Data are from COMPASS [24]. The theoretical curves indicate the magnitude of the effect on the basis of the estimate (5).

2.2 Sivers effect in the Drell-Yan process. Universility is a particularly interesting aspect of the Sivers function. On the basis of time-reversal arguments it is predicted [14] that this (and other "T-odd") distribution(s) have opposite signs in SIDIS and DY

$$f_{1T}^{\perp}(x, \mathbf{p}_T^2)_{\rm SIDIS} = -f_{1T}^{\perp}(x, \mathbf{p}_T^2)_{\rm DY}\ . \tag{6}$$

The experimental check of Eq. (6) would provide a thorough test of our understanding of the Sivers effect within QCD. In particular, the experimental verification of (6) is a crucial prerequisite for testing the factorization approach to the description of processes containing p_T-dependent correlators [26].

On the basis of the first information of the Sivers effect in SIDIS [23,24] it was shown that the Sivers effect leads to sizeable SSA in $p^\uparrow\pi^- \to l^+l^-X$, which could be studied at COMPASS, and in $p^\uparrow\bar{p} \to l^+l^-X$ or $p\bar{p}^\uparrow \to l^+l^-X$ in the planned PAX experiment at GSI [42] making the experimental check of Eq. (6) feasible and promising [18]. Both experiments are dominated by annihilations of valence quarks (from p) and valence antiquarks (from $\bar{p}$, π^-). This yields sizeable counting rates, and the processes are not sensitive to Sivers antiquarks, that are not constrained by the present data, see [18]- [21].

On a shorter term the Sivers effect in DY can be studied in $p^\uparrow p \to l^+l^-X$ at RHIC. In pp-collisions inevitably antiquark distributions are involved, and the counting rates are smaller. We have shown, however, that the Sivers SSA in DY can nevertheless be measured at RHIC with an accuracy sufficient to unambiguously test Eq. (6) [25].

The theoretical understanding of SSA in $p^\uparrow p \to \pi X$, which originally motivated the introduction of the Sivers effect, is more involved compared to SIDIS or DY. No factorization proof is formulated for this process. The SSA can also be generated by twist-3 effects [34] that, however, could be manifestations of the same effect in different k_T regions [35].

3 Transversity and Collins effect

The transversity distribution function $h_1^a(x)$ enters the expression for the Collins SSA in SIDIS together with the equally unknown Collins fragmentation function [6] (FF) $H_1^a(z)$[1]

$$A_{UT}^{\sin(\phi+\phi_S)} = 2\frac{\sum_a e_a^2 x h_1^a(x) B_{\rm G} H_1^a(z)}{\sum_a e_a^2\, x f_1^a(x)\, D_1^a(z)}\ . \tag{7}$$

However, $H_1^a(z)$ is accessible in $e^+e^- \to \bar{q}q \to$ 2jets where the quark transverse spin correlation induces a specific azimuthal correlation of two hadrons in opposite jets [17]

$$\mathrm{d}\sigma = \mathrm{d}\sigma_{\rm unp} \underbrace{\left[1 + \cos(2\phi_1)\frac{\sin^2\theta}{1+\cos^2\theta}\, C_{\rm G} \times \frac{\sum_a e_a^2 H_1^a H_1^{\bar{a}}}{\sum_a e_a^2 D_1^a D_1^{\bar{a}}}\right]}_{\equiv A_1} \tag{8}$$

where ϕ_1 is azimuthal angle of hadron 1 around z-axis along hadron 2, and θ is electron polar angle. Also here we assume the Gauss model and $C_{\rm G}(z_1, z_2) = \frac{16}{\pi} z_1 z_2/(z_1^2 + z_2^2)$.

First experimental indications for the Collins effect were obtained from studies of preliminary SMC data on SIDIS [36] and DELPHI data on charged hadron production in e^+e^- annihilations at the Z^0-pole [37]. More recently HERMES reported data on the Collins (SSA) in SIDIS from proton target [23, 7] giving the first unambiguous evidence that H_1^a and $h_1^a(x)$ are non-zero, while in the COMPASS experiment [24] the Collins effect from a deuteron target was found compatible with zero within error bars. Finally, year ago the BELLE collaboration presented data on sizeable azimuthal correlation in e^+e^- annihilations at a center of mass energy of 60 MeV below the Υ-resonance [7].

The question which arises is: *Are all these data from different SIDIS and e^+e^- experiments compatible, i.e. due to the same Collins effect?*

In order to answer this question we extract H_1^a from HERMES [7] and BELLE [7] data, and compare the ratios H_1^a/D_1^a from these and other experiments. Such "analyzing powers" might be expected to be weakly scale-dependent.

3.1 Collins effect in SIDIS. A simultanous extraction of $h_1^a(x)$ and $H_1^{\perp a}(z)$ from SIDIS data is presently not possible. We use therefore for $h_1^a(x)$ predictions from chiral quark-soliton model [38] which provides a good description of $f_1^a(x)$ and $g_1^a(x)$. The HERMES data on the Collins SSA [7] can be described in this approach if, at $\langle Q^2\rangle = 2.5\,\mathrm{GeV}^2$,

$$\left.\frac{\langle 2B_{\rm G} H_1^{\rm fav}\rangle}{\langle D_1^{\rm fav}\rangle}\right|_{\rm HERMES} = (7.2 \pm 1.7)\%\ , \quad \left.\frac{\langle 2B_{\rm G} H_1^{\rm unf}\rangle}{\langle D_1^{\rm unf}\rangle}\right|_{\rm HERMES} = -(14.2 \pm 2.7)\%\ . \tag{9}$$

[1] We assume a factorized Gaussian dependence on parton and hadron transverse momenta [16] with $B_{\rm G}(z) = (1 + z^2\ \langle \mathbf{p}_{h_1}^2\rangle/\langle \mathbf{K}_{H_1}^2\rangle)^{-1/2}$ and define $H_1^a(z) \equiv H_1^{\perp(1/2)a}(z) = \int \mathrm{d}^2\mathbf{K}_T \frac{|\mathbf{K}_T|}{2z m_\pi} H_1^{\perp a}(z, \mathbf{K}_T)$. The Gaussian widths are assumed flavor and x- or z-independent. We neglect throughout the soft factors [26].

where "fav" ("unf") means favored $u \to \pi^+$ etc. (unfavored $u \to \pi^-$, etc.) fragmentation, and $\langle \ldots \rangle$ denotes average over z within the HERMES cuts $0.2 \le z \le 0.7$.

The absolute numbers for $\langle 2B_{\rm G} H_1^{\rm fav} \rangle$ and $\langle 2B_{\rm G} H_1^{\rm unf} \rangle$ are of similar magnitude. This can be understood in the string fragmentation picture and the Schäfer-Teryaev sum rule [39]. Fit (9) describes the HERMES proton target data [7] on the Collins SSA (Figs. 4a, b) and is in agreement with COMPASS deuteron data [24] (Figs. 4c, d).

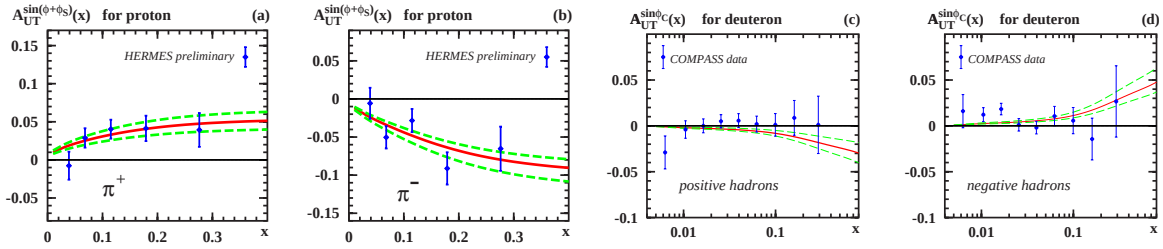

Figure 4: Collins SSA $A_{UT}^{\sin(\phi+\phi_S)}$ as function of x vs. HERMES [7] and new COMPASS [24] data.

3.2 Collins effect in e^+e^-. The $\cos 2\phi$ dependence of the cross section (8) could arise also from hard gluon radiation or detector acceptance effects. These effects, being flavor independent, cancel out from the double ratio of A_1^U, where both hadrons $h_1 h_2$ are pions of unlike sign, to A_1^L, where $h_1 h_2$ are pions of like sign, i.e.

$$\frac{A_1^U}{A_1^L} \approx 1 + \cos(2\phi_1) P_{U/L}(z_1, z_2) \; . \qquad (10)$$

The BELLE data [7] can be described with the following Ansatz and best fit, which is shown in Fig. 5,

$$H_1^a(z) = C_a \, z \, D_1^a(z), \;\; C_{\rm fav} = 0.15, \;\; C_{\rm unf} = -0.45. \qquad (11)$$

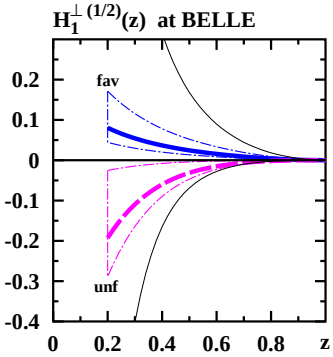

Figure 5: Collins FF $H_1^a(z)$ needed to explain the BELLE data [7]. The shown 1-σ error bands are correlated.

Other Ansätze gave less satisfactory fits. The azimuthal observables in e^+e^--annihilation are bilinear in H_1^a and therefore symmetric with respect to the exchange of the signs of $H_1^{\rm fav}$ and $H_1^{\rm unf}$. The BELLE data [7] unambiguously indicate that $H_1^{\rm fav}$ and $H_1^{\rm unf}$ have opposite signs, but they cannot tell us which is positive and which is negative. The definite signs in (11) and Fig. 5 are dictated by SIDIS data [7] and model [38] with $h_1^u(x) > 0$. In Fig. 6 (top) the BELLE data [7] are compared to the theoretical result for $P_{U/L}(z_1, z_2)$.

3.3 BELLE vs. HERMES. In order to compare Collins effect in SIDIS at HERMES [23, 7] and in e^+e^--annihilation at BELLE [7] we consider the ratios H_1^a/D_1^a which might be less scale dependent. The BELLE fit in Fig. 5 yields in the HERMES z-range:

$$\left.\frac{\langle 2H_1^{\rm fav}\rangle}{\langle D_1^{\rm fav}\rangle}\right|_{\rm BELLE} = (5.3 \cdots 20.4)\%, \quad \left.\frac{\langle 2H_1^{\rm unf}\rangle}{\langle D_1^{\rm unf}\rangle}\right|_{\rm BELLE} = -(3.7 \;\cdots\; 41.4)\% \; . \qquad (12)$$

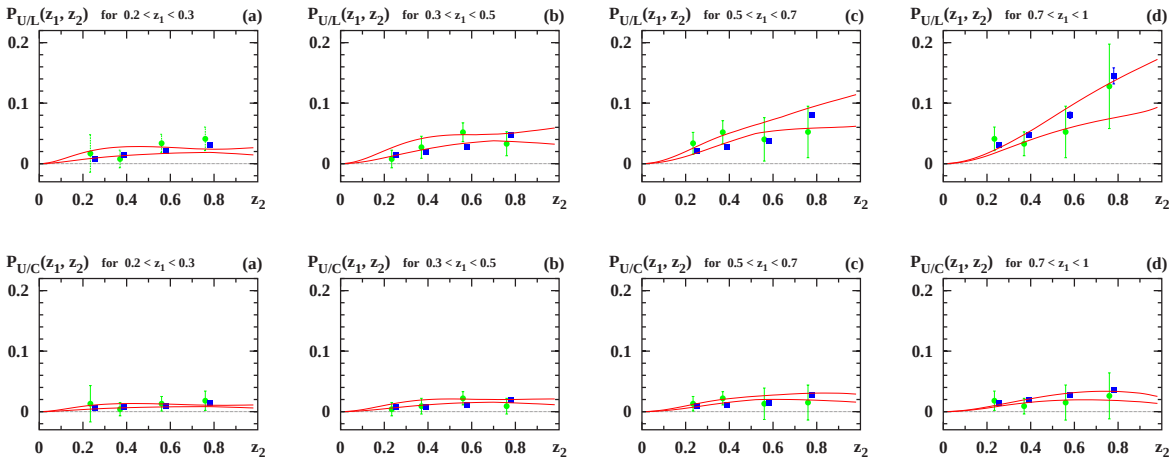

Figure 6: **Top**: $P_{U/L}(z_1, z_2)$ defined in Eq. (10) for fixed z_1-bins as function of z_2 vs. BELLE data [7]. **Bottom**: The observable $P_{U/L}(z_1, z_2)$ defined analogously, see text, vs. preliminary BELLE data [45]. Blue squares are new preliminary data, see Sec. 4.

The above numbers (errors are correlated!) and the result in Eq. (9) are compatible, if one takes into account the factor $B_{\rm G} < 1$ in Eq. (9).

Assuming a weak scale-dependence also for

$$\left.\frac{H_1^a(z)}{D_1^a(z)}\right|_{\rm BELLE} \approx \left.\frac{H_1^a(z)}{D_1^a(z)}\right|_{\rm HERMES} \qquad (13)$$

and considering the 1-σ uncertainty of the BELLE fit in Fig. 5 and the sensitivity to unknown Gaussian widths of $H_1^a(z)$ and $h_1^a(x)$, c.f. Footnote 1 and Ref. [18], one obtains also a satisfactory description of the z-dependence of the HERMES data [7] as shown in Fig. 7.

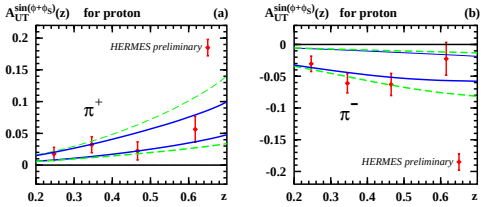

Figure 7: The Collins SSA $A_{UT}^{\sin(\phi+\phi_S)}(z)$ as function of z. The theoretical curves are based on the fit of $H_1^a(z)$ to the BELLE data under the assumption (13). The dashed lines indicate the sensitivity of the SSA to the Gaussian widths.

These observations allow to draw the conclusion that it is, in fact, the same Collins effect at work in SIDIS [23, 24, 7] and in e^+e^--annihilation [7, 45]. Estimates indicate that the early preliminary DELPHI result [37] is compatible with these findings [18].

3.3 Transversity in Drell-Yan process. The double-spin asymmetry observable in Drell-Yan (DY) lepton-pair production in proton-proton collisions is given in LO by

$$A_{TT}(x_F) = \frac{\sum_a e_a^2 h_1^a(x_1) h_1^{\bar a}(x_2)}{\sum_a e_a^2 f_1^a(x_1) f_1^{\bar a}(x_2)} \qquad (14)$$

where $x_F = x_1 - x_2$ and $x_1 x_2 = \frac{Q^2}{s}$. In the kinematics of RHIC A_{TT} is small and difficult to measure.

In the J-PARC experiment with $E_{\rm beam} = 50\,{\rm GeV}$ A_{TT} would reach $-5\,\%$ in the model [38], see Fig. 8, and could be measured [40]. The situation is similarly promising in proposed polarized beam U70-experiment [41].

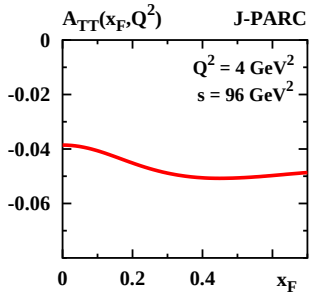

Figure 8: Double spin asymmetry A_{TT} in DY, Eq. (14), vs. x_F for the kinematics of J-PARC.

Finally, in the PAX-experiment proposed at GSI [42] in polarized $\bar{p}p$ collisions one may expect $A_{TT} \sim (30 \cdots 50)\%$ [4]. There $A_{TT} \propto h_1^u(x_1) h_1^{\bar{u}}(x_2)$ to a good approximation, due to u-quark ($\bar{u}$-quark) dominance in the proton (anti-proton) [4].

4 New data and developements

Since our studies were completed [18, 21, 18] new data became available from SIDIS at HERMES [35] and e^+e^--annihilations at BELLE [45]. What is the impact of the new experimental results? Do they confirm our current understanding of the Sivers- and Collins-effects, or will they require a revision?

4.1 New results from BELLE. Interesting recent news are the preliminary BELLE data [45] for the ratio of azimuthal asymmetries of unlike sign pion pairs, A_1^U, to all charged pion pairs, A_1^C. The new observable $P_{U/C}$ is defined analogously to $P_{U/L}$ in Eq. (10) as $A_1^U/A_1^C \approx 1 + \cos(2\phi)\, P_{U/C}$. Fig. 6 (bottom) shows that the fit (11) from [18] ideally describes the new experimental points! Thus, the new data confirm the picture of the Collins function in Fig. 5, but will allow to reduce the uncertainty of the extraction.

4.2 π^0 Collins SSA. The (unpolarized or Collins) fragmentation functions for neutral pions are just the average of the favoured and unfavoured fragmentation functions into charged pions, due to isospin symmetry. Since in the HERMES kinematics the favoured and unfavoured Collins functions are of opposite sign and nearly equal in magnitude, $\langle 2B_{\rm G} H_1^{\rm fav} \rangle \approx -\langle 2B_{\rm G} H_1^{\rm unf} \rangle$ c.f. Sec. 3.1, one expects the π^0 Collins SSA to be nearly zero [18]. Most recent HERMES data confirm this prediction within error bars [35].

4.3 π^0 Sivers SSA. Isospin symmetry applies not only to fragmenation functions but to the entire effects. Thus, knowing the Sivers SSAs for charged pions one is able to predict the effect for π^0. In Figs. 9a, b we compare our predictions made on the basis of the results from [21] discussed in Sec. 2.1 with the most recent HERMES data [35]. The agreement is satisfactory. In particular, data on the z-dependence of the Sivers SSA provide a direct test of the Gauss model for transverse parton and hadron momenta [21]. As can be seen in Fig. 9b, within the present precision of data the Gauss Ansatz is useful.

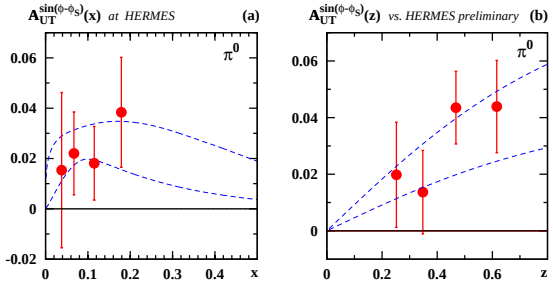

Figure 9: The Sivers SSA $A_{UT}^{\sin(\phi+\phi_S)}(z)$ for π^0 as functions of x and z. The preliminary HERMES data are from [35]. The theoretical curves are based on the extraction of the Sivers effect [21] from the HERMES data on $\pi^\pm$ SSAs [23].

4.4 Sivers effect for kaons. In the HERMES experiment also the Sivers effect for charged kaons was measured. For K^- the effect is compatible with zero within error bars. But for K^+ in the region of $x = (0.05 - 0.15)$ the SSA is about (2-3) times larger than the π^+ SSA [35], while for $x \geq 0.15$ the K^+ and π^+ SSAs are of comparable size within error bars. Can one understand this behaviour?

The "only difference" between the π^+ and K^+ SSAs is the exchange $\bar{d} \leftrightarrow \bar{s}$. Therefore, in our approach of Sec. 2.1, where we neglect the effects of Sivers strange and antiquarks one expects π^+ and K^+ SSAs of same magnitude. However, by including explicitly $\bar{u}$, $\bar{d}$, s and $\bar{s}$ Sivers distributions one could explain the observed enhancement of the K^+ Sivers SSA with respect to the π^+ SSA, provided the Sivers seaquark distributions would reach about 50% of the magnitude of the Sivers quark distributions. At small x this could be a reasonable scenario, see [26] for a detailed discussion. A simultaneous refitting of pion and kaon SSAs will give us a conclusive answer (see, however, the talk by Prokudin [20]).

5 Conclusions

Within the uncertainties of our study we find that the SIDIS data from HERMES [23, 7] and COMPASS [24] on the Sivers and Collins SSA from different targets are in agreement with each other and with BELLE data on azimuthal correlations in e^+e^--annihilations.

At the present stage of art large-N_c predictions for the flavour dependence of the Sivers function are compatible with data, and provide useful constraints for their analysis.

The favored and unfavored Collins FFs appear to be of comparable magnitude but have opposite signs, and $h_1^u(x)$ seems close to saturating the Soffer bound, other $h_1^a(x)$ are hardly constrained. This conclusion is supported by a simultanuous analysis of HERMES, COMPASS and BELLE data [20] with additional conclusion on the tendency of $h_1^d(x)$ to be negative. These findings are in agreement with old DELPHI and with the most recent BELLE data and with independent theoretical studies [19].

New HERMES and BELLE data confirm our first understanding of these effects, except for the HERMES data on the kaon Sivers SSA which may provide new interesting information on Sivers seaquarks. Further data from SIDIS (COMPASS, JLAB, HERMES) and e^+e^- colliders (BELLE) will help to improve this first picture.

The understanding of the novel functions $f_{1T}^{\perp a}$, h_1^a and H_1^a emerging from SIDIS and e^+e^--annihilations, however, will be completed only thanks to future data spin asymmetries in the Drell-Yan process. Experiments are in progress or planned at RHIC, J-PARC, COMPASS, U70 and PAX at GSI.

While the Sivers and Collins effects are the most prominent effects, it is important to keep in mind that there are further equally fascinating effects to be explored [46–48]. Preliminary COMPASS results on compatible with zero deuteron target SSAs beyond the Sivers and Collins effects were presented in [49].

Acknowledgments. This work is supported by BMBF (Verbundforschung), COSY-Jülich project, the Transregio Bonn-Bochum-Giessen, and is part of the by EIIIHT project under contract number RII3-CT-2004-506078. A.E. is also supported by RFBR grant 06-02-16215, by RF MSE RNP.2.2.2.2.6546 (MIREA) and by the Heisenberg-Landau Program of JINR.

References

[1] G. Bunce *et al.*, Phys. Rev. Lett. **36** (1976) 1113.
[2] V. D. Apokin *et al.*, Sov. J. Nucl. Phys. **49** (1989) 103 [Yad. Fiz. **49** (1989) 165].

[3] D. L. Adams *et al.*, Phys. Lett. B **261**, 201 and **264**, 462 (1991).
[4] M. Anselmino, Czech. J. Phys. **52** (2002) C13 [arXiv:hep-ph/0201150].
[5] A. Airapetian *et al.* [HERMES Collaboration], Phys. Rev. Lett. **94** (2005) 012002.
[6] V. Y. Alexakhin *et al.* [COMPASS Collaboration], Phys. Rev. Lett. **94** (2005) 202002. E. S. Ageev *et al.* [COMPASS Collaboration], Nucl. Phys. B **765** (2007) 31.
[7] M. Diefenthaler, AIP Conf. Proc. **792** (2005) 933 [arXiv:hep-ex/0507013].
[8] K. Abe *et al.* [BELLE Collaboration], Phys. Rev. Lett. **96** (2006) 232002.
[9] X. D. Ji, J. P. Ma and F. Yuan, Phys. Rev. D **71** (2005) 034005; Phys. Lett. B **597** (2004) 299. J. C. Collins and A. Metz, Phys. Rev. Lett. **93** (2004) 252001.
[10] P. J. Mulders and R. D. Tangerman, Nucl. Phys. B **461** (1996) 197. D. Boer and P. J. Mulders, Phys. Rev. D **57** (1998) 5780 [arXiv:hep-ph/9711485].
[11] D. Boer, R. Jakob and P. J. Mulders, Nucl. Phys. B**504** (1997) 345; Phys. Lett. B**424** (1998) 143.
[12] D. W. Sivers, Phys. Rev. D **41** (1990) 83; Phys. Rev. D **43** (1991) 261.
[13] S. J. Brodsky, D. S. Hwang, I. Schmidt, Phys. Lett. B **530** (2002) 99; Nucl. Phys. B **642** (2002) 344.
[14] J. C. Collins, Phys. Lett. B **536** (2002) 43.
[15] A. V. Belitsky, X. Ji and F. Yuan, Nucl. Phys. B **656** (2003) 165. X. D. Ji and F. Yuan, Phys. Lett. B **543** (2002) 66. D. Boer, P. J. Mulders and F. Pijlman, Nucl. Phys. B **667** (2003) 201.
[16] J. C. Collins, Nucl. Phys. B **396** (1993) 161 [arXiv:hep-ph/9208213]. A. V. Efremov, L. Mankiewicz and N. A. Tornqvist, Phys. Lett. B **284** (1992) 394.
[17] M. Anselmino, M. Boglione, U. D'Alesio, E. Leader and F. Murgia, Phys. Rev. D **71** (2005) 014002. B. Q. Ma, I. Schmidt and J. J. Yang, Eur. Phys. J. C **40** (2005) 63.
[18] A. V. Efremov, K. Goeke, S. Menzel, A. Metz and P. Schweitzer, Phys. Lett. B **612** (2005) 233.
[19] M. Anselmino, M. Boglione, U. D'Alesio, A. Kotzinian, F. Murgia and A. Prokudin, Phys. Rev. D **72** (2005) 094007.
[20] W. Vogelsang and F. Yuan, Phys. Rev. D **72** (2005) 054028 [arXiv:hep-ph/0507266].
[21] J. C. Collins, A. V. Efremov, K. Goeke, S. Menzel, A. Metz and P. Schweitzer, Phys. Rev. D **73** (2006) 014021 [arXiv:hep-ph/0509076]. J. C. Collins *et al.*, arXiv:hep-ph/0510342.
[22] M. Anselmino *et al.*, arXiv:hep-ph/0511017.
[23] A. V. Efremov, K. Goeke and P. Schweitzer, Phys. Rev. D**73** (2006) 094025.
[24] M. Anselmino, M. Boglione, U. D'Alesio, A. Kotzinian, F. Murgia, A. Prokudin and C. Turk, Phys. Rev. D **75** (2007) 054032 [arXiv:hep-ph/0701006]. A. Prokudin, these Proceedings.
[25] J. C. Collins *et al.*, Phys. Rev. D **73** (2006) 094023; Czech. J. Phys. **56** (2006) C125.
[26] A. V. Efremov, K. Goeke and P. Schweitzer, Czech. J. Phys. **56** (2006) F181 [arXiv:hep-ph/0702155].
[27] A. Airapetian *et al.* [HERMES Collaboration], Phys. Rev. Lett. **84** (2000) 4047; Phys. Rev. D **64** (2001) 097101; Phys. Lett. B **562** (2003) 182, **622** (2005) 14, and **648** (2007) 164.
[28] H. Avakian *et al.* [CLAS Collaboration], Phys. Rev. D **69**, 112004 (2004) [arXiv:hep-ex/0301005].

[29] A. V. Efremov, K. Goeke and P. Schweitzer, Phys. Lett. B **522** (2001) 37, **544** (2002) 389E.
[30] A. V. Efremov, K. Goeke and P. Schweitzer, Eur. Phys. J. C **24** (2002) 407; Phys. Lett. B **568** (2003) 63; Eur. Phys. J. C **32** (2003) 337.
[31] J. Adams *et al.* [STAR Collaboration], Phys. Rev. Lett. **92** (2004) 171801 [arXiv:hep-ex/0310058]. G. Bunce, these Proceedings.
[32] P. V. Pobylitsa, arXiv:hep-ph/0301236.
[33] M. Burkardt, Phys. Rev. D **66** (2002) 114005; Phys. Rev. D **69** (2004) 057501; Phys. Rev. D **69** (2004) 091501.
[34] A. V. Efremov and O. V. Teryaev, Yad. Fiz. **39** (1984) 1517; Phys. Lett. B **150** (1985) 383.
J. W. Qiu and G. Sterman, Phys. Rev. Lett. **67** (1991) 2264; Nucl. Phys. B **378** (1992) 52.
Y. Kanazawa and Y. Koike, Phys. Lett. B **478** (2000) 121; Phys. Lett. B **490** (2000) 99.
[35] C. J. Bomhof, P. J. Mulders and F. Pijlman, Phys. Lett. B **596** (2004) 277.
A. Bacchetta, C. J. Bomhof, P. J. Mulders and F. Pijlman, Phys. Rev. D **72** (2005) 034030.
O. Teryaev, these Proceedings and references therein.
[36] A. Bravar, Nucl. Phys. B**79** (1999) 520c.
[37] A. V. Efremov, O. G. Smirnova and L. G. Tkachev, Nucl. Phys. B**74** (1999) 49c [arXiv:hep-ph/9812522]; *ibid.* B**79** (1999) 554.
[38] P. Schweitzer *et al.*, Phys. Rev. D**64** (2001) 034013 [arXiv:hep-ph/0101300].
[39] X. Artru, J. Czyżewski and H. Yabuki, Z. Phys. C**73** (1997) 527; Acta Phys. Polon. B**29** (1998) 2115 [arXiv:hep-ph/9805463]. A. Schäfer and O. V. Teryaev, Phys. Rev. D**61** (2000) 077903.
[40] D. Dutta *et al.*, J-PARC Letter of Intent (2002).
[41] V. V. Abramov *et al.*, arXiv:hep-ex/0511046. A. Vasiliev, this proceedings and references therein.
[42] P. Lenisa and F. Rathmann *et al.* [PAX Collaboration], arXiv:hep-ex/0505054.
F. Rathmann *et al.*, Phys. Rev. Lett. **94** (2005) 014801 [arXiv:physics/0410067].
[43] A. V. Efremov, K. Goeke and P. Schweitzer, Eur. Phys. J. C **35** (2004) 207; arXiv:hep-ph/0412427. B. Pasquini, M. Pincetti and S. Boffi, Phys. Rev. D **76** (2007) 034020 [arXiv:hep-ph/0612094]. M. Anselmino, V. Barone, A. Drago and N. N. Nikolaev, Phys. Lett. B **594** (2004) 97.
[44] M. Diefenthaler, arXiv:hep-ex/0612010; arXiv:0706.2242 [hep-ex]. V. Korotkov, these Proceedings.
[45] A. Ogawa, M. Grosse-Perdekamp, R. Seidl and K. Hasuko, arXiv:hep-ex/0607014.
[46] A. Kotzinian, Nucl. Phys. **B441**, 234 (1995).
[47] A. Kotzinian, B. Parsamyan and A. Prokudin, Phys. Rev. D **73** (2006) 114017.
[48] H. Avakian, A. V. Efremov, K. Goeke, A. Metz, P. Schweitzer and T. Teckentrup, arXiv:0709.3253.
[49] A. Kotzinian [on behalf of the COMPASS collaboration], arXiv:0705.2402 [hep-ex].

DESCRIPTION OF THE SPIN STRUCTURE FUNCTION g_1 AT ARBITRARY x AND ARBITRARY Q^2

B.I. Ermolaev[1†], M. Greco[2] and S.I. Troyan[3]

(1) *Ioffe Physico-Technical Institute, 194021 St.Petersburg, Russia*
(2) *Department of Physics and INFN, University Rome III, Rome, Italy*
(3) *St.Petersburg Institute of Nuclear Physics, 188300 Gatchina, Russia*
† *E-mail: ermolaev@mail.cern.ch*

Abstract

The explicit expressions describing the structure function g_1 at arbitrary x and Q^2 are obtained. In the first place, they combine the well-known DGLAP expressions for g_1 with the total resummation of leading logarithms of x, which makes possible to cover the kinematic region of arbitrary x and large Q^2. In order to cover the small-Q^2 region the shift $Q^2 \to Q^2 + \mu^2$ in the large-Q^2 expressions is suggested and values of μ are estimated. The expressions obtained do not require singular factors x^{-a} in the fits for initial parton densities.

1 Introduction

The goal of obtaining universal expressions describing the structure function g_1 at all x and Q^2 is an attractive task from both theoretical and phenomenological point of view. Until recently, the only theoretical instrument to describe g_1 was the Standard Approach (SA) which involves the DGLAP evolution equations [1] and standard fits [2] for the initial parton densities δq and δg. The fits are defined from phenomenological considerations at $x \sim 1$ and $Q^2 = \mu^2 \sim 1\text{GeV}^2$. The DGLAP equations are one-dimensional, they describe the Q^2 -evolution only, converting δq and δg into the evolved distributions Δq and Δg. The DGLAP equations are theoretically grounded in the kinematical the region **A** only:

$$\mathbf{A:} \qquad s > Q^2 \gg \mu^2, \qquad x \leq 1 \tag{1}$$

where we have denoted $s \equiv 2pq$, with p and q being the momenta of the initial hadron and photon respectively. This leaves the other kinematical regions uncovered. It is convenient to specify those regions as follows:

The small-x region **B**:

$$\mathbf{B:} \qquad s \gg Q^2 \gg \mu^2, \qquad x \ll 1 \tag{2}$$

and the small-Q^2 regions **C** and **D** :

$$\mathbf{C:} \qquad 0 \leq Q^2 \leq \mu^2, \qquad x \ll 1, \tag{3}$$

$$\mathbf{D:} \qquad 0 \leq Q^2 \leq \mu^2, \qquad x \leq 1. \tag{4}$$

As the matter of fact, the SA has been extended from Region **A** to the small-x Region **B**, though without any theoretical basis. The point is that after converting δq and δg

into Δq and Δg with the DGLAP evolution equations, they should be evolved to the small-x region as well. The x -evolution is supposed to come from convoluting Δq and Δg with the coefficient functions C_{DGLAP}. However, in the leading order $C^{LO}_{DGLAP} = 1$; the NLO corrections account for one- or two- loop contributions and neglect higher loops. This is the correct approximation in the region **A** but becomes wrong in the Region **B** where contributions $\sim \ln^k(1/x)$ are large and should be accounted for to all orders in α_s. C_{DGLAP} do no include the total resummation of the leading logarithms of x (LL), so SA requires special fits for δq and δg. The general structure of such fits (see Refs. [2]) is as follows:

$$\delta q = N x^{-a} \varphi(x) \tag{5}$$

where N is a normalization constant; $a > 0$, so x^{-a} is singular when $x \to 0$ and $\varphi(x)$ is regular in x at $x \to 0$. In Ref. [3] we showed that the role of the factor x^{-a} in Eq. (5) is to mimic the total resummation of LL performed in Refs [4, 5]. Similarly to LL, the factor x^{-a} provides the steep rise to g_1 at small x and sets the Regge asymptotics for g_1 at $x \to 0$, with the exponent a being the intercept. The presence of this factor is very important for extrapolating DGLAP into the region **B:** When the factor x^{-a} is dropped from Eq. (5), DGLAP stops to work at $x \leq 0.05$ (see Ref. [3] for detail). Accounting for the LL resummation is beyond the DGLAP framework, because LL come from the phase space not included in the DGLAP -ordering

$$\mu^2 < k_{1\ \perp}^2 < k_{2\ \perp}^2 < ... < Q^2 \tag{6}$$

for the ladder partons ($k_{2i\ \perp}$ are the transverse components of the ladder momenta k_i). LL can be accounted only when the ordering Eq. (6) is lifted and all $k_{i\ \perp}$ obey

$$\mu^2 < k_{i\ \perp}^2 < (p+q)^2 \approx (1-x)2pq \approx 2pq \tag{7}$$

at small x. Replacing Eq. (6) by Eq. (7) leads inevitably to the change of the DGLAP parametrization

$$\alpha_s^{DGLAP} = \alpha_s(Q^2) \tag{8}$$

by the alternative parametrization of α_s given by Eq. (14). This parametrization was obtained in Ref. [6] and was used in Refs. [4, 5] in order to find explicit expressions accounting for the LL resummation for g_1 in the region **B**. Obviously, those expressions require the non-singular fits for the initial parton densities. Let us note that the replacement of Eq. (6) by Eq. (7) brings a more involved μ -dependence of g_1. Indeed, Eq. (6) makes the contributions of gluon ladder rungs be infrared (IR) stable, with μ acting as a IR cut-off for the lowest rung and $k_{i\ \perp}$ playing the role of the IR cut-off for the $i+1$-rung. In contrast, Eq. (7) implies that μ acts as the IR cut-off for every rung.

The small-Q^2 Regions **C** and **D** are, obviously, beyond the reach of SA because DGLAP cannot be exploited here. Alternatively, in Refs. [7, 8] we obtained expressions for g_1 in the region **C** and proved that Region C can be described through the shift $Q^2 \to Q^2 + \mu^2$ in our large-Q^2 formulae. Combining these results with SA obtained in Ref. [3] makes it possible to describe g_1 in Region **D**. For the sake of simplicity, we present below formulae for g_1^{NS}, the non-singlet component of g_1 only.

2 Description of g_1 in the region B

The total resummation of the double-logarithms (DL) and single- logarithms of x in the region **B** was done in Refs. [4,5]. In particular, the non-singlet component, g_1^{NS} of g_1 is

$$g_1^{NS}(x,Q^2) = (e_q^2/2)\int_{-\imath\infty}^{\imath\infty}\frac{d\omega}{2\pi\imath}(1/x)^{\omega}C_{NS}(\omega)\delta q(\omega)\exp\left(H_{NS}(\omega)\ln(Q^2/\mu^2)\right)\ , \qquad (9)$$

with new coefficient functions C_{NS},

$$C_{NS}(\omega) = \frac{\omega}{\omega - H_{NS}^{(\pm)}(\omega)} \qquad (10)$$

and anomalous dimensions H_{NS},

$$H_{NS} = (1/2)\Big[\omega - \sqrt{\omega^2 - B(\omega)}\Big] \qquad (11)$$

where

$$B(\omega) = (4\pi C_F(1+\omega/2)A(\omega) + D(\omega))/(2\pi^2)\ . \qquad (12)$$

$D(\omega)$ and $A(\omega)$ in Eq. (12) are expressed in terms of $\rho = \ln(1/x)$, $\eta = \ln(\mu^2/\Lambda^2_{QCD})$, $b = (33-2n_f)/12\pi$ and the color factors $C_F = 4/3$, $N = 3$:

$$D(\omega) = \frac{2C_F}{b^2N}\int_0^{\infty} d\rho e^{-\omega\rho}\ln\big(\frac{\rho+\eta}{\eta}\big)\Big[\frac{\rho+\eta}{(\rho+\eta)^2+\pi^2} \mp \frac{1}{\eta}\Big]\ , \qquad (13)$$

$$A(\omega) = \frac{1}{b}\Big[\frac{\eta}{\eta^2+\pi^2} - \int_0^{\infty}\frac{d\rho e^{-\omega\rho}}{(\rho+\eta)^2+\pi^2}\Big]. \qquad (14)$$

H_S and C_{NS} account for DL and SL contributions to all orders in α_s. Eqs. (14) and (13) depend on the IR cut-off μ through variable η. It is shown in Refs. [4,5] that there exists an Optimal scale for fixing μ: $\mu \approx 1$ Gev for g_1^{NS} and $\mu \approx 5$ GeV for g_1^s. The arguments in favor of existence of the Optimal scale were given in Ref. [8]. Eq. (9) predicts that g_1 exhibits the power behavior in x and Q^2 when $x \to 0$:

$$g_1^{NS} \sim \left(Q^2/x^2\right)^{\Delta_{NS}/2},\ g_1^S \sim \left(Q^2/x^2\right)^{\Delta_S/2} \qquad (15)$$

where the non-singlet and singlet intercepts are $\Delta_{NS} = 0.42$, $\Delta_S = 0.86$ respectively. However the asymptotic expressions (15) should be used with great care: According to Ref. [3], Eq. (15) should not be used at $x \geq 10^{-6}$. So, Eq. (9) should be used instead of Eq. (15) at available small x. Expressions accounting the total resummation of LL for the singlet g_1 in the region **B** were obtained in Ref. [5]. They are more complicated than Eq. (9) because involve two coefficient functions and four anomalous dimensions.

3 Unified description of Regions A and B

As was suggested in Ref. [3], the natural way to describe g_1 in the Regions A and B is to combine the small-x results with the DGLAP expressions for the coefficient functions

and anomalous dimensions of g_1. In particular, g_1^{NS} is again given by Eq. (9), however with the new coefficient function $\widetilde{C}_{NS}$ and new anomalous dimension $\widetilde{H}_{NS}$:

$$\widetilde{C}_{NS} = C_{NS} + C_{NS}^{DGLAP} - \Delta C_{NS}$$
$$\widetilde{H}_{NS} = H_{NS} + \gamma_{NS}^{DGLAP} - \Delta H_{NS} \tag{16}$$

where C_{NS} and H_{NS} are defined in Eqs. (10,11), C_{NS}^{DGLAP} and γ_{NS}^{DGLAP} are the DGLAP non-singlet coefficient function and anomalous dimension. The terms ΔC_{NS}, ΔH_{NS} should be introduced to avoid the double counting. In the case when the DGLAP expressions are used in C_{NS}^{DGLAP} and γ_{NS}^{DGLAP} with the LO accuracy,

$$\Delta C_{NS} = 1, \quad \Delta H_{NS} = \frac{A(\omega)}{2\pi}\Big[\frac{1}{\omega} + \frac{1}{2}\Big] \tag{17}$$

They are the first terms of expansions of Eqs. (10,11) in the series in $A(\omega)$. In order to account for the NLO terms for C_{NS}^{DGLAP} and γ_{NS}^{DGLAP}, the next terms of the expansions should be included into ΔC_{NS} and ΔH_{NS}. When Eq. (16) is substituted into Eq. (9), we arrive at the description of g_1^{NS} covering both Regions **A** and **B**. Obviously, the main contribution to $\widetilde{C}_{NS}$, $\widetilde{H}_{NS}$ at Region **A** comes from their DGLAP components. On the contrary, the total resumation terms dominate at $x \ll 1$. When Eq. (16) is used, the initial parton densities should not include singular factors.

4 Description of g_1 in the Regions B and C

Region **C** is defined in Eq. (3). It involves small Q^2, so there are no large contributions $\ln^k(Q^2/\mu^2)$ in this region. In other words, the DGLAP ordering of Eq. (6) does not make sense in the region **C** , which makes impossible exploiting DGLAP here. In contrast, Eq. (6) is not sensitive to the value of Q^2 and therefore the total resummation of LL does make sense in the region **C**. In Ref. [7] we suggested that the shift

$$Q^2 \to Q^2 + \mu^2 \tag{18}$$

would allow for extrapolating our previous results (obtained in Refs. [4, 5] for g_1 in the region **B**) into the region **C**. Then in Ref. [8] we proved this suggestion. Therefore, applying Eq. (18) to g_1^{NS} leads to the following expression for g_1^{NS} valid in the regions **B** and **C**:

$$g_1^{NS}(x+z,Q^2) = (e_q^2/2)\int_{-\imath\infty}^{\imath\infty}\frac{d\omega}{2\pi\imath}\Big(\frac{1}{x+z}\Big)^{\omega} C_{NS}(\omega)\delta q(\omega)\exp\Big(H_{NS}(\omega)\ln\big((Q^2+\mu^2)/\mu^2\big)\Big)\,, \tag{19}$$

where $z = \mu^2/2pq$. Obviously, Eq. (19) reproduces Eq. (9) in the region **B**. Expression for g_1^S looks similarly but more complicated, see Refs. [7, 8] for detail. Let us notice that the idea of considering DIS in the small-Q^2 region through the shift Eq. (18) is not new. It was introduced by Nachtmann in Ref. [10] and used after that by many authors (see e.g. [11]), being based on different phenomenological considerations. On the contrary, our approach is based on the analysis of the Feynman graphs contributing to g_1. We also suggest that the following values for μ should be used: for the non-singlet component of g_1 $\mu = 1$ GeV and $\mu = 5.5$ GeV for the singlet g_1.

5 Generalization to the Region D

The generalization of the results of Sect. IV to the Region **D** can easily be done with replacements

$$C_{NS} \to \widetilde{C}_{NS}, \qquad H_{NS} \to \widetilde{H}_{NS} \tag{20}$$

in Eq. (19), with $\widetilde{C}_{NS}$, $\widetilde{H}_{NS}$ defined in Eq. (16). So, we arrive at the final result: the expression for g_1 which can be used in the Regions **A,B,C,D** universally is

$$g_1^{NS}(x+z,Q^2) = (e_q^2/2)\int_{-\imath\infty}^{\imath\infty}\frac{d\omega}{2\pi\imath}\Big(\frac{1}{x+z}\Big)^{\omega}\widetilde{C}_{NS}(\omega)\delta q(\omega)\exp\big(\widetilde{H}_{NS}(\omega)\ln\big((Q^2+\mu^2)/\mu^2\big)\big). \tag{21}$$

We remind that the expressions for the initial parton densities in Eq. (21) should not contain singular terms because the total resummation of leading logarithms of x is explicitly included into $\widetilde{C}_{NS}$ and $\widetilde{H}_{NS}$.

6 Prediction for the COMPASS experiments

The COMPASS collaboration now measures the singlet g_1^S at $x \sim 10^{-3}$ and $Q^2 \leq 3$ GeV^2, i.e. in the kinematic region beyond the reach of DGLAP. However, our formulae for g_1^{NS} and g_1^S obtained in Refs. [7, 8] cover this region. Although expressions for singlet and non-singlet g_1 are different, with formulae for the singlet being much more complicated, we can explain the essence of our approach, using Eq. (19) as an illustration. According to results of [5], $\mu \approx 5$ GeV for g_1^S, so in the COMPASS experiment $Q^2 \ll \mu^2$. It means, $\ln^k(Q^2+\mu^2)$ can be expanded into series in Q^2/μ^2, with the first term independent of Q^2:

$$g_1^S(x+z,Q^2,\mu^2) = g_1^S(z,\mu^2) + \sum_{k=1}(Q^2/\mu^2)^k E_k(z) \tag{22}$$

where $E_k(z)$ account for the total resummation of LL of z and

$$g_1^S(z,\mu^2) = (< e_q^2/2 >)\int_{-\imath\infty}^{\imath\infty}\frac{d\omega}{2\pi\imath}\big(1/z\big)^{\omega}\big[C_S^q(\omega)\delta q(\omega) + C_S^g(\omega)\delta g(\omega)\big], \tag{23}$$

so that $\delta q(\omega)$ and $\delta g(\omega)$ are the initial quark and gluon densities respectively and $C_S^{q,g}$ are the singlet coefficient functions. Explicit expressions for $C_S^{q,g}$ are given in Refs. [5, 7]. Therefore, we can makes the following predictions easy to be checked by COMPASS:

6.1 Prediction 1

In the whole COMPASS range $0 \leq Q^2 \leq 3$ GeV^2, the singlet g_1 does not depend on x regardless of the value of x.

6.2 Prediction 2

Instead of studying experimental the x-dependence of g_1^S, it would be much more interesting to investigate its dependence on $2pq$ because it makes possible to estimate the ratio $\delta g/\delta q$ (see Ref. [7] for detail).

7 Remark on the higher twists contributions

In the region **B** one can expand terms $\sim (Q^2+\mu^2)^k$ in Eq. (19) into series in $(\mu^2/Q^2)^n$ and represent $g_1^{NS}(x+z,Q^2,\mu^2)$ as follows:

$$g_1^{NS}(x+z,Q^2,\mu^2) = g_1^{NS}(x,Q^2/\mu^2) + \sum_{k=1}(\mu^2/Q^2)^k T_k \tag{24}$$

where $g_1^{NS}(x,Q^2/\mu^2)$ is given by Eq. (9); for explicit expressions for the factors T_k see Ref. [8]. The power terms in the rhs of Eq. (24) look like the power $\sim 1/(Q^2)^k$ -corrections and therefore the lhs of Eq. (24) can be interpreted as the total resummation of such corrections. These corrections are of the perturbative origin and have nothing in common with higher twists contributions ($\equiv HTW$). The latter appear in the conventional analysis of experimental date on the Polarized DIS as a discrepancy between the data and the theoretical predictions, with $g_1^{NS}(x,Q^2/\mu^2)$ being given by the Standard Approach:

$$g_1^{NS\ exp} = g_1^{NSSA} + HTW\ . \tag{25}$$

Confronting Eq. (25) to Eq. (24) leads to an obvious conclusion: In order estimate genuine higher twists contributions to g_1^{NS}, one should account, in the first place, for the perturbative power corrections predicted by Eq. (24); otherwise the estimates cannot be reliable. It is worth mentioning that we can easily explain the empirical observation made in the conventional analysis of experimental data: The power corrections exist for $Q^2 > 1$ GeV^2 and disappear when $Q^2 \to 1$ GeV^2. Indeed, in Eq. (24) $\mu = 1$ GeV , so the expansion in the rhs of Eq. (24) make sense for $Q^2 > 1$ GeV^2 only; at smaller Q^2 it should be replaced by the expansion of Eq. (19) in $(Q^2/\mu^2)^n$.

8 Conclusion

The extrapolation of DGLAP from the standard Region **A** to the small-x Region B involves necessarily the singular fits for the initial parton densities without any theoretical basis. On the contrary, the resummation of the leading logarithms of x is the straightforward and most natural way to describe g_1 at small x. Combining this resummation with the DGLAP results leads to the expressions for g_1 which can be used at large Q^2 and arbitrary x (Regions **A** and **B**), leaving the initial parton densities non-singular. Then, incorporating the shift of Eq. (18) into these expressions allows us to describe g_1 in the small-Q^2 regions (Regions **C** and **D**) and to write down Eq. (21) describing g_1 at the Regions **A,B,C,D.** We have used it for studying the g_1 singlet at small Q^2 which is presently investigated by the COMPASS collaboration. It turned out that g_1 in the COMPASS kinematic region depends on $z = \mu^2/2pq$ only and practically does not depend on x, even at $x \ll 1$. Numerical calculations show that the sign of g_1 is positive at z close to 1 and can remain positive or become negative at smaller z, depending on the ratio between δg and δq. To conclude, let us notice that extrapolating DGLAP into the small-x region, although it could provide a satisfactory agreement with experimental data, leads to various wrong statements, or misconceptions. We enlisted the most of them in Ref. [9]. Below we mention one important wrong statements not included in Ref. [9]:

Misconception: *The impact of the resummation of leading logarithms of x on the small-x behavior of g_1 is small.*

This statement appears when the resummation is combined with the DGLAP expressions, similarly to Eq. (16), and at the same time the fits for the initial parton densities contain singular factors like the one in Eq. (5). Such a procedure is inconsistent and means actually a double counting of the logarithmic contributions: the first implicitly, through the fits, and the second in explicit way. It also affects the small-x asymptotics of g_1, leading to the incorrect values of the intercepts of g_1 (see Ref. [3] for more detail).

Acknowledgement

B.I. Ermolaev is grateful to the Organizing Committee of the workshop Spin-2007 for financial support of his participation in the workshop.

References

[1] G. Altarelli and G. Parisi, Nucl. Phys. **B126**, 297 (1977);
V.N. Gribov and L.N. Lipatov, Sov. J. Nucl. Phys. **15**, 438 (1972);
L.N.Lipatov, Sov. J. Nucl. Phys. **20**, 95 (1972);
Yu.L. Dokshitzer, Sov. Phys. JETP **46**, 641 (1977).

[2] G. Altarelli, R.D. Ball, S. Forte and G. Ridolf, Nucl. Phys. **B496**, 337 (1997); ibid Acta Phys. Polon. **B29**, 1145 (1998);
E. Leader, A.V. Sidorov and D.B. Stamenov, Phys. Rev. D **73**, 034023 (2006);
J. Blumlein, H. Botcher. Nucl. Phys. **B636**, 225 (2002);
M. Hirai at al., Phys. Rev. D **69**, 054021 (2004).

[3] B.I. Ermolaev, M. Greco and S.I. Troyan, Phys. Lett. **B622**, 93 (2005).

[4] B.I. Ermolaev, M. Greco and S.I. Troyan, Nucl.Phys. **B594**, 71 (2001); ibid **B571**, 137 (2000).

[5] B.I. Ermolaev, M. Greco and S.I. Troyan, Phys. Lett. **B579**, 2004 (321).

[6] B.I. Ermolaev, M. Greco and S.I. Troyan. Phys. Lett. **B522**, 57 (2001).

[7] B.I. Ermolaev, M. Greco and S.I. Troyan, Eur.Phys.J. C **50**, 823 (2007).

[8] B.I. Ermolaev, M. Greco and S.I. Troyan, hep-ph/0607024.

[9] B.I. Ermolaev, M. Greco and S.I. Troyan, Acta Phys. Polon. B **38**, No 7, 2243 (2007); ibid hep-ph/0704.0341.

[10] O.Nachtmann. Nucl. Phys. **B63**, 237 (1973).

[11] B. Badelek and J. Kwiecinski. Z. Phys. C **43**, 251 (1989); ibid Rev. Mod. Phys. **68**, No 2, 445 (1996); ibid Phys. Lett. **B418**, 229 (1998).

Discussion

Com. (D.Sivers, Portland Phys. Inst.) The idea of the talk is to complement DGLAP with total resummation of $\ln(1/x)$, which is a natural way.

Com. (O.Teryaev, JINR, Dubna) This approach corresponds to another definitions of non-perturbative inputs with singular terms in x subtracted. The whole procedure of factorization should be therefore re-analyzed in order to describe other processes, like hadron-hadron collisions at RHIC

Q. (J.Nassalski, SINS, Warsaw) You said you can use "simplified" initial quark distributions. But their shape is known from experiments and it is not very simple.

A. The conventional shape of Δq is determined from experiment with using DGLAP. DGLAP lacks the total resummation of logs of x, so they mimic it by introducing singular factors x^{-a} in the fits. When the resummation is account for, these factors can be dropped. It simplifies the fits.

Q. (H.Santos, LIFEP, Lisboa) Standard QCD fits to g_1 using DGLAP equations find 2 solutions for ΔG - one ΔG positive and the other ΔG negative. Do you think that your approach could constrain the estimates of ΔG, namely the sign, and give more reliable results on $\Delta\Sigma$?

A. Yes, I think so.

Q. (A.Sidorov, JINR, Dubna) What are the arguments of the g_1 structure function in the l.h.s. of the formula.

A. Generally speaking g_1 depends on 3 arguments.

Q. (A.Sidorov, JINR, Dubna) What about x, is it shifted or not?

A. Yes, it is shifted.

Q. (A.Sidorov, JINR, Dubna) So, you shift the argument x with a small value $z = \mu^2/2pq << x = Q^2/2pq$ (which means $\mu^2 << Q^2$) and make an expansion of $g_1[x(1 + \mu^2/Q^2)]$ around x. You immediately get $(1/Q^2)^n$ terms on the r.h.s. of the equation, which provides a connection between $g_1(x+z, Q^2)$ and $g_1(x, Q^2)$. However, these Q^2 terms have nothing to do with the dynamical $(1/Q^2)^n$ corrections to $g_1(x, Q^2)$ coming from QCD, which are corrections to $g_1(x, Q^2)_{LT}$ at the SAME x.

FORWARD DISPERSION RELATIONS FOR COMPTON SCATTERING AND FINITE ENERGY SUM RULES FOR NUCLEONS AND LIGHT NUCLEI: NEW RESULTS

S.B. Gerasimov †

Bogoliubov Laboratory of Theoretical Physics, JINR, Dubna
† E-mail: gerasb@theor.jinr.ru

Abstract

The results following from new integral finite energy sum rules (FESR) for the nucleon and lightest nuclei total photoabsorption cross sections are presented. The correlation between of the difference of the proton and neutron $j = 0$ fixed-pole residues in the real part of respective Compton scattering amplitudes and multi-pion photoproduction on nucleons is discussed. The integral sum rules for the total photoabsorption on the helium-4 and deuteron serve as the measure of the nuclear medium influence on the mean value of the scalar pion densities in respective nuclei.

1. The known specific feature of the Compton scattering amplitude, alien to pure hadronic amplitudes, is the admission in its analytic structure of the fixed poles in the complex angular momentum plane. The positive evidence for the presence of the $j = 0$-fixed pole in proton Compton scattering amplitude was given by Damashek and Gilman (DG) [1] via the noticing the energy independent contribution of the value $C_p \simeq 3\ \mu b{\cdot}GeV$ in the real part of the high energy forward γp-scattering amplitude $\mathcal{R}ef_1(\nu)$, ν being the photon energy, calculated through the evaluation of the once-subtracted dispersion relation for spin-independent γp-scattering amplitude

$$f(\nu, \theta = 0^o) = f_1(\nu) + \imath\boldsymbol{\sigma} \cdot [\boldsymbol{\epsilon^*}_2 \times \boldsymbol{\epsilon}_1] f_2(\nu)\,.$$

The experimental confirmation of the DG-evaluation at $\nu = 2.2$ GeV was done via an ingenious measuring of the interference between the pure real Bethe-Geitler amplitude and weakly-virtual "Compton" amplitude of the electron -positron pair production in the γp-collision [2]. As is now known, the total photoabsorption cross-section $\sigma_{tot}^{\gamma N}(\nu)$ is rising with energy contrary to assumption $\sigma_{tot}(\infty) = const$ adopted by DG. For our further purposes, we consider the dispersion sum rule for the difference $f_{pn} = f_1^{\gamma p}(\nu) - f_1^{\gamma n}(\nu)$ of scattering amplitudes on the proton and neutron, where the difference of the corresponding cross sections is, presumably, free of infinitely-rising "soft-Pomeron" contributions and dominated, in the moderately-high energy photons, by t-channel exchange of the isovector a_2-Regge trajectory.

The standard FESR techniques enable us to confine ourselves with amplitudes in the finite region of the complex energy plane

$$f(\nu) = \frac{1}{2\pi\imath} \oint dz \frac{f(z)}{z - \nu} \tag{26}$$

where $f(\nu)$ is the spin-averaged, forward Compton scattering amplitude and the integration contour along the real axis and the large circle in the complex energy-plane.

Assumed parameterization of $f_{pn}(\nu)$ looks as follows [3]:

$$Imf_p(\nu) - Imf_n(\nu) = (\nu/4\pi)(\sigma_p^{tot} - \sigma_n^{tot}) = b_{a_2}\nu^{1/2}, \tag{27}$$

$$\mathcal{R}e(f_p(\nu) - f_n(\nu)) = (1/4\pi)b_{a_2}(-\nu^{1/2}) + C_p - C_n, \tag{28}$$

where $\sigma_p^{tot}(\nu) - \sigma_n^{tot}(\nu) = 24.6/\nu^{1/2}; C_p = -3.0\mu b \cdot GeV; C_n$-is a free parameter.
The energy interval considered: $\nu_{min} = \nu_{thr}(\pi)$ $\nu_{max} = 1.64\ GeV$, corresponding to $s(\gamma N) \simeq 2\ GeV^2$ The meson photoproduction cross-sections on the neutron are largely unknown and should be extracted *e.g.* from the deuteron data. Of all possible photomeson reactions, the best known is the single pion photoproduction. Therefore we treat the neutron cross-sections entering our sum rules as follows. The $\sigma_{\gamma n}^{tot}(\nu)$ is split into two parts: $\sigma_{\gamma n}^{tot} = \sigma(\gamma n \to \pi N) + \sigma(\gamma n \to 2\pi N + \dots)$
The single pion production cross-section is taken according to theoretical calculation with fairly good multipole amplitudes of the MAID Collaboration [4].

The detailed experimental study of the meson photoproduction on the deuteron target is planned at the MAMI electron accelerator (Mainz, Germany) up to photon energies $\sim 1.5\ GeV$. So, anticipating the appearance of the γn-data, needed for the checking of FESR sum rule for the difference of the γp- and γn- Compton amplitudes and extracting the value $C_p - C_n$ required further for definition of the nuclear sum rules, we present first the dependence of the experimentally measurable ratios $R_{n/p}^{tot}(R_{n/p}^{non-res})$, defined as:

$$R_{n/p}^{tot}(R_{n/p}^{non-res}) = \frac{\sigma_0^{tot}(\gamma n \to 2\pi + X)}{\sigma_0^{tot}(\gamma p \to 2\pi + X)}\left(\frac{\sigma_0^{non-res}(\gamma n \to 2\pi + X)}{\sigma_0^{non-res}(\gamma p \to 2\pi + X)}\right)$$

as the function of several plausible values of C_n, taking $C_p = -3.0\ \ \mu bGeV$ for granted. The results are presented in Table.

Table

C_p	C_n	$R_{n/p}^{tot}$	$R_{n/p}^{non-res}$
0	0	.95	.98
-3	-2	.72	.62
-3	0	.60	.39

For illustrative reasons, we indicate the results of the modelling the neutron-to-proton ratios as following from the ratios of the electric dipole moment fluctuation in the lowest hadronic Fock-components of the nucleon with at least one charged pion: $N \leftrightarrow \pi + N, 2\pi + N, \pi + \Delta(1231)$.

$$\frac{\langle \boldsymbol{D}^2(n \leftrightarrow n\pi^+\pi^-)\rangle}{\langle \boldsymbol{D}^2(p \leftrightarrow p\pi^+\pi^-)\rangle} \simeq r_{uncorr}$$

$$r_{uncorr} \simeq \frac{(1+4\varepsilon)\langle \boldsymbol{r}^2_{\pi^+\pi^-}\rangle}{(1+2\varepsilon)\langle \boldsymbol{r}^2_{\pi^+\pi^-}\rangle + 2\varepsilon\langle(\boldsymbol{r}_{\pi^+\pi^-} \cdot \boldsymbol{r}_{p\pi^-})\rangle} \geq 1.$$

$$r_{corr} \simeq \frac{\langle \boldsymbol{D}^2(n \leftrightarrow \pi\Delta)\rangle}{\langle \boldsymbol{D}^2(p \leftrightarrow \pi\Delta)\rangle} \simeq\ .66\ (.41)$$

The first value in r_{corr} refers to the sum over all possible charge $\pi\pi$-states produced in the final decay stage $\pi\Delta \to \pi\pi N$, while the second ratio corresponds to the selection of the $\pi^+\pi^-$ final states. The numerical relevance of r_{corr} to the last two rows in the Table testifies on the crucial importance of the correlation of the valence and nonvalence partonic composites of the nucleon in producing of the ultimate characteristics of the Compton scattering amplitude.

2. We turn now to a certain modification of the Gell-Mann, Goldberger and Thirring (GGT) sum rule for total photonuclear cross sections [5]. Our choice of the "superconvergent" combination of Compton amplitudes $f_{\gamma A(p,n)}$ is different from GGT.It includes amplitudes of two nuclei with $A_1 = Z_1 + N_1, A_2 = Z_2 + N_2$:

$$\frac{1}{A_1} f_{A_1} - \frac{1}{A_2} f_{A_2} = \frac{Z_1 N_2 - N_1 Z_2}{A_1 A_2}(f_p - f_n)$$

where each amplitude in the above relation will be presented in the form of the FESR with the finite large circle radius $R = \nu_{max}$ with ν_{max} chosen to be about the beginning of the Regge-model relevance for representing the non-diffraction contributions to total photoabsorption cross sections on nucleons and nuclei.

For arbitrary $A_1 = Z_1 + N_1$ and $A_2 = Z_2 + N_2$ our general sum rule reads

$$2\pi^2[\frac{f_{A_1}(\nu=0) + S_\pi(A_1)}{A_1} - \frac{f_{A_2}(\nu=0) + S_\pi(A_2)}{A_2} +$$
$$+\frac{Z_1 N_2 - Z_2 N_1}{A_1 A_2} \cdot (\frac{2b_{a_2}\nu_{max}^{1/2}}{2\pi^2} - C_p + C_n)] = \frac{\sigma_0^{\nu_{max}}(\gamma A_1)}{A_1} - \frac{\sigma_0^{\nu_{max}}(\gamma A_2)}{A_2} \qquad (29)$$

where $f_{A_i}(\nu = 0) \simeq -(\alpha Z_i^2)/(A_i m_n)$ is the Thompson zero-energy amplitude,

$$S_\pi(A_i) \simeq \frac{\alpha}{3} \int d^3x \langle A_i | \boldsymbol{\phi}(x)\boldsymbol{\phi}(x) | A_i \rangle \qquad (30)$$

and the energy integration in all integrals $\sigma_0^{\nu_{max}}$ over cross-sections extends from the photodisintegration threshold to the upper bound ν_{max}. It is principal point that in the photonuclear case there appears a new ingredient $S_\pi(A_i)$ including nonadditive contributions depending on atomic numbers. Formally, the terms proportional to scalar product of the pionic fields result naturally from the reduction formulas containing the equal-time commutators of the spatial- and time-components of the electromagnetic current operator [6–10]. Assuming the explicit presence of the pionic degrees of freedom in the effective lagrangian governing both the single-nucleon and multinucleon dynamics in the resonance region $\nu \leq \nu_{max}$, we obtain in particular additional constant terms entering the parameterization of the amplitude on the large circle in the complex energy plane and propagating into explicit expressions of our new sum rules.

The important particular case we shall concentrate thereupon for numerical estimates is the case of nuclei with equal number of protons and neutrons, specifically, the deuteron and He-4. Due to absence of helium-data at high energies we have to confine ourselves with the integration of all the experimentally known cross-sections over the intervals with $\nu \leq .8\ GeV$ [11, 12]. Thus we obtain

$$\frac{1}{4} S_\pi(^4He_2) - \frac{1}{2} S_\pi(d) \simeq (180 - 172 = 8)\ \mu b \cdot GeV, \qquad (31)$$

where the contributions of Thompson amplitudes are largely compensited in (31) and we left only with the difference of integrals over respective cross-sections. The physical significance of the derived sum rules lies in that they present relation of the explicitly relativistic, field-theoretic nuclear matrix elements in terms of experimentally measurable quantities and therefore they may have bearing on the checks of presently developing approaches of chiral Effective Field Theory (EFT) in the few-nucleon sector (see, *e.g.*, [13] and references therein).

The author is grateful to Dr. S.S. Kamalov for providing some additional MAID data and helpful discussions.

References

[1] M.Damashek and F.J.Gilman, Phys.Rev.**D1** (1970)1319.

[2] H.Alvensleben, et al. Phys.Rev.Lett. **30**(1973)328.

[3] W.P. Hesse, *et al.*, Phys.Rev.Lett. **25** (1970) 613.

[4] D.Drechsel, S.S.Kamalov, and L.Tiator, Nucl.Phys. **A 645** (1999) 145.
S.S.Kamalov, private communication.

[5] M.Gell-Mann, M.L.Goldberger and W.Thirring, Phys.Rev.**95**(1954) 1612.

[6] S.B.Gerasimov, in Proc.Int.Conf. on Electromagnetic Interactions at Low and Medium Energies, AN USSR, Moscow, 1972, v.3, p.382.

[7] S.B.Gerasimov and J.Moulin, Nucl.Phys. **B98** (1975) 349.

[8] S.A.Kulagin, TRK 91-39, Uni. Regensburg, 1991.

[9] M.Ericson, M.Rosa-Clot, and S.A.Kulagin, Nuovo.Cim. **A111**(1998)75.

[10] M.Ericson, G.Chanfray, J. Delorm, and M.Rosa-Clot, Nucl.Phys. **A663&664** (2000) 369c.

[11] D.Drechsel and Y.E.Kim, Phys.Rev.Lett.**40** (1978) 531.

[12] M.MacCormick, *et al.*, Phys.Rev.**C 53** (1996) 41.

[13] E.Epelbaum, arXiv: 0710.4247 [nucl-th].

POLARIZATION AT PHOTON COLLIDERS. EXAMPLE: CHARGE ASYMMETRY IN $\gamma\gamma \to \mu^+\mu^- + \nu$'s

I.F. Ginzburg†

Sobolev Institute of Mathematics. Novosibirsk, Russia
† *E-mail: ginzburg@math.nsc.ru*

Abstract

Photon collider (PLC) will be necessary option in the future International Linear Collider. We describe main features of PLC underlying high degree of polarization of photon beams there. As an example we compare the momentum distributions of positively and negatively charged leptons ($\ell^\pm = \mu^\pm$, $e^\pm$) in the reactions of type $\gamma\gamma \to \ell^+\ell^- + N\nu$, at $\sqrt{s} > 200$ GeV with polarized photons. These distribution demonstrates a considerable *charge asymmetry*.

Photon collider (PLC) will be necessary option of future Linear Collider (e.g. ILC) based on the laser photon backscattering on accelerated electrons of e-beam [1, 2]. Focused laser beam meet electron beam of ILC at collision point C, obtained in the Compton effect photons move in the direction of parental electrons and collide with similar photon beam ($\gamma\gamma$ collision) or with electron beam ($e\gamma$ collisions) in the interaction point IP (Fig. 1). At the reasonable energy of laser flash in few Jouls almost each electron transfer its energy to the photon so that the luminosity will be close to that of parental e^+e^- ILC.

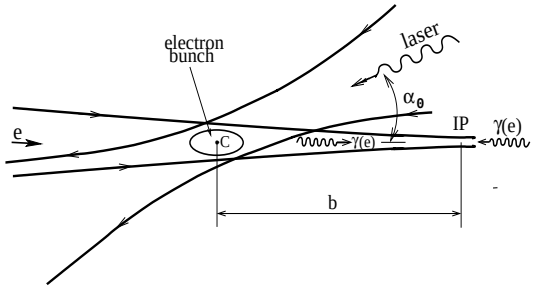

Figure 1: Photon beam production for PLC

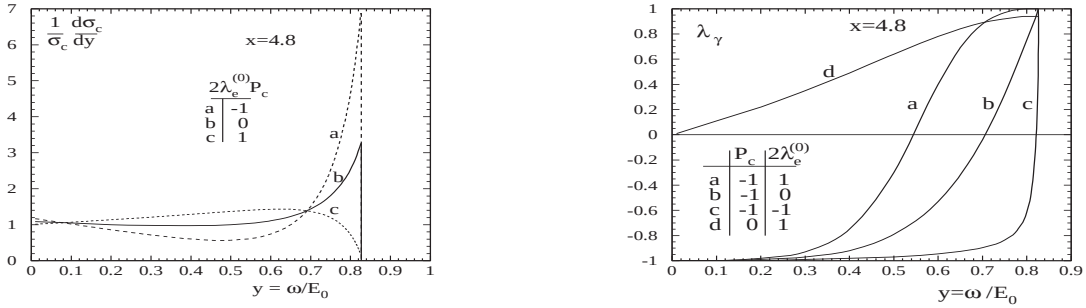

Figure 2: Photon energy spectrum (left) and polarization (right), $y = E_\gamma/E_0$

In the description of this conversion process important parameter is $x = \dfrac{4E\omega_0}{m_e^2}$, where E_0 is electron beam energy and $\omega \approx 1$ eV is laser photon energy. For $E_0 = 250$ GeV we have $x \approx 5$ (higher values are forbidden since photons can disappear in the collisions with laser photons from the tail of flash with production of e^+e^- pair). Maximal photon energy

is $E_{\gamma max} = \frac{x}{x+1}E$, and photon spectrum is concentrated near upper bound, at the left plot of Fig. 2 this spectrum from one $e\gamma$ collision is shown at different helicities of parental beams). In the high energy part of spectrum photon polarization reproduces that of laser flight (the circular polarization is preferable). With decreasing of photon energy mean photon polarization decreases depending on initial electron polarization, being very high for high energy part of spectrum (Fig. 2, right plot). Therefore PLC will be collider for $\gamma\gamma$ and $e\gamma$ collisions of high energy with high luminosity and *with high and easily variable polarization of high energy photons*.

Due to the finite distance b between conversion point (C) and interaction point (IP) and also due to rescatterings of laser photons on electrons after first collision with laser photon, photon spectra even non-factorizable. Fortunately in the high energy part of spectra ($E_\gamma > E_\gamma^{max}/\sqrt{2}$) these spectra are factorizable with high precision and these photons have high degree of polarization. The form of effective spectra in this region is described with high accuracy with the aid of one additional parameter $\rho \propto m_e b/E_0$ only independent on details of organization of experimental set up [3]. The luminosity of Photon Collider is normalized for this very region only.

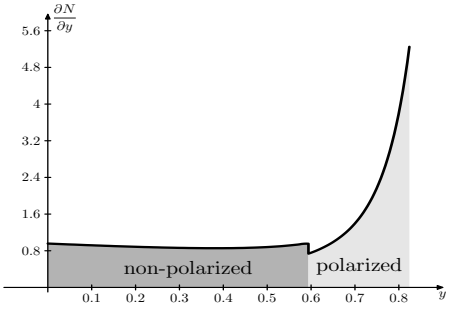

Figure 3: Model "realistic" photon beam spectrum for PLC

As for low energetic tail of effective photon spectrum it depends strongly on details of experimental set-up which will vary in the process of construction of ILC. Moreover in this part photon spectra in fact non-factotrizable in luminosity spectra.

So, in our simulations for the high energy part of the spectrum $E_\gamma > E_\gamma^{max}/\sqrt{2}$ we used the approximation from [3] with $\rho = 1$ and $x = 4.8$ with polarization for ideal Compton effect [1]. To imitate low energy part of spectrum we used spectra from [1] for the case when $b = 0$ and consider these photons to be unpolarized (Fig. 3).

• The Photon colliders allow to study well known processes in hadron physics and QCD at much higher energies and precision than now with polarization dependence which is unattainable now. That are diffractive processes like $\gamma\gamma \to \rho\rho$, $\rho\omega$, etc. at high enough transfers, polarized structure functions (at $e\gamma$ collisions), etc. (see preliminary list in [2]).

Besides, these colliders provide very effective field for the study of new effects of both SM and New Physics. In particularly, it is naturally to expect that the charge asymmetry of leptons, produced in the collision of *neutral but highly polarized colliding particles* $\gamma\gamma \to \ell^+\ell^- + neutrals$ (where $\ell = \mu$, e), can be a good tool for the discovery of New Physics effects [5].

• As an example below we study most important background process of the mentioned type – the SM process, in which *neutrals* are ν's and main mechanism is given by $\gamma\gamma \to W^+W^-$ process with subsequent lepton decay of W [4], [6]. The latter process (+ other SM processes) will ensure very high event rate at the anticipated luminosity of ILC. The charge asymmetry here appears due to transformation of initial photon helicity into distribution of final leptons via P-violating but CP-preserving leptonic decay of W.

We present most of results, applying cuts on the muons scattering angles given by $\pi - \theta_0 > \theta > \theta_0$, with $\theta_0 = 10$ mrad, and a cut on muons transverse momentum $p_\perp^c > 10$ GeV, both on each muon or W and on the couple of muons. These simultaneous cuts reduce many backgrounds. We expect that the New Physics effects will be more important

at high $p_\perp$. How discussed SM charge asymmetry depend on cut value $p_\perp^c$?

Our numerical results have been obtained with the CompHEP/CalcHEP packages [7], [8] in a version which allows one to take into account the circular polarization of the initial photons and choose different random seed numbers for Monte Carlo (MC) [8].

$\gamma\gamma \to \mu^+\mu^-\nu\bar{\nu}$, monochromatic photons.

Figure 4 presents the distributions of muons in the $p_\parallel$, $p_\perp$ plane, $\partial^2\sigma/(\partial p_\parallel \partial p_\perp)$ at different photon polarizations for monochromatic beams for the process $\gamma\gamma \to \mu^+\mu^-\nu\bar{\nu}$.

These figures show explicitly strong difference in the distributions of negative and positive muons as well as strong dependence of distributions on photon polarizations. Therefore, the charge asymmetry in the process is **a strong effect**.

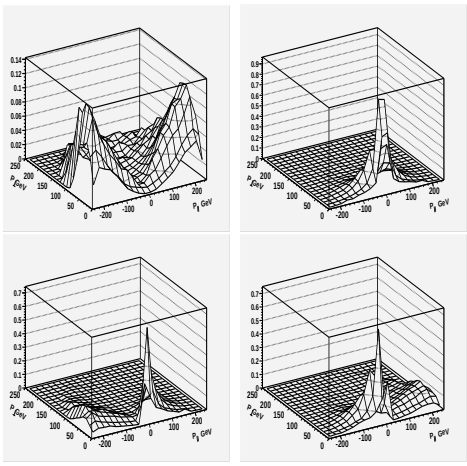

Figure 4. Muon distribution in $\gamma_-\gamma_- \to W\mu + \nu's$ (upper plots) and $\gamma_+\gamma_- \to W\mu + \nu's$ (lower plots), left – μ^-, right – μ^+

To obtain more definite quantitative description, we consider normalized mean values of longitudinal $p_\parallel^\mp$ and transverse $p_\perp^\mp$ momenta of μ^- or μ^+, in the forward hemisphere ($p_\parallel > 0$, subscript +), and take their relative difference as a measure of the longitudinal Δ_L and transverse Δ_T charge asymmetry:

$$P^\pm_{L,T+} = \frac{\int p^\pm_{\parallel,\perp} d\sigma}{E_\gamma^{max} \int d\sigma}, \quad \Delta_{L,T} = \frac{P^-_{L,T+} - P^+_{L,T+}}{P^-_{L,T+} + P^+_{L,T+}}$$

MC calculations simulate experiment and have statistical uncertainty similar to that in the future experiment. We find it useful to obtain statistical uncertainties $\delta_{L,T}$ of the considered integral characteristics at given expected number of events (about 10^6) by repeating our calculation 5 times with different seed number inputs for MC (with CalcHEP [8]). Also we consider as an independent set of observations data obtained by simultaneous change λ_1, $\lambda_2 \to -\lambda_1, -\lambda_2$, $\mu^- \leftrightarrow \mu^+$ (this change should not change distributions due to CP conservation in SM).

$\gamma_{\lambda_1}\gamma_{\lambda_2}$	N	P_N^- δP_N^-	P_N^+ δP_N^+	Δ_N $\delta\Delta_N$
$\gamma_-\gamma_-$	L	0.606 0.29%	0.201 0.55%	0.501 0.57%
	T	0.333 0.61%	0.159 0.28%	0.335 0.44%
$\gamma_+\gamma_-$	L	0.223 0.74%	0.609 0.19%	-0.463 0.47%
	T	0.164 0.08%	0.262 0.31%	-0.231 2.76%

Table I. Charge asymmetry quantities and statistical uncertainties for $\gamma_{\lambda_1}\gamma_{\lambda_2} \to W\mu\nu$ process, N=T or L.

Table I presents obtained average momenta for the positive and negative muons and corresponding asymmetry quantities together with their statistical uncertainties (in percents).

Cascade process contribution. The final state $\mu\mu$ ($W + \mu$ + *missing* $p_\perp$) mainly arises through the process$\gamma\gamma \to \mu^+\mu^-\nu_\mu\bar{\nu}_\mu$ ($\gamma\gamma \to W\mu\nu$). In addition, *cascade processes* such as $\gamma\gamma \to \tau^+\mu^-\nu_\tau\bar{\nu}_\mu$ ($\gamma\gamma \to W\tau\nu$), $\tau \to \mu\nu_\mu\nu_\tau$, contribute at the level 37% (17%) relative to the leading contribution. The straightforward calculation of such

processes is out of potential of known packages. The good way give here *double-resonant (DRD) approximation*, in which one consider only diagrams $\gamma\gamma \to W^+W^-$ (DRD diagrams) with subsequent decay of W to leptons. Direct calculation shows these DRD-diagrams are responsible for about 98% of the total $\gamma\gamma \to W\mu\nu$ cross-section. The same is valid for the momentum distributions. The detail study shows that the inaccuracy implemented by the using of DRD approximation for cascade process contribution into the total result is within statistical uncertainty of future experiments [6].

In the framework of DRD approximation, the polarization of τ in the rest frame of W is collinear with the known momentum of corresponding neutrino, and the momentum distribution of muons from the decay of τ in this system is calculated easily. The distribution of final muons in our process is given by the convolution of the mentioned accurate distribution of μ in τ decay with the CompHEP-generated distribution. Simple analysis shows that the cascade processes change the asymmetry only weakly, and their contribution to the asymmetry reduces even more with the growth of applied cuts.

Effect of photon non-monochromaticity. At the Photon Collider photons will be non-monochromatic with spectra like those shown in Fig. 3.

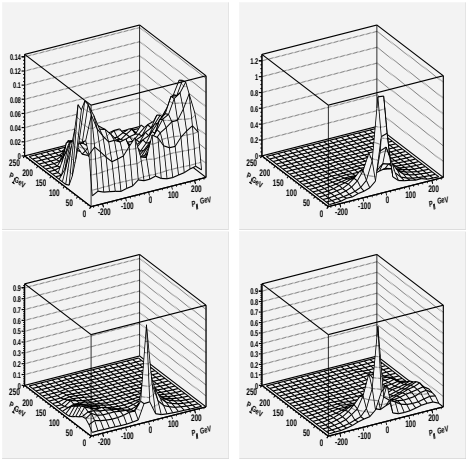

Figure 5. The distributions of muons calculated with "realistic" spectra distribution. Upper plots - $\gamma_-\gamma_-$. Lower plots – $\gamma_+\gamma_-$. Left – μ^-,right – μ^+

The distributions of muons with this non-monochromaticity are presented on Figure 5. These distributions resemble the distributions presented on Figure 4. with additional wide peak at low energies.

Table II shows the corresponding asymmetry quantities. These values are slightly smaller in comparison to monochromatic case. But they are:

$\gamma_{\lambda_1}\gamma_{\lambda_2}$	N	P_N^-	P_N^+	Δ_N
$\gamma_-\gamma_-$	L	0.365	0.157	0.398
	T	0.284	0.179	0.228
$\gamma_+\gamma_-$	L	0.174	0.338	-0.321
	T	0.200	0.236	-0.082

Table II. Charge asymmetry quantities for "realistic" photon spectra.

Dependence on $p^c_{\perp\mu}$ cut. New Physics effects are expected to be switched on at the relatively large transverse momenta. That is why we study the dependence of observed effects on the cut value $p^c_{\perp\mu}$.

Figs. 6 and 7 show the $p^c_{\perp\mu}$ dependence of the asymmetry quantity Δ_L and the cross section of the main $\gamma\gamma \to W^+\mu^-\bar{\nu}$ process for various initial photon polarizations. One can see that the asymmetry remains large even with large cuts, while the cross section quickly reduces.

Conclusions:

• The asymmetry effect is huge and easily observable.

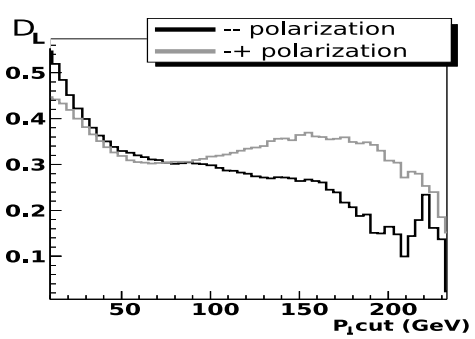

Figure 6. The $p^c_{\perp\mu}$ dependence of asymmetry.

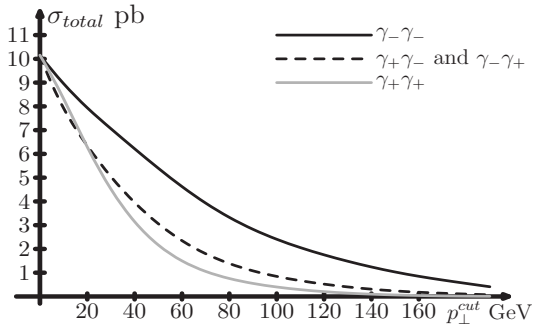

Figure 7. The smoothed $\gamma\gamma \to W^+\mu^-\bar{\nu}$ cross section dependence on $p^c_{\perp\mu}$.

• Cascade process weakly affect the asymmetry.
• Introduced quantities (especially Δ_L) large even with large $p^c_{\perp\mu}$ cuts (but the number of events reduces strong at large $p^c_{\perp\mu}$).
• Taking into account same effects for e^+e^-, $e^+\mu^-$, μ^+e^- enhance statistics. This will enhance the value of the cross section for $\gamma\gamma \to \ell^+\ell^-\nu\bar{\nu}$ from 1.2 to 4.8 pb and for $\gamma\gamma \to W^+\ell^-\bar{\nu}$, etc. to 30 pb.
• The statistical uncertainty of future experiments can be estimated from below as that of Monte Carlo simulation with anticipated number of events. Taking this uncertainty into account allows to develop useful approximations at the calculation of some contributions. Besides, one can see that the statistical uncertainty is at the level of radiative corrections, so our tree-level approximation is sufficient
• Non-monochromaticity of photon spectra decreases the considered asymmetries but retain them large enough.

This research has been supported by Russian grants RFBR 05-02-16211, NSh-5362.2006.2

References

[1] I. F. Ginzburg, G. L. Kotkin, V. G. Serbo and V. I. Telnov, Nucl. Instrum. Meth. **205** (1983) 47; I. F. Ginzburg, G. L. Kotkin, S. L. Panfil, V. G. Serbo and V. I. Telnov, Nucl. Instrum. Meth. **A 219** (1984) 5.

[2] B. Badelek *et al. Int. J. Mod. Phys.* **A 19** (2004) 5097-5186

[3] I.F. Ginzburg, G.L. Kotkin. *Eur. Phys. J.* **C 13** (2000) 295–300

[4] I.F. Ginzburg, G.L. Kotkin, S.L. Panfil, V.G. Serbo, *Nucl. Phys.* **B 228** (1983) 285.

[5] I. F. Ginzburg, hep-ph/0211099.

[6] D. A. Anipko, M. Cannoni, I. F. Ginzburg, K. A. Kanishev, A. V. Pak, O.Panella, Submitted to *Phys. Rev.* **D** (2007)

[7] E. Boos et al. Nucl. Instr. Meth. **A534** (2004) 250; hep-ph/0403113

[8] A. Pukhov, hep-ph/0412191

Discussion

Q. (X.Artru, IPN, Lion) 1) Is it interesting linearly polarized photons? 2) What region of x is interesting?

A. Linearly polarized photons can be obtained as well. However in this case photon spectra are not so sharp. The degree of linear polarization is lower than that circular. It can be improved at lower x. If we use 70% linear + 70% circular polarization we will have sharp enough spectrum with good linear and circular polarization. Directions of these polarization can be changed independently and easily.

Q. (S.Belostotsky, PNPI, St.Petersburg) In what new physics can be used this charge asymmetry?

A. 1) In the study of SUSY processes like $\gamma\gamma \to \tilde{u}\tilde{u} \to \mu^+\chi\mu^-\chi$ ($\chi = LSP$). That are our nearest plans.
2) For the study anomalous interaction of W with γ generally not, except of P-violating terms in this interaction.

ELECTROPRODUCTION OF LIGHT VECTOR MESONS

S.V. Goloskokov †

Bogoliubov Laboratory of Theoretical Physics, Joint Institute for Nuclear Research, Dubna 141980, Moscow region, Russia
† *E-mail:goloskkv@theor.jinr.ru*

Abstract

An analysis of light vector meson photoproduction at small Bjorken $x \leq 0.2$ is done on the basis of the generalized parton distributions (GPDs). Our results on the cross section and spin density matrix elements (SDME) are in good agreement with experiments.

This report is devoted to the study of the vector meson leptoproduction at Bjorken $x \leq 0.2$ based on our results [1–3]. At large photon virtualities the amplitude for longitudinally polarized virtual photons and vector meson (LL amplitude) factorizes [4] into a hard meson photoproduction off partons and GPDs. Unfortunately, in the collinear approximation the LL cross section exceeds the data by an order of magnitude [5]. Moreover, in this approximation the amplitude for transversally polarized photons (TT amplitude) exhibits infrared singularities [6], which signals the factorization breakdown.

In this report, we discuss the spin effects in the vector meson leptoproduction. Our calculations [2, 3] are based on the modified perturbative approach (MPA) [7] which includes the quark transverse degrees of freedom accompanied by Sudakov suppressions. The contribution from the end-point region to the LL amplitude is suppressed in our model and the cross section is close to the experiment. The TT amplitudes can be calculated in the model because the transverse quark momentum regularizes the singularities. Within the MPA we calculate the cross sections and the spin observables in the energy range $5\text{GeV} < W < 90\text{GeV}$. Our results on the cross section and SDME are in good agreement with experiments [8, 9, 4, 15].

The model is based on the handbag approach where the $\gamma^* p \to V p$ amplitude factorizes into hard partonic subprocess and GPDs. In the region of small $x \leq 0.01$ gluons give the dominant contribution [1]. At larger $x \sim 0.2$, in addition to the gluon GPD the inclusion of quark contribution is important [2, 3]. For small t the amplitude of the vector meson production off the proton with positive helicity reads as a convolution of the partonic subprocess $\mathcal{H}^V$ and GPDs $H^i\,(\widetilde{H}^i)$

$$\mathcal{M}^V_{\mu'+,\mu+} = \frac{e}{2}\mathcal{C}^V \sum_\lambda \int d\overline{x} \mathcal{H}^{Vi}_{\mu'\lambda,\mu\lambda} H^i(\overline{x},\xi,t), \tag{1}$$

where i denotes the gluon and quark contribution, μ (μ') is the helicity of the photon (meson), $\overline{x}$ is the momentum fraction of the parton with helicity λ, and the skewness ξ is related to Bjorken-x by $\xi \simeq x/2$. The flavor factors are $C^\rho = 1/\sqrt{2}$ and $C^\phi = -1/3$. In the analysis of the cross section at small x the main contribution is determined by the unpolarized GPDs H^i.

The k- dependent wave function [12] that contains the leading and higher twist terms describing the longitudinally and transversally polarized vector meson is used to calculate the partonic subprocess $\mathcal{H}$ in (1); $\mathcal{H}$ is estimated within the MPA [7] where we keep the $k_\perp^2$ terms in the denominators of the amplitudes and in the numerator of the TT amplitude. The gluonic corrections are treated in the form of the Sudakov factors which additionally suppress the end-point integration regions.

The GPDs are modeled using the double distribution

$$H_i(\overline{x},\xi,t) = \int_{-1}^{1} d\beta \int_{-1+|\beta|}^{1-|\beta|} d\alpha \delta(\beta + \xi\,\alpha - \overline{x})\, f_i(\beta,\alpha,t). \qquad (2)$$

Here the double distribution function $f_i(\beta,\alpha,t)$ is connected with the corresponding parton distributions (PDFs) which are taken from the CTEQ6M results [14]. The simple Regge ansatz is used to consider t dependencies of PDFs. For details see [2, 3].

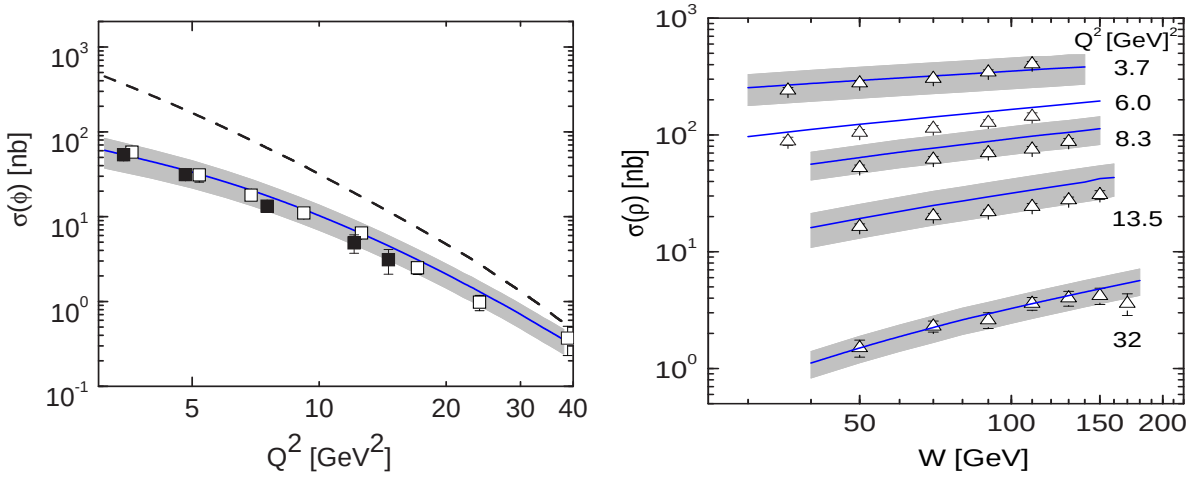

Figure 1: Left: The cross sections of ϕ production at $W = 75$GeV with error band from CTEQ6 PDFs uncertainties. Data are from H1 [8] -solid symbols and ZEUS [9] -open symbols. Dashed line- LO result. Right: The cross sections of ρ production via W at different Q^2.

The cross section for the $\gamma^* p \to \phi p$ production integrated over t is shown in Fig.1 (full line). Good agreement with DESY experiments [8, 9] is observed. The shared bands in the figures reflect uncertainties of our results caused by the errors in the CTEQ6 PDFs. The leading twist results are also presented in Fig. 1. The $k_\perp^2/Q^2$ corrections in the hard amplitude decrease the cross section by a factor of about 10 at $Q^2 \sim 3\text{GeV}^2$.

Our results reproduce well the energy dependence of the ρ cross section [9] as shown in Fig.1. The cross section at HERA energies is dominated by the gluon and sea quark contributions.

The model describes properly spin effects determined by the TT transition amplitude. Our results for the ratio of the longitudinal and transverse cross sections and SDME in the energy range $5\text{GeV} < W < 75\text{GeV}$ can be found in [3]. In Fig.2, we present the SDME on the ρ production at $W = 5, 10, 75$GeV. At HERMES energy $W = 5$GeV the valence quark contribution to the amplitudes is essential. At COMPASS $W = 10$GeV quark effects are not so large and they are negligible at HERA $W = 75$GeV. This is the main reason of the energy dependencies of SDME shown in Fig.2. A similar energy dependence is observed experimentally.

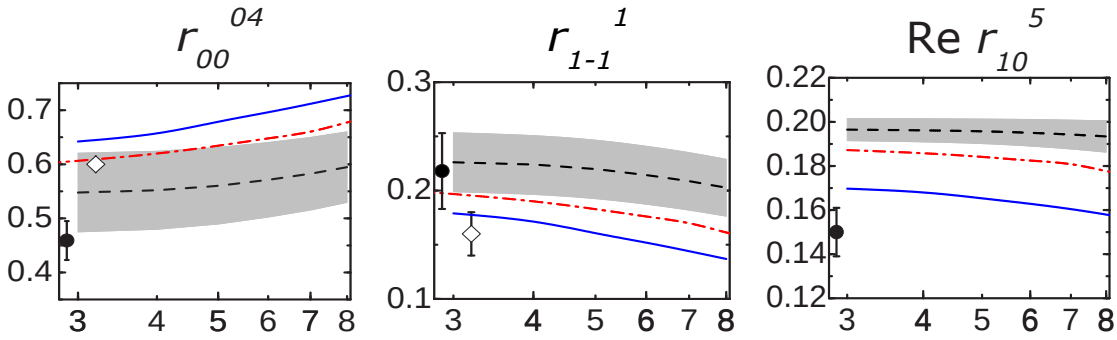

Figure 2: The Q^2 dependence of SDME on the ρ production and $W = 75(10, 5)$ GeV-solid(dash-dotted, dashed) line. Preliminary data are taken from HERMES [4] (solid circles) and COMPASS [15] (diamonds).

The A_{LL} asymmetry for a longitudinally polarized beam and target is sensitive to the polarized GPD. The leading term in A_{LL} asymmetry integrated over the azimuthal angle is determined through the interference between the H and $\widetilde{H}$ distributions. In Fig. 3, we show our results for the ρ production at $W = 5$GeV and $W = 10$GeV. At HERMES energies the valence quark contribution generates large asymmetry of the order of 0.1 which is compatible with the experimental results [4]. At COMPASS [15], the valence quark contribution is small and asymmetry close to zero is predicted. Note that we observe an essential cancellation of the gluon and sea quark contributions. This leads to small A_{LL} asymmetry for the ϕ production.

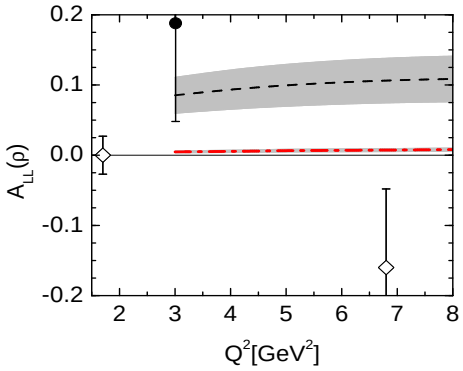

Figure 3: The A_{LL} asymmetry for the ρ production at $W = 5$ GeV (dashed line) and $W = 10$ GeV (dashed-dotted line).

In summary: Light vector meson electroproduction at small x was analyzed here within the GPD approach. The partonic subprocesses have been calculated using the MPA with the wave function dependent on the transverse quark momentum. The higher order $k_\perp^2/Q^2$ corrections which are considered in the propagators of the partonic subprocess decrease the cross section by a factor of about 10 at $Q^2 \sim 3\mathrm{GeV}^2$. The same higher order effects in the denominators of the hard subprocess regularize the singularities in the TT amplitude. This gives a possibility to calculate the TT amplitude and study spin effects in the vector meson production in our model.

In our previous calculations [1] we analysed the low $x \leq 0.01$ region where the gluon contribution has a predominant role. In this report, we extend our analysis to $x \sim 0.2$ [2, 3]. In the moderate x region we consider gluon, sea and valence quark GPDs. The GPDs are modeled via double distribution based on the CTEQ6M distributions. In the model we find a good description of the cross section and the spin observables from HERMES to HERA energies [2]. It is found that the gluon and sea contributions control the amplitude behaviour at energies $W \geq 10$GeV. Valence quarks are essential only at HERMES energies, where their contribution to the $\rho(\omega)$ cross section is about 40(65%). This shows that the ω production at low energies is much more sensitive to valence quarks than ρ production.

The model describes well the ratio of the longitudinal and transverse cross sections and SDME in the energy range 5GeV $< W <$ 75GeV [3]. We predict large A_{LL} asymmetry at HERMES energies determined by the valence quark contribution which is compatible with experiment. At COMPASS the A_{LL} asymmetry is small, about zero. Our first results on SDME for transversally polarized target and A_{UT} asymmetry cans be found in [3].

Thus, we can conclude that the vector meson photoproduction at small x is a good tool to probe the GPDs. Study of SDME gives important information on the structure of different helicity amplitudes in the vector meson production.

This work is supported in part by the Russian Foundation for Basic Research, Grant 06-02-16215 and by the Heisenberg-Landau program.

References

[1] S.V. Goloskokov, P. Kroll, Euro. Phys. J. C**42**, 281 (2005).

[2] S.V. Goloskokov, P. Kroll, Euro. Phys. J. C**50** 829, (2007).

[3] S.V. Goloskokov, P. Kroll, arXiv:0708.3569 [hep-ph], to be publ. in Euro. Phys. J C.

[4] X. Ji, Phys. Rev. D**55**, 7114 (1997); A.V. Radyushkin, Phys. Lett. B**380**, 417 (1996); J.C. Collins *et al.*, Phys. Rev. D**56**, 2982 (1997).

[5] L. Mankiewicz, G. Piller, T. Weigl, Eur. Phys. J. C**5**, 119 (1998).

[6] L. Mankiewicz, G. Piller, Phys. Rev. D**61**, 074013 (2000); I.V. Anikin, O.V. Teryaev, Phys. Lett. B**554**, 51 (2003).

[7] J. Botts, G. Sterman, Nucl. Phys. B**325**, 62 (1989).

[8] C. Adloff et al. [H1 Collab.], Eur. Phys. J. C**13**, 371 (2000); S.Aid et al. [H1 Collab.], Nucl. Phys. B**468**, 3 (1996).

[9] J. Breitweg et al. [ZEUS Collab.], Eur. Phys. J. C**6** 603, (1999); S. Chekanov et al. [ZEUS Collab.], Nucl.Phys. B**718**, 3 (2005); S. Chekanov et al. [ZEUS Collab.], arXiv:0708.1478 [hep-ex].

[10] A. Airapetian et al. [HERMES Collab.], Eur. Phys. J. C**17** 389, (2000); A. Borissov, [HERMES Collab.], "Proc. of Diffraction 06", PoS (DIFF2006), 014.

[11] D. Neyret [COMPASS Collab.], "Proc. of SPIN2004", Trieste, Italy, 2004; V. Y. Alexakhin et al. [COMPASS Collab.], arXiv:0704.1863 [hep-ex].

[12] J. Bolz, J.G. Körner, P. Kroll, Z. Phys. A**350**, 145 (1994).

[13] I. V. Musatov, A. V. Radyushkin, Phys. Rev. D**61**, 074027 (2000)

[14] J. Pumplin, D. R. Stump, J. Huston, H. L. Lai, P. Nadolsky, W. K. Tung, JHEP **0207**, 012 (2002).

Discussion

Q. (L.Jenkovszky, ITP, Kiev) What king of QCD evolution you have in mind when citing Vinnikov? As far as I know, there is no evolution equation like that of DGLAP for DVCS.

A. I mean a simple evolution equation for ordinary parton distributions multiplied by an exponential in t.

SPIN POLARIZATION PHENOMENA IN DENSE NUCLEAR MATTER

A.A. Isayev

Kharkov Institute of Physics and Technology, Kharkov, 61108, Ukraine
Kharkov National University, Svobody Sq., 4, Kharkov, 61077, Ukraine

Abstract

Spin polarized states in nuclear matter with the effective Skyrme interaction are studied for a wide range of isospin asymmetries and densities. Based on a Fermi liquid theory, it is shown that there are a few possible scenarios of spin ordered phase transitions: (a) nuclear matter undergoes at some critical density a phase transition to a spin polarized state with the oppositely directed spins of neutrons and protons (SLy4 interaction); (b) at some critical density, a spin polarized state with the like-directed neutron and proton spins appears (SkI5 interaction); (c) nuclear matter under increasing density, at first, undergoes a phase transition to the state with the opposite directions of neutron and proton spins, which goes over at larger density to the state with the same direction of nucleon spins (SkI3 interaction).

The issue of spontaneous appearance of spin polarized states in nuclear matter is a topic of a great current interest due to its relevance in astrophysics. In particular, the scenarios of supernova explosion and cooling of neutron stars are essentially different, depending on whether nuclear matter is spin polarized or not. On the one hand, the models with the effective nucleon-nucleon (NN) interaction predict the occurrence of spin instability in nuclear matter at densities in the range from ϱ_0 to $6\varrho_0$ for different parametrizations of the NN potential [1]– [4] ($\varrho_0 = 0.16\,\mathrm{fm}^{-3}$). On the other hand, for the models with the realistic NN interaction, the ferromagnetic phase transition seems to be suppressed up to densities well above ϱ_0 [5]– [7].

Here the issue of spin polarizability of nuclear matter is considered with the use of an effective NN interaction. The main objective is to study the possible scenarios of spin ordered phase transitions in nuclear matter with Skyrme forces, attracting parametrizations of a NN potential being relevant for calculations at strong isospin asymmetry and high density. In particular, we choose SLy4 effective interaction, constructed originally to reproduce the results of microscopic neutron matter calculations [8]. We utilize SkI3 and SkI5 parametrizations as well, giving a correct description of isotope shifts in neutron-rich medium and heavy nuclei [4]. The basic formalism is presented in detail in Ref. [4]. We are interested in studying spin polarized states with like-directed and oppositely directed spins of neutrons and protons. One should solve the self-consistent equations for the coefficients $\xi_{00}, \xi_{30}, \xi_{03}, \xi_{33}$ in the expansion of the single particle energy in Pauli matrices in spin and isospin spaces

$$\begin{aligned} &\xi_{00}(\mathbf{p}) = \varepsilon_0(\mathbf{p}) + \tilde{\varepsilon}_{00}(\mathbf{p}) - \mu_{00},\ \xi_{30}(\mathbf{p}) = \tilde{\varepsilon}_{30}(\mathbf{p}), \\ &\xi_{03}(\mathbf{p}) = \tilde{\varepsilon}_{03}(\mathbf{p}) - \mu_{03},\ \xi_{33}(\mathbf{p}) = \tilde{\varepsilon}_{33}(\mathbf{p}). \end{aligned} \tag{1}$$

Here $\varepsilon_0(\mathbf{p})$ is the free single particle spectrum, and $\tilde{\varepsilon}_{00}, \tilde{\varepsilon}_{30}, \tilde{\varepsilon}_{03}, \tilde{\varepsilon}_{33}$ are the Fermi liquid (FL) corrections to the free single particle spectrum, related to the normal FL amplitudes

$U_0(\mathbf{k}), ..., U_3(\mathbf{k})$ by formulas

$$\tilde{\varepsilon}_{00}(\mathbf{p}) = \frac{1}{2\mathcal{V}} \sum_{\mathbf{q}} U_0(\mathbf{k}) f_{00}(\mathbf{q}),\ \tilde{\varepsilon}_{30}(\mathbf{p}) = \frac{1}{2\mathcal{V}} \sum_{\mathbf{q}} U_1(\mathbf{k}) f_{30}(\mathbf{q}),\ \mathbf{k} = \frac{\mathbf{p}-\mathbf{q}}{2}, \qquad (2)$$
$$\tilde{\varepsilon}_{03}(\mathbf{p}) = \frac{1}{2\mathcal{V}} \sum_{\mathbf{q}} U_2(\mathbf{k}) f_{03}(\mathbf{q}),\ \tilde{\varepsilon}_{33}(\mathbf{p}) = \frac{1}{2\mathcal{V}} \sum_{\mathbf{q}} U_3(\mathbf{k}) f_{33}(\mathbf{q}).$$

The distribution functions $f_{00}, f_{03}, f_{30}, f_{33}$, in turn, can be expressed in terms of the components ξ of the single particle energy and satisfy the normalization conditions for the total density $\varrho_n + \varrho_p = \varrho$, excess of neutrons over protons $\varrho_n - \varrho_p \equiv \alpha\varrho$, ferromagnetic (FM) $\varrho_\uparrow - \varrho_\downarrow \equiv \Delta\varrho_{\uparrow\uparrow}$ and antiferromagnetic (AFM) $(\varrho_{n\uparrow} + \varrho_{p\downarrow}) - (\varrho_{n\downarrow} + \varrho_{p\uparrow}) \equiv \Delta\varrho_{\uparrow\downarrow}$ spin order parameters, respectively (α being the isospin asymmetry parameter, $\varrho_\uparrow = \varrho_{n\uparrow} + \varrho_{p\uparrow}$ and $\varrho_\downarrow = \varrho_{n\downarrow} + \varrho_{p\downarrow}$, with $\varrho_{n\uparrow}, \varrho_{n\downarrow}$ and $\varrho_{p\uparrow}, \varrho_{p\downarrow}$ being the neutron and proton number densities with spin up and spin down). The quantities of interest are the neutron and proton spin polarization parameters $\Pi_n = \frac{\varrho_{n\uparrow} - \varrho_{n\downarrow}}{\varrho_n}, \Pi_p = \frac{\varrho_{p\uparrow} - \varrho_{p\downarrow}}{\varrho_p}$, characterizing spin ordering in neutron and proton subsystems.

Fig. 1a shows the density dependence of the neutron and proton spin polarization parameters at zero temperature for SLy4 force. The main qualitative feature is that for SLy4 force there are only solutions corresponding to the oppositely directed spins of neutrons and protons in a spin polarized state. The reason is that for SLy4 force the FL amplitude U_1, determining spin–spin correlations, is repulsive for all relevant densities, while the FL amplitude U_3, describing spin–isospin correlations, becomes quite attractive at high densities. The critical density of spin instability in symmetric nuclear matter ($\alpha = 0$), corresponding to AFM spin ordering ($\Delta\varrho_{\uparrow\downarrow} \neq 0$, $\Delta\varrho_{\uparrow\uparrow} = 0$), is $\varrho_c \approx 0.33$ fm^{-3}. It is less than the critical density of FM instability in neutron matter, $\varrho_c \approx 0.59$ fm^{-3}. Even small admixture of protons to neutron matter leads to the appearance of long tails in the density profiles of the neutron spin polarization parameter near the transition point to a spin

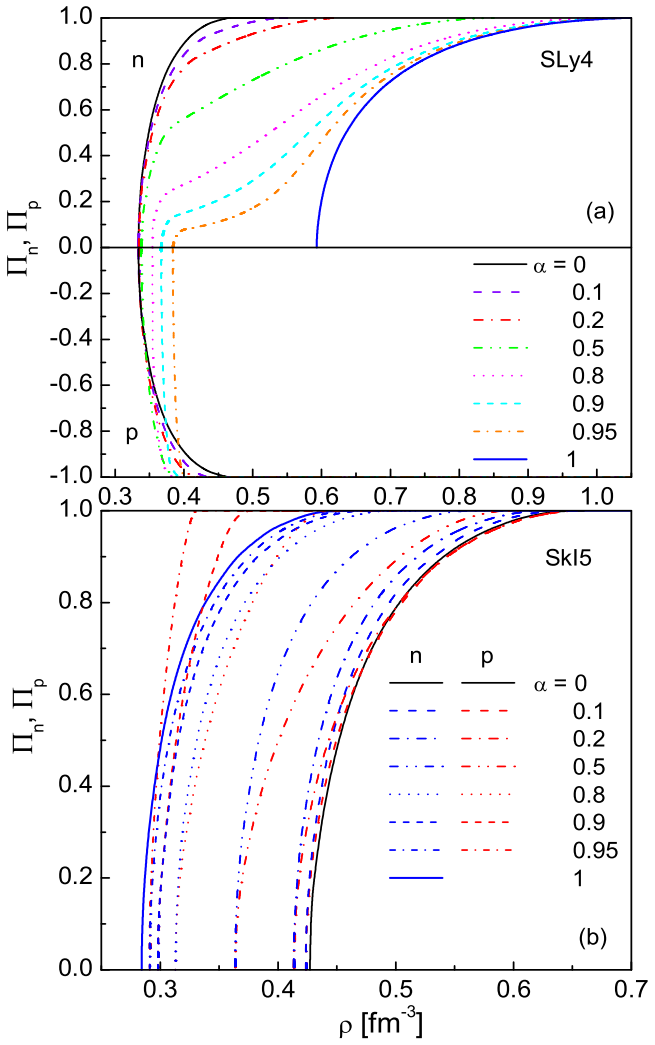

Figure 1. Neutron and proton spin polarization parameters as functions of density at zero temperature for (a) SLy4 force and (b) SkI5 force (color online at http://theor.jinr.ru/∼spin).

ordered state. As a consequence, a spin polarized state is formed much earlier in density than in pure neutron matter.

As seen from Fig. 1b, for SkI5 force, oppositely to SLy4 force, there are only solutions corresponding to the same direction of neutron and proton spins in a polarized state. In the case under consideration the FL amplitude U_3 is repulsive for all relevant densities, while the FL amplitude U_1 becomes quite attractive at high densities. For SkI5 force, a phase transition to the FM spin state in neutron matter takes place at the critical density $\varrho_c \approx 0.28$ fm^{-3}. It is less than the critical density of spin instability in symmetric nuclear matter $\varrho_c \approx 0.43$ fm^{-3}, corresponding to FM spin ordering ($\Delta\varrho_{\uparrow\uparrow} \neq 0$, $\Delta\varrho_{\uparrow\downarrow} = 0$). There are no long tails in the density profiles of the neutron spin polarization parameter at large isospin asymmetry. In the given case, a small admixture of protons to neutron matter even leads to the increase of the critical density of spin instability.

Fig. 2 shows the neutron and proton spin polarization parameters as functions of density at zero temperature for SkI3 force. There are two types of solutions of the self-consistent equations in symmetric nuclear matter, corresponding to FM and AFM ordering of neutron and proton spins. Due to proximity of FL amplitudes U_1 and U_3, the respective critical densities are very close to each other ($\varrho_c \approx 0.910\,\text{fm}^{-3}$ for FM ordering and $\varrho_c \approx 0.917\,\text{fm}^{-3}$ for AFM ordering) and larger than the critical density of spin instability in neutron matter ($\varrho_c \approx 0.37\,\text{fm}^{-3}$). When some admixture of protons is added to neutron matter, the last critical density is shifted to larger densities and a spin polarized state with the oppositely directed spins of neutrons and protons appears. Under increasing density of nuclear matter, the neutron spin polarization continuously increases till all neutron spins will be aligned in the same direction. Protons, at first, become more polarized with density and their spin polarization is opposite to the spin polarization of neutrons. But, after reaching the maximum, spin polarization of protons decreases and at some critical density spins of protons change direction, so that the spin ordered phase with the like-directed spins of neutrons and protons is formed. Then, beyond the critical density, the spin polarization of protons is continuing to increase until the totally polarized state with parallel ordering of neutron and proton spins will be formed. Thus, for SkI3 force nuclear matter undergoes at some critical density a phase transition from the state with antiparallel ordering of neutron and proton spins to the state with parallel ordering of spins. With increasing isospin asymmetry, this critical density increases as well. Note that there are no long tails in the density profiles of the neutron spin polarization parameter at large asymmetries.

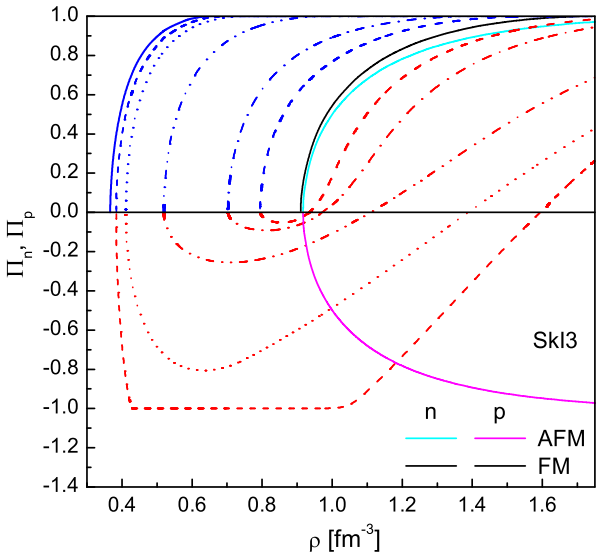

Figure 2. Same as in Fig. 1, but for SkI3 force. Also the curves, corresponding to FM and AFM ordering in symmetric nuclear matter, are shown (color online at http://theor.jinr.ru/∼spin).

It is necessary to emphasize that different behavior at high densities of the interaction amplitudes, describing spin–spin and spin–isospin correlations, lays behind this divergence in calculations with different Skyrme forces. These results clearly indicate the necessity to construct a new generation of the energy functionals with the properly constrained time-odd part at high densities. Probably, these constraints will be obtained from the data on the time decay of magnetic field of isolated neutron stars [10].

References

[1] M. Kutschera, and W. Wojcik, Phys. Lett. **325B**, 271 (1994).

[2] S. Reddy, M. Prakash, J.M. Lattimer, and J.A. Pons, Phys. Rev. C **59**, 2888 (1999).

[3] A.A. Isayev, JETP Letters **77**, 251 (2003).

[4] A.A. Isayev, and J. Yang, Phys. Rev. C **69**, 025801 (2004); Ibid. **70**, 064310 (2004).

[5] V.R. Pandharipande, V.K. Garde, and J.K. Srivastava, Phys. Lett. **38B**, 485 (1972).

[6] I. Vidaña, and I. Bombaci, Phys. Rev. C **66**, 045801 (2002).

[7] S. Fantoni, A. Sarsa, and E. Schmidt, Phys. Rev. Lett. **87**, 181101 (2001).

[8] E. Chabanat, P. Bonche, P. Haensel, J. Meyer, and R. Schaeffer, Nucl. Phys. **A635**, 231 (1998).

[9] P.-G. Reinhard and H. Flocard, Nucl. Phys. **A584**, 467 (1995).

[10] S.B. Popov and M.E. Prokhorov, Surveys in High Energy Physics **15**, 381 (2001).

DISPERSION REPRESENTATIONS FOR HARD EXCLUSIVE REACTIONS

M. Diehl[1] and D.Yu. Ivanov[2†]

(1) *Theory Group, Deutsches Elektronen-Synchroton DESY, 22603 Hamburg, Germany*
(2) *Sobolev Institute of Mathematics, 630090 Novosibirsk, Russia*
† *E-mail: d-ivanov@math.nsc.ru*

Abstract

A number of hard exclusive scattering processes can be described in terms of generalized parton distributions (GPDs) and perturbative hard-scattering kernels. Both the physical amplitude and the hard-scattering kernels fulfill dispersion relations. We show that their consistency at all orders in perturbation theory is guaranteed if the GPDs satisfy certain integral relations. These relations are fulfilled thanks to Lorentz invariance.

1 Introduction

For hard exclusive processes that can be calculated using collinear factorization, one may write down dispersion relations both for the physical process and for the parton-level subprocess. The question of consistency between both representations turns out to be nontrivial. Important progress has recently been reported in [1], where it was shown that this consistency is ensured by Lorentz invariance in the form of the polynomiality property for generalized parton distributions (GPDs). The studies in [1] were carried out using the Born-level approximation of the hard-scattering subprocess. In particular, they showed that to this accuracy not only the imaginary but also the real part of the process amplitude can be represented in terms of GPDs $F(x,\xi,t)$ along the line $x=\xi$ in the x–ξ plane. It is natural to ask how the situation changes when including radiative corrections to the hard-scattering kernel. Here we discuss dispersion representations for hard exclusive processes to all orders in perturbation theory, generalizing the leading-order results derived for the unpolarized quark GPDs in [1]. More details, as well as results for polarized quarks and for gluons, where special issues arise, can be found in our journal publication [2].

2 Dispersion relations

The exclusive processes we discuss here are deeply virtual Compton scattering (DVCS) and light meson production,

$$\gamma^*(q)+p(p)\to\gamma(q')+p(p')\,,\qquad \gamma^*(q)+p(p)\to M(q')+p(p')\,, \tag{1}$$

where four-momenta are indicated in parentheses. Since the processes in (1) involve particles with nonzero spin, the appropriate quantities for discussing dispersion relations are

invariant amplitudes, which have simple analyticity and crossing properties. An explicit decomposition for Compton scattering can be found in [3].

We use the Mandelstam variables $s = (p+q)^2$, $t = (p-p')^2$, $u = (p-q')^2$, and consider an invariant amplitude $\mathcal{F}^{[\sigma]}(\nu, t)$ with definite signature σ under $s \leftrightarrow u$ crossing,

$$\mathcal{F}^{[\sigma]}(-\nu, t) = \sigma \mathcal{F}^{[\sigma]}(\nu, t)\,, \tag{2}$$

where $2\nu = s - u$. At $t \leq 0$ the imaginary part of the amplitude is due to the s-channel discontinuity for $\nu > 0$ and to the u-channel discontinuity for $\nu < 0$. The fixed-t dispersion relation with one subtraction reads

$$\begin{aligned} &\mathrm{Re}\,\mathcal{F}^{[\sigma]}(\nu, t) - \mathrm{Re}\,\mathcal{F}^{[\sigma]}(\nu_0, t) \\ &= \frac{1}{\pi} \int_{\nu_{th}}^{\infty} d\nu'\, \mathrm{Im}\,\mathcal{F}^{[\sigma]}(\nu', t) \left[\frac{1}{\nu' - \nu} + \sigma \frac{1}{\nu' + \nu} - \frac{1}{\nu' - \nu_0} - \sigma \frac{1}{\nu' + \nu_0} \right], \end{aligned} \tag{3}$$

where ν_{th} is the value of ν at threshold. Its validity requires

$$\nu^{-2} \mathcal{F}^{[+]}(\nu, t) \to 0\,, \qquad \nu^{-1} \mathcal{F}^{[-]}(\nu, t) \to 0\,. \tag{4}$$

for $|\nu| \to \infty$. We consider dispersion relations for the processes (1) in the Bjorken limit of large $-q^2$ at fixed q^2/ν and t. It is useful to trade ν for the scaling variable

$$\xi = -\frac{(q+q')^2}{2(p+p')\cdot(q+q')} = -\frac{q^2}{s-u} = -\frac{q^2}{2\nu}\,, \tag{5}$$

where we have neglected q'^2 and t compared with q^2 in the numerator. The factorization theorems state that in the Bjorken limit certain invariant amplitudes become dominant and can be written as convolutions of partonic hard-scattering kernels with quark or gluon GPDs. We discuss the contribution of unpolarized quark distributions $F^q = \{H^q, E^q\}$ to the leading invariant amplitudes for DVCS or meson production,

$$\mathcal{F}^{q[\sigma]}(\xi, t) = \int_{-1}^{1} dx\, \frac{1}{\xi}\, C^{q[\sigma]}\Big(\frac{x}{\xi}\Big)\, F^q(x, \xi, t) \tag{6}$$

where for brevity we do not display the dependence of $\mathcal{F}^{q[\sigma]}$ and $C^{q[\sigma]}$ on q^2. The hard-scattering kernel satisfies the symmetry relation

$$C^{q[\sigma]}(-x/\xi) = -\sigma\, C^{q[\sigma]}(x/\xi)\,. \tag{7}$$

In the Bjorken limit the Mandelstam variables for the hard-scattering subprocess are

$$\hat{s} = xs + \tfrac{1}{2}(1-x)q^2\,, \qquad \hat{u} = xu + \tfrac{1}{2}(1-x)q^2\,, \tag{8}$$

so that one has $x/\xi = (\hat{u} - \hat{s})/q^2$. To leading order (LO) in α_s, the kernel reads

$$C^{q[\sigma]}(\omega) \;\propto\; \frac{1}{1-\omega-i\epsilon} - \sigma \frac{1}{1+\omega-i\epsilon}\,, \qquad \mathrm{Im}\, C^{q[\sigma]}(\omega) \;\propto\; \pi\big[\delta(\omega-1) - \sigma\delta(\omega+1)\big] \tag{9}$$

for both DVCS and meson production. At higher orders in α_s one finds branch cuts in the $\hat{s}$ and $\hat{u}$ channels for $\omega > 1$ and $\omega < -1$, respectively. For the dispersion relations we need to know the behavior of the kernels when $|\omega| \to \infty$. The NLO kernels for DVCS can

be found in [4], and those for meson production in [5]. For negative signature, one finds $C^{q[-]}(\omega) \sim \omega^{-1}$ up to logarithms for both DVCS and meson production. For positive signature, the NLO corrections give $C^{q[+]}(\omega) \sim \omega^{-1}$ for DVCS, and $C^{q[+]}(\omega) \sim \omega^0$ for meson production, again up to logarithms. The power behavior as ω^0 is due to two-gluon exchange in the t-channel. For DVCS such graphs only start at NNLO, so that at this level one will also have $C^{q[+]}(\omega) \sim \omega^0$. For both signatures one can thus write down an unsubtracted dispersion relation for the kernel,

$$\operatorname{Re} C^{q[\sigma]}\Big(\frac{x}{\xi}\Big) = \frac{1}{\pi}\int_1^\infty d\omega \operatorname{Im} C^{q[\sigma]}(\omega)\left[\frac{1}{\omega - x/\xi} - \sigma\frac{1}{\omega + x/\xi}\right]. \tag{10}$$

On the other hand, the invariant amplitude satisfies its own fixed-t dispersion relation (3). Therefore the real part of the leading invariant amplitudes for DVCS or meson production can be obtained from a dispersion relation for the hard-scattering kernel,

$$\operatorname{Re} \mathcal{F}^{q[\sigma]}(\xi,t) = \frac{1}{\pi}\int_1^\infty d\omega \operatorname{Im} C^{q[\sigma]}(\omega)\int_{-1}^1 dx\, F^q(x,\xi,t)\left[\frac{1}{\omega\xi - x} - \sigma\frac{1}{\omega\xi + x}\right], \tag{11}$$

or for the invariant amplitude itself,

$$\operatorname{Re} \mathcal{F}^{q[\sigma]}(\xi,t) = \frac{1}{\pi}\int_1^\infty d\omega \operatorname{Im} C^{q[\sigma]}(\omega)\left\{\int_{-1}^1 dx\, F^q\Big(x,\frac{x}{\omega},t\Big)\left[\frac{1}{\omega\xi - x} - \sigma\frac{1}{\omega\xi + x}\right] + \mathcal{I}^{q[\sigma]}(\omega,\xi_0,t)\right\}, \tag{12}$$

where ξ_0 corresponds to the subtraction point ν_0 in (3) and

$$\mathcal{I}^{q[\sigma]}(\omega,\xi,t) = \int_{-1}^1 dx\left[F^q(x,\xi,t) - F^q\Big(x,\frac{x}{\omega},t\Big)\right]\left[\frac{1}{\omega\xi - x} - \sigma\frac{1}{\omega\xi + x}\right]. \tag{13}$$

As shown in [2], the term $\mathcal{I}^{q[\sigma]}$ is related with spin-zero exchange in the t-channel.

Consistency of the two representations provides nontrivial constraints on the GPDs. Indeed, in (12) the GPD enters in the DGLAP region only, whereas in (11) both the DGLAP and ERBL regions contribute. Let us see that the consistency is guaranteed by the polynomiality property of Mellin moments, which follows directly from the Lorentz covariance of the operator matrix elements that are parameterized by GPDs. With the conventional definitions (given e.g. in [6]) we have for quarks

$$\int_{-1}^1 dx\, x^{n-1} H^q(x,\xi,t) = \sum_{k=0}^{n-1}(2\xi)^k A^q_{n,k}(t) + (2\xi)^n C^q_n(t), \tag{14}$$

$$\int_{-1}^1 dx\, x^{n-1} E^q(x,\xi,t) = \sum_{k=0}^{n-1}(2\xi)^k B^q_{n,k}(t) - (2\xi)^n C^q_n(t), \tag{15}$$

where k is even because of time reversal invariance. Clearly, (11) and (12) are consistent if $\mathcal{I}^{q[\sigma]}(\omega,\xi,t)$ is independent of ξ for all $\omega \geq 1$. To show that this is the case, we Taylor

expand $F^q(x, x/\omega, t)$ in its second argument,

$$\mathcal{I}^{q[\sigma]}(\omega,\xi,t) = \frac{1}{\omega}\sum_{n=1}^{\infty}\frac{1}{n!}\left(\frac{\partial}{\partial\eta}\right)^n\int_{-1}^{1}dx\left(\frac{x}{\omega}-\xi\right)^{n-1}F^q(x,\eta,t)\Big|_{\eta=\xi} + \frac{\sigma}{\omega}\sum_{n=1}^{\infty}\frac{1}{n!}\left(\frac{\partial}{\partial\eta}\right)^n\int_{-1}^{1}dx\left(\frac{x}{\omega}+\xi\right)^{n-1}F^q(x,\eta,t)\Big|_{\eta=-\xi}, \tag{16}$$

where we have interchanged the order of differentiation and integration. For definiteness let us consider the case $F^q = H^q$. Using the polynomiality property (14) and the fact that C_n^q is only nonzero for even n, we find

$$\mathcal{I}^{q[+]}(\omega,\xi,t) = 2\sum_{n=2}^{\infty}\left(\frac{2}{\omega}\right)^n C_n^q(t)\,, \qquad \mathcal{I}^{q[-]}(\omega,\xi,t) = 0\,, \tag{17}$$

which is independent of ξ as required. In the case $F^q = E^q$ there is an additional minus sign on the r.h.s. of (17), in accordance with (15).

The dispersion representations discussed here can provide a practical check for GPD models in which Lorentz invariance is not exactly satisfied. In particular, we find that even for small ξ the model proposed in [7] leads to serious conflicts with dispersion relations when it is used for calculating the real part of scattering amplitudes [2].

The representation (12) has important consequences on the information about GPDs that can be extracted from DVCS and meson production. To leading approximation in α_s, the imaginary part of the amplitude is only sensitive to the distributions at $x = \xi$, and the only additional information contained in the real part is a constant associated with pure spin-zero exchange, given by (17) at $\omega = 1$. In [1] this was referred to as a holographic property. Beyond leading order, the evaluation of both imaginary and real parts of the amplitude involves the full DGLAP region $|x| \geq \xi$. In addition, the real part depends on the appropriate spin-zero term at all $\omega \geq 1$.

Consider now the comparison of a given model or parameterization of GPDs with data on DVCS or meson production. In a leading-order analysis (which should of course always be restricted to kinematics where the LO approximation is adequate) it is sufficient to characterize each GPD by its values at $x = \xi$, supplemented by a constant for the spin-zero exchange contribution discussed above. On one hand this can be a welcome simplification, and on the other hand it indicates the limitations of an LO analysis: when confronting data with a given GPD one is sensitive to $x \neq \xi$ (and to the details of the spin-zero exchange contribution) only at NLO or higher accuracy.

Acknowledgements. This work is supported by the Helmholtz Association, contract number VH-NG-004. The work of D.I. is supported in part by the grants RFBR-06-02-16064 and NSh 5362.2006.2.

References

[1] O.V. Teryaev, hep-ph/0510031;
I.V. Anikin and O.V. Teryaev, Phys. Rev. D **76** (2007) 056007.

[2] M. Diehl and D.Yu. Ivanov, Eur. Phys. J. C **52** (2007) 919.

[3] A.V. Belitsky, D. Müller and A. Kirchner, Nucl. Phys. **B629** (2002) 323.

[4] A.V. Belitsky and A.V. Radyushkin, Phys. Rept. **418** (2005) 1.

[5] D.Yu. Ivanov, L. Szymanowski and G. Krasnikov, JETP Lett. **80** (2004) 226;
N. Warkentin, M. Diehl, D.Yu. Ivanov and A. Schäfer, Eur. Phys. J. A **32** (2007) 273.

[6] M. Diehl, Phys. Rept. **388** (2003) 41.

[7] A. Freund, M. McDermott and M. Strikman, Phys. Rev. D **67** (2003) 036001.

Discussion

Q. (L.Jenkowzsky, ITP, Kiev) It is credible that a bootstrap relation between a GPD and the (imaginary part of) DVCS exists, following from the fact that, in the lowest order approximation, the imaginary part of the DVCS amplitude is proportional to the GPD?

A. This is not evident for me.

PRODUCTION OF SPIN-3 MESONS IN DIFFRACTIVE DIS

I.P. Ivanov

University of Liege, Belgium
Sobolev Institute of Mathematics, Novosibirsk, Russia
† *E-mail: Igor.Ivanov@ulg.ac.be*

Abstract

Non-trivial spin effects do not die out with energy growth. Here, we discuss one example of such effects — production of spin-3 mesons in diffractive DIS. Using both explicit k_t-factorization calculations and their vector-dominance-model interpretation, we argue that diffractive production of $\rho_3(1690)$ is a unique probe of several novel aspects of diffraction.

It is well known that even at highest energies a significant fraction of hadron-hadron collisions must be elastic. Elastic scattering is a member of the family of diffractive processes, in which the colliding hadrons can survive the scattering or turn into a small-mass diffractive system, $M_{diff} \ll \sqrt{s}$. In deep-inelastic scattering, DIS, where the virtual photon can be also viewed as a hadron, a significant part of all $\gamma^* p$ collisions is also diffractive.

The t-channel exchange that drives diffraction, the Pomeron, is often pictured as a "spin-blind" object. This leads to a prejudice that all non-trivial spin effects must die out at high energies, where the Pomeron exchange dominates over the secondary Reggeons. Partly in order to eliminate this prejudice, we present here our recent results on production of spin-3 mesons in diffractive DIS, [1, 2], which is a genuine example of *non-trivial spin effects in diffraction*.

1 Basics of diffractive meson production

Dynamics of diffractive DIS is conveniently described within the color dipole approach, [3]. The incoming photon turns into a $q\bar{q}$ pair (a color dipole), which experiences scattering off the target and then is projected onto the final meson V. Thanks to the Lorentz-dilatation of the transverse motion inside the projectile, the amplitude for this transition can be written in the probabilistic form

$$\frac{1}{s}\mathcal{A}(\gamma \to V) = \langle V|\hat{\sigma}|\gamma\rangle = \int dz\, d^2\boldsymbol{r}\, \Psi_V^*(z,\boldsymbol{r})\sigma_{\rm dip}(\boldsymbol{r})\Psi_\gamma(z,\boldsymbol{r})\,.$$

Here, $\hat{\sigma}_{\rm dip}$ is the *diffraction operator*, which acts in the projectile Fock space. In the $\boldsymbol{r}$-space it is diagonal and is known as *dipole cross section*.

Practical calculations are most convenient in the transverse momentum space. In this approach, known as the k_t-factorization approach, the amplitude has form:

$$\frac{1}{s}\mathcal{A}(\gamma \to V) = \frac{e\, c_V}{4\pi^2}\int \frac{dz\, d^2\boldsymbol{k}_\perp}{z(1-z)}\int \frac{d^2\boldsymbol{\kappa}}{\boldsymbol{\kappa}^4}\alpha_s\, \mathcal{F}\cdot I^V_{\lambda_V;\lambda_\gamma}\cdot \Psi_V(p^2)\,. \qquad (1)$$

Here z is the lightcone momentum fraction of the photon carried by the quark, $\boldsymbol{k}$ is the relative transverse momentum of the $q\bar{q}$ pair, while $\boldsymbol{\kappa}$ is the transverse momentum of the gluon. Coefficient c_V is the standard flavor-dependent average charge of the quark. The color dipole cross section is encoded via the unintegrated gluon distribution function $\mathcal{F}$. In our calculations we used fits of $\mathcal{F}$ obtained in [4] and adapted to the off-forward kinematics needed for the meson production, see details in [5].

This approach can be used to calculate production of quarkonia in different spin-orbital states. The only requirement is that $P = C = -1$.

- Ground state vector mesons ($L = 0$, $n_r = 0$): $\rho, \omega, \phi, J/\psi, \Upsilon$.
- Radially excited VM ($L = 0$, $n_r > 0$): $\approx \rho'(1450)$, ...
- Orbitally excited VM ($L = 2$, $n_r = 0$): $\approx \rho''(1700)$, ...
- High-spin mesons, e.g. spin-3 mesons with $L = 2$ such as $\rho_3(1690)$.

The properties of the given meson appear in (1) in two ways: via the radial wave function $\Psi_V(p^2)$, and via the spin-orbital structure, which is encoded in an appropriate spinorial structure of the $q\bar{q}V$ vertex, [6], and is present in (1) implicitly inside the integrands $I^V_{\lambda_V;\lambda_\gamma}$. For example, for the D-wave vector meson the vertex has form $\bar{u}\Gamma^\mu_D u \cdot V_\mu$, where V_μ is the polarization vector and $\Gamma^\mu_D = \gamma^\mu - 4(M+m)p^\mu/(M^2-4m^2)$. The corresponding structure for the spin-3 meson is $u\Gamma^{\mu\nu\rho}u \cdot T_{\mu\nu\rho}$, where $T_{\mu\nu\rho}$ is the polarization tensor and $\Gamma^{\mu\nu\rho}$ was derived in [1].

2 Production of orbitally or spin-excited mesons

2.1 Characteristic features

Let us first discuss the vital property of diffraction: *it does not conserve orbital momentum L of the $q\bar{q}$ pair*. Indeed, symbolically the amplitude is

$$\mathcal{A} \propto \int \frac{dz d^2\boldsymbol{k}_\perp}{z(1-z)} \langle L'|\hat{\sigma}_{\rm dip}|L\rangle = \int \frac{4}{M} d^3p \, \langle L'|\hat{\sigma}_{\rm dip}|L\rangle \neq 0\,, \tag{2}$$

because diffraction operator $\hat{\sigma}_{\rm dip}$ is not spherically symmetric. Namely, when calculating the diagrams, one observes that the transverse momentum circulating in the quark loop is much more important than the longitudinal one. This is the unavoidable consequence of the fact that any collision has a preferred direction.

Since the incoming photon can be also represented as a coherent combination of various vector mesons, including radially and orbitally excited mesons, see discussion in [2], one can, therefore, expect that orbitally excited and spin-excited mesons will be present among the final states in diffractive DIS.

Orthogonality of $q\bar{q}$ with different L suppresses the helicity conserving, but not the helicity violating amplitudes. Therefore, a much stronger helicity violation is expected for orbital excitations than for grounds state mesons.

2.2 Numerical results

Numerical results are obtained by direct evaluation of amplitudes (1) and integration of the differential cross section within the diffraction cone, $|t| < 1$ GeV^2. We took into account all helicity amplitudes, including all helicity violating transitions.

The main sources of uncertainty in the absolute values of the cross sections are the choice of the parametrization of the radial wave function and the e^+e^- decay width, which is used to adjust the size of the wave function. Our experience with ground state VM production [5] shows that different choices of the wave function lead to results differing by factor of 2. The results for the orbitally excited mesons are even more uncertain since the value of $\Gamma(\rho''(1700) \to e^+e^-)$ is known only within factor of 5. However, the relative production rates of $\rho''(1700)$ and $\rho_3(1690)$ are more stable, within factor of 2.

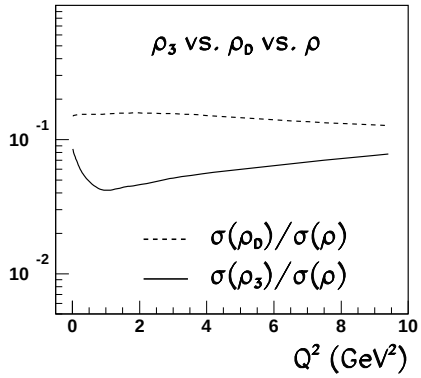

Figure 1. Ratios $\sigma(\rho''(1700))/\sigma(\rho)$ and $\sigma(\rho_3(1690))/\sigma(\rho)$ as functions of Q^2.

Fig. 1 shows the results for the ratios $\sigma(\rho''(1700))/\sigma(\rho)$ and $\sigma(\rho_3(1690))/\sigma(\rho)$ as functions of Q^2. Both ratios are $\mathcal{O}(0.1)$ and are comparable. Since $\rho''(1700)$ and $\rho_3(1690)$ are degenerate, this means that one must perform a very careful analysis of multipion diffractive final states in order to separate these two mesons.

Studying ρ_3 production in more detail, we found some other peculiar features.

- Numerical calculations confirm very large contribution from helicity violating transitions in ρ_3 even at moderate Q^2. We even predict *domination of helicity violation* at small Q^2 — a new regime in diffraction.
- The radial wave functions of the orbitally excited mesons are broader than of the ground states. Thus, typical dipole sizes in ρ_3 photoproduction are ~ 1.5 times larger (up to 2 fm) than for ρ photoproduction.
- σ_L/σ_T ratio is abnormally large for ρ_3.

2.3 Coupled channel analysis

The cross sections for $\rho''(1700)$ and $\rho_3(1690)$ production are of the same orders of magnitude, yet, the mechanisms of their diffractive production are quite different. We found this by performing, in the spirit of generalized vector dominance model, a coupled channel analysis of the action of diffraction operator in the Fock space generated by three mesons: ground state ρ, orbitally excited state $\rho''(1700)$ and spin-3 meson $\rho_3(1690)$. Details are reported in [2]. Here we just show the matrix for the integrated cross sections and with the sum over all final polarization states:

$$\sigma_{ba} = \langle V_b|\hat{\sigma}_{\rm dip}|V_a\rangle = \begin{pmatrix} 19 & 1 & 0.2 \\ 1 & 27 & 0.3 \\ 1.3 & 0.4 & 19 \end{pmatrix} \text{ mb}\,, \quad V_a, V_b = \rho, \rho'', \rho_3\,.$$

The diagonal elements have uncertainty of $\sim 50\%$, while the off-diagonal elements are uncertain within factor 2-3.

Since the hadronic part of the incoming photon at small virtuality can be roughly represented as $|\gamma\rangle_h \sim |\rho_S\rangle + 0.2|\rho_D\rangle$, one can conclude that

- $\rho''(1700)$ is produced mostly via "direct materialization" of the D-wave component of the photon followed by diagonal scattering, $\gamma \to \rho'' \to \rho''$.
- $\rho_3(1690)$ is produced via truly off-diagonal transition $\gamma \to \rho \to \rho_3$.
- Thus, ρ_D and ρ_3 probe *different properties of diffraction.*

3 Experimental opportunities

In contrast to the ground state vector meson production, [5], the data on excited VM, in particular, on the orbitally or spin-excited mesons, are very scarce. For example, the only published data on excited $\rho_3(1690)$ go back to 1986, when the fixed-target experiment OMEGA at CERN measured it in diffractive multipion photoproduction, [7].

Modern era experiments, both collider or fixed target, have great potential in making much progress in this field. What one needs is to study diffractive multipion production and extract the resonant contribution. One broad peak at $M \approx 1.1 - 1.9$ GeV should be separated into three excited ρ states: $\rho'(1450)$, $\rho''(1700)$, and $\rho_3(1690)$.

Specifically, the best tool to extract the ρ_3 contribution would be the partial-wave analysis. We expect that the most sensitive to the ρ_3 would be $\pi^+\pi^-$ final state at not too small t, say, at $|t| \approx 0.5$ GeV^2. One can try to see the ρ_3 by comparing multipion spectra in diffractive production and in e^+e^- annihilation experiments, since ρ_3 is present in diffraction but absent in the annihilation. Preliminary analysis [2] gave interesting results.

Acknowledgements. The work was supported by FNRS and partly by grants RFBR 05-02-16211 and NSh-5362.2006.2.

References

[1] F. Caporale, I. P. Ivanov, Eur. Phys. J. C **44** (2005) 505.

[2] I. P. Ivanov and S. Pacetti, arXiv:0706.3717 [hep-ph].

[3] N. N. Nikolaev and B. G. Zakharov, Z. Phys. C **49** (1991) 607; A. H. Mueller, Nucl. Phys. B **335** (1990) 115; N. N. Nikolaev, Comments Nucl. Part. Phys., **21** (1992) 41.

[4] I. P. Ivanov and N. N. Nikolaev, Phys. Rev. D **65** (2002) 054004.

[5] I. P. Ivanov, N. N. Nikolaev and A. A. Savin, Phys. Part. Nucl. **37** (2006) 1

[6] I. P. Ivanov and N. N. Nikolaev, JETP Lett. **69** (1999) 294.

[7] M. Atkinson *et al.* [Omega Photon Collaboration], Z. Phys. C **30** (1986) 531.

Discussion

Q. (X.Artru, IPN, Lion) Did you make prediction on the polarization of ρ_3, etc...?
A. Yes.

DIFFRACTIVE ELECTROPRODUCTION OF VECTOR PARTICLES WITH SPIN

R. Fiore[a♣] and L. Jenkovszky[b◇]

[a] *Dipartimento di Fisica, Università della Calabria, Istituto Nazionale di Fisica Nucleare,Gruppo Collegato di Cosenza, I-87036 Arcavacata di Rende, Cosenza, Italy*
[b] *Bogolyubov Institute for Theoretical Physics, Academy of Sciences of Ukraine, Kiev-143, Ukraine*

♣*e-mail address:* fiore@cs.infn.it
◇*e-mail address:* jenk@bitp.kiev.ua

Abstract

A Regge-pole model developed earlier for the electroproduction of vector mesons and for DVCS is generalized to include spin and to calculate the spin density matrix of the reactions.

In a recent paper [1] a Regge-pole model for the invariant deeply virtual scattering (DVCS) amplitude was suggested. Here we present its extension including spin and enabling the calculation of spin density matrixes for ϕ and J/Ψ diffractive photoproduction, where, by the Okubo-Zweig-Iizuka (OZI) rule, only the Pomeron contributes.

Let the helicity amplitude for the process $\gamma^* + N \to V + N$ in the c.m.s. of the t channel be $M_{\lambda_{\bar{N}},\lambda_V}(s,t)$ (for a review see e.g. Fef. [2]). The elements of the spin density matrix of V in its rest frame can be expressed, according to Ref. [3], in terms of helicity amplitudes in the t channel:

$$\rho^V_{\lambda\mu}(s,t) = N^{-1} \sum_{\lambda_{\bar{N}}\lambda_N} M^*_{\lambda_{\bar{N}}\lambda_V,\mu}(s,t), \tag{1}$$

where N is normalized to $\sum_\lambda \rho^V_{\lambda\lambda} = 1$,

$$N = \sum_{\lambda_{\bar{N}}\lambda_N} \mid M_{\lambda_{\bar{N}},\lambda_V,\lambda}(s,t) \mid^2 [s - (m_N - \mu)^2] = [s - (m_N + \mu)^2] \frac{d\sigma}{dt},$$

and μ is the virtual photon "mass." Experimentally, the polarization density matrix can be determined from the angular distribution of the decay products of the resonance V. When a vector meson V decays into two particles, e.g. $V \to 2\pi$, the angular distribution of the decay products is [4]

$$\frac{d\sigma}{d\Omega} = \frac{3}{4\pi}(\rho_{11}\sin^2\theta + \rho_{00}\cos^2\theta - \rho_{1-1}\sin^2\theta\cos 2\phi - \sqrt{2}\Re\rho_{10}\sin 2\theta\cos\phi),$$

where θ and ϕ are the polar and azimuthal angles of one of the emitted particle. In a factorized Regge pole model

$$M_{\lambda_{\bar{N}}\lambda_N,\lambda_V}(s,t) = \sum_k \xi_k(t) b^k_{\lambda_{\bar{N}}\lambda_N}(t) b^k_{\lambda_V}(t) \left(\frac{s}{s_0}\right)^{\alpha_k(t)},$$

where $\alpha_k(t)$ are the relevant Regge trajectories, $b^k_{\lambda_V}(t)$ and $b^k_{\lambda_{\tilde{N}}\lambda_N}(t)$ are the $\gamma^* Pp$ and pPp vertices respectively and $\xi_k(t)$ is the signature factor.

Each Regge pole is characterized by definite quantum numbers: signature P_j, parity P, isospin T, and G parity. By the conservation of P and G parity, a number of constrains and relations between the amplitudes and the residue can be derived [4]. Since in the present paper we consider purely diffractive processes, dominated solely by a Pomeron exchange, we get from Eq. (1) the following simple expressions for the spin density matrices in terms of the helicity amplitutes [4]:

$$\rho_{11} = 2N^{-1}(|M^a_{1/21/2,1}|^2 + |M^a_{1/2-1/2,1}|^2 + |M^b_{1/21/2,1}|^2),$$

$$\rho_{1-1} = 2N^{-1}(|M^{-a}_{1/21/2,1}|^2 + |M^a_{1/2-1/2,1}|^2 - |M^b_{1/21/2,1}|^2),$$

$$\rho_{00} = 2N^{-1}|M^b_{1/21/2,1}|^2, \quad \rho_{10} = 2N^{-1}M^b_{1/21/2,1}M^{b*}_{1/21/2,1},$$

where $M^{a(b)}_{\lambda_{\tilde{N}},\lambda_N,\lambda_V}(s,t)$ are correspondingly leading (a) or sub-leading (b) type Regge contributions to the helicity amplitude. Note the relation [4]

$$\rho_{00}(\rho_{11} - \rho_{1-1}) = 2|\rho_{10}|^2.$$

In ϕ or J/ψ photoproduction at high energies the dominant contribution comes from the Pomeron (type a) exchange, whence

$$\rho_{11} = 2N^{-1}(|M^a_{1/21/2,1}|^2 + |M^a_{1/2-1/2,1}|^2$$

$$\rho_{1-1} = 2N^{-1}(|M^{-a}_{1/21/2,1}|^2 + |M^a_{1/2-1/2,1}|^2,$$

$$\rho_{00} = \rho_{10} = 0.$$

Now we present a dynamical model [1] for the amplitudes M. According to Regge-factorization, the invariant amplitude can be written as

$$M(s,t,Q^2)_{\gamma^* p\to\gamma p} = -A_0 V_1(t,Q^2)V_2(t)(-is/s_0)^{\alpha(t)}, \tag{2}$$

where A_0 is a normalization factor, $V_1(t,Q^2)$ is the $\gamma^* P\gamma$ vertex, $V_2(t)$ is the pPp vertex and $\alpha(t)$ is the exchanged Pomeron trajectory, which we assume in a logarithmic form:

$$\alpha(t) = \alpha(0) - \alpha_1 \ln(1-\alpha_2 t). \tag{3}$$

Similarly to the procedure adopted in Ref. [5], we consider only the helicity conserving amplitude. Here we are referring to the dominant Pomeron contribution. Notice the appearance in Eq. (2) of a new variable, Q^2, absent from the conventional on-mass-shall S-matrix theory and from the formalism developed by Kaidalov et al. [4]. The role of the Q^2-dependence in the spin-dependent residuae is not quite clear.

For convenience, and following the arguments based on duality, the t dependence of the pPp vertex is introduced via the $\alpha(t)$ trajectory: $V_2(t) = e^{b\alpha(t)}$ where b is a parameter. A generalization of this concept will be applied also to the upper, $\gamma^* P\gamma$ vertex by introducing the trajectory

$$\beta(z) = \alpha(0) - \alpha_1 \ln(1-\alpha_2 z), \quad z = t - Q^2. \tag{4}$$

Hence the scattering amplitude (1), with the correct signature, becomes [1]

$$M(s,t,Q^2)_{\gamma^* p\to\gamma p} = -A_0 e^{b\alpha(t)} e^{b\beta(z)} (-is/s_0)^{\alpha(t)} = -A_0 e^{(b+L)\alpha(t)+b\beta(z)}, \tag{5}$$

where $L \equiv \ln(-is/s_0)$.

¿From Eq. (5) the slope of the forward cone is

$$B(s,Q^2,t) = \frac{d}{dt}\ln|A|^2 = 2\left[b + \ln\left(\frac{s}{s_0}\right)\right]\frac{\alpha'}{1-\alpha_2 t} + 2b\,\frac{\alpha'}{1-\alpha_2 z}, \tag{6}$$

which, in the forward limit, $t = 0$ reduces to

$$B(s,Q^2) = 2\left[b + \ln\left(\frac{s}{s_0}\right)\right]\alpha' + 2b\,\frac{\alpha'}{1+\alpha_2 Q^2}. \tag{7}$$

Thus, the slope shows shrinkage in s and antishrinkage in Q^2.

In the $Q^2 \to 0$ limit the Eq. (5) becomes

$$M(s,t) = -A_0 e^{2b\alpha(t)} (-is/s_0)^{\alpha(t)}, \tag{8}$$

where we recognize a typical Regge-behaved photoproduction (or, for $Q^2 \to m_H^2$, an on-shell hadronic) amplitude. The related deep inelastic scattering structure function is recovered by setting $Q_2^2 = Q_1^2 = Q^2$ and $t = 0$, to get a typical elastic virtual forward Compton scattering amplitude:

$$M(s,Q^2) = -A_0 e^{b(\alpha(0)-\alpha_1\ln(1+\alpha_2 Q^2))} e^{(b+\ln(-is/s_0))\alpha(0)} \propto -(1+\alpha_2 Q^2)^{-\alpha_1}(-is/s_0)^{\alpha(0)}. \tag{9}$$

For not too large Q^2 the contribution from longitudinal photons to DVCS is small. Moreover, at high energies, typical of the HERA collider, the amplitude is dominated by the helicity conserving Pomeron exchange and, since the final photon is real and transverse, the initial one is also transverse - to the extent that helicity is conserved. Hence the relevant structure function is F_1 that, at leading order, is related to F_2 by the Callan-Gross relation.

For $t = 0$ (with $x \approx Q^2/s$, valid for large s), the structure function assumes the form:

$$F_2(s,Q^2) \approx \frac{(1-x)Q^2}{\pi\alpha_e}\Im M(s,Q^2)/s, \tag{10}$$

where α_e is the electromagnetic coupling constant and the normalization is $\sigma_t(s) = \frac{4\pi}{s}\Im M(s,Q^2)$. It has the correct (required by gauge invariance) $Q^2 \to 0$ limit and has Bjorken scaling behavior for large enough s and Q^2.

A standard procedure for the fit [1] to the HERA data on DVCS [6], based on Eq. (5), is shown in Fig. 1 (for more details see Ref. [1]). The HERMES data will be analyzed within the present formalism in a forthcoming paper.

We thank A. Borissov and S. Manaenkov for fruitful discussion. L.J. thanks the organizers of the Spin07 conference in Dubna for their warm hospitality.

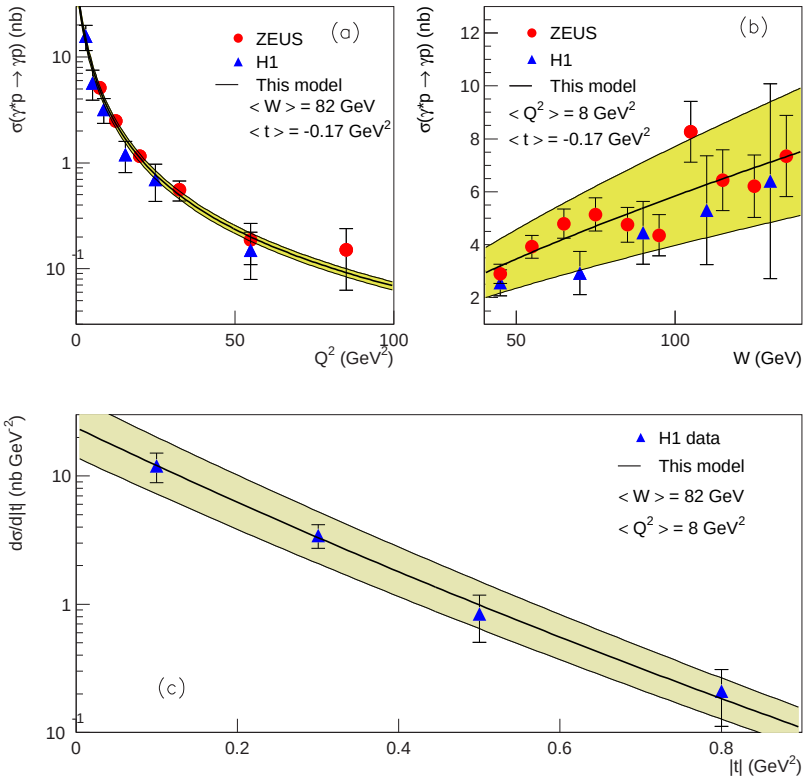

Figure 1: The $\gamma * p \to \gamma p$ cross section as a function of Q^2 (a), of W (b) and the cross section differential in t (c) measured by H1 and ZEUS experiments [6]. The ZEUS measurements have been rescaled to the W and Q^2 H1 values.

References

[1] M. Capua, R. Fiore, S. Fazio, L. Jenkovszky, and F. Paccanoni, Phys. Lett. B **645** (2007) 161 [arXiv: hep-ph/0605319]; L. Jenkovszky, In the Proc. of the EDS (Blois) conf. at DESY, 2007.

[2] C. Bourrely, E. Leader and J. Soffer, Phys. Rep. **59** (1980) 96.

[3] K. Gottfried, J.D. Jackson, Nuovo Cim. **33** (1964) 309.

[4] A.B. Kaidalov and B.M. Karnakov, Sov. J. Nucl. Phys. **3** (1966) 814 (Yad. Fiz. **11** (1966) 1119; A.B. Kaidalov, B.M. Karnakov, Yad. Fiz. **152** (1968) 152; A.B. Kaidalov and B.M. Karnakov, Sov. J. Nucl. Phys. **11** (1970) 121 (Yad. Fiz. **11** (1970) 216).

[5] D. Muller, *Pomeron dominance in deeply virtual Compton scattering and the femto holographic image of the proton*, arXiv:hep-ph/0605013.

[6] H1 Coll.: A. Aktas et al., Eur. Phys. J. C **44** (2005) 1; S. Chekanov et al., Phys. Lett. B **573** (2003) 46.

SPIN EFFECTS IN ELASTIC BACKWARD P-D SCATTERING

A.P.Ierusalimov[1], G.I.Lykasov[1†] and M.Viviani[2]

(1) *Joint Institute for Nuclear Research, Dubna, 141980, Moscow region, Russia*
(2) *INFN, Sezione di Pisa, Largo Bruno Pontecorvo, I-56127, Pisa, Italy*
† *E-mail:lykasov@jinr.ru*

Abstract

The elastic backward proton-deuteron scattering is analyzed including both relativistic effects in the deuteron and the reaction mechanism. It is shown that inclusion of the graphs corresponding to the emission, rescattering and absorption of the virtual pion by a deuteron nucleon in addition to the one-nucleon exchange graph allows a rather satisfactory description of all the experimental data on the differential cross section, tensor analyzing power of the deuteron and transfer polarization in this reaction .

1. Introduction. As is known, the study of polarization phenomena in hadron and hadron-nucleus interactions gives more detailed information on dynamics of their interactions and the structure of colliding particles. The elastic backward proton-deuteron scattering has been experimentally and theoretically studied in Saclay [1], Dubna and at the JLab (USA) [2,3]. Up to now all these data cannot be described within the one-nucleon exchange model (ONE) including even the relativistic effects in the deuteron [4–6].

In this paper we analyze the elastic backward proton-deuteron scattering within the relativistic approach including the ONE and the high order graphs corresponding to the emission, rescattering and absorption of the virtual pion by a deuteron nucleon.

2. One-nucleon exchange model. The studies of the elastic backward proton-deuteron scattering within the nonrelativistic ONE and the relativistic invariant one-nucleon exchange model (RONE) are presented in Ref. [4] and Ref. [5] respectively. The differential cross section calculated within the RONE (Fig.1a) can be presented in the following form [6]:

$$\frac{d\sigma}{d\Omega}|_{c.m.s.} = \frac{6\pi^2}{s} m^2 (m^2 - u)^2 \mid \Psi_d(q_s^2) \mid^4 \quad , \tag{1}$$

where $\Psi_d(q_s^2)$ is the deuteron wave function; s is the square of the initial energy in the $p-D$ c.m.s., u is the square of momentum transfer from initial deuteron to final proton; $q_s^2 = \frac{1}{4}s_{12} - m^2$, $s_{12} = (k_1 + k_2)^2$, k_1, k_2 are the four-momenta of neutron and proton in the deuteron, m is the nucleon mass. Unfortunately, the ONE and the RONE do not allow a satisfactory description of all the observables at the kinetic energy of backward scattered protons $T_p > 0.6$ GeV [6] .

3. One-nucleon and one-pion exchange graphs. As was shown in Ref. [7], the contribution of the high-order graphs in the $p-D$ backward elastic scattering corresponding to the emission, rescattering and absorption of the virtual pion by a deuteron nucleon

can be sizable at initial energies corresponding to possible creation of the Δ-isobar at the $\pi - N$ vertex, see Fig.1c. The corrections to the ONE graph of Fig.1a were also analyzed in other papers, see for example Ref. [8] and references therein. As was shown in Refs. [9, 10] the contribution of the one-pion exhange graphs to the deuetron stripping reaction of type $D+p \to p+X$ can be also sizable at the initial energies close to a possible Δ-isobar creation in the intermediate state.

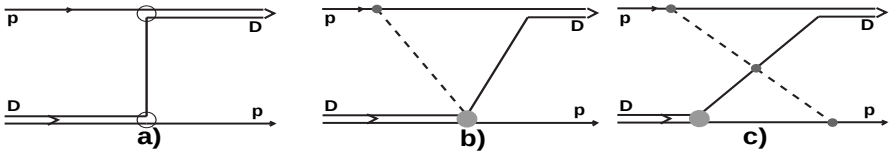

Figure 1: One-nucleon exchange graph (a) one-pion exchange graph for the process $p + D \to D + p$ (b), and its equivalent graph (c).

4. Results and discussion. We calculated the center-of-mass differential cross section, the tensor analyzing power of the deuteron T_{20} and the transfer polarization κ_0 in the elastic backward $p - D$ squattering including the RONE graph (Fig.1a) and the graphs of Fig.1c. These results are presented in Figs.(2,3). In Figs.(2,3) curves 1 and 3 correspond to the total calculation and the RONE computation using the Reid soft core deuteron wave function, whereas the lines 2 and 4 are the same calculations but for the Argon-18 $N - N$ potential. As is evident from Figs.(2,3) the RONE allows us to describe $d\sigma/d\Omega_{c.m.s.}$ and T_{20} at initial deuteron momenta up to $1.5 GeV/c$, whereas the transfer polarization κ_0 is not described within the RONE in the wide interval of deuteron momenta $1.(GeV/c) < p_d^{l.s.} < 4.(GeV/c)$. Figures.(2,3) show that the total calculation of all the observables including the graphs of Fig.1a and Fig.1c results in a rather satisfactory description of the experimental data . The graphs of Fig.1c were calculated using the monopole form factor for the virtual pion with the cut-off parameter about $1. GeV/c$. The $\pi - N$ amplitude entering into the $\pi - N$ vertex of the Fig.1c graph was taken from the $\pi - N$ phase shift analysis.

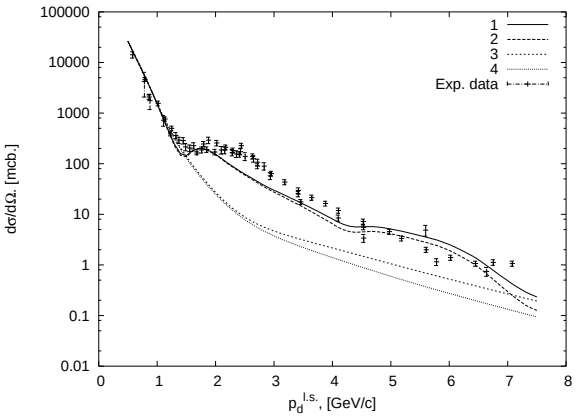

Figure 2: The center-of-mass differential cross section $d\sigma/d\Omega_{c.m.s.}$ for the elastic backward $p - D$ scattering as a function of the deuteron momentum $p_d^{l.s}$ in the laboratory system.

One can conclude that the calculation of all the observables for the elastic backward $p-D$ scattering within the relativistic invariant approach including the RONE graphs and the one-pion exchange graphs of Fig.1c type results in a rather satisfactory description of the experimental data at initial deuteron momenta up to $7 GeV/c$. Note that we do not include the six-quark admixture in the deuteron wave function. This effect can probably be important at larger initial momenta because the contribution of the Fig.1c graphs decreases when $p_d^{l.s}$ increases, as is shown in Fig.2.

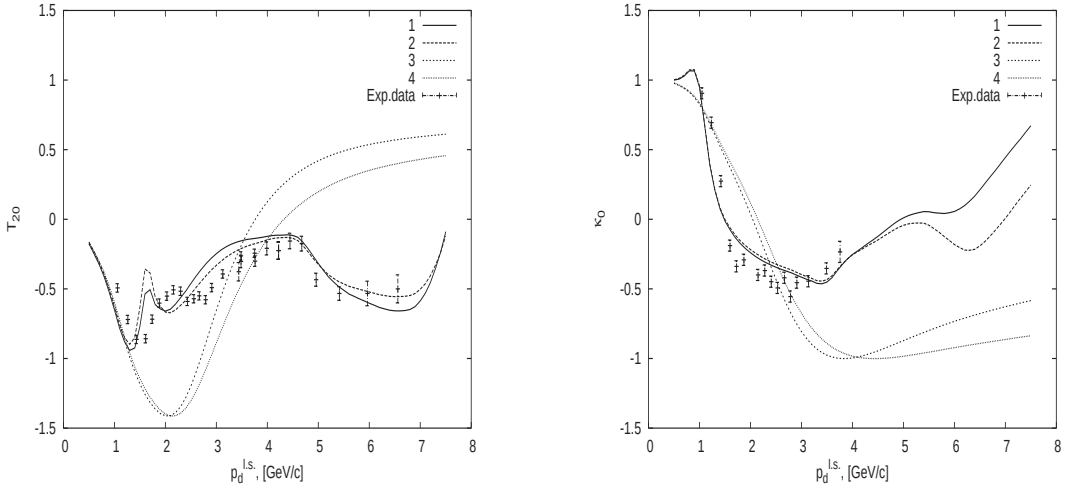

Figure 3: The tensor analyzing power of the deuteron T_{20} as a function of $p_d^{l.s}$ (lhs) and the transfer polarization κ_0 as a function of $p_d^{l,s}$ (rhs).

Acknowledgement. We are grateful to F.Gross, E.A.Strokovsky, V.A.Karmanov and Yu.N.Uzikov for very useful discussions.

References

[1] J.Arvieux, *et al.,* Nucl.Phys. **A431**, 613 (1983).

[2] L.S.Azhgirei, *et al.,* Proc. Few Body (ICFBP 14), 1994, p.423; *ibid* Phys.Lett B**361**, 21 (1995); B**391**, 22 (1997).

[3] V.Punjabi, *et al.,* Phys.Lett. B**350**, 178 (1995).

[4] A.K.Kerman and L.S.Kisslinger, Phys.Rev.**180**,1483 (1969)

[5] W.W.Buck, Franz Gross, Phys.Rev.**D20**,2361 (1969)

[6] A.Yu.Illarionov, G.I.Lykasov, Phys.Rev.**D64**,044004 (2001)

[7] G.W.Barry, Ann.Phys., **73**,482 (1972)

[8] Yu.N.Uzikov, Phys.Atom.Nucl., **60**, 1458 (1997)

[9] M.G.Dolidze, G.L., Z.Phys.A**335**,95 (1990); Z.Phys.A**336**,339 (1990)

[10] L.G.Dachno, V.A.Nikonov, Yad.Fiz., **50**, 1757 (1989).

Discussion

Q. (L.N.Strunov, JINR) What can you say about a contribution of one-pion exchange graphs to the deuteron breakup reaction ?

A. The contribution of the discussed triangle graphs to the all observables in the deuteron breakup reaction is sizable at initial energies corresponding to a possible creation of the Δ-isobar in the intermediate state, e.g., at the initial kinetic energy about 1 GeV.

Q. (I.M.Sitnik, JINR) What is a role of the discussed effects in the elastic backward proton-deuteron scattering and the deuteron stripping reactions on nuclei at high initial energies ?

A. At least, the discussed effects in the elastic backward proton-deuteron scattering decrease at initial deuteron momenta above 7 GeV/c and they can be neglected, as

is evident from Fig.2. As for the deuteron stripping reactions on nuclei, probably the contribution of discussed triangle graphs can be also neglected at high initial energies.

Q. (S.L.Belostozky, PNPI) As I understood, the pion entering into one-pion exchange graphs is virtual. What is the sensitivity of your results to the pion form factor used in your calculations ?

A. We used the monopole form factor for the virtual pion. The sensitivity of all the results to the value of the cut-off parameter entering into the form factor is about 10-20 percent. The results presented in the slides correspond to the cut-off parameter about 1 GeV/c.

Q. (S.S.Shimansky, JINR) Why your old results on T_{20} in the deuteron stripping reaction on a proton including similar one-pion exchange graphs did not describe the experimental data at large internal deuteron momenta ? On the other hand your new calculations of T_{20} and κ_0 in the elastic backward proton-deuteron scattering allow a rather satisfactory description of the experimental data in the whole kinematic region.

A. It is due to the following. In our old calculations we did not include the interference between different graphs, we summed the squares of separate graphs. However, the inclusion of the interference terms is very important. Now we include the interference terms because we take the pion-nucleon scattering amplitude entering into the $\pi - N$ vertex of the graph in Fig.1c from the $\pi - N$ phase shift analysis and can calculate both the real part and the imaginary part of the matrix element corresponding to any graph of Fig.1c.

SPIN STRUCTURE OF THE "FORWARD" CHARGE-EXCHANGE REACTION $n+p \to p+n$ AND THE DEUTERON CHARGE-EXCHANGE BREAKUP $d+p \to (pp)+n$

V.L. Lyuboshitz and V.V. Lyuboshitz†

Joint Institute for Nuclear Research,
141980 Dubna, Moscow Region, Russia
† *E-mail: Valery.Lyuboshitz@jinr.ru*

Abstract

The structure of the nucleon charge-exchange process $n+p \to p+n$ is investigated basing on the isotopic invariance of the nucleon-nucleon scattering. Using the operator of permutation of the spin projections of the neutron and proton, the connection between the spin matrices, describing the amplitude of the nucleon charge-exchange process at zero angle and the amplitude of the elastic scattering of the neutron on the proton in the "backward" direction, has been obtained. Due to the optical theorem, the spin-independent part of the differential cross-section of the process $n+p \to p+n$ at zero angle for unpolarized particles is expressed through the difference of total cross-sections of unpolarized proton-proton and neutron-proton scattering. Meantime, the spin-dependent part of this cross-section is proportional to the differential cross-section of the deuteron charge-exchange breakup $d+p \to (pp)+n$ at zero angle at the deuteron momentum $\mathbf{k}_d = 2\,\mathbf{k}_n$ ($\mathbf{k}_n$ is the initial neutron momentum). Analysis shows that, in the wide range of neutron laboratory momenta $k_n > 700\,MeV/c$, the main contribution into the differential cross-section of the process $n+p \to p+n$ at zero angle is provided namely by the spin-dependent term.

1. Isotopic structure of NN-scattering. Taking into account the isotopic invariance, the nucleon-nucleon scattering is described by the following operator:

$$\hat{f}(\mathbf{p},\mathbf{p}') = \hat{a}(\mathbf{p},\mathbf{p}') + \hat{b}(\mathbf{p},\mathbf{p}')\hat{\boldsymbol{\tau}}^{(1)}\hat{\boldsymbol{\tau}}^{(2)}\,. \tag{1}$$

Here $\hat{\boldsymbol{\tau}}^{(1)}$ and $\hat{\boldsymbol{\tau}}^{(2)}$ are vector Pauli operators in the isotopic space, $\hat{a}(\mathbf{p},\mathbf{p}')$ and $\hat{b}(\mathbf{p},\mathbf{p}')$ are 4-row matrices in the spin space of two nucleons; $\mathbf{p}$ and $\mathbf{p}'$ are the initial and final momenta in the c.m. frame, the directions of $\mathbf{p}'$ are defined within the solid angle in the c.m. frame, corresponding to the front hemisphere.

One should note that the process of elastic neutron-proton scattering into the back hemisphere is interpreted as the charge-exchange process $n+p \to p+n$.

According to (1), the matrices of amplitudes of proton-proton, neutron-neutron and neutron-proton scattering take the form:

$$\hat{f}_{pp\to pp}(\mathbf{p},\mathbf{p}') = \hat{f}_{nn\to nn}(\mathbf{p},\mathbf{p}') = \hat{a}(\mathbf{p},\mathbf{p}') + \hat{b}(\mathbf{p},\mathbf{p}')\,;$$

$$\hat{f}_{np\to np}(\mathbf{p},\mathbf{p}') = \hat{a}(\mathbf{p},\mathbf{p}') - \hat{b}(\mathbf{p},\mathbf{p}')\,; \tag{2}$$

meantime, the matrix of amplitudes of the charge transfer process is as follows:

$$\hat{f}_{np\to pn}(\mathbf{p},\mathbf{p}') = 2\hat{b}(\mathbf{p},\mathbf{p}') = \hat{f}_{pp\to pp}(\mathbf{p},\mathbf{p}') - \hat{f}_{np\to np}(\mathbf{p},\mathbf{p}')\,. \tag{3}$$

It should be stressed that the differential cross-section of the charge-exchange reaction, defined in the front hemisphere $0 \le \theta \le \frac{\pi}{2}$, $0 \le \phi \le 2\pi$ (here θ is the angle between the momenta of initial neutron and final proton, ϕ is the azimuthal angle), should coincide with the differential cross-section of the elastic neutron-proton scattering into the back hemisphere by the angle $\widetilde{\theta} = \pi - \theta$ at the azimuthal angle $\widetilde{\phi} = \pi + \phi$ in the c.m. frame. Due to the antisymmetry of the state of two fermions with respect to the total permutation, including the permutation of momenta ($\mathbf{p}' \to -\mathbf{p}'$), permutation of spin projections and permutation of isotopic projections ($p \leftrightarrows n$), the following relation between the amplitudes $\hat{f}_{np\to pn}(\mathbf{p},\mathbf{p}')$ and $\hat{f}_{np\to np}(\mathbf{p},-\mathbf{p}')$ holds [1] :

$$\hat{f}_{np\to pn}(\mathbf{p},\mathbf{p}') = -\hat{P}^{(1,2)}\hat{f}_{np\to np}(\mathbf{p},-\mathbf{p}')\,, \tag{4}$$

where $\hat{P}^{(1,2)}$ is the operator of permutation of spin projections of two particles with equal spins; the matrix elements of this operator are [2]: $\langle m_1' m_2' \mid \hat{P}^{(1,2)} \mid m_1 m_2\rangle = \delta_{m_1' m_2}\delta_{m_2' m_1}$. For particles with spin 1/2 [1,2]

$$\hat{P}^{(1,2)} = \frac{1}{2}(\hat{I}^{(1,2)} + \hat{\boldsymbol{\sigma}}^{(1)}\hat{\boldsymbol{\sigma}}^{(2)}), \tag{5}$$

where $\hat{I}^{(1,2)}$ is the four-row unit matrix, $\hat{\boldsymbol{\sigma}}^{(1)}$, $\hat{\boldsymbol{\sigma}}^{(2)}$ – vector Pauli operators. It is evident that $\hat{P}^{(1,2)}$ is the unitary and Hermitian operator:

$$\hat{P}^{(1,2)} = \hat{P}^{(1,2)+}, \quad \hat{P}^{(1,2)}\hat{P}^{(1,2)+} = \hat{I}^{(1,2)}. \tag{6}$$

Taking into account the relations (5) and (6), the following matrix equality holds:

$$\hat{f}^{+}_{np\to pn}(\mathbf{p},\mathbf{p}')\hat{f}_{np\to pn}(\mathbf{p},\mathbf{p}') = \hat{f}^{+}_{np\to np}(\mathbf{p},-\mathbf{p}')\hat{f}_{np\to np}(\mathbf{p},-\mathbf{p}'). \tag{7}$$

As a result, the differential cross-sections of the charge-exchange process $n + p \to p + n$ and the elastic np-scattering in the corresponding back hemisphere coincide at any polarizations of initial nucleons:

$$\frac{d\sigma_{np\to pn}}{d\Omega}(\mathbf{p},\mathbf{p}') = \frac{d\sigma_{np\to np}}{d\Omega}(\mathbf{p},-\mathbf{p}'). \tag{8}$$

However, the separation into the spin-dependent and spin-independent parts is <u>different</u> for the amplitudes $\hat{f}_{np\to pn}(\mathbf{p},\mathbf{p}')$ and $\hat{f}_{np\to np}(\mathbf{p},-\mathbf{p}')$!

2. Nucleon charge-exchange process at zero angle. Now let us investigate in detail the nucleon charge transfer reaction $n + p \to p + n$ at zero angle. In the c.m. frame of the (np)-system, the amplitude of the nucleon charge transfer in the "forward" direction $\hat{f}_{np\to pn}(0)$ has the following spin structure:

$$\hat{f}_{np\to pn}(0) = c_1\hat{I}^{(1,2)} + c_2\,[\hat{\boldsymbol{\sigma}}^{(1)}\hat{\boldsymbol{\sigma}}^{(2)} - (\hat{\boldsymbol{\sigma}}^{(1)}\mathbf{l})(\hat{\boldsymbol{\sigma}}^{(2)}\mathbf{l})] + c_3\,(\hat{\boldsymbol{\sigma}}^{(1)}\mathbf{l})(\hat{\boldsymbol{\sigma}}^{(2)}\mathbf{l})\,, \tag{9}$$

where $\mathbf{l}$ is the unit vector directed along the incident neutron momentum. In so doing, the second term in Eq. (9) describes the spin-flip effect, and the third term characterizes

the difference between the amplitudes with the parallel and antiparallel orientations of the neutron and proton spins.

The spin structure of the amplitude of the elastic neutron-proton scattering in the "backward" direction $\hat{f}_{np\to np}(\pi)$ is analogous:

$$\hat{f}_{np\to np}(\pi) = \widetilde{c}_1 \hat{I}^{(1,2)} + \widetilde{c}_2[\hat{\boldsymbol{\sigma}}^{(1)}\hat{\boldsymbol{\sigma}}^{(2)} - (\hat{\boldsymbol{\sigma}}^{(1)}\mathbf{l})(\hat{\boldsymbol{\sigma}}^{(2)}\mathbf{l})] + \widetilde{c}_3(\hat{\boldsymbol{\sigma}}^{(1)}\mathbf{l})(\hat{\boldsymbol{\sigma}}^{(2)}\mathbf{l}). \tag{10}$$

However, the coefficients $\widetilde{c}$ in Eq.(10) do not coincide with the coefficients c in Eq.(9). According to Eq.(4), the connection between the amplitudes $\hat{f}_{np\to pn}(0)$ and $\hat{f}_{np\to np}(\pi)$ is the following:

$$\hat{f}_{np\to pn}(0) = -\hat{P}^{(1,2)}\hat{f}_{np\to np}(\pi)\,, \tag{11}$$

where the unitary operator $\hat{P}^{(1,2)}$ is determined by Eq.(5).

As a result of calculations with Pauli matrices, we obtain:

$$c_1 = -\frac{1}{2}(\widetilde{c}_1 + 2\widetilde{c}_2 + \widetilde{c}_3); \quad c_2 = -\frac{1}{2}(\widetilde{c}_1 - \widetilde{c}_3); \quad c_3 = -\frac{1}{2}(\widetilde{c}_1 - 2\widetilde{c}_2 + \widetilde{c}_3). \tag{12}$$

Hence, it follows from here that the "forward" differential cross-section of the nucleon charge-exchange reaction $n + p \to p + n$ for unpolarized initial nucleons is described by the expression:

$$\frac{d\sigma_{np\to pn}}{d\Omega}(0) = |c_1|^2 + 2|c_2|^2 + |c_3|^2 =$$

$$= \frac{1}{4}|\widetilde{c}_1 + 2\widetilde{c}_2 + \widetilde{c}_3|^2 + \frac{1}{2}|\widetilde{c}_1 - \widetilde{c}_3|^2 + \frac{1}{4}|\widetilde{c}_1 - 2\widetilde{c}_2 + \widetilde{c}_3|^2 = |\widetilde{c}_1|^2 + 2|\widetilde{c}_2|^2 + |\widetilde{c}_3|^2. \tag{13}$$

Thus,

$$\frac{d\sigma_{np\to pn}}{d\Omega}(0) = \frac{d\sigma_{np\to np}}{d\Omega}(\pi),$$

just as it must be in accordance with the relation (8).

3. Spin-independent and spin-dependent parts of the cross-section of the reaction $n + p \to p + n$ at zero angle. It is clear that the amplitudes of the proton-proton and neutron-proton elastic scattering at zero angle have the structure (9) with the replacements $c_1, c_2, c_3 \to c_1^{(pp)}, c_2^{(pp)}, c_3^{(pp)}$, $c_1, c_2, c_3 \to c_1^{(np)}, c_2^{(np)}, c_3^{(np)}$, respectively. It follows from the isotopic invariance (see Eq. (3)) that

$$c_1 = c_1^{(pp)} - c_1^{(np)}, \quad c_2 = c_2^{(pp)} - c_2^{(np)}, \quad c_3 = c_3^{(pp)} - c_3^{(np)}. \tag{14}$$

In accordance with the optical theorem, the following relation holds, taking into account Eq.(14):

$$\frac{4\pi}{k}\mathrm{Im}\ c_1 = \frac{4\pi}{k}(\mathrm{Im}\ c_1^{(pp)} - \mathrm{Im}\ c_1^{(np)}) = \sigma_{pp} - \sigma_{np}\,, \tag{15}$$

where σ_{pp} and σ_{np} are the total cross-sections of interaction of two unpolarized protons and of an unpolarized neutron with unpolarized proton, respectively (due to the isotopic invariance, $\sigma_{pp} = \sigma_{nn}$); $k = |\mathbf{p}| = |\mathbf{p}'|$ is the modulus of neutron momentum in the c.m. frame of the colliding nucleons [1)].

[1)] We use the unit system with $\hbar = c = 1$.

Taking into account Eqs. (9), (13) and (15), the differential cross-section of the process $n+p \to p+n$ in the "forward" direction for unpolarized nucleons can be presented in the following form, distinguishing the spin-independent and spin-dependent parts:

$$\frac{d\sigma_{np\to pn}}{d\Omega}(0) = |c_1|^2 + 2|c_2|^2 + |c_3|^2 = \frac{d\sigma^{(si)}_{np\to pn}}{d\Omega}(0) + \frac{d\sigma^{(sd)}_{np\to pn}}{d\Omega}(0)\,. \tag{16}$$

In doing so, the spin-independent part $\frac{d\sigma^{(si)}_{np\to pn}}{d\Omega}(0)$ in Eq.(16) is determined by the difference of total cross-sections of the unpolarized proton-proton and neutron-proton interaction:

$$\frac{d\sigma^{(si)}_{np\to pn}}{d\Omega}(0) = |c_1|^2 = \frac{k^2}{16\pi^2}(\sigma_{pp} - \sigma_{np})^2(1+\alpha^2)\,, \tag{17}$$

where $\alpha = \mathrm{Re}\ c_1/\mathrm{Im}\ c_1$. The spin-dependent part of the cross-section of the "forward" charge-exchange process is

$$\frac{d\sigma^{(sd)}_{np\to pn}}{d\Omega}(0) = 2|c_2|^2 + |c_3|^2. \tag{18}$$

Meantime, according to Eqs. (10), (12) and (13), the spin-dependent part of the cross-section of the "backward" elastic np-scattering is

$$\frac{d\sigma^{(sd)}_{np\to np}}{d\Omega}(\pi) = 2|\widetilde{c}_2|^2 + |\widetilde{c}_3|^2. \tag{19}$$

We see that $\frac{d\sigma^{(sd)}_{np\to pn}}{d\Omega}(0) \neq \frac{d\sigma^{(sd)}_{np\to np}}{d\Omega}(\pi)$.

Further it is advisable to deal with the differential cross-section $\left.\frac{d\sigma}{dt}\right|_{t=0}$, being a relativistic invariant ($t = -(p_1 - p_2)^2 = (\mathbf{p} - \mathbf{p}')^2 - (E - E')^2$ is the square of the 4-dimensional transferred momentum). In the c.m. frame we have: $t = 2k^2(1 - \cos\theta)$ and $\frac{d\sigma}{dt} = (\pi/k^2)\ \frac{d\sigma}{d\Omega}$. So, in this representation, the spin-independent and spin-dependent parts of the differential cross-section of the "forward" charge transfer process $\left.\frac{d\sigma_{np\to pn}}{dt}\right|_{t=0}$ are as follows: $\left.\frac{d\sigma^{(si)}_{np\to pn}}{dt}\right|_{t=0} = (\pi/k^2)\,|c_1|^2$, $\left.\frac{d\sigma^{(sd)}_{np\to pn}}{dt}\right|_{t=0} = (\pi/k^2)\,(2|c_2|^2 + |c_3|^2)$, and we may write, instead of Eq.(16):

$$\left.\frac{d\sigma_{np\to pn}}{dt}\right|_{t=0} = \left.\frac{d\sigma^{(sd)}_{np\to pn}}{dt}\right|_{t=0} + \frac{1}{16\pi}(\sigma_{pp} - \sigma_{np})^2(1+\alpha^2)\,. \tag{20}$$

Now it should be noted that, in the framework of the impulse approach, there exists a simple connection between the spin-dependent part of the differential cross-section of the charge-exchange reaction $n + p \to p + n$ at zero angle $\left.\frac{d\sigma^{(sd)}_{np\to pn}}{dt}\right|_{t=0}$ (not the "backward" elastic neutron-proton scattering, see Section 2) and the differential cross-section of the deuteron charge-exchange breakup $d + p \to (pp) + n$ in the "forward" direction $\left.\frac{d\sigma_{dp\to(pp)n}}{dt}\right|_{t=0}$ at the deuteron momentum $\mathbf{k}_d = 2\mathbf{k}_n$ ($\mathbf{k}_n$ is the the initial

neutron momentum) . In the case of unpolarized particles we have [3,4,5]:

$$\frac{d\sigma_{dp\to(pp)n}}{dt}\Big|_{t=0} = \frac{2}{3}\,\frac{d\sigma^{(sd)}_{np\to pn}}{dt}\Big|_{t=0}. \qquad (21)$$

In doing so, this formula remains still valid if one takes into account the deuteron D-wave state [5].

It is easy to understand also that, due to the isotopic invariance, the same relation (like Eq. (21)) takes place for the process $p + d \to n + (pp)$ at the proton laboratory momentum $\mathbf{k}_p = \mathbf{k}_n$ and for the process $n + d \to p + (nn)$ at the neutron laboratory momentum $\mathbf{k}_n$.

Thus, in principle, taking into account Eqs. (20) and (21),the modulus of the ratio of the real and imaginary parts of the spin-independent charge transfer amplitude at zero angle ($\mid \alpha \mid$) may be determined using the experimental data on the total cross-sections of interaction of unpolarized nucleons and on the differential cross-sections of the "forward" nucleon charge transfer process and the charge-exchange breakup of an unpolarized deuteron $d + p \to (pp) + n$ in the "forward" direction.

At present there are not yet final *reliable* experimental data on the differential cross-section of the deuteron charge-exchange breakup on a proton. However, the analysis shows: if we suppose that the real part of the spin-independent amplitude of charge transfer $n + p \to p + n$ at zero angle is smaller or of the same order as compared with the imaginary part ($\alpha^2 \leq 1$), then it follows from the available experimental data on the differential cross-section of charge transfer $\frac{d\sigma_{np\to pn}}{dt}\Big|_{t=0}$ and the data on the total cross-sections σ_{pp} and σ_{np} that the main contribution into the cross-section $\frac{d\sigma_{np\to pn}}{dt}\Big|_{t=0}$ is provided namely by the spin-dependent part $\frac{d\sigma^{(sd)}_{np\to pn}}{dt}\Big|_{t=0}$.

If the differential cross-section $\frac{d\sigma}{dt}$ is given in the units of $mbn/\,(\frac{GeV}{c})^2$ and the total cross-sections are given in mbn, then the spin-independent part of the "forward" charge transfer cross-section may be expressed in the form :

$$\frac{d\sigma^{(si)}_{np\to pn}}{dt}\Big|_{t=0} \approx 0.0512\,(\sigma_{pp} - \sigma_{np})^2(1 + \alpha^2). \qquad (22)$$

Using (22) and the data from the works [6,7,8], we obtain the estimates of the ratio $\frac{d\sigma^{(si)}_{np\to pn}}{dt}\Big|_{t=0} \Big/ \frac{d\sigma_{np\to pn}}{dt}\Big|_{t=0}$ at different values of the neutron laboratory momentum k_n:

1) $k_n = 0.7\ \frac{GeV}{c}$; $\quad \frac{d\sigma_{np\to pn}}{dt}\Big|_{t=0} = 268\ mbn/\,(\frac{GeV}{c})^2$; $\quad \sigma_{pp} - \sigma_{np} = -22.6\ mbn$;

$$\frac{d\sigma^{(si)}_{np\to pn}}{dt}\Big|_{t=0} \Big/ \frac{d\sigma_{np\to pn}}{dt}\Big|_{t=0} \approx 0.1\,(1 + \alpha^2).$$

2) $k_n = 1.7\ \frac{GeV}{c}$; $\quad \frac{d\sigma_{np\to pn}}{dt}\Big|_{t=0} = 37.6\ mbn/\,(\frac{GeV}{c})^2$; $\quad \sigma_{pp} - \sigma_{np} = 10\ mbn$;

$$\frac{d\sigma^{(si)}_{np\to pn}}{dt}\Big|_{t=0} \Big/ \frac{d\sigma_{np\to pn}}{dt}\Big|_{t=0} \approx 0.136\,(1 + \alpha^2).$$

3) $k_n = 2.5\ \frac{GeV}{c}$; $\left.\frac{d\sigma_{np\to pn}}{dt}\right|_{t=0} = 17.85\ mbn/\ (\frac{GeV}{c})^2$; $\sigma_{pp} - \sigma_{np} = 5.5\ mbn$;

$$\left.\frac{d\sigma^{(si)}_{np\to pn}}{dt}\right|_{t=0} \Big/ \left.\frac{d\sigma_{np\to pn}}{dt}\right|_{t=0} \approx 0.085\,(1+\alpha^2).$$

So, it is well seen that, assuming $\alpha^2 \lesssim 1$, the spin-dependent part $\left.\frac{d\sigma^{(sd)}_{np\to pn}}{dt}\right|_{t=0}$ provides at least $(70 \div 90)\%$ of the total magnitude of the "forward" charge transfer cross-section.

The preliminary experimental data on the differential cross-section of "forward" deuteron charge-exchange breakup $d+p \to (pp)+n$, obtained recently in Dubna (JINR, Laboratory of High Energies), also confirm the conclusion about the predominant role of the spin-dependent part of the differential cross-section of the nucleon charge-exchange reaction $n+p \to p+n$ in the "forward" direction.

This work is supported by Russian Foundation of Basic Research (Grant No. 05-02-16674)

References

[1] V.L. Lyuboshitz, V.V. Lyuboshitz, Proc. of the XI International Conference on Elastic and Diffractive Scattering (Blois, France, May 15 - 20, 2005), Gioi Publishers, 2006, p.223 .

[2] V.L. Lyuboshitz and M.I. Podgoretsky, Phys. At. Nucl. **59** (3), 449 (1996).

[3] N.W. Dean, Phys. Rev. D **5**, 1661 (1972); Phys. Rev. D **5**, 2832 (1972).

[4] V.V. Glagolev, V.L. Lyuboshitz, V.V. Lyuboshitz, N.M. Piskunov, JINR Communication **E1-99-280**, Dubna, 1999 .

[5] R. Lednicky, V.L. Lyuboshitz, V.V. Lyuboshitz, Proc. of the XVI International Baldin Seminar on High Energy Physics Problems, vol.I, JINR **E1,2-2004-76**, Dubna, 2004, p.199.

[6] P.F. Shepard et al, Phys. Rev. D **10**, 2735 (1974).

[7] T.J. Delvin et al, Phys. Rev. D **8**, 136 (1973).

[8] J.L. Friedes et al, Phys. Rev. Lett. **15**, 38 (1965).

RELATIONS BETWEEN GPDS AND TMDS: MODEL RESULTS AND BEYOND

S. Meißner[1†], A. Metz[2], M. Schlegel[3], and K. Goeke[1]

(1) *Institut für Theoretische Physik II, Ruhr-Universität Bochum, 44780 Bochum, Germany*
(2) *Department of Physics, Temple University, Philadelphia, PA 19122-6082, USA*
(3) *Theory Center, Jefferson Lab, 12000 Jefferson Avenue, Newport News, VA 23606, USA*
† *E-mail: stephan.meissner@tp2.ruhr-uni-bochum.de*

Abstract

Comparing the respective structures of the correlators defining generalized and transverse momentum dependent parton distributions, one finds possible relations between these two objects. Although it looks like the relations found do not hold in general, we show that they can be established at least in simple spectator model calculations. In addition, we discuss these relations in the context of generalized transverse momentum dependent parton distributions.

1 Introduction and definitions

Parton distributions are an essential tool for the QCD-description of hadronic scattering processes. In particular, generalized parton distributions (GPDs) and transverse momentum dependent parton distributions (TMDs), which appear in connection with hard exclusive and semi-inclusive reactions, respectively, attracted a lot of interest during the last years. Although these two types of parton distributions are *a priori* two distinct objects, recent work suggests possible relations between them [1–6]. In this note, we will briefly summarize the current knowledge on these relations (as presented in the review article [6]) and, in addition, also present new results from the analysis of generalized transverse momentum dependent parton distributions (GTMDs).

Before discussing the relations between GPDs and TMDs we recall their definitions. First of all, the leading twist GPDs of the nucleon for unpolarized quarks are defined through

$$\begin{aligned} F^q(x,\xi,\boldsymbol{\Delta}_T;\lambda,\lambda') &= \frac{1}{2}\int \frac{dz^-}{2\pi}\, e^{ik\cdot z}\, \big\langle p';\lambda'\big|\, \bar{\psi}\big(-\tfrac{1}{2}z\big)\,\gamma^+\,\mathcal{W}_{\rm GPD}\,\psi\big(\tfrac{1}{2}z\big)\,\big|p;\lambda\big\rangle\,\Big|_{z^+=\boldsymbol{z}_T=0} \\ &= \frac{1}{2P^+}\,\bar{u}(p',\lambda')\left(\gamma^+\,H^q(x,\xi,t) + \frac{i\sigma^{+\mu}\Delta_\mu}{2M}\,E^q(x,\xi,t)\right)u(p,\lambda)\,, \end{aligned} \tag{1}$$

with the average nucleon momentum $P = \frac{1}{2}(p+p')$ and the nucleon momentum transfer $\Delta = p' - p$. The GPDs depend on the three kinematical variables

$$x = \frac{k^+}{P^+}\,, \qquad \xi = -\frac{\Delta^+}{2P^+}\,, \qquad t = \Delta^2\,. \tag{2}$$

Throughout this note, we disregard any dependence of the correlator in Eq. (1) on a renormalization scale μ, as this does not affect the analysis of possible relations between GPDs and TMDs.

To derive these relations, it is convenient to work with the GPDs in impact parameter instead of momentum space. This representation of the GPDs can be obtained by Fourier transforming the correlator in Eq. (1) for $\xi = 0$,

$$\mathcal{F}^q(x, \boldsymbol{b}_T; S) = \int \frac{d^2\boldsymbol{\Delta}_T}{(2\pi)^2}\, e^{-i\boldsymbol{\Delta}_T\cdot\boldsymbol{b}_T}\, F^q(x, 0, \boldsymbol{\Delta}_T; S) = \mathcal{H}^q(x, \boldsymbol{b}_T^2) + \frac{\epsilon_T^{ij} b_T^i S_T^j}{M}\left(\mathcal{E}^q(x, \boldsymbol{b}_T^2)\right)', \tag{3}$$

where S parametrizes all possible combinations of the helicities λ and λ' as described in Refs. [3, 6]. The GPDs $\mathcal{H}^q$ and $\mathcal{E}^q$ are the Fourier transformed GPDs H^q and E^q, respectively, and the prime denotes the first derivative with respect to $\boldsymbol{b}_T^2$. The correlator in Eq. (3) can be interpreted as the probability density of finding an unpolarized quark with longitudinal momentum fraction x at transverse position $\boldsymbol{b}_T$ inside a transversely polarized nucleon.

The second set of parton distributions we are interested in are the TMDs. The leading twist TMDs of a nucleon for unpolarized quarks are defined through

$$\begin{aligned}\Phi^q(x, \boldsymbol{k}_T; S) =& \frac{1}{2}\int \frac{dz^-}{2\pi}\,\frac{d^2\boldsymbol{z}_T}{(2\pi)^2}\, e^{ik\cdot z}\left\langle P; S\right|\bar\psi\left(-\tfrac{1}{2}z\right)\gamma^+\,\mathcal{W}_{\text{TMD}}\,\psi\left(\tfrac{1}{2}z\right)\left|P; S\right\rangle\Big|_{z^+=0^+}\\ =& f_1^q(x, \boldsymbol{k}_T^2) - \frac{\epsilon_T^{ij} k_T^i S_T^j}{M}\, f_{1T}^{\perp q}(x, \boldsymbol{k}_T^2)\,,\end{aligned} \tag{4}$$

where again we disregard any dependence on a renormalization scale μ. Similar to the GPDs in impact parameter space the TMDs have a probability interpretation, too. The correlator in Eq. (4) gives the probability of finding an unpolarized quark with longitudinal momentum fraction x and transverse momentum $\boldsymbol{k}_T$ inside a transversely polarized target.

2 Relations between GPDs and TMDs

Comparing the respective structures of the correlators in Eqs. (3) and (4) one finds that they are identical after exchanging the impact parameter $\boldsymbol{b}_T$ and the transverse parton momentum $\boldsymbol{k}_T$. This, together with the similar probability interpretations of the correlators, leads to the assumption that there might exist some relations between these two objects.

Performing such a comparison for all leading twist parton distributions for quarks [3] as well as for gluons [6], one finds the following set of possible relations, which can be grouped into four different types according to the number of derivatives on the GPD side:

$$\mathcal{H}^{q/g} \;\leftrightarrow\; f_1^{q/g}\,, \qquad \tilde{\mathcal{H}}^{q/g} \;\leftrightarrow\; g_{1L}^{q/g}\,,$$

$$\left(\mathcal{H}_T^q - \tfrac{\boldsymbol{b}_T^2}{M^2}\,\Delta_b\tilde{\mathcal{H}}_T^q\right), \leftrightarrow \left(h_{1T}^q + \tfrac{\boldsymbol{k}_T^2}{2M^2}\, h_{1T}^{\perp q}\right) \tag{5}$$

$$\left(\mathcal{E}^{q/g}\right)' \;\leftrightarrow\; -f_{1T}^{\perp q/g}\,, \qquad \left(\mathcal{E}_T^q + 2\tilde{\mathcal{H}}_T^q\right)' \;\leftrightarrow\; -h_1^{\perp q}\,,$$

$$\left(\mathcal{H}_T^g - \tfrac{\boldsymbol{b}_T^2}{M^2}\,\Delta_b\tilde{\mathcal{H}}_T^g\right)' \leftrightarrow -\tfrac{1}{2}\left(h_{1T}^g + \tfrac{\boldsymbol{k}_T^2}{2M^2}\, h_{1T}^{\perp g}\right), \tag{6}$$

$$\left(\tilde{\mathcal{H}}_T^q\right)'' \;\leftrightarrow\; \tfrac{1}{2}h_{1T}^{\perp q}\,, \qquad \left(\mathcal{E}_T^g + 2\tilde{\mathcal{H}}_T^g\right)'' \;\leftrightarrow\; \tfrac{1}{2}h_1^{\perp g}\,, \tag{7}$$

$$\left(\tilde{\mathcal{H}}_T^g\right)''' \leftrightarrow -\tfrac{1}{4}h_{1T}^{\perp g}\,. \tag{8}$$

3 Model results...

To check whether the possible relations in Eqs. (5)–(8) really exist, we performed model calculations in two simple spectator models: a scalar diquark spectator model of the nucleon and a quark target model in perturbative QCD. In these models we were able to confirm all relations to lowest order in perturbation theory [6].

For the relations of first type in Eq. (5) this is not very surprising as it is a well known model-independent property of the involved GPDs and TMDs that they can be reduced to the same forward parton distributions,

$$q(x) = \int d^2\boldsymbol{b}_T \, \mathcal{H}^q(x, \boldsymbol{b}_T^2) = \int d^2\boldsymbol{k}_T \, f_1^q(x, \boldsymbol{k}_T^2) \tag{9}$$

and analogous for all other relations in Eq. (5).

In the case of the relations of second type in Eq. (6) we were able to reproduce the results of Refs. [2, 5] and to generalize them [6]. We suppose, however, that the explicit form for the relations in Eq. (6) presented in Refs. [2, 5, 6] is only valid in the performed lowest order model calculations and not in general, because it will probably break down once higher order contributions are taken into account [6]. Nevertheless, this type of relations has very interesting phenomenological implications [1–6].

For the relations of third type in Eq. (7) we found that

$$\int d^2\boldsymbol{b}_T \, \boldsymbol{b}_T^2 \left(\tilde{\mathcal{H}}_T^q(x, \boldsymbol{b}_T^2) \right)'' = \int d^2\boldsymbol{k}_T \, \boldsymbol{k}_T^2 \, \tfrac{1}{2} h_{1T}^{\perp q}(x, \boldsymbol{k}_T^2) \tag{10}$$

and analogous for the other relation in Eq. (7). The explicit form in Eq. (10) for the relations in Eq. (7), which has been presented in Ref. [6] for the first time, looks very similar to the relations of first type in Eq. (9), but so far it is not known whether Eq. (10) is restricted to model calculations or whether it could even be valid in general.

Eventually, we were not able to find an explicit form for the relation of fourth type in Eq. (8). Nevertheless, this relation is trivially fulfilled in our model calculations, as the corresponding GPD $\tilde{\mathcal{H}}_T^g$ and TMD $h_{1T}^{\perp g}$ vanish.

4 ... and beyond

So far, from the relations between GPDs and TMDs in Eqs. (5)–(8) only those of first type in Eq. (5) are known to be valid in general. Therefore, in order to obtain more information on the status of the other types of relations, we analyzed generalized transverse momentum dependent parton distributions (GTMDs). For a spinless target, these are defined through

$$W^{q[\Gamma]}(x, \xi, \boldsymbol{k}_T, \boldsymbol{\Delta}_T) = \frac{1}{2} \int \frac{dz^-}{2\pi} \frac{d^2\boldsymbol{z}_T}{(2\pi)^2} \, e^{ik\cdot z} \left\langle p' \right| \bar{\psi}\left(-\tfrac{1}{2}z\right) \Gamma \, \mathcal{W}_{\text{GTMD}} \, \psi\left(\tfrac{1}{2}z\right) \left| p \right\rangle \Big|_{z^+=0^+}, \tag{11}$$

which reduces to the correlator for GPDs in Eq. (1) by integration over $\boldsymbol{k}_T$ and to the one for TMDs in Eq. (4) by setting $\Delta = 0$. Note that the correlator in Eq. (11) is directly related to the Wigner distributions discussed in Refs. [7, 8].

Using the constraints from hermiticity, parity, and time-reversal, the correlator in Eq. (11) can be parametrized by 16 GTMDs, which are complex-valued functions of x, ξ,

$\boldsymbol{k}_T^2$, $\boldsymbol{k}\cdot\boldsymbol{\Delta}$, and $\boldsymbol{\Delta}_T^2$. The four leading twist quark GTMDs of an unpolarized target are

$$W^{q[\gamma^+]} = F_1^q(x,\xi,\boldsymbol{k}_T^2,\boldsymbol{k}_T\cdot\boldsymbol{\Delta}_T,\boldsymbol{\Delta}_T^2)\,, \tag{12}$$

$$W^{q[\gamma^+\gamma_5]} = \frac{i\varepsilon_T^{ij}k_T^i\Delta_T^j}{M^2}\,\tilde{G}_1^q(x,\xi,\boldsymbol{k}_T^2,\boldsymbol{k}_T\cdot\boldsymbol{\Delta}_T,\boldsymbol{\Delta}_T^2)\,, \tag{13}$$

$$W^{q[i\sigma^{j+}\gamma_5]} = \frac{i\varepsilon_T^{ij}k_T^i}{M}\,H_1^{k,q}(x,\xi,\boldsymbol{k}_T^2,\boldsymbol{k}_T\cdot\boldsymbol{\Delta}_T,\boldsymbol{\Delta}_T^2) + \frac{i\varepsilon_T^{ij}\Delta_T^i}{M}\,H_1^{\Delta,q}(x,\xi,\boldsymbol{k}_T^2,\boldsymbol{k}_T\cdot\boldsymbol{\Delta}_T,\boldsymbol{\Delta}_T^2)\,. \tag{14}$$

From this parametrization one immediately recovers the model-independent validity of the relations of first type in Eq. (5), as the involved GPDs and TMDs are simply limiting cases of the same GTMDs,

$$\int d^2\boldsymbol{b}_T\,\mathcal{H}^q(x,\boldsymbol{b}_T^2) = \int d^2\boldsymbol{k}_T\,f_1^q(x,\boldsymbol{k}_T^2) = \int d^2\boldsymbol{k}_T\,\mathrm{Re}\Big[F_1^q(x,0,\boldsymbol{k}_T^2,0,0)\Big]\,. \tag{15}$$

For the relations of second type in Eq. (6) one finds, however, that

$$\Big(\mathcal{E}_T^q + 2\tilde{\mathcal{H}}_T^q\Big)' \sim \mathrm{Re}\Big[\tfrac{1}{2}\Big(\tfrac{k_T^1}{\Delta_T^1}+\tfrac{k_T^2}{\Delta_T^2}\Big)\,H_1^{k,q} + H_1^{\Delta,q}\Big] \qquad \text{and} \qquad h_1^{\perp q} \sim \mathrm{Im}\Big[H_1^{k,q}\Big]\,, \tag{16}$$

so that the involved GPDs and TMDs are limiting cases of two independent functions, the real and the imaginary part of some GTMDs. This supports the understanding that the relations in Eq. (6) do not hold in general. At the present stage our analysis does not permit any statement about the relations of third or fourth type in Eqs. (7) and (8), as here we would have to consider, in particular, target polarization.

5 Conclusions

We showed that model-independent considerations suggest possible relations between GPDs and TMDs. From these relations, so far only the relations of first type are known to be valid in general. The relations of second type are probably only valid in simple model calculations, which is supported by our analysis of GTMDs. It will be very interesting to redo this analysis for the relations of third and fourth type, as at least the relations of third type are similar to those of first type and could therefore be valid in general.

References

[1] M. Burkardt, Phys. Rev. D **66**, 114005 (2002); Nucl. Phys. A **735**, 185 (2004).
[2] M. Burkardt and D. S. Hwang, Phys. Rev. D **69**, 074032 (2004).
[3] M. Diehl and P. Hägler, Eur. Phys. J. C **44**, 87 (2005).
[4] M. Burkardt, Phys. Rev. D **72**, 094020 (2005).
[5] Z. Lu and I. Schmidt, Phys. Rev. D **75**, 073008 (2007).
[6] S. Meissner, A. Metz, and K. Goeke, Phys. Rev. D **76**, 034002 (2007).
[7] X. d. Ji, Phys. Rev. Lett. **91**, 062001 (2003).
[8] A. V. Belitsky, X. d. Ji, and F. Yuan, Phys. Rev. D **69**, 074014 (2004).

Discussion

Q. (A.Efremov, JINR, Dubna) If the relation of type-3 is valid for any n, then it has to be a direct relation between GPD and TMD functions. Is it correct?

A. Yes, for the model calculations we performed so far, this is correct. But we expect, that in general, if the relations of third type should exist at all, they will probably only hold for some moments of GPDs and TMDs like the relations of first type. However, this question is still under investigation.

ELASTIC PROTON-PROTON AND PROTON-ANTIPROTON SCATTERING: ANALYSIS OF COMPLETE SET OF HELICITY AMPLITUDES

S.B. Nurushev[1] and V.A. Okorokov[2†]

(1) *Institute for High Energy Physics, 142284 Protvino, Moscow Region, Russia*
(2) *Moscow Engineering Physics Institute (State University), 115409, Moscow, Russia*
† *Okorokov@bnl.gov; VAOkorokov@mephi.ru*

Abstract

The differential cross-sections are calculated for proton-proton and proton-antiproton elastic scattering using the phenomenological model based on the analytic parameterizations for global scattering parameters (total cross-section and ρ - parameter), crossing symmetry and derivative relations. We confront our model predictions with experimental data in wide range of energy and momentum transfer. The suggested method may be useful for PAX Program (GSI) as well as for high-energy experiments at RHIC and LHC.

The elastic proton-proton and proton-antiproton interactions allow a unique access to a number of fundamental physics observables. Some important experimental pp and $p\bar{p}$ data are drastically different in the energy region of $\sqrt{s} < 50$ GeV and become close each to other at higher energies approaching the asymptotical expectation. We have proposed earlier two analytical presentations for full set of helicity amplitudes for $p\bar{p}$ elastic scattering and have made predictions for t-dependences of some spin observables in first presentation [1]. In present paper we focus our attention on predictions for pp, $p\bar{p}$ elastic reactions in second approach.

We use the following analytic parameterization of averaged spin non-flip amplitude for elastic proton-proton scattering:

$$\Phi_+(s,t) = \sum_{i=1}^{3} A_i \delta_i \exp\left(-B_i(s,t)\, t/2\right), \tag{1}$$

where A_i are free complex constant parameters, the slope parameters $B_i(s,t)$ are functions of s and t, $\delta_i = 1$, $i = 1,3$, and $\delta_2 = \exp(-i\beta\pi t/2)$ describes experimental data in the region of diffraction deep, β - free parameter. We have approximated the experimental data for slope parameter in order to derive the analytic energy dependence for $B_i(s,t)$, $i = 1,2$ and the $B_3(s,t)$ was remained as a free parameter. The results for different approximations are shown on Fig. 1a, 1b for energy dependence of slope parameter at low and intermediate t values correspondingly. We choose the following approximation for the slope parameter:

$$B_i(s,t) = B_0^i + a_1^i (s/s_1)^{a_2^i} + 2\alpha_i \left[\ln(s/s_1)\right]^{a_3^i}, \quad i = 1,2, \tag{2}$$

where $s_1 = 1$ GeV^2, $a_3^1 = 1$ - fixed and $a_3^2 = 1.500 \pm 0.005$. One can see the parameterization (2) describes all experimental data quite reasonably for low t domain (χ^2/ndf=2.54).

The new experimental data are necessaire at high (RHIC, LHC) energies for intermediate t values in order to derive more unambiguous energy dependence of slope parameter. But now the function (2) approximates this dependence reasonably (χ^2/ndf=4.66) and predicts the values of $B_2(s,t)$ in high energy domain which agree qualitatively with theoretical expectation $B^{pp}(s,t) \simeq B^{p\bar{p}}(s,t)$ at asymptotic energies.

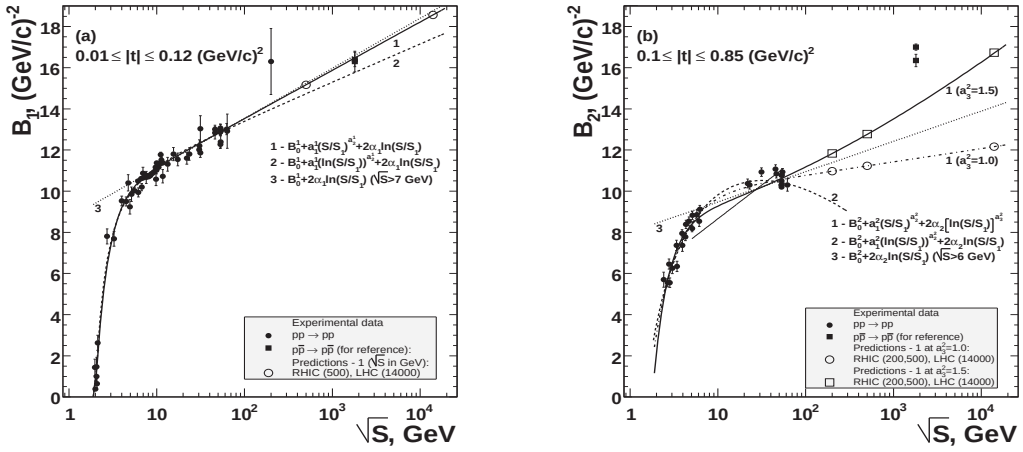

Figure 1. Energy dependence of slope parameter for low (a) and medium (b) $|t|$ values. The data are drawn from the Durham Database Group (UK). Thin solid line in (b) is a Regge model prediction from [2].

We have followed the standard way [3] and have assumed that the approximation (1) describes the spin non-flip helicity amplitude at $|t| \geq 0$ (GeV/c)^2. There are significant data set for total cross-section (σ_{tot}^{pp}) and $\rho^{pp} = [\Re\Phi_+(s,t=0)]/[\Im\Phi_+(s,t=0)]$. We choose these two characteristics for present analysis in order to decrease the amount of free parameters in (1). The PAX project (GSI), in particular, plans to study the $p\bar{p}$ collisions at energies $\sqrt{s} > 3$ GeV. Therefore we have to investigate this energy domain at least in order to obtain the reasonable energy dependence of free parameters in spin non-flip amplitude.

We choose the following parameterization for proton-proton total cross-section:

$$\begin{aligned} \sigma_{tot}^{pp}(s) &= \sum_{j=1}^{3} \left(\sigma_{tot}^{pp}\right)_j , \\ \left(\sigma_{tot}^{pp}\right)_1 &= a_1 \left(\frac{s_1}{s-4m_p^2}\right)^{a_2} ; \quad \left(\sigma_{tot}^{pp}\right)_2 = \frac{a_3}{\xi^{a_6-1}} \frac{J_1(\xi)}{(\xi)}, \quad \xi = a_4 (s/s_1 - a_5) ; \\ \left(\sigma_{tot}^{pp}\right)_3 &= Z^{pp} + B \ln^2(s/s_0) + Y_1^{pp} (s_1/s)^{\eta_1} - Y_2^{pp} (s_1/s)^{\eta_2} . \end{aligned} \tag{3}$$

The sum of first two terms is the modification of standard total cross section parameterization from [4] for $\sqrt{s} > 5$ GeV.

The different approximations are shown at Fig.2, the fit quality for (3) is χ^2/ndf=6.95 when using all available experimental data. As seen the Donnachie - Landshoff (DL), Kang - Nikolescu (KN) and standard Particle Data Group (PDG) parameterizations do not describe the proton-proton total cross section at low energies. On the other side the suggested approach describes the σ_{tot}^{pp} at qualitative level reasonably but this fit is

still statistically unacceptable. Therefore the problem of description the low energy data remains open.

Based on the defined analytical parameterization for total cross-section (3) one can try to obtain the corresponding parameterization for ρ^{pp}-parameter from analyticity and the dispersion relations written in the derivative form. We use the following analytic parameterization for ρ^{pp}-parameter:

$$\rho^{pp} = \frac{1}{2\sigma_{tot}^{pp}} \left[2\sigma_{tot}^{pp}\Lambda + \sum_{i=1}^{3} \left(\frac{K_i}{s} + \pi\delta_i \frac{d\left(\sigma_{tot}^{pp}\right)}{d\ln\left(s/s_1\right)} \right) \right], \quad \Lambda = \lambda_1 \frac{J_1\left(\lambda_2\left(s/s_1 - \lambda_3\right)\right)}{\left(\lambda_2\left(s/s_1 - \lambda_3\right)\right)^{\lambda_4}}, \qquad (4)$$

where the additional term Λ describes the low energy data, the σ_{tot}^{pp} are defined above. The first term and $K_i, \delta_i, i = 1-3$ can be derived from fit of experimental data. The fit quality for (4) is χ^2/ndf=7.8 for all experimental data. For comparison the fit quality is equal 54.4 for PDG parameterization, for example. There are a phase shift analysis results at energy lower than 5 GeV and we plan to look at these techniques and improve our description of the experimental data for low energies.

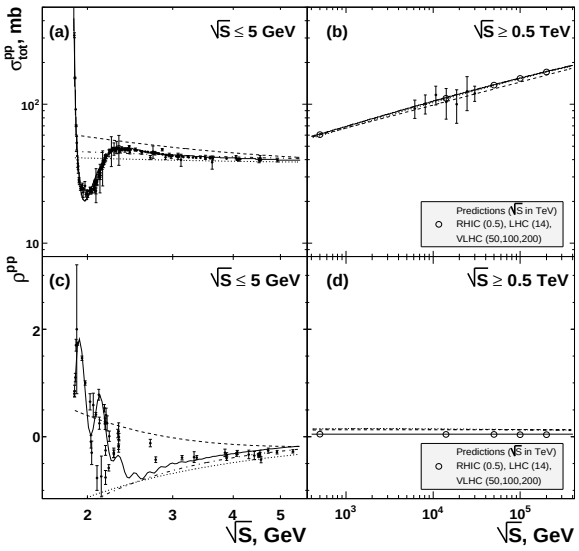

Figure 2. Energy dependences for σ_{tot}^{pp} (a,b) and for ρ^{pp} (c,d). Experimental data are from [4]. Solid line is the present work parameterization, other curves: dashed Ц- DL, dotted Ц- KN models [5], dot-dashed Ц- PDG parameterization [4].

As seen from Fig. 2 the different models predict quite similar results for σ_{tot}^{pp} (Fig. 2b) and for ρ (Fig. 2d) at high energies, but they valid only above 10 GeV or so. These models differ at low energies $\sqrt{s} < 5$ GeV dramatically (Fig. 2a, 2c). Thus we approximated the global scattering parameters at qualitative level for all available energy domain and defined A_1.

The remaining parameters in (1) are defined by fit of experimental proton-proton data for differential cross-section $d\sigma/dt$, in particular. We have used the method from [1] in order to obtain the full set of helicity amplitudes for proton-proton elastic scattering.

We have considered the data for pp differential cross-section in wide energy domain ($\sqrt{s} \simeq 2-62$ GeV) and for range of square of transfer momentum $t \simeq 10^{-2} - 10$ (GeV/c)^2. Experimental data and corresponding fits are shown on Fig. 3a for some initial energies. One can see that our parameterization describes experimental points well at any energies understudy and up to $t \sim 9$ (GeV/c)^2 at quantitative level. Disagreement between the experimental data and approximation curves at high t is expected: the high t domain is described by power dependence inspired pQCD.

We have considered the large set of available experimental data for $p\bar{p}$ differential cross-section. Analytic curves contradict with experimental data and some other models (Fig. 3b). Our approach describes experimental data fairly well at energies $\sqrt{s} \geq 19$

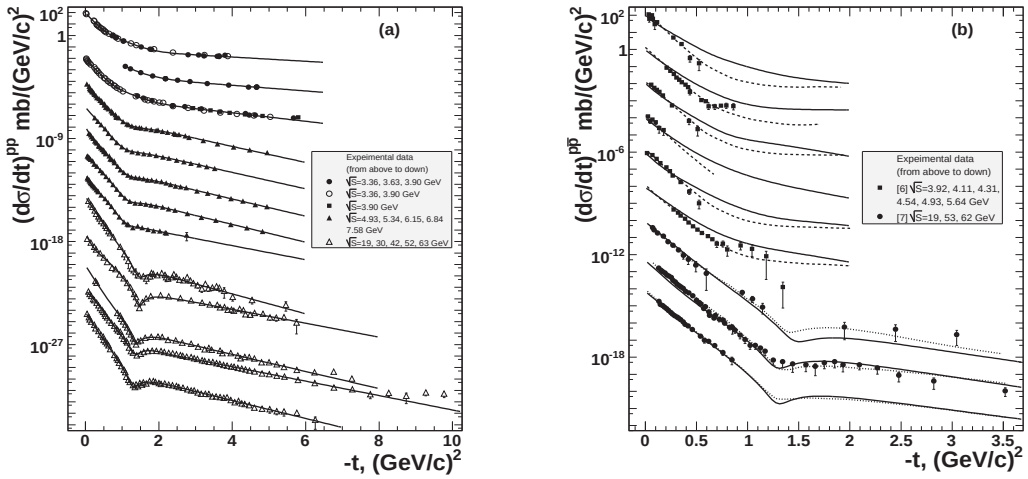

Figure 3. Differential cross sections for elastic pp (a) and $p\bar{p}$ (b) scattering. A factor 10^{-2} between each successive energy is omitted. Experimental data are from the Durham Database Group (UK) for pp and from [6, 7] for $p\bar{p}$. Solid lines are predictions of present work, other curves at (b): dashed Ц- Regge-pole [6], dotted Ц- mAQ [7] model prediction.

GeV at all t values and it's close to the modified additive quark (mAQ) model. But our approach contradicts to experimental data and Regge model predictions at low energies.

In summary, the new analytic approach for full set of helicity amplitudes for elastic pp collisions allows to describe well proton-proton experimental differential cross section at $\sqrt{s} \simeq 2 - 62$ GeV and up to $t \sim 9$ (GeV/c)^2. Full set of helicity amplitudes for $p\bar{p}$ elastic scattering is derived based on the known helicity amplitude parameterization for pp and crossing-symmetry. Analytic approach describes experimental $p\bar{p}$ data well at $\sqrt{s} \geq 19$ GeV and for low and intermediate t value, $t < 1.5$ (GeV/c)^2.

References

[1] V.A. Okorokov, S.B. Nurushev, Proc. of the 17th International Spin Physics Symposium, SPIN2006, AIP Conference Proc. **V.915**, 709 (2007) [arXiv: hep-ph/0612045]; arXiv: hep-ph/0701226.

[2] R.J.N Phillips, V. Barger, Phys. Lett. **46B**, 412 (1973).

[3] N.N. Amos et al, Phys. Rev. Lett. **61**, 525 (1988).

[4] W.-M. Yao et al, J. Phys. G **33**, 1 (2006).

[5] R.F. Avila, E.G.S. Luna, M.J. Menon, Phys.Rev. D **67** (2003) 054020.

[6] D.M. Austin et al, Phys.Rev, D **2**, 2613 (1970).

[7] P. Desgroland, M. Giffon, E. Martynov, arXiv: hep-ph/0004150.

CONTACT INTERACTION SEARCHES AT e^+e^- INTERNATIONAL LINEAR COLLIDER: ROLE OF POLARIZATION

A.A. Pankov and A.V. Tsytrinov

ICTP Affiliated Centre, Pavel Sukhoi Gomel State Technical University, Gomel 246746, Belarus

† *E-mail: pankov@ictp.it*

Abstract

We explore the potential of e^+e^- International Linear Collider (ILC) to study four-fermion contact interactions in fermion pair production process $e^+e^- \to \bar{f}f$. We stress the role played by the initial state polarization to increase the reach of this machine to discover of the new phenomena. Discovery limits are discussed in a model-independent way.

A very general framework in which to search for the effect of new physics is the four-fermion contact interaction. In this framework the Standard Model (SM) Lagrangian for

$$e^+ + e^- \to \bar{f} + f \tag{1}$$

($f = e, \mu, \tau, c, b$) is extended by a term describing a new effective contact interaction (CI) with an unknown coupling constants $g^2_{\rm eff}$ and an energy scale Λ. For the process (1) we consider the flavor-diagonal, helicity conserving $eeff$ contact-interaction effective Lagrangian [1]:

$$\mathcal{L}_{\rm CI} = \frac{1}{1+\delta_{ef}} \sum_{\alpha,\beta} g^2_{\rm eff}\, \epsilon_{\alpha\beta} \left(\bar{e}_\alpha \gamma_\mu e_\alpha\right) \left(\bar{f}_\beta \gamma^\mu f_\beta\right). \tag{2}$$

In Eq. (2): $\alpha, \beta = {\rm L}, {\rm R}$ denote left- or right-handed fermion helicities, $\delta_{ef} = 1$ for Bhabha scattering $e^+e^- \to e^+e^-$. The CI coupling constants in Eq. (2) are parameterized in terms of corresponding mass scales as $\epsilon_{\alpha\beta} = \eta_{\alpha\beta}/\Lambda^2_{\alpha\beta}$ and one assumes $g^2_{\rm eff} = 4\pi$. Also, by convention, one takes $|\eta_{\alpha\beta}| = 1$ or $\eta_{\alpha\beta} = 0$, leaving the energy scales $\Lambda_{\alpha\beta}$ as free, *a priori* independent, parameters.

For the Bhabha scattering, Eq. (2) envisages the existence of three independent CI models, each one contributing to individual helicity amplitudes or combinations of them, with *a priori* free, and nonvanishing, coefficients (basically, $\epsilon_{\rm LL}, \epsilon_{\rm RR}$ and $\epsilon_{\rm LR} = \epsilon_{\rm RL}$ combined with the $\pm$ signs). For the processes (1) with $f \neq e$ there are four independent CI couplings. Correspondingly, in principle, a model-independent analysis of the data should account for the situation where the full set of couplings of Eq. (2) is included in the expression for the cross section. Potentially, in this case, the different CI couplings may interfere and such interference could substantially weaken the bounds. To this aim, in the case of the processes (1) at the ILC considered here, a possibility is offered by *initial beam polarization* to disentangle the constraints on the corresponding CI constants. In this note, we wish to present a model-independent analysis of the CI based on the polarized differential distributions of the final fermions. We stress the role played by the initial state polarization to increase the reach of the ILC to discover of the CI effects.

The relative deviation of an observable $\mathcal{O}$ from the SM predictions due to the new physics (NP) reads:

$$\Delta(\mathcal{O}) = \frac{\mathcal{O}(\mathrm{SM}+\mathrm{NP}) - \mathcal{O}(\mathrm{SM})}{\mathcal{O}(\mathrm{SM})}, \tag{3}$$

and, as anticipated, we concentrate on the polarized differential cross section, $\mathcal{O} \equiv \mathrm{d}\sigma(P^-, P^+)/\mathrm{d}\cos\theta$.

To derive the constraints on the models, one has to compare the theoretical deviations from the SM predictions, that are functions of Λs, to the foreseen experimental uncertainties on the differential cross sections. To this purpose we introduce χ^2 function as:

$$\chi^2(\mathcal{O}) = \sum_{\{P^-,\ P^+\}} \sum_{\text{bins}} \left(\frac{\Delta(\mathcal{O})^{\text{bin}}}{\delta\mathcal{O}^{\text{bin}}} \right)^2 . \tag{4}$$

Here, for the individual processes, the cross sections for the different initial polarization configurations are combined in the χ^2, and $\delta\mathcal{O}$ denotes the expected experimental relative uncertainty (statistical plus systematic one). As indicated in Eq. (4), we divide the angular range into bins. For Bhabha scattering, the cut angular range $|\cos\theta| < 0.9$ is divided into ten equal-size bins. Similarly, for annihilation into fermions pairs ($f = \mu, \tau, c, b$) we consider the analogous binning of the cut angular range $|\cos\theta| < 0.98$.

Table 1: 95% C.L. model-dependent discovery reaches (in TeV). Left entry in each column refers to the unpolarized beams ($|P^-|, |P^+|$)=(0,0), while the right entry corresponds to ($|P^-|$,$|P^+|$)=(0.8, 0.3) at $\sqrt{s} = 0.5$ TeV, $\mathcal{L}_{\text{int}} = 500$ fb^{-1} and ($|P^-|$,$|P^+|$)=(0.8, 0.6) at $\sqrt{s} = 1$ TeV, $\mathcal{L}_{\text{int}} = 1000$ fb^{-1}, respectively.

Model	Processes							
	$e^+e^- \to e^+e^-$		$e^+e^- \to l^+l^-$		$e^+e^- \to \bar{b}b$		$e^+e^- \to \bar{c}c$	
	$\sqrt{s} = 0.5$ TeV; $\mathcal{L}_{\text{int}} = 500$ fb^{-1}							
Λ^{ef}_{VV}	128.3;	136.7	136.4;	144.2	115.8;	137.4	128.3;	136.7
Λ^{ef}_{AA}	76.1;	90.3	122.4;	129.5	116.7;	139.5	116.9;	124.8
Λ^{ef}_{LL}	66.2;	82.7	81.9;	98.6	96.9;	105.7	84.1;	96.6
Λ^{ef}_{RR}	64.0;	81.5	78.4;	97.7	64.4;	98.0	71.5;	95.3
Λ^{ef}_{LR}	94.9;	100.1	74.1;	90.2	76.0;	95.9	54.5;	79.0
Λ^{ef}_{RL}	$\Lambda_{RL} = \Lambda_{LR}$		74.0;	90.6	70.9;	85.5	78.2;	86.5
	$\sqrt{s} = 1$ TeV; $\mathcal{L}_{\text{int}} = 1000$ fb^{-1}							
Λ^{ef}_{VV}	223.3;	237.2	230.2;	254.1	196.2;	245.5	216.7;	241.4
Λ^{ef}_{AA}	133.6;	187.5	206.5;	228.0	196.6;	249.3	197.5;	220.2
Λ^{ef}_{LL}	119.3;	151.9	138.3;	176.0	163.4;	187.5	141.7;	171.8
Λ^{ef}_{RR}	114.9;	150.5	132.3;	174.6	109.4;	180.1	120.7;	171.3
Λ^{ef}_{LR}	160.0;	179.7	125.3;	161.5	126.2;	171.3	94.2;	145.4
Λ^{ef}_{RL}	$\Lambda_{RL} = \Lambda_{LR}$		125.0;	162.2	121.3;	153.1	131.8;	153.8

For the Bhabha process, we combine the cross sections with the following initial electron and positron longitudinal polarizations: $\{P^-, P^+\} = (|P^-|, -|P^+|)$; $(-|P^-|, |P^+|$; $(|P^-|, |P^+|)$; $(-|P^-|, -|P^+|)$. For the processes in Eq. (1), with $f \neq e$, we limit to combining the $(P^-, P^+) = (|P^-|, -|P^+|)$ and $(-|P^-|, |P^+|)$ polarization configurations.

Regarding the ILC energy and time-integrated luminosity, we take $\sqrt{s} = 0.5$ TeV with $\mathcal{L}_{\rm int} = 500\ fb^{-1}$, and $\sqrt{s} = 1$ TeV with $\mathcal{L}_{\rm int} = 1000\ fb^{-1}$. The assumed reconstruction efficiencies, that determine the expected statistical uncertainties, are 100% for e^+e^- final pairs; 95% for final l^+l^- events ($l = \mu, \tau$); 35% and 60% for $c\bar{c}$ and $b\bar{b}$, respectively. The major systematic uncertainties are found to originate from uncertainties on beams polarizations and on the time-integrated luminosity: we assume $\delta P^-/P^- = \delta P^+/P^+ = 0.1\%$ and $\delta\mathcal{L}_{\rm int}/\mathcal{L}_{\rm int} = 0.5\%$, respectively.

As theoretical inputs, for the SM amplitudes we use the effective Born approximation taking into account electroweak corrections to propagators and vertices, with $m_{\rm top} = 175$ GeV and $m_{\rm H} = 120$ GeV. Concerning the $\mathcal{O}(\alpha)$ QED corrections, the (numerically dominant) effects from initial-state radiation are accounted for by a structure function approach including both hard and soft photon emission, and by a flux factor method, respectively.

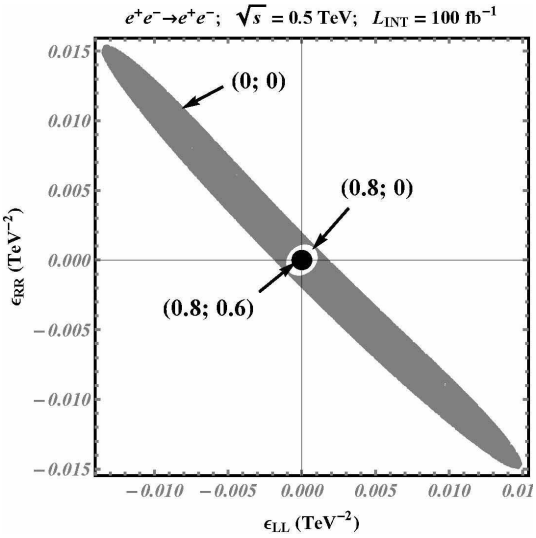

Figure 1. Two-dimensional projection of the 95% C.L. allowed region for unpolarized beams ($P^- = P^+ = 0$), polarized only electrons ($P^- \neq 0$, $P^+ = 0$) and both beams polarized ($P^- \neq 0$, $P^+ \neq 0$).

The expected discovery reaches on the contactlike effective interactions are assessed by assuming a situation where no deviation from the SM predictions is observed within the experimental uncertainty. Accordingly, the corresponding upper limits on the accessible values of Λs are determined by the condition $\chi^2(\mathcal{O}) \leq \chi^2_{\rm CL}$, and we take $\chi^2_{\rm CL} = 3.84$ for a 95% C.L. In Table 1, we present the numerical results for model-dependent (varying only one CI parameter at a time) constraints on the $eeff$ contact interactions from the processes (1).

The model-independent reach on the CI couplings, and the corresponding constraints on their allowed values in the case of no effect observed, can be estimated by the method based on the covariance matrix [2, 3] adapted for such kind of analysis. In this approach model-independent allowed domains in the three- or four-dimensional CI parameter space to 95% confidence level are obtained from the error contours determined by the quadratic form in $\epsilon_{\alpha\beta}$ that can be written for Bhabha scattering as:

$$(\epsilon_{LL}\ \epsilon_{LR}\ \epsilon_{RR})\, W^{-1} \begin{pmatrix} \epsilon_{LL} \\ \epsilon_{LR} \\ \epsilon_{RR} \end{pmatrix} = w^2, \tag{5}$$

where W^{-1} being the inverse covariance matrix and $w^2 = 7.82$. In this case the quadratic form (5) defines a three-dimensional surface in the (ϵ_{LL}, ϵ_{LR}, ϵ_{RR}) parameter space. The matrix W has the property that the square roots of the individual diagonal matrix elements, $\sqrt{W_{\alpha\alpha}}$, determine the projection of the surface onto the corresponding α-parameter axis in the three-dimensional space, and has the meaning of the bound at 95% C.L. on that parameter regardless of the values assumed for the others. As an example, in Fig. 1

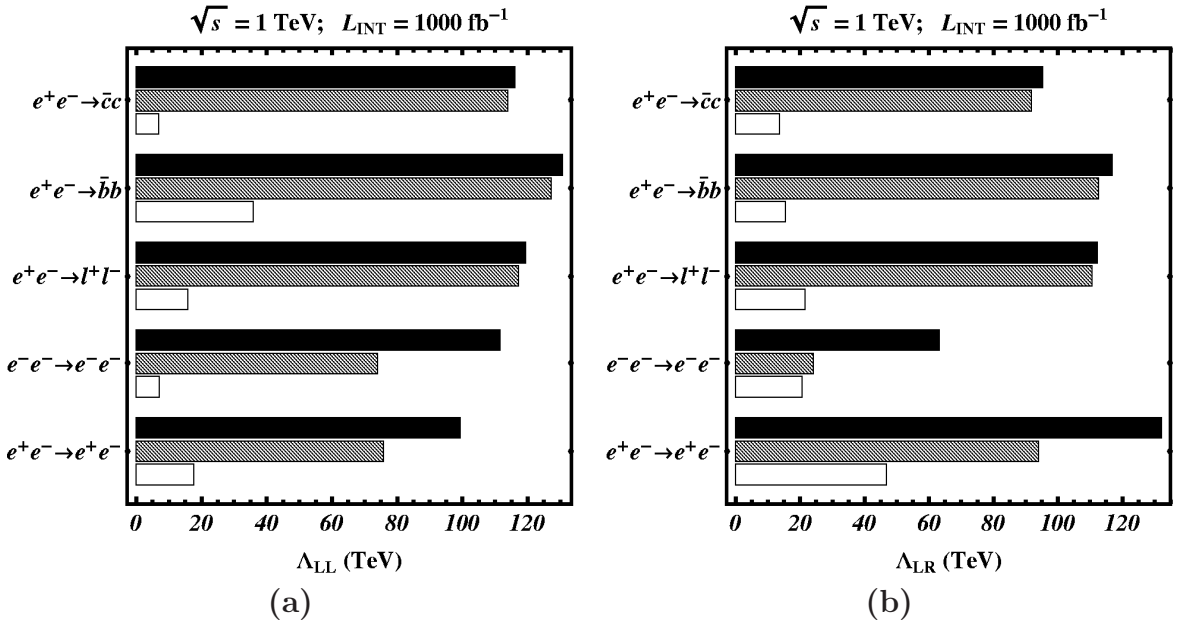

Figure 2a. Model-independent discovery reaches on Λ_{LL} at 95% C.L. obtained at different combinations of polarizations $(|P^-|;|P^+|)$=(0; 0): open bars, (0.8; 0): gray bars and (0.8; 0.6): black bars. **Figure 2b.** Same as in Fig. 2a but for Λ_{LR}.

we show the planar region that is obtained from Bhabha scattering by projecting onto the plane $(\epsilon_{LL}, \epsilon_{RR})$ the 95% C.L. allowed three-dimensional surface resulting from Eq. (5). The model-independent limits on CI are shown in Fig. 2 for all fermion pair production processes. Also, Fig. 1 and Fig. 2 clearly show the role of initial beam polarizations to increase the sensitivity of observables to CI parameters.

Acknowledgments. This work is partially supported by the ICTP through the OEA-Affiliated Centre-AC88.

References

[1] E. Eichten, K. Lane and M. E. Peskin, *Phys. Rev. Lett.* **50**, 811 (1983).
[2] F. Cuypers, P. Gambino, *Phys. Lett.* **B388**, 211 (1996).
[3] A. A. Babich, P. Osland, A. A. Pankov and N. Paver, *Phys. Lett.* **B518**, 128 (2001).

Discussion

Comm. (J.Soffer, Temple Univ.,Philadelphia) I was glad to hear your talk and I would like to remind you that we have also emphasized the importance of polarization in e^+e^- colliders in connection with the discovering of Susy particles (see NPB259, 365 (1985), NP262, 495 (1985))

TRANSVERSITY, COLLINS AND SIVERS EFFECTS FROM COMPASS, HERMES AND BELLE DATA

M. Anselmino[1], M. Boglione[1], U. D'Alesio[2], A. Kotzinian[3], F. Murgia[2], A. Prokudin[4], and C. Türk[1]

(1) *Dipartimento di Fisica Teorica, Università di Torino and INFN, Sezione di Torino, Via P. Giuria 1, I-10125 Torino, Italy.* (2) *INFN, Sezione di Cagliari and Dipartimento di Fisica, Università di Cagliari, C.P. 170, I-09042 Monserrato (CA), Italy.* (3) *Dipartimento di Fisica Generale, Università di Torino and INFN, Sezione di Torino, Via P. Giuria 1, I-10125 Torino, Italy.* (4) *Di.S.T.A., Università del Piemonte Orientale "A. Avogadro" and INFN, Gruppo Collegato di Alessandria, 15100 Alessandria, Italy.*

Abstract

The recent data on the transverse single spin asymmetries $A_{UT}^{\sin(\phi_h+\phi_S)}$ and $A_{UT}^{\sin(\phi_h-\phi_S)}$ from HERMES and COMPASS Collaborations are analyzed within LO parton model with unintegrated parton distribution and fragmentation functions. A fit of SIDIS data from HERMES and COMPASS Collaboration and BELLE e^+e^- data is performed leading to the extraction of favoured and unfavoured Collins fragmentation functions and transversity distribution. u and d Sivers distribution functions and sea Sivers functions are evaluated.

The transversity distribution function, usually denoted as $h_{1q}(x, Q^2)$ or $\Delta_T q(x, Q^2)$, together with the unpolarized distribution functions $q(x, Q^2)$ and the helicity distributions $\Delta q(x, Q^2)$, contains basic and necessary information for a full understanding of the quark structure, in the collinear, $\boldsymbol{k}_\perp$ integrated configuration, of a polarized nucleon. The distribution of transversely polarized quarks in a transversely polarized nucleon, $\Delta_T q(x, Q^2)$, is so far unmeasured. The reason is that, being related to the expectation value of a chiral-odd quark operator, it appears in physical processes which require a quark helicity flip: this cannot be achieved in the usual inclusive DIS, due to the helicity conservation of perturbative QED and QCD processes.

The problem of measuring the transversity distribution has been largely discussed in the literature [1]. The most promising approach is considered the double transverse spin asymmetry A_{TT} in Drell-Yan processes in $p\bar{p}$ interactions at a squared c.m. energy of the order of 200 GeV^2, which has been proposed by the PAX Collaboration [1, 3–5]. However, this requires the availability of polarized antiprotons, which is an interesting, but formidable task in itself. Meanwhile, the most accessible channel, which involves the convolution of the transversity distribution with the Collins fragmentation function [6], is the azimuthal asymmetry $A_{UT}^{\sin(\phi_h+\phi_S)}$ in SIDIS processes, namely $\ell\, p^\uparrow \to \ell\, \pi\, X$. This is the strategy being pursued by HERMES, COMPASS and JLab Collaborations.

A crucial improvement, towards the success of this strategy, has been recently achieved thanks to the independent measurement of the Collins function (or rather, of the convolution of two Collins functions), in $e^+e^- \to h_1 h_2\, X$ unpolarized processes by Belle Collaboration at KEK [7]. By combining the SIDIS experimental data from HERMES [23, 8] and COMPASS [9], with the Belle data, we have, for the first time, a large enough set

of data points as to attempt a global fit which involves, as unknown functions, both the transversity distributions and the Collins fragmentation functions of u and d quarks.

In Refs. [21,22], we studied the transverse single spin asymmetry $A_{UT}^{\sin(\phi_h-\phi_S)}$ observed by the HERMES [23] and COMPASS [24] Collaborations in polarized SIDIS scattering processes, $\ell p\,(\boldsymbol{S}) \to \ell' h X$. The quality of the data was such that, for the first time, we could perform a rather well constrained extraction of the Sivers distribution function [11, 26] for u and d quarks, assuming the existence of a symmetric and negligibly small Sivers sea. Very recently, higher precision data on single spin asymmetries for SIDIS pions *and kaons* production have become available, see Refs. [27] and [28]: it is, therefore, of great interest to reconsider the analysis performed in Ref. [22] to increase our understanding of the properties of the Sivers functions, for both valence and sea contributions. In particular, reduced error bars and hadron separation in both the HERMES and COMPASS sets of experimental data, combined with the use of some newly released sets of pion and kaon fragmentation functions [34] where quark and antiquark contributions are given separately for u, d and s flavours, allow us not only a reliable determination of the valence u and d flavour Sivers distribution functions, but also a first insight into the sea and strange contributions to the Sivers functions, namely $\Delta^N f_{\bar{u}/p^\uparrow}$, $\Delta^N f_{\bar{d}/p^\uparrow}$, $\Delta^N f_{s/p^\uparrow}$ and $\Delta^N f_{\bar{s}/p^\uparrow}$.

We consider here Collins [6] $\sin(\phi_S+\phi_h)$ asymmetry in SIDIS,

$$A_{UT}^{\sin(\phi_S+\phi_h)} = 2\,\frac{\int d\phi_S\, d\phi_h\, [d\sigma^\uparrow - d\sigma^\downarrow]\,\sin(\phi_S+\phi_h)}{\int d\phi_S\, d\phi_h\, [d\sigma^\uparrow + d\sigma^\downarrow]}\,, \tag{1}$$

measured by the HERMES [23, 8] and COMPASS [9] Collaborations. This asymmetry singles out the Collins fragmentation function:

$$D_{h/q,s}(z,\boldsymbol{p}_\perp) = D_{h/q}(z,p_\perp) + \frac{1}{2}\,\Delta^N D_{h/q^\uparrow}(z,p_\perp)\,\hat{\boldsymbol{s}}\cdot(\hat{\boldsymbol{p}}_q\times\hat{\boldsymbol{p}}_\perp)\,, \tag{2}$$

and transversity distribution,

$$\Delta_T q(x) \equiv h_{1q}(x) = \int d^2\boldsymbol{k}_\perp\,\Delta_T q(x,k_\perp)\,, \tag{3}$$

The transversity distributions and the Collins functions are unknown. We choose the following simple parameterization

$$\Delta_T q(x,k_\perp) = \frac{1}{2}\,\mathcal{N}_q^T(x)\,\left[f_{q/p}(x)+\Delta q(x)\right]\,\frac{e^{-k_\perp^2/\langle k_\perp^2\rangle_T}}{\pi\langle k_\perp^2\rangle_T} \tag{4}$$

$$\Delta^N D_{h/q^\uparrow}(z,p_\perp) = 2\,\mathcal{N}_q^C(z)\,D_{h/q}(z)\,h(p_\perp)\,\frac{e^{-p_\perp^2/\langle p_\perp^2\rangle}}{\pi\langle p_\perp^2\rangle}\,, \tag{5}$$

with

$$\mathcal{N}_q^T(x) = N_q^T\,x^\alpha(1-x)^\beta\,\frac{(\alpha+\beta)^{(\alpha+\beta)}}{\alpha^\alpha\beta^\beta} \tag{6}$$

$$\mathcal{N}_q^C(z) = N_q^C\,z^\gamma(1-z)^\delta\,\frac{(\gamma+\delta)^{(\gamma+\delta)}}{\gamma^\gamma\delta^\delta} \tag{7}$$

$$h(p_\perp) = \sqrt{2e}\,\frac{p_\perp}{M}\,e^{-p_\perp^2/M^2}\,, \tag{8}$$

and $|N_q^T|, |N_q^C| \leq 1$. We let the coefficients N_q^T and N_q^C to be flavor dependent ($q = u, d$), while all the exponents $\alpha, \beta, \gamma, \delta$ and the dimensional parameter M are taken to be flavor independent.

$f_{q/p}(x, k_\perp)$ is the unpolarized transverse momentum dependent (TMD) distribution function, while $D_{h/q}(z, p_\perp)$ is the unpolarized TMD fragmentation function:

$$f_{q/p}(x, k_\perp) = f_{q/p}(x) \, \frac{e^{-k_\perp^2/\langle k_\perp^2 \rangle}}{\pi \langle k_\perp^2 \rangle} \,, \tag{9}$$

$$D_{h/q}(z, p_\perp) = D_{h/q}(z) \, \frac{e^{-p_\perp^2/\langle p_\perp^2 \rangle}}{\pi \langle p_\perp^2 \rangle} \,, \tag{10}$$

where $f_{q/p}(x)$ and $D_{h/q}(z)$ are the usual integrated parton distribution and fragmentation functions, available in the literature; in particular we refer to Refs. [11,4] and [13]. Finally, the average values of $k_\perp^2$ and $p_\perp^2$ are taken from Ref. [21], where they were obtained by fitting the azimuthal dependence of SIDIS unpolarized cross section:

$$\langle k_\perp^2 \rangle = 0.25 \, \text{GeV}^2 \qquad \langle p_\perp^2 \rangle = 0.20 \, \text{GeV}^2 \,. \tag{11}$$

Notice that such values are assumed to be constant and flavor independent.

Notice that our parameterizations are devised in such a way that the transversity distribution function automatically obeys the Soffer bound [14]

$$|\Delta_T q(x)| \leq \frac{1}{2} \left[f_{q/p}(x) + \Delta q(x) \right] \,, \tag{12}$$

and the Collins function satisfies the positivity bound

$$|\Delta^N D_{h/q^\uparrow}(z, p_\perp)| \leq 2 D_{h/q}(z, p_\perp) \,, \tag{13}$$

since $\mathcal{N}_q^T(x)$, $\mathcal{N}_q^C(z)$ and $h(p_\perp)$ are normalized to be smaller than 1 in size for any value of x, z and $p_\perp$ respectively.

For the asymmetry we obtain (see Ref. [20]) in agreement with Refs. [15, 16],

$$A_{UT}^{\sin(\phi_S + \phi_h)} = \frac{-\dfrac{P_T}{M} \dfrac{1-y}{sxy^2} \sqrt{2e} \dfrac{\langle p_\perp^2 \rangle_C^2}{\langle p_\perp^2 \rangle} \dfrac{e^{-P_T^2/\langle P_T^2 \rangle_C}}{\langle P_T^2 \rangle_C^2} \displaystyle\sum_q e_q^2 \, \mathcal{N}_q^T(x) \left[f_{q/p}(x) + \Delta q(x) \right] \, \mathcal{N}_q^C(z) \, D_{h/q}(z)}{\dfrac{e^{-P_T^2/\langle P_T^2 \rangle}}{\langle P_T^2 \rangle} \dfrac{[1 + (1-y)^2]}{sxy^2} \displaystyle\sum_q e_q^2 \, f_{q/p}(x) \, D_{h/q}(z)} \,, \tag{14}$$

where

$$\begin{aligned} \langle p_\perp^2 \rangle_C &= \frac{M^2 \langle p_\perp^2 \rangle}{M^2 + \langle p_\perp^2 \rangle} \,, \\ \langle P_T^2 \rangle &= \langle p_\perp^2 \rangle + z^2 \langle k_\perp^2 \rangle \,, \\ \langle P_T^2 \rangle_C &= \langle p_\perp^2 \rangle_C + z^2 \langle k_\perp^2 \rangle \,. \end{aligned} \tag{15}$$

Eq. (14) expresses $A_{UT}^{\sin(\phi_S + \phi_h)}$ in terms of the parameters $\alpha, \beta, \gamma, \delta, N_q^T, N_q^C$ and M.

In $e^+e^- \to h_1 h_2\, X$ process Collins fragmentation functions of two fragmenting quarks generate an asymmetry (see Ref. [20]):

$$\frac{d\sigma^{e^+e^-\to h_1h_2X}}{dz_1\, dz_2\, d^2\boldsymbol{p}_{\perp 1}\, d^2\boldsymbol{p}_{\perp 2}\, d\cos\theta} = \frac{3\pi\alpha^2}{2s} \sum_q e_q^2 \left\{ (1+\cos^2\theta)\, D_{h_1/q}(z_1, p_{\perp 1})\, D_{h_2/\bar{q}}(z_2, p_{\perp 2}) + \frac{1}{4}\sin^2\theta\, \Delta^N D_{h_1/q^\uparrow}(z_1, p_{\perp 2})\, \Delta^N D_{h_2/\bar{q}^\uparrow}(z_2, p_{\perp 2})\, \cos(\varphi_1+\varphi_2) \right\} \quad (16)$$

in the reference frame so that the $e^+e^- \to q\,\bar{q}$ scattering occurs in the $\hat{x}\hat{z}$ plane, with the back-to-back quark and antiquark moving along the $\hat{z}$-axis.

We can now gather simultaneous information on the transversity distribution function $\Delta_T q(x, k_\perp)$ and the Collins fragmentation function $\Delta^N D_{h/q^\uparrow}(z, p_\perp)$. To such a purpose we perform a global best fit analysis of experimental data involving these functions, namely the data from the SIDIS measurements by the HERMES [23,8] and COMPASS [9] Collaborations, and the data from $e^+e^- \to h_1 h_2\, X$ unpolarized processes by the Belle Collaboration [7]. Our best fits (see Ref. [20]) of the experimental data from HERMES, COMPASS and Belle are shown in Figs. 1, Figs. 2 and 3 respectively.

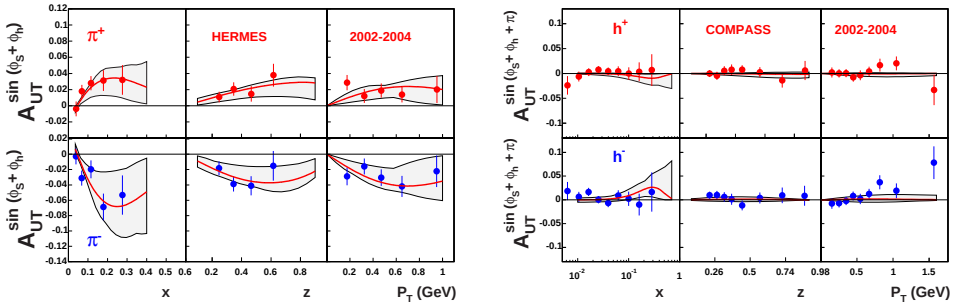

Figure 1: Our results compared with HERMES data [23] on $A_{UT}^{\sin(\phi_S+\phi_h)}$ for $\pi^\pm$ production (left panel) and COMPASS data on $A_{UT}^{\sin(\phi_S+\phi_h)}$, for the production of positively and negatively charged hadrons off a deuterium target [9] (right panel).

The SIDIS transverse Single Spin Asymmetry (SSA) $A_{UT}^{\sin(\phi_h-\phi_S)}$ measured by HERMES and COMPASS is defined as

$$A_{UT}^{\sin(\phi_h-\phi_S)} = 2\, \frac{\int d\phi_S\, d\phi_h\, [d\sigma^\uparrow - d\sigma^\downarrow]\, \sin(\phi_h-\phi_S)}{\int d\phi_S\, d\phi_h\, [d\sigma^\uparrow + d\sigma^\downarrow]}\,, \quad (17)$$

and shows the azimuthal modulation in the distribution function triggered by the correlation between the nucleon spin and the quark's intrinsic transverse momentum. This is embodied in the Sivers distribution function $\Delta^N f_{q/p^\uparrow}(x, k_\perp)$, which gives the number density of an unpolarized quark q with intrinsic transverse momentum $\boldsymbol{k}_\perp$ inside a transversely polarized proton $p^\uparrow$, with three-momentum $\boldsymbol{P}$ and spin polarization vector $\boldsymbol{S}$

$$f_{q/p^\uparrow}(x, \boldsymbol{k}_\perp) = f_{q/p}(x, k_\perp) + \frac{1}{2}\, \Delta^N f_{q/p^\uparrow}(x, k_\perp)\, \boldsymbol{S}\cdot(\hat{\boldsymbol{P}}\times\hat{\boldsymbol{k}}_\perp) \quad (18)$$

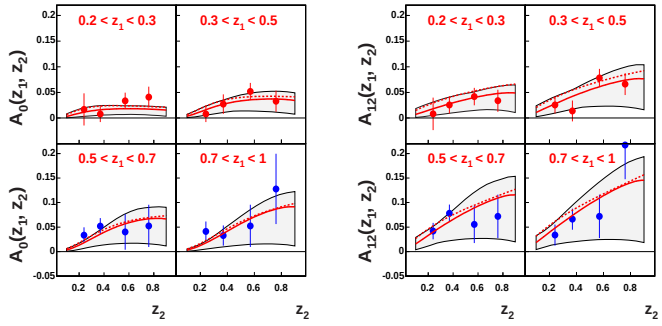

Figure 2: Data on two different azimuthal correlations in unpolarized $e^+e^- \to h_1 h_2\, X$ processes, as measured by Belle Collaboration [7], compared to the curves obtained from our fit. The solid (dashed) lines correspond to the global fit obtained including the $A_{12}(A_0)$ asymmetry; the shaded area corresponds to the theoretical uncertainty on the parameters.

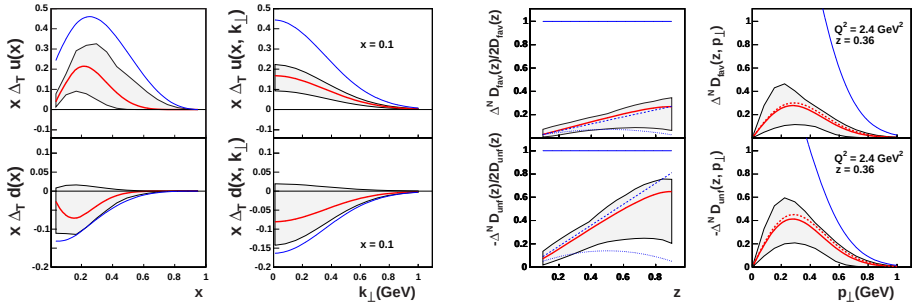

Figure 3: First panel: $x\,\Delta_T u(x)$ (upper plot) and $x\,\Delta_T d(x)$ (lower plot), vs. x at $Q^2 = 2.4\,\mathrm{GeV}^2$. The Soffer bound is also shown for comparison (bold blue line). Second panel: $x\,\Delta_T u(x,k_\perp)$ (upper plot) and $x\,\Delta_T d(x,k_\perp)$ (lower plot), vs. $k_\perp$ at a fixed value of x. Third panel: the z dependence of the moment of the Collins functions, also shown the results of Refs. [18] (dashed line) and [19] (dotted line). Fourth panel: the $p_\perp$ dependence of the Collins functions.

In our analysis we will use u,d and s flavours for quark and antiquark. The Sivers function is parametrized in terms of the unpolarized distribution function, as in Ref. [22], in the following factorized form:

$$\Delta^N f_{q/p^\uparrow}(x,k_\perp) = 2\,\mathcal{N}_q(x)\,h(k_\perp)\,f_{q/p}(x,k_\perp)\;, \tag{19}$$

where

$$\mathcal{N}_q(x) = N_q\,x^{a_q}(1-x)^{b_q}\,\frac{(a_q+b_q)^{(a_q+b_q)}}{a_q^{a_q}\,b_q^{b_q}}\;, \tag{20}$$

$$h(k_\perp) = \sqrt{2e}\,\frac{k_\perp}{M_1}\,e^{-k_\perp^2/M_1^2}\;, \tag{21}$$

where N_q, a_q, b_q and M_1 (GeV/c) are free parameters to be determined by fitting the experimental data.

The $A_{UT}^{\sin(\phi_h-\phi_S)}$ single spin asymmetry corresponding to K^+ production measured by the HERMES Collaboration [35] is much larger than the analogous asymmetry for π^+ in spite of "naive" expectation that K^+ and π^+ asymmetry are of the same size due to u quark dominance. This apparent mismatch between experimental data and theory expectations can easily be explained by some simple considerations on the properties of kaon fragmentation functions. In a simple partonic model one can imagine a K^+ meson being produced in SIDIS processes in two possible different ways: either from a u or from an $\bar{s}$ quark originating from the target proton. In the first case, the fragmentation process consists in the ricombination of the u quark with a secondary $s\bar{s}$ pair from the (sea) vacuum, whereas in the second case the $\bar{s}$ quark originating from the initial proton recombines with a u quark from a secondary $u\bar{u}$ pair. In both cases a final K^+ is generated. It is intuitive to see that, due to mass effects, it should be more "expensive" to extract an $s\bar{s}$ than a $u\bar{u}$ pair: therefore, one expects the number density of K^+ mesons inside an $\bar{s}$ quark to be larger than that of K^+ mesons inside a u quark. As a matter of fact, this simple property is not respected by any of the fragmentation function sets available in the literature, see for instance Refs. [13, 30–32, 29], with one exception: very recently De Florian, Sassot and Stratmann [33, 34] have presented a new global, very advanced analysis of quark and anti-quark fragmentation functions for protons and charged hadrons (separated among pions, kaons and residual mesons), in which $D_{s+\bar{s}}^{K^+}$ and $D_{u+\bar{u}}^{K^+}$ are fitted independently, to account for the expectation that the formation of $s\bar{s}$ secondary pairs should be suppressed compared to $u\bar{u}$. Indeed, they find $D_{s+\bar{s}}^{K^+}(z) > D_{u+\bar{u}}^{K^+}(z)$ over the whole z range, in contrast to all other previous work.

Using the sets of Refs. [33, 34] we can describe both π and K production data. Our best fits (see Ref. [36]) of the experimental data from HERMES, COMPASS in Figs. 4, Figs. 5, and Figs. 6 respectively.

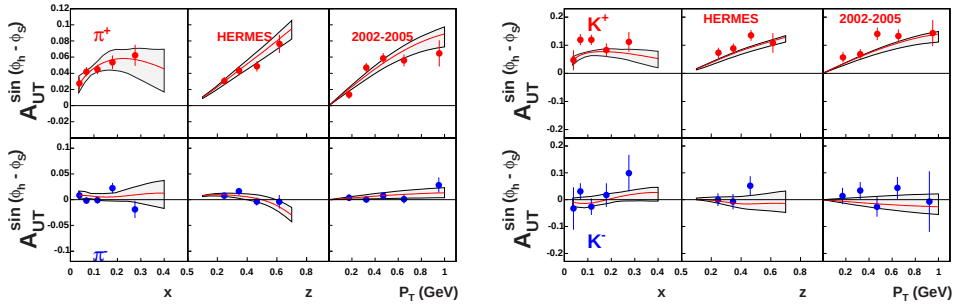

Figure 4: The results obtained from our simultaneous fit of the SIDIS $A_{UT}^{\sin\phi_h-\phi_S}$ Sivers asymmetries (solid lines) are compared to HERMES experimental data [35] for pion and kaon production (left and right panel respectively). The shaded area corresponds to the theoretical uncertainty on the parameters, see text for further details.

We have performed a combined analysis of all experimental data on spin azimuthal asymmetries which involve the transversity distributions of u and d quarks and the Collins fragmentation functions, classified as favored (when the fragmenting quark is a valence quark for the final hadron) and unfavored (when the fragmenting quark is not a valence quark for the final hadron). We have fixed the total number of 9 parameters by best fitting the HERMES, COMPASS and Belle data.

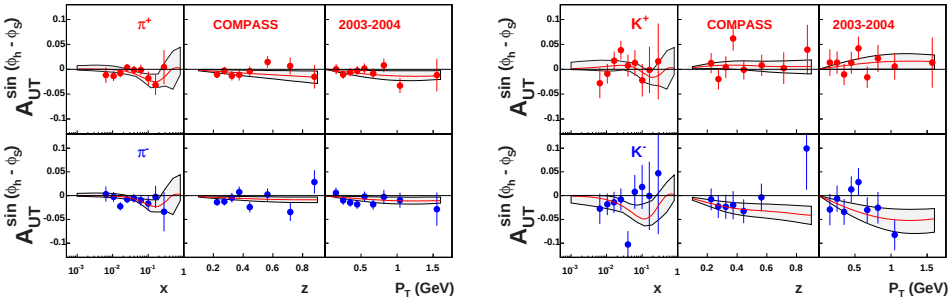

Figure 5: The results obtained from our fit (solid lines) are compared to the COMPASS measurements of $A_{UT}^{\sin\phi_h-\phi_S}$ for pion (left panel) and kaon (right panel) production [28].

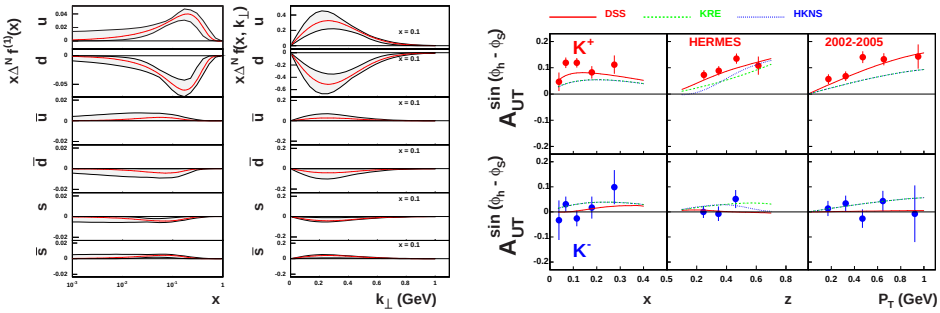

Figure 6: Sivers distribution functions for u, d and s flavours as determined by our simultaneous fit on HERMES and COMPASS (left panel). The results obtained from our fit using DSS FF Ref. [34] are compared to the results we would find by using the Sivers functions as obtained in our fit, but using the Kretzer and HKNS set [13]

All data can be accurately described, leading to the extraction of the favored and unfavored Collins functions, in agreement with similar results previously obtained in the literature [19, 18]. In addition, we have obtained, *for the first time*, an extraction of the so far unknown transversity distributions for u and d quarks, $h_{1u}(x)$ and $h_{1d}(x)$. They turn out to be opposite in sign, with $|h_{1d}(x)|$ smaller than $|h_{1u}(x)|$, and both smaller than their Soffer bound [14].

Usage of DSS FF [33, 34] allows to describe Sivers asymmetry data on π and K production, u and d Sivers distribution functions and sea Sivers functions are evaluated [36].

References

[1] V. Barone, A. Drago, and P. G. Ratcliffe, Phys. Rept. **359**, 1 (2002), hep-ph/0104283.

[2] PAX, V. Barone *et al.*, (2005), hep-ex/0505054.

[3] M. Anselmino, V. Barone, A. Drago, and N. N. Nikolaev, Phys. Lett. **B594**, 97 (2004), hep-ph/0403114.

[4] A. V. Efremov, K. Goeke, and P. Schweitzer, Eur. Phys. J. **C35**, 207 (2004), hep-ph/0403124.
[5] B. Pasquini, M. Pincetti, and S. Boffi, (2006), hep-ph/0612094.
[6] J. C. Collins, Nucl. Phys. **B396**, 161 (1993).
[7] Belle, R. Seidl *et al.*, Phys. Rev. Lett. **96**, 232002 (2006).
[8] HERMES, L. Pappalardo *et al.*, Proceedings of the XIV International Workshop on Deep Inelastic Scattering, Tsukuba City, Japan, April 20th - April 24th. (2006).
[9] COMPASS, E. S. Ageev *et al.*, (2006), hep-ex/0610068.
[10] A. Bacchetta, U. D'Alesio, M. Diehl, and C. A. Miller, Phys. Rev. **D70**, 117504 (2004), hep-ph/0410050.
[11] M. Gluck, E. Reya, and A. Vogt, Eur. Phys. J. **C5**, 461 (1998), hep-ph/9806404.
[12] M. Gluck, E. Reya, M. Stratmann, and W. Vogelsang, Phys. Rev. **D63**, 094005 (2001), hep-ph/0011215.
[13] S. Kretzer, Phys. Rev. **D62**, 054001 (2000).
[14] J. Soffer, Phys. Rev. Lett. **74**, 1292 (1995).
[15] A. Kotzinian, Nucl. Phys. **B441**, 234 (1995), hep-ph/9412283.
[16] P. J. Mulders and R. D. Tangerman, Nucl. Phys. **B461**, 197 (1996).
[17] D. Boer, R. Jakob, and P. J. Mulders, Nucl. Phys. **B504**, 345 (1997).
[18] A. V. Efremov, K. Goeke, and P. Schweitzer, Phys. Rev. **D73**, 094025 (2006).
[19] W. Vogelsang and F. Yuan, Phys. Rev. **D72**, 054028 (2005).
[20] M. Anselmino, M. Boglione, U. D'Alesio, A. Kotzinian, F. Murgia, A. Prokudin and C. Turk, Phys. Rev. D **75** (2007) 054032 [arXiv:hep-ph/0701006].
[21] M. Anselmino *et al.*, Phys. Rev. **D71**, 074006 (2005), hep-ph/0501196.
[22] M. Anselmino *et al.*, Phys. Rev. **D72**, 094007 (2005), hep-ph/0507181.
[23] HERMES, A. Airapetian *et al.*, Phys. Rev. Lett. **94**, 012002 (2005).
[24] COMPASS, V. Y. Alexakhin *et al.*, Phys. Rev. Lett. **94**, 202002 (2005), hep-ex/0503002.
[25] D. W. Sivers, Phys. Rev. **D41**, 83 (1990).
[26] D. W. Sivers, Phys. Rev. **D43**, 261 (1991).
[27] HERMES, M. Diefenthaler, (0600), arXiv:0706.2242 [hep-ex].
[28] COMPASS, A. Martin, Czech. J. Phys. **56**, F33 (2006), hep-ex/0702002.
[29] M. Hirai, S. Kumano, T. H. Nagai, and K. Sudoh, (2007), hep-ph/0702250.
[30] B. A. Kniehl, G. Kramer, and B. Potter, Nucl. Phys. **B582**, 514 (2000), hep-ph/0010289.
[31] S. Albino, B. A. Kniehl, and G. Kramer, Nucl. Phys. **B734**, 50 (2006), hep-ph/0510173.
[32] S. Albino, B. A. Kniehl, and G. Kramer, Nucl. Phys. **B725**, 181 (2005), hep-ph/0502188.
[33] D. de Florian, R. Sassot, and M. Stratmann, (0700), arXiv:0707.1506 [hep-ph].
[34] D. de Florian, R. Sassot, and M. Stratmann, Phys. Rev. **D75**, 114010 (2007), hep-ph/0703242.
[35] M. Diefenthaler, (2006), hep-ex/0612010.
[36] M. Anselmino *et al.*, paper in preparation.

Discussion

Comm. (S.Belostotsky, PNPI, St.Petersburg) 1. It is hard to accept that the explanation of problem Sivers DF measurement done by HERMES using K^+ and π^+ is related to big differences in FF. MC-tuning at HERMES to multiplicity is done well.
2. How $p_\perp$ and $k_\perp$ parameters were found from the fit to hadron TMD?

A. 1. It is exactly what I mean. None of the existing FF sets is able to describe kaon multiplicities of HERMES. De Florian et al. set was constructed to describe kaon production. In some sense it is equivalent to "tuning" Monte Carlo.

2. $< p_\perp >$ and $< k_\perp >$ were fitted to SIDIS experimental data on unpolarized cross sections measured by EMC. They describe very well $< p_\perp >$ measured by HERMES. See references in this contribution.

Q. (J.Nassalski, SINS, Warsaw) 1. Do we know the Q^2-dependence of transverse quark distributions?
2. Did you compare transversely and longitudinally polarized quark distributions?

A. 1. The evolution of transversity is known and is taken into account in our model. Gluons decouple from transversity thus its evolution is different from "usual" evolution of unpolarized and helicity distributions.
2. Thank you for your suggestion, it is easy to do in this framework and should be very instructive.

Q. (A.Efremov, JINR, Dubna) What was assumed about Sivers $\bar{s}$ and $\bar{d}$ in fitting K^+ data?

A. In this analysis we separate sea Sivers functions for $\bar{s}$ and $\bar{d}$ quarks, x and $k_\perp$ dependence is assumed to be the same. $\bar{s}$ Sivers function and $\bar{d}$ Sivers function were found to have opposite signs.

DOMINANT CONTRIBUTION IN PION PRODUCTION SINGLE-SPIN ASYMMETRIES

Philip G. Ratcliffe[1,2 †], Marco Ramilli[1]

(1) *Dipartimento di Fisica e Matematica, Università degli Studi dell'Insubria*
(2) *Istituto Nazionale di Fisica Nucleare, Sezione di Milano*
† *E-mail: philip.ratcliffe@uninsubria.it*

Abstract

Working with a completely collinear twist-3 factorized cross-section formula, we identify two largely dominant partonic sub-processes, which contribute to the single-spin asymmetries in semi-inclusive pion production, in the region of large p_T and medium–large x_F.

1 Introduction

During the past years, different models have been developed in an attempt to explain the mechanism behind the single-spin asymmetries observed experimentally in high-energy hadronic interactions. The approach based on the study of the hadronic cross-section contribution given by the twist-3 components in the operator product expansion of parton matrix elements turns out to be particularly interesting: taking into account such terms provides a consistent model. However, at the same time the complexity of the calculational framework unfortunately increases, since twist-3 contribution are characterized by the presence of an additional gauge-field term, which in turn implies an *extra gluon* in the sub-processes, see for example [1, 2].

Restricting our analysis therefore to a particular class of processes (pion production in proton–proton collisions), our principal aim is to identify which, if any, among all possible partonic sub-processes provide the dominant contributions to the asymmetry and to understand the origin of the suppression of the other terms. We can thus list a set of criteria (which we call *"selection rules"*) summarizing these mechanisms. To simplify our analysis, we shall extract a totally collinear cross-section formula, in the axial gauge and in the limit of $x_F \to 1$, valid for large p_T.

2 The model

We shall now go into detail, first by providing an expression for the twist-3 contribution to the cross-section through the study of the pole behavior of the Bjorken variables, and then by analyzing the causes of the suppression of many other sub-processes.

2.1 The poles

Working in axial gauge, thus setting $A^+ = 0$, allows us to write the twist-3 contribution to the cross-section in the following way:

$$d\sigma^{(\tau=3)} \simeq \mathrm{Tr}\left\{\Phi_A^\alpha(x_1, x_2)\mathrm{S}^\beta(x_1, x_2)\right\} g_{\perp\alpha\beta}, \tag{1}$$

where $\Phi_A^\alpha(x_1, x_2)$ is the multi-parton matrix element and the index α is completely transverse, due to gauge choice. Moreover, in the axial gauge, the relation between $\Phi_A^\alpha(x_1, x_2)$ and $\Phi_F^\alpha(x_1, x_2)$ assumes a very simple form (see [3], Eq. 7.3.30):

$$(x_2 - x_1)\Phi_A^\alpha(x_1, x_2) = -i\Phi_F^\alpha(x_1, x_2), \tag{2}$$

demonstrating that if $\Phi_F^\alpha(x_1, x_2)$ is different from zero for $x_1 = x_2$, then $\Phi_A^\alpha(x_1, x_2)$ must have a pole.

The analysis of the hard part is also crucial for the pole structure; there are two different possibilities for the extra gluon, generated at twist-3, to interact significantly: with the on-shell fragmenting parton (the so-called final-state interactions, FSI) and with the on-shell parton coming from the unpolarized nucleon (initial-state interactions, ISI); the important feature of these interactions is the presence of an extra internal propagator, whose Dirac structure has the form

$$\cdots \frac{\not{k}}{2(P\cdot k)} \left(\frac{2k_\alpha - (x_2 - x_1)\gamma_\alpha \not{P}}{x_2 - x_1 - i\varepsilon} \right) \cdots , \tag{3}$$

where k^μ is the four-momentum of the on-shell parton and P^μ is the four-momentum of the polarized hadron.

By also taking into account the pole behavior originating in the multi-parton matrix element, it is possible to separate the trace over the Dirac indices into two traces, each one with a different pole structure: the first, known as the *single-pole* contribution, where the $(x_2 - x_1)$ term in the numerator cancels the pole contribution of the matrix element, and the other, called the *double-pole* contribution, where no such cancellation occurs. In order to maintain the cross-section a real quantity, we are forced to take the imaginary part of these poles, remembering that

$$\mathrm{Im}\left(\frac{1}{(x_2 - x_1 \pm i\varepsilon)} \right) = \mp i\pi\delta(x_2 - x_1), \tag{4}$$

$$\mathrm{Im}\left(\frac{1}{(x_2 - x_1 \pm i\varepsilon)^2} \right) = \mp i\pi\delta'(x_2 - x_1). \tag{5}$$

Using these relations and integrating the derivative of the delta function by parts, we obtain the following expression for the twist-3 contribution to the cross-section:

$$d\sigma^{(\tau=3)} = \int dx\, dx'\, \frac{dz}{z^3}\, \varepsilon_T^{P_h S_\perp} \left\{ \frac{dG_F(x,x)}{dx} H_{DP}(x, x', z) + G_F(x,x) H_{SP}(x, x', z) \right\} f(x')\, D(z), \tag{6}$$

where we have omitted the color factors and the sum over flavor indices; $\varepsilon_T^{\mu\nu}$ is the antisymmetric tensor in the transverse directions, $G_F(x, x)$ is the multi-parton distribution function evaluated at the pole (owing to the delta functions), $f(x')$ is the unpolarized quark density and H represents the hard-scattering partonic cross-sections, with DP and SP standing respectively for double pole and single pole.

2.2 "Selection Rules"

Given such an expression for the cross-section at twist three, we list here the set of principles we have adopted to identify the possibly dominant contributions:

- first, we expect DP contributions to be much more relevant than SP ones, owing to the presence of the derivative of the multiparton density function, which endows the asymmetry with a behavior in x roughly as $A_N \sim \frac{1}{(1-x)}$ (for x_F approaching unity, the Bjorken x of the incoming parton also approaches unity), thus enhancing the contribution of such terms for growing x_F;

- for $x_F \to 1$ and $|T| \ll |U| \ll |S|$, we expect the t-channel diagrams to be dominant; for the same reason, remembering the power suppression of the hard parts given in Eq. 3, we expect FSI to give a greater contribution than ISI;

- we neglected the contributions given by polarized gluons and by sea quarks since these may reasonably be expected to be small.

In order to test our model and the selection rules described above, we have evaluated the single-spin asymmetries for the reaction $p^{\uparrow}p \to \pi^0 + X$ for the STAR kinematical range ($\sqrt{S} = 200\,\mathrm{GeV}$ and $1.3\,\mathrm{GeV}/c < P_{hT} < 2.8\,\mathrm{GeV}/c$, see for example [4]). Restricting our analysis to the contribution given only by the t-channel diagram involved in the process, in Fig. 1a we present a comparison between the data points and the resulting prediction given by our model; we note that there is good agreement with data for values of x_F greater than $0.4 - 0.5$.

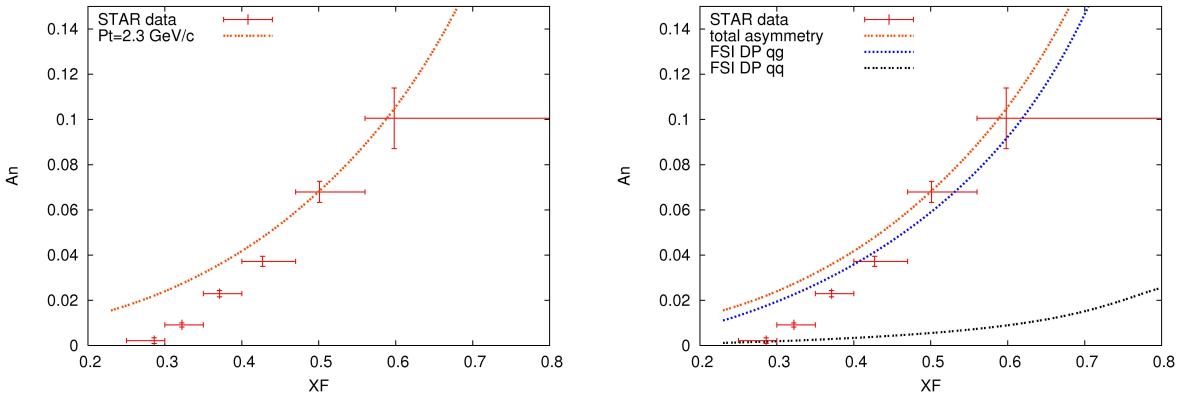

(a) (b)

Figure 1. **(a)** The theoretical curve represents the prediction for the SSA in π^0 production evaluated at $P_{hT} = 2.3$ GeV/c, compared to STAR data points. **(b)** Here we plot the same curve as in Fig. 1a, compared to the FSI DP term in a quark–gluon (here labeled qg) sub-process and the FSI DP in a quark–quark subprocess.

In Fig. 1b we also plot the total asymmetry, but together with the contribution given by the two major sub-processes we have identified, i.e. the t-channel FSI DP terms. Comparing these curves, we can see how the two sub-processes mentioned provide almost entirely the value of the asymmetry in the kinematical range of $x_F > 0.4$; for lower values of this variable, we expect all the neglected contribution to become more important.

3 Conclusions

To summarize then:

- we have obtained an expression providing predictions for the single-spin asymmetries for pion production consistent with data, in a completely collinear framework, without appealing to any collinear expansion;

- using such an expression and a simple set of criteria, we have also been able to identify two largely dominant subprocesses, which are almost entirely responsible for the asymmetries in the $x_F \to 1$ limit.

References

[1] A.V. Efremov and O.V. Teryaev, Phys. Lett. B **150**, 383 (1985).

[2] J.W. Qiu and G. Sterman, Phys. Rev. D **59**, 014004 (1998).

[3] V. Barone, A. Drago and P.G. Ratcliffe, Phys. Rept. **359**, 1 (2002).

[4] L. Nogach (STAR collab.), in proc. of the XVII Int. Symp. on High-Energy Spin Physics, eds. K. Imai, T. Murakami, N. Saito and K. Tanida (Kyoto, 2006), p. 543.

SPIN-ORBIT DYNAMICS FROM THE GLUON ASYMMETRY

Y. Binder[1], G.P. Ramsey[2†] and D. Sivers[3]

(1) *Loyola University Chicago, Chicago, IL USA*
(2) *Loyola University Chicago, Chicago, IL USA and Argonne National Lab, IL, USA*
(3) *Portland Physics Institute, Portland, OR USA and University of Michigan, USA*
† *E-mail: gpr@hep.anl.gov*

Abstract

Determination of the orbital angular momentum of the proton is a difficult but important part of understanding fundamental structure. Insight can be gained from suitable models of the gluon asymmetry applied to the $J_z = 1/2$ sum rule. We have constrained the models of the asymmetry to gain possible scenarios for the angular momentum of the proton constituents. Results and phenomenology for determining L_z are presented.

1 Status of Proton Spin Structure

For the past twenty years, much work has been done to understand the spin structure of the nucleons. There has been progress in determining the contribution of the lightest quarks to the spin, but there is still uncertain knowledge about the gluon contribution. Transversity studies have contributed additional insight about quark dynamics, but little is known about the the orbital angular momentum of the constituents. [1] This paper will summarize a project that provides a method of gaining insight into the nature of the orbital angular momentum of the nucleon constituents.

Recent experiments [15, 4] have significantly lowered the measurement errors of the quark longitudinal spin contribution ($\Delta\Sigma$) to the proton. The COMPASS collaboration analysis quotes a result

$$\Delta\Sigma = 0.30 \pm 0.01(\text{stat}) \pm 0.02(\text{evol}), \qquad \text{all data} \tag{1}$$

while the HERMES collaboration analysis quotes a result

$$\Delta\Sigma = 0.330 \pm 0.025(\text{exp}) \pm 0.011(\text{th}) \pm 0.028(\text{evol}), \qquad \text{all data.} \tag{2}$$

These groups and others [1] have been working on providing a significant measure of the proton's spin weighted gluon density,

$$\Delta G(x,t) \equiv G_{++}(x,t) - G_{+-}(x,t), \tag{3}$$

where x is the Bjorken scaling variable and $t \equiv \log(\alpha_s(Q_0^2)/\log(\alpha_s(Q^2))$ is the Q^2 evolution variable. The combination of these measurements is summarized in terms of the $J_z = \frac{1}{2}$ sum rule:

$$J_z = \frac{1}{2} \equiv \frac{1}{2}\Delta\Sigma + \Delta G + L_z. \tag{4}$$

Here $\Delta\Sigma = \int_0^1 dx \Delta q(x,t)$ and $\Delta G = \int_0^1 dx \Delta G(x,t)$ are the projections of the spin carried by all quarks and the gluons on the z-axis, respectively. Also L_z is the net z-component of the orbital angular momentum of the constituents. We do not attempt to separate the flavor components of L_z within the sum rule.

2 Modeling the Gluon Asymmetry

Experimental groups at the COMPASS, HERMES and RHIC collaborations are measuring both the gluon polarization and the asymmetry, $A \equiv \Delta G/G$ to determine the gluon polarization [15,4,1]. Since there is no suitable theoretical model for ΔG, we have devised a way to model the asymmetry, $A(x,t)$ to gain insight into the structure of ΔG. This, coupled with the $J_z = \frac{1}{2}$ sum rule can then shed light on the nature of the orbital angular momentum of the constituents, L_z. To model $A(x,t)$, we write the polarized gluon asymmetry using the decomposition

$$A(x,t) \equiv \Delta G/G = A_0(x) + \epsilon(x,t), \tag{5}$$

where

$$A_0(x) \equiv \Big[(\frac{\partial \Delta G}{\partial t})/(\frac{\partial G}{\partial t})\Big] \tag{6}$$

is a scale invariant calculable reference form [5]. Here $\epsilon(x,t)$ represents the difference between the calculated and measured asymmetry. Since ΔG is unknown, a useful form is to write equation (5) as

$$\Delta G = A_0(x)\, G(x,t) + \Delta G_\epsilon(x). \tag{7}$$

Although the quantity $\Delta G_\epsilon(x)$ is not a physical parameter, it allows the theoretical development of the calculable quantity, A_0. Once an asymmetry is generated from equations (6) and (7), the measurable quantity $A(x,t)$ can be compared to data. Thus, each Ansatz for $\Delta G_\epsilon(x)$ gives a corresponding form for ΔG and a parameterization for L_z. These can be compared to existing data to provide a range of suitable models for these contributions.

With the definition for the asymmetry in equation (6), the DGLAP equations can then be used to evaluate the evolution terms on the right side.

$$A_0 = \left[\frac{\Delta P_{Gq} \otimes \Delta q + \Delta P_{GG} \otimes \Delta G}{P_{Gq} \otimes q + P_{GG} \otimes G}\right]. \tag{8}$$

The polarized gluon distribution in the numerator of equation (8) is replaced by $\Delta G \equiv A_0 \cdot G + \Delta G_\epsilon$. For certain unpolarized distributions, there are points at which the denominator vanishes. To avoid this, we write equation (8) as:

$$\begin{aligned} \frac{\partial \Delta G}{\partial t} &= (2/\beta_0)\Big[\Delta P_{gq}^{LO} \otimes \Delta q + \Delta P_{gg}^{LO} \otimes (A_0 \cdot G + \Delta G_\epsilon)\Big] \\ &= A_0 \cdot \frac{\partial G}{\partial t} = (2/\beta_0) A_0 \Big[P_{gq}^{LO} \otimes q + P_{gg}^{LO} \otimes G\Big]. \end{aligned} \tag{9}$$

The NLO form is essentially the same as equation (9) with the splitting functions P^{LO} replaced with their NLO counterparts. The quark and gluon unpolarized distributions are CTEQ5 and the polarized quark distributions are a modified GGR set. [6]

There are constraints on $A_0(x)$ that must be imposed to satisfy the physical behavior of the gluon asymmetry, $A(x)$. These are:

- positivity: $|A_0(x)| \leq 1$ for all x, and
- endpoint values: $A_0(0) = 0$ and $A_0(1) = 1$

Note that the constraint of $A_0 \to 1$ is built in to satisfy the assumption that the large x parton distributions are dominated by the valence up quarks in the proton. The convolutions are dominated by the quark terms, forcing the asymmetry to unity as $x \to 1$. To investigate the possible asymmetry models, we parameterize A_0 in the form

$$A_0 \equiv Ax^\alpha - (B-1)x^\beta + (B-A)x^{\beta+1}, \tag{10}$$

which automatically satisfies the constraints that $A_0(0) = 0$ and $A_0(1) = 1$. Once $\Delta G_\epsilon(x)$ is chosen, equation (9) is used to determine the parameters in equation (10).

3 Results and Conclusions

The models for $\Delta G_\epsilon(x)$ that led to asymmetries that satisfied these constraints were all in the range $|\int_0^1 \Delta G_\epsilon dx| \leq 0.25$, with positive and negative values included. Larger values of ΔG_ϵ violate one or more of the constraints. A representative sample of models that satisfy the constraints are listed in Table 1.

Table 1: Gluon Asymmetry Parameters

ΔG_ϵ	$\int_0^1 \Delta G_\epsilon dx$	A_0	$\int_0^1 \Delta G dx$
0	0	$3x^{1.5} - 3x^{2.2} + x^{3.2}$	0.18
$2(1-x)^7$	0.25	$4x^{1.6} - 4x^{2.1} + x^{3.1}$	0.42
$-2(1-x)^7$	-0.25	$1.75x^{1.1} - 1.5x^{2.1} + 0.75x^{3.1}$	0.01
$-90x^2(1-x)^7$	-0.25	$3.5x^{1.3} - 4.5x^{2.2} + 2x^{3.2}$	0.05
$9x(1-x)^7$	0.125	$3.75x^{1.4} - 3x^{1.6} + 0.25x^{2.6}$	0.29
$-9x(1-x)^7$	-0.125	$3.25x^{1.4} - 3.75x^{2.2} + 1.5x^{3.2}$	0.11
$4.5x(1-x)^7$	0.0625	$2x^{0.9} - 1.5x^{1.2} + 0.5x^{2.2}$	0.37
$-4.5x(1-x)^7$	-0.0625	$2.25x^{1.1} - 2.25x^{1.9} + x^{2.9}$	0.23

Note that the integrals for ΔG are all positive, ranging from about 0.01 to 0.42. The models that gave negative values for these integrals did not agree with the existing asymmetry data, reported at this workshop to be:

- $\Delta G/G = 0.016 \pm 0.058 \pm 0.055$ at $x = 0.09$ from COMPASS, $Q^2 > 1$ GeV^2
- $\Delta G/G = 0.060 \pm 0.31 \pm 0.06$ at $x = 0.13$ from COMPASS, $Q^2 < 1$ GeV^2
- $\Delta G/G = 0.078 \pm 0.034 \pm 0.011$ at $x = 0.204$ from HERMES, factorization method
- $\Delta G/G = 0.071 \pm 0.034 \pm 0.010$ at $x = 0.222$ from HERMES, approximate method.

The models in Table 1 that are within one σ of the preliminary data reported in these proceedings are in the third, fourth and sixth rows, respectively. Plots of the full asymmetry are shown in Figure 1. None of the models shown are ruled out by the data since they fall within two σ of the data and our values of $Q^2 > 1$ GeV^2. All of these models except for the fourth row in the table generate asymmetries $A(x, t = 0)$ that are close to $A(x) = x$. Ironically, early assumptions of the polarized gluon assumed this functional

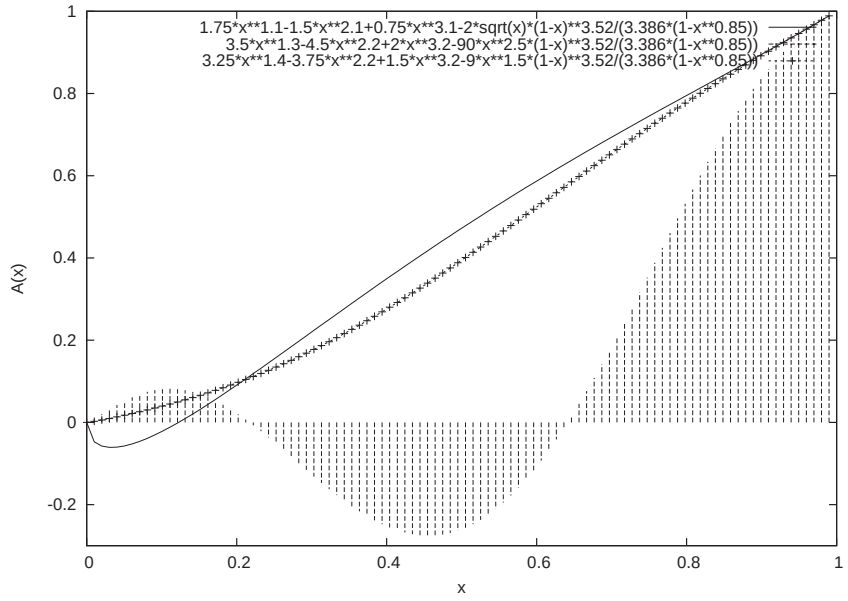

Figure 1: The gluon asymmetries most closely in agreement with data. Solid line, impulses and linepoints represent the models in rows 3, 4 and 6 of Table 1 respectively.

form as a naive estimate. Next-to-leading order corrections to these asymmetries tend to bring them less positive, but with the same general shape.

Using the data on $\Delta\Sigma$, the relation between $< \Delta G >$ and $< L_z >$ can be written as:

$$< \Delta G >= 0.35 - < L_z > \pm 0.02. \tag{11}$$

The models agreeing most closely with existing data imply that ΔG is in the approximate range $(0 \rightarrow 0.11)$. Thus, with existing data, we have the approximate relation $0.24 \leq L_z \leq 0.35 \pm 0.02$. Clearly, future measurements of ΔG and $\Delta G/G$ must increase the kinematic range in x and Q^2 with improved precision to better specify the appropriate model of the asymmetry and extract the x dependence of the constituents' orbital angular momentum.

References

[1] X. Ji, AIP Conf. Proc. **915**: 16, 2007, X. Ji, Phys. Rev. Lett. **78**, 610 (1997).

[2] See talk by Y. Bedfer, this proceedings.

[3] See talk by S. Belostotski, this proceedings.

[4] See talk by G. Bunce, this proceedings.

[5] G. Ramsey, Proceedings of the 16th International Spin Physics Symposium, Trieste, Italy, c2005, World Scientific Press, p. 310.

[6] L.E. Gordon, M. Goshtaspbour and G.P. Ramsey, Phys. Rev. **D58**, 094017 (1997).

GENERALIZED PARTON DISTRIBUTIONS AND NUCLEON FORM FACTORS

O.V. Selyugin[1†] and O.V. Teryaev[1††]

(1) *Bogoliubov Laboratory of Theoretical Physics,*
Joint Institute for Nuclear Research, 141980 Dubna, Moscow region, Russia
† *E-mail: selugin@theor.jinr.ru*
†† *E-mail: teryaev@theor.jinr.ru*

Abstract

The Dirac and Pauli form factors of the proton and neutron are obtained in the framework of the generalized parton distributions (GPDs) with some simple momentum transfer dependence. It is shown that both sets of the existing experimental data on the form factors, obtained by the Rosenbluth and polarization transfer, can be described by changing only the slope of the GPDs E. The description of neutron form factors is substantially better when the proton data obtained by the studies of polarization transfer are used.

1 Introduction

The determination of the hadron structure is related with our understanding of the non-perturbative properties of the QCD. Generalized parton distributions (GPDs) [1] for $\xi = 0$ provide information about the distribution of the partons in impact parameter space [2]. It is correlated with t-dependence of GPDs. Now we cannot obtain this dependence from the first principles; instead, it may be obtained from the phenomenological description of the nucleon electromagnetic form-factors.

Following [3], we limit ourselves to the case of GPDs with $\xi = 0$ corresponding to the non-forward parton densities so that the form factors can be represented as

$$F_1^q(t) = \int_0^1 dx\ \mathcal{H}^q(x,t), \tag{1}$$

$$F_2^q(t) = \int_0^1 dx\ \mathcal{E}^q(x,t), \tag{2}$$

We assume the validity of Gaussian ansatz which was used in [3] to describe the form factors of proton. However, this ansatz leads to a faster decrease in F_1 at larger momentum transfer. Although this region is, strictly speaking, outside the domain of validity of QCD factorization involving GPDs, one may consider also the problem of t-dependence of GPDs at large t [4]. It was shown that at large $x \to 1$ and momentum transfer the behavior of GPDs requires a (larger) power dependence on $(1-x)$ in the $t-$ dependent exponent:

$$\mathcal{H}^q(x,t)\ \sim exp[a\ (1-x)^n\ t]\ q(x). \tag{3}$$

with $n \geq 2$. It was noted that $n = 2$ naturally gives rise to Drell-Yan-West duality between parton distributions at large x and the form factors. Various more elaborated parameterizations were considered later, see e.g. [5].

2 Momentum transfer dependence of GPDs and proton form factors

Our proposal consists in the attempt to find a simple ansatz which will be good enough to describe the form factors of the proton and neutron taking into account a number of new data that have appeared in the last years. Let us keep the simple Gaussian ansatz but using some new conditions. To support the proposal [3] and [4] we chose the t-dependence of GPDs in the form

$$\mathcal{H}^q(x,t) \ = q(x)\ exp[a_+\ \frac{(1-x)^2}{x^b}\ t]; \quad \mathcal{E}^q(x,t) \ = \mathcal{E}^q(x)\ exp[a_-\ \frac{(1-x)^2}{x^b}\ t]. \qquad (4)$$

with the free parameters $b = 0.4$ (determined mostly by the power 2 of the factor $1-x$), $a_\pm$ (a_+ - for $\mathcal{H}$ and a_- - for $\mathcal{E}$). All these parameters were fixed by analyzing the data on the ratio of proton Pauli and Dirac form-factors. The function $q(x)$ was taken in the same normalization point $\mu^2 = 1$ GeV^2 as in [6], which is based on the MRST2002 global fit [11]. In all our calculations we restricted ourselves to the contributions of u and d quarks in $\mathcal{H}^q$ and $\mathcal{E}^q$ with $\mathcal{E}^u(x) \ = k_u/N_u(1-x)^{\kappa_1}\ u(x), \quad \mathcal{E}^d(x) \ = \frac{k_d}{N_d}(1-x)^{\kappa_2}\ d(x)$, (where $\kappa_1 = 1.53$ and $\kappa_2 = 0.31$ [6]) According to the normalization of the Sachs form factors, we have $k_u = 1.673, \quad k_d = 2.033, \quad N_u = 1.53, \quad N_d = 0.946$. The parameters $a_+ = 0.675$ and a_- correspond to the two experimental methods of the determination of the ratio of the Pauli and Dirac form factors. Below we consider version (I - polarization transfer method) leading to $a_- = 0.59$ and version (II - Rosenbluth separation) leading to $a_- = 0.7$.

The proton Dirac form factor, calculated in this work and multiplied by t^2, is shown in Fig.1a in comparison with the other works ([6], [8]) and experimental data. One can see, that our calculations sufficiently well reproduces the behavior of experimental data not only at high t but also at low t.

The ratio of the Pauli to the Dirac proton form factors multiplied by t is shown in Fig.1b. There are two different sets of experimental data. Firstly, one may extract the form factors of the proton from the unpolarized differential cross section by the Rosenbluth

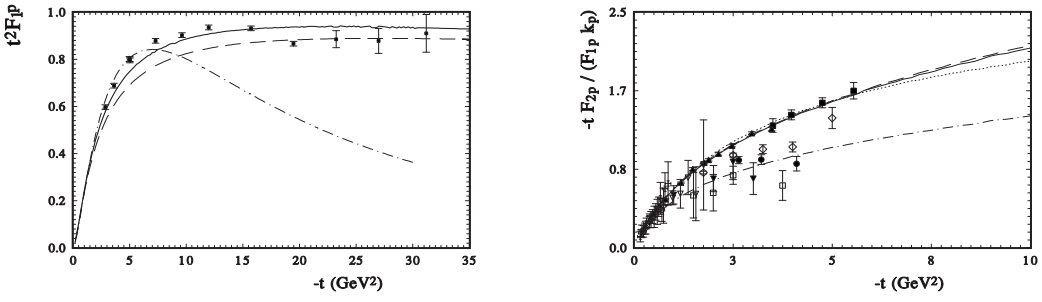

(a) **(b)**

Figure 1a. Proton Dirac form factor multiplied by t^2 (hard line - the present work, dot-dashed line - [3]; long-dashed line - [6]; the data for F_1^p are from [9].

Figure 1b. Ratio of the Pauli to Dirac proton form factors multiplied by t (hard and dot-dashed lines correspond to version (I) and (II)) of the present work , dotted line - [10]; long-dashed line - [6]) ; the data are from [11].

method. The other method uses the polarized differential cross section to obtain these form factors. In our model we can obtain the results of both methods by changing the slope of $\mathcal{E}$. So we examined two versions differing by the slopes a_-.

One can now use the information on the neutron form factors in order to choose the more realistic version.

3 Neutron form factors

Using the model developed for proton we can calculate the neutron form factors. For that the isotopic invariance can be used to relate the proton GPDs to the neutron ones, Hence, we do not change any parameters and preserve the same t-dependence of GPDs as in the case of proton.

Again, we take two values of the slope a_- as in the case of the proton form factors with the same size, which correspond to version (I) and version (II) below.

Our calculation of the G_E^n is shown in Fig. 2a. Evidently, the first version is in better agreement with experimental data. Therefore, neutron data support the results obtained by polarization transfer method.

This conclusion is supported by the calculations of G_M^n shown in Fig.2b. In this case, it is clearly seen that our parameterization normalized using the *proton* form-factors ratio from the polarization experiments describes these *neutron* data quite well.

4 Conclusions

The proposed version of Gaussian t-dependence of GPDs reproduces the electromagnetic structure of the proton and neutron sufficiently well. We show that changing only the slope parameters a_- of $\mathcal{E}^q$ it is possible to obtain both the Rosenbluth and Polarization data on the ratio of Pauli and dirac electromagnetic proton form-factors. The description of neutron form-factors is essentially better with the slope parameter fitted to proton polarization transfer data. This is in accordance with the recent theoretical analysis [14].

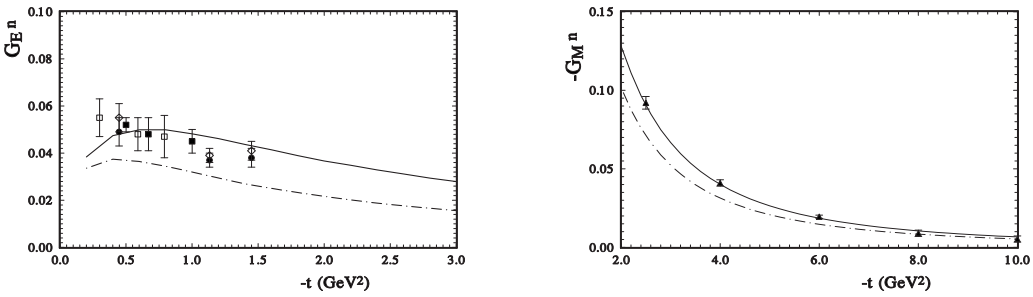

(a) **(b)**

Figure 2a. G_E^n (hard and dot-dashed lines correspond to version (I) and (II)); experimental data from [12].

Figure 2b. G_M^n (hard and dot-dashed lines correspond to version (I) and (II)); experimental data from [13].

Acknowledgments. We are indebted to M. Anselmino, S.V. Goloskokov, P. Kroll, E. A. Kuraev, E. Predazzi and E. Tomasi-Gustafsson for useful discussions. This work was partially supported by the Deutsche Forschungsgemeinschaft, grant 436 RUS 113/881/0, the Russian Foundation for Basic Research (Grant 03-02-16816) and the Russian Federation Ministry of Education and Science (Grant MIREA 2.2.2.2.6546).

References

[1] D. Muller et al., Fortschr. Phys. **42**, 101 (1994); X. Ji, Phys.Rev. Lett. **78**, 610 (1998); A.V. Radyushkin, Phys.Rev, D **56**, 5524 (1997).

[2] M. Burkardt , Phys. Rev. D **62**, 071503 (2000).

[3] A. V. Radyushkin, Phys. Rev. D **58**, 11400 (1998).

[4] M. Burkardt , Phys.Lett. B **595**,245 (2004).

[5] M.Diehl, Th Feldmann, R. Jakob and P.Kroll, Eur.Phys. J. C **39**,1 (2005).

[6] M. Guidal, M.V. Polyakov, A.V. Radyushkin, and M. Vanderhaeghen, Phys. RevD (2005).

[7] A.D. Martin *et al.*, Phys. Lett. B **531**, 216 (2002).

[8] P.Stoler, Phys.Rev. D **65** (2002) 053013; Phys.Rev. Lett., **91**,172303 (2003).

[9] A.F. Sill *et al.*, Phys.Rev. D **48**, 29 (1993).

[10] S.J. Brodsky , hep-ph/0208158 .

[11] M.K. Jones *et al.*, Phys.Rev. Lett., **84**, 1398 (2000); O. Gayou *et al.*, Phys.Rev. C **64**, 038202 (2001); O. Gayou *et al.*, Phys.Rev. Lett., **88**, 092301 (2002); V. Punjabil *et al.*, Phys.Rev. C **71**, 055202 (2005).

[12] B. Plaster *et al.*, Phys.Rev. C **73**, 025205 (2006); R. Madey, *et al.*, Phys.Rev. Lett. **91**, 122002 (2003); I. G. Warren, *et al.*, Phys.Rev. Lett. **92**, 042301 (2004) .

[13] S. Rock, *et al.*, Phys.Rev. Lett. **49**, 1139 (1982).

[14] Yu. M. Bystritskiy, E. A. Kuraev and E. Tomasi-Gustafsson, Phys. Rev. C **75** (2007) 015207.

Discussion

Comm.(L.Jenkovszky, ITP, Kiev) For simplicity, however, the model should contains also singularities that manifest experimentally as well as "hard" effects at large $|t|$.

RESEARCH ON DRELL-YAN AND J/ψ PHYSICS AT J-PARC AND COMPASS

A. Sissakian, O. Shevchenko, A. Nagaytsev, O. Ivanov

Joint Institute for Nuclear Research, Dubna, Russia

Abstract

The feasibility is studied of the asymmetries which give the direct access to transversity as well as to k_T dependent T-odd PDFs via investigation of unpolarized and single-polarized Drell-Yan (DY) processes. The estimations performed for J-PARC and RHIC kinematics demonstrate that there exist the such kinematical regions where these asymmetries are presumably measurable. It is also studied the model on J/ψ production allowing to extract parton distribution functions from the combined analysis with both data on Drell-Yan and J/ψ production processes. It is shown that this, so attractive from theoretical point of view, model, can be safely used in the low energy region $E \lesssim 100GeV$.

The leading twist k_T integrated transversity PDF $\Delta_T q \equiv h_{1q}$, as well as the leading twist unpolarized $q \equiv f_{1q}$ and longitudinally polarized (helicity) $\Delta q \equiv g_{1q}$ PDFs, is of the crucial importance for understanding of the nucleon spin structure. At the same time, nowadays the study of transverse momentum k_T dependent PDFs is also among the special issues in hadron physics. Of particular interest, are two leading-twist T-odd k_T dependent PDFs: Sivers function $f_{1T}^{\perp q}(x, k_T^2)$ and Boer-Mulders function $h_{1q}^{\perp}(x, k_T^2)$. Recently it was shown [2] that not only the double polarized DY processes but also the unpolarized and single-polarized DY processes can give us an access to these PDFs. In the papers [2] we considered the DY processes with antiproton-proton and pion-proton collisions. At the same time the DY processes with proton-proton collisions are also very important since they provide the access to sea PDFs. The such experiments are planned at RHIC and J-PARC. Here we will consider the single-polarized DY process $pp^{\uparrow} \to l^+l^-X$ and estimate two types of single-spin asymmetries (SSA), which give us respectively access to Sivers PDF [1]

$$A_{UT}^{\sin(\phi-\phi_S)\frac{q_T}{M_N}} = 2\frac{\sum_q e_q^2[\bar{f}_{1T}^{\perp(1)q}(x_{p^{\uparrow}})f_{1q}(x_p) + (q \to \bar{q})]}{\sum_q e_q^2[\bar{f}_{1q}(x_{p^{\uparrow}})f_{1q}(x_p) + (q \to \bar{q})]}, \tag{1}$$

and to transversity and Boer-Mulders PDFs [2]:

$$A_{UT}^{\sin(\phi+\phi_S)\frac{q_T}{M_N}} = -\frac{\sum_q e_q^2[\bar{h}_{1q}^{\perp(1)}(x_p)h_{1q}(x_{p^{\uparrow}}) + (q \to \bar{q})]}{\sum_q e_q^2[\bar{f}_{1q}(x_p)f_{1q}(x_{p^{\uparrow}}) + (q \to \bar{q})]}. \tag{2}$$

At first sight it seems that DY processes with proton-proton collisions are strongly suppressed because there is no valence antiquark in the initial state there. However, on the contrary to valence PDFs, the sea PDFs dominate at small x and rapidly die out when x increases. Thus, in the case of $pp^{\uparrow}$ collisions it is very important to find the

regions where the sea PDFs are given at small Bjorken x, while, by virtue of the relation $x_p x_{p^\uparrow} = Q^2/s$, the valence PDFs occur at large x. In such the regions we can neglect the contributions to SSA containing sea PDFs at large x and, thereby, to essentially cancel the number of extra unknown PDFs entering the asymmetries. Let us consider two limiting cases $x_p \gg x_{p^\uparrow}$ and $x_p \ll x_{p^\uparrow}$

In the first case, neglecting the terms containing the sea PDFs at large x_p, taking into account the quark charges and u quark dominance at large x, Eqs. (1) and (2) are essentially given by $A_{UT}^{\sin(\phi-\phi_S)\frac{q_T}{M_N}}\Big|_{x_p \gg x_{p^\uparrow}} \simeq 2\frac{\bar{f}_{1T}^{\perp(1)u}(x_{p^\uparrow})}{\bar{f}_{1u}(x_{p^\uparrow})}$, $A_{UT}^{\sin(\phi+\phi_S)\frac{q_T}{M_N}}\Big|_{x_p \gg x_{p^\uparrow}} \simeq -\frac{h_{1u}^{\perp(1)}(x_p)\bar{h}_{1u}(x_{p^\uparrow})}{f_{1u}(x_p)\bar{f}_{1u}(x_{p^\uparrow})}$. Analogously, in the second limiting case one gets $A_{UT}^{\sin(\phi-\phi_S)\frac{q_T}{M_N}}\Big|_{x_p \ll x_{p^\uparrow}} \simeq 2\frac{f_{1T}^{\perp(1)u}(x_{p^\uparrow})}{f_{1u}(x_{p^\uparrow})}$, $A_{UT}^{\sin(\phi+\phi_S)\frac{q_T}{M_N}}\Big|_{x_p \ll x_{p^\uparrow}} \simeq -\frac{\bar{h}_{1u}^{\perp(1)}(x_p)h_{1u}(x_{p^\uparrow})}{f_{1u}(x_p)f_{1u}(x_{p^\uparrow})}$. It is easy to check that these approximations are indeed work quite well.

To study the feasibility of SSA (1) and (2) for the kinematical conditions of J-PARC facility, we performed the preliminary estimations using available in the literature information on Sivers, Boer-Mulders and transversity PDFs. To this end we use the three different fits for the Sivers function: fits I and II from Ref. [1] and also the latest fit from Ref. [3], which we denote as fit III. For the first moment of the sea Sivers PDF entering Eq. (1) we use the model (with the positive sign) proposed in Ref. [4]: $\frac{f_{1T}^{\perp(1)\bar{q}}(x)}{f_{1T}^{\perp(1)q}(x)} = \frac{f_{1\bar{u}}(x)+f_{1\bar{d}}(x)}{f_{1u}(x)+f_{1d}(x)}$. Since neither the Boer-Mulders function nor its first moment are still not measured, we use in our calculation the Boer's model [5]. We also apply the following assumption for the first moment of the sea Boer-Mulders PDF $\frac{h_{1\bar{q}}^{\perp(1)}(x)}{h_{1q}^{\perp(1)}(x)} = \frac{f_{1\bar{q}}(x)}{f_{1q}(x)}$. To estimate the transversity, we applied two versions of evolution model [6]. First is the model where the Soffer inequality is saturated [6]: $h_{1q}(x,Q_0^2) = \frac{1}{2}\left[q(x,Q_0^2) + \Delta q(x,Q_0^2)\right]$, $h_{1\bar{q}}(x,Q_0^2) = \frac{1}{2}\left[\bar{q}(x,Q_0^2) + \Delta\bar{q}(x,Q_0^2)\right]$ at low initial scale ($Q_0^2 = 0.23GeV^2$), and then h_{1q}, $h_{1\bar{q}}$ are evolved with DGLAP. In the second version the valence and sea transversity PDFs are assumed to be equal to helicity PDF Δq at the same initial scale. The results for J-PARC kinematics are presented in Fig. 1.

Looking at Fig. 1 we see that SSA $A_{UT}^{\sin(\phi-\phi_S)\frac{q_T}{M_N}}$ is rather large, of order 5-10% in the region $x_p > x_{p^\uparrow}$ and is much smaller in the region $x_p < x_{p^\uparrow}$. On the contrary, the

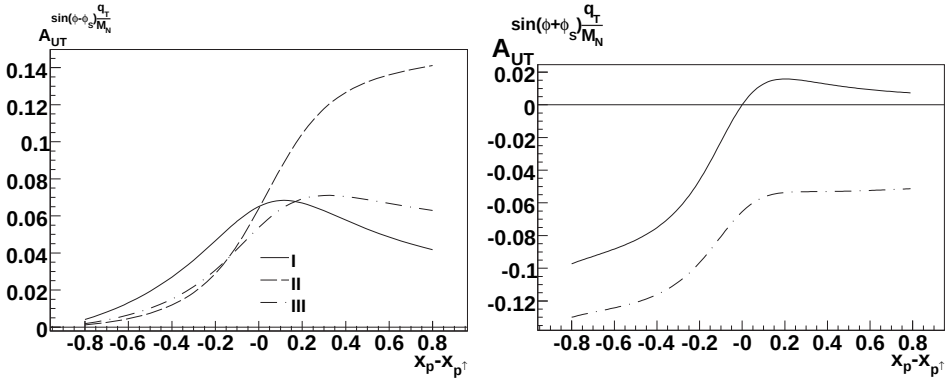

Figure 1. Estimation of SSA $A_{UT}^{\sin(\phi-\phi_S)\frac{q_T}{M_N}}$ (left) and $A_{UT}^{\sin(\phi+\phi_S)\frac{q_T}{M_N}}$ (right) for J-PARC, s=$100GeV^2$, with $Q^2 = 2GeV^2$.

estimations performed for SSA $A_{UT}^{\sin(\phi+\phi_S)\frac{q_T}{M_N}}$ (see Fig. 1), show that this asymmetry is negligible in the region $x_p > x_{p^\uparrow}$ and take quite considerable values (also about 5-10%) in the region $x_p < x_{p^\uparrow}$.

In the case of fixed target mode (J-PARC facility) the regions $x_p > x_{p^\uparrow}$ and $x_p < x_{p^\uparrow}$ correspond to the options with the unpolarized beam/polarized target and the polarized beam/unpolarized target, if the forward-geometry spectrometer would be applied. Certainly, it would be very desirable to avoid the acceptance restriction applying the forward-backward geometry spectrometer. In particular, studying the unpolarized and single-polarized Drell-Yan processes in the limiting case $x_p \ll x_{p^\uparrow}$ one can directly extract the ratio of transversity and Boer-Mulders PDFs.

There exists also another very interesting possibility to extract PDFs we are interested in. Namely, one can use [7,8] the close analogy (duality) between Drell-Yan (DY) $H_1H_2 \to \gamma^*X \to l^+l^-X$ and J/ψ $H_1H_2 \to J/\psi X \to l^+l^-X$ production mechanisms. It is assumed that a such analogy/duality occurs at relatively low energies, where the gluon-gluon fusion (gg) mechanism of J/ψ production is suppressed by the quark-antiquark fusion ($\bar{q}q$). Then, since J/ψ is a vector particle like γ and the helicity structure of $\bar{q}q(J/\psi)$ and $(\bar{q}q)\gamma^*$ couplings is the same, one can get the J/ψ production cross-section from the DY process cross-section applying the simple replacement

$$16\pi^2\alpha^2 e_q^2 \to (g_q^{J/\psi})^2\,(g_\ell^{J/\psi})^2,\ \frac{1}{M^4} \to \frac{1}{(M^2-M_{J/\psi}^2)^2+M_{J/\psi}^2\Gamma_{J/\psi}^2}\,, \tag{3}$$

where $M^2 \equiv Q^2$ is the squared mass of dilepton pair, $M_{J/\psi}^2 \simeq 9.59\,GeV^2$ is the squared J/ψ mass and $\Gamma_{J/\psi}$ is the full J/ψ width. It is believed that the model (3) can be applied in both unpolarized [8] and polarized [7] cases. The advantage of model (3) is that in the region of u-quark dominance all couplings exactly cancel out in the ratios of cross-sections, so that they become absolutely the same for DY and J/ψ production processes. Certainly, the such possibility to use J/ψ production for PDFs extraction is very attractive because the dilepton production rate in the J/ψ production region is two orders of magnitude higher than in the continuum region above the J/ψ mass. However, the "duality" model (3) is applicable only in the such kinematical regions where the quark-antiquark fusion process dominates while the gluon-gluon fusion is suppressed. To find these regions we, besides of the model (3), will consider the most popular "gluon evaporation" model which includes all elementary processes [9]. To cancel unknown constants, we will study not absolute cross-sections but the ratios of the angle and x_F integrated ($x_F > 0$) cross-sections on J/ψ production $\sigma_{pp}/\sigma_{\pi^\pm p}$, $\sigma_{pA}/\sigma_{\pi^\pm A}$ and $\sigma_{pp}/\sigma_{\bar{p}p}$.

First we consider the ratios $\sigma_{pp}/\sigma_{\pi^\pm p}$. The results in comparison with experimental data (taken from [9], Tables 2 and 3) are presented in Fig.2. First of all, one can conclude that in the low energy region, near the first experimental point $\sqrt{s} \simeq 8.7\,GeV$, the curves corresponding to "duality" model and to "gluon evaporation" model with and without gluons almost merge and equally well describe the existing experimental data. This is not surprising since the gluon contribution should be suppressed in the low energy region. At the same time, the results in the high energy region occur to be rather surprising: even at energies 150 GeV and 200 GeV the gluon contribution seems to be insignificant in the ratios $\sigma_{pp}/\sigma_{\pi^\pm p}$ and the curves with and without gluon contributions equally well describe the existing data. The absolutely analogous picture occur also for the ratios $\sigma_{pA}/\sigma_{\pi^\pm A}$ with the different target nuclei.

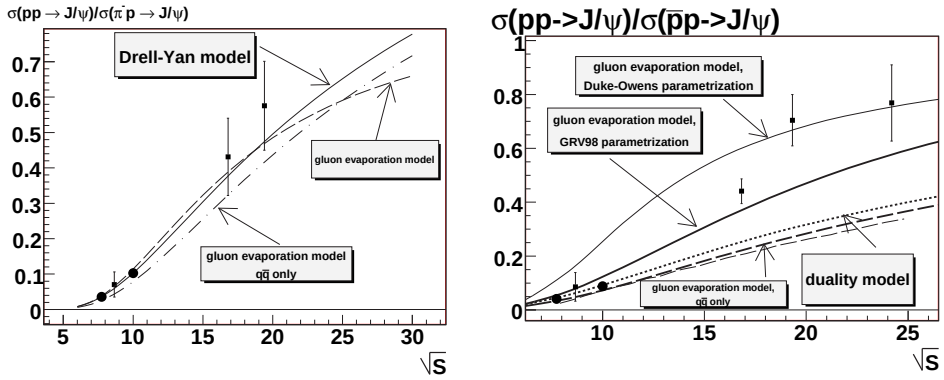

Figure 2. Ratios of cross-sections $\sigma_{pp}/\sigma_{\pi^- p}$ (left) and $\sigma_{pp}/\sigma_{\bar{p}p}$ (right) on J/ψ production calculated with two models in comparison with the experimental data.

The results for the ratios $\sigma_{pp}/\sigma_{\bar{p}p}$ in comparison with experimental data [10] are presented in Fig.2. While in the low energy region we again see the good agreement between the models with and without gluons and the data, the situation in high energy region is absolutely different. First, the gluon contribution becomes very significant in this kinematical region. Second, the "gluon evaporation" model gives a good description of the high energy data only with the old parameterization [11]. However, when we apply the modern and widely used GRV98 parameterization instead, we immediately get the strong disagreement of "gluon evaporation" model prediction with the high energy data. Thus, it seems that to pass this crucial test the gluon sector in the "gluon evaporation" model should be essentially modified. In any case, all existing nowadays models on J/ψ production should pass this test on high energy behaviour, and this is a subject of our future investigation.

References

[1] A. V. Efremov et al, Phys. Lett. B612 (2005) 233
[2] A.N. Sissakian et al, Phys. Rev. **D72** (2005) 054027; Eur. Phys. J. C46 (2006) 147
[3] J.C. Collins et al, Phys. Rev. D73 (2006) 014021
[4] J.C. Collins et al, Phys. Rev. D73 (2006) 094023
[5] D. Boer, Phys. Rev. D **60**, 014012 (1999)
[6] O. Martin, A. Schäfer, M. Stratmann and W. Vogelsang, Phys. Rev. D57 (1998) 3084
[7] N. Anselmino, V. Barone, A. Drago, N. Nikolaev, Phys. Lett. B594 (2004) 97
[8] V. Barone, Z. Lu, B. Ma, Eur. Phys. J. C49 (2007) 967
[9] R. Vogt, Phys. Rept. 310 (1999) 197
[10] C. Morel et al (UA6 collab.), Phys. Lett. B252 (1990) 505
[11] D.W. Duke, J.F. Owens, Phys. Rev. D30 (1984) 49

Discussion

Comm. (O.Teryaev, JINR, Dubna) The pion-nucleon Drell-Yan process at COMPASS may provide (see recent paper of Bakulev, Stefanis and myself Phys. Rev. D76: 074032, 2007) the access to such an important ingredient of pion structure as light-cone distribution amplitude, being similar to Generalized Parton Distributions.

Q. (A.Vasiliev, IHEP, Protvino) If you substitute beam protons by pions with about the same energy, how will it affects your calculations on Drell-Yan?

A. When we replace the incident protons by incident pions, then, due to the antiquark in the valence state in pion, we have: 1) the integrated over x_F absolute cross-sections are higher 2) the asymmetries behaves in another way. Namely, they acquire their maximal value near $x_F = 0$ and decrease at high x.

PROGRESS IN THE DETERMINATION OF POLARIZED PDFs AND HIGHER TWIST

E. Leader[1], A.V. Sidorov[2†] and D.B. Stamenov[3]

(1) *Imperial College London, Prince Consort Road, London SW7 2BW, England*
(2) *Bogoliubov Theoretical Laboratory, JINR, Dubna, Russia*
(3) *Institute for Nuclear Research and Nuclear Energy, Bulgarian Academy of Sciences, Sofia, Bulgaria*
† *E-mail: sidorov@theor.jinr.ru*

Abstract

The impact of the recent very precise CLAS and COMPASS g_1/F_1 data on polarized parton densities and higher twist effects is discussed. It is demonstrated that the low Q^2 CLAS data improve essentially our knowledge of higher twist corrections to the spin structure function g_1, while the large Q^2 COMPASS data influence mainly the strange quark and gluon polarizations. It is also shown that the uncertainties in the determination of the polarized parton densities are significantly reduced. We find also that the present inclusive DIS data cannot rule out a negative polarized and changing in sign gluon densities. The present status of the proton spin sum rule is discussed.

1 Introduction

One of the features of polarized DIS is that a lot of the present data are in the preasymptotic region ($Q^2 \sim 1-5$ GeV^2, 4 GeV^2 < W^2 < 10 GeV^2). This is especially the case for the experiments performed at the Jefferson Laboratory. As was shown in [1], to confront correctly the QCD predictions to the experimental data including the preasymptotic region, the *non-perturbative* higher twist (powers in $1/Q^2$) corrections to the nucleon spin structure functions have to be taken into account too.

In this talk we discuss the impact of the recent very precise CLAS [2] and COMPASS [3] inclusive polarized DIS data on the determination of both the longitudinal polarized parton densities (PDFs) in the nucleon and the higher twist (HT) effects. These experiments give important information about the nucleon structure in quite different kinematic regions. While the CLAS data entirely belong to the preasymptotic region and as one can expect they should mainly influence the higher twist effects, the COMPASS data on the spin asymmetry A_1^d are large Q^2 data and they should affect mainly the polarized parton densities. In addition, due to COMPASS measurements we have for the first time accurate data at small x ($0.004 < x < 0.015$), which allow to determine the behavior of the PDFs at small x region and therefore to calculate more precisely the first moment of the nucleon spin structure g_1.

2 NLO QCD analysis of the data

The method used to extract simultaneously the polarized parton densities and higher twist corrections to the spin-dependent nucleon structure function g_1 is described in [1]. According to this method, the g_1/F_1 and $A_1(\approx g_1/F_1)$ data have been fitted using the experimental data for the unpolarized structure function $F_1(x,Q^2)$

$$\left[\frac{g_1(x,Q^2)}{F_1(x,Q^2)}\right]_{exp} \Leftrightarrow \frac{g_1(x,Q^2)_{\rm LT}+h(x)/Q^2}{F_1(x,Q^2)_{exp}} \ . \tag{1}$$

As usual, F_1 is replaced by its expression in terms of the usually extracted from unpolarized DIS experiments F_2 and R and the phenomenological parameterizations of the experimental data for $F_2(x,Q^2)$ [4] and the ratio $R(x,Q^2)$ of the longitudinal to transverse γN cross-sections [5] are used. Note that such a procedure is equivalent to a fit to $(g_1)_{exp}$, but it is more precise than the fit to the g_1 data themselves actually presented by the experimental groups because here the g_1 data are extracted in the same way for all of the data sets.

In Eq. (1) "LT" denotes the leading twist contribution to g_1

$$g_1(x,Q^2)_{\rm LT} = g_1(x,Q^2)_{\rm pQCD} + h^{\rm TMC}(x,Q^2)/Q^2 + \mathcal{O}(M^4/Q^4) \ , \tag{2}$$

where $g_1(x,Q^2)_{\rm pQCD}$ is the well known (logarithmic in Q^2) NLO pQCD contribution

$$g_1(x,Q^2)_{\rm pQCD} = \frac{1}{2}\sum_q^{N_f} e_q^2[(\Delta q+\Delta\bar{q})\otimes(1+\frac{\alpha_s(Q^2)}{2\pi}\delta C_q)+\frac{\alpha_s(Q^2)}{2\pi}\Delta G\otimes\frac{\delta C_G}{N_f}], \tag{3}$$

and $h^{\rm TMC}(x,Q^2)$ are the calculable kinematic target mass corrections [6], which effectively belong to the LT term. In Eq. (3), $\Delta q(x,Q^2), \Delta\bar{q}(x,Q^2)$ and $\Delta G(x,Q^2)$ are quark, antiquark and gluon polarized densities in the proton, which evolve in Q^2 according to the spin-dependent NLO DGLAP equations. $\delta C(x)_{q,G}$ are the NLO spin-dependent Wilson coefficient functions and the symbol $\otimes$ denotes the usual convolution in Bjorken x space. $\rm N_f$ is the number of active flavors ($\rm N_f = 3$ in our analysis). $h(x)/Q^2$ in Eq. (1) corresponds to the first term in the $(\Lambda^2_{\rm QCD}/Q^2)^n$ expansion of higher twist contribution to g_1. Its logarithmic Q^2 dependence, which is not known in QCD, is neglected. Compared to the principal $1/Q^2$ dependence it is expected to be small and the accuracy of the present data does not allow its determination. Therefore, the extracted from the data values of $h(x)$ correspond to the mean Q^2 for each x-bean.

Let us discuss now how inclusion of the CLAS EG1 proton and deuteron g_1/F_1 data [2] and the *new* COMPASS data on A_1^d [3] influence our previous results [12] on polarized PDFs and higher twist obtained from the NLO QCD fit to the world data [8], before the CLAS and the latest COMPASS data were available.

3 Impact of the new data on polarized PDFs and HT

The new CLAS EG1/p, d data on g_1/F_1 (633 experimental points) [2] and the recent COMPASS data on the longitudinal asymmetry A_1^d (15 experimental points) [3] are at very different kinematic regions. While the CLAS data are high-precision data at low

Q^2:$\{x \sim 0.1 - 0.6,\ Q^2 \sim 1 - 5\ \mathrm{GeV}^2,\ \mathrm{W} > 2\ \mathrm{GeV}\}$, the COMPASS data are mainly at large Q^2:$\{0.0046 \leq x \leq 0.57,\ Q^2 \sim 1 - 55\ \mathrm{GeV}^2\}$ and the only precise data covering the low x region. Therefore, they will play a different role in the improvement of the determination of the polarized PDFs and higher twist effects. The new PDFs and HT and their uncertainties will be compared with those of LSS'05 determined from our previous analysis of the world data [8] available before the CLAS EG_1/p, d and COMPASS'06 data have appeared.

As the CLAS data are mainly low Q^2 data where the role of HT becomes important, they should help to fix better the higher twist effects. Indeed, due to the CLAS data, the determination of HT corrections to the proton and neutron spin structure functions, $h^p(x)$ and $h^n(x)$, is significantly improved in the CLAS x region, compared to the values of HT obtained from our LSS'05 analysis [12] in which a NLO($\overline{\mathrm{MS}}$) QCD approximation for $g_1(x, Q^2)_{\mathrm{LT}}$ was used. This effect is illustrated in Fig. 1. One can conclude now that the HT corrections for the proton target are definitely different from zero and negative in the x region: 0.1-0.4. Also, including the CLAS data in the analysis, the HT corrections for the neutron target are better determined in the x region: 0.2-0.4. Note that $h^n(x)$ at $x \sim 0.5$ was already fixed very precisely from the JLab Hall A data on the ratio $g_1^{(n)}/F_1^{(n)}$. We have found that the impact of the COMPASS'06 data on the values of higher twist corrections and their uncertainties is negligible. The only exception are the central values of HT at small x for both the proton and the neutron targets which are slightly lower than the old ones. Note that this is the only region where the COMPASS DIS events are at small Q^2: 1-4 GeV^2.

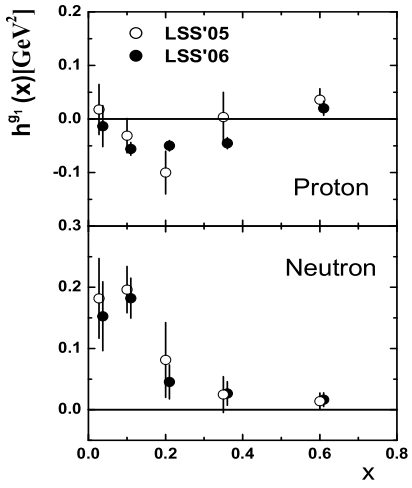

Figure 1. Effect of new data on the higher twist values.

The effect of the new data on the polarized PDFs and their uncertainties is demonstrated in Figures 2 and 3, respectively. The central values of both the $(\Delta u + \Delta\bar{u})$ and $(\Delta d + \Delta\bar{d})$ parton densities do not change in the experimental region (the corresponding LSS'06 curves can not be distinguished from those of LSS'05). As one can see from Fig. 2 the new data influence only the polarized gluon and strange quark sea densities (while the magnitude of strange sea decreases at $x < 0.1$, the gluon density increases at $x > 0.1$). As expected, the central values of the polarized PD are practically *not* affected by the CLAS data. This is a consequence of the fact that at low Q^2 the deviation from logarithmic in Q^2 pQCD behaviour of g_1 is accounted for by the higher twist term in g_1 in Eq. (1). So, the change of the central values of the polarized gluon and strange quark sea densities is entirely due to the new COMPASS data. On the contrary, the accuracy of the determination of polarized PDFs is essentially improved due to the CLAS data (the dashed curves in Fig. 3). This improvement is a consequence of the much better determination of higher twist contributions to the spin structure function g_1, as discussed above. The impact of COMPASS data on the uncertainties for the PDFs is also shown in Fig. 3 (the solid curves). As seen, they help to improve in addition the accuracy of the determination of the gluon and strange sea quark polarized densities at small x: $x < 0.2$

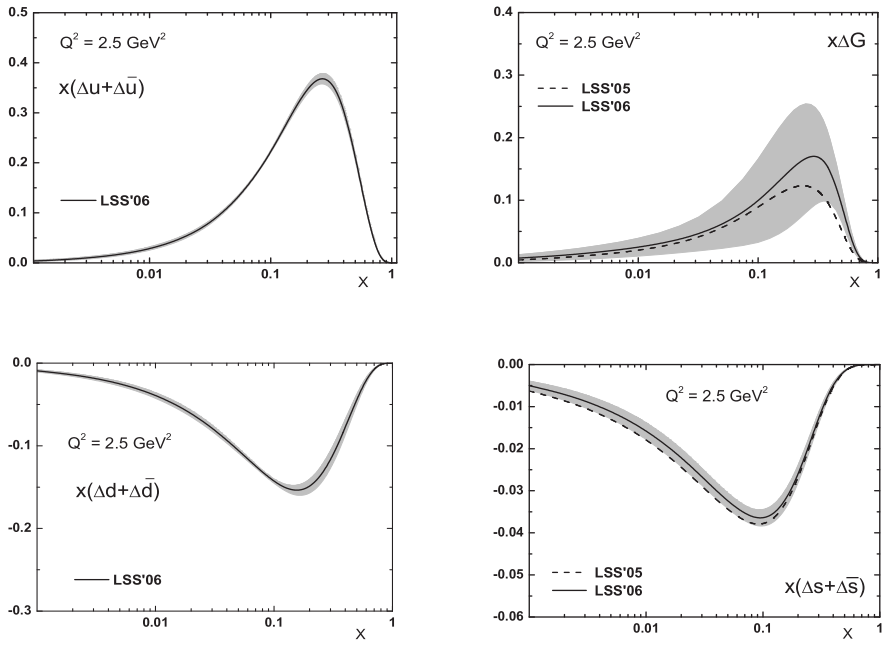

Figure 2. Effect of new data on the NLO($\overline{\text{MS}}$) polarized parton densities.

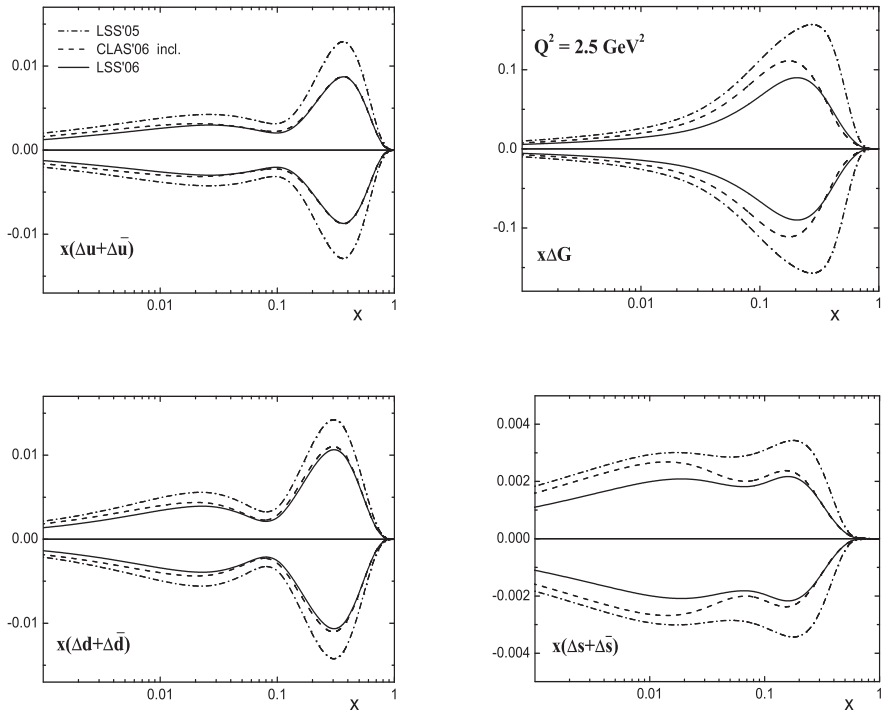

Figure 3. Impact of GLAS and COMPASS data on uncertainties for NLO polarized PDFs.

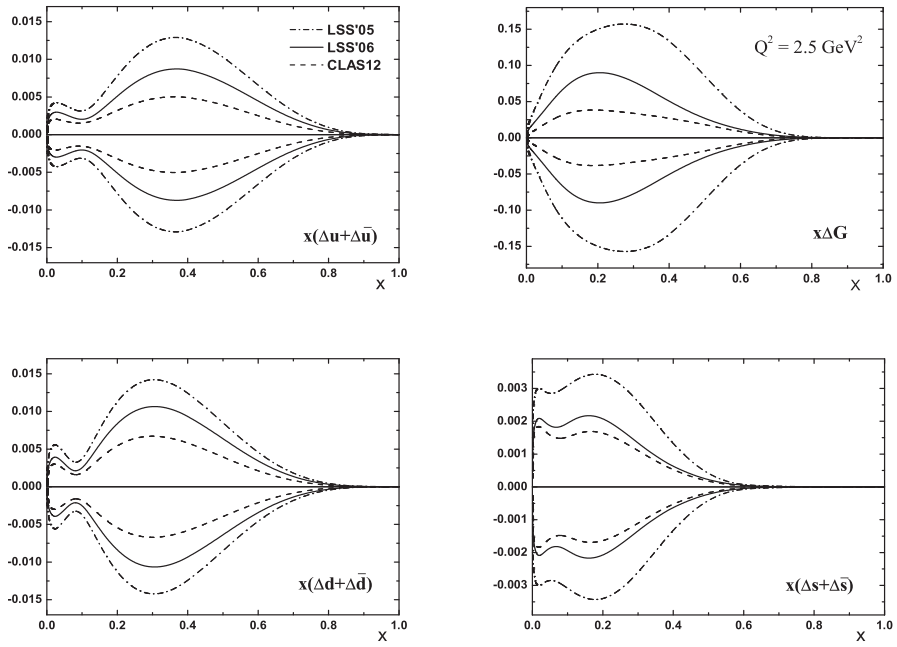

Figure 4. Expected uncertainties for NLO($\overline{\rm MS}$) polarized PDFs after including the data set to be collected with CLAS12 experiment including statistical and systematic errors

for the gluons and $x < 0.1$ for the strange sea.

An essential further improvement (the dashed lines in Fig. 4) can be achieved after including in the analysis the data set to be collected with CLAS12 experiment [9] planned to be performed using a 12 GeV electron beam at Jefferson Laboratory, USA.

At the end of this Section we would like to mention that all results on the PDFs presented here have been obtained when 5 x-bins have been used to extract the HT values. Due to the good accuracy of the CLAS data, one can split the measured x region of the world data set into 7 bins instead of 5, as used up to now, and therefore, can determine more precisely the x-dependence of the HT corrections to g_1. The numerical results of the best fit to the data using 7 x-bins are presented in [13]. It is important to emphasize that the central values for the PDFs(5 bins) and PDFs(7 bins) excepting the gluons are very close to each other. However, the uncertainties for the PDFs(5 bins) are smaller than those for PDFs(7 bins), especially for $\Delta s(x)$ and $\Delta G(x)$. That is why we prefer to present here the PDFs and there uncertainties corresponding to 5 bins in x using for the HT values.

4 The sign of the gluon polarization

We have observed also that the present inclusive DIS data cannot rule out the solutions with negative and changing in sign gluon polarizations (see Fig 5a). The shape of the negative gluon density differs from that of positive one. In all the cases the magnitude of ΔG (the first moment of the gluon density) is small: $|\Delta G| \leq 0.4$ and the corresponding polarized quark densities $(\Delta u + \Delta\bar{u})$ and $(\Delta d + \Delta\bar{d})$ are very close to each other. The

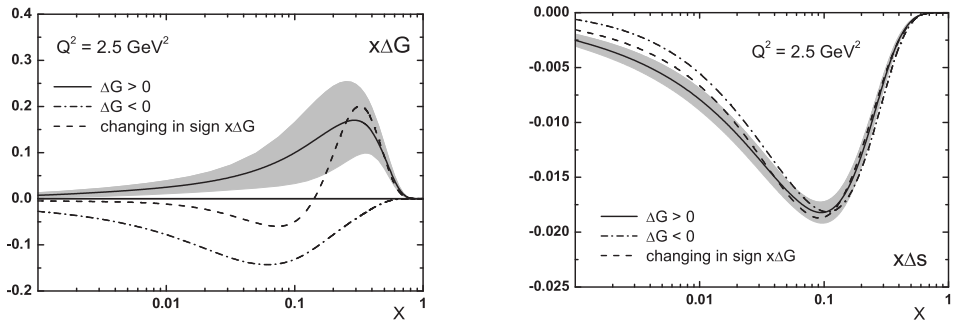

Figure 5. Strange quark sea densities $x\Delta s(x)$ corresponding to the fits with $\Delta G > 0$, $\Delta G < 0$ and changing in sign $x\Delta G$

corresponding strange sea densities are shown in Fig. 5b. Note, however, that the uncertainties for PDFs corresponding to the solution with $\Delta G < 0$ are larger than those in the case of $\Delta G > 0$ (for more details see [13]). In Fig. 6 the ratio $\Delta G(x)/G(x)$ calculated for the different $\Delta G(x)$ obtained in our analysis and using $G(x)_{\rm MRST'02}$ [11] for the unpolarized gluon density, is compared to the existing direct measurements of $\Delta G(x)/G(x)$. The error band correspond to statistic and systematic errors of $\Delta G(x)$. The most precise value for $\Delta G/G$, the COMPASS one, is well consistent with any of the polarized gluon densities determined in our analysis. One can see from Fig. 6 that in order to choose between gluons with positive and negative polarization direct measurements of $\Delta G(x)$ at large x : $x > 0.3$ are needed.

5 The proton spin sum rule and spin puzzle

Using the values for the singlet and gluon polarizations $\Delta\Sigma(Q^2)$ and $\Delta G(Q^2)$ at $Q^2 = 1\ GeV^2$ obtained in our analysis ($\overline{\rm MS}$ scheme):$\Delta\Sigma = 0.207 \pm 0.039$ and $\Delta G = 0.237 \pm 0.153$ we have found the following value for the spin of the proton at $Q^2 = 1\ GeV^2$:

$$S_z = \frac{1}{2} = \frac{1}{2}\Delta\Sigma(Q^2) + \Delta G(Q^2) + L_z(Q^2) = 0.34 \pm 0.15 + L_z(Q^2). \qquad (4)$$

So, in order to satisfy the proton spin sum rule (4) the sum of the quark and gluon orbital angular momentum $L_z = L_z^q + L_z^g$ should be different from zero and positive. Note that the quark orbital momentum L_z^q will be determined soon from the data using the forward extrapolation of the generalized parton densities (GPD).

Let us finally discuss the so called "spin puzzle" - the discrepancy between the values of the singlet polarization $\Delta\Sigma$: 0.2-0.3 in the DIS region and 0.6 at low $Q^2 (Q^2 \sim \Lambda^2_{\rm QCD})$ (see Fig. 7a). For better understanding of the situation it is useful to use the JET factorization scheme [12], in which $\Delta\Sigma(Q^2)$ does not depend on Q^2. Then, in this scheme it is meaningful to directly interpret the singlet polarization $\Delta\Sigma$ as the contribution of the quark spins to the nucleon spin and to compare its values obtained in the DIS and low Q^2 regions. The value of $\Delta\Sigma_{\rm JET}$ obtained in our LSS'06 analysis of the DIS data is 0.26 ± 0.08.

On the other hand the well known value of 0.6 for $\Delta\Sigma(Q^2 \sim \Lambda^2_{\rm QCD}) = \Delta u_v + \Delta d_v + \Delta q_{sea}$ is predicted in the relativistic constituent quark model (CQM) [13]. However, this model does NOT account for the vacuum (quark sea) polarization. It was qualitatively shown in the instanton models [14, 15] that due to the non-perturbative vacuum spin effects the contribution of the sea quark polarization to $\Delta\Sigma$ is *negative*. So, the value of $\Delta\Sigma$ in the non-perturbative region ($Q^2 \sim \Lambda^2_{\rm QCD}$) is really smaller than 0.6. Also, it was found from a combined analysis of forward scattering parity-violating elastic $\overrightarrow{e}p$ asymmetry data from G^0 and HAPPEx experiments at JLab, and elastic νp and $\bar{\nu}p$ scattering data from Experiment 734 at BNL, that the strange axial form factor $G_A^S(Q^2)$, which is strongly related with Δs ($G_A^S(Q^2=0) = \Delta s$), is *negative* in the region $0.4 < Q^2 < 1\ GeV^2$ [16] (see Fig. 7b), *i.e* there is a strong indication that the strange quark contribution to $\Delta\Sigma$ at low Q^2 is *negative*. In conclusion, we are very close to the solution of the so called "spin puzzle".

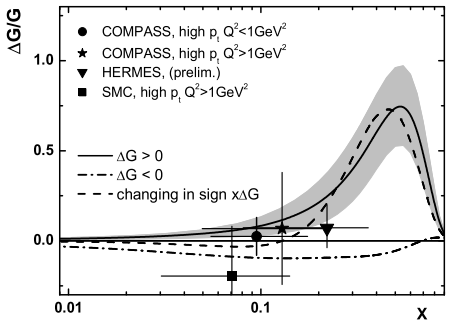

Figure 6. Comparison between the experimental data and NLO($\overline{\rm MS}$) curves for the gluon polarization $\Delta G(x)/G(x)$ at $Q^2 = 3$ GeV^2 corresponding to $\Delta G > 0$, $\Delta G < 0$ and an oscillating-in-sign $x\Delta G$.

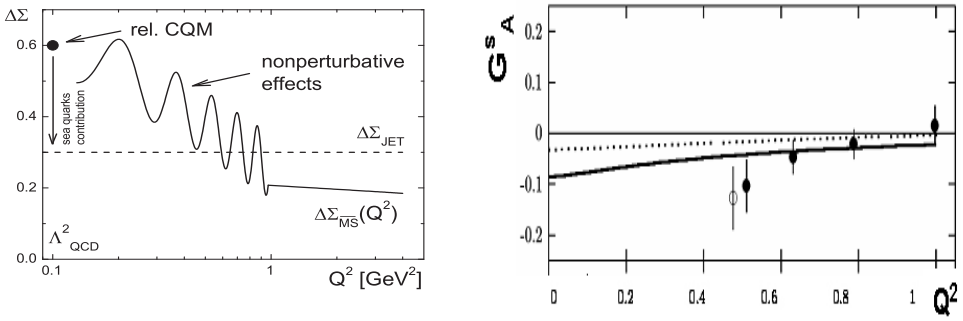

Figure 7. A possible explanation of the nucleon's spin puzzle (a). Results of analysis for the strange axial form factor of the proton (b).

Conclusion

We have studied the impact of the CLAS and latest COMPASS data on the polarized parton densities and higher twist contributions. It was demonstrated that the inclusion of the low Q^2 CLAS data in the NLO QCD analysis of the world DIS data improves essentially our knowledge of HT corrections to g_1 and does not affect the central values of PDFs, while the large Q^2 COMPASS data influence mainly the strange quark and gluon polarizations, but practically do not change the HT corrections. The uncertainties in the determination of polarized parton densities is significantly reduced due to both of the data sets. These results strongly support the QCD framework, in which the leading twist pQCD contribution is supplemented by higher twist terms of $\mathcal{O}(\Lambda^2_{\rm QCD}/Q^2)$.

Finally, one of the important messages coming from this analysis is that it is impossible to describe the very precise CLAS data if the HT corrections are not taken into account. Note that if the low Q^2 data are not too accurate, it would be possible to describe them using only the leading twist term in g_1 (logarithmic in Q^2), *i.e.* to mimic the power in Q^2 dependence of g_1 with a logarithmic one (using different forms for the input PDFs and/or more free parameters associated with them) which was done in the analysis of another groups before the CLAS data were available.

Acknowledgments: This research was supported by the JINR-Bulgaria Collaborative Grant and by the RFBR Grants (No 05-01-00992, No 05-02-17748, 06-02-16215, 07-02-01046).

References

[1] E. Leader, A.V. Sidorov and D.B. Stamenov, Phys. Rev. **D67**, 074017 (2003).

[2] K.V. Dharmwardane et al. (CLAS Collaboration), Phys. Lett. **B641**, 11 (2006).

[3] V.Yu. Alexakhin et al. (COMPASS Collaboration), Phys. Lett. **B647**, 8 (2007).

[4] M. Arneodo et al. (NMC Collaboration), Phys. Lett. **B364**, 107 (1995).

[5] K. Abe et al. (SLAC E143 Collaboration), Phys. Lett. **B452**, 194 (1999).

[6] A. Piccione and G. Ridolfi, Nucl. Phys. **B513**, 301 (1998);
J.Blumlein and A. Tkabladze, Nucl. Phys. **B553**, 427 (1999).

[7] E. Leader, A.V. Sidorov and D.B. Stamenov, Phys. Rev. **D73**, 034023 (2006).

[8] J. Ashman et al. (EMC Collaboration), Phys. Lett. **B206**, 364 (1988); Nucl. Phys. **B328**, 1 (1989);
P.L. Anthony et al. (SLAC E142 Collaboration), Phys. Rev. **D54**, 6620 (1996);
K. Abe et al. (SLAC/E154 Collaboration), Phys. Rev. Lett. **79**, 26 (1997);
B. Adeva et al. (SMC Collaboration) Phys. Rev. **D58**, 112001 (1998);
K. Abe et al. (SLAC E143 Collaboration), Phys. Rev. **D58**, 112003 (1998);
P.L. Anthony et al. (SLAC E155 Collaboration), Phys. Lett. **B463**, 339 (1999); **B493**, 19 (2000);
X. Zheng et al. (JLab/Hall A Collaboration), Phys. Rev. Lett. **92**, 012004 (2004);
A. Airapetian et al. (HERMES Collaboration), Phys. Rev. D**71**, 012003 (2005);
E.S. Ageev et al. (COMPASS Collaboration), Phys. Lett. **B612**, 154 (2005).

[9] M. Amarian et al., A 12 GeV Research Proposal to Jefferson Lab, PR12-06-109. *The Longitudinal Spin Structure of the Nucleon.*

[10] E. Leader, A.V. Sidorov and D.B. Stamenov, Phys. Rev. **D75**, 074027 (2007).

[11] A.D. Martin, R.G. Roberts, W.J. Stirling and R.S. Thorne, Eur. Phys. J. **C 28**, 455 (2003).

[12] R. D. Carlitz, J. C. Collins and A.H. Mueller, Phys. Lett. **B214**, 229 (1988); M. Anselmino, A. V. Efremov and E. Leader, Phys. Rep. **261**, 1 (1995); H.-Y. Cheng, Int. J. Mod. Phys. **A 11**, 5109 (1996); D. Müller and O. V. Teryaev, Phys. Rev. **D56**, 2607 (1997).

[13] A.W. Shreiber and A.W. Thomas, Phys. Lett. **B 215**, 141 (1988); R.D. Jaffe and A. Manohar, Nucl. Phys. **B 337**, 509 (1990).

[14] S.N. Shore and G. Veneziano, Phys. Lett. **B 244**, 75 (1990); S. Forte and E.V. Shuryak, Nucl. Phys. **B 357**, 153 (1991).

[15] A.E. Dorokhov, Czech. J. Phys. **52**, c79 (2002); A.E. Dorokhov, N.I. Kochelev and Yu.A. Zubov, Int. Journ. Mod. Phys. **A 8**, 603 (1993); A.E. Dorokhov and N.I. Kochelev, Phys. Lett. **B 304**, 167 (1993).

[16] S. Pate, AIP Conf. Proceedings **915**, 391 (2007) (arXiv:hep-ex/0611053).

Discussion

Q. (S.Belostotsky, PNPI, S.Petersburg) How to explain in better details the discrepancy between $\Delta\Sigma = 0.3$ from DIS experiments and theoretical expectation?

A. The theoretical estimations for $\Delta\Sigma$ are usually given in the non-perturbative region ($Q^2 \sim \Lambda^2$), which is different from DIS one. However, using the factorization JET scheme, in which $\Delta\Sigma$ does not depend on Q^2, one can compare the values of $\Delta\Sigma$ obtained in non-perturbative and DIS regions. The well known value of 0.6 for $\Delta\Sigma(Q^2 \sim \Lambda^2)$ is predicted in constituent quark model (CQM). However, this model does NOT account for vacuum (quark sea) polarization. It was qualitatively shown in the instanton models that the contribution of the sea quark polarization to $\Delta\Sigma$ is NEGATIVE. So, the value of $\Delta\Sigma$ in the non-perturbative region should be smaller than 0.6. On the other hand, as I have discussed in my talk, there is also an experimental evidence that the strange axial form factor $G_A^S(Q^2)$, which is strongly related with Δs [note that $G_A^S(Q^2 = 0) = \Delta s$], is NEGATIVE in the region $0.4 < Q^2 < 1\ GeV^2$. In conclusion, we are very close to the solution of the so called "spin puzzle".

Q. (B.Ermolaev, IPTI, St.Petersburg) 1. No doubt that Q^2-corrections exist and they are important. However, they cannot be attributed to higher twists before accounting for perturbative contributions.
2. You should not use DGLAP at small x or small Q^2. It makes your results unreliable.

A. 1. The "Q^2-corrections" to g_1, which you point out to be of a "perturbative origin", have nothing to do with the dynamical $(1/Q^2)^n$ corrections to $g_1(x, Q^2)_{LT}$ coming from QCD. The Q^2 terms, you are speaking, arise in the expansion of $g_1(x + z, Q^2)$ when $z = \mu^2/2pq << x = Q^2/2pq$ (or $\mu^2 << Q^2$):

$$g_1(x + z, Q^2) = g_1(x, Q^2) + \sum_{k=1} T_k(\mu^2/Q^2)^k.$$

In contrast to the Q^2 terms in this equation, which provide a connection between $g_1(x + z, Q^2)$ and $g_1(x, Q^2)$ for small z, the higher twist corrections are $(1/Q^2)^n$ corrections to $g_1(x, Q^2)_{LT}$ at the SAME x.
2. The analysis of the world unpolarized data including the HERA data at very small x ($x \sim 10^{-5}$) have demonstrated that DGLAP equations are still working at such a small x. In the polarized case the smallest x value is much larger: $x = 0.0046$. So, as all other groups, we have used the standard DGLAP equations for the leading twist term of g_1.

Q. (A.Prokudin, Univ. Torino) Nowadays speaking about extraction of the parton distributions we speak about accuracy of the result. The mere definition of accuracy some times is ambiguous. For example, CTEQ and AAC use two different methods to estimate accuracy. What is your procedure to do that?

A. Our error bands for the polarized PDFs correspond to $\Delta\chi^2 = 1$.

Q. (A.Efremov, JINR, Dubna) What changes in your analysis? Why earlier you do not speak about negative ΔG?

A. In some of our previous analysis we have also found solutions with ΔG negative. However, we have not shown them because the corresponding χ^2 were significantly larger than those corresponding to ΔG positive. The situation has changed due to the CLAS and COMPASS data: i) χ^2 corresponding to ΔG positive and negative are practically the same and ii) the absolute value of ΔG is smaller now.

CHIRAL DYNAMICS AND SINGLE-SPIN ASYMMETRIES

Dennis Sivers

Portland Physics Institute 4730 SW Macadam, #101 Portland, OR 97239
Spin Physics Center University of Michigan Ann Arbor, MI 48109

Abstract

Parity-conserving single-spin asymmetries provide a specific measure of coherent spin-orbit dynamics in quantum chromodynamics. The origin of these effects can be traced to the interplay of chiral dynamics and confinement in the theory. The most elegant display of the relevant mechanisms occurs in the Collins functions and in the polarizing fragmentation functions and fracture functions for particles with spin. In the nucleon, these same dynamical mechanisms generate virtual quantum structures leading to the Boer-Mulders functions and orbital distributions. Two complementary formalisms for these distribution functions appear. The familiar gauge-link formalism incorporates all nonperturbative dynamics into nonlocal correlators. The constructive formalism introduced by the author describes distributions normalized to an intrinsic property of the nucleon, namely, the currents specified in the Bakker-Leader-Trueman sum rule. The connection between these two approaches can be explored in the process dependence of single-spin asymmetries in various hard-scattering processes. The study of the SU(2) Weyl-Dirac equation in spherical coordinates allows typical Wilson operators that determine this process dependence to be evaluated in the coordinate gauge.

This conference has already heard two excellent theoretical talks on transverse single-spin asymmetries by Professors Efremov [1] and Teryaev [2]. A specific goal of this presentation is to acquaint you with a different, and complementary, set of theoretical tools that emphasizes the dynamical origin of these observables. A convenient way of introducing this alternative approach focuses on the concept of spin-directed momentum. The observation that single-spin measurements (either analyzing powers or polarizations) necessarily define a spin-directed momentum can be easily confirmed. The requirement can be illustrated by the sketch shown in Fig. 1. For a parity-conserving asymmetry, the form of this spin-directed momentum is highly constrained by rotational invariance and finite symmetries. The required expression is

$$k_{TN} = \boldsymbol{k}_T \cdot \left(\hat{\sigma} \times \hat{P}\right) \tag{1}$$

in which $\boldsymbol{P}$ is the 3-momentum of a hadron, $\boldsymbol{k}$the 3-momentum of a constituent and $\boldsymbol{\sigma}$ and axial vector denoting a spin direction. This expression can easily seen to be invariant under C (charge conjugation), P (parity) and T (time reflection). It is, however, odd under a symmetry designated A_τ[3,4]. The observation that all single-spin observables are odd under the combination $O = PA_\tau$ requires that all such observables fall into one of two distinct categories:

1. P-odd and A_τ-even,
2. P-even and A_τ-odd.

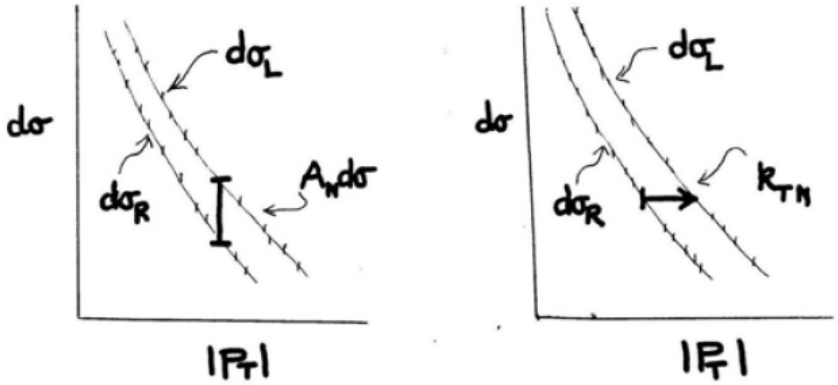

Figure 1: Graphical illustration of how a measurement of A_N for a parity-conserving single-spin asymmetry can also be used to define the underlying spin-directed momentum transfer in the process.

In the light-quark sector of the standard model, A_τ-odd observables can be shown to be uniquely associated with coherent spin-orbit dynamics. Mulders and Tangerman [5] have classified four distinct leading-twist functions characterizing A_τ-odd quantum structures. This collection consists of two types of fragmentation function: the Collins functions [6] and the polarizing fragmentation functions, and two types of distribution function; the Boer-Mulders functions [7] and the orbital distribution functions. These functions have distinct characteristics but they share a common origin in the combination of confinement and chiral dynamics that generate the non-perturbative spin-orbit correlations.

The existence of a probabilistic description of the A_τ-odd dynamics in fragmentation functions is guaranteed by the existence of a projection operator [3,4]

$$\mathrm{P}_{\mathrm{A}}^{-} = \frac{1 - \mathrm{A}_\tau}{2} \tag{2}$$

that isolates spin-orbit effects. The work of Artru, Czyzewski, and Yabuki [8] displays these dynamical elements very elegantly. This model actually has all the ingredients of the full nonperturbative calculation of the pion Collins function. The ingredients include mixing between gluonic degrees of freedom and a 0^{++} $^3P_0$ quark-antiquark pair that generates internal orbital angular momentum. As the pair rotates, configuration mixing alters the local SU(3) color geometry, enhancing the probability of flux-tube breaking. Chiral dynamics enter the picture by giving an energy advantage for the antiquark in the $^3P_0$ pair to form a light-mass pion involving the leading quark. This pion then inherits the spin-directed momentum of the antiquark. The phenomenological estimates for pion Collins functions presented in Prof. Efremov's talk [1] provide strong quantitative support for this picture. The reader should consult his summary for the original references.

For particles with spin, a density matrix formulation of these basic dynamical mechanisms with a quantization axis specified by the orientation of $\boldsymbol{L}$ produces a tightly-constrained formulation of both the Collins function and the polarizing fragmentation function. For baryons, it is convenient to consider, in addition to usual polarizing fragmentation functions describing the fragmentation of a quark jet, the polarizing fracture function describing the fragmentation of the "diquark-jet" created by stripping away a quark from a nucleon target to create an SU(3) color ion. This extension of the fracture-function formalism established by Trendadue and Veneziano [9] to the sector of A_τ-odd

dynamics seems also to be efficiently characterized by mechanisms similar to those of the Collins functions.

Since the nucleon is a stable particle, the orbital angular momentum that appears explicitly in the final state for fragmentation and fracture functions appears as virtual quantum structures leading to the nucleon's A_τ-odd distribution functions. The field-theoretical descriptions of the virtual processes allow for two distinct formalisms to characterize these distributions. The distinction between the two approaches reflects the alternate descriptions for single-spin observables illustrated in Fig. 1. The, now conventional, gauge-link formalism [10,11] presents these functions in terms of nonlocal correlators that lead to the expectation value for k_{TN}. This formalism engages the full power of gauge theory and makes a direct connection to the operator product expansion. [12]. The predictive power of the gauge-link approach is demonstrated by the Collins conjugation relation, [10] that relates the orbital distribution measured in SIDIS with that measured in the DY process. The other, more modest, formalism, developed by the author in [3,4], is based on local, gauge-invariant, number densities that describe properties intrinsic to the proton and are not based on any specific process. The orbital distributions and Boer-Mulders functions in this formalism are constructed such that they are normalized to the expectation values of spin-orbit effects,

$$\begin{array}{l} \int dx d^2k_T \Delta^N G^{front}_{q/p\uparrow}(x, k_{TN}(x); \mu^2) = \frac{1}{2} \langle \boldsymbol{L}_q \cdot \hat{\sigma}_p(\mu^2) \rangle \\ \int dx d^2k_T \Delta^N G^{front}_{g/p\uparrow}(x, k_{TN}(x); \mu^2) = \frac{1}{2} \langle \boldsymbol{J}_g \cdot \hat{\sigma}_p(\mu^2) \rangle \\ \int dx d^2k_T \Delta^N G^{front}_{q\uparrow/p}(x, k_{TN}(x); \mu^2) = \frac{1}{2} \langle \boldsymbol{L}_q \cdot \hat{\sigma}_q(\mu^2) \rangle \end{array} \tag{3}$$

To avoid confusion, the symbols for the distributions in these constructions are purposely chosen to be different from the Mulders-Tangerman symbols traditionally used in the gauge-link formalism. This, constructive, formalism describes characteristics of the spin-orbit dynamics of the proton so that, for example, the Bakker, Leader, Trueman sum rule [13] can be written,

$$J_y = \frac{1}{2} = \frac{1}{2} \sum_{q_i} \delta^T q_i(\mu^2) + 2 \sum_{q_i, g=c} \int dx d^2k_T \Delta^N G^{front}_{c/p\uparrow}(x, k_{TN}(x); \mu^2) \tag{4}$$

where $\delta^T q_i(\mu^2)$is the moment of the quark transversity distribution. The constructive formalism takes advantage of the fact that all A_τ-odd dynamics can be factorized into an effective distribution to give a recipe for the initial-state and final-state interactions that contribute to a given single-spin asymmetry. The specific construction of these functions described in refs. [3,4] clarifies the distinction between constructive distributions and the conventional functions specified by nonlocal correlators.

As discussed in the presentation by Teryaev, [2] at this conference and emphasized, for example by Brodsky [14] the orbital distributions and Boer-Mulders functions defined in the gauge-link formalism are, in fact, effective distributions. These functions are connected to the imaginary parts generated in the helicity-amplitude basis by soft initial-state and/or final-state interactions. In the gauge-link formalism it thus makes perfect sense to say that the distributions are <u>created</u> by the initial-state or final-state interactions involved. Whereas, in the constructive approach of the author it is more correct to say that the underlying A_τ-odd number densities are <u>revealed</u> by the soft initial-state or final-state interactions. Brodsky and his collaborators have demonstrated in numerous calculations

[14] the connection between in soft initial-state and final-state interactions involved in single-spin effects with those that appear in other phenomenological contexts.

The constructive approach allows a more direct connection of the virtual corrections leading to quantum structures in the nucleon with the explicit spin-orbit dynamics as displayed by the Collins functions. For example, the calculations presented in Ref. 4 provide the normalization for the quark, antiquark and gluon orbital distributions $\Delta^N G^{front}_{c/p\uparrow}$and for the quark Boer-Mulders functions $\Delta^N G^{front}_{q\uparrow/p}$ in terms of the expectation values for orbital angular momentum found in the Georgi-Manohar [15] chiral quark model. This venerable model is defined in terms of transitions from constituent quarks, (U,D) to partonic quarks (u,d,s) as exemplified by

$$\begin{array}{l} U\uparrow\rightarrow[1-\eta_B-\alpha_c(1+\varepsilon_s+\varepsilon_o)]u\uparrow ...(L=0) \\ +[\eta_B u\downarrow+\alpha_c d\downarrow(\bar{d}u)+\varepsilon_s\alpha_c s\downarrow(\bar{s}u)+\varepsilon_o\alpha_c u\downarrow(\bar{u}u)]...(L=+1) \end{array} \tag{5}$$

The transitions for $U\downarrow, D\uparrow$ and $D\downarrow$ can be obtained from (5) using isospin and rotational invariance. The fixing of the parameters $\eta_B, \alpha_c, \varepsilon_s, \varepsilon_o$ in the model is an interesting exploration of angular momentum sum rules. The observation that the transitions (5) are precisely the Collins functions $q_i\uparrow\rightarrow q_j\downarrow\pi_{\bar{j}i}$ emphasizes the underlying connections.

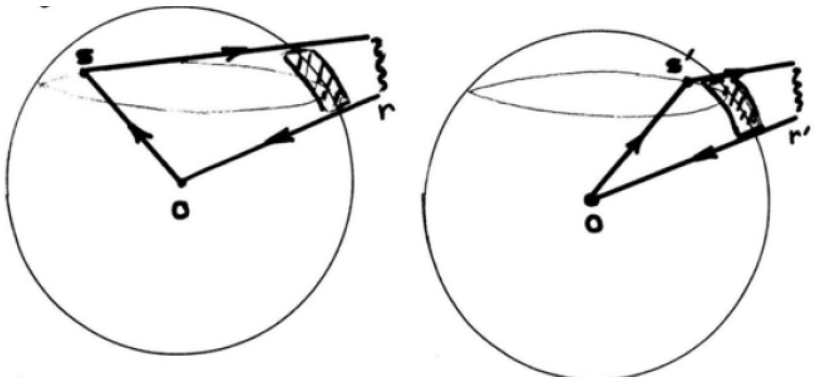

Figure 2: In spherical coordinates, the coordinate gauge allows for the calculation Wilson operators consisting of triangles with two radially directed lines based on the operator techniques discussed in references 16 and 17.

The familiar gauge-link formalism of the effective approach and the transversity-amplitude based calculations of the constructive approach are therefore seen to be very complementary. Each constrains the other in many important ways. Comparing the two leads to a challenging program of study of the process-dependence in single-spin asymmetries. The process dependence for the gauge-link formalism can be described recursively using spectator models and the twist expansion. A convenient tool that goes beyond perturbation theory for beginning to understand the same process dependence in the constructive approach uses explicit solutions of the Weyl-Dirac equation in color SU(2) and spherical coordinates to calculate the Wilson operators that appear for these observables in the coordinate gauge. The techniques for doing these calculations exploit specific operators discussed in Refs.[16,17]. The Weyl-Dirac equation allows the separation of degrees of freedom for the energy and 3-momentum and the coordinate gauge in spherical coordinates simplifies the calculation of the spatial component of Wilson operators as indicated in Fig. 2.

Significant progress is being made in the understanding of the factorization properties [18] of the gauge-link formalism, as well as the connection to the twist expansion [19] and in the relationships with generalized parton distributions [20] found in this approach. The application of the $A_\tau$symmetry and the formulation of single- spin observables in terms of transversity amplitudes provides important constraints in all these endeavors. The ability to formulate calculations in complementary formalisms has already proven to be a real benefit but the important information contained in the fragmentation and fracture functions has not yet been fully exploited.

References

1. A.V. Efremov, Invited talk, this conference
2. O.V. Teryaev, Invited talk, this conference
3. D. Sivers, "Single-Spin Observables and Orbital Structures in Hadronic Distributions", ArXiv hep-ph/060908, Phys. Rev.**D74**, 094008(2006)erratum **D75** e039901
4. D. Sivers, "Chiral Mechanisms Leading to Orbital Quantum Structures in the Nucleon", ArXiv 074.1791 (2007) Submitted to Phys Rev D but rejected
5. P.J. Mulders and R.D. Tangerman, Nucl. Phys. **B461**, 197 (1996)
6. J.C. Collins, Nucl. Phys. **B396**, 161 (1993)
7. D. Boer and P.J. Mulders, Phys. Rev. **D57**, 5780 (1994)
8. A. Artru, J. Czyzewski and H. Yabuki, Z. Phys **C73**, 527 (1997)
9. L. Trentadue and G. Veneziano, Phys. Lett. **B323**, 201 (1994)
10. J.C. Collins, Phys. Lett. **B536**, 43 (2002)
11. A.V. Belitsky, X. Ji, and F. Yuan, Nucl. Phys. **B636**, 165 (2003); D. Boer, P.J. Mulders and F. Pijlman, Nucl. Phys. **B667**, 201 (2003)
12. Two excellent comprehensive summaries of the gauge-link formalism can be found in F. Pijlman, Free University of Amsterdam thesis (2006) and C.J. Bonhoff, Free University of Amsterdam thesis (2007
13. B.L. Bakker, E. Leader and T.L. Trueman, Phys. Rev. **D70**, 114001 (2004)
14. See, for example, S.J. Brodsky, ArXiv 0709.2229 (2007) and references contained therein.
15. A. Manohar and H. Georgi, Nucl Phys. **B234**, 189 (1984)
16. J. Ralston and D. Sivers, Phys. Rev. **D28**, 953 (1983); ibid. **D30**, 472 (1984)
17. D. Sivers, Phys. Rev. **D35**, 707 (1987); ibid. **D35**, 3231 (1987)
18. A. Bacchetta, C. Bomhof, U. D'Alesio, P. Mulders and F. Murgia, ArXiv 0703.153
19. P. Ratcliffe and O. Teryaev, arXiv:hep-ph/0703293 (2007)
20. S. Meissner, A. Metz and K. Goeke, arXiv:0706.1193

THE NUCLEON SPIN STRUCTURE AND QCD SPIN PHYSICS

Jacques Soffer

Department of Physics, Temple University,
Philadelphia, Pennsylvania 19122-6082, USA
E-mail: jsoffer@temple.edu

Abstract

Our knowledge of the nucleon spin structure has greatly improved over the last twenty years or so, but still many fundamental questions remain unsolved. I will try to review some of the puzzling aspects of the structure of the nucleon spin, in particular, what is known, what remains to be discovered and the prospects for the near future. I will also focus on some current activities in QCD spin physics.

1 Introduction

Among the essential goals of QCD spin physics one has first, to understand the nucleon spin structure in terms of its basic partonic constituents and second, to test the *SPIN SECTOR* of perturbative QCD, at the highest possible precision level. Concerning the first point, one needs to know how the quark and gluon distributions in a polarized nucleon make its spin one-half and several questions arise in particular: what is the role of the orbital angular momentum? The second point is very relevant to reinforce the validity of the already well established perturbative QCD theory, because many spin asymmetries have been calculated, at the next-to-leading order (NLO), and have not yet been compared with experimental data. Therefore it is very legitimate to ask to what extent they will agree. We will try to answer the following questions: What is known? What is missing? What needs to be measured next? What are the prospects?

The basic information comes from Deep Inelastic Scattering (DIS), unpolarized $lN \to l'X$, or polarized $\overrightarrow{l}\overrightarrow{N} \to l'X$. In the unpolarized case, widely measured over the last three decades, one gets access to $F_2^{p,n}(x,Q^2) = \sum_q e_q^2[xq(x,Q^2) + x\bar{q}(x,Q^2)]$. Here the $q(x,Q^2)$'s (same for antiquarks) are defined as $q = q_+ + q_-$, where $q_\pm$ are the quark distributions in a polarized proton with helicity parallel $(+)$ or antiparallel $(-)$ to that of the proton. In the polarized case, one measures the corresponding polarized structure function, $g_1^{p,n}(x,Q^2) = 1/2\sum_q e_q^2[\Delta q(x,Q^2) + \Delta\bar{q}(x,Q^2)]$. Similarly $\Delta q(x,Q^2)$'s (same for antiquarks) are defined as $\Delta q = q_+ - q_-$. The gluon distributions are also defined as $G = G_+ + G_-$ and $\Delta G = G_+ - G_-$, but in DIS they are not accessible directly and only enter in the QCD Q^2 evolution of the quark distributions.

There is a long list of interesting topics, *e.g.* characteristic features of unpolarized and polarized parton distributions, flavor separation of Δq, $\Delta\bar{q}$, gluon polarization in the nucleon, generalized parton distributions, quark transversity $\delta q(x,Q^2)$ and double transverse spin asymmetries A_{TT}, single spin asymmetries (SSA) A_N and QCD mechanisms, etc...

In this opening lecture, for lack of time, we will have to make a strong selection, but given the high density of the scientific program, it will certainly allow to cover all missing important subjects.

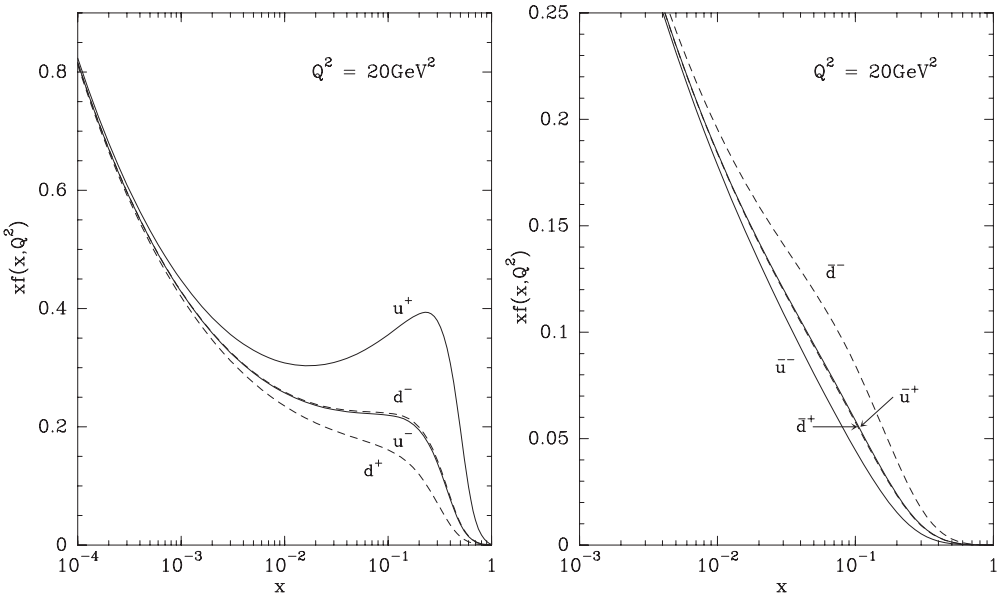

Figure 1: On the left (right) the light quark (antiquark) distributions with different helicities versus x for $Q^2 = 20\text{GeV}^2$, taken from Ref. [1].

2 Digression on parton distributions functions

A new set of parton distribution functions (PDF) was constructed in the framework of a statistical approach of the nucleon [1], which has the following characteristic features:
- For quarks (antiquarks), the building blocks are the helicity dependent distributions $q_\pm$ ($\bar{q}_\pm$) and we define $q = q_+ + q_-$ and $\Delta q = q_+ - q_-$ (similarly for antiquarks).
- At the initial energy scale taken at $Q_0^2 = 4\text{GeV}^2$, these distributions are given by the sum of two terms, a quasi Fermi-Dirac function and a helicity independent diffractive contribution, which leads to a universal behavior for all flavors at very low x.
- The flavor asymmetry for the light sea, *i.e.* $\bar{d} > \bar{u}$, observed in the data is built in. This is clearly understood in terms of the Pauli exclusion principle, based on the fact that the proton contains two u quarks and only one d quark.
- The chiral properties of QCD lead to strong relations between q and $\bar{q}$. For example, it is found that the well established result $\Delta u > 0$ implies $\Delta\bar{u} > 0$ and similarly $\Delta d < 0$ leads to $\Delta\bar{d} < 0$.
- Concerning the gluon, the unpolarized gluon distribution is given in terms of a quasi Bose-Einstein function, with *no free parameter*, but for simplicity, one assumes zero gluon polarization, *i.e.* $\Delta G(x, Q_0^2) = 0$, at the initial energy scale.
- All unpolarized and polarized distributions depend upon *eight* free parameters, which were determined in 2002 (See [1]), from an NLO fit of a selected set of accurate DIS

data. For illustration, the ± light quark (antiquark) distributions are displayed on Fig. 1 and we clearly notice the essential features mentioned above [1]. More recently, new tests against experimental (unpolarized and polarized) data turned out to be very satisfactory, in particular in hadronic reactions [2, 3].

The statistical approach has been extended to the interesting case where the PDF have, in addition to the usual Bjorken x dependence, an explicit transverse momentum k_T dependence [4] and this might be used in future calculations with no k_T integration.

Concerning the strange quark and antiquark distributions, a simplifying assumption consists to take $s(x, Q^2) = \bar{s}(x, Q^2)$ and similarly for the corresponding polarized distributions $\Delta s(x, Q^2) = \Delta\bar{s}(x, Q^2)$. However a careful analysis of the data led us to the conclusion that $s(x, Q^2) \neq \bar{s}(x, Q^2)$ and the corresponding polarized distributions are unequal, small and negative [5].

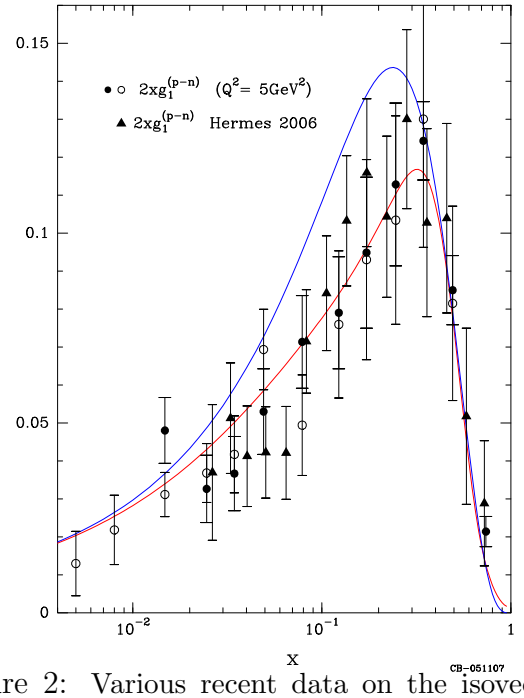

Figure 2: Various recent data on the isovector structure function $2xg_1^{(p-n)}(x)$ compared to the statistical model prediction Ref. [3] (lower curve) and the AAC calculation Ref. [6] (upper curve, taken from Ref. [7]).

Now let us come back to the important prediction of the statistical approach, namely $\Delta\bar{u} > 0$ and $\Delta\bar{d} < 0$, which contrasts with the flavor symmetric assumption $\Delta\bar{u} = \Delta\bar{d} = \Delta s = \Delta\bar{s}$ made, for example, in Ref. [6]. With this assumption, the $\Delta\bar{q}$ don't contribute to the Bjorken sum rule, so one has to increase the absolute values of the valence contributions to Δu and Δd, in order to satisfy this sum rule. As shown on Fig. 2, this leads to over estimate $2xg_1^{(p-n)}(x)$ in the valence region, but it is not the case for the statistical approach. This has been confirmed by recent Compass data [8].

There is another way to test directly the predictions of the statistical approach for the polarized quark distributions and their flavor separation. This has been obtained from the semi-inclusive polarized DIS and the Hermes data are shown on the left hand side of Fig. 3. On the right hand side of Fig. 3, we also display the very accurate JLab data which show that, even in the high x region, $\Delta(u + \bar{u})$ remains positive whereas $\Delta(d + \bar{d})$ remains negative, in accordance with the statistical approach expectations.
These features can and will be also investigated in future runs with polarized pp collisions at BNL-RHIC, which we briefly discuss now.
Consider the parity-violating helicity asymmetry $A_L^{PV}(W)$

$$A_L^{PV}(y) = \frac{\Delta d\sigma/dy}{d\sigma/dy} = \frac{d\sigma_-^W/dy - d\sigma_+^W/dy}{d\sigma_-^W/dy + d\sigma_+^W/dy} \ , \qquad (1)$$

[1] For a practical use of these PDF, see www.cpt.univ-mrs.fr/ bourrely/research/bbs-dir/bbs.html.

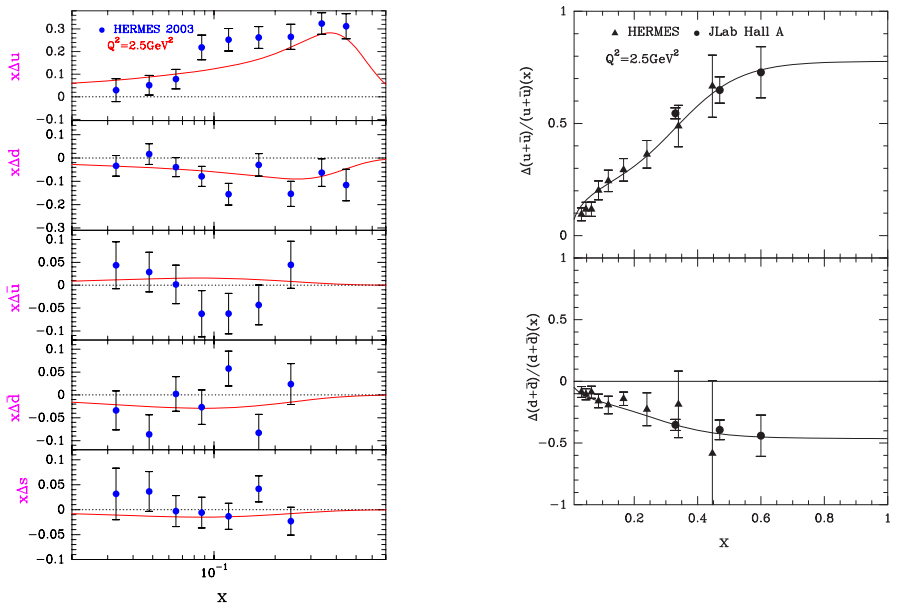

Figure 3: Left: Quark and antiquark polarized parton distributions as a function of x for $Q^2 = 2.5\text{GeV}^2$. Data from Ref. [9]. Right: Ratios $(\Delta u + \Delta\bar{u})/(u + \bar{u})$ and $(\Delta d + \Delta\bar{d})/(d + \bar{d})$ as a function of x. Data from Hermes for $Q^2 = 2.5\text{GeV}^2$ [9] and a JLab experiment [8]. In both the curves are predictions from the statistical approach Ref. [3].

where $\pm$ stands for the helicity of one polarized proton beam and y is the W rapidity. For W^+, at the lowest order of the Drell-Yan production mechanism, it reads

$$A_L^{PV}(W^+) = \frac{\Delta u(x_a)\bar{d}(x_b) - \Delta\bar{d}(x_a)u(x_b)}{u(x_a)\bar{d}(x_b) + \bar{d}(x_a)u(x_b)} \ , \tag{2}$$

where $x_a = \sqrt{\tau}e^y$, $x_b = \sqrt{\tau}e^{-y}$ and $\tau = M_W^2/s$. For W^- production one interchanges u and d. The general trend of $A_L^{PV}(y)$ can be easily understood and, for example at $\sqrt{s} = 500\text{GeV}$ near $y = +1$, $A_L^{PV}(W^+) \sim \Delta u/u$ and $A_L^{PV}(W^-) \sim \Delta d/d$, evaluated at $x = 0.435$. Similarly for near $y = -1$, $A_L^{PV}(W^+) \sim -\Delta\bar{d}/\bar{d}$ and $A_L^{PV}(W^-) \sim -\Delta\bar{u}/\bar{u}$, evaluated at $x = 0.059$.

The features appear clearly on the left hand side of Fig. 4, where the calculations were done at two different energies. For completeness we also show the predicted $A_L^{PV}(Z)$ on the right hand side of Fig. 4, but in this case the interpretation is not so straightforward. Moreover the production rate of Z's is much lower than W's.

However there is an important point to mention here, since the W's are not directly seen. For the most relevant signature, if one selects the leptonic decay $W \to e\nu$, one measures in fact

$$A_L^{PV}(y_e) = \frac{\Delta d\sigma/dy_e}{d\sigma/dy_e} = \frac{d\sigma_-^W/dy_e - d\sigma_+^W/dy_e}{d\sigma_-^W/dy_e + d\sigma_+^W/dy_e} \ , \tag{3}$$

where y_e is the charged lepton rapidity. Fortunately, by using the RhicBos code due to P. Nadolski, one finds that $A_L^{PV}(y_e)$ has essentially the same trend as $A_L^{PV}(y)$.

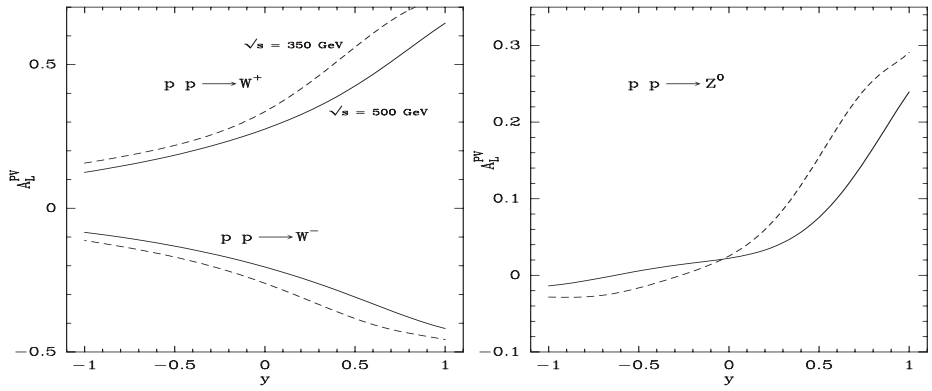

Figure 4: Left: Predictions from the statistical approach for the parity violating asymmetry A_L^{PV} for the $pp \to W^{\pm}$ production, versus the W rapidity y, at $\sqrt{s} = 350$GeV (dashed curve) and $\sqrt{s} = 500$GeV (solid curve). Right: Same for the $pp \to Z$ production. (Taken from Ref. [1])

So much for the quarks, let us now turn to the gluon distributions and we first consider the unpolarized distribution $G(x, Q^2)$. In the statistical approach it has a very simple expression (See Ref. [1]), which is consistent with the available data, most coming indirectly from the QCD Q^2 evolution of $F_2(x, Q^2)$, defined earlier, in particular in the low x region. However it is known that ep DIS cross section is characterized by two independent structure functions, $F_2(x, Q^2)$ and the longitudinal structure function $F_L(x, Q^2)$. For low Q^2, the contribution of the later to the cross section at HERA is only sizeable at x smaller than approximately 10^{-3} and in this domain the gluon density dominates over the sea quark density. More precisely, it was shown that using some approximations, one has [12]

$$xG(x, Q^2) = \frac{3}{10} 5.9 [\frac{3\pi}{2\alpha_s} F_L(0.4x, Q^2) - F_2(0.8x, Q^2)] \simeq \frac{8.3}{\alpha_s} F_L(0.4x, Q^2) \ . \tag{4}$$

Before HERA was shut down, a dedicated run period with reduced proton beam energy was approved and we are waiting for these new H1 results on F_L. We show on Fig. 5 the predictions of the statistical approach and the new data, whose precision is expected to be rather good, will allow to test its predictive power, once more.

The polarized gluon distribution ΔG is also extremely important to determine and we have the following helicity sum rule

$$\frac{1}{2} = \frac{1}{2}\Delta\Sigma + \Delta G(Q^2) + L_q(Q^2) + L_G(Q^2) \ , \tag{5}$$

where $\Delta\Sigma = \sum_q \int_0^1 [\Delta q(x, Q^2) + \Delta\bar{q}(x, Q^2)] dx$ is twice the quark (+ antiquark) contribution to the nucleon helicity and ΔG, $L_{q,G}$ are the contributions of gluon and orbital angular momentum of quark and gluon. So far $\Delta\Sigma \sim 0.3$ and the sum rule is not satisfied.

There are several attempts to extract $\Delta G(Q^2)$ from DIS using different processes and the most recent results will be presented later in this Workshop. The RHIC spin program is also putting a high priority to this determination and the cleanest reaction is inclusive prompt photon production, which is dominated by the subprocess $Gq \to \gamma q$. The double helicity asymmetry, which has schematically the following expression

$$A_{LL} \approx \frac{\Delta G(x_1)}{G(x_1)} \cdot \left[\frac{\sum_q e_q^2 \left[\Delta q(x_2) + \Delta\bar{q}(x_2)\right]}{\sum_q e_q^2 \left[q(x_2) + \bar{q}(x_2)\right]} \right] \cdot \hat{a}_{LL}(Gq \to \gamma q) + (1 \leftrightarrow 2) \ , \tag{6}$$

is directly proportional to ΔG. This has not been measured yet, but from the measurements on $\overrightarrow{p}\overrightarrow{p} \to \pi(orjet)X$, we have all indications that ΔG is small and still badly known, unfortunately.

The next very serious question is indeed: are there relevant contributions from $L_{q,G}$?

3 Quark transversity $\delta q(x, Q^2)$ and A_{TT}

The existence of this new quark distribution $\delta q(x, Q^2)$, was first mentioned by Ralston and Soper in 1979, by studying the angular distribution in $p(\uparrow)p(\uparrow) \to \mu^+\mu^- X$ with transversely polarized protons. It was merely forgotten until 1990, where it was first realized that it completes the description of the quark distribution in a nucleon as a density matrix

$$\mathcal{Q}(x, Q^2) = q(x, Q^2) I \otimes I + \Delta q(x, Q^2)\sigma_3 \otimes \sigma_3 + \delta q(x, Q^2)(\sigma_+ \otimes \sigma_- + \sigma_- \otimes \sigma_+) \ . \quad (7)$$

This quark transversity $\delta q(x, Q^2)$ is chiral odd, leading twist and decouples from DIS. So it was never measured and we only have the following positivity bound [13] [2]

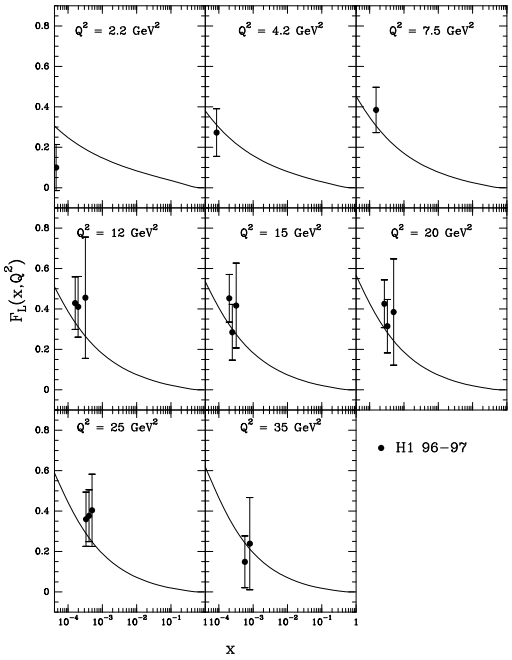

Figure 5: Statistical approach predictions for the longitudinal structure function $F_L(x, Q^2)$ with earlier H1 data (Taken from Ref. [7]).

$$q(x, Q^2) + \Delta q(x, Q^2) \geq 2|\delta q(x, Q^2)| \ , \quad (8)$$

which survives up to NLO corrections. It is indeed accessible in $p(\uparrow)p(\uparrow) \to \mu^+\mu^- X$, with both protons transversely polarized. The double transverse spin asymmetry A_{TT} reads

$$A_{TT} = \frac{d\sigma(\uparrow\uparrow) - d\sigma(\uparrow\downarrow)}{d\sigma(\uparrow\uparrow) + d\sigma(\uparrow\downarrow)} = \widehat{a}_{TT} \frac{\sum_q e_q^2 \delta q(x_1, M^2)\delta\bar{q}(x_2, M^2) + (1 \leftrightarrow 2)}{\sum_q e_q^2 q(x_1, M^2)\bar{q}(x_2, M^2) + (1 \leftrightarrow 2)} \ , \quad (9)$$

where $\widehat{a}_{TT} = -1$ and M^2 is the dilepton mass square. It involves the product of δq and $\delta\bar{q}$, as expected from the dominant $q\bar{q}$ annihilation Drell-Yan mechanism. Predictions using the saturation of the bound, lead to some estimates of only a few percents, but it is on the list of future measurements at the BNL-RHIC spin program.

The asymmetry at the Z pole, which reads

$$A_{TT}(Z) = \frac{\sum_q (b_q^2 - a_q^2)\delta q(x_1, M_Z^2)\delta\bar{q}(x_2, M_Z^2) + (1 \leftrightarrow 2)}{\sum_q (b_q^2 + a_q^2) q(x_1, M_Z^2)\bar{q}(x_2, M_Z^2) + (1 \leftrightarrow 2)} \ , \quad (10)$$

is also expected to be small. However, for the $W^\pm$ production, considered above, $A_{TT} = 0$, because the W has a $V - A$ coupling, *i.e.* $a_q = b_q$, which remains to be checked.

[2] Positivity is extremely useful to constrain spin observables, as discussed by X. Artru in these proceedings (See also Ref. [14]).

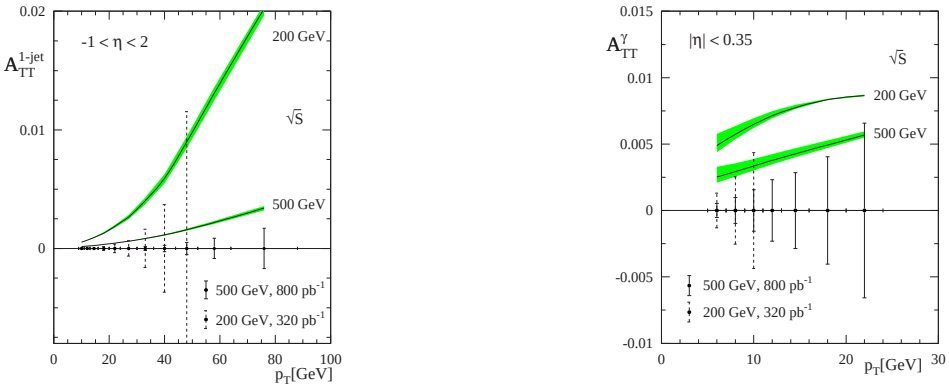

Figure 6: Left: Upper bounds for A_{TT} for single jet production at RHIC, with the expected statistical errors. Right: same for prompt photon production (Taken from Ref. [15]).

There is no such a transversity distribution for gluons which carry a spin one and this fact has important consequences for A_{TT} of different reactions. For example in the case of single-jet production, according to pQCD, the cross section in the low p_T region is dominated by gluon- gluon collisions, in the medium p_T region by gluon-quark collisions and in the high p_T region by quark-quark collisions. As a result, A_{TT} is expected to be non-zero only in this last kinematic region and this is what we see on the left hand side of Fig. 6. We have a similar situation for prompt photon production, shown on the right hand side of Fig. 6. These results, which were obtained by using the positivity bound, probe the sensitivity only to quark transversity in the hight p_T region. As was noticed in Ref. [15], we expect double spin transverse asymmetries to be much smaller than double helicity asymmetries, *i.e.* $|A_{TT}| << |A_{LL}|$ and this theoretical observation must be carefully confirmed experimentally.

4 Single spin asymmetry in QCD

What is a single spin asymmetry (SSA)?

Consider the collision of a proton of momentum $\overrightarrow{p}$, carrying a transverse spin $\overrightarrow{s_T}$ and producing an outgoing hadron with transverse momentum $\overrightarrow{k_T}$. The SSA defined as

$$A_N = \frac{d\sigma(\overrightarrow{s_T}) - d\sigma(-\overrightarrow{s_T})}{d\sigma(\overrightarrow{s_T}) + d\sigma(-\overrightarrow{s_T})} \tag{11}$$

is zero, unless the cross section contains a term $\overrightarrow{s_T} \cdot (\overrightarrow{p} \times \overrightarrow{k_T})$. It can be shown that this requires the existence of an *helicity flip* and *final state interactions*, which generate a phase difference between the flip and the non-flip amplitudes, to avoid violation of time reversal invariance. In the naive parton model one expects very small SSA, because of the double suppression $\alpha_s m_q/Q$, where m_q is the quark mass and Q the energy scale of the process.

Actually a large SSA has been discovered 30 years ago at FNAL with a 300 GeV/c unpolarized proton beam in $pBe \to \Lambda^{\uparrow} X$ [17] and many more SSA have been observed later, in particular large SSA in $p^{\uparrow} p \to \pi X$ and $\bar{p}^{\uparrow} p \to \pi X$ at FNAL by E704 [15] and

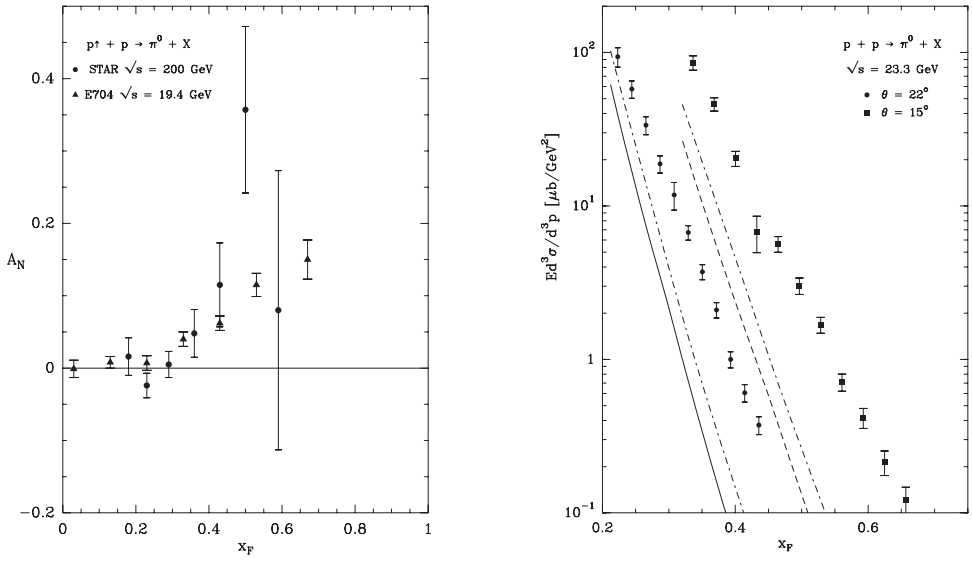

Figure 7: Left: The single spin asymmetry A_N as a function of x_F at two different energies. The data are from Refs. [15, 19]. Right: A comparison between a pQCD NLO calculation and data for two different angles (Taken from Ref. [22]) .

more recently by STAR at BNL-RHIC [19]. These data have the same trend, as shown in Fig. 7, although they were obtained in very different energy ranges. Therefore one can be tempted to conclude that they originate from the same mechanism satisfying scaling.

Before discussing this point, we recall that in the collinear approximation, the mechanism to generate SSA is based on higher-twist quark-gluon correlators (Efremov-Teryaev 1982, Qiu-Sterman 1991). However, if one introduces transverse momentum dependence (TMD), two QCD mechanisms have been proposed:
- TMD parton distributions ⇒ Sivers effect 1990
- TMD fragmentation distributions ⇒ Collins effect 1993

The gauge-invariance properties of the TMD PDF have been first clarified for DIS and Drell-Yan processes in Ref. [20]. In general both Sivers and Collins effects contribute to a specific reaction, although there are some cases in which only one of them contributes. For example in semi inclusive DIS, the Collins effect is the only mechanism that can lead to asymmetries A_{UT} and A_{UL}. On the other hand, it does not appear in some electroweak interaction processes, where there is only the Sivers effect. In prompt photon production in pp collisions, which is dominated by $qG \to q\gamma$, the SSA is sensitive to either the quark or the gluon Sivers functions, according to the value of the photon x_F [21].

Now let us ask: do we understand the SSA displayed on Fig. 7, given the fact that STAR is at a very small angle 2.6 deg., whereas E704 is at a much larger angle, between 9 deg. and 64 deg.? A negative answer is partially obtained by looking at the cross section. The pQCD NLO calculation underestimates the cross section at *low* energies and *medium* angles, namely for the E704 kinematic region. This is shown on Fig. 7 and it means that one should not ignore other contributions. This is not the case at 90 deg. and at very small angles at high energy, which is the STAR kinematic range. To conclude, one should

not try to "explain" the SSA, ignoring the unpolarized cross section [22]. Of course one should not forget resummation effects, which might help clarifying the situation.

Acknowledgements. This work was completed during my visit at the Universidad Santa Maria, Valparaiso, supported by the cooperation program Ecos-Conicyt C04E04 between France and Chile. I am grateful to the organizers of DSPIN07, for their invitation to this conference dedicated to L.I. Lapidus, I had the great privilege to meet several times. My special thanks go also to Prof. A.V. Efremov for providing a full financial support and for making, once more, this meeting so successful.

References

[1] C. Bourrely, F. Buccella and J. Soffer, Euro. Phys. J. **C23**, 487 (2002).
[2] C. Bourrely, F. Buccella and J. Soffer, Modern Phys. Lett. **A18**, 771 (2003).
[3] C. Bourrely, F. Buccella and J. Soffer, Euro. Phys. J. **C41**, 327 (2005).
[4] C. Bourrely, F. Buccella and J. Soffer, Modern Phys. Lett. **A21**, 143 (2006).
[5] C. Bourrely, F. Buccella and J. Soffer, Phys. Lett. **B648**, 39 (2007).
[6] H. Hirai, S. Kumano and N. Saito, Phys. Rev. **D74**, 014015 (2006).
[7] C. Bourrely, F. Buccella and J. Soffer, (in preparation).
[8] Compass Coll., M. Alekseev et *al.*, arXiv:0707.4077 [hep-ex].
[9] Hermes Coll., K. Ackerstaff et *al.*, Phys. Lett. **B464**, 123 (1999).
[10] JLab Hall A Coll., X. Zheng, et *al.*, Phys. Rev. **C70**, 065207 (2004).
[11] Hermes Coll., A. Airapetian et *al.*, Phys. Rev. Lett. **92**, 012005 (2004).
[12] A. M. Cooper-Sarkar et *al.*, Z. Phys. **C39**, 281 (1988).
[13] J. Soffer, Phys. Rev. Lett. **74**, 1292 (1995).
[14] X. Artru, M. Elchikh, J. M. Richard, J. Soffer and O. Teryaev, *Spin observables and spin structure functions: inequalities and dynamics*, Physics Reports (2008).
[15] J. Soffer, M. Stratmann and W. Vogelsang, Phys. Rev. **D65**, 114024 (2002).
[16] A. Mukherjee, M. Stratmann and W. Vogelsang, Phys. Rev. **D67**, 114006 (2003).
[17] G.Bunce et al., Phys. Rev. Lett. **36**, 1113 (1976).
[18] E704 Coll., D. L. Adams, Phys. Lett. **B261**, 201 (1991).
[19] STAR Coll., J. Adams et *al.*, Phys. Rev. Lett. **92**, 171801 (2004).
[20] S. Brodsky, D.S. Hwang and I. Schmidt, Phys. Lett. **B530**, 99 (2002).
[21] I. Schmidt, J. Soffer and J. J. Yang, Phys. Lett. **B612**, 258 (2005).
[22] C. Bourrely and J. Soffer, Euro. Phys. J. **C36**, 371 (2004).

Discussion

Comm. (S.Belostotsky, PNPI, St.Petersburg) 1. HERMES latest result differs from that presented by the speaker: $\Delta G \simeq 0.1 \pm 0.2$.

Q. (G.Lykasov, JINR, Dubna) Do the spin asymmetries die out with energy increase?

A. Yes, all spin-asymmetries are general coming down but that does not mean not importance to study them. Only the difficulties are getting more serious.

Q. (J.Nassalski, SINS, Warsaw) 1. The first hint on $\bar{u} < \bar{d}$ came from the NMC result on the Gottfried sum rules violation.

2. The first quark helicity distributions were obtained by the SMC.
3. You did not show the new HERMES result on $\Delta G/G$ which is lower than their first result.

A. 1. I fully agree and even have an article following the MNC data (PRL66, 687 (1991)).
2. I agree.
3. I agree but this was left to HERMES people, since a talk is scheduled on that.

Q. (S.Nurushev, IHEP, Protvino) Your statement about cross-section and analyzing power in reaction $p_{\uparrow}p \to \pi^0 X$ at $\sqrt{s} = 20GeV$ and $\sqrt{s} = 200GeV$ a little bit confused me. First the p_T region is small in both cases ($p_T \leq 3.5GeV/c$). How do you apply QCD for such small p_T region?
Second, the asymmetries are the same in both cases. How do you explain this fact in your model?

A. I have said that the pQCD NLO calculation agrees well with the STAR cross section which is at low p_T and $\sqrt{s} = 200$ GeV, but underestimate the E704 cross section data corresponding to the same p_T region. I don't explain the A_N for both experiment, but I claim that one should first understand the cross section in both cases.

SPIN EFFECTS FOR NEUTRINOS AND ELECTRONS MOVING IN DENSE MATTER

A.V. Grigoriev [1], A.M. Savochkin [2], A.I. Studenikin[2†] and A.I. Ternov[3]

(1) *Skobeltsin Institute of Nuclear Physics, Moscow State University*
(2) *Department of Theoretical Physics, Moscow State University*
(3) *Department of Theoretical Physics, Moscow Institute for Physics and Technology*
† *E-mail: studenik@srd.sinp.msu.ru*

Abstract

We give a review on a recently developed powerful method for investigation of different phenomena that can appear when neutrinos and electrons move in background matter with special focus on the spin phenomena.

This paper is devoted to the problem of neutrino and electrons motion in a dense matter with special focus on the spin phenomena.

It has been proven in recent oscillation experiments that neutrino has nonzero mass. Therefore, the Dirac neutrino should have nontrivial electromagnetic properties, in particular, nonzero magnetic moment. It is also well known [1] that in the minimally extended Standard Model with $SU(2)$-singlet right-handed neutrino the one-loop radiative correction generates neutrino magnetic moment which is proportional to the neutrino mass $\mu_\nu = \frac{3}{8\sqrt{2}\pi^2} e G_F m_\nu = 3 \times 10^{-19} \mu_0 \left(\frac{m_\nu}{1\mathrm{eV}} \right)$, where $\mu_0 = e/2m$ is the Bohr magneton, m_ν and m are the neutrino and electron masses. There are also models (see [2]) in which much large values for magnetic moment of neutrino are predicted.

The LEP data require that the number of light neutrinos coupling to Z boson is exactly three, whereas any additional neutrino, if this particle exist, must be heavy. In light of this opportunity we considered the neutrino magnetic moment for various ratios of particles masses. We have obtained [3] values of the neutrino magnetic moment for light (for this particular case see also [1, 4]), intermediate and heavy massive neutrino: 1) $\mu_\nu = \frac{eG_F}{4\pi^2\sqrt{2}} m_\nu \frac{3(2-7a+6a^2-2a^2\ln a - a^3)}{4(1-a)^3}$, for $m_\nu \ll m_\ell \ll M_W$, 2) $\mu_\nu = \frac{3eG_F}{8\pi^2\sqrt{2}} m_\nu \left\{ 1 + \frac{5}{18} b \right\}$, for $m_\ell \ll m_\nu \ll M_W$, 3) $\mu = \frac{eG_F}{8\pi^2\sqrt{2}} m_\nu$, for $m_\ell \ll M_W \ll m_\nu$, where $a = \left(\frac{m_l}{M_W} \right)^2$ and $b = \left(\frac{m_\nu}{M_W} \right)^2$. It should be also mentioned that the neutrino magnetic moment can be affected by the external environment. In particular, the value of the neutrino magnetic moment can be significantly shifted by the presence of strong external magnetic fields [5] (see also [6, 7]).

So far, solar neutrino experiments set a limit on the neutrino magnetic moment on the level of $\mu_{\nu_e} \leq 1.5 \times 10^{-10}$ [8]. More stringent constraint $\mu_{\nu_e} \leq 5.8 \times 10^{-11}$ has been provided by the GEMMA accelerator experiment [9]. The constraint from astrophysical considerations (the red giants cooling) is $\mu_{\nu_e} \leq 3 \times 10^{-12}$ [10].

Developing of the theory of neutrino spin properties in an external environment we have evaluated the Lorentz invariant approach to the neutrino spin evolution that was based on the proposed generalized Bargmann-Michel-Telegdi equation [11]. Within the developed Lorentz invariant approach it is also possible to find the solution for the neutrino

spin evolution problem for a general case when the neutrino is subjected to general types of non-derivative interactions with external fields [12]. These interactions are given by the Lagrangian

$$-\mathcal{L} = g_s s(x)\bar{\nu}\nu + g_p \pi(x)\bar{\nu}\gamma^5\nu + g_v V^\mu(x)\bar{\nu}\gamma_\mu\nu + g_a A^\mu(x)\bar{\nu}\gamma_\mu\gamma^5\nu + \frac{g_t}{2}T^{\mu\nu}\bar{\nu}\sigma_{\mu\nu}\nu + \frac{g'_t}{2}\Pi^{\mu\nu}\bar{\nu}\sigma_{\mu\nu}\gamma_5\nu, \tag{1}$$

where $s, \pi, V^\mu = (V^0, \mathbf{V}), A^\mu = (A^0, \mathbf{A}), T_{\mu\nu} = (\mathbf{a}, \mathbf{b}), \Pi_{\mu\nu} = (c, d)$ are the scalar, pseudoscalar, vector, axial-vector, tensor and pseudotensor fields, respectively. For the corresponding spin evolution equation we have found

$$\begin{aligned}\frac{d\mathbf{S}}{dt} = 2g_a\left\{A^0[\mathbf{S}\times\beta] - \frac{(\mathbf{A}\beta)[\mathbf{S}\times\beta]}{1+\gamma^{-1}} - \frac{1}{\gamma}[\mathbf{S}\times\mathbf{A}]\right\} + 2g_t\left\{[\mathbf{S}\times\mathbf{b}] - \frac{(\beta\mathbf{b})[\mathbf{S}\times\beta]}{1+\gamma^{-1}} + [\mathbf{S}\times[\mathbf{a}\times\beta]]\right\} \\ + 2ig'_t\left\{[\mathbf{S}\times\mathbf{c}] - \frac{(\beta\mathbf{c})[\mathbf{S}\times\beta]}{1+\gamma^{-1}} - [\mathbf{S}\times[\mathbf{d}\times\beta]]\right\}.\end{aligned} \tag{2}$$

This is a rather general equation for the neutrino spin evolution that can be also used for description of neutrino spin oscillations in different environments such as moving and polarized matter with external electromagnetic fields (see [13, 14]).

Considering the neutrino spin evolution within the quasi-classical treatment on the basis of the above mentioned generalized Bargmann-Michel-Telegdi equation, we have predicted [15] a new mechanism for the electromagnetic radiation by a neutrino moving in the background matter. We have termed this radiation the "spin light of neutrino" ($SL\nu$) in matter [15]. The term "spin light" was used [16] for designation of the magnetic-dependent term in the radiation of an electron in a magnetic field. The $SL\nu$ effect also studied in the cases when electromagnetic and gravitational fields also present in matter [17]. Here we should like to mention that the considered $SL\nu$ is indeed a new type of electromagnetic radiation of a neutrino that can be emitted by the particle in matter. This radiation mechanism has never been considered before. As it was mentioned in our first papers on this subject [15], the $SL\nu$ in matter can not be considered as the neutrino Cherenkov radiation in matter because it can exist even when the emitted photon refractive index is equal to unit. The $SL\nu$ radiation is due to radiation of the neutrino by its own rather then radiation of the background particles.

As it was clear from the very beginning [15], the $SL\nu$ is a quantum phenomenon by its nature and later on we elaborated [18] the quantum theory of this radiation (see also [19]). To put it on a solid ground, we of have elaborated a rather powerful method that implies the use of the exact solutions of the modified Dirac equation for the neutrino wave function in matter.

Recently we have spread this developed method of the "exact solutions" to description of an electron moving matter [20–22] and derived the modified Dirac equation for an electron moving in matter and found its solutions. On the basis of this exact solution of this equation we have considered a new mechanism for the electromagnetic radiation that can be emitted by an electron in the background matter. This mechanism is similar to the $SL\nu$ in matter and we termed it the "spin light of electron" in matter [20].

As it was shown in [18,20–22], in the case of the standard model interactions of electron neutrinos and electrons with matter composed of neutrons, the corresponding modified Dirac equations for each of the particles can be written in the following form:

$$\left\{i\gamma_\mu\partial^\mu - \frac{1}{2}\gamma_\mu(c_l + \gamma_5)\widetilde{f}^\mu - m_l\right\}\Psi^{(l)}(x) = 0, \tag{3}$$

where for the case of neutrino $m_l = m_\nu$ and $c_l = c_\nu = 1$, whereas for electron $m_l = m_e$ and $c_l = c_e = 1 - 4\sin^2\theta_W$. For unpolarized matter $\widetilde{f}^\mu = \frac{G_F}{\sqrt{2}}(n_n, n_n\mathbf{v})$, n_n and $\mathbf{v}$ are, respectively, the neutron number density and overage speed. The solutions of these equations are as follows,

$$\Psi^{(l)}_{\varepsilon,\mathbf{p},s}(\mathbf{r},t) = \frac{e^{-i(E^{(l)}_\varepsilon t - \mathbf{pr})}}{2L^{\frac{3}{2}}} \begin{pmatrix} \sqrt{1+\frac{m_l}{E^{(l)}_\varepsilon - c\alpha_n m_l}}\ \sqrt{1+s\frac{p_3}{p}} \\ s\sqrt{1+\frac{m_l}{E^{(l)}_\varepsilon - c\alpha_n m_l}}\ \sqrt{1-s\frac{p_3}{p}}\ e^{i\delta} \\ s\varepsilon\eta\sqrt{1-\frac{m_l}{E^{(l)}_\varepsilon - c\alpha_n m_l}}\ \sqrt{1+s\frac{p_3}{p}} \\ \varepsilon\eta\sqrt{1-\frac{m_l}{E^{(l)}_\varepsilon - c\alpha_n m_l}}\ \sqrt{1-s\frac{p_3}{p}}\ e^{i\delta} \end{pmatrix}. \tag{4}$$

where the energy spectra are

$$E^{(l)}_\varepsilon = \varepsilon\eta\sqrt{\mathbf{p}^2\Big(1 - s\alpha_n\frac{m_l}{p}\Big)^2 + m^2} + c_l\alpha_n m_l, \quad \alpha_n = \pm\frac{1}{2\sqrt{2}}G_F\frac{n_n}{m_l}. \tag{5}$$

Here p, s and ε are the particles momenta, helicities and signs of energy, "$\pm$" corresponds to e and ν_e. The value $\eta = \text{sign}\big(1 - s\alpha_n\frac{m_l}{p}\big)$ is introduced to provide a proper behavior of the neutrino wave function in the hypothetical massless case.

It should be pointed out that the derived modified Dirac equations for a neutrino and electron in matter and their exact solutions obtained establish an effective method for investigation of different phenomena that can arise when the particles move in dense media (for more details see [21]), including the cases peculiar for astrophysical and cosmological environments. For example, effects of the Dirac neutrino reflection and trapping, as well as neutrino-antineutrino annihilation and neutrino pair creation in matter at the interface between two media with different densities can be considered on this basis (see [23] and references therein).

Using the exact solutions of the above mentioned Dirac equations for a neutrino and electron we have performed detailed investigations of the $SL\nu$ and SLe in matter. In particular, in the case of ultra-relativistic neutrinos ($p \gg m$) and a wide range of the matter density parameter α for the total rate of the $SL\nu$ we obtained [18]

$$\Gamma_{SL\nu} = 4\mu_\nu^2\alpha^2 m_\nu^2 p, \qquad m_\nu/p \ll \alpha \ll p/m_\nu. \tag{6}$$

The main properties of the $SL\nu$ investigated in [15, 17, 18] can be summarized as follows: 1) a neutrino with nonzero mass and magnetic moment when moving in dense matter can emit spin light; 2) in general, $SL\nu$ in matter is due to the dependence of the neutrino dispersion relation in matter on the neutrino helicity; 3) the $SL\nu$ radiation rate and power depend on the neutrino magnetic moment and energy, and also on the matter density; 4) the matter density parameter α, that depends on the type of neutrino and matter composition, can be negative; therefore the types of initial and final neutrino (and antineutrino) states, conversion between which can effectively produce the $SL\nu$ radiation, are determined by the matter composition; 5) the $SL\nu$ in matter leads to the neutrino-spin polarization effect; depending on the type of the initial neutrino (or antineutrino) and matter composition the negative-helicity relativistic neutrino (the left-handed neutrino ν_L) is converted to the positive-helicity neutrino (the right-handed neutrino ν_R) or vice versa; 6) the obtained expressions for the $SL\nu$ radiation rate and power exhibit non-trivial

dependence on the density of matter and on the initial neutrino energy; the $SL\nu$ radiation rate and power are proportional to the neutrino magnetic moment squared which is, in general, a small value and also on the neutrino energy, that is why the radiation discussed can be effectively produced only in the case of ultra-relativistic neutrinos; 7) for a wide range of matter densities the radiation is beamed along the neutrino momentum, however the actual shape of the radiation spatial distribution may vary from projector-like to cap-like, depending on the neutrino momentum-to-mass ratio and the matter density; 8) in a wide range of matter densities the $SL\nu$ radiation is characterized by total circular polarization; 9) the emitted photon energy is also essentially dependent on the neutrino energy and matter density; in particular, in the most interesting for possible astrophysical and cosmology applications case of ultra-high energy neutrinos, the average energy of the $SL\nu$ photons is one third of the neutrino momentum. Considering the listed above properties of the $SL\nu$ in matter, we argue that this radiation can be produced by high-energy neutrinos propagating in different astrophysical and cosmological environments.

Performing the detailed study of the SLe in neutron matter [22] we have found for the total rate

$$\Gamma_{SLe} = e^2 m_e^2/(2p) \left[\ln\left(4\alpha_n p/m_e\right) - 3/2\right], \quad m_e/p \ll \alpha_n \ll p/m_e, \tag{7}$$

where it is supposed that $\ln \frac{4\alpha_n p}{m_e} \gg 1$. It was also found that for relativistic electrons the emitted photon energy can reach the range of gamma-rays. Furthermore, the electron can loose nearly the whole of its initial energy due to the SLe mechanism.

Several aspects of the background plasma effects in the $SL\nu$ radiation mechanism have been discussed in [18]. Recently this problem has been also considered in [24] and the total rates of the $SL\nu$ and SLe in plasma where derived. The final result of [24] for the $SL\nu$ rate, that accounted for the photon dispersion in plasma, in the case of ultra-high energy neutrino (i.e., when the time scale of the process can be much less than the age of the Universe) exactly reproduces our result (6) obtained in [18]. At the same time, the SLe total rate given by eq. (65) in the second paper of [24] in the leading logarithmic term confirms our result (7) obtained in [22].

Recently we have applied the developed method of exact solutions of quantum wave equations in the background matter to a particular case when a neutrino is propagating in a rotating medium of constant density [25]. Suppose that the neutrino propagates inside a uniformly rotating medium composed of neutrons. This can be considered for modelling of neutrino propagation inside a rotating neutron star. The corresponding modified Dirac equation for the neutrino wave function is given by (3) with the potential $\tilde{f}^\mu$ that accounts for the medium rotation. The equation can be solved in the considered case and for the energy spectrum of the relativistic active left-handed neutrinos with vanishing mass we have obtained

$$p_0 = \sqrt{p_3^2 + 2\gamma N} - G_F n/\sqrt{2}, \quad \gamma = G_F \omega n/\sqrt{2}, \quad N = 0, 1, 2, ..., \tag{8}$$

where ω is the angular frequency of the star rotation. The energy depends on the neutrino momentum component p_3 along the rotation axis of matter and the quantum number N that determines the value of the neutrino momentum in the orthogonal plane. Thus, it is shown that the transversal motion of an active neutrino is quantized very much like an electron energy is quantized in a constant magnetic field forming the Landau energy

levels. From these properties of the neutrino energy spectrum we predict that there is an effect of trapping neutrinos with the correspondent energies inside rotating dense stars.

The two of the authors (A.G. and A.S.) are thankful to Anatoly Efremov and Oleg Teryaev for the invitation to attend the XII Workshop on High Energy Spin Physics and for the kind hospitality provided in Dubna.

References

[1] K. Fujikawa, R. Shrock, Phys.Rev.Lett. **45**, 963 (1980).

[2] J. Kim, Phys.Rev. **D14**, 3000 (1976); M. Beg, W. Marciano, Phys.Rev. **D17**, 1395 (1978); M. Voloshin, M. Vysotsky, L. Okun, Sov.Phys.JETP **64**, 446 (1986); M. Fukugita, T. Yanagida, Phys.Rev.Lett. **58**, 1807 (1987); M. Voloshin, Sov.J.Nucl.Phys. **48**, 512 (1988).

[3] M. Dvornikov, A. Studenikin, Phys.Rev. **D69**, 073001 (2004); JETP **99** (2004) 254.

[4] L. Cabral-Rosetti, J. Bernabeu, J. Vidal, A. Zepeda, Eur.Phys.J. **C 12**, 633 (2000).

[5] A. Borisov, V. Zhukovsky, V. Kurilin, A. Ternov, Sov.J.Nucl.Phys. **41**, 743 (1985).

[6] A. Egorov, G. Likhachev, A. Studenikin, in: Elementary Particle Physics, Publ. by ICAS (Moscow, Russia, 1999), 52.

[7] J. Nieves, Phys.Rev. **D68**, 113003 (2003).

[8] J. F. Beacom and P. Vogel, Phys. Rev. Lett. **83**, 5222 (1999); D. W. Liu *et al.*, Phys. Rev. Lett. **93**, 021802 (2004).

[9] A.Beda et al, Phys.Atom.Nucl. **70**, 1873 (2007).

[10] G. G. Raffelt, Phys. Rep. **320**, 319 (1999).

[11] A.Egorov,A.Lobanov,A.Studenikin,Phys.Lett. B491 (2000) 137; A.Lobanov, A.Studenikin, Phys.Lett.B **515**, 94 (2001);

[12] M.Dvornikov, A.Studenikin, JHEP **09** (2002) 016.

[13] A. Studenikin, *Neutrinos in magnetic fields: from the first studies to the new effects in neutrino oscillations*, in: Results and Perspectives in Particle Physics, Les Recontres de Physique de la Vallee d'Aoste, ed. by M.Greco, Frascati Physics Series, V.XXXIV, p. 155; Nucl.Phys. B (Proc.Suppl.) **143**, 570 (2005); hep-ph/0407010.

[14] A. Studenikin, Phys.Atom.Nucl. **70**, 1275 (2007).

[15] A. Lobanov, A. Studenikin, Phys.Lett.B **564**, 27 (2003), hep-ph/0212393; Phys.Lett.B **601**, 171 (2004) .

[16] I.M.Ternov, Sov.Phys.Usp. **38**, 405 (1995); V.A.Bordovitsyn, I.M.Ternov, V.G.Bagrov, Sov.Phys.Usp. **38**, 1037 (1995).

[17] M.Dvornikov, A.Grigoriev, A.Studenikin, Int.J.Mod.Phys.D **14**, 309 (2005) .

[18] A. Studenikin, A. Ternov, Phys.Lett. B **608**, 107 (2005), hep-ph/0410297, hep-ph/0410296; A. Grigoriev, A. Studenikin, A. Ternov, Phys.Lett. B **622**, 199 (2005), hep-ph/0502231; A. Grigoriev, A. Studenikin, A. Ternov, Grav. & Cosm. **11**, 132 (2005).

[19] A.Lobanov, Dokl.Phys. **50**, 286 (2005), hep-ph/0411342; Phys.Lett.B **619**, 136 (2005), hep-ph/0506007.

[20] A. Studenikin, J.Phys.A: Math.Gen. **39**, 6769 (2006).

[21] A. Studenikin, Ann.Fond. de Broglie **31**, no 2-3, (2006), hep-ph/0611100.

[22] A. Grigoriev, S. Shinkevich, A. Studenikin, A. Ternov, I. Trofimov, Spin light of electron in matter, in: Particle Physics at the Year of 250th Anniversary of Moscow University, ed. by A.Studenikin, World Scientific (Singapore), p. 73 (2006); Izv.Vuzov.Fizika (Russia) No.6, p.66 (2007), hep-ph/0611128.

[23] A. Grigoriev, A. Studenikin, A. Ternov, Phys.Atom.Nucl. **69**, 1940 (2006).

[24] A. Kuznetsov, N. Mikheev, Mod.Phys.Lett A **23**, 1769 (2006); Int.J.Mod.Phys. A **22** 3211 (2007).

[25] A. Grigoriev, A. Savochkin, A. Studenikin, Izv.Vuzov.Fizika (Russia) No. 8, 90 (2007).

Discussion

Q. (S.Nurushev, IHEP, Protvino) I have two questions:
1) As I remember, Prof. I.M. Ternov wrote a paper "Spin-light of electrons" several years ago. Is your mechanism relevant to that process which was experimentally observed?
2) If the neutrino has a mass, how much it may influence your results?

A. 1) We termed a new mechanism of electromagnetic radiation by a neutrino moving in matter as "Spin Light of Neutrino" because this light originates from the neutrino momentum procession (in matter) that in fact reminds us the "Spin Light of Electron" (in magnetic field) that was discussed in papers of Igor Mikhailovich and that was observed in Novosibirsk in 80th.
2) In fact, we need non-zero neutrino mass because a massive neutrino should have no magnetic moment so that in this case there is no spin light.

Q. (V.Huseynov, Nakhchivan Univ.) 1) Does the medium radiate or does a neutrino radiate when neutrino propagate in the medium?
2) Does anomalous magnetic moment of a neutrino change its sign when the magnetic field strength is greater then the corresponding Schwinger critical field strength? Do any tachyon modes appear in this case?

A. 1) The spin light of neutrino (SL_ν) in matter is radiated by the neutrino itself and this is a new mechanism of electromagnetic radiation that has never discussed before. The SL_ν is not a Cherenkov radiation (the Cherenkov radiation of neutrino in matter was considered before by many people and it is the radiation that is emitted not by a neutrino but by particles of the background matter through which a neutrino is propagating).
2) In strong magnetic filed of the order of the critical Schwinger value ($m_e^2/e = 4.41 \cdot 10^{13}$ Gauss), the influence of the field on the neutrino magnetic moment is not visible. However, in the very extreme case of the magnetic field of the order of $m_W^2/e \approx 10^{24}$ Gauss there is a significant increase of the neutrino magnetic moment (this has been checked for the one-loop contribution to the neutrino magnetic moment).

SIVERS FUNCTION: FROM SMALL TO LARGE TRANSVERSE MOMENTA

P.G. Ratcliffe[1] and O.V. Teryaev[2†]

(1) *Dipartimento di Fisica e Matematica,*
Università degli Studi dell'Insubria, via Valleggio 11, 22100 Como, Italy
and
Istituto Nazionale di Fisica Nucleare—sezione di Milano–Bicocca,
piazza della Scienza 3, 20126 Milano, Italy
(2) *Bogoliubov Laboratory of Theoretical Physics,*
Joint Institute for Nuclear Research, 141980 Dubna, Moscow region, Russia
† *E-mail: teryaev@theor.jinr.ru*

Abstract

The soft-gluon twist-3 contributions to single-spin asymmetries (SSA) in hard processes may be expressed in the form of *effective* T-odd Sivers distributions, whose signs and scales are modified by process-dependent colour factors. The Sivers mechanism is applied at large transverse momenta and the emission of balancing gluons provide the colour flow explaining this factor.

Introduction. Single-spin asymmetries (SSA) represent one of the most subtle and intriguing effects in QCD. In the simplest inclusive processes parity conservation requires a transversely polarised beam or target. The transverse polarisation component is not enhanced by Lorentz boosts, and one immediately encounters the necessity of describing twist-3 effects. This can be achieved via use of either local [1] or non-local [2–5] operators.

The latter approach also permits the description of the imaginary phases required to produce T-odd effects, such as SSA. These phases mimic true T(CP) violation (see *e.g.* [6]) and allow T-odd effects in a T-conserving theory, such as QCD. The phases emerging from gluon loops describing initial- and final-state interactions (ISI and FSI) in hard subprocesses are suppressed by powers of light-quark masses and the QCD coupling constant [7]. However, deeper analysis [8] shows that quark masses should be substituted by hadronic mass scales. Moreover, ISI and FSI between the hard and soft regions of QCD factorisation, which is just the physical picture corresponding to twist three, lead to SSA free of both suppression factors [9]. The imaginary phase is generated by gluon correlations with soft quarks; the situation when instead the gluon is soft was also considered later [10].

An alternative description of SSA effects is provided by a T-odd transverse-momentum dependent (TMD) distribution function, first introduced by Sivers [11]. As soon as there is no kinematical variable whose cut produces an imaginary phase in the hadron–parton transition amplitude, this may simply become an effective function [6], so that the phase also emerges owing to the ISI and FSI involving hard subprocess. The first case of the appearance of an effective T-odd distribution was found [12] for soft-gluon SSA in the Drell–Yan (DY) process integrated over transverse momenta [13]. It was later identified [14] with the first moment of the Sivers function, which plays a special role in what follows. The role of FSI between the hard and soft regions of semi-inclusive deeply inelastic scattering (SIDIS) was clearly revealed in the model of Brodsky, Hwang and Schmidt [15],

where it was interpreted [16] as a manifestation of the Sivers function. The crucial role of hard processes in defining this function was made manifest by the discovery of a sign difference between SIDIS and DY.

This is all qualitatively similar to earlier findings [17] in the twist-3 case. However, the apparent difference between the FSI arising in twist-3 interactions is the absence of true power suppression. The situation is, though, even more peculiar. In the hard Abelian process of semi-inclusive production of a real photon by a deeply virtual photon (SIDVCS, the semi-inclusive counterpart of the well-known DVCS [18] process) an overall suppression as $b(x_B, x_B - x_g)Mp_T/Q^2$ was shown [19] to be compensated by a gluonic pole in the quark–gluon correlator $b \sim 1/x_g$, which is approached at low $p_T \ll Q$ as the gluon momentum fraction is defined by kinematics $x_g \sim p_T^2/Q^2$, indicating the possibility to obtain unsuppressed (in Q) twist-3 effects. Similar conclusions that the Sivers function and gluonic poles describe similar physics for different p_T have been reached within the framework of a general proof [20].

These analyses imply a picture in which the Sivers function is limited to the low-p_T region, where a special type of factorisation [21] is assumed valid and either the continuation of the twist-3 result to lower p_T [19] or matching [20] of high- and low-p_T results is adopted.

Recently, a different, complementary approach [22] was suggested to apply the Sivers function at *high* p_T. This is of special importance for hadronic processes where p_T is the only hard scale. The general quantitative relations between the Sivers function and gluonic poles, using master formulæ [23] for the latter lead, besides the sign, to the important process-dependent colour factors (*cf.* [24, 25], where such colour factors were calculated by considering gauge links) modifying the Sivers function and underlining its effective nature.

In the approach suggested these factor correspond to the colour flow carried by the hard partons balancing transverse momentum. It is a universal feature of the processes, while the sign factor between SIDIS and DY at low p_T is an exception due to the participation of only a colour-neutral hard photon and emerging colour correlations between the initial and final quarks (in SIDIS) or initial quark and antiquark (in DY).

From the Sivers function to gluonic poles. To prove the relation between twist three and the Sivers function we shall not attempt to obtain the latter as some special limit [19, 20] of a twist-3 contribution, but instead transform some approximation of it to the form [23] appearing in the twist-3 calculation. In other words, we are going to provide *a posteriori* proof of the following factorised formula involving the Sivers function

$$d\Delta\sigma \sim \int d^2k_T\, dx\, f_S(x, k_T)\, Tr\left[\gamma_\rho H(xP, k_T)\right] \epsilon^{\rho sPk_T}, \tag{1}$$

where other (unpolarized and collinear) distribution or fragmentation functions should normally also be present. To achieve this goal, we expand the subprocess coefficient function H in powers of k_T, retaining only the first non-vanishing term: and after some algebra get [22]:

$$d\Delta\sigma \sim M \int dx\, f_S^{(1)}(x)\, Tr\left[\not{P} \frac{\partial H(xP, k_T)}{\partial k_T^\alpha}\right]_{k_T=0} \epsilon^{\alpha sPn}. \tag{2}$$

The key observation now is that this expression exactly coincides with the recently obtained master formula [23] for the contribution of twist-3 gluonic poles in high-p_T processes. The Sivers distribution can then be identified with the gluonic pole strength $T(x,x)$ multiplied by a process-dependent colour factor. In turn, the sign of the Sivers function is fixed according as to which of the ISI or FSI is relevant:

$$f_S^{(1)}(x) = \sum_i C_i \frac{1}{2M} T(x,x), \tag{3}$$

where C_i is a relative colour factor, defined with respect to an Abelian subprocess (say SIDVCS discussed above, where it is just C_F), which is naturally absorbed into the definition of the quark–gluon correlator [3]. As we shall discuss below, this is also the factor appearing in low-p_T SIDIS and DY at the Born level.

The relation established is one of the principal results of this paper. It completes the *a posteriori* proof of (1) and relates the twist-3 factorization to the *modified* (by colour factors) factorization in terms of Sivers function The second moment of the Sivers function enters the original expression (1) with a factor M instead of $1/M$, indicating its twist-3 nature. This may be seen immediately by defining the Sivers function in coordinate (impact-parameter) space, in a manner similarly to earlier discussions [27] of the Collins fragmentation function:

$$\langle P,s|\psi(0)\gamma_\rho\psi(z)|P,s\rangle \sim M\epsilon^{\rho sPz}\int dx\; e^{izx} f_S^{(1)}(x). \tag{4}$$

Note too that higher Sivers-function moments enter with higher derivatives of the coefficient function and therefore correspond to higher twist (5, 7, 9, ...). The entire k_T-dependent Sivers function thus corresponds to a resummed infinite tower of higher twists. This property has also been studied in coordinate space [27], where k_T-dependent functions represent a complete similarity with non-local quark condensates. The latter manifest a similar resummation of an infinite tower of higher twists (see *e.g.* [28] and refs. therein), but for vacuum rather than hadronic matrix elements.

Colour factors and the transition from large to small transverse momenta. Let us consider some particular applications of this relation, starting with high-p_T SIDIS. In this case there are only final-state interactions, while the colour factors differ for mesons produced in fragmentation of quarks ($-1/2N_c$); or gluons ($N_c/2$). This shows that there is a specific enhancement in the latter, which is of special importance for K^- mesons.

To experimentally verify such a picture, it would be of major importance to distinguish between mesons originating from either quark or gluon fragmentation at large p_T. While a complete separation is impossible, there are methods that can help. Firstly, one may use jet shape, which differs for quark and gluon jets owing to the different spins of the fragmenting objects. This difference in spin can also be seen in the tensor polarization of vector mesons [30]. However, most promising would seem to be exploration of the different z-dependence in quark and gluon fragmentation functions. The faster decrease of the latter should result in dramatic variations of SSA, so that at low z gluon fragmentation would be dominant with a colour factor $N_c/2$, while at large z one would expect a sign change and transition to quark fragmentation with a factor $-1/2N_c$.

Let us now turn to hadronic processes, starting with the simplest: direct-photon production. There are only initial-state interactions with gluons, resulting in the very simple relation

$$F_S^{hh\to\gamma X} = \frac{N_c}{2}\, f_S^{DY}. \tag{5}$$

Exploration of this process in various kinematical regions can provide information on the gluon Sivers function [31]. There is little doubt that this is also an effective function, related to the three-gluon correlators considered earlier in relation to pion SSA [32] and the DIS structure function g_2 [33,34]. The generalization of our approach to the case of three-gluon correlators is therefore an important task. Consideration of quark–gluon processes is more complicated; a list of colour factors relevant for twist-3 subprocesses may be found in [24, 25]. Let us only mention that FSI for pions produced in quark fragmentation may be reexpressed in a manifestly gauge-invariant manner via the summation formula

$$t^a S\, t^a = -\frac{1}{2N_c}\, S + \frac{1}{2} I\, Tr S. \tag{6}$$

The first term corresponds to the usual Sivers function [35] with colour factor $-1/2N_c$ and the second to the Abelian Compton subprocess, with s- and u-channel diagrams contributing with the same factors while the t-channel is absent. Both terms are separately gauge invariant. The general proof of gauge invariance in hadronic collisions remains to be found

The colour factor is defined by the colour charge of the parton participating in the ISI and FSI. This charge is, generally speaking, independent of the properties of the polarized hadron emitting the gluon that participates in the ISI and FSI and, in this sense, breaks factorization. SIDIS and DY processes at low p_T are exceptional: the colour charge of the quark participating in the FSI in SIDIS is the same as that of the quark originally emitted by polarized hadron. By the same token, the colour charge of the antiquark participating in the ISI in DY processes at low p_T is just the opposite, which explains the Collins sign rule. At the same time, the emission of a hard gluon changes these colour charges in high-p_T SIDIS, DY processes and, needless to say, other hadronic processes. This modification of colour charge causes a colour modification of the effective Sivers function.

Discussion and Conclusions. We have suggested and proved here a method of applying the Sivers distribution at large transverse momenta. We have shown that the Sivers function is, in effect, none other than an expression of the contribution of gluonic poles. It is therefore process dependent and this dependence includes, besides the sign related to the ISI and FSI responsible for the imaginary phase, a colour factor. This situation means that *validity* of factorization in terms of twist-3 correlators leads to its *violation* or *modification* in terms of Sivers function. The colour factor is defined by the colour charge of the initial and final partons participating in the hard scattering. Its simplest manifestation is provided by the sign difference between SIDIS and DY processes at low p_T. At the same time, at high p_T and in hadronic reactions these factors are much more complicated.

Such a picture is complementary to that considered previously, in which matching between the Sivers function and twist-3 matrix elements occurred in the region where, strictly speaking, factorization formulæ were not valid. This complementary method of

establishing a relation between the Sivers function and twist-3 matrix elements lends support to the possibility of global fits of Sivers functions [19], including lepton–hadron and hadron–hadron processes, as well as DIS, where twist three also contributes.

Acknowledgments. O.T. is grateful to the Cariplo Science Foundation for support during his stay at the University of Insubria in Como and to the Department of Physics and Mathematics of the University for kind hospitality. This work was partially supported by the Deutsche Forschungsgemeinschaft, grant 436 RUS 113/881/0, the Russian Foundation for Basic Research (Grant 03-02-16816) and the Russian Federation Ministry of Education and Science (Grant MIREA 2.2.2.2.6546).

References

[1] E. V. Shuryak and A. I. Vainshtein, Nucl. Phys. **B201**, 141 (1982).
[2] A. P. Bukhvostov, É. A. Kuraev and L. N. Lipatov, JETP Lett. **37**, 482 (1983).
[3] A. V. Efremov and O. V. Teryaev, Sov. J. Nucl. Phys. **39**, 962 (1984).
[4] P. G. Ratcliffe, Nucl. Phys. **B264**, 493 (1986).
[5] I. I. Balitsky and V. M. Braun, Nucl. Phys. **B311**, 541 (1989).
[6] O. V. Teryaev, in proc. of the *Circum-Pan-Pacific RIKEN Symp. on High Energy Spin Physics* (Wako, Nov. 1999), eds. S. Kumano, T.-A. Shibata, Y. Watanabe and K. Yazaki; RIKEN Rev. **28**, 101 (2000).
[7] G. L. Kane, J. Pumplin and W. Repko, Phys. Rev. Lett. **41**, 1689 (1978).
[8] A. V. Efremov and O. V. Teryaev, Sov. J. Nucl. Phys. **36**, 140 (1982).
[9] A. V. Efremov and O. V. Teryaev, Phys. Lett. **B150**, 383 (1985).
[10] J. Qiu and G. Sterman, Phys. Rev. Lett. **67**, 2264 (1991).
[11] D. Sivers, Phys. Rev. **D41**, 83 (1990) and These Proceedings
[12] D. Boer, P. J. Mulders and O. V. Teryaev, Phys. Rev. **D57**, 3057 (1997).
[13] N. Hammon, O. Teryaev and A. Schäfer, Phys. Lett. **B390**, 409 (1997).
[14] D. Boer, P. J. Mulders and F. Pijlman, Nucl. Phys. **B667**, 201 (2003).
[15] S. J. Brodsky, D. S. Hwang and I. Schmidt, Phys. Lett. **B530**, 99 (2002).
[16] J. C. Collins, Phys. Lett. **B536**, 43 (2002);
[17] O. V. Teryaev, in proc. of the *10th. Int. Workshop on Deep Inelastic Scattering—DIS 2002* (Kraków, Apr.–May 2002), eds. A. Eskreys, J. Kwieciński and J. Szwed; Acta Phys. Polon. **B33**, 3749 (2002).
[18] X. Ji, Phys. Rev. **D55**, 7114 (1997).
[19] O. V. Teryaev, in proc. of the *Int. Workshop on Transverse Polarisation Phenomena in Hard Processes—Transversity 2005* (Como, Sept. 2005), eds. V. Barone and P. G. Ratcliffe (World Sci., 2006), p. 276.
[20] X. Ji, J.-W. Qiu, W. Vogelsang and F. Yuan, Phys. Rev. Lett. **97**, 082002 (2006).
[21] J. C. Collins and A. Metz, Phys. Rev. Lett. **93**, 252001 (2004).
[22] P. G. Ratcliffe and O. V. Teryaev, arXiv:hep-ph/0703293.
[23] Y. Koike and K. Tanaka, Phys. Lett. **B646**, 232 (2007);

[24] C. J. Bomhof and P. J. Mulders, in proc. of the *XVII Int. Symp. on High-Energy Spin Physics—SPIN 2006* (Kyoto, Oct. 2006), eds. K. Imai, T. Murakami, N. Saito and K. Tanida; AIP Conf. Proc. **915**, 563 (2007).

[25] C. J. Bomhof, P. J. Mulders, W. Vogelsang and F. Yuan, Phys. Rev. **D75**, 074019 (2007);

[26] X.-d. Ji, J.-p. Ma and F. Yuan, Phys. Rev. **D71**, 034005 (2005).

[27] O. V. Teryaev, in proc. of the *X Adv. Research Workshop on High Energy Spin Physics—SPIN-03* (Dubna, Sept. 2003), eds. A. V. Efremov and O. V. Teryaev; Phys. Part. Nucl. **35**, S24 (2004).

[28] A. P. Bakulev and S. V. Mikhailov, Phys. Rev. **D65**, 114511 (2002).

[29] J. Collins and J.-W. Qiu, Phys. Rev. **D75**, 114014 (2007).

[30] A. Schäfer, L. Szymanowski and O. V. Teryaev, Phys. Lett. **B464**, 94 (1999).

[31] I. Schmidt, J. Soffer and J.-J. Yang, Phys. Lett. **B612**, 258 (2005).

[32] X. Ji, Phys. Lett. **B289**, 137 (1992).

[33] A. V. Belitsky, A. V. Efremov and O. V. Teryaev, Phys. Atom. Nucl. **58**, 1253 (1995).

[34] A. V. Belitsky, X. Ji, W. Lu and J. Osborne, Phys. Rev. **D63**, 094012 (2001).

[35] M. Anselmino, M. Boglione, U. D'Alesio, E. Leader and F. Murgia, Phys. Rev. **D71**, 014002 (2005).

DIRECTED FLOW AND ROTATION OF TRANSIENT MATTER

S.M. Troshin† and N.E. Tyurin

Institute for High Energy Physics, Protvino, 142281 Russia
†E-mail: Sergey.Troshin@ihep.ru

Abstract

Directed flow v_1 treated as an effect of the transient matter rotation in hadronic and nuclei reactions.

Multiparticle production in hadron and nucleus collisions and corresponding observables provide a clue to the mechanisms of confinement and hadronization. Discovery of the deconfined state of matter has been announced by the four major experiments at RHIC [1]. Despite the highest values of energy and density have been reached, a genuine quark-gluon plasma QGP (gas of the free current quarks and gluons) was not found [1]. The deconfined state reveals the properties of the perfect liquid, being strongly interacting collective state and therefore it was labelled as sQGP [3]. The nature of the new form of matter is not known. The importance of the experimental discoveries at RHIC is that the matter remains strongly correlated and reveals high degree of the coherence when it is well beyond the critical values of density and temperature. In this report we would like to stress that the behavior of collective observables in hadronic and nuclear reactions could have some similarities. Among several experimental probes of collective dynamics in AA interactions [4, 5] are the momentum anisotropies v_n defined by means of the Fourier expansion of the transverse momentum spectrum over the momentum azimuthal angle ϕ. With measurements of these observables one can obtain a valuable information on the early stages of reactions and observe signals of QGP formation [6–14]. We discuss the role of the coherent rotation of the transient matter in hadron and nuclei collisions and the directed flow dependence. Hypothesis on connection of the strongly interacting transient matter rotation with the directed flow generation is the main point of this report.

We consider non-central hadron collisions and apply notions acquired from heavy-ion studies. In particular, we amend the model [15] developed for hadron interactions (based on the chiral quark model ideas) and consider the effect of collective rotation of a quark matter in the overlap region. The determination of the reaction plane in the non-central hadronic collisions [16] could be experimentally realizable with the utilization of the standard procedure [17]. Geometrical picture of hadron collision at non-zero impact parameters [15] implies that the generated massive virtual quarks in overlap region (due to shock-wave type of interaction of the condensate clouds[2]) carry large orbital angular momentum at high energies. The total orbital angular momentum can be estimated as follows

$$L(s,b) \simeq \alpha b \frac{\sqrt{s}}{2} D_C(b). \quad (1)$$

[1] It is to be noted here that confinement due to causality principle might exclude the very existence of QGP defined that way [2].

[2] This mechanism is similar to the shock-wave production process proposed by Heisenberg [18]

The parameter α is related to the fraction of the initial energy carried by the condensate clouds which goes to rotation of the quark system and

$$D_C(b) \equiv D_c^{h_1} \otimes D_c^{h_1},$$

where function D_c^h describes peripheral condensate distribution inside the hadron h, and b is an impact parameter of the colliding hadrons. The overlap region, which is described by the function $D_C(b)$, has an ellipsoidal form similar to the overlap region in the nucleus collisions. It should be noted that $L \to 0$ at $b \to \infty$ and $L = 0$ at $b = 0$. Similar impact parameter dependence with maximum at the impact parameter values around 1 fm the directed flow v_1 has.

Due to strong interaction between quarks the orbital angular momentum L leads to coherent rotation of the quark-pion liquid located in the overlap region as a whole in the xz-plane since strong correlations between particles are presented there. It should be noted that for the given value of the orbital angular momentum L kinetic energy has a minimal value if all parts of liquid rotates with the same angular velocity. We assume therefore that the different parts of the quark-pion liquid in the overlap region indeed have the same angular velocity ω. It has grounds also in the perfect, non-viscous, character of the liquid revealed at RHIC. Such coherent rotation is absent in the parton picture used in [20], where finite transverse gradient of parton longitudinal momentum is a driving force of the orbital angular momentum conversion to the global system polarization through spin-orbital coupling. The polarization not yet been detected experimentally [19].

The generation time of the transient state Δt_{tsg} obey to the inequality $\Delta t_{tsg} \ll \Delta t_{int}$, where Δt_{int} is the total interaction time. The assumed particle production mechanism at moderate transverse momenta is an excitation of a part of the rotating transient state of massive constituent quarks (interacting by pion exchanges) by the one of the valence constituent quarks with subsequent hadronization of the quark-pion liquid droplets. Due to the fact that the transient matter is strongly interacting, the excited parts should be located closely to the periphery of the rotating transient state otherwise absorption would not allow to quarks and pions to leave the region (quenching). The mechanism is sensitive to the particular rotation direction and the directed flow should have opposite signs for the particles in the fragmentation regions of the projectile and target respectively. It is evident that the effect of rotation (shift in p_x value) is most significant in the peripheral part of the rotating quark-pion liquid and is to be weaker in the less peripheral regions (rotation with the same angular velocity ω), i.e. the directed flow v_1 (averaged over all transverse momenta) directly depends on the distance to the center of the rotating matter or on the depth Δl where the excitation of the rotating quark-pion liquid takes place. In its turn, the length Δl should be proportional to the energy loss of constituent valence quark in the medium (quark-pion liquid) prior an excitation occurs, i.e. before constituent quark would deposit its energy into the energy of the excited quarks (those quarks lead to the production of the secondary particles)

$$\Delta l \sim \Delta E. \tag{2}$$

Proportionality of the energy loss due to elastic rescattering and Δl is a consequence of the liquid nature of the transient state which has fixed interparticle distances. Energy loss ΔE should (in a rough approximation) be proportional to the difference between the rapidities of the final particle and the projectile. Thus, the observable v_1, which

magnitude is determined by the shift of transverse momentum due to rotation and depend therefore on the value of Δl in this mechanism, would depend in its turn on the rapidity difference $y - y_{beam}$ and not on the incident energy. The mechanism therefore can provide a qualitative explanation of the incident-energy scaling of v_1 observed at RHIC [21]. Evidently, the directed flow $|v_1|$ decreases when the absolute value of the above difference increases, i.e. $|v_1|$ increases at fixed energy and increasing rapidity of final particle and it decreases at fixed rapidity of final particle and increasing beam energy.

An important assumption based on the RHIC data is the strongly interacting nature of the transient matter, namely, it was supposed that valence constituent quark excites quark-pion liquid in the closest hemisphere to the entry point.

The magnitude of $|v_1|$ is to be proportional to inverse depth length Δl^{-1} which is determined by elastic quark scattering cross-section σ and quark pion liquid density n, i.e. $\Delta l \sim 1/\sigma n$ and therefore averaged value of v_1 should be proportional to the particle density of the transient state $\langle |v_1| \rangle \sim \sigma n$. This estimate shows that the magnitude of the directed flow could provide information on the properties of the transient state. The centrality dependence of v_1 should be decreasing towards high and lower centralities. Decrease toward high centralities is evident, no overlap of hadrons or nuclei should be at high enough impact parameters. Decrease of v_1 toward lower centralities is specific prediction of the proposed mechanism based on rotation since central collisions with smaller impact parameters would lead to slower rotation or its complete absence in the head-on collisions.

If the proposed mechanism of the directed flow generation is realized, vanishing directed flow can serve as a signal of a genuine quark-gluon plasma (gas of free quarks and gluons) formation. Then the orbital momentum, could be converted e.g. into the global polarization at the partonic level and detected experimentally measuring hyperon or photon polarizations [20].

It would be interesting to perform studies of transient matter at the LHC not only in heavy ion collisions, but also in pp–collisions, and to find possible existence or absence of the rotation effects through the directed flow and polarization measurements. Collective rotation should also contribute to the elliptic flow. However, since the regularities already found experimentally for v_1 and v_2 in nuclei interactions imply different dynamical origin for these flows, we should conclude that the rotation does not provide a significant contribution to elliptic flow.

Acknowledgement

We are grateful to J. Dunlop and O. Teryaev for the interesting discussions. One of the authors (S.T.) is also grateful to the Organizing Committee of the XII Workshop on High Energy Spin Physics and especially to its Chairman A.V. Efremov for the support and warm hospitality in Dubna.

References

[1] Quark Gluon Plasma. New Discoveries at RHIC: A Case of Strongly Interacting Quark Gluon Plasma. Proceedings, RBRC Workshop, Brookhaven, Upton, USA,

May 14-15, 2004: D. Rischke, G. Levin, eds; 2005, 169pp; J. Adams et al. (STAR Collaboration) Nucl. Phys. A 757, 102 (2005); K. Adcox et al (PHENIX Collaboration), Nucl. Phys. A 757, 184 (2005).

[2] D. Miśkoviec, [arXiv: 0707.0923].

[3] D. d'Enterria, [arXiv: nucl-ex/0611012].

[4] J.-Y. Ollitrault, Phys. Rev. D46, 229 (1992); recent review can be found in S.A. Voloshin, Nucl. Phys. A715, 379 (2003).

[5] D. Molnar, [arXiv: nucl-th/0408044].

[6] J. Hofmann, H. Stöcker, U. W. Heinz, W. Scheid, W. Greiner, Phys. Rev. Lett. 36, 88, (1976).

[7] H. Stöcker, J. A. Maruhn, W. Greiner, Phys. Lett. B 81, 303, (1979).

[8] H. Stöcker, J. A. Maruhn, W. Greiner, Phys. Rev. Lett. 44, 725 (1980).

[9] H. Stöcker, W. Greiner, Phys. Rept. 137, 277, (1986).

[10] H. Sorge, Phys. Rev. Lett. 82, 2048 (1999) [arXiv:nucl-th/9812057].

[11] M. Bleicher, H. Stöcker, Phys. Lett. B 526, 309 (2002) [arXiv:hep-ph/0006147].

[12] H. Stöcker, Nucl. Phys. A 750, 121 (2005) [arXiv:nucl-th/0406018].

[13] X. l. Zhu, M. Bleicher, H. Stöcker, J. Phys. G 32, 2181 (2006) [arXiv:nucl-th/0601049].

[14] H. Petersen, Q. Li, X. Zhu, M. Bleicher, Phys. Rev. C 74, 064908 (2006) [arXiv:hep-ph/0608189].

[15] S. M. Troshin, N. E.Tyurin, Phys. Rev. D 49, 4427 (1994).

[16] S.A. Voloshin, [arXiv: nucl-th/0410089].

[17] S.A. Voloshin, A.M. Poskanzer, Phys. Lett. B 474, 27 (2000).

[18] W. Heisenberg, Zeit. Phys. 133, 65 (1952).

[19] B.I. Abelev et al, (STAR Collaboration), [arXiv:0705.1691].

[20] Z.-T. Liang, X.-N. Wang, Phys. Rev. Lett. 94, 102301 (2005), ibid. 96, 039901 (2006) A. Ipp, A. Di Piazza, J. Evers, C.H. Keitel, [arXiv:0710.5700].

[21] G. Wang (for the STAR Collaboration), arXiv: nucl-ex/0701045;// B.B. Back et al., (PHOBOS Collaboration), Phys. Rev. Lett., 97, 012301 (2006);
A.H. Tang (for the STAR collaboration), J. Phys. G: Nucl. Part. Phys. 31, S35 (2005); J. Adams et al. (STAR Collaboration), Phys. Rev. C 73, 034903 (2006).

COMPARATIVE ANALYSIS OF TRANSVERSITIES AND LONGITUDINALLY POLARIZED DISTRIBUTIONS OF THE NUCLEON

M. Wakamatsu†

(1) *Department of Physics, Faculty of Science, Osaka University, Toyonaka, Osaka 560-0043, JAPAN*
† *E-mail: wakamatu@phys.sci.osaka-u.ac.jp*

Abstract

We carry out a comparative analysis of the transversities and the longitudinally polarized parton distribution functions in light of the first empirical extraction of the transversity distributions recently done by Anselmino et al. It is shown that the precise determination of the isoscalar tensor charge, which is defined as the 1st moment of the isoscalar combination of the transversity distributions, is of fundamental importance for clarifying the internal spin structure function of the nucleon.

As is well known, the transversity is one of the three fundamental parton distribution functions (PDFs) with the lowest twist 2. Different from the other two, i.e. more familiar unpolarized PDF and the longitudinally polarized PDF, its chiral-odd nature prevents us from extracting it directly through the standard inclusive deep-inelastic-scattering measurements [1], [2]. For this reason, we have had little empirical information on it until recently. Very recently, however, Anselmino et al. succeeded to get a first empirical information on the transversities [3] from the combined global analysis of the azimuthal asymmetries in semi-inclusive DIS scatterings measured by HERMES and COMPASS groups [4], [5], and those in $e^+e^- \to h_1h_2X$ processes by the Belle Collaboration [6]. Their main observation for the transversities can be summarized as follows. First, the u-quark transversity is positive and d-quark one is negative with the magnitude of $\Delta_T u(x)$ being much larger than that of $\Delta_T d(x)$. Second, both of $\Delta_T u(x)$ and $\Delta_T d(x)$ are significantly smaller than the Soffer bound [7]. The 2nd observation is only natural, since the magnitudes of unpolarized PDFs are generally much larger than the polarized PDFs. In our opinion, what is more interesting from the physical viewpoint is the comparison of the transversities with the longitudinally polarized PDFs. This comparative analysis of the two fundamental PDFs is the main purpose of my present talk [8].

Before going into the comparative analysis of the transversities and the longitudinally polarized PDFs, it would be useful to give an overview of new measurements of the longitudinally polarized PDFs, especially in the flavor singlet channel related to the nucleon spin problem. Recently, the COMPASS and HERMES groups carried out high-statistics measurements of the longitudinal spin structure function of the deuteron, thereby having succeeded to significantly reduce the error bars of $\Delta\Sigma$, the net quark spin contribution to the nucleon spin [9]- [11].

As pointed out in [12], these new results for the deuteron spin structure function is remarkably close to our theoretical predictions given some years ago based on the chiral quark soliton model (CQSM) [12], [14]. (See also [15]- [18].) Fig.1 show the comparison between our predictions for $x\, g_1^d(x, Q^2)$ given several years ago and the new COMPASS

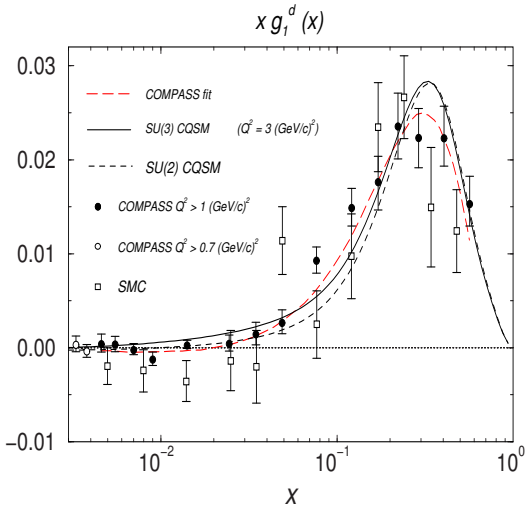

Figure 1: The predictions of the $SU(2)$ and $SU(3)$ CQSM in comparison with the new COMPASS data for $x\,g_1^d(x)$ (filled circles) and their NLO QCD fits (long-dashed curve). The old SMC data [28] are also shown by open squares.

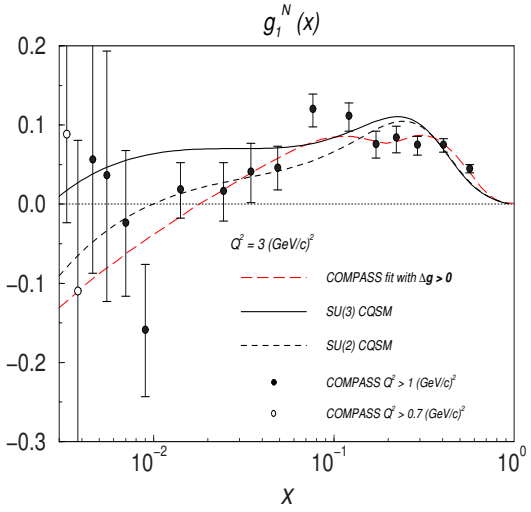

Figure 2: The predictions of the $SU(2)$ and $SU(3)$ CQSM in comparison with the new COMPASS data for $g_1^N(x)$ (filled circles) and their NLO QCD fits (long-dashed curve).

data [9] (the filled circles) together with the old SMC data [28] (the open squares). The solid and dashed curves respectively stand for the predictions of the flavor $SU(3)$ and $SU(2)$ CQSM evolved to the energy scale $Q^2 = 3\,\mathrm{GeV}^2$, which is the average energy scale of the new COMPASS measurement. The long-dashed curve shown for reference is the next-to-leading order QCD fit by the COMPASS group [10]. As one can see, the new COMPASS data show a considerable deviation from the old SMC data in the small x region. One finds that the predictions of the CQSM are consistent with the new COMPASS data especially in the small x region. This tendency can more clearly be seen in comparison of $g_1^N(x) \equiv g_1^d(x)/(1 - \frac{3}{2}\,\omega_D)$ illustrated in Fig.2. The filled circles here represent the new COMPASS data for $g_1^N(x)$, while the long-dashed curve is the result of the next-to-leading order QCD fit by the COMPASS group [10]. The predictions of the $SU(3)$ and $SU(2)$ CQSM are represented by the solid and dashed curves, respectively. For the quantity $g_1^N(x)$, the experimental uncertainties are still fairly large in the small x region. Still, one can say that the predictions of the CQSM is qualitatively consistent with the new COMPASS data as well as their QCD fit.

The COMPASS group also extracted the matrix element of the flavor-singlet axial charge a_0 [10], which can be identified with the net longitudinal quark polarization $\Delta\Sigma$ in the $\overline{\mathrm{MS}}$ factorization scheme. Taking the value of a_8 from the hyperon beta decay, under the assumption of $SU(3)$ flavor symmetry, they extracted from the QCD fit of the new COMPASS data for $g_1^d(x)$ the value of $\Delta\Sigma$ as

$$\Delta\Sigma(Q^2 = 3\,\mathrm{GeV}^2)_{COMPASS} \;=\; 0.35 \;\pm\; 0.03\,(stat.) \;\pm\; 0.05\,(syst.). \qquad (1)$$

On the other hand, the same quantity derived from the fits to all g_1 data is a little smaller

$$\Delta\Sigma(Q^2 = 3\,\mathrm{GeV}^2)_{COMPASS} \;=\; 0.30 \;\pm\; 0.01\,(stat.) \;\pm\; 0.02\,(evol.). \tag{2}$$

A similar analysis was also reported by the HERMES group [11]. Their result is

$$\Delta\Sigma(Q^2 = 5\,\mathrm{GeV}^2)_{HERMESS} \;=\; 0.330 \pm 0.011\,(theor.) \pm 0.025\,(exp.) \pm 0.028\,(evol.). \tag{3}$$

The results of the two groups for $\Delta\Sigma$ are mutually consistent and seems to be larger than the previously known central values [28]. We now compare these new results with the prediction of the CQSM given in our previous papers [13], [14]. Shown in Fig.3 are the prediction of the CQSM for $\Delta\Sigma$ and Δg as functions of the energy scale Q^2. They are obtained by solving the standard DGLAP equation at the NLO with the prediction of the model as the initial condition given at the scale $Q^2_{ini} = 0.30\,\mathrm{GeV}^2 \simeq (600\,\mathrm{MeV})^2$. Since the CQSM is an effective quark model, which contains no gluon degrees of freedom, Δg is simply assumed to be zero at the initial scale. One sees that the new COMPASS and the HERMES results for $\Delta\Sigma$ are surprisingly close to the prediction of the CQSM. Also interesting is the longitudinal gluon polarization Δg. In spite that we have assumed that Δg is zero at the starting energy, it grows rapidly with increasing Q^2. As pointed out in [20], the growth of the gluon polarization with Q^2 can be traced back to the positive sign of the anomalous dimension $\gamma^{(0)1}_{qg}$. The positivity of this quantity dictates that the polarized quark is preferred to radiate a gluon with helicity parallel to the quark polarization. Since the net quark spin component in the proton is positive, it follows that $\Delta g > 0$ at least for the gluon perturbatively emitted from quarks. The growth rate of Δg is so fast especially in the relatively small Q^2 region that its magnitude reaches around $(0.3 - 0.4)$ already at $Q^2 = 3\,\mathrm{GeV}^2$, which may be compared with the estimate given by the COMPASS group :

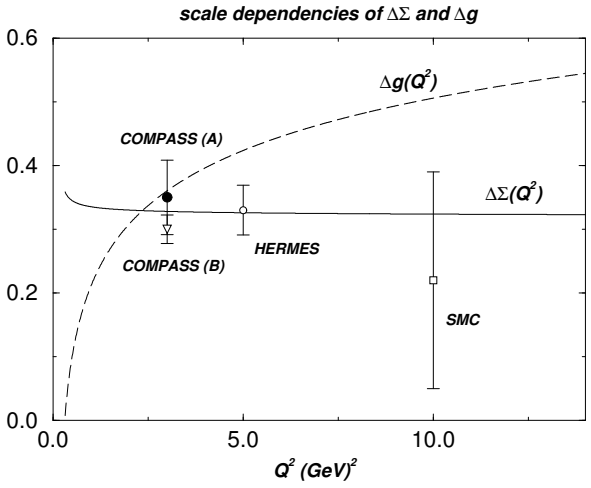

Figure 3: The scale dependencies of $\Delta\Sigma$ and Δg predicted by the CQSM in combination with the NLO DGLAP equation are compared with the recent QCD fits by the COMPASS group (filled circle and open triangle) and by the HERMES group (open circle). The old SMC result is also shown by an open square.

$$\Delta g(Q^2 = 3\,\mathrm{GeV}^2)_{COMPASS} \;\simeq\; (0.2 - 0.3). \tag{4}$$

Now that we have convinced that the CQSM reproduces very well the longitudinally polarized PDFs of the nucleon and the deuteron, we return to the main topic of this talk, i.e. the difference of the longitudinally polarized PDFs and the transversities. First, I recall that the most important quantities characterizing these PDFs are their 1st moments, known as the axial and tensor charges. Next, I emphasize that the understanding of isospin dependencies is crucially important to disentangle the *nonperturbative chiral dynamics* of QCD hidden in the PDFs. Neglecting the strange quark degrees of freedom, for simplicity,

there exist two independent combinations. the isoscalar and isovector combinations for both of the axial and tensor charges.

Let us first recall some basic facts about the axial and tensor charges. The difference of the axial and tensor charges is of purely relativistic nature [1]. In fact, in the naive quark model or the nonrelativistic quark model, there is no difference between the axial and tensor charges, that is, the isovector axial and tensor charges are both 5/3, while the isoscalar axial and tensor charges are both unity :

$$g_A^{(I=1)} \;=\; g_T^{(I=1)} \;=\; \frac{5}{3}, \qquad g_A^{(I=0)} \;=\; g_T^{(I=0)} \;=\; 1. \tag{5}$$

On the other hand, in the familiar MIT bag model, which is nothing but the valence quark model with the relativistic kinematics, an important difference appear between the axial and tensor charges due to the presence of the lower component of the ground state wave function $g(r)$ as

$$g_A^{(I=0)} \;=\; 1 \cdot \int \left(f^2 - \frac{1}{3}\, g^2 \right) r^2\, dr, \qquad g_A^{(I=1)} \;=\; \frac{5}{3} \cdot \int \left(f^2 - \frac{1}{3}\, g^2 \right) r^2\, dr, \tag{6}$$

$$g_T^{(I=0)} \;=\; 1 \cdot \int \left(f^2 + \frac{1}{3}\, g^2 \right) r^2\, dr, \qquad g_T^{(I=1)} \;=\; \frac{5}{3} \cdot \int \left(f^2 + \frac{1}{3}\, g^2 \right) r^2\, dr. \tag{7}$$

Nevertheless, an important observation is that the *ratio* of the isoscalar to isovector charge is just *common* for the axial and tensor charges, i.e. they are three fifth in both of the NQM and the MIT bag model :

$$\frac{g_A^{(I=0)}}{g_A^{(I=1)}} \;=\; \frac{g_T^{(I=0)}}{g_T^{(I=1)}} \;=\; \frac{3}{5}. \tag{8}$$

Most probably, this feature is related to a common shortcoming of these models, that is, the lack of the spontaneous chiral symmetry breaking mechanism. One can convince it by comparing the predictions of the MIT bag model with those of the CQSM, which is an effective model of QCD taking account of the effect of spontaneous chiral symmetry breaking in a maximal way.

	MIT bag	CQSM	Experiment
$g_A^{(I=1)}$	1.06	1.31	1.267 (scale independent)
$g_A^{(I=0)}$	0.64	0.35	0.330 ± 0.040 $(Q^2 = 5\mathrm{GeV}^2)$
$g_T^{(I=1)}$	1.34	1.21	
$g_T^{(I=0)}$	0.88	0.68	
$g_A^{(I=0)}/g_A^{(I=1)}$	0.60	0.27	~ 0.26 $(Q^2 = 5\mathrm{GeV}^2)$
$g_T^{(I=0)}/g_T^{(I=1)}$	0.60	0.56	

Table 1: The predictions of the MIT bag model and of CQSM for the axial and tensor charges in comparison with the empirical information.

As mentioned, in the MIT bag model, the ratio of the isoscalar and isovector axial charges and also the ratio of isoscalar and isovector tensor charges are both exactly 0.6. On the other hand, the CQSM predicts that the ratio of the axial charges is much smaller than that of the tensor charges. This comes from the fact that the CQSM predicts very small isoscalar axial charge just consistent with the EMC observation, while its prediction for the isoscalar tensor charge is not extremely different from the prediction of other low energy effective models including the MIT bag model.

In any case, the predictions of the CQSM for the axial and tensor charges can roughly be summarized as follows. The isovector tensor and axial charges have the same order of magnitudes, while the isoscalar tensor charge is not so small as the isoscalar axial charge. From this analysis, we immediately expect the following qualitative features for the transversity and the longitudinally polarized PDFs. The isovector transversity distribution and the isovector longitudinally polarized distribution would have the same order of magnitude, while the isoscalar $\Delta_T q(x)$ is much larger than the isoscalar $\Delta q(x)$, i.e.

$$\Delta q^{(I=0)}(x) \;\ll\; \Delta_T q^{(I=0)}(x), \qquad \Delta q^{(I=1)}(x) \;\simeq\; \Delta_T q^{(I=1)}(x). \tag{9}$$

In other words, we would expect the magnitude of d-quark transversity is much smaller than that of d-quark longitudinally polarized PDF :

$$|\Delta_T d(x)| \;\ll\; |\Delta d(x)|. \tag{10}$$

To make the argument more quantitative, we compare in Fig.4 the CQSM predictions for the transversities and the longitudinally polarized PDFs. Here, the model predictions are evolved to the energy scale of $Q^2 = 2.4\,\mathrm{GeV}^2$, for later convenience. One can confirm that the magnitudes of the u-quark transversities and the u-quark longitudinally polarized PDF are roughly the same, whereas the magnitude of d-quark transversity is roughly a *factor of two* smaller than that of the d-quark longitudinally polarized PDF.

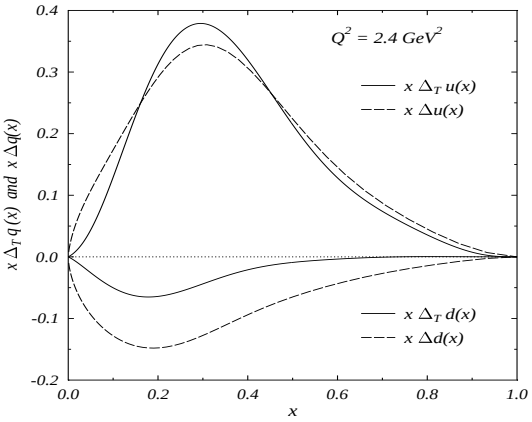

Figure 4: The predictions of the flavor $SU(2)$ CQSM for the transversities (solid curves) and the longitudinally polarized distribution functions (dashed curves) for the u- and d-quarks evolved to $Q^2 = 2.4\,\mathrm{GeV}$.

Now, I compare in Fig.5 the CQSM predictions for the transversities with the recently obtained global fit by Anselmino et al. [3]. As one sees, the uncertainties of the global fit are still quite large. Still, a remarkable feature of the transversity distributions seems to be already seen in their fit. A common feature of the CQSM prediction and their global fit is that the ratio $\Delta_T d(x)/\Delta d(x)$ is very small. As a general trend, however, the magnitudes of the transversities obtained by their global fit look fairly smaller than the corresponding CQSM predictions. In particular, the CQSM prediction for the u-quark transversity appears to lie outside the upper limit of their fit. We shall come back to this point later.

At this point, it would be useful to make some comments on the calculation of transversities by Bochum group based on the same CQSM [21]. A main difference between our cal-

culation [13], [22] and theirs [21] resides in the isovector part of transversities $\Delta_T q^{(I=1)}(x)$. In their calculation, they included only the leading-order contribution to this quantity, and neglected the subleading $1/N_c$ correction, while we have included the latter as well. This is because we know that a similar $1/N_c$ correction (or more concretely, the 1st-order rotational correction) is very important for resolving the famous underestimation problem of some isovector observables, like the isovector axial-charge and/or the isovector magnetic moment of the nucleon, inherent in the hedgehog-type soliton model [23], [24]. The neglect of this $1/N_c$ correction would led to a similar underestimation of the isovector tensor charge, thereby having a fear of being lead to a misleading conclusion on the size of the transversities. We emphasized that, to avoid such a danger, it is very important to analyze the transversities and the longitudinally polarized PDFs *simultaneously* within the same theoretical framework.

To see the difference with the longitudinally polarized PDFs, we show in Fig.6 the LSS2005 fit for the longitudinally polarized u- and d-quark distributions [25]. One can confirm that the CQSM prediction for the u-quark transversity has the same order of magnitude as that of the LSS fit for the u-quark longitudinally polarized PDF, while the CQSM prediction for the d-quark transversity is a factor of two smaller than the LSS fit for the longitudinally polarized PDF [25].

As already emphasized, the reason of this difference can be traced back to the fact that the isoscalar tensor charge is not so small as the isoscalar axial charge in the CQSM. Then, the next question is why the CQSM predicts so small isoscalar axial charge. First, I recall that in the standard $\overline{MS}$ scheme the isoscalar axial charge can be identified with the net quark polarization $\Delta\Sigma$. Within the framework of the CQSM, we can prove the following nucleon spin sum rule, naturally saturated by the quark fields alone [26] :

$$\frac{1}{2} \;=\; \frac{1}{2}\Delta\Sigma \;+\; L^Q. \tag{11}$$

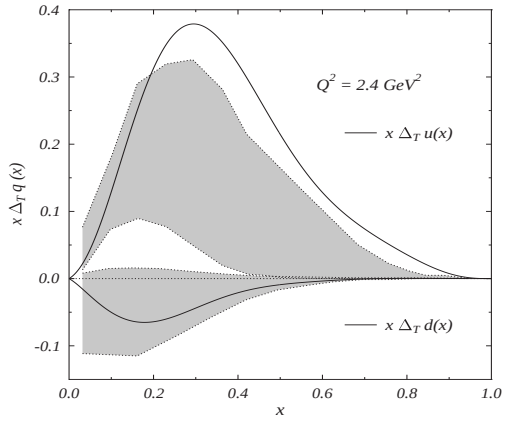

Figure 5: The predictions of the flavor $SU(2)$ CQSM for the transversities (solid curves) in comparison with the global-fit of [3] (shaded areas).

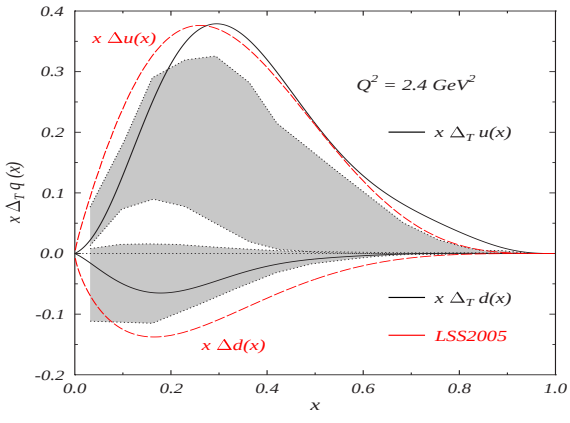

Figure 6: The predictions of the flavor $SU(2)$ CQSM for the transversities (solid curves) in comparison with the LSS2005 fit [25] of the longitudinally polarized u- and d-quark distributions.

On the other hand, in accordance with the physical nucleon picture of the model as a rotating hedgehog, the CQSM predicts quite large quark OAM, which in turn dictates that $\Delta\Sigma$ must be small [26]. As a matter of course, in real QCD, the correct nucleon spin sum rule contains the gluon contributions as well :

$$\frac{1}{2} \;=\; \frac{1}{2}\Delta\Sigma \;+\; L^Q \;+\; \Delta g \;+\; L^g. \tag{12}$$

However, all the recent investigations indicate that the Δg is likely to be small at least in the relatively low energy scale. Combining these observation, one must therefore conclude that the sum of L^Q and L^g must be fairly large at low energy scale.

Our next question is then, "Is there any sum rule that constrains the magnitudes of the isoscalar tensor charge ? Here, one may remember the nucleon spin sum rule proposed by Bakker, Leader and Trueman some years ago [27], which in fact contains the transversity distributions as

$$\frac{1}{2} \;=\; \frac{1}{2}\sum_{a=q,\bar{q}}\int_0^1 \Delta_T q^a(x) \;+\; \sum_{a=q,\bar{q},g}\langle L_{s_T}\rangle^a, \tag{13}$$

where L_{s_T} is the component of the orbital angular momentum $\boldsymbol{L}$ along the transverse spin direction s_T. Unfortunately, there are several peculiarities in the BLT sum rule. First of all, it is not such a sum rule obtained as the 1st moment of some parton distribution functions. In fact, the r.h.s. of this sum rule does not correspond to a nucleon matrix element of *local operator*. In particular, the 1st term of this sum rule does not correspond to the isoscalar tensor charge, because here the sum of the quarks and antiquarks, not the difference, appear as

$$\begin{aligned}\sum_{a=q,\bar{q}}\int_0^1 \Delta_T\, q^a(x)\, dx &= \int_0^1 \Big\{\, [\Delta_T u(x) + \Delta_T d(x)] \;+\; [\Delta_T \bar{u}(x) + \Delta_T \bar{d}(x)] \,\Big\} \\ &\neq \qquad\qquad g_T^{(I=0)}\,. \end{aligned} \tag{14}$$

Nonetheless, our analysis based on the CQSM indicates that antiquark transversities are fairly small. This means that the 1st term of the BLT sum rule may not be extremely different from the tensor charge. Then, if the postulated inequality between the isoscalar axial and tensor charges is in fact confirmed experimentally, it would mean the following inequality, that is the transverse OAM is much smaller than the longitudinal OAM :

$$L^Q_{s_T} \;+\; L^g_{s_T} \;\ll\; L^Q \;+\; L^g. \tag{15}$$

At this point, we come back to the discrepancy between the CQSM predictions and the global fit by Anselmino et al. We can estimate the magnitudes of tensor charges from their central fit, under the assumption that the antiquark contributions to them are negligible, as justified by the CQSM. We then get the following values for the u- and d-quark tensor charges,

$$\delta u \;\simeq\; 0.39, \qquad \Delta d \;\simeq\; -\,0.16, \tag{16}$$

or for the isoscalar and the isovector tensor charges,

$$g_T^{(I=0)} \;\simeq\; 0.23, \qquad g_T^{(I=1)} \;\simeq\; 0.55, \tag{17}$$

at the energy scale $Q^2 \simeq 2.4\,\mathrm{GeV}^2$. If they are evolved down to the low energy model scale around 600 MeV, we would obtain the following numbers :

$$\delta u \;\simeq\; 0.49, \qquad \Delta d \;\simeq\; -\,0.20, \tag{18}$$

or

$$g_T^{(I=0)} \;\simeq\; 0.28, \qquad g_T^{(I=1)} \;\simeq\; 0.69. \tag{19}$$

We recall that all the theoretical estimates in the past, based on the low energy models as well as the lattice QCD, predict the isovector tensor charge between 1.0 and 1.5 [28]- [33]. At any rate, we emphasize that the transversities obtained by their global fit correspond to fairly small magnitudes of tensor charges as compared with the past theoretical estimates.

To sum up, we have carried out a comparative analysis of the transversities and the longitudinally polarized PDFs in light of the new global fit of transversities and the Collins fragmentation functions carried out by Anselmino et al. Their results, although with large uncertainties, already appears to indicate a remarkable qualitative difference between transversities and longitudinally polarized PDFs such that $|\Delta_T d(x)/\Delta d(x)| \ll |\Delta_T u(x)/\Delta u(x)|$, which is qualitatively consistent with the predictions of the CQSM. I have emphasized that the cause of this feature can be traced back to the relation $g_T^{(I=0)} \gg g_A^{(I=0)} = \Delta\Sigma$. Further combining with the BLT sum rule, this indicates the inequality, $L^Q_{S_T} + L^g_{S_T} \ll L^Q + L^g$, i.e. the transverse OAM may be much smaller than the longitudinal OAM. We are not sure whether this unique observation can be understood as the dynamical effects of Lorentz boost or Melosh transformation. Naturally, the global analysis carried out by Anselmino et al. is just a 1st step for extracting transversities. More complete understanding of the spin dependent fragmentation mechanism is mandatory for getting more definite knowledge of the transversities. Also very desirable is some independent determination of transversities, for example, through double transverse spin asymmetry in Drell-Yan processes. We hope that such near-future experiments will provide us with more stringent constraint on the isovector as well as the isoscalar tensor charges, thereby deepening our knowledge on the internal spin structure function of the nucleon.

Acknowledgement. This work is supported in part by a Grant-in-Aid for Scientific Research for Ministry of Education, Culture, Sports, Science and Technology, Japan (No. C-16540253)

References

[1] R.L. Jaffe and X. Ji, Nucl. Phys. B **375**, 527 (1992).

[2] V. Barone, A. Drago, and P.G. Ratcliffe, Phys. Rep. **359**, 1 (2002).

[3] M. Anselmino, M. Boglione, U. D'Alesio, A. Kotzinian, F. Murgia, A. Prokudin, and C. Türk, Phys. Rev. D **75**, 054032 (2007).

[4] HERMES Collaboration, A. Airapetian et al., Phys. Rev. Lett. **94**, 012002 (2005).

[5] COMPASS Collaboration, E.S. Ageev et al., Nucl. Phys. B **765**, 31 (2007).

[6] Belle Collaboration, R. Seidl et al. Phys. Rev. Lett. **96**, 232002 (2006).

[7] J. Soffer, Phys. Rev. Lett. **74**, 1292 (1995).

[8] M. Wakamatsu, Phys. Lett. B **653**, 398 (2007).
[9] COMPASS Collaboration : E.S. Ageev et al., Phys. Lett. B **612**, 154 (2005).
[10] COMPASS Collaboration : V.Yu. Alexakhin et al., Phys. Lett. B **647**, 8 (2007).
[11] HERMES Collaboration : A. Airapetian et al., Phys. Rev. D **75**, 012007 (2007).
[12] M. Wakamatsu, Phys. Lett. B **646**, 24 (2007).
[13] M. Wakamatsu and T. Kubota, Phys. Rev. D **60**, 034020 (1999).
[14] M. Wakamatsu, Phys. Rev. D **67**, 034005 (2003) ;
M. Wakamatsu, Phys. Rev. D **67**, 034006 (2003).
[15] D.I. Diakonov, V.Yu. Petrov, P.V. Pobylitsa, M.V. Polyakov, and C. Weiss, Nucl. Phys. B **480**, 341 (1996).
[16] D.I. Diakonov, V.Yu. Petrov, P.V. Pobylitsa, M.V. Polyakov, and C. Weiss, Phys. Rev. D **56**, 4069 (1997).
[17] H. Weigel, L. Gamberg, H. Reinhardt, Mod. Phys. Lett. A **11**, 3021 (1996).
[18] M. Wakamatsu and T. Watabe, Phys. Rev. D **62**, 054009 (2000).
[19] SMC Collaboration, B. Adeva et al., Phys. Rev. D **58**, 112001 (1998).
[20] H.-Y. Cheng, Int. J. Mod. Phys. A **11**, 5109 (1996).
[21] P. Schweitzer, D. Urbano, M.V. Polyakov, C. Weiss, P.V. Pobylitsa, and K. Goeke, Phys. Rev. D **64**, 034013 (2001).
[22] M. Wakamatsu, Phys. Lett. B **509**, 59 (2001).
[23] M. Wakamatsu and T. Watabe, Phys. Lett. B **312**, 184 (1993).
[24] Chr.V. Christov, A. Blotz, K. Goeke, P. Pobylitsa, V.Yu. Petrov, M. Wakamatsu, and T. Watabe, Phys. Lett. B **325**, 467 (1994).
[25] E. Leader, A.V. Sidorov, and D.B. Stamonev, Phys. Rev. D **73**, 034023 (2006)
[26] M. Wakamatsu and H. Yoshiki, Nucl. Phys. A **524**, 561 (1991).
[27] B.L.G. Bakker, E. Leader, and T.L. Trueman, Phys. Rev. D **70**, 114001 (2004).
[28] H. He and X, Ji, Phys. Rev. D **52**, 2960 (1995).
[29] H.-C. Kim, M.V. Polyakov, and K. Goeke, Phys. Lett. B **387**, 577 (1996).
[30] I. Schmidt and J. Soffer, Phys. Lett. B **407**, 331 (1997).
[31] B. Pasquini, M. Pincetti, and S. Boffi, Phys. Rev. D **72**, 094029 (2005).
[32] S. Aoki, M. Doi, T. Hatsuda, and Y. Kuramashi, Phys. Rev. D **56**, 433 (1997).
[33] QCDSF Collaboration, M. Göckler, Ph. Hägler, R. Horsley, D. Pleiter, P.E.L. Rakow, A. Schäfer, G. Schierholz, and J.M. Zanotti, Nucl. Phys. A **755**, 537c (2005).

Discussion

Comm. (A.Prokudin, Univ. Torino) I would like to comment on the comparison between the results of the presented work and Anselmino et al. global analysis results. In SIDIS we measure product of transversity and Collins Fragmentation Function. In order to extract transversity one should know the evolution of Collins FF. The results of the global analysis could change if the evolution of Collins FF differs drastically from the evolution of unpolarized FF.

Q. (G.Burce, BNL) Is the statement that if $g_T^{I=0} >> g_A^{I=0} = \Delta\Sigma$ with BLT Sum Rule, $L_T^Q + L_T^G << L^Q + L^G$ model independent?

A. Depends on validity of BLT sum rule. Under discussion.

Q. (J.Soffer, Temple Univ.,Philadelphia) 1. Your model does not reproduce well the magnitude of $\bar{d}/\bar{u}$? Do you know why?
2. A_{TT} for $p\bar{p} \to \mu^+\mu^-$ requires polarized $\bar{p}$. Any comment?

A. 1. I agree and the reason is that the ratio of two small quantities is difficult to predict.
2. I agree.

Q. (A.Efremov, JINR, Dubna) Could you compare transversity of your model and those of the Bochum group?

A. The biggest difference between my calculation of transversities and that by Bochum group is that I have included the $1/N_c$ correction (or the $Q(\Omega')$ correction) to the isovector transversity. The importance of such $1/N_c$ correction is already known from the analysis of isovector axial-vector coupling constant $g_A^{I=1}$, which is nothing but the 1st moment of isovector longitudinally polarized PDF, or the familiar β-decay coupling constant. Without this $1/N_c$ correction, we cannot reproduce the observed β-decay coupling constant. Roughly

$$g_A^{I=1} \simeq g_A^{I=1}(\Omega^\circ) + g_A^{I=1}(\Omega')$$
$$\simeq 0.8 + 0.4 \simeq 1.2 \ \ (\text{exp.} : 1.27)$$

If we do not include such $1/N_c$ correction in the calculation of isovector tensor charge, we would obtain smaller isovector tensor charge, and also smaller isovector transversity distribution. As a consequence, the difference between the u-quark transversity and the d-quark transversity would become smaller, and the find prediction would become closer to the global fit by Anselmino et al. However, such success is fortuitous, I think. In fact, the predictions of many effective models as well as the prediction of lattice QCD is close to the answer obtained by including both of $O(\Omega^\circ)$ and $O(\Omega')$ terms.

To sum up, such $1/N_c$ correction term (or the $O(\Omega')$ term) which is necessary to resolve the underestimation problem of should also be included in the calculation of $g_T^{I=1}$, or $\Delta_T q^{I=1}(x)$, for theoretical consistency.

EXPERIMENTAL RESULTS

OBSERVATION OF SPIN ALIGNMENT OF DEUTERONS TRAVELING THROUGH MATTER

L.S. Azhgirey[1], Yu.V. Gurchin, A.Yu. Isupov, A.N. Khrenov, A.S. Kiselev, A.K. Kurilkin, P.K. Kurilkin, V.P. Ladygin, A.G. Litvinenko, V.F. Peresedov, S.M. Piyadin, S.G. Reznikov, P.A. Rukoyatkin, A.V. Tarasov, T.A. Vasiliev, V.N. Zhmyrov and L.S. Zolin

JINR, 141980, Dubna, Moscow Region, Russia

Abstract

The tensor polarization of the deuteron beam arising as deuterons pass through a carbon target was measured. The experiment was performed at an extracted unpolarized 5-GeV/c deuteron beam of the Nuclotron. The effect observed is compared with the calculations made within the framework of the Glauber multiple scattering theory.

1 Introduction

The deuteron is a loosely bound pair of nucleons with aligned spins (spin 1 triplet state). The a small quadruple moment of the deuteron implies that it is not spherical in configuration space, i.e. these two nucleons are not in a pure S state of the relative orbital angular momentum, and there is an additional D wave component. These properties of the deuteron give rise to a number of polarization effects in the nuclear reactions involving the deuteron.

First of all, the calculations of the angular dependence of the elastic dp scattering [1,2] made within the framework of the Glauber multiple scattering theory [3] show that if one would direct the unpolarized deuteron beam onto an unpolarized hydrogen target, the scattered deuterons would be aligned. Secondly, a marked tensor analyzing power was observed in the inclusive inelastic reaction $A(d, d')X$ in the region of 4-momentum transfer near $|t| = 0.3$ GeV/c in the scattering of polarized deuterons with initial momenta of 4.5 and 5.5 GeV/c on nuclei at 0° [4]. At last, it was shown by Baryshevsky [5] that as particles of spin ≥ 1 pass through matter, effects of spin rotation and oscillations may occur. These effects may give rise to polarization of the beam crossing the target. The first attempt to measure spin dichroism, i.e. occurrence of tensor polarization of an unpolarized deuteron beam by an unpolarized target, was made with deuterons up to 20 MeV in a carbon target [6]. Although the magnitude of the deuteron polarization was not determined precisely, authors argue that evidence for existence of dichroism was obtained in this experiment.

In this report we describe an experimental investigation devoted to the first attempt to measure tensor polarization of an unpolarized 5-Gev/c deuteron beam after its passing through a carbon target.

2 Experiment

The experiment has been performed at an unpolarized deuteron beam extracted from the Nuclotron of JINR. The layout of the experimental equipment is shown in Fig. 1. In this

[1]E-mail: azhgirey@jinr.ru

figure $F3, F4, F5$ and $F6$ are the foci of the magnetic system of the beam line. Magnetic lenses and magnets are schematically denoted as $L1, l2, L3$ and $M1, M2, M3$. The part of the beam line up to $F5$ was tuned to the momentum of ~ 5 GeV/c, and the part behind $F5$ was tuned to 3.3 GeV/c.

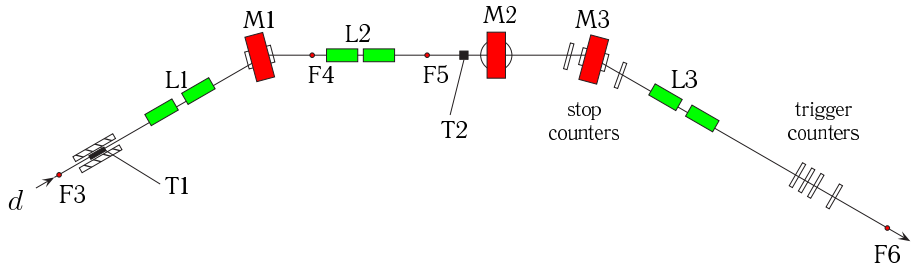

Figure 1: Layout of the experimental equipment

The slowly extracted beam of ~ 5 GeV/c deuterons with an intensity of $5\times10^8-3\times10^9$ particles per beam spill was incident on 40, 83 and 123 g/cm^2-thick carbon targets $T1$ placed near $F3$. The values of the extracted beam momenta were taken to be exactly 5.0 GeV/c after crossing the target irrespective of the target thickness. The measurements without the target were also made. The beam intensities near $F3, F4$ and $F5$ were monitored by ionization chambers. The intensity of the secondary beam between $F4$ and $F5$ was $5 \times 10^6 - 3 \times 10^7$ particles per beam spill.

The tensor polarization of the deuteron beam scattered at the target $T1$ at 0° was determined by means of the second scattering on the 10-cm thick beryllium target $T2$ placed near $F5$ [18]. It is known that the reaction $d + \mathrm{Be} \to p + X$ for proton emission at the zero angle with the momentum $p_p \sim \frac{2}{3}p_d$ has a large tensor analyzing power $T_{20} = -0.82 \pm 0.04$, which is independent of the atomic number of the target ($A > 4$) and the momentum of incident deuterons between 2.5 and 9.0 GeV/c [8].

The secondary particles emitted from the target $T2$ at 0° were transported to the focus $F6$ by means of bending magnets and magnetic lens doublets. The momentum and polar angle acceptances of the setup defined by the Monte Carlo simulation were $\Delta p/p \sim \pm 2\%$ and ± 8 mr, respectively.

Coincidences of the signals from the scintillation counters placed near the focus $F6$ were used as a trigger. Along with the secondary protons, the apparatus detected the deuterons from inelastic scattering. The detected particles were identified off-line on the basis of time-of-flight measurements with a base line of ~ 28 m between the start counters and four stop counters. The TOF resolution (~ 0.2 ns) allowed one to separate protons and deuterons completely.

Since the experiment was carried out with beams of considerably different intensities, the question of the linearity of monitors had a dominant role. The examination of the linearity was made in separate measurements. The readings of current-to-digit convertors of ionization chambers at F3 and F5 were linear with current in the range from 0.1 to 10^4 nA.

The general expression for the invariant differential cross section of the reaction with the polarized deuteron may be found in Ref. [9]. In our case it converts to

$$\sigma' = \sigma_0\big(1 + \frac{1}{\sqrt{2}} p_{ZZ} T_{20}\big), \tag{1}$$

(where the polarized and unpolarized cross sections are referred to as σ' and σ_0, respectively, p_{ZZ} is the tensor polarization of the beam, and T_{20} is the analyzing power in the representation of irreducible tensors $T_{\kappa q}$).

The ionization chamber placed upstream of the analyzer target $T2$ served as a monitor. The numbers of protons normalized to the monitor counts detected in exposures with carbon targets of different thickness are shown in Fig. 2. Here dark points, stars and crosses refer to the 123- , 83- and 40-g/cm^2-thick carbon targets, respectively, and the light points correspond to the measurements without target $T1$. The values of these ratios averaged for all the exposures are shown with dashed lines. It is seen that the points corresponding to different target thickness are grouped in different regions of the picture. The spread of the points exceeds statistical errors that are less than point sizes. This spread is likely to be caused by the non-stabilities of currents in the magnetic elements of the beam line. Considerable deviations of the points obtained in the last exposures from the averaged values are due to the fact that the control over the head end of the magnet-optical channel was lost during these exposures.

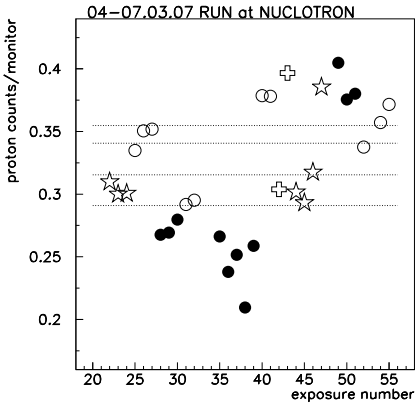

Figure 2: Ratios of proton counts to the monitor for targets $T1$ of different thickness: black points - 123 g/cm^2, stars - 83 g/cm^2, crosses - 40 g/cm^2, light points - 0 g/cm^2.

The possible systematic errors resulting from such current fluctuations were estimated in the following way. It is known that the differential cross section of the proton emission at forward angles in the deuteron breakup is a sharp function of the secondary proton momentum [10, 11]. As to the cross section of the A(d,d') reaction, it has considerably smoother behaviour [12]. Thus, deviations of the proton/deuteron ratio from the constant value can reflect changes in the currents of magnetic elements, or in the momentum of detected particles. On the other hand, the difference Δt in the arrival of signals caused by protons and deuterons is also connected with the spread Δp in the momentum of these particles; for our experimental arrangement $\delta p/\Delta t = -0.172$ GeV/c/ns. The correlation between the ratio $N(p)/N(d)$ and the momentum p calculated from the experimental difference Δt was found to be

$$\frac{N(p)}{N(d)} = (190.14 \pm 0.54) - (53.84 \pm 0.16)p(\mathrm{GeV/c}). \qquad (2)$$

Recall that the magnetic channel was tuned to the rated momentum of 3.3 GeV/c. It follows from Eq. (3) that correction factors to proton counts should vary from 1.26 to 0.88 as the proton momentum varies from 3.24 to 3.33 GeV/c. An estimate of the possible systematic error is thus seen to be $\pm 20\%$.

The tensor polarizations P_{ZZ} of the deuterons that passed through target $T1$ were calculated in accordance with Eq. (2) for each of four channels separately, and they were averaged thereafter; the counts without $T1$ were taken as σ_0. The values of the tensor polarization as a function of the target $T1$ thickness are shown in Fig. 3.

3 Theory

On the assumption that the NN scattering amplitude has the form

$$f(\mathbf{q}) = \frac{k\sigma_{NN}}{4\pi}(1+\alpha_{NN})\exp(-\frac{1}{2}Bq^2), \qquad (3)$$

where $\mathbf{q}$ is the momentum transfer, and if one takes a multi-Gaussian representation of the deuteron wave function [13], in line with the multiple scattering theory [3,14], the difference of the total cross sections of the nuclear scattering of deuterons in different spin states (0) and ($\pm$1) may be written in the form:

$$\Delta\sigma = \sum_{N=1}^{A}(-1)^N\frac{A!}{(A-N)!}\Delta\sigma^{(N)}, \qquad (4)$$

where the cross section difference for the Nth collision is given by

$$\Delta\sigma^{(N)} = \pi R_1 R_2 \sum_{m=0}^{N}\sum_{n=0}^{N-m}\frac{\Delta^{(N)}_{m,n}a_1^{m+n}a_2^{N-m-n}}{[(m+n)R_2+(N-m-n)R_1]\ n!\ m!\ (N-m-n)!}. \qquad (5)$$

Here

$$\Delta^{(N)}_{m,n} = 3\sum_{i=1}^{5}\sum_{k=1}^{5}C_iD_k\Big(\frac{\pi}{\tau_{i,k}}\Big)^{3/2}\frac{\lambda^{(N)}_{m,n}}{(\lambda^{(N)}_{m,n}+\tau_{i,k})^2}+\frac{3}{2}\sum_{i=1}^{5}\sum_{k=1}^{5}D_iD_k\Big(\frac{\pi}{\nu_{i,k}}\Big)^{3/2}\frac{\lambda^{(N)}_{m,n}(3\lambda^{(N)}_{m,n}+7\nu_{i,k})}{\nu_{i,k}(\lambda^{(N)}_{m,n}+\nu_{i,k})^3} \qquad (6)$$

with

$$\lambda^{(N)}_{m,n} = \frac{1}{4}\Big(\frac{N-m-n}{B}+\frac{4mnR_2+(m+n)(N-m-n)R_1}{R_1\left[(m+n)R_2+(N-m-n)R_1\right]}\Big). \qquad (7)$$

The parameters R_1, R_2, a_1 and a_2 are expressed in terms of constants peculiar to this problem:

$$R_1 = \frac{2}{3}<r_A^2>+2B, \quad R_2 = \frac{2}{3}<r_A^2>+B, \quad a_1 = \frac{\sigma_{NN}}{2\pi R_1}, \quad a_2 = -\frac{\sigma_{NN}^2}{16\pi^2 B R_2}, \qquad (8)$$

where $<r_A^2>$ is the rms radius of a nucleus.

The following values of the parameters were used in the calculations: $\sigma_{NN} = 4.40$ fm^2, $\alpha_{NN} = -0.339$, $B = 0.297$ fm^2 [15], $<r_C^2> = 5.86$ fm^2. The calculated difference of total cross sections of $d-^{12}C$ scattering in the deuteron spin states (0) and ($\pm$1) turns out to be $\Delta\sigma = 3.87$ fm^2.

It can be shown that the tensor polarization of the deuteron beam arising from this cross section difference is

$$P_{ZZ} = \frac{1-\exp(-N\Delta\sigma x)}{1+\frac{1}{2}\exp(-N\Delta\sigma x)}, \qquad (9)$$

where N is the number of nuclei in cm^3 of matter with thickness of $x$cm. The calculation results for our experiment are shown in Fig. 3 by the solid curve.

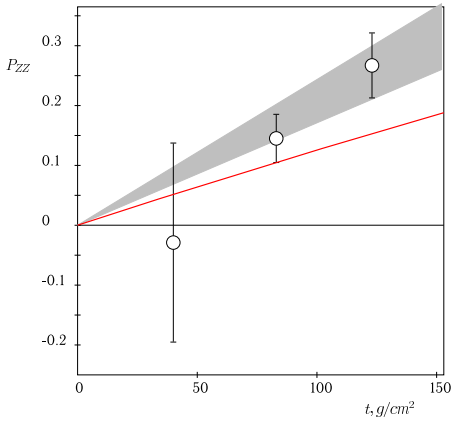

Figure 3: Tensor polarization of deuterons vs thickness of target $T1$. The dashed region shows the error corridor, the solid curve is the calculation result.

4 Conclusion

The tensor polarization of an unpolarized deuteron beam arising as deuterons pass through carbon targets of different thickness was measured. The phenomenon of spin dichroism (defined as production of spin polarization in an unpolarized beam) was first observed using an extracted unpolarized 5-GeV/c deuteron beam of the Nuclotron.

A formalism was elaborated to describe the effect observed within the framework of the Glauber multiple scattering theory. The calculation results are in qualitative agreement with the experimental data obtained.

The observed effect can be used to produce tensor polarized deuteron beams of small intensity at high energies.

Acknowledgments

The authors express their gratitude to Prof. V.G.Baryshevsky for the suggestion of this experiment and helpful discussions. The research was supported in part by the Russian Foundation for Basic Research under grants No. 06-02-16728 and 06-02-16842.

References

[1] V.Franco, R.J.Glauber, Phys.Rev.Letters **22**, 370(1969).

[2] D.Harrington, Phys.Lett. B **29**, 188(1969).

[3] R.J.Glauber, in: Lectures in Theoretical Physics, ed. by W.E.Brittin et al., V.1, Intrascience Publishers, Inc., New York, 1959, p.315.

[4] L.S.Azhgirey et al., Phys.Lett. B **361**, 21(1995).

[5] V.G.Baryshevsky, J.Phys.G: Nucl.Part.Phys. **19**, 273(1993).

[6] V.Baryshevsky et al., arXiv:hep-ex/0501045 v2(2005).

[7] L.S.Zolin et al., JINR Rapid Commun. No. 2[88]-98, 27(1998).

[8] C.F.Perdrisat et al., Phys.Rev.Lett. **59**, 2840(1987); V.Punjabi et al.,Phys.Rev. C **39**,608(1989); V.G.Ableev et al., Pis'ma Zh.Eksp.Teor.Fiz. **47**,558(1988); JINR Rapid Commun. No. 4[43]-90, 5(1990); T.Aono et al., Phys.Rev.Lett. **74**, 4997(1995).

[9] W.Haeberli, Ann.Rev.Nucl.Sci. **17**, 373(1967).

[10] V.G.Ableev et al., Nucl.Phys. A **393**,491 (1983); S.A.Zaporozhets et al., Proc. VIII Intern. seminar on high energy physics problems, Dubna, 1986, V.1, p.341 [in russian].

[11] L.S.Azhgirey, M.A.Ignatenko, N.P.Yudin, Z.Phys. A **343**, 35(1992).

[12] L.S.Azhgirey et al., Yad.Fiz. **27**, 1027(1978) [in russian].

[13] G.Alberi,L.P.Rosa,Z.D.Thomé, Phys.Rev.Lett. **34**, 503(1975).

[14] V.Franco,R.J.Glauber, Phys.Rev. **142**, 1195(1966).

[15] pdg.lbl.gov/2006.tables.html

Discussion

Q. (S.Belostotsky, PNPI, St.Petersburg) I understand that the cross section for $M = \pm 1$ and $M = 0$ must be different. However, where is the quantization axis? The target is uniform.

A. In our case the direction of the quantization axis coincides with the beam direction because it is the only separated direction.

Q. (A.Efremov, JINR, Dubna) Could the effect you have discovered serve as a sort of filtering effect?

A. Of course, the observed effect of spin dichroism may be regarded as a sort of spin filtering effect.

Q. (A.Silenko, Belarusian State Univ., Minsk) Needs the discussed effect to be taken into account in measuring the polarization of tensor polarized deuteron beam?

A. We believe that the considered effect should be taken into account for precision deuteron polarization measurements with thick targets.

MEASUREMENT OF $\Delta G/G$ AT COMPASS

Y. Bedfer (on behalf of the COMPASS collaboration)

CEA/DAPNIA, Saclay and CERN, Geneva.
E-mail: Yann.Bedfer@cern.ch

Abstract

The gluon polarization $\Delta G/G$ is the key to a further clarification of the spin structure of the nucleon. The COMPASS collaboration at CERN has set out to undertake the direct measurement of this quantity. It is being determined from the measurement of double spin asymmetries in the scattering of polarized muons off a polarized deuteron target.

Three different channels sensitive to the gluon distribution are explored: open charm production and high transverse momentum (high p_T) production in either the quasi-real (virtuality $Q^2 < 1$ GeV^2) photoproduction or the deep inelastic scattering ($Q^2 > 1$ GeV^2) regimes. I describe their experimental and theoretical aspects. And I report on the preliminary results and prospects for future analysis.

1 Introduction

The spin 1/2 of the nucleon can be decomposed as follows

$$\frac{1}{2} = \frac{1}{2}\Delta\Sigma + \Delta G + L_z \quad ,$$

where the right hand side terms designate the contributions of the spin of the quarks, the spin of the gluons and the angular momentum of the quarks and gluons, respectively.

In the recent years much effort has been put in determining $\Delta\Sigma$. This quantity can be derived from the measurement of the spin dependent structure function g_1 by polarized inclusive deep inelastic lepton-nucleon scattering (DIS) experiments. Measurements were carried out at CERN, SLAC, DESY and JLAB. COMPASS itself is presently carrying on with this program. The results lead to the conclusion that $\Delta\Sigma$ is surprisingly small, significantly smaller than predicted by the Ellis-Jaffe sum rule [1] for example. An analysis of world polarized DIS data performed by the COMPASS collaboration and including its latest data points corroborates this conclusion, *cf.* [2, 3].

A solution to the problem was put forward in 1988 [4–6]. It involves a leading order contribution to the polarized DIS cross-section originating from the axial anomaly of QCD, $\alpha_s/2\pi\ \Delta G$, which is anomalous in the sense that it does not vanish in the asymptotic limit: in leading order evolution ΔG grows with $ln\, Q^2$ whereas α_s is inversely proportional to $ln\, Q^2$. This anomalous gluon contribution introduces some freedom in the definition of $\Delta\Sigma$, but it can in any case reconcile polarized DIS data with QCD predictions given a large enough, positive value for the first moment of ΔG [7].

The unpolarized gluon distribution, G, can be determined from the dependence of the inclusive DIS cross-section upon Q^2. In the polarized case, however, DIS data cover

too small a range in Q^2 for this method to significantly constrain ΔG. The fit of world polarized DIS data by COMPASS mentioned *supra* exemplifies this situation.

A direct measurement of the gluon polarization, $\Delta G/G$, is therefore the most promising way to further clarify the nucleon's spin puzzle. Several experimental projects have recently been started to carry it out, using different approaches. In COMPASS, we access the gluon distribution via two different channels: open charm production and high transverse momentum (high p_T) hadron production. The two share a set of common features. Factorization theorems ensure that, in the presence of a large scale, the cross-section can be written as a convolution of partonic cross-sections, calculable pertubatively, and quark and gluon distributions. And for both channels, this scale can be set irrespective of Q^2, by the charm mass and the p_T cut, respectively. Both have also been successfully used to directly measure the unpolarized gluon distribution at the HERA collider experiments (with the difference that high p_T refers to the production of jets there) [8, 9]. But they represent diametrically opposed trade-offs between the conflicting requirements of statistics and purity. Open charm is the purest. It provides a model-independent access to $\Delta G/G$ and for this reason remains our golden channel. I will present it first. And I will present next the high p_T case, which we subdivide into several sub-cases depending upon the Q^2 of the exchanged photon. I start with some experimental essentials.

2 Experimental essentials

The COMPASS spectrometer is described in details in [10]. I recall that it uses a beam of 160 GeV muons, with an intensity of 2 10^8 *per* spill of ∼15 s and a polarization of 76÷80%, and a polarized deuteron target [11]. And that it comprises two stages, for low and high momenta respectively, equipped with tracking, calorimetry and particle identification (muon absorbers in both stages and RICH in only the first one).

Its experimental setup was designed to allow a precise determination of asymmetries. An important point in this respect, is the control of fake asymmetries. We achieve it thanks to the simultaneous measurement of both parallel and anti-parallel spin states in two oppositely polarized target cells, upstream u and downstream d, and to a frequent reversal of target spin orientations, so that fluctuations in acceptance and incident muon flux cancel out in the formula for the counting asymmetry A:

$$A = \frac{1}{2}\left(\frac{N_u^{\Uparrow\uparrow} - N_d^{\Uparrow\downarrow}}{N_u^{\Uparrow\uparrow} + N_d^{\Uparrow\downarrow}} + \frac{N_d^{\Uparrow\uparrow} - N_u^{\Uparrow\downarrow}}{N_d^{\Uparrow\uparrow} + N_u^{\Uparrow\downarrow}}\right) \quad , \tag{1}$$

where $\Uparrow\uparrow$ and $\Uparrow\downarrow$ denote the two spin states. (Note that weighted asymmetries are used instead of (1) in all calculations presented below.)

The reversal of target spins is most frequently performed by field rotation. This rotation induces a small change in the acceptances of the u and d cells, which is hence correlated with the configuration of spin states. In order to correct for this effect, a full re-polarization is performed periodically, allowing a spin reversal in constant field.

An even better control of the instrumental asymmetries is achieved starting with the 2006 run, where the target is divided in 3 (1/4 ↑, 1/2 ↓, 1/4 ↑ and *vice-versa*), so that both spin states have permanently the same average acceptance.

The cross-section helicity asymmetry, $A_\parallel$, is related to the counting asymmetry by factors describing the polarization of the incoming particles, P_μ for the beam (∼80%), P_T

and f for the target polarization ($\sim$50%) and for the, process dependent, dilution factor ($\sim$40%). It is best expressed as $A_\parallel/D$,

$$A_\parallel/D = A \;/\; (P_\mu \times P_T f \times D) \quad , \tag{2}$$

where one takes also into account a kinematical factor, D, describing the polarization transfer from the muon to the photon. D is process dependent and typically averages to $\sim$60%. Therefore the overall dilution factor relating the physics aymmetry of interest to the expermimental asymmetry is $\sim$10%.

During its first three years of running from 2002 to 2004, the experiment has accumulated $\sim$2 fb^{-1} of data with its target polarized longitudinally. In 2005, the experimental apparatus has undergone a major upgrade, and a further $\sim$1 fb^{-1} have been recorded in 2006. The results shown in this presentation are preliminary and correspond to the 2002$\div$2004 part of the data. The gain in statistics expected from 2006 is equal to the $\sim$50% luminosity factor times an enhancement factor brought by the upgrade. The latter factor is channel dependent and an estimation of its magnitude is given *infra* for some of the $\Delta G/G$ channels.

The upgrade concerns 3 aspects: RICH, acceptance and electromagnetic calorimetry.

The efficiency of the RICH was limited in the forward direction by the presence of a large uncorrelated background, due to the halo accompanying the muon beam. In order to better suppress it, the older photon detectors (*viz.* MWPCs with CsI photocathode) were replaced by a much faster system based of multianode photomultipliers, in the central region (25% of the focal plane detection), and, for the outer region, were equipped with new faster electronics.

The aperture of the polarized target was increased from $\pm$70 mrad to $\pm$180 mrad by the installation of a new solenoid magnet. And a drift chamber has been built to complete the large area detection matching this aperture downstream.

Electromagnetic calorimetry was installed in both spectrometer stages next to the already existing hadronic one. It is not yet included in the $\Delta G/G$ analysis.

Last, in 2007, COMPASS has taken data with a proton, NH_3, target. Given the low value of $P_T f$ that this corresponds to and the limited statistics collected in the longitudinal mode, it will not contribute significantly to the $\Delta G/G$ measurement.

3 Open Charm

This channel was discussed by many authors [12,13] as a good candidate to access $\Delta G/G$. Since there is no or only a small intrinsic charm in the nucleon in COMPASS kinematical domain [14], diagrams with an incoming charm quark do not contribute and the leading order process is the photon-gluon fusion (PGF) $\gamma^* g \to c\bar{c}$, which is directly proportional to the gluon distribution.

In COMPASS we tag open charm, and hence PGF, by the reconstruction of a D^o meson. The $D^o \to K\pi$ decay channel is used, with K and π identified in the RICH. The main difficulty lies in the associated combinatorial background. This is a major concern in our experiment, where the vertex resolution is not sufficient to resolve the decay vertex from the primary vertex, because of the thickness of the target.

Special care is therefore taken to optimize the use of the data. First, the favorable cases when the D^o comes from a $D^* \to D^o\pi$ decay are counted separately, *cf.* Fig. 1. Secondly,

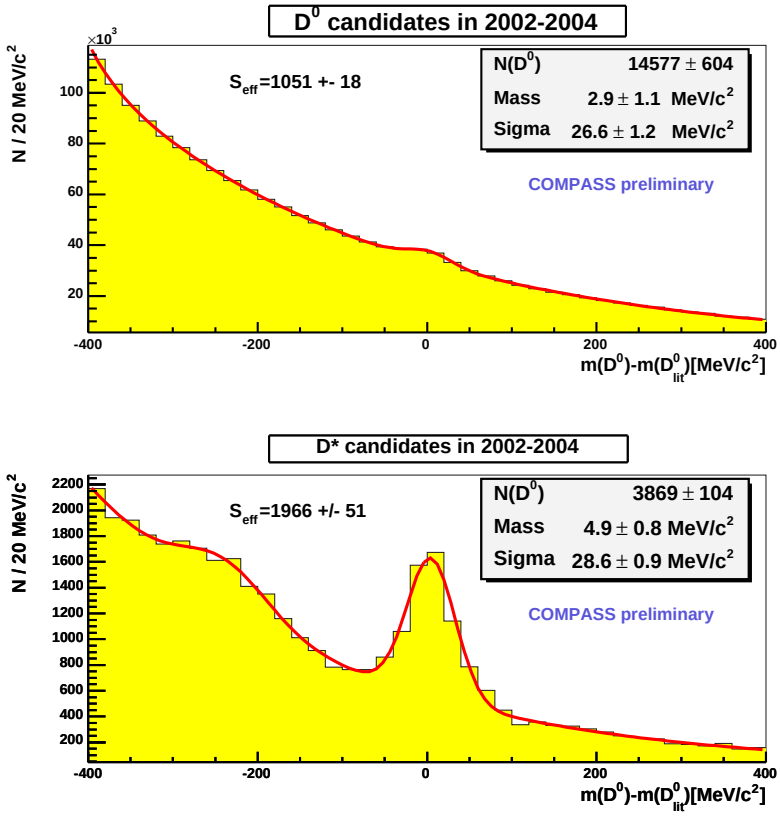

Figure 1. D^o peak in the $K\pi$ invariant mass distribution for all events (top) and D^*-tagged events (bottom) for 2002÷2004 data. S_{eff} is the effective number of events $S_{eff} = S^2/(S+B)$ where S and B are signal and background counts. A bump shows up at low mass in the D^* case, attributable to $D^o \to K\pi\pi^o$. It is not included in the S count.

kinematical cuts are applied, on the fraction z_D of the energy of the virtual photon carried by the D meson, and on its decay angle measured in its rest frame, relative to its direction of flight. The signal over background ratios S/B achieved by these cuts are of the order of 1/10 and 1/1 for the D^o and D^* samples respectively. The corresponding statistical significances $S^2/(S+B)$ are given in Fig. 1. Thirdly, a weighting procedure is applied for the derivation of $\Delta G/G$:

$$\Delta G/G = \frac{1}{P_T} \; \frac{\sum_i^{\Uparrow\uparrow} w_i - \sum_i^{\Uparrow\downarrow} w_i}{\sum_i^{\Uparrow\uparrow} w_i^2 + \sum_i^{\Uparrow\downarrow} w_i^2} \qquad w_i = f\, P_\mu\, a_{LL}\, \langle S/(S+B) \rangle \tag{3}$$

where a_{LL} is the analyzing power of the $\gamma^* g \to c\bar{c}$ PGF and $S/(S+B)$ is the signal strength. This procedure gives a gain in precision equal to $\sqrt{\langle w^2 \rangle / \langle w \rangle^2}$. It is particularly welcome in the open charm case where a_{LL} spans a large domain and even crosses zero, *cf.* Fig. 2. However, when applying it, care has to be taken of a possible correlation between variables that are averaged over, the signal strength in the present case, and variables calculated on an event by event basis, $f\, P_\mu\, a_{LL}$. And indeed the signal strength turns out to be (anti-)correlated with a_{LL}. In order to avoid any bias, the analysis is therefore done independently for several bins in a_{LL}, within which the correlation vanishes.

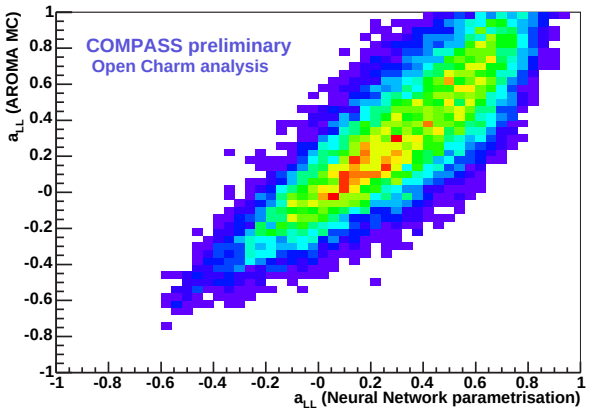

Fig. 2

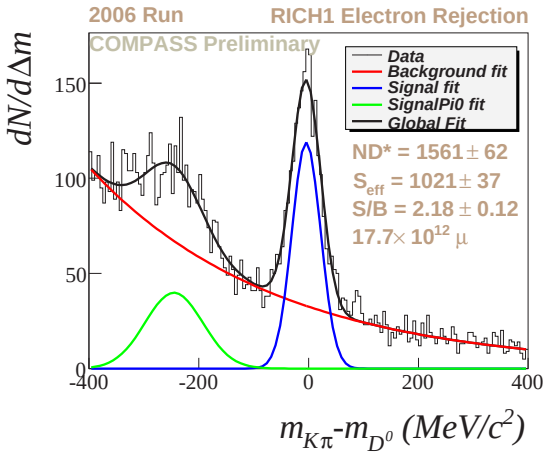

Fig. 3

Figure 2. Parameterization of the analyzing power a_{LL} of the D^o production: the true value is plotted *vs.* the value reconstructed from measurable quantities using the parameterization. The correlation factor is ∼82%.

Figure 3. $K\pi$ invariant mass for D^* tagged events in ∼1/2 of 2006 data: the gain in effective signal *per* incident muon over the 2002÷2004 case shown in Fig. 1 is ∼2.25.

A Monte Carlo simulation of the experiment is used to calculate estimates of all quantities that cannot be directly computed from the hadron level kinematics, such as a_{LL}, x_g, the momentum fraction carried by the gluon and μ^2 the hard scale assigned to the PGF. It is based on the event generator AROMA [15], which uses the PGF matrix element to generate charmed hadrons. a_{LL} is computed from parton level kinematics using polarized matrix elements from [16] and then parameterized as a function of the measurable hadron kinematics and a depolarization factor, D, describing the polarization transfer to the virtual photon, so that it can be estimated on an event by event basis in equation (3). The parameterization is obtained via a neural network. It yields an ∼82% correlation with a_{LL} true value, *cf.* Fig. 2. The determination of a_{LL} is at present limited to LO in perturbative QCD, and hence, so is our extraction of $\Delta G/G$.

In these conditions, a preliminary analysis, bearing 2002÷2004 data, gives:

$$\Delta G/G = -0.57 \pm 0.41(stat.) \pm 0.17(syst.) \quad \text{at } x_g = 0.15 \pm 0.08\, RMS \text{ and } \mu^2 = 13\, GeV^2.$$

The systematics include the statistical uncertainty on the background asymmetry, measured on side bands, and the instrumental asymmetry, which are evaluated on a higher statistics sample, and the choice of the fit function.

This result means a clear lack of precision, which we intend to remedy in two steps. A first step will be the inclusion of 2006 data, combined with a cleaner selection applied to all data and a more efficient weighting method. An indication of the effectiveness of the first two points can be seen on Fig. 3. The precision on $\Delta G/G$ expected from this first step is 0.25. In the longer term, we plan to explore new selection channels, like D^o decays with a π^o in the final state or kaons below the Cerenkov threshold.

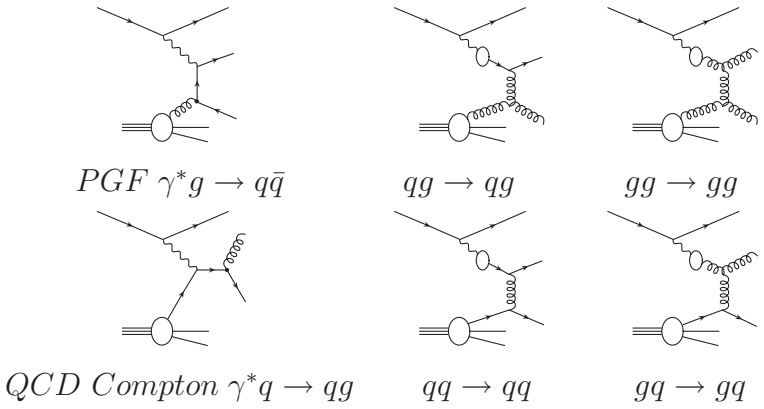

Figure 4. High p_T hadron production processes in leading order pQCD.

4 High p_T

The alternative channel used to access $\Delta G/G$ consists in requiring hadron production at a high transverse momentum with respect to the virtual photon [17]. This suppresses $\gamma^* q \to q$ events, where the fragmenting quark goes into the direction of the photon. Note that the suppression is not perfect, however. The cross-sections receive then contributions from different partonic channels, involving either direct or resolved photons. They correspond to the leading order processes depicted in Fig. 4, where the processes sensitive to the gluon distribution in the nucleon are shown first.

In order to gain information about the gluon distribution from this bundle of processes, we have considered two different approaches. They ultimately differ in the way they fold the partonic level QCD calculations into the soft fragmentation process and the instrumental acceptance. But their actual implementations in COMPASS differentiates them in many other ways and I will then refer to them in what follows as the Monte-Carlo extraction and the NLO photoproduction.

4.1 Monte-Carlo extraction

The Monte-Carlo method relies on the following approximation for the LO expansion of the cross-section helicity asymmetry:

$$A_{\parallel} \simeq (R_{PGF} \langle a_{LL}^{PGF} \rangle + \sum R_i \langle D\, a_{LL}^i D\, \Delta p/p \rangle) \Delta G/G + A_{Background} \qquad (4)$$

where the summation runs over all resolved photon processes sensitive to the gluon distribution, the R factors represent the fraction of events for a given process, a_{LL} its analyzing power, $\Delta p/p$ are the polarizations of the partons in the resolved photon and $A_{Background}$ is the contribution to the asymmetry of all remaining processes. In order to retrieve $\Delta G/G$, the R fractions, $A_{background}$ and the parton level kinematics defining a_{LL} need be determined by a simulation of the experiment. In COMPASS, we consider independently two different kinematical regimes, the DIS regime at $Q^2 > 1$ GeV^2 and the photoproduction regime at $Q^2 < 1$ GeV^2. And for the simulation, we resort to Monte-Carlo event generators, LEPTO [18] and PYTHIA [19] respectively. The two cases share a number of common features. As was already mentioned, they both rely on a LO approximation.

And for both, the event selection follows a same path. In particular, two hadrons are required, with $p_T > 0.7$ GeV and $\Sigma\, p_T^2 > 2.5$ GeV^2. But the two cases are attractive in their own right. The photoproduction case yields much higher statistics, a factor 10. But the DIS event generation is theoretically better grounded: Q^2 provides the hard scale and eliminates the need for modeling events from soft processes that pass the p_T selection through fragmentation. It ignores the resolved photons altogether, however.

More details about the Monte-Carlo extraction of $\Delta G/G$ can be found in these proceedings [21]. The photoproduction case alone is published so far, *cf.* [22].

4.2 NLO photoproduction

In the second approach, the soft hadronization is modeled by fragmentation functions and the instrumental setup is taken into account by applying the acceptance cuts directly to the parton level kinematics. The calculations for the COMPASS case have been done, at NLO, for two subcases: single hadron production [23] and hadron pair production [24]. In these calculations, a parameterizations of $\Delta G(x)$ is assumed and the differential asymmetry is determined as a function of p_T. $\Delta G/G$ can then be extracted by adjusting the parameterization for the calculated asymmetry to fit the data, either independently or via a global fit including both high-p_T and inclusive DIS. The analysis of the COMPASS data along these lines has not yet been completed. To get an indication of their sensitivity to the gluon polarization, one can still compare the projected error bars with different parameterizations, *cf.* Fig. 5.

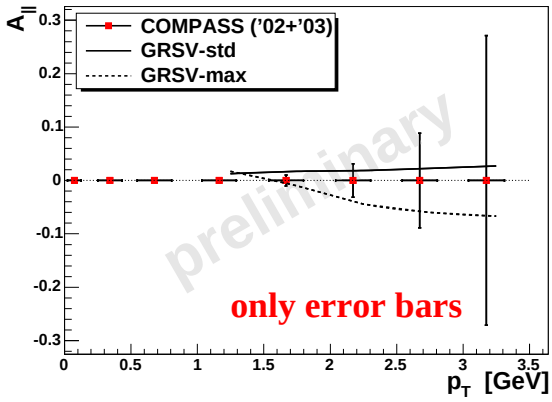

Figure 5. Single hadron at high p_T in photoproduction ($Q^2 < 0.5$ GeV^2). The error bars corresponding to ~1/3 of recorded data are plotted against two of the GRSV2000 [4] parameterizations. These span a large range of $\Delta G/G$, all compatible with DIS data. The two retained here correspond to the best fit (*std*) and $\Delta G/G = 1$ at the input scale of evolution (*max*).

In order to ensure the validity of the method, one has to check the calculations in the unpolarized case. In COMPASS, unpolarized cross-sections are measured with reasonable accuracy. However, as is noted in [23], at the low *cms* energy achieved by our fixed target setup, threshold effects become important. These can be accounted for by all-order resummations of large logarithms, but such calculations are not yet available for the photoproduction case. Keeping this *caveat* in mind, we intend to release our unpolarized cross-section and asymmetry data beginning of 2008.

5 Conclusion

COMPASS has pursued of a broad array of $\Delta G/G$ measurements. Preliminary results have been obtained in the open charm and high p_T channels. When combined with QCD fits of world DIS data, they are compatible with a low value for the first moment of ΔG at a scale of 3 GeV^2, *cf.* Fig. 6, and dismiss as very unlikely the axial anomaly scenario

whereby a ΔG of the order of $2 \div 3$ would account for the small value of the first moment of g_1.

Many more results are expected in view of the good quality of 2006 data and of the improvements achieved in the analysis of older data.

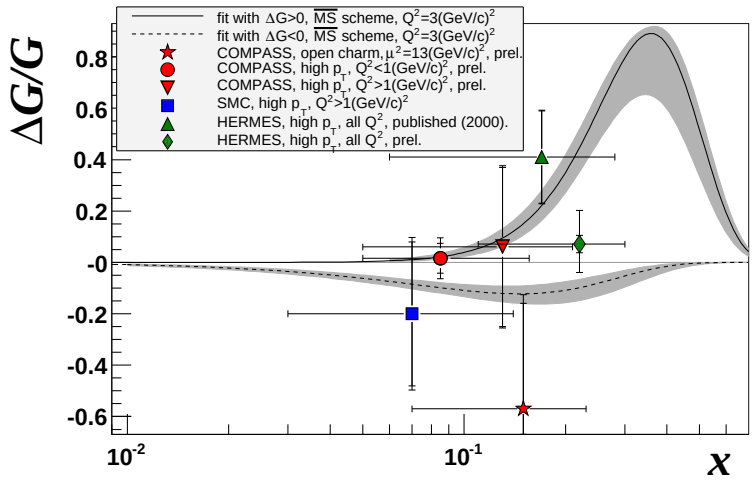

Figure 6. Comparison of the $\Delta G/G$ measurements from COMPASS [21, 22, 27], SMC [25] and HERMES [26]. For each point, the vertical error bar includes the statistical uncertainty only and the horizontal bar represents the x_g range. The curves show the two parameterizations of $\Delta G/G(x_g)$ at a scale of 3 GeV^2 solutions of the COMPASS NLO fit of world DIS data [2], which give for the first moment ΔG a maximum value of $\sim$0.3. (*N.B.:* the open charm point is measured at much higher scale.)

References

[1] J. R. Ellis and R. L. Jaffe, Phys. Rev. D **9** (1974) 1444 [Erratum-ibid. D **10** (1974) 1669].

[2] V. Y. Alexakhin *et al.* [COMPASS Collaboration], Phys. Lett. B **647** (2007) 8 [arXiv:hep-ex/0609038].

[3] H. Santos, *in these proceedings.*

[4] A. V. Efremov and O. V. Teryaev, JINR-E2-88-287

[5] G. Altarelli and G. G. Ross, Phys. Lett. B **212** (1988) 391.

[6] R. D. Carlitz, J. C. Collins and A. H. Mueller, Phys. Lett. B **214** (1988) 229.

[7] H. Y. Cheng, Int. J. Mod. Phys. A **11** (1996) 5109 [arXiv:hep-ph/9607254].

[8] B. W. Harris, arXiv:hep-ph/9909310.

[9] A. M. Cooper-Sarkar, arXiv:hep-ex/0511058.

[10] P. Abbon *et al.* [COMPASS Collaboration], Nucl. Instrum. Meth. A **577** (2007) 455 [arXiv:hep-ex/0703049].

[11] Yu. Kisselev, *In these proceedings.*

[12] A. D. Watson, Z. Phys. C **12** (1982) 123.

[13] M. Glück and E. Reya, Z. Phys. C **39** (1988) 569.

[14] R. Brugnera, *In the Proceedings of International Conference on Heavy Quarks and Leptons (HQL 06), Munich, Germany, 16-20 Oct 2006, pp 032* [arXiv:hep-ex/0701027].

[15] G. Ingelman, J. Rathsman and G. A. Schuler, Comput. Phys. Commun. **101** (1997) 135 [arXiv:hep-ph/9605285].

[16] I. Bojak and M. Stratmann, Nucl. Phys. B **540** (1999) 345 [arXiv:hep-ph/9807405].

[17] A. Bravar, D. von Harrach and A. Kotzinian, Phys. Lett. B **421** (1998) 349 [arXiv:hep-ph/9710266].

[18] G. Ingelman, A. Edin and J. Rathsman, Comput. Phys. Commun. **101** (1997) 108 [arXiv:hep-ph/9605286].

[19] T. Sjostrand, L. Lonnblad, S. Mrenna and P. Skands, arXiv:hep-ph/0308153.

[20] M. Glück, E. Reya, M. Stratmann and W. Vogelsang, Phys. Rev. D **63** (2001) 094005 [arXiv:hep-ph/0011215].

[21] K. Klimaszewski, *In these proceedings.*

[22] E. S. Ageev *et al.* [COMPASS Collaboration], Phys. Lett. B **633** (2006) 25 [arXiv:hep-ex/0511028].

[23] B. Jäger, M. Stratmann and W. Vogelsang, Eur. Phys. J. C **44** (2005) 533 [arXiv:hep-ph/0505157].

[24] C. Hendlmeier, M. Stratmann and A. Schafer, arXiv:0706.3766 [hep-ph].

[25] B. Adeva *et al.* [Spin Muon Collaboration (SMC)], Phys. Rev. D **70** (2004) 012002 [arXiv:hep-ex/0402010].

[26] A. Airapetian *et al.* [HERMES Collaboration], Phys. Rev. Lett. **84** (2000) 2584 [arXiv:hep-ex/9907020].

[27] S. Koblitz [COMPASS Collaboration], arXiv:0707.0175 [hep-ex].

Discussion

Q. (S.Belostotsky, PNPI, St.Petersburg) What is a typical number for purity factor in the case of open charm production?

A. This factor ranges from 0.1 to 0.2.

RECENT RESULTS FROM HERMES

S. Belostotski on behalf of the HERMES collaboration

Petersburg Nuclear Physics Institute
E-mail: belostot@mail.desy.de

Abstract

This review summarizes recent results of the analysis of HERMES experimental data collected with longitudinally polarized hydrogen and deuterium targets. From the precise measurement of the spin structure function g_1 in inclusive deep-inelastic scattering, the total quark contribution to the nucleon spin (the singlet axial charge) is found to be $a_0 = \Delta\Sigma = 0.330 \pm 0.025(exp.) \pm 0.028(evol.)$ with the negative strange quark contribution being equal to $-0.085 \pm 0.008(exp.) \pm 0.009(evol.)$. The individual quark and anti-quark helicity distributions are extracted for the first time using the data on semi-inclusive deep-inelastic scattering with well identified charged pions and kaons in the final states. The gluon polarization $\Delta g/g = 0.075 \pm 0.034(stat) \pm 0.011(syst.exp.) \pm 0.1(syst.model.)$ is evaluated from the data sample with inclusive high-p_T hadrons.

1 Introduction

A measurement done by the European Muon Collaboration (EMC) in 1988 indicated that only a small fraction of the proton spin is carried by quarks [3]. A huge number of experimental and theoretical studies have been done since then using polarized deep-inelastic scattering (DIS) with high-energy electron and muon beams as a tool for probing spin structure of the nucleon (see, e.g., [2]). The most recent results with charged lepton beams have been obtained in this field by the HERMES and COMPASS experiments. Besides, the spin program successfully developed at RHIC provides very important complementary information on the nucleon spin structure, in particular on the gluon polarization. All these results are intensively discussed at this Conference.

The HERMES experiment at DESY studies the spin structure of the nucleon using the 27.6 GeV longitudinally polarized positron (electron) beam of the HERA e-p collider and a polarized (longitudinally or transversely) or unpolarized gaseous target [3]. Due to reliable particle identification and relatively large acceptance, the HERMES spectrometer measures both inclusive and semi-inclusive DIS, in the latter case a hadron identified with the help of the RICH detector is detected in coincidence with the scattered positron (electron).

The HERMES experiment was commissioned in the year 1995. In the years 1995-2000, refered to as RUN I, HERMES accumulated experimental data with a longitudinally polarized target and, after the HERA luminosity upgrade, with a transversely polarized target (2002-2005). In order to improve the selection of exclusive reactions, i.e., to better study deeply virtual Compton scattering, a Recoil Detector (RD) was installed at HERMES in the year 2006. HERMES kept running with the RD and unpolarized target till June 2007 when the HERA accelerator was shutdown. The period of data taking

2002-2007 is refered to as RUN II. Most of HERMES data are collected from polarized hydrogen and deuterium targets, but in order to study nuclear effects ^{4}He, ^{14}N, ^{20}Ne, ^{84}Kr and ^{131}Xe targets are also used.

At this Conference, there are several presentations related to recent results from HERMES [4–8].

An overview of transverse physics at HERMES (RUN II) is done by V.Korotokov [5].

In my talk I will focus on the analysis results based on double-spin asymmetries measured with longitudinally polarized targets (RUN I). The topics to be discussed are listed below:

- evaluation of the singlet axial charge a_0 (total contribution of the quarks to the nucleon spin) using the precise measurement of the spin structure function $g_1(x, Q^2)$ for the proton and deuteron in inclusive DIS (Section 2);
- extraction of the quark helicity distributions from semi-inclusive DIS data with well identified charged pions and kaons in the final state (Section 3);
- recent analysis of the gluon polarization $\frac{\Delta g}{g}$ evaluated using a data sample of inclusive charged hadrons with high transverse momenta ($p_T > 1$ GeV) (Section 4).

2 Inclusive DIS, $\Delta\Sigma$ and strange sea polarization.

The low energy properties of the light baryons are well explained in the Constituent Quark Model (CQM), in which a baryon is made up of three constituent quarks (u-up, d-down, and s-strange) , all three quarks being in S-state. For a baryon polarized along the z axis, one would then expect that $S_z = \frac{1}{2} = \frac{1}{2}\Delta\Sigma = \frac{1}{2}\sum_i \Delta q_i$, where Δq_i is the contribution of a quark of flavor i ($\Delta q_i = \Delta u,\ \Delta d,\ \Delta s$) to the baryon spin. Using the non-relativistic wave function for the proton and applying $SU(3)$ flavor symmetry one may calculate $\Delta u,\ \Delta d,\ \Delta s$ for all members of the spin-1/2 baryon octet and evaluate the magnetic moments in a good agreement with the experiment at reasonable values for the constituent quark masses.

On the other hand, it is obvious that the naive CQM with $\Delta\Sigma = 1$ cannot be used as a basis for comprehension of the baryon spin. A partonic structure of the nucleon suggests that the nucleon spin decomposes into contributions from quark and gluon spins and quark and gluon orbital momenta [9]. Individual contributions to the nucleon spin are subject to experimental study in various polarization experiments. The most effective tool for probing quark polarizations and $\Delta\Sigma$ is deep-inelastic scattering (DIS) with a polarized charged lepton beam and a polarized target. In the case of inclusive DIS the measured double-spin asymmetry is straightforwardly related to the spin structure function $g_1(x, Q^2)$. In the Quark-Parton model (QPM), i.e., in leading order QCD (α_s^0) and neglecting higher twists ($1/Q^2 \to 0$), $g_1(x, Q^2)$ is expressed through the quark $\Delta q_i(x)$ and antiquark $\Delta\bar{q}_i(x)$ spin distribution functions, giving for the proton

$$g_1^p(x) = \frac{1}{2}\sum_i e_i^2(\Delta q_i^p(x) + \Delta\bar{q}_i^p(x)) = \frac{1}{2}[(2/3)^2(\Delta u(x) + \Delta\bar{u}(x)) + (1/3)^2(\Delta d(x) + \Delta\bar{d}(x)) + (1/3)^2(\Delta s(x) + \Delta\bar{s}(x))]. \quad (1)$$

First moments of the spin-structure functions for the proton, neutron and deuteron are given by integrals

$$\Gamma_1^{p,n} = \int_0^1 g_1^{p,n}(x)dx = \frac{1}{36}(4a_0 \pm 3a_3 + a_8) \tag{2}$$

and

$$\frac{\Gamma_1^d}{1-\frac{3}{2}\omega_d} = \frac{1}{2}(\Gamma_1^p + \Gamma_1^n) = \frac{1}{36}(4a_0 + a_8), \tag{3}$$

where ω_d accounts for a small correction for the D-state in the deuteron and indices p, n and d correspond to proton, neutron and deuteron, respectively.

The fundamental singlet (a_0) and non-singlet (a_3, a_8) axial charges in Eqs. 2 and 3 are invariants of the $SU(3)$ flavor symmetry. They can be written as

$$\begin{aligned} a_0 &= (\Delta u + \Delta\bar{u}) + (\Delta d + \Delta\bar{d}) + (\Delta s + \Delta\bar{s}) \equiv \Delta\Sigma, \\ a_3 &= (\Delta u + \Delta\bar{u}) - (\Delta d + \Delta\bar{d}), \\ a_8 &= (\Delta u + \Delta\bar{u}) + (\Delta d + \Delta\bar{d}) - 2(\Delta s + \Delta\bar{s}), \end{aligned} \tag{4}$$

where $\Delta u,\ \Delta\bar{u}, ...\ \Delta\bar{s}$ are the first moments of the spin-dependent quark distribution functions in the proton.

Under the assumption of $SU(3)$ flavor symmetry the non-singlet quantities a_3 and a_8 are expressed through the two hyperon decay constants F and D, related to the flavor-changing weak decays in the spin-1/2 baryon octet. According to a recent fit to the hyperon decay data $F = 0.464 \pm 0.008$ and $D = 0.806 \pm 0.008$, and $a_3 = F + D = g_A/g_V = 1.267 \pm 0.0003$, $a_8 = 3F - D = 0.586 \pm 0.031$.

A simple estimation of the singlet axial charge $a_0 = \Delta\Sigma$ may be done assuming that the strange sea in the proton is unpolarized ($\Delta s + \Delta\bar{s} = 0$). In this approximation one obtains $\Delta\Sigma = a_8 = 0.586$ and $\Gamma_p = 0.186$ $\Gamma_n = -0.024$ (Ellis-Jaffe sum rule). In general case ($\Delta s + \Delta\bar{s} \neq 0$) an additional equation is needed to specify all three axial charges. It may be obtained in a polarized DIS experiment, e.g., by measuring the deuteron integral Γ_1^d (see Eq.3).

The HERMES experiment has measured the double-spin asymmetries in DIS of the polarized positrons off polarized hydrogen or deuterium targets [10]. The measured asymmetries are corrected for detector smearing and QED radiative effects. The structure functions $g_1^p(x, Q^2)$ and $g_1^d(x, Q^2)$ are extracted from the data and the integrals Γ_p and Γ_d are evaluated in the range of the Bjorken scaling variable x from $x_{min} = 0.021$ to $x_{max} = 0.9$ for data with $Q^2 > 1$ GeV^2. For $x > 0.9$ the partial integrals of g_1 both for the proton and the deuteron are compatible with zero, e.g., the magnitude of $\int_{0.9}^1 g_1^d(x, Q^2)dx$ at Q^2=5 GeV^2 is estimated to be less than 10^{-4}. In order to estimate a possible contribution from the low-x region ($x < 0.021$), not explored in the experiment, the integrals are evaluated as functions of the lower limit in x. The deuteron integral appears to saturate at $x < 0.04$, thus showing that the contribution from the unmeasured low-x region is negligibly small. This allows us to calculate the singlet axial charge using the experimental values of $\Gamma_1^d(Q^2)$ and a_8:

$$a_0(Q^2) = \frac{1}{\Delta C_S^{\overline{MS}}}\left(\frac{9\Gamma_1^d}{1-\frac{3}{2}\omega_d} + \frac{1}{4}a_8\Delta C_{NS}^{\overline{MS}}\right). \tag{5}$$

The singlet and non-singlet coefficients $\Delta C_S^{\overline{MS}}$ and $\Delta C_{NS}^{\overline{MS}}$ in Eq.5 are calculated in the $\overline{MS}$ scheme up to second order in the strong coupling constant $\alpha_s(Q^2)$ (NNLO) [1]. With $\alpha_s = 0.29 \pm 0.01$ for $Q^2 = 5$ GeV^2 and $\omega_d = 0.05 \pm 0.01$, it is found

$$a_0^{\overline{MS}} = \Delta\Sigma = 0.330 \pm 0.025(exp.) \pm 0.028(evol.). \tag{6}$$

The theoretical (factorization scheme) uncertainty is estimated to be about ± 0.01.

The first moments of the quark helicity distributions are given by the relations $(\Delta s + \Delta\bar{s}) = \frac{1}{3}(a_0 - a_8)$, $(\Delta u + \Delta\bar{u}) = \frac{1}{6}(2a_0 + a_8 + a_3)$ and $(\Delta d + \Delta\bar{d}) = \frac{1}{6}(2a_0 + a_8 - a_3)$. In NNLO it has been obtained

$$(\Delta s + \Delta\bar{s}) = -0.085 \pm 0.008(exp.) \pm 0.009(evol.) \tag{7}$$

and

$$\begin{aligned}(\Delta u + \Delta\bar{u}) &= 0.842 \pm 0.008(exp.) \pm 0.009(evol.)\\ (\Delta d + \Delta\bar{d}) &= -0.427 \pm 0.008(exp.) \pm 0.009(evol.)\end{aligned} \tag{8}$$

3 SIDIS and quark helicity distributions.

The measurement of double-spin asymmetries in semi-inclusive deep-inelastic scattering (SIDIS), in which both scattered electron and produced hadron are well identified, gives direct access to the individual quark polarizations and helicity distributions. The double-spin asymmetry $A_1^h(x)$ is a linear combination of quark polarizations $\Delta q_i(x)/q_i(x)$ in the pure target spin state $S_z = +1/2$ weighted with purity distributions $P_i^h(x)$:

$$A_1^h(x) = \sum_i P_i^h(x)\frac{\Delta q_i(x)}{q_i(x)}, \quad P_i^h(x) = \frac{e_i^2 q_i(x)\int D_i^h(z)dz}{\sum_{i'} e_{i'}^2 q_{i'}(x)\int D_{i'}^h(z)dz}. \tag{9}$$

Here $D_i^h(z)$ is the fragmentation function and $z = E^h/\nu$ is the fractional energy of the detected hadron. All quantities in Eq.9 are averaged over Q^2. The purity $P_i^h(x)$ describes the probability that the hadron h originates from the interaction of the virtual photon with a quark of flavor i (struck quark).

HERMES has measured double-spin asymmetries in SIDIS from hydrogen and deuterium targets with π^+, π^-, K^+, K^- in the final state [11]. The asymmetries are extracted from the data sample under the following kinematical requirements: $Q^2 > 1$ GeV^2, $W^2 > 10$ GeV^2, $y = \frac{\nu}{E_e} < 0.85$, $0.2 < z < 0.8$. The DIS condition $Q^2 > 1$ GeV^2 restricts the minimum value of the Bjorken scaling variable to $x_{min} = 0.023$.

The measured asymmetries $A_1^h(x)$, corrected for detector smearing and QED radiative effects, have been used for the extraction of the quark polarizations and helicity distributions with the help of the system of equations Eq.9. The purities for hadron production from the proton and deuteron targets are calculated using the LUND MC program which has been tuned to the HERMES unpolarized SIDIS data, the spectrometer acceptance being taken into account. The CTEQ5L parametrization has been used for the computation of the unpolarized quark distributions $q_i(x)$.

[1] In LO (α_s^0) the two coefficients are equal to unity and Eq.5 is reduced to Eq.3.

The five independent helicity distribution functions $\Delta u(x), \Delta d(x), \Delta s(x), \Delta\bar{u}(x), \Delta\bar{d}(x)$ have been extracted. As the data do not significantly constrain $\Delta\bar{s}(x)$, it has been assumed that $\Delta\bar{s}(x) \equiv 0$. The obtained results are practically unchanged if instead of the latter constraint the assumption $\frac{\Delta s(x)}{s(x)} = \frac{\Delta\bar{s}(x)}{\bar{s}(x)}$ is used.

Fig. 1 shows the x-weighted distributions $x\Delta q_i(x)$ extracted using the purity formalism. The maximum value of x is chosen to be $x_{max} = 0.6$ since at higher x all the helicity distributions are compatible with zero. The systematic uncertainties, shown with an error band at the bottom of each panel, are dominated by the uncertainties in the purity calculations.

The theoretical parameterizations overlaid in Fig.1, obtained by the LO QCD global fit to inclusive DIS data [9, 13], describe well the HERMES semi-inclusive results. It is important to note that the analysis of inclusive data involves the hyperon-decay constants, and, therefore, requires validity of the SU(3) flavor symmetry. In contrast, the semi-inclusive DIS is a direct measurement of the quark polarizations, albeit in a restricted range of the Bjorken x variable.

In the explored range of the Bjorken x variable first moments of the quark helicity distributions may be calculated and compared with those found in the inclusive DIS analysis (Sect.2). For the total quark contribution $\widetilde{\Delta\Sigma}$ it is obtained

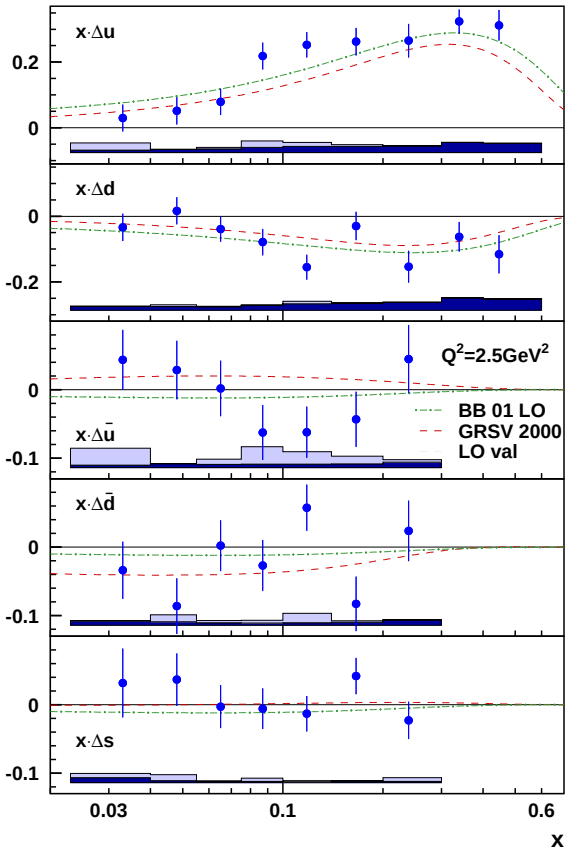

Figure 1. The quark helicity distributions $x\Delta q(x)$ evaluated at $Q_0^2 = 2.5\text{GeV}^2$. The theoretical curves are two variants of helicity distribution parameterizations taken from [9] (the dashed line) and [13] (dashed-dotted line), respectively. The parameterizations are obtained by global QCD fit to inclusive DIS data.

$$\widetilde{\Delta\Sigma} = \int_{0.023}^{0.6} [\Delta u(x) + \Delta\bar{u}(x) + \Delta d(x) + \Delta\bar{d}(x) + \Delta s(x)]dx \quad = \\ 0.347 \pm 0.024 \pm 0.066 \quad \Rightarrow \quad a_0 = \mathbf{0.330}\ (incl), \tag{10}$$

showing that the integral $\widetilde{\Delta\Sigma}$, similar to the deuteron integral Γ_1^d in inclusive DIS analysis (Eq.5), is very likely close to saturation. On the other hand, $(\widetilde{\Delta u} + \widetilde{\Delta\bar{u}}) = 0.599 \pm 0.022 \pm 0.065$, and $(\widetilde{\Delta d} + \widetilde{\Delta\bar{d}}) = -0.280 \pm 0.026 \pm 0.057$ are far from saturation (see Eq.8) which implies a substantial contribution from the unexplored region of $x < 0.023$. Similar to that, the strange quark contribution is also found compatible with zero: $\widetilde{\Delta s} = 0.028 \pm 0.033 \pm 0.009$, while from the inclusive DIS analysis it is a statistically significant negative value (Eq.7).

In distinction from inclusive DIS, the purity method used in SIDIS analysis allows the separation of q and $\bar{q}$ contributions. First moments for *up* and *down* anti-quarks are

found compatible with zero: $\Delta\bar{u} = -0.002 \pm 0.036 \pm 0.023$, $\Delta\bar{d} = -0.054 \pm 0.033 \pm 0.011$.

4 Gluon polarization.

The contribution of gluons to the nucleon spin is still poorly known to date. In principle, information on the spin-dependent gluon distribution function $\Delta g(x, \mu^2)$ may be obtained by a pertubative QCD NLO fit to the structure function $g_1(x, Q^2)$. Unfortunately, not sufficient precision and the restricted kinematic range of available data on $g_1(x, Q^2)$ result in large uncertainties in the Δg parameterizations. In Fig. 2 Feynman diagrams for DIS subprocesses are shown. In LO the virtual photon does not interact directly with gluons. Sensitivity to the gluon polarization may only appear in NLO due to the Photon-Gluon Fusion (PGF) subprocess.

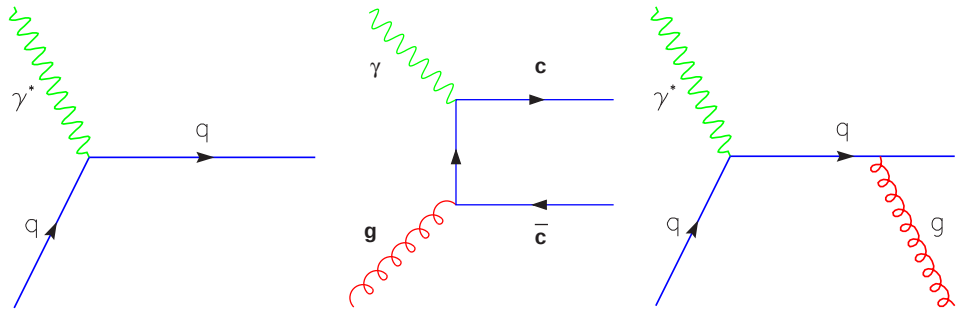

Figure 2. Feynman diagrams for DIS subprocesses. LO (α_s^0), left panel and two NLO (α_s^1) QCD subrocesses: Photon-Gluon Fusion (middle panel) and QCD Compton scattering (right panel).

One possibility to increase sensitivity to the gluon polarization is the detection of charmed hadrons in the final state. Charmed hadron electroproduction is dominated by the PGF subprocess. The scale μ, defined in this case by the mass of the charm quark pair, is sufficiently large. Unfortunately, a typical problem of these experiments is lack of statistics.

Another option to enhance sensitivity to the gluon contribution when measuring the double-spin asymmetry in electroproduction is to detect inclusive hadrons with high transverse momenta p_T. The results on $\frac{\Delta g}{g}$ of the COMPASS collaboration obtained by using both possibilities have already been reported in details [14].

The HERMES experiment has realized the second variant (high-p_T) because there is practically no open charm production at HERMES energy. The gluon polarization has been evaluated from inclusively detected charged hadrons. As detection of the positron is not required (or "anti-tagged") in this case, the kinematics of the virtual photon is not defined and the hadron transverse momentum p_T is measured in the respect to the direction of the primary beam. This data sample is characterized by a small positron scattering angle, and hence small Q^2, and, therefore, for most the of events the difference between measured p_T and "true" p_T (in the respect to the virtual photon) is not large. However, this is not true for a fraction of events with positrons scattered at large angles, out of the HERMES acceptance. In this case a LO DIS event with a small p_T of the hadron in the respect to the virtual photon can simulate a high-p_T event.

The double-spin asymmetries measured in the anti-tagged regime are shown in Fig. 3. The curves are calculated using the PYTHIA 6.2 MC for three assumptions: $\frac{\Delta g}{g} \pm 1$

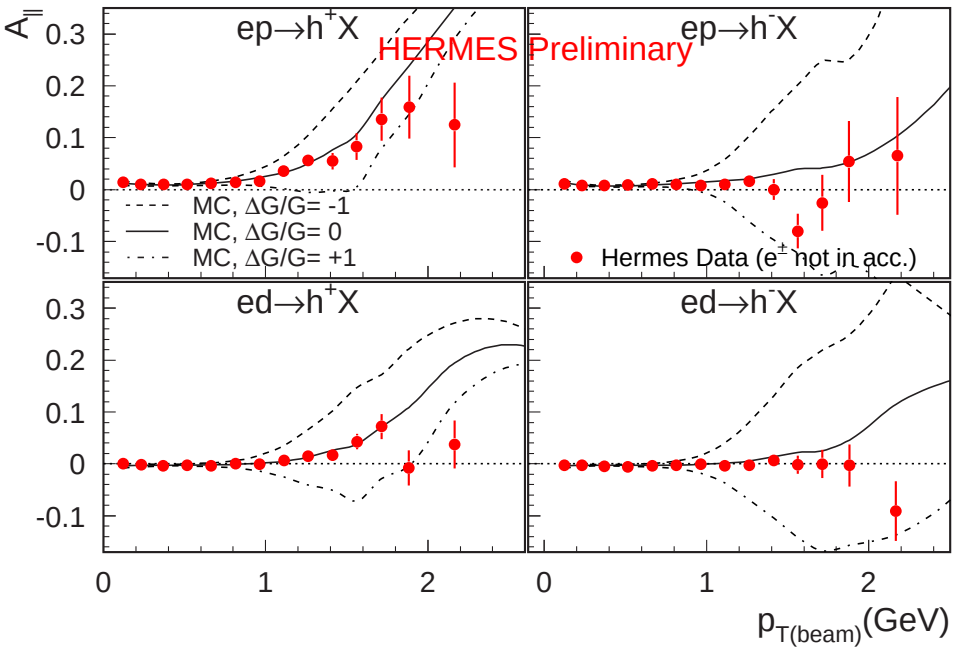

Figure 3. Measured double-spin asymmetries for positive and negative hadrons produced inclusively from the hydrogen and deuterium targets. The curves are MC asymmetries calculated for three different assumption on the gluon polarization.

and $\frac{\Delta g}{g} = 0$. As one can see, all the asymmetries in the region of p_T about 2 GeV favor the positive values of $\frac{\Delta g}{g}$.

The asymmetry calculated in the MC simulation is the weighted sum of the asymmetries of subprocesses classified in PYTHIA as hard photon interactions (pertubative QCD sketched in Fig. 2), soft VMD and resolved photon interactions. In order to specify where the signal to background ratio is optimized, variations of the individual terms of the sum with p_T have been studied. The fraction of the *signal* subprocesses, i.e., the subprocesses with asymmetries proportional to $\frac{\Delta g}{g}$, has been shown to increase with transverse momentum reaching about 20% at $p_T \simeq 1.75$ GeV.

Two methods have been applied to extract the gluon polarization $\frac{\Delta g}{g}$ from the data. *Method I.* It is assumed that $\frac{\Delta g}{g}$ is a slow function of x and Q^2 variables which results in "factorization", i.e., for a bin in p_T the value of $\frac{\Delta g}{g}$ can be found from the following equation

$$R^{sig}\{\hat{a}\frac{\Delta f_p^\gamma(x_p,Q^2)}{f_p^\gamma(x_p,Q^2)}\}\cdot\frac{\Delta g}{g} = A_{meas} - A_{MC}^{BGR}. \qquad (11)$$

Here A_{meas} is the measured asymmetry, A_{MC}^{BGR} is the calculated background asymmetry, R^{sig} is the fraction of all signal subprocesses, $\hat{a}$ is the elementary partonic asymmetry (e.g. the asymmetry calculated for subprocesses $\gamma q \to q\bar{q}$, $qg \to qg$, etc.), Δf_p^γ and f_p^γ are spin-dependent and spin-independent photon PDFs for a parton p. The function in braces is averaged over all signal subprocesses.

Method II. The function $\varphi(x) \equiv \frac{\Delta g(x)}{g(x)}$ is parameterized using two forms: $\varphi(x) = x(1 + p_1(1-x)^2$ and $\varphi(x) = x(1 + p_1'(1-x)^2 + p_2'(1-x)^3$. The free parameters p_1, p_1' and p_2' has been found by minimizing the difference between the measured and calculated asymmetries.

Methods I and II give very consistent results:
$\frac{\Delta g}{g} = 0.078 \pm 0.034 \pm 0.011 \pm 0.1(Models)$ at $\langle x \rangle = 0.204$ (Method I)
$\frac{\Delta g}{g} = 0.071 \pm 0.034 \pm 0.010 \pm 0.1(Models)$ at $\langle x \rangle = 0.222$ and $\mu = 1.35\text{GeV}^2$ (Method II).
The systematic error related to the "Models" in parenthesis has been estimated by variation of the parameters controlling the PYTHIA subprocesses, JETSET fragmentation processes and the spin-dependent and spin-averaged PDFs for the nucleon and the photon.

The HERMES results together with existing world data on $\frac{\Delta g}{g}$ and theoretical curves are presented in Fig. 4.

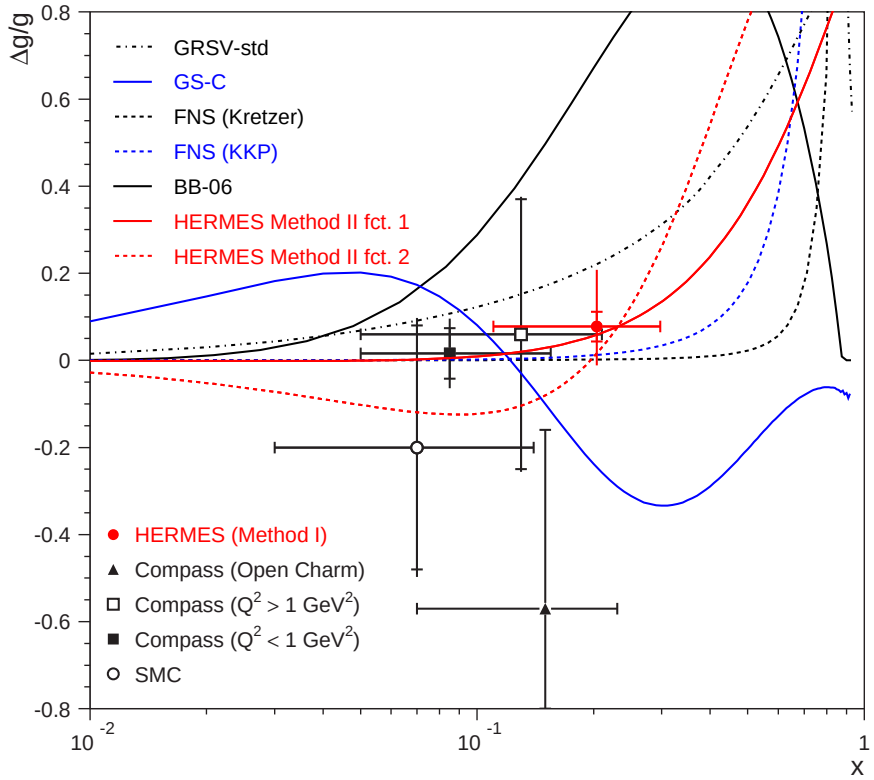

Figure 4. Compilation of world data on the gluon polarization. The HERMES data point (method I) is compared with those of COMPASS [15] and SMC [16]. Statistical (full) uncertainties are shown with inner (outer) error bars. The two HERMES fit functions (fct.1 and fct.2, Method II) are plotted.Also shown are the functions obtained by several NLO perturbative QCD fits.

5 Summary.

The main HERMES results obtained from the data collected during the RUN I on inclusive and semi-inclusive scattering with longitudinally polarized H and D targets are summarized as follows.

The total contribution of quarks to the nucleon spin (the singlet axial charge a_0) is found to be $a_0^{\overline{MS}} = \Delta\Sigma = 0.330 \pm 0.025(exp.) \pm 0.028(evol.)$ at $Q^2 = 5$ GeV^2. The first moment of the strange quark helicity distribution is a small but statistically significant negative value : $(\Delta s + \Delta\bar{s}) = -0.085 \pm 0.008(exp.) \pm 0.009(evol.)$. For the light quarks it is obtained $(\Delta u + \Delta\bar{u}) = 0.842 \pm 0.008(exp.) \pm 0.009(evol.)$ and $(\Delta d + \Delta\bar{d}) = -0.427 \pm$

$0.008(exp.) \pm 0.009(evol.)$. As far as the contribution to the deuteron integral from the region $x < x_{min} = 0.021$, not explored in the experiment, is shown to be negligibly small, the obtained results are not expected to be restricted by the limited x-Bjorken range accessed by the HERMES spectrometer. It is also important that SU(3) flavor symmetry violation cannot seriously affect the results (see, e.g., [17]).

Five quark helicity distributions $\Delta u(x)$,$\Delta d(x)$, $\Delta\bar{s}(x)$,$\Delta\bar{d}(x)$,$(\Delta\bar{s}(x) \equiv 0)$ have been extracted for the first time from semi-inclusive DIS data with well identified charged pions and kaons in the final states.The LO global QCD fit to the inclusive DIS results is in good agreement with extracted helicity distributions. In the x-Bjorken range explored by the experiment, the sea quark helicity distributions are found compatible with zero.

The gluon polarization obtained from the data sample of inclusive hadrons produced with high transverse momenta is found to be $\frac{\Delta g}{g} = 0.075 \pm 0.034 \pm 0.010 \pm 0.1(Models)$ at $\langle x \rangle = 0.222$ and $\mu = 1.35\text{GeV}^2$.

References

[1] J.Ashman et al.(EMC), Phys.Lett. **B206**, 364 (1988).
[2] B.Filippone and X.-D.Ji, Adv. Nucl. Phys. **26**, 1 (2001).
[3] K.Ackerstaff et al.(HERMES), Nucl. Instrum. Meth. **A417**, 230 (1998).
[4] M.Varanda, these proceedings.
[5] V.Korotkov, these proceedings.
[6] A.Borissov, these proceedings.
[7] D.Veretennikov, these proceedings.
[8] I.Vilardi, these proceedings.
[9] R.L.Jaffe and A.Manohar, Nucl. Phys. **B337**, 509 (1990).
[10] A.Airapetian *et al.*, Phys. Rev. **D75**, 012007 (2007).
[11] A.Airapetian *et al.*, Phys. Rev. **D71**, 012003 (2005).
[12] M.Glück, E.Reya, M.Stratmann, and W.Vogelsang, Phys. Rev. **D63**, 094005 (2001).
[13] J.Blümlein and H.Bottcher, Nucl. Phys. **B636**, 225 (2002).
[14] Y.Bedfer, this proceedings.
[15] E.S.Ageev *et al.*,(COMPASS), Phys.Lett. **B633**, 25 (2006).
[16] B.Adeva *et al.*, (SMC), Phys.Rev. **D70**, 012002 (2004).
[17] E.Leader, A.V.Sidorov and D.B.Stamenov, Phys.Lett. **B488**, 283 (2000).

Discussion

Q. (J.Nassalsky, SINS, Warsaw) 1. Does the new result on $\Delta G/G$ from large-p_t replace the old one? What is wrong with the old one?
2. In your semi-inclusive analysis you assume $\Delta\bar{s} = 0$ but you determine Δs - it seems to be inconsistent.
3. Could you comment more on the discrepancy with the Bjorken Sum Rule?

A. 1. The old result includes only a part of statistics. In addition, new analysis includes new approaches with Monte-Carlo calculations of each process contributions. In other words, the data are fully reanalyzed. So, yes, HERMES suggests the new number

for ΔG.
2. Yes. This has been done to reduce to a reasonable number of free parameter. This fit also may be done assuming $\Delta s = \Delta\bar{s}$. This would not practically affect the result.
3. HERMES has measured a_3 in the region x with $x_{min} = 0.023$. In this region $\int dx a_3(x)$ is not saturated and the integral is smaller than that given by g_A/g_V ratio. But this of course does not mean BjSR violation.

Q. (H.Santos, LIFEP, Lisboa) Which hints do you have to explain the discrepancy between inclusive and semi-inclusive results in what concerns strange polarization? Could it be due to the necessary assumptions made in the inclusive case, namely $SU(3)_F$? Or is more likely to be related to model-dependent fragmentation functions? What about the purity method?

A. To my mind, there is no discrepancy at all, and, as I have realized COMPASS and HERMES results are in excellent agreement. HERMES has measured zero strange quark polarization in the limited x range with x_{min}=0.023. This is direct semi-inclusive data. On the other hand, from HERMES inclusive measurements of g_1^d + SU(3) flavor symmetry it is found $\Delta s = -0.08 \pm 0.02 \pm \ldots$. That means that all contribution from s-quarks comes from low x range, $x < 0.023$, not reachable in semi-inclusive HERMES measurements.

THE FIRST RESULTS ON THE SPIN ASYMMETRIES IN ELASTIC pp SCATTERING AT SQRT S=200 GeV AND SMALL t AT RHIC

S. Bultmann[1], I. H. Chiang[1], R.E. Chrien[1], A. Drees[1], R. L. Gill[1], W. Guryn[1], J. Landgraf[1], T.A. Ljubiшiш[1], D. Lynn[1], C. Pearson[1], P. Pile[1], A. Rusek[1], M. Sakitt[1], S. Tepikian[1], K. Yip[1], A.A. Bogdanov[2], S. B. Nurushev[2], M. F. Runtzo[2], M. N. Strikhanov[2], I. G. Alekseev[3], V. P. Kanavets[3], L. I. Koroleva[3], B. V. Morozov[3], D. N. Svirida[3], A. Khodinov[4], M. Rijssenbeek[4], L. Whitehead[4], S. Yeung[4], K. De[5], N. Guler[5], J. Li[5], N. Ozturk[5], A. Sandacz[6], M. Haguenauer [7], J. Chwastowski[8], B. Pawlik[8]

(1) *Brookhaven National Laboratory, USA*
(2) *Moscow Engineering Physics Institute, Moscow, Russia*
(3) *Institute for Theoretical and Experimental Physics, Moscow, Russia*
(4) *Stony Brook University, Stony Brook, NY 11794, USA*
(5) *University of Texas at Arlington, Arlington, TX 76019, USA*
(6) *Soltan Institute for Nuclear Studies, Warsaw, Poland*
(7) *Ecole Polytechnique, 91128 Palaiseau Cedex, France*
(8) *Institute of Nuclear Physics, Cracow, Poland*
† *E-mail: asp9702@nm.ru*

Abstract

We present the measurements of the single spin analyzing power A_N and the double spin asymmetries A_{NN} and A_{SS} at $\sqrt{s} = 200$ GeV, obtained by the pp2pp Collaboration using polarized proton beams at the Relativistic Heavy Ion Collider (RHIC). Data points were measured in the four momentum transfer t range $0.01 < |t| < 0.03$ $(\mathrm{GeV/c})^2$. The measured double spin asymmetries, which are consistent with zero, allow us to estimate upper limits on the double helicity-flip amplitudes at small $|t|$ as well as on the difference between the total cross sections for collisions of transversely polarized protons and antiprotons.

The pp2pp experiment [1] at RHIC is designed to systematically study polarized proton-proton (pp) elastic scattering from $\sqrt{s}$ =60 GeV to $\sqrt{s}$ = 500 GeV, covering the $|t|$-range from the region of Coulomb Nuclear Interference (CNI) to 1.5 $(\mathrm{GeV/c})^2$. The experiment pp2pp is located at the У2 oTclockΦ position of the RHIC ring. The two protons collide at the interaction point (IP) and since the scattering angles are small, the scattered protons stay within the beam pipe until they reach the detectors. The measured coordinates are related to the scattering angles by the beam transport matrix. The coordinates are measured by silicon microstrip detectors (SSD) positioned just above and below the beam orbits by insertion devices Ц Roman Pots (RP) [2]. Each RP contains four planes of SSDs (two vertical and two horizontal) to provide redundancy for the track reconstruction. The identification of elastic events is based on the collinearity criterion, hence it requires the simultaneous detection of the scattered protons in a pair of RP detectors on either side of the IP. The background originates from particles from inelastic interactions, beam halo particles and products of beam-gas interactions. The estimated background fraction varies from 0.5% to 9% depending on the y-coordinate. Since in our

analysis the coordinate area was essentially limited to y > 30 strips, the background in the final sample does not exceed 2%. The sample of 1.14 million events, for $N^{\uparrow\uparrow}$ and $N^{\downarrow\downarrow}$ bunch combinations was used to determine A_N, and sample of 2.3 million elastic events was collected for analysis of double spin asymmetries in the t-interval $0.010 \leq -t \leq 0.030$, subdivided into three intervals $0.010 \leq -t < 0.015$, $0.015 \leq -t < 0.020$, $0.020 \leq -t \leq 0.030$. In each t-interval the asymmetry was calculated as a function of azimuthal angle ϕ using 5°-bins. Then the square root formula [4] for the single spin raw asymmetry $\varepsilon(\phi)$ can be written as

$$\varepsilon(\phi) = \frac{(P_B + P_Y) A_N \cos\phi}{1 + P_B P_Y (A_{NN} \cos^2\phi + A_{SS} \sin^2\phi)} = \frac{\sqrt{N^{\uparrow\uparrow}(\phi) N^{\downarrow\downarrow}(\pi-\phi)} - \sqrt{N^{\downarrow\downarrow}(\phi) N^{\uparrow\uparrow}(\pi-\phi)}}{\sqrt{N^{\uparrow\uparrow}(\phi) N^{\downarrow\downarrow}(\pi-\phi)} - \sqrt{N^{\downarrow\downarrow}(\phi) N^{\uparrow\uparrow}(\pi-\phi)}} \tag{1}$$

Beam polarizations for our run were $P_Y = 0.345 \pm 0.066$ and $P_B = 0.532 \pm 0.106$, leading to an upper constraint of 0.028 for the term $P_B P_Y (A_{NN} cos^2\phi + A_{SS} sin^2\phi)$, even if both double-spin asymmetries A_{NN} and A_{SS} were as large as 0.15. This term is small in comparison to the systematic errors on A_N and was therefore neglected in (1). A cosine fit to the raw asymmetry was used to determine values of A_N.

The values of A_N obtained in this experiment and their statistical errors for the three t-intervals are summarized in Table I.

Table I. A_N results.

$-t$ interval $(GeV/c)^2$	0.010-0.015	0.015-0.020	0.020-0.030	0.010-0.030
$< -t > (GeV/c)^2$	0.0127	0.0175	0.0236	0.0185
A_N	0.0277	0.0250	0.0178	0.0212
ΔA_N - stat.	±0.0061	±0.0043	±0.0030	±0.0023
ΔA_N - syst.	±0.0023	±0.0021	±0.0015	±0.0018

The general formula for A_N in the CNI region is given by Eq. 28 of [5]. With reasonable assumptions that the amplitude ϕ_2 and the difference $\phi_1 - \phi_3$ could be neglected at collider energies, the formula becomes simpler

$$A_N = \frac{\sqrt{-t}}{m} \frac{[k(1-\rho\delta) + 2(\delta Re r_5 - Im r_5)]\frac{t_c}{t} - 2(Re r_5 - \rho Im r_5)}{(\frac{t_c}{t})^2 - 2(\rho+\delta)\frac{t_c}{t} + (1+\rho)} \tag{2}$$

In this formula $t_c = -8\pi\alpha/\sigma_{tot}$, k is the anomalous magnetic moment of the proton, ρ is the ratio of the real to imaginary parts of forward (nonflip) elastic amplitude, and δ is the relative phase between the Coulomb and hadronic amplitudes. Since the total cross section σ_{tot} and the ρ parameter have not been measured in this energy range, we have used values of $\sigma_{tot} = 51.6$ mb and $\rho = 0.13$. These values come from fits to the existing pp data taken at energies below 63 GeV and world pp data. The Coulomb phase δ is calculated as in Ref. [5],

$$\delta = \alpha ln \frac{2}{|t|(b + 8/\Lambda^2)} - \alpha\gamma \tag{3}$$

where b is the slope of the forward peak in elastic scattering, α is the fine structure constant, EulerTs constant $\gamma = 0.5772$ and $\Lambda = 0.71 GeV^2$. The value of b comes from our previous measurement [1].

To quantify a possible contribution of the single helicity- flip amplitude ϕ_5, the formula given by (2) was fitted to the measured A_N values with Re r_5 and Im r_5 as fit parameters. The statistical and systematical errors (except the beam polarization error) of A_N were added in quadrature for the fit. The results of the fit are following: Re $r_5 = -0.033 \pm 0.035$ and Im $r_5 = -0.43 \pm 0.56$. The double spin raw asymmetry $\delta(\phi)$ is

$$\begin{aligned} \delta(\phi) &= P_B P_Y (A_{NN} \cos^2\phi + A_{SS} \sin^2\phi) \\ &= \frac{N^{\uparrow\uparrow}(\phi)/L^{\uparrow\uparrow} + N^{\downarrow\downarrow}(\phi)/L^{\downarrow\downarrow} - N^{\uparrow\downarrow}(\phi)/L^{\uparrow\downarrow} - N^{\downarrow\uparrow}(\phi)/L^{\downarrow\uparrow}}{N^{\uparrow\uparrow}(\phi)/L^{\uparrow\uparrow} + N^{\downarrow\downarrow}(\phi)/L^{\downarrow\downarrow} + N^{\uparrow\downarrow}(\phi)/L^{\uparrow\downarrow} + N^{\downarrow\uparrow}(\phi)/L^{\downarrow\uparrow}} \end{aligned} \tag{4}$$

where $L^{i,j}$ is the relative luminosity for the sum of bunches with a given spin combination. The raw asymmetry $\delta(\phi)$ was calculated as a function of the azimuthal angle ϕ using 5°-bins in the three t-intervals same as for $\varepsilon(\phi)$. A_{NN} and A_{SS} are the fit parameters and $P_B P_Y = 0.198 \pm 0.064$. The raw asymmetry was obtained using bunch intensities for an estimate of the relative luminosities. In order to facilitate separation of contributions of the helicity amplitudes ϕ_2 and ϕ_4 to the double spin asymmetries, we performed also alternative fits to $\delta(\phi) = P_B P_Y (a_1 + a_2 cos^2\phi)$ using $a_1 = (A_{NN} + A_{SS})/2$ and $a_2 = (A_{NN} - A_{SS})/2$ as fit parameters. The results on the double spin asymmetries for the whole t-interval $0.010 \leq -t \leq 0.030 (GeV/c)^2$, at an average $< -t >= 0.0185 (GeV/c)^2$, are presented in Table II. The most accurately determined asymmetry is $A_{SS} = 0.0035 \pm 0.0081$, which is consistent with zero at 1σ confidence level. The asymmetry $A_{NN} = 0.0298 \pm 0.0166$ as well as the combinations $(A_{NN} + A_{SS})/2 = 0.0167 \pm 0.0091$ and $(A_{NN} - A_{SS})/2 = 0.0131 \pm 0.0096$ are also small and consistent with zero.

Table II.Double spin asymmetries A_{NN}, A_{SS}, $(A_{NN} + A_{SS})/2$ and $(A_{NN} - A_{SS})/2$ for the t-interval $0.010 \leq -t \leq 0.030 (GeV/c)^2$ at $< -t >= 0.0185 (GeV/c)^2$.

	A_{NN}	A_{SS}	$(A_{NN} + A_{SS})/2$	$(A_{NN} + A_{SS})/2$
A_{sym}	0.0298	0.0035	0.0167	0.0131
$\Delta A_{sym}(stat. + norm.)$	$\pm$0.0166	$\pm$0.0081	$\pm$0.0091	$\pm$0.0096
$\Delta A_{sym}(syst.)$	$\pm$0.0045	$\pm$0.0031	$\pm$0.0034	$\pm$0.0072

At collider energies one expects [5] the two helicity conserving amplitudes ϕ_1 and ϕ_3 to be equal, $\phi_1 \approx \phi_3 = \phi_+ = (\phi_1 + \phi_3)/2$. A more precise limit on $Im\phi_2$ at t close to zero and therefore on $\Delta\sigma_T = \sigma_{tot}^{\uparrow\downarrow} - \sigma_{tot}^{\uparrow\uparrow}$ tot can be obtained using the t-dependence of the asymmetry A_{SS} and extrapolating A_{SS} to $t = -0.01$ $(GeV/c)^2$ where the term containing the real parts of amplitudes vanishes. For that purpose the corresponding experimental distributions $\delta(\phi)$ in the three t-intervals were fitted with a function $PP_Y A_{SS} + (A_{NN} - A_{SS}) cos^2\phi$ with A_{SS} as a fit parameter. Here the term $A_{NN} - A_{SS}$ was not fitted, but calculated as a predefined function of t. At small $|t|$ this term is proportional to t, $A_{NN} - A_{SS} = Ct$, because of the kinematical factors in ϕ_5 and ϕ_4 resulting from angular momentum conservation [5]. The constant C was calculated using the value of $A_{NN} - A_{SS}$ from the $\delta(\phi)$ fit for the combined t-interval. With the linear extrapolation to $t_0 = -0.01$ $(GeV/c)^2$ we obtain $A_{SS}(t_0) = 0.0037 \pm 0.0104$. Neglecting the contribution of ϕ_4 to A_{SS} and the variation of ϕ_2 over the small range of t one obtains $Im\phi_2/Im\phi_+ = 0.0037 \pm 0.0104$, $Imr_2 = 0.0019 \pm 0.0052$ and $\Delta\sigma = 0.19 \pm 0.53$ mb.

We consider the effect on A_{SS} of a possible contribution of the Pomeron-Odderon cut exchange in the t-channel as discussed in [6] and [7]. In case of such exchange the phase of the ϕ_2 amplitude is shifted by 90° relative to the amplitude ϕ_+, and $\mathrm{Im}\phi_2 = -\rho\mathrm{Re}\phi_2$ and thus $A_{SS} \approx t_c/t\mathrm{Re}\phi_2/\mathrm{Im}\phi_+$. Using the A_{SS} value at t = -0.185 $(GeV/c)^2$ one obtains Re $\phi_2/\mathrm{Im}\phi_+ = -0.050 \pm 0.130$ or $\mathrm{Re}r_2 = -0.025 \pm 0.065$. Though this value is well consistent with zero it leaves wide room for a possible Pomeron-Odderon cut contribution. Theoretical predictions for double-spin asymmetries in elastic proton-proton scattering at high energies and small momentum transfers have been recently presented in Ref. [7]. The magnitudes of A_{NN} and A_{SS} have been estimated using results from an earlier determination of the spin-couplings of the leading Regge poles [8] and the required Regge cuts were estimated using the absorptive Regge model. As the Odderon spin coupling is totally unknown, the predictions are given for various assumptions: (a) no Odderon, (b) weak Odderon spin coupling - equal to that of the Pomeron, (c) strong Odderon spin coupling - equal to the ρ Reggeon spin coupling. For none or a weak Odderon coupling the predicted values of the A_{NN} and A_{SS} asymmetries are very small. At $\sqrt{s} = 200GeV$ and $0.01 \leq |t| \leq 0.03(GeV/c)^2$ their values are in the range 0.001 - 0.002. On the contrary, for a strong Odderon spin coupling (like ρ) the double-spin asymmetries become significantly larger, at least by a factor of 10. Our results on the t-dependence of A_{SS} support predictions of Ref. [7] which assume none or a weak spin coupling of the Odderon.

In conclusion, these are the first measurements of the transverse double spin asymmetries and the first results on the double helicity-flip amplitudes in the small $|t|$ region in elastic pp scattering at collider energies. From the measured double spin asymmetries we determined the parameters $\mathrm{Im}r_2 = 0.0019 \pm 0.0053$ and $\Delta\sigma_T = -.0.19 \pm 0.53$ mb, both being consistent with zero within errors. We also estimated the upper limit on $\mathrm{Im}r_4$ which is $\mathrm{Im}r_4 < 1.25$. Assuming the Pomeron-Odderon cut exchange one finds $\mathrm{Re}r_2 = .0.025 \pm 0.065$. The signs and central values of the real and imaginary parts of r_2 agree with expectations for Pomeron-Odderon cut exchange. Their magnitudes are consistent with an assumption of about 5 ratio of the cut amplitude to the dominant one. The fitted r_5 is compatible, at about one σ level, with the hypothesis of no hadronic spin flip.

References

[1] S. Bultmann et al., Phys. Lett. **B579** 245-250. (2004).

[2] R. Battiston et al., Nucl. Instr. Meth. **A238** (1985) 35.

[3] S. Bultmann et al., Nucl. Instr. Meth. **A535** (2004) 415-420.

[4] G.G. Ohlsen and P.W. Keaton, Jr., Nucl. Instr. Meth. **109**, 41 (1973).

[5] N. H. Buttimore et al., Phys. Rev. **D59**, 114010 (1999).

[6] E. Leader and T.L. Trueman, Phys. Rev. **D61** (2000) 077504.

[7] T.L. Trueman, hep-ph/0604153.

[8] T.L. Trueman, Proceedings of the 16th International Spin Physics Symposium SPIN 2004, eds. F. Bradamante et al, World Scientific, 2005, p. 519.

Discussion

Q. (M.Grosse Perdekamp, Univ. of Illinois, Upton) In testing the hypothesis that no hadron spin flip is required it seems that the statistical significance of the data sample is not sufficient?

A. Yes. To improve our results we are going to continue measurements in STAR collaboration.

Q. (J.Soffer, Temple Univ., Philadelphia) I assume you also have measured the differential cross section in this experiment in the same kinematical region?

A. Yes, also we measured slope parameter b of the diffractive peak of the elastic cross section, but this is not a subject of my talk.

Q. (M.Sapozhnikov, JINR, Dubna) Is the sensitivity to $\Delta\bar{s}$ large enough to be measured at RHIC?

A. Yes, it is large enough.

NEW RESULTS ON EXCLUSIVE ρ^0 AND ϕ MESON PRODUCTION AT HERMES

A. Borissov, on behalf of the HERMES Collaboration

DESY, D-22603 Hamburg, Germany
E-mail: borissov@mail.desy.de

Abstract

Exclusive diffractive production of light vector mesons (ρ^0 and ϕ) on Hydrogen and Deuterium targets is measured in the HERMES kinematic region of $0.5 < Q^2 < 7$ GeV^2 and $3.0 < W < 6.3$ GeV. Data for Q^2 and W dependences of longitudinal cross sections are presented and compared with GPD based calculations and world data. Spin density matrix elements have been determined for exclusive ρ^0 and ϕ production. Within the given experimental uncertainties a hierarchy of relative sizes of helicity amplitudes is observed. Non-conservation of s-channel helicity is observed for ρ^0, but not for ϕ mesons. An indication of a contribution of unnatural parity exchange amplitudes in exclusive ρ^0 production is seen for proton data.

1 Introduction

Exclusive production of vector mesons such as ρ, ω or ϕ in deep-inelastic lepton scattering, see Fig. 1 a, is of particular interest as measurements of angular and momentum distributions of the scattered lepton and the vector meson decay products allow the study of the production mechanism and, in a model-dependent way, the nucleon structure. In the context of perturbative QCD (pQCD), the formalism of Generalized Parton Distributions (GPDs) has been introduced to describe the structure of the nucleon [1]. Here, at sufficiently large values of the factorization scale, exclusive meson production is assumed to be dominated by handbag-diagrams, see Fig. 1b, which involve various GPDs, e.g. H, $\widetilde{H}$, E, $\widetilde{E}$. Experimentally, GPDs can be investigated assuming certain functional forms for GPDs with a number of adjustable parameters, and fitting these parameters through a comparison of calculated observables with experimental data [2]. The HERMES data on hard-exclusive production of vector mesons (ρ^0 and ϕ) are compared with the calculations of the GK model [3]- [6] which is based on the 'handbag factorization'.

The determination of the longitudinal cross section (σ_L) of ρ^0 [7] and ϕ meson production allows the estimation of the contributions of the two major production mechanisms involved: quark-exchange and gluon-exchange, see Fig. 1b. For these two mechanisms, the amplitudes of ρ^0 and ϕ meson production have been calculated in the GK model and, from properly normalized bilinear combinations of amplitudes, the spin density matrix elements (SDMEs) have been obtained and compared with HERMES data.

The spin transfer from the virtual photon to the vector meson is commonly described [5] in terms of SDMEs. Those are usually described in the center-of-mass system of the virtual photon and target nucleon by the helicity amplitudes $T_{\lambda_V \lambda'_N, \lambda_\gamma \lambda_N}$ where λ_V (λ_γ) is the helicity of the vector meson (virtual photon). For longitudinal polarization

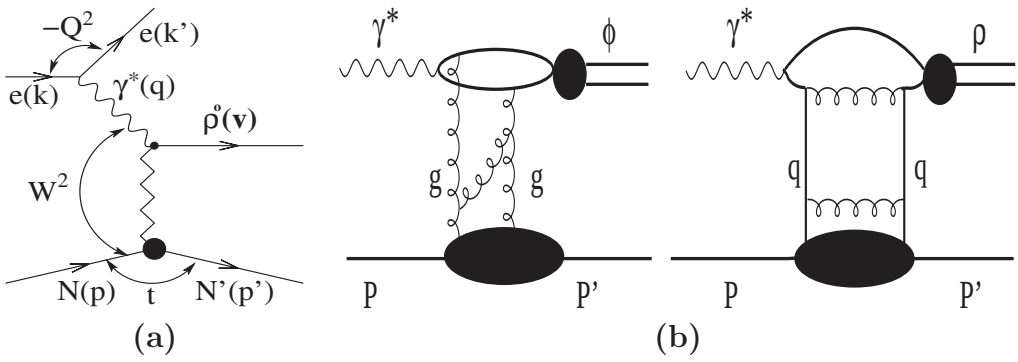

Figure 1a. Generic process $\gamma^\star p \to \rho^0 p$.
Figure 1b. Two-gluon exchange diagram and quark-exchange diagram.

of virtual photon (vector meson) $\lambda_{\gamma(V)} = 0$, and $\lambda_{\gamma(V)} = \pm 1$ for transverse polarization. Helicities of incident (λ_N) and outgoing nucleon (λ'_N) are summed over. The full expression for the decay angular distribution is given in Ref. [5] in terms of SDMEs r^α_{ij}, which are related to the initial spin density matrix elements $\rho^\alpha_{\lambda_V \lambda'_V}$ of the vector meson: $\rho^\alpha_{\lambda_V \lambda_{V'}} = \frac{1}{2N_\alpha} \sum_{\lambda_\gamma \lambda_{\gamma'}} T_{\lambda_V \lambda_\gamma} \Sigma^\alpha_{\lambda_\gamma \lambda'_\gamma} T^*_{\lambda'_V \lambda'_\gamma}$. Here N_α denotes a normalization factor, and $\Sigma^\alpha_{\lambda_\gamma \lambda'_\gamma}$ ($\alpha = 0,\ 1, \ldots, 8$) are nine Hermitian matrices defined in Ref. [5]. The index values $\alpha = 0, 1, 2, 3$ represent transverse photons: unpolarized, the two directions of linear polarization, and circular polarization. Pure longitudinal photons correspond to $\alpha = 4$, while the remaining values $\alpha = 5, 6, 7, 8$ are attributed to the interference of longitudinal and transverse photons. Summation over final nucleon helicities and averaging over initial proton helicities is implied. As the contributions of longitudinal and transverse photons are not distinguishable at fixed beam energy, the following matrix elements (referred to SDMEs) are used [5]: $r^{04} \equiv (\rho^0 + \epsilon R \rho^4)/(1 + \epsilon R)$, $r^\alpha \equiv \rho^\alpha/(1 + \epsilon R)$ for $\alpha = 1, 2, 3$, and $r^\alpha \equiv \sqrt{R}\rho^\alpha/(1 + \epsilon R)$ for $\alpha = 5, 6, 7, 8$, where ϵ is the virtual-photon polarization parameter and $R \equiv \frac{\sigma_L}{\sigma_T}$ is the longitudinal-to-transverse cross section ratio.

In the case of s-channel helicity conservation (SCHC), the helicity of the vector meson is the same as that of the virtual photon. The validity of SCHC was tested and, as shown below, the observation of several non-zero SDMEs for ρ^0 production indicates contributions from SCHC-violating helicity-flip amplitudes. In addition, the relative contributions of natural and unnatural-parity exchange were estimated from the combination of certain SMDEs. Natural-parity exchange (NPE) indicates that the interaction between the virtual photon and the target nucleon is mediated by a particle of 'natural' parity ($J^P = 0^+, 1^-, \ldots$ e.g. ρ^0, ω, A_2), while 'unnatural' parity exchange (UnPE) denotes the contribution of exchanged mesons with $J^P = 0^-, 1^+, \ldots$, e.g. π or A_1.

2 Detection of ρ^0 and ϕ Mesons and their Longitudinal Cross Sections

In the HERMES spectrometer [9] ρ^0 and ϕ mesons are observed by detecting their decay products in the following channels: $\rho^0 \to \pi^+\pi^-$ (100%) and $\phi \to K^+K^-$ (49%), respectively. The ρ^0 mesons are identified [7] by requiring $0.6 < M_{\pi\pi} < 1$ GeV, with $M_{\pi\pi}$ being

the invariant mass of the $\pi^+\pi^-$ system. The $\phi \to K^+K^-$ background in the ρ^0 spectrum is removed by the requirement that $M_{KK} > 1.04$ GeV, if the hadrons are assumed to be kaons. The ϕ mesons are selected by requiring $0.99 < M_{KK} < 1.04$ GeV. The absence of a signal in the Cherenkov threshold detector is required to identify kaon tracks in 1996-1997 data samples. For 1998-2000 data information from RICH detector [10] was used for kaon identification.

In order to extract information on the longitudinal production cross section, data on r_{00}^{04}, the longitudinal fraction of the ρ^0 cross section, have been used [7]. Using a parameterization of R, the longitudinal cross section for ρ^0 and ϕ production has been determined using $\sigma_L = \frac{R}{1+\epsilon R}\sigma_{total}$, where σ_{total} represents the total measured cross section [7]. The resulting values for ρ^0 and ϕ production are shown in Figs. 2 a and b, respectively, and are compared to the calculations of Ref. [4] and world data. The calculations for ρ^0 are in agreement with the data if the quark-exchange, two-gluon and sea quark interference, and the gluon-exchange contributions are included. For ϕ meson production only the gluon-exchange mechanism is expected to contribute, as the proton contains only a small population of s-quarks. Calculations based on this assumption [4] are in agreement with the data as presented in Fig. 2b. Contributions of different mechanisms to the longitudinal cross section of ρ^0 and ϕ meson leptoproduction are also related to the following results on SDMEs.

3 Spin Density Matrix Elements

In exclusive vector meson production, the angular distributions of the scattered lepton and the vector meson decay products are described in terms of the angles: Φ, the angle between the scattering plane and the ρ^0 production plane, Θ and ϕ, the polar and azimuthal angles of the decay π^+ in the vector meson rest frame with the z-axis aligned opposite to the outgoing nucleon momentum in the γ^*p center-of-mass system [5], see Fig. 3a.

The SDMEs are obtained from the measured angular distributions by minimizing the difference between the 3-dimensional $(\cos\Theta, \phi, \Phi)$ decay angle matrices of the data and of a sample of fully reconstructed Monte Carlo events, using the maximum likelihood method. An $8 \times 8 \times 8$ binning was used for the variables $\cos\Theta$, ϕ, Φ. The Monte Carlo events were generated with uniform angular distributions and were reweighted in an iterative procedure with the angular distribution $W(\cos\Theta, \phi, \Phi, r_{ij}^{\alpha})$ [5], where the SDMEs were treated as free parameters. These SDMEs were determined without the assumption of SCHC. The best fit parameters were obtained using a binned maximum log-likelihood method. The minimization itself and the error calculation were performed using the MINUIT package. Angular distributions from Monte Carlo, weighted with the final SDMEs, are compared with the data in Fig. 3b.

3.1 Hierarchy of SDMEs

The extracted SDMEs will be presented below based on the hierarchy of NPE helicity amplitudes:

$$|T_{00}| \sim |T_{11}| \gg |T_{01}| > |T_{10}| \sim |T_{1-1}|, \quad (1)$$

where the subscripts denote the helicitites of vector meson and virtual photon. This hierarchy was established for the first time in Ref. [17]. It is experimentally confirmed [12,

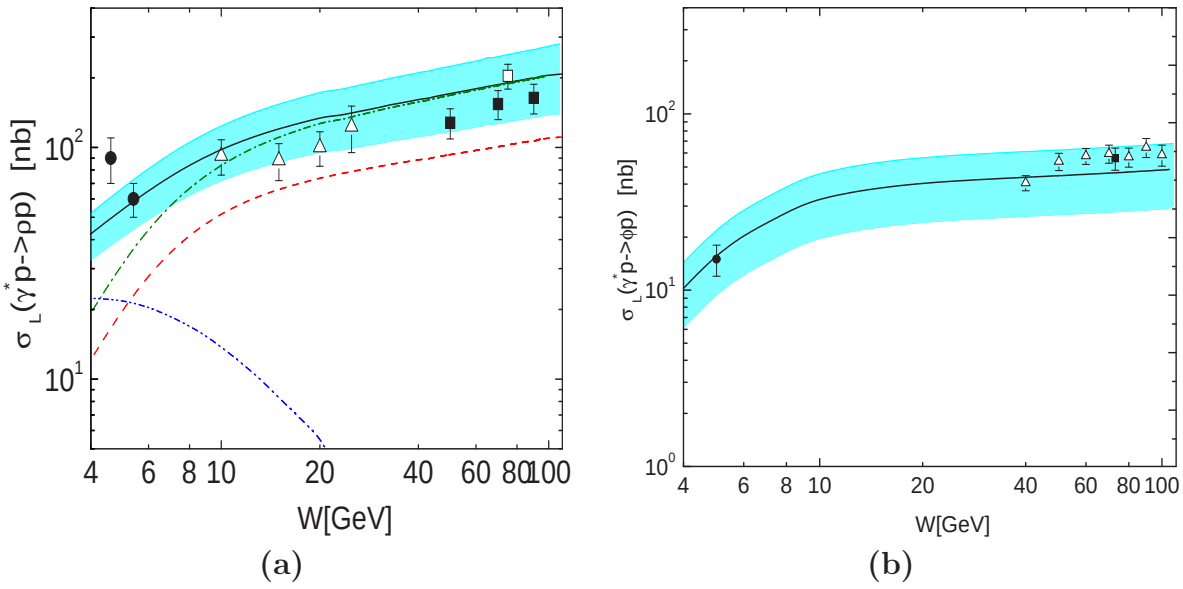

Figure 2a [4]. The longitudinal ρ^0 electroproduction cross section at Q^2=3.8 GeV^2. Data are from HERMES [7] (solid circles), E665 [11] (open triangles), ZEUS [12] (open square) and H1 [13] (solid squares). The dashed (dash-dotted,dash-dot-dotted) line represents the gluon, gluon+sea interference, and valence quark contribution [4]. The full line represents the sum of all contributions. The shaded area represents the error band resulting from the uncertainty in the CTEQ parton distributions.

Figure 2b [4]. The longitudinal ϕ meson electroproduction cross section at Q^2=4 GeV^2. Data are from HERMES [14] (solid circles), ZEUS [15] (open triangles), and H1 [16] (solid squares). The solid line represents the gluon contribution [4]. The shaded area represents the error band resulting from the uncertainty in the CTEQ parton distributions.

13] at the HERA collider and discussed in Refs. [3–5]. The measured 23 SDMEs are subdivided into five classes according to the hierarchy shown above. Class A includes SDMEs dominated by the helicity-conserving amplitudes T_{00} and T_{11} which describe the transitions $\gamma^*_L \to \rho^0_L$ and $\gamma^*_T \to \rho^0_T$, respectively. Class B contains SDMEs corresponding to the interference of the above two amplitudes. Class C consists of all those SDMEs in which the main term contains a linear contribution of the s-channel helicity non-concerving amplitude T_{01}, corresponding to the $\gamma^*_T \to \rho^0_L$ transition, except r^1_{00} for which the T_{01} contribution described above is quadratic. The classes D and E represent the SDMEs in which the main terms contain a linear contribution of the small helicity-flip amplitudes T_{10} ($\gamma^*_L \to \rho^0_T$) and T_{-11} ($\gamma^*_T \to \rho^0_{-T}$), respectively.

The SDMEs extracted for the kinematic region $1 < Q^2 < 5$ GeV^2, $3 < W < 6.3$ GeV (corresponding to $0.03 < x_{Bj} < 0.25$), and $0 < -t' < 0.4$ GeV^2, are presented for ρ^0 and ϕ meson data in Fig. 4. The shown SDMEs are multiplied by certain factors in order to present them according to the dominant amplitudes. The elements of class A are presented in the figure in such a way that their main terms are proportional to $|T_{11}|^2$, in particular $1-r^{04}_{00}$. The coefficients for class B are chosen to have the main contribution for the SDMEs proportional to $\mathrm{Re}\{\mathrm{T}_{11}\mathrm{T}^*_{00}\}$ and $\mathrm{Im}\{\mathrm{T}_{11}\mathrm{T}^*_{00}\}$, respectively. This corresponds to the general rule which is applicable to classes B to E: the dominant contribution of

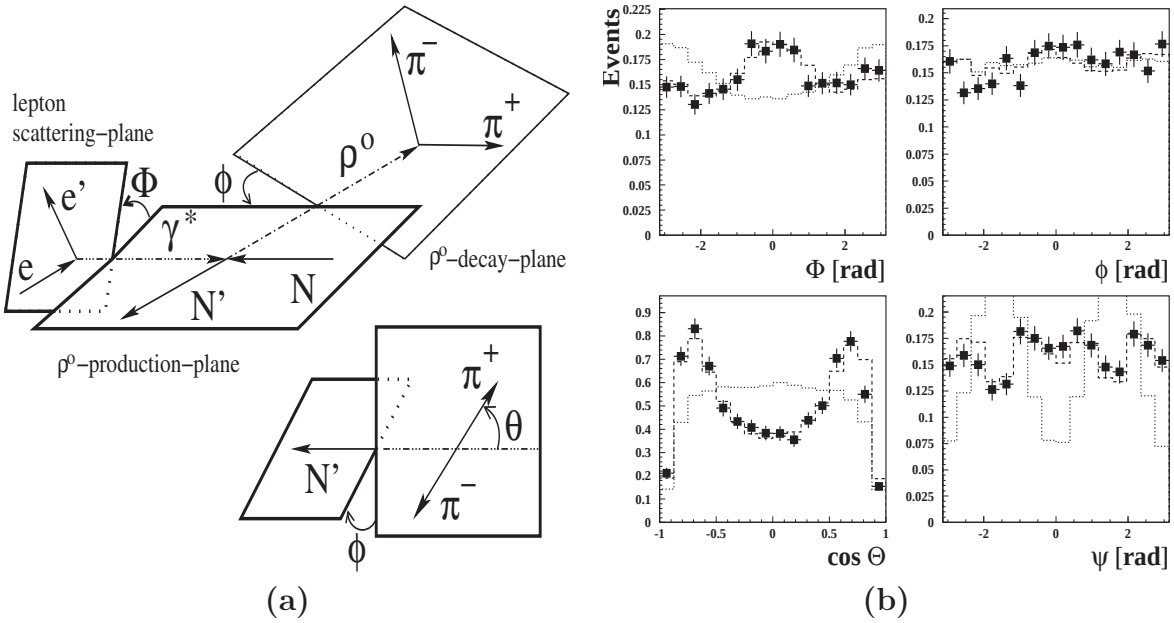

Figure 3a. Definition of angles in the process $\gamma^\star p \to \rho^o p$. Here Φ is the angle between the ρ^0 production plane and the lepton scattering plane, Θ and ϕ are polar and azimuthal angles of the decay π^+ in the vector meson rest frame.

Figure 3b. Angular distributions of ρ^0 meson production and decay. Data points represent used in the fit subsample of the proton data with positive polarization of the beam. The dotted lines are the Monte Carlo input distributions, the dashed lines are the results of the 23-parameter fit.

any element presented in Fig. 4 is equal to the real or imaginary part of a product of two amplitudes. Class C contains products $T_{01}T_{00}^*$ (for $r_{00}^5/\sqrt{2}$ and $r_{00}^8/\sqrt{2}$) and $T_{01}T_{11}^*$. The dominant contributions for classes D and E contain products $T_{10}T_{11}^*$ and $T_{1-1}T_{11}^*$, respectively.

The unpolarized SDMEs of class B have large values, very similar to those of class A. This suggests the presence of a substantial interference between the two dominant amplitudes T_{00} and T_{11} for ρ^0 and ϕ meson production. The two polarized class B SDMEs are significantly non-zero for ρ^0 and ϕ as well. As seen from Fig. 4, the values of elements in class C which contains the dominant term $T_{01}T_{11}^*$ are close to each other for the unpolarized SDMEs (Re$\{r_{10}^{04}\}$, Re$\{r_{10}^1\}$, Im$\{r_{10}^2\}$). While they are much smaller than class B SDMEs, they are still significantly larger than class D and class E SDMEs. This shows that the anticipated hierarchy is supported by the data.

3.2 Test of the SCHC Hypothesis

Elements of classes C,D,E indicate non-conservation of s-channel helicity in ρ^0 production if they are non-zero. In particular, the SDME r_{00}^5 is observed to be non-zero at the level of eight standard deviations in the combined uncertainty, proving s-channel helicity non-conservation. This was already observed earlier by the HERA collider experiments [12,13] at a lower significance level, and with high significance very recently [12]. For the first

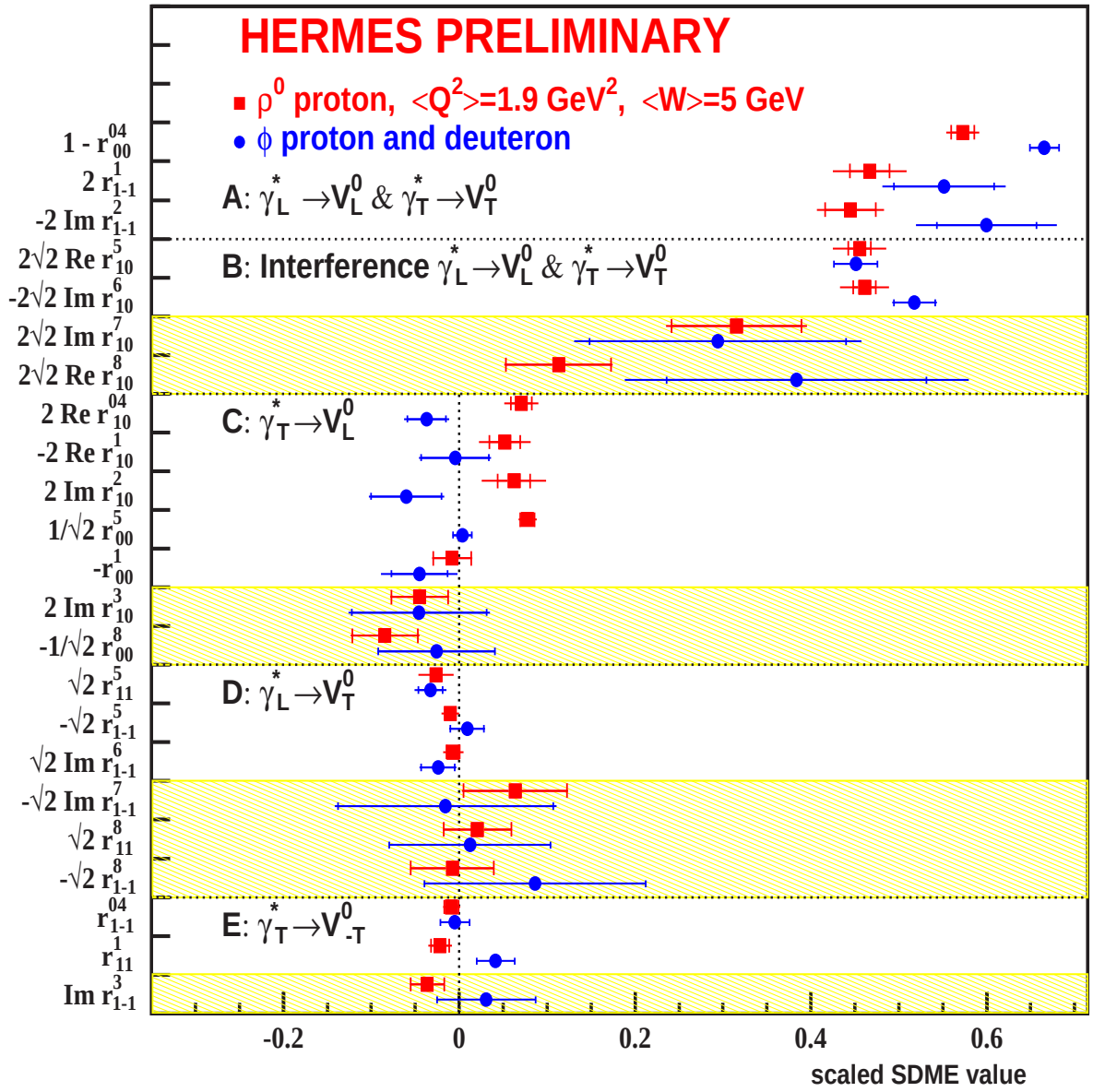

Figure 4. The 23 SDMEs extracted for ρ^0 production on proton (squares) and ϕ meson production on proton and deuteron (circles) in the entire HERMES kinematics with $\langle x \rangle = 0.08, \langle Q^2 \rangle = 1.9$ GeV^2, $\langle -t' \rangle = 0.13$ GeV^2. The SDMEs are renormalized to represent the leading contribution of the corresponding amplitude. The inner error bars represent the statistical uncertainties, while the outer ones indicate the statistical and systematic uncertainties added in quadrature. The unshaded (shaded) areas indicate beam-polarization independent (dependent) SDMEs. The vertical dashed line at zero corresponds to SDMEs expected to be zero under the hypothesis of SCHC.

time, HERMES observes s-channel helicity non-conservation also in other class C SDMEs, in particular Re$\{r^{04}_{10}\}$. The beam-polarization dependent elements r^8_{00} and Im$\{r^3_{10}\}$ are determined using information on the longitudinally polarized lepton beam, for the first time. Both elements are consistent with zero within large uncertainties, indicating only a small possible contribution from the term Im$\{T_{01}T^*_{11}\}$.

Contrary to ρ^0 production, ϕ meson SDMEs are in agreement with s-channel helicity conservation.

3.3 Phase Difference between T_{11} and T_{00}

The phase difference δ between the amplitudes T_{11} and T_{00} can be evaluated as follows:

$$\cos\delta = \frac{2\sqrt{\epsilon}(\mathrm{Re}\{\mathrm{r}^5_{10}\} - \mathrm{Im}\{\mathrm{r}^6_{10}\})}{\sqrt{r^{04}_{00}(1 - r^{04}_{00} + r^1_{1-1} - \mathrm{Im}\{\mathrm{r}^2_{1-1}\})}}. \tag{2}$$

This results in the precise determination of $|\delta| = 28.1 \pm 2.8_{stat} \pm 3.7_{syst}$ degrees for ρ^0 data on proton. Using beam-polarization dependent SDMEs, also the sign of δ can be determined:

$$\sin\delta = \frac{2\sqrt{\epsilon}(\mathrm{Re}\{\mathrm{r}^8_{10}\} + \mathrm{Im}\{\mathrm{r}^7_{10}\})}{\sqrt{r^{04}_{00}(1 - r^{04}_{00} + r^1_{1-1} - \mathrm{Im}\{\mathrm{r}^2_{1-1}\})}}. \tag{3}$$

In this way, the HERMES experiment for the first time determines the sign of δ to be positive: $\delta = 24.4 \pm 5.2_{stat} \pm 2.1_{syst}$ degrees for ρ^0 production.

3.4 Unnatural-Parity Exchange

Disregarding the assumption of SCHC, the hypothesis of the absence of unnatural-parity exchange (UnPE) in the t-channel implies that $U_1 \equiv 1 - r^{04}_{00} + 2r^{04}_{1-1} - 2r^1_{11} - 2r^1_{1-1} = 0$. The HERMES result for ρ^0 production on the proton, $U_1 = 0.132 \pm 0.026_{stat} \pm 0.053_{syst}$, is different from zero at a level of 2σ of the total uncertainty, demonstrating the significance of the unnatural-parity-exchange contribution. A signal of UnPE is important as evidence of quark-antiquark exchange, corresponding to a description of the polarized GPDs. The kinematic dependences of U_1 for the proton on Q^2, t' and x_{bj} are presented in Fig. 5a. Although the errors are large due to the large number of SDMEs involved, all measured values of U_1 are positive. Note that a positive U_1 value of about 0.1 was recently obtained including the GPD $\widetilde{H}$ in GK model calculations [5].

Contrary to ρ^0 production, U_1 values calculated from ϕ meson SDMEs are consistent with zero, see Fig. 5b. This is in agreement with corresponding calculations in the GK model [5] where only two-gluon exchange was considered.

4 Summary

Using a maximum likelihood fit, 15 beam-polarization-independent SDMEs and, for the first time, 8 beam-polarization-dependent SDMEs are determined. The measured SDMEs are grouped according to their theoretically expected hierarchy which is observed within given experimental uncertainties. This facilitates the investigation of the relative importance of various helicity amplitudes describing different $\gamma^* \to \rho^0(\phi)$ transitions.

Non-zero values of ρ^0 SDMEs corresponding to the amplitude T_{01} indicate a small but statistically significant deviation from the hypothesis of s-channel helicity conservation.

The phase difference between the helicity-conserving amplitudes T_{00} and T_{11} is confirmed to be significantly non-zero. For the first time, the sign of the phase difference is precisely determined using the beam-polarization-dependent ρ^0 SDMEs.

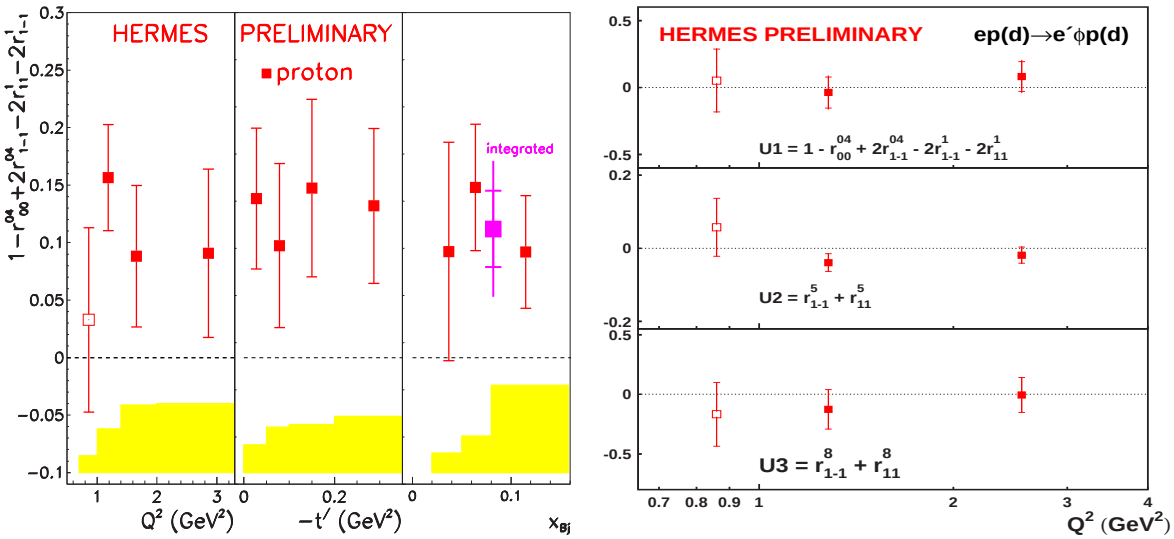

Figure 5a. The Q^2, t', and x_{Bj} dependence of the SDME combination $U_1 = 1 - r^{04}_{00} + 2r^{04}_{1-1} - 2r^{1}_{11} - 2r^{1}_{1-1}$ for ρ^0 production on the proton. The data given in the open point for the first Q^2 bin (< 1 GeV^2) are not included in the t' and x_{Bj} plots, which represent data with a $Q^2 > 1$ GeV^2. The error bars represent the statistical uncertainty while the bands below indicate the systematic uncertainties. For the integrated point, the inner error bar represents the statistical uncertainty while the outer one indicates the additional systematic uncertainty.

Figure 5b. The Q^2 dependence of the enumerated on the SDME combinations U_1, U_2, U_3 for ϕ meson production. The values integrated in the range $1 < Q^2 < 7$ GeV^2 are shown as closed symbols. The data given as open point are for the first bin, $Q^2 < 1$ GeV^2. The inner (outer) error bars represent the statistical (total) uncertainty.

The evaluation of certain relations between SDMEs provides an indication for the existence of unnatural-parity-exchange amplitudes for ρ^0 production, supporting a significant role of the quark-exchange mechanism in ρ^0 production at intermediate energies.

For the first time HERMES results on light vector meson production (ρ^0 and ϕ) are comprehensively compared with model calculations [3]- [6] based on GPDs at kinematic values of $W = 5$ GeV and Q^2=3 GeV^2. It is remarkable to note that these calculations are in fair agreement with the longitudinal and full cross sections of ρ^0 and ϕ mesons, the values of most of the SDMEs and hierarchy of corresponding amplitudes, violation of SCHC in ρ^0 production, the W-dependence of ρ^0 and ϕ SDMEs and with the σ_L/σ_T ratios [5,6]. Nevertheless, HERMES data provide several constraints for a further development of this model, in particular for the phase difference in the interference of $\gamma^*_L \to \rho^0_L$ and $\gamma^*_T \to \rho^0_T$ transitions, the $\widetilde{H}$ contribution in the unnatural parity exchange amplitude, and the E contribution in the transverse target-spin asymmetry of exclusive ρ^0 electroproduction discussed in [18].

This work is supported in part by the Heisenberg-Landau program.

References

[1] D. Müller et al, Fortschr. Phys. **42** (1994) 101; X. Ji, Phys. Rev. Lett. **78** (1997) 610; X. Ji, Phys. Rev. **D55** (1997) 7114; A.V. Radyushkin, Phys. Rev. **D56** (1997) 5524.

[2] M. Diehl, Phys. Rept. **388**, (2003) 41.

[3] S.V. Goloskokov and P. Kroll, Eur.Phys.J. **C 42** (2005) 02298.

[4] S.V. Goloskokov and P. Kroll, Eur.Phys.J. **C 50** (2007) 829.

[5] S.V. Goloskokov and P. Kroll, e-Print: arXiv:0708.3569, acc. by Eur.Phys.J. C.

[6] S.V. Goloskokov, these proceedings.

[7] HERMES Collab. K. Ackerstaff et al, Eur.Phys.J. C **17**, (2000) 3898.

[8] K. Schilling and G. Wolf, Nucl. Phys. **B61** (1973) 381.

[9] HERMES Collab. H. Ackerstaff et al, NIM **A 417** (1998) 230.

[10] N. Akopov et al., Nucl. Instr. and Meth. **A 479** (2002) 511.

[11] M.R. Adams et al., E665 Coll., Z. Phys. **C 74** (1997) 237.

[12] J. Breitweg et.al., ZEUS Coll., Eur. Phys. J. **C12** (2000) 393; S. Chekanov et al., ZEUS Coll., DESY-07-118 (August 2007), submitted to PMC Physics A.

[13] C. Adloff et al., H1 Coll., Eur. Phys. J. **C13** (2000) 371.

[14] A. Borissov, for HERMES collab., Procs. of the 9th International Workshop on High-Energy Spin Physics (SPIN 01), Dubna, Russia, 2-7 Aug. 2001; A. Borissov, for HERMES collab.,Nucl. Phys. Proc. Suppl. **99A** (2001) 156.

[15] S. Chekanov et al., ZEUS Coll., Nucl. Phys. B **718** (2005) 3.

[16] C. Adloff et al., H1 Coll., Phys. Lett. B. **483** (2000) 360.

[17] D.Yu. Ivanov and R.Kirschner, Phys.Rev.D **58** (1998) 114026.

[18] S.V. Korotkov, these proceedings.

Discussion

Q. (L.Jenkowzsky, ITP, Kiev) Are the elements of your spin density matrix constant parameters, or they are functions of the dynamical variables: W, t and Q^2?

A. They are functions. What I have shown, is only in the first approximations. Here (a slide shown) you can see their functional dependence.

THE RHIC SPIN PROGRAM

G. Bunce[1†]

(1) *RIKEN BNL Research Center and Brookhaven National Laboratory*
† *E-mail: bunce@bnl.gov*

Abstract

The RHIC spin program, colliding polarized protons to study the spin structure of the proton, is underway. For 2006 we have achieved high luminosity collisions at $\sqrt{s}$=200 GeV, with 55 to 60% polarization. We present sensitive measurements on the gluon polarization in polarized protons, large observed transverse spin asymmetries, and discuss the future program.

1 Introduction

The goal of the RHIC spin program is to study the spin structure of the proton, using strongly interacting probes of polarized quarks and gluons by colliding beams of polarized protons [1]. We began polarized proton collisions in 2001, with about 15% beam polarization and ran for an integrated luminosity of 0.15 pb^{-1}. In 2006, the Renaissance Run, the polarization was 55-60%, and the luminosity delivered to the experiments was 46 pb^{-1}. In this report, I will discuss the beautiful results from this run, from RHIC and from the three spin experiments, PHENIX, STAR, and BRAHMS. RHIC polarization for 2006 is shown in Figure 1.

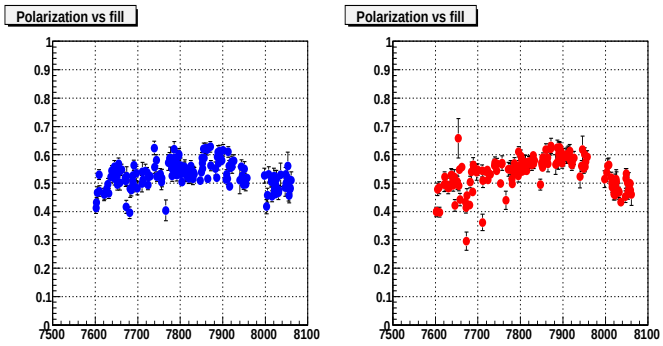

Figure 1: Final polarization by RHIC fill, for 2006, weighted by collision luminosity. The left panel is for the clockwise (from above) beam, right panel for the counter-clockwise beam. Measurements for fill numbers from 8000 are for $\sqrt{s}$=62 GeV runs. These measurements use polarized proton-carbon scattering from an ultra-thin carbon target that is rotated into the RHIC beams a few times per fill.

2 The Polarization of the Gluons

The collisions of (polarized) protons, producing jets and particles of sufficiently high transverse momentum p_T, are described by perturbative QCD. For example, at $\sqrt{s}$=200 GeV, the π^0 cross section vs. p_T is described by the next to leading order (NLO) pQCD prediction [2] with no free parameters, for over seven orders of magnitude [3], at mid-rapidity. Similarly for jet production [4] and direct photon production for p_T above 5 GeV/c [5].

At forward rapidity, the cross section for π^0 production at $\sqrt{s}$=200 GeV is also described by pQCD [6].

Double beam helicity asymmetries (A_{LL}) for production of jets, direct photons, and fragmentation products of the jets, are sensitive to the polarization of the gluons in polarized protons. The gluon-gluon scattering subprocess and the quark-gluon scattering subprocess both depend on the helicities of the initial state partons, basically due to angular momentum conservation. This is the approach used to constrain the gluon polarization at RHIC. Lower p_T production of π^0 or jets is dominated by the gluon-gluon graph, and A_{LL} at mid-rapidity is essentially quadratic in the gluon polarization. At higher p_T, the quark-gluon graph dominates, and A_{LL} is linear in gluon polarization. For direct photon production, the dominant graph is quark-gluon Compton scattering, and A_{LL} is linear in gluon polarization. So far, sensitive measurements have been made for π^0 and jet production; the direct photon measurements require accumulating significantly higher luminosity.

The data for A_{LL} for jet production, obtained by the STAR collaboration, was presented by J. Dunlop here. Figure 2 shows the preliminary result for π^0 from the 2006 run, from the PHENIX collaboration [7], as well as published data from the 2005 run [8].

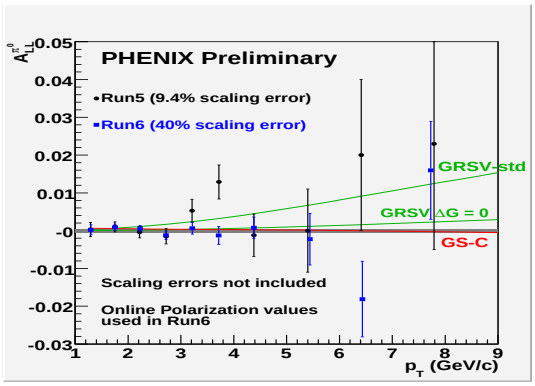

Figure 2: The double beam helicity asymmetry for π^0 production, at $\sqrt{s}$=200 GeV, mid-rapidity. These are preliminary results from the PHENIX experiment, 2006 RHIC run, and published results from 2005. The curves are discussed in the text.

Both the jet and π^0 results indicate little or no asymmetry, and therefore little or no gluon polarization in the measured region. The measured region corresponds to a gluon momentum fraction of x_{gluon} from about 0.02 to 0.3. Each point in p_T in Fig. 2 corresponds to a broad range in x_{gluon}. To be more quantitative, we have used a model for the kinematic behavior of the gluon polarization to provide limits on the level of gluon polarization (within the context of the model).

The curves on Fig. 2 show the asymmetry expected for two levels of gluon polarization, following the GRSV model [9]. The GRSV model assumes that the gluon polarization does not change sign over x_{gluon}. The curve GRSV-std uses the best fit to DIS data, and has an integral over x_{gluon} of ΔG=0.4 for the scale Q^2=1 GeV^2. The curve GRSV-ΔG=0 sets the gluon polarization, $\Delta G(x)$=0, at a low input scale of Q^2=0.4 (GeV/c)^2. Deep inelastic scattering results are fit with this level of gluon polarization, which is evolved to the scale of the data. The combination of gluon and refit quark polarization is then used to obtain the expected asymmetry for RHIC, in this case for π^0 production. Note that the ΔG=0 curve does not give zero A_{LL}. This is due to evolution–the splitting of polarized quarks to polarized gluons at higher scales. The curve GS-C [10] assumes a node in the gluon polarization vs. x_{gluon}. The sign change gives an average gluon polarization in the measured region near zero, with a calculated A_{LL} near zero.

The proton spin crisis began with the 1988 result from the EMC experiment [11]

which indicated nearly zero quark spin contribution to the proton spin. The modern result for the level of quark spin contribution to the proton spin is about 0.15 for Q^2=3 and 5 GeV^2 [12] [13]. Therefore, the level of gluon polarization of 0.4 for GRSV-std corresponds (roughly) to the remainder of the proton spin being carried by the gluons, with no additional contribution from orbital angular momentum.

Figure 3 shows a χ^2 distribution vs. the integral of the gluon polarization over the measured region, for the π^0 data from Fig. 2, and for the 2005 data. This approach is described in the paper on the 2005 results [8]. The curve is generated by creating a range of curves for $A_{LL}(p_T)$, from a range of gluon polarizations following the GRSV model, each refitting the DIS data to obtain new quark polarizations. The χ^2 values used for the curve of Fig. 3 are then obtained by comparing the $A_{LL}(p_T)$ data to these curves for different gluon polarizations.

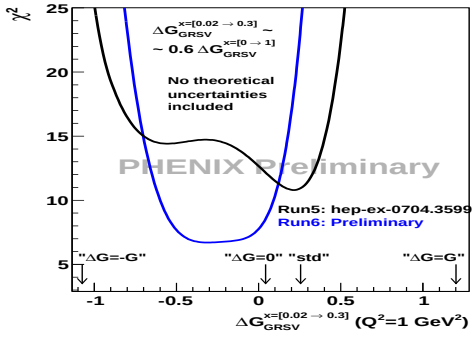

Figure 3: χ^2 vs. the gluon polarization for one model, integrated over the measured region in x_{gluon}, from the preliminary 2006 data of Fig. 2. Also shown is the curve from the 2005 data.

Within the context of the model, the data prefer small to zero, or negative, gluon polarization. It should also be emphasized that this statement applies to the measured range in gluon polarization, as is indicated on the figure. For the GRSV model, the measured region corresponds to about 60% of the integral of gluon polarization. However, for a model with a node in gluon polarization, for example GS-C, the measured region corresponds to nearly zero integral, whereas the integral over all x_{gluon} is of order 1 (next to leading order, at Q^2=4 GeV^2).

From Fig. 3, we see that, for the GRSV model for gluon polarization, a small or zero (or negative) gluon polarization is preferred. It will be important to further constrain the gluon contribution, through more data. Higher p_T inclusive data will provide sensitivity where the RHIC asymmetry is linear in gluon polarization, and where gluon polarization is expected from evolution from quark polarization. Lower x_{gluon} data can be obtained from forward production, particularly from forward direct photon production; also, data from higher energy running at RHIC will contribute lower x_{gluon} data. A major focus will also be on correlations, for example photon plus jet events, where the kinematics of the partons can be obtained at lowest order. These measurements are planned for 2008 through 2009 or 2010, for $\sqrt{s}$=200 GeV, and for 500 GeV running after that. The 500 GeV running will provide a lower x_{gluon} reach, and also data for the parity-violating production of W bosons. The W production will provide direct measurements of the polarization of the anti-u and anti-d quarks.

3 Transverse Spin Renaissance

Large transverse spin asymmetries and polarizations in inclusive production have been observed for over thirty years [14] [15]. However, for many years it was argued that these effects were from (unknown) complicated soft physics scattering processes. Three results

changed this view. The first was from the HERMES experiment, where a significant and unexpected azimuthal asymmetry was observed in the production of pions in deep inelastic scattering of electrons from polarized protons [16]. The second was the observation at RHIC by the STAR experiment of large transverse spin asymmetry in the production of π^0 at $\sqrt{s}$=200 GeV, at forward rapidity, and where the cross section was described by pQCD [17]. The third result was the observation by the BELLE experiment that, for q-$\bar{q}$ production in electron-positron annhilation, the azimuth of the leading pion in one quark jet is correlated with the azimuth of the leading oppositely-charged pion in the other (anti)quark jet [18]. This correlation indicates an analyzing power for the fragmentation of transversely polarized quarks.

At the same time, partly a result of the new transverse spin experimental results, and partly driving the experimental measurements, there has been a remarkable theoretical effort in the field. I will not try to present a comprehensive discussion of this work. However, for example, the measurements at HERMES and at BELLE were partly driven by the suggestion of Efremov [33] and Collins and Heppelmann [20] that a possible quark fragmenation analyzing power would give access to measuring the contribution of the quark spin to the transverse spin of the proton (transversity).

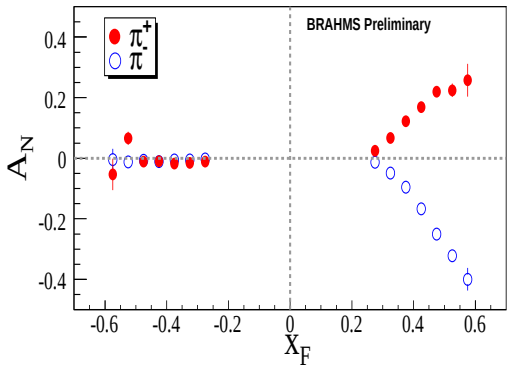

Figure 4: A_N vs. x_F for inclusive production of charged pions, at $\sqrt{s}$=62 GeV, preliminary data from 2006, from the BRHAMS experiment. The data are for production angles of 2.3 and 3 degrees.

New results from RHIC include precise measurements of π^0 asymmetries for forward production, by the STAR experiment, and presented here by J. Dunlop. These results were for collisions at $\sqrt{s}$=200 GeV. Figure 4 shows preliminary results from the BRAHMS experiment for charged pion asymmetries, at $\sqrt{s}$=62 GeV [21]. This experiment has previously presented results for 200 GeV. The asymmetries at 62 GeV are very large, and significantly larger than the asymmetries at 200 GeV. This is presumably due to the dependence of the asymmetry on x_F. At the lower energy, the BRAHMS detector is sensitive to signficantly higher x_F. These asymmetries are remarkable.

4 A Transverse Spin Drell-Yan Experiment

A very exciting direction for the transverse spin program is connecting semi-inclusive DIS and RHIC results. The existence of a transverse spin asymmetry requires the interference of production amplitudes, and a key paper by Brodsky, Hwang, and Schmidt [22] presented an argument that this interference can occur at leading twist (the asymmetry is not suppressed as $1/Q$ when Q is large) through initial and final state interactions that generate the necessary interfering amplitude and phase. Collins [23] suggested that for DIS, a final state interaction is involved, between the struck quark and the proton remnant (see Figure 5). For Drell-Yan production, an initial state interaction is required, between the anti-quark from the unpolarized hadron and the remnant from the polarized

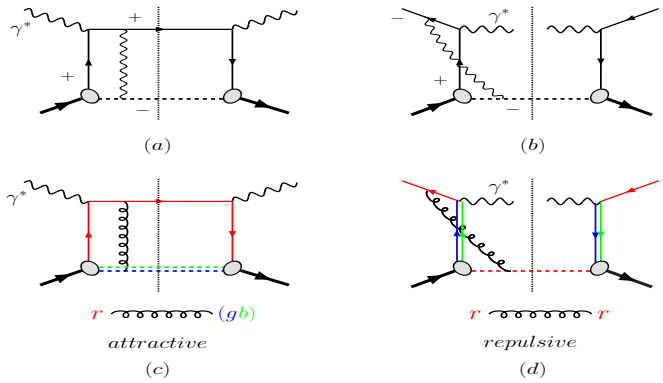

Figure 5: The bottom diagrams present, at lowest order, the argument that the initial state interaction for DIS (left graph), and the final state interaction for Drell-Yan (right graph), give a color force that is attractive (left) and repulsive (right). The argument holds at all orders, and results in the prediction that the transverse spin asymmetries for DIS and for Drell-Yan should be of opposite sign. The top diagrams present a QED analog.

proton (see Fig. 5). The final state interaction of DIS and the intitial state interaction of Drell-Yan have different color interactions, giving in general an attractive force for DIS and a negative force for Drell-Yan, resulting in opposite sign transverse spin asymmetries. This can be seen for lowest order in Fig. 5, where the color charge of the quark and remnant in DIS are necessarily opposite, producing an attractive force for the final state interaction. For Drell-Yan, for the lowest order graph shown in Fig. 5, the initial state interaction has necessarily the same color charge for anti-quark and remnant, resulting in a repulsive force. Although shown at lowest order, the prediction holds at all orders.

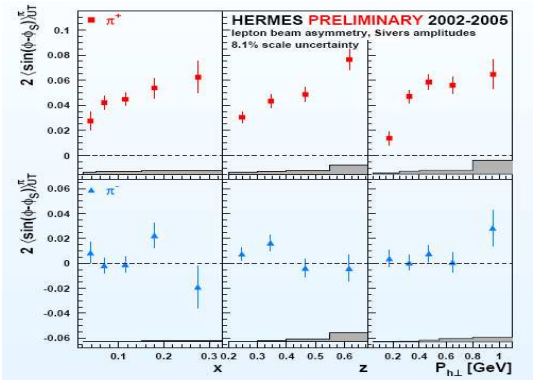

Figure 6: Asymmetry for π^+ and π^- production in DIS, for a transversely polarized proton target, from the HERMES experiment.

Figure 6 shows the DIS transverse spin asymmetry for π^+ and π^- production, corresponding to the initial state k_T suggested by Sivers [24], reported by HERMES [16]. Figure 7 shows the predicted Drell-Yan asymmetry, for RHIC with one beam transversely polarized and one beam unpolarized [25]. The statistics shown require 250 pb^{-1} for collisions at $\sqrt{s}$=200 GeV. Both PHENIX and STAR could do this, with the uncertainties shown. The PHENIX experiment would need an active nose cone absorber to provide necessary isolation requirements for the identification of forward direct muons (that is, to reject muons from heavy quark decays, with the heavy quarks embedded in jets). The STAR experiment would require a forward charged particle spectrometer set-up, to measure the charge signs of the electron-positron pair. This luminosity is high–it requires significantly higher luminosity than available now, but which may be available in the future with luminosity upgrades to RHIC.

A Drell-Yan measurement with transverse spin at RHIC, testing this prediction, tests our understanding of the transverse spin asymmetries. A successful outcome would also confirm the color interaction of QCD with attraction for opposite color charges and repulsion for like color charges. Failure of the test would not challenge QCD, but would challenge our understanding of these asymmetries, and likely challenge our pQCD description of these interactions, both DIS and RHIC. Therefore, this should be done, and the results of the measurement would have consequences.

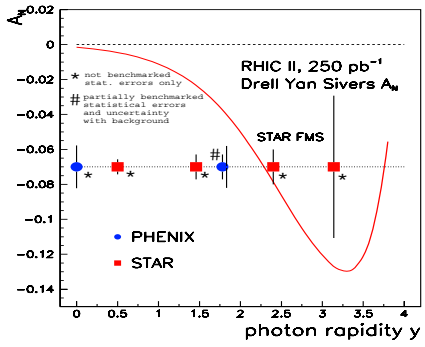

Figure 7: Predicted transverse spin asymmetry and sensitivities, for RHIC, for Drell-Yan production.

5 Final Remarks

The past six or so years have resulted in great progress toward understanding the spin structure of the proton.

The helicity structure now appears to have little contribution from the gluon spin; however, there is a lot more work to do here to be confident of such a conclusion. We need measurements at lower gluon momentum fraction, measurements with direct photons, and measurements of correlated observables to pin down the momentum fraction of each colliding parton. Another direction which is likely to give surprises is to measure the polarization of the anti-u and anti-d quarks directly, using parity-violating W production at RHIC. This program should start around 2010.

The field of the transverse spin structure of the proton is blossomming. There are major new experimental results from DIS, hadron probes, and for fragmentation. There are major new theoretical advances connecting these measurements to a pQCD description, to orbital angular momentum of the quarks (and gluons) in the proton, and connecting DIS and hadron probe results. Personally, I am particularly looking forward to a theoretical understanding of the simplest (in principle) QCD spin process–the observed analyzing power for fragmenting polarized quarks.

Acknowledgements

The work is supported by the U.S. DOE, the U.S. NSF, and RIKEN Laboratory, Japan. The 2006 run was additionally supported (and made possible by) a generous donation from Renaissance Technologies.

I would like to thank Hiromi Okada, Itaru Nakagawa, Les Bland, Werner Vogelsang, Abhay Deshpande, Sasha Bazilevsky, Matthias Grosse Perdekamp, and many others for their advice and plots, used in the presentation and here.

References

[1] G. Bunce, N. Saito, J. Soffer, and W. Vogelsang, *Ann. Rev. Nucl. Part. Sci. 2000* **50**, 525 (2000).

[2] B. Jager *et al.*, *Phys. Rev.* **D67**, 054005 (2003).

[3] S.S. Adler *et al.* [PHENIX Collaboration], *Phys. Rev. Lett.* **91**, 241803 (2003).

[4] B.L. Abalev *et al.* (STAR Collaboration), *Phys. Rev. Lett.* **97**, 252001 (2003).

[5] S.S. Adler *et al.* (PHENIX Collaboration), *Phys. Rev. Lett.* **98**, 012002 (2007).

[6] J. Adams *et al.* (STAR Collaboration), *Phys. Rev. Lett.* **97**, 152302 (2006).

[7] K. Boyle *et al.* (PHENIX Collaboration), Spin2006 Symposium, Kyoto, Japan.

[8] A. Adare *et al.* (PHENIX Collaboration), *Phys. Rev.* **D76**, 051106(R) (2007)

[9] B. Jager, A. Schafer, M. Stratmann and W. Vogelsang, *Phys. Rev.* **D67**, 054005 (2003); M. Gluck, E. Raya, M. Stratmann and W. Vogelsang, *Phys. Rev.* **D63**, 094005 (2001).

[10] T. Gehrmann and W.J. Stirling, *Phys. Rev.* **D53**, 6100 (1996).

[11] J. Ashman *et al.* [European Muon Collaboration], *Phys. Lett.* **B206**, 364 (1988); *Nucl. Phys.* **B328**, 1 (1989).

[12] V.Yu. Alexakhin *et al.* (COMPASS Collaboration), *Phys. Lett.* **B647**, 8 (2007).

[13] A. Airapetian *et al.* (HERMES Collaboration), *Phys. Rev.* **D75**, 012007 (2007).

[14] G. Bunce *et al.*, *Phys. Rev. Lett.* **36**, 1113 (1976).

[15] D.L. Adams *et al.* [FNAL E704 Collaboration], *Phys. Lett.* **B264**, 462 (1991).

[16] A. Airapetian *et al.* [HERMES Collaboration], *Phys. Rev. Lett.* **84**, 4047 (2000); A. Airapetian *et al.*, *Phys. Lett.* **B622**, 14 (2005); M. Diefenthaler *et al.*, Int. Workshop on DIS 2007, Munich, Germany (2007).

[17] J. Adams *et al.* [STAR Collaboration], *Phys. Rev. Lett.***92**, 171801 (2004).

[18] R. Seidl et al. [BELLE, KEK], *Phys. Rev. Lett.* **96**, 232002 (2006).

[19] A.V. Efremov, L. Mankiewicz and N.A. Tornqvist, *Phys. Lett.* **B284**, 394 (1992).

[20] J.C. Collins, S.F. Heppelmann and G.A. Ladinsky *Nucl. Phys.* **B420**, 565 (1994).

[21] J. H. Lee (BRAHMS Collaboration), DIS 2006, Tsukuba, Japan.

[22] S.J. Brodsky, D.S. Hwang and I. Schmidt, *Phys. Lett.***B 530**, 99 (2002).

[23] J.C. Collins, *Phys. Lett.***B 536**, 43 (2002).

[24] D.W. Sivers, *Phys. Rev.* **D41**, 83 (1990).

[25] W. Vogelsang and F. Yuan, *Phys. Rev.* **D 72**, 054028-1-17 (2005); J. C. Collins et al., Phys. Rev. D 73, 094023-1-10 (2006)a; see also http://spin.riken.bnl.gov/rsc/write-up/dy_final.pdf.

Discussion

Q. (L.Jenkowzsky, ITP, Kiev) Given the flexibility in the definition of jets, to what extent can the polarization of a jet be identify with that of the parton - quark or gluon - of which it is a footprint?

A. The correlation between the polarizations of the jets and partons can be best seen in e^+e^- annihilation.

Q. (J.Nassalski, SINS, Warsaw) What are your plans concerning single-photon asymmetries?

A. My personal view is that direct photon production will only be valuable if the pion and jet A_{LL} are nonzero. This is due to the small cross section for direct photon. An exception is that forward (direct photon + jet) asymmetries may constrain ΔG at lower momentum fraction.

Q. (I.Ginzburg, IM, Novosibirsk) What is the absolute precision in the luminosity monitoring (i.e. in total x-sections)?

A. It is now $\sim$9% from the scan method (measuring beam size by moving one beam across the other). However, we have had a recent advance in our understanding for this technique and may be able to reduce this uncertainty considerably. A few % is possible.

Q. (S.Belostotsky, PNPI, St.Petersburg) High p_T region looks free (practically) from gluon-gluon contribution and, in such way, qg (quark-gluon) starts dominating. What are the prospects than to reach much better statistical accuracy in this high p_T region.

A. If we have a non-zero positive A_{LL}, the uncertainty for negative ΔG will be greatly reduced. If we continue to have $A_{LL} = 0$, there will still be a larger uncertainty for negative ΔG. (The uncertainty for positive ΔG would be small in this case).

GENERALIZED PARTON DISTRIBUTIONS AT COMPASS

N. d'Hose[1]

(1) *CEA-Saclay, DAPNIA-SPhN, F91191 Gif-sur-Yvette Cedex*
On behalf of the COMPASS collaboration
† *E-mail: ndhose@cea.fr*

Abstract

The Generalized Parton Distribution (GPD) framework is a novel and powerful tool for the investigation of the nucleon structure. Accessible through hard exclusive reactions the GPDs provide a three-dimensional picture of how the quarks and the gluons build up the nucleon. The high energies available at CERN, and the option of using either positive or negative polarized muon beams, make the fixed-target COMPASS set-up a unique place for studying GPDs, through Deeply virtual Compton scattering (DVCS). This contribution presents the goal of such experiments as well as the detectors necessary to complement the high resolution forward spectrometer COMPASS.

1 Quark and gluon imaging of the nucleon with GPDs

The GPD functions have been introduced 10 years ago [1, 21, 3] and they provide a comprehensive description of the quark and gluon structure of the nucleon (see Ref. [4–6] for reviews). GPDs describe the quantum-mechanical amplitude for "taking out" a parton (quark or gluon) of the wave function of the fast-moving nucleon and "putting it back" with a different momentum, giving a small momentum transfer to the nucleon (see Fig. 1).

Such a process can be probed by hard exclusive reactions such as Deeply Virtual Compton Scattering (DVCS) or meson production where a photon of virtuality Q^2 interacts with the active quark and where a real photon or a meson is ejected in order to compensate the energy flow in the hard scattering. The short-distance information specific to the process can be unambiguously separated from the long-distance information about nucleon structure contained in the GPDs (factorization theorem). The GPDs depend upon three kinematical variables: x, ξ and t. x is the average longitudinal [1] momentum fraction of the active quarks. $2\xi = 2x_{Bj}/(2 - x_{Bj})$ is the longitudinal momentum fraction of the transfer to the nucleon. $t = \Delta^2 = (\Delta_L + \Delta_T)^2$ is the squared transfer between the initial and final nucleons. The transverse transfer Δ_T leads to information about the spatial transverse distribution of partons.

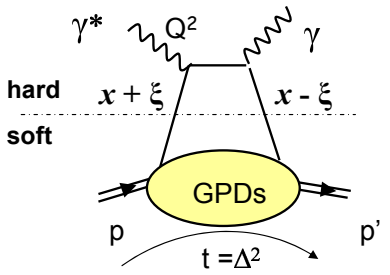

Figure 1. Handbag diagram for the DVCS amplitude at leading twist.

[1] "Longitudinal" refers to the direction of the fast moving nucleon for example in the centre of mass of the virtual photon-nucleon collision

At leading twist four GPDs are necessary to parametrize the nucleon structure information. H and $\tilde{H}$ are generalizations of the parton distributions measured in DIS. In the forward limit, corresponding to $\xi = 0$ and $t = 0$, H^q, for a quark of flavor q, reduces to the quark distribution $q(x)$ and $\tilde{H}^q$ to the longitudinally polarized quark distribution $\Delta q(x)$ while for the gluon sector $H^g(x, 0, 0) = g(x)$ and $\tilde{H}^g(x, 0, 0) = \Delta g(x)$. H and $\tilde{H}$ conserve the helicity of the proton, whereas E and $\tilde{E}$ allow for the possibility of the proton helicity flip. In such a case the overall helicity is not conserved: the proton changes helicity but the massless quark does not, so that the angular momentum conservation implies a transfer of orbital angular momentum. This is only possible for nonzero transverse momentum transfer, which is new with respect to the ordinary parton distributions. The Ji sume rule relates the GPDs and the total angular momentum of the partons [21]:

$$\frac{1}{2}\sum_q \int_{-1}^{+1} dx x(H^q(x, \xi, t = 0) + E^q(x, \xi, t = 0)) = J^{quark} \tag{1}$$

The second moment at $t = 0$ gives the total (spin + orbital) angular momentum carried by the quarks. There is an equivalent sum rule for the gluons. The first moments of the GPDs are related to the nucleon elastic form factors. For example:

$$\sum_q e_q \int_{-1}^{+1} dx H^q(x, \xi, t) = F_1(t) \tag{2}$$

where F_1 is the Dirac form factor. However the GPDs contain much more information than the parton densities and the elastic form factors. They describe the correlation between a parton longitudinal momentum fraction, x, and the transverse momentum transfer to the nucleon, Δ_T. For $\xi = 0$, $H(x, 0, -\Delta_T^2)$ is the Fourier transform of the probability density to find a quark with momentum fraction x at a given distance b from the center of momentum in the transverse plane: $H(x, 0, -\Delta_T^2) = \int d^2b e^{-i\Delta_T.b} f(x, b)$. This 1+2-dimensional "mixed" longitudinal momentum and transverse coordinate representation corresponds to a set of tomographic images of the parton distribution in the nucleon at a fixed longitudinal momentum fraction x (see Fig. 2).

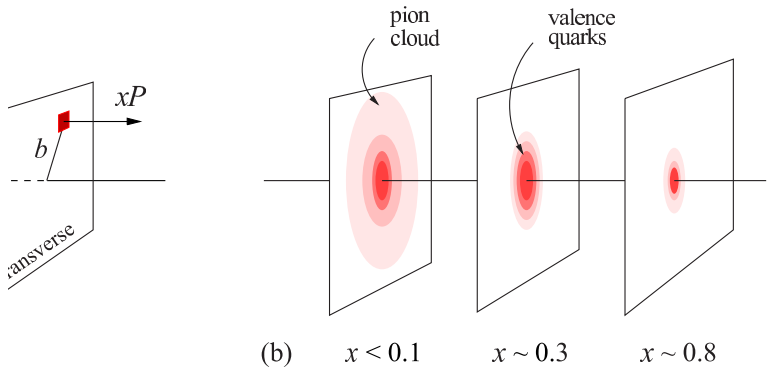

Figure 2. Nucleon tomography: (a) The transverse Fourier transform of the GPD describes the distribution of quarks with longitudinal momentum fraction x with respect to transverse position, (b) It produces a set of 1+2-dimensional "tomographic" image of the quark structure of the nucleon which allows to separate the contributions from the valence quarks or from the pion cloud or sea quarks. (The figures are from Refs [7, 8].)

The width of the b distribution goes to zero as $x \to 1$ since the active quark becomes the center of momentum. At $x \sim 0.3$ one mainly "sees" the core of the valence quarks distributed over transverse distances $b << 1$ fm. At $x < 0.1$ the pion cloud becomes visible, extending over larger transverse distances $b \sim 1$ fm. At even smaller momentum fractions, $x < 0.01$ the observed partons are mostly the gluons and flavor singlet quarks produced by gluon radiation.

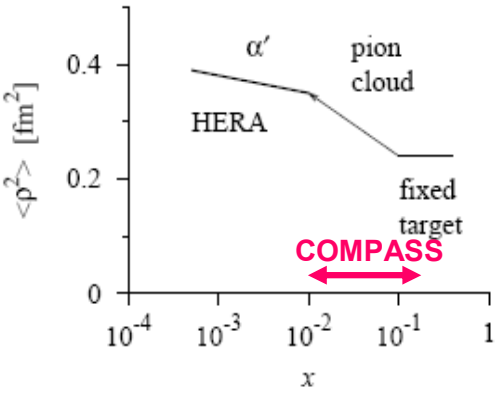

Figure 3. The average squared transverse radius of the gluon distribution in the nucleon (extracted from J/ψ photoproduction data) and the COMPASS kinematical domain.

A large effort in the community since 10 years on both experimental and theoretical aspects has been undertaken and has provided more than 300 publications so far. Several models are emerging and the complex task of extracting information on the GPDs from the experimental observables is extensively discussed in the recent literature. Predictions made from lattice QCD [9–11] for the first moments of the nucleon GPDs confirm that the transverse size of the nucleon depends significantly on the momentum fraction x. In the chiral dynamics approach [12], the gluon density is generated by the "pion cloud" of the nucleon, and a significant increase in the overall transverse size of the nucleon is observed for x below the ratio of pion and proton masses m_π/m_p (see Fig. 3). The favored domain to see a transition in the transverse size is ranging from 10^{-2} to 10^{-1}, which is the kinematical COMPASS domain.

Experimental information about GPDs comes from hard exclusive processes, such as DVCS or meson production. The factorization [13] is valid when the finite momentum transfer $t = \Delta^2$ to the target remains small compared to the photon virtuality Q^2. For meson production the factorization implies the extra condition that the virtual photon be longitudinally polarized. For DVCS, the experience with inclusive DIS and other two-photon processes suggests that the leading-twist approximation should be reliable at $Q^2 \sim 1$ GeV^2, which seems consistent with the first experimental results. For meson production, data on the pion form factor at high Q^2 suggest that higher-twist effects could give significant corrections to the GPD description up to Q^2 larger than a few GeV^2.

2 Role of COMPASS with the unique availability of high energy positive and negative muon beams

Thanks to the high energy of the muon beam available at COMPASS (between 100 and 190 GeV) the kinematical range covered by the proposed GPD programme experiment will be large enough to provide a bridge between the HERA collider experiments [14–17] at very small x_{Bj} and the JLAB [18–21] and HERMES [22–24] fixed target experiments at large x_{Bj}. Since the shutdown of HERA, the availability of positive and negative polarized muons at CERN gives to COMPASS the opportunity to measure the different configurations of charge and spin of the beam.

The experimental programme using COMPASS at CERN with a muon beam of 100

GeV will give access to three bins in x_{Bj} (presented in Fig. 4):

$$x_{Bj} = 0.05 \pm 0.02 \qquad x_{Bj} = 0.1 \pm 0.03 \qquad x_{Bj} = 0.2 \pm 0.07$$

in a large range of Q^2 from 1 to 7 GeV^2 in order to control the Q^2 independence (scaling) predicted by the QCD factorization. Assuming 6 months of data taking and a muon flux of $2 \cdot 10^8$ μ per SPS spill, a reasonable statistics can be obtained for Q^2 values up to 7 GeV^2. It is worth noting that an increase of the number of muons per spill by a factor 2

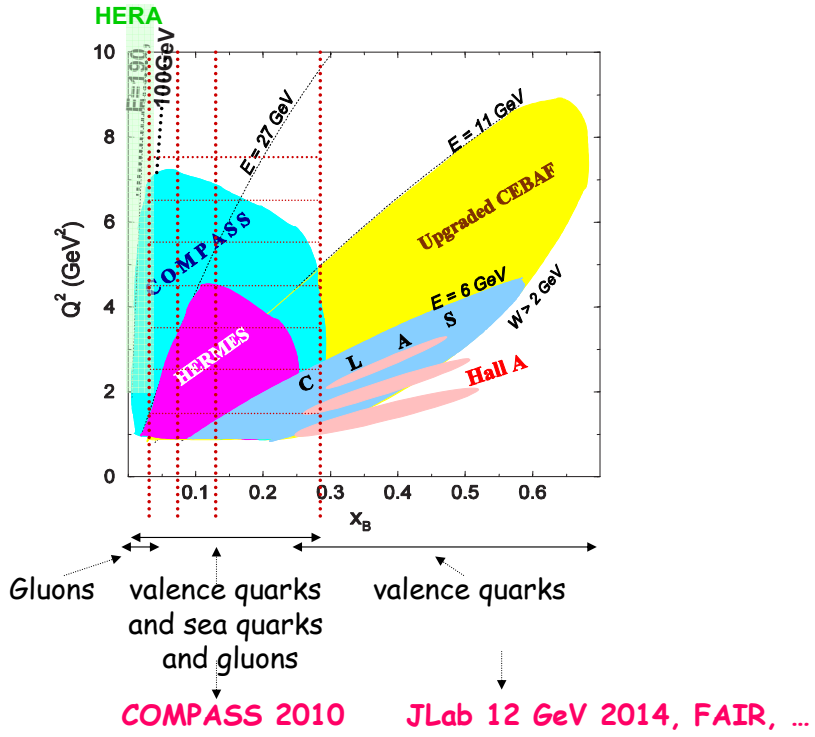

Figure 4. Kinematical coverage for all the experiments. Three bins in x_{Bj} can be investigated at COMPASS around 0.05, 0.1 and 0.2 and each one can be subdivided in sub-bins in Q^2 from 1 to 7 GeV^2.

3 The DVCS measurements at COMPASS

3.1 Experimental method

The DVCS amplitude at leading order has the form:

$$\mathcal{H} \sim \int_{-1}^{+1} \frac{H(x,\xi,t)}{x-\xi+i\epsilon} dx \quad \sim \quad \mathcal{P} \int_{-1}^{+1} \frac{H(x,\xi,t)}{x-\xi} dx - i\pi H(\xi,\xi,t) \tag{3}$$

where H stands for a generic GPD and $\mathcal{P}$ for Cauchy's principal value integral.

Since GPDs are real valued due to time reversal invariance, the real and imaginary parts of the DVCS amplitude contain distinct information on GPDs. The imaginary part depends on the GPDs at the specific values $x = \xi$. The real part is a convolution of the GPDs with the kernel $1/(x-\xi)$ (see Eq. 3). To extract the GPDs from this convolution the strategy will be similar to the one used in DIS. The GPDs will be adequately parametrized and the parameters will be determined by a fit to the data. The real and imaginary parts

can be accessed separately through the azimuthal dependence of the interference between DVCS and BH.

With muon beams one naturally reverses both charge and helicity at once. Practically μ^+ are selected with a polarization of -0.8 and μ^- with a polarization of +0.8. The precise method to extract these quantities with polarized positive and negative muon beams has been proposed by Diehl *et al.* [25, 26] and well established up to twist-3 contributions by Belitsky, Mueller and Kirchner [27]. Let us consider an unpolarized target and a muon beam of charge e_ℓ and longitudinal polarization P_ℓ. We can write:

$$\begin{aligned}\frac{d\sigma(\ell p \to \ell p\gamma)}{d\varphi} &= d\sigma^{BH} + d\sigma^{DVS}_{unpolarized} \quad + \quad P_\ell \times d\sigma^{DVS}_{polarized} \\ &+ \quad e_\ell \times \mathcal{R}_e(Int_C) \quad + \quad e_\ell P_\ell \times \mathcal{I}_m(Int_S)\end{aligned} \tag{4}$$

Considering the sum or the difference of the cross section given by muons of opposite charge and polarization and using also the azimuthal angular dependence in φ the angle between the leptonic and hadronic planes, we can get the dominant twist-2 contributions of the Beam Charge and Single Spin Asymetries for DVCS:

$$\begin{aligned}d\sigma(\mu^{+\downarrow},\varphi) + d\sigma(\mu^{-\uparrow},\varphi) &\propto \Im m(F_1\mathcal{H} + \xi(F_1+F_2)\tilde{\mathcal{H}} - t/4m^2F_2\mathcal{E}) \cdot sin\varphi + \cdots \\ d\sigma(\mu^{+\downarrow},\varphi) - d\sigma(\mu^{-\uparrow},\varphi) &\propto \mathrm{Re}e(F_1\mathcal{H} + \xi(F_1+F_2)\tilde{\mathcal{H}} - t/4m^2F_2\mathcal{E}) \cdot cos\varphi + \cdots\end{aligned} \tag{5}$$

F_1, F_2 are the Dirac, Pauli form factors, $\mathrm{Re}e\mathcal{H} = \mathcal{P}\int_{-1}^{+1} \frac{H(x,\xi,t)}{x-\xi}dx$, $\Im m\mathcal{H} = -i\pi H(\xi,\xi,t)$

Thanks to these last equations we can see that the small values of the kinematical factors ξ and t give a dominant contribution of the GPD H when using a proton target. In contrary with a neutron (or deuterium) target F_1 is negligible and this is a good case for a measurement of the GPD E contribution.

3.1.1 Projections for DVCS Beam Charge & Spin Asymmetry measurements

We propose to measure at COMPASS the quantities

$$\sigma(\mu^{+\downarrow}) - \sigma(\mu^{-\uparrow})\ ,\ \sigma(\mu^{+\downarrow}) + \sigma(\mu^{-\uparrow}) \text{ and } \frac{\sigma(\mu^{+\downarrow}) - \sigma(\mu^{-\uparrow})}{\sigma(\mu^{+\downarrow}) + \sigma(\mu^{-\uparrow})} \tag{6}$$

This last ratio is called in the following, the Beam Charge & Spin Asymmetry (BC&SA).

Figure 5 shows the azimuthal distribution of the Beam Charge & Spin Asymmetry which could be measured at COMPASS using the 100 GeV muon beams for different (x_{Bj}, Q^2) domains. Statistical errors are evaluated for 150 days of data taking with a 25% global efficiency. The data allow for a good discrimination between different models. Predictions are made using the VGG model with different parametrizations.

The VGG model relies on the double distributions in x and ξ proposed by Radyushkin [3] to respect polynomiality conditions. Model 1 [28, 29] uses a simple ansatz to parametrize GPDs based on nucleon form factors and parton distributions and fulfills the GPD sum rules. Model 2 [28, 4, 29] is more realistic because it correlates the x and t dependence with a simple Regge-motivated ansatz. This takes into account the fact that the slow partons tend to stand at a larger distance from the nucleon centre than the fast partons. A gradual increase of the t-dependence of $H(x,0,t)$ is seen as one goes from larger to

smaller values of x. The parameterization: $H(x,0,t) = q(x)e^{t<b_\perp^2>} = q(x)/x^{\alpha t}$ is used where $< b_\perp^2 >= \alpha \cdot ln1/x$ represents the increase of the nucleon transverse size with energy. α is considered as a slope in Regge theory and is evaluated to 0.8 GeV^2 (Model 2) and 1.1 GeV^2 (Model 2*) (values which give rather good description of the proton Dirac form factor). α is related to the transverse size of partons inside the nucleon and a precise determination of the α parameter can be done at COMPASS. Other models including gluons contributions are under study.

4 The other measurements at COMPASS

4.1 The observables to get a spin/flavor decomposition

The GPDs reflect the structure of the nucleon independently of the reaction which probes the nucleon. In this sense they are universal quantities and can be accessed, through DVCS or through the hard exclusive leptoproduction of mesons as $\pi^{0,\pm}, \eta, ..., \rho^{0,\pm}, \omega, \phi, ...$

The longitudinally polarized vector meson channels $\rho^{0,\pm}, \omega, \phi, ...$ are sensitive at leading order only to the GPDs H and E while the pseudo-scalar channels $\pi^{0,\pm}, \eta, ...$ are sensitive only to $\tilde{H}$ and $\tilde{E}$ [13]. In comparison we recall that DVCS depends on the four GPDs. This property makes the hard meson production reactions complementary to the DVCS process as it provides an additional tool or filter to disentangle the different GPDs.

Both quark and gluon GPDs contribute to the meson production at the same order in α_s. The decomposition on quark flavor and gluon contributions can be realized through the different combinations obtained with a set of mesons. For example:

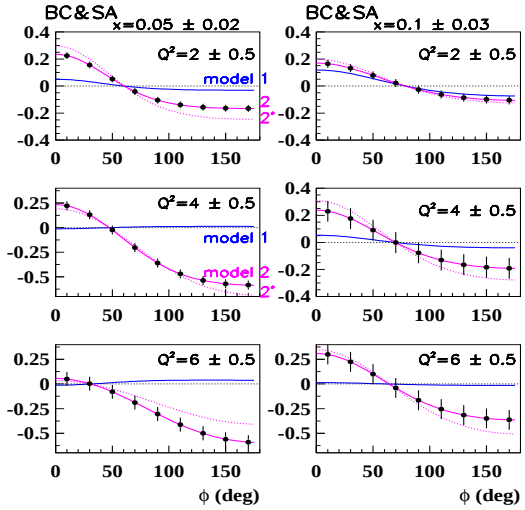

Figure 5. Projected error bars for a measurement of the azimuthal angular distribution of the BC&SA measurable at COMPASS at E_μ= 100 GeV and $|t| \leq 0.6$ GeV^2 for 2 domains of x_{Bj} (0.05 on left and 0.10 on right) and 3 domains of Q^2 (2,4,6 GeV^2) obtained in 150 days of data taking with a global efficiency of 25% and with $2{\cdot}10^8$ μ per SPS spill ($P_{\mu^+} = -0.8$ and $P_{\mu^-} = +0.8$) and a 2.5m long liquid hydrogen target. Predictions are made using the VGG model with different parameterizations (see the text).

$$H_{\rho^0} = \frac{1}{\sqrt{2}}(\frac{2}{3}H^u + \frac{1}{3}H^d + \frac{3}{8}H^g); \quad H_\omega = \frac{1}{\sqrt{2}}(\frac{2}{3}H^u - \frac{1}{3}H^d + \frac{1}{8}H^g); \quad H_\phi = -\frac{1}{3}H^s - \frac{1}{8}H^g$$

The complete experimental programme at COMPASS will comprise the measurement of DVCS cross section with polarized positive and negative muon beams and at the same time the measurement of a large set of mesons (ρ, ϕ, ω, π, η,...). This will provide different and complementary facets of the GPDs study.

4.2 The observables to get the GPD E

This GPD E is of high importance to determine the angular orbital momentum contribution to the nucleon spin puzzle. It enters in the Ji sum rule (1):

$$\frac{1}{2}\sum_q \int_{-1}^{+1} dx x(H^q(x,\xi,t=0)+E^q(x,\xi,t=0)) = J^{quark}$$

which is ξ-independent. Polarized DIS determines the forward limit of H^q. So:

$$M_q = \int_{-1}^{+1} dx x q(x) = \int_{-1}^{+1} dx x H^q(x,\xi=0,t=0)$$

meaning that the contribution of H^q to the Ji sum rule is known. Constraints on E^q come from the Pauli form factor

$$F_2(t) = \sum_q e_q \int_{-1}^{+1} dx E^q(x,\xi,t)$$

where e_q is the quark charge in units of the elementary charge [30,31]. Further constraints on E^q will provide information related to the quark orbital momentum in the nucleon (see predictions in [4,32]).

At leading order there are several promising ways to get the GPD E at COMPASS:

1. the Beam Charge and Single Spin Asymmetry for DVCS on the neutron (see Equ.(5));
2. the Transverse Target Spin Asymmetry for DVCS on the proton:

$$d\sigma(\varphi,\varphi_S) - d\sigma(\varphi,\varphi_S+\pi) \propto \Im m(F_2\mathcal{H} - F_1\mathcal{E})\cdot sin(\varphi-\varphi_S)\cdot cos\varphi$$
$$+\Im m(F_2\tilde{\mathcal{H}} - F_1\xi\tilde{\mathcal{E}})\cdot cos(\varphi-\varphi_S)\cdot sin\varphi$$

3. the Transverse Target Spin Asymmetry for vector meson (M) production induced by longitudinal virtual photon[2] on the proton:

$$d\sigma(\varphi,\varphi_S) - d\sigma(\varphi,\varphi_S+\pi) \propto \Im m(\mathcal{E}^*_{\mathcal{M}}\mathcal{H}_{\mathcal{M}})\cdot sin(\varphi-\varphi_S)$$

where φ is the azimuthal angle between the lepton and hadron planes and φ_S the azimuthal angle of the target spin vector around the virtual photon direction.

Method 1 has been successfully investigated at JLab [21] on a deuterium target while the transverse asymmetries of methods 3 and 4 have been studied at HERMES both for DVCS and rho vector meson production [24].

Preliminary studies on the transverse target spin difference (see Fig.6) were already made with the present COMPASS set-up and the ^{6}LiD polarized target [33]. Contributions from coherent scattering from the target nuclei and incoherent scattering from the quasi-free nucleons inside the target, have to be disentangled. Separation between longitudinal and tranverse photon contributions is being performed thanks to the method proposed by Diehl *et al.* [34].

[2]For which factorization is valid.

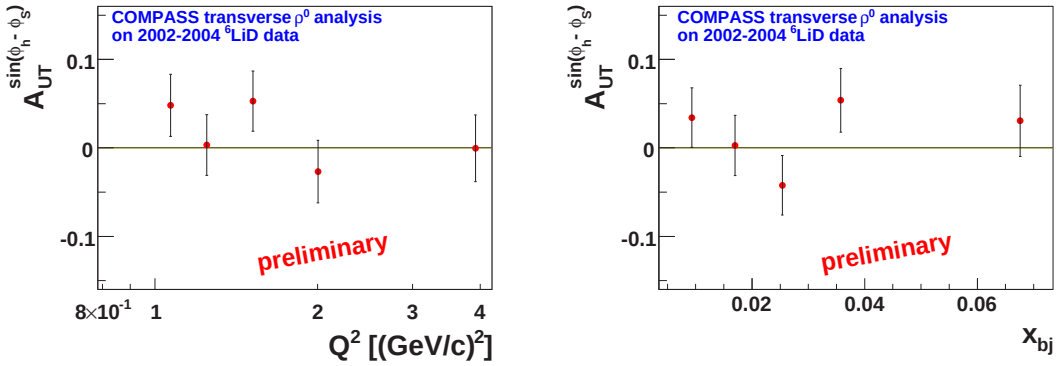

Figure 6. Transverse Target Spin Asymmetry obtained for the full 2002-3-4 sample with the ^{6}LiD target, which contains both, coherent contributions of the target nuclei and incoherent contributions of protons and neutrons. It contains also longitudinal and transverse virtual photon contributions.

5 General Request for the COMPASS apparatus

The goal of a GPD experiment is to measure absolute cross sections for the exclusive production of photons (DVCS) and a large set of mesons. This implies an accurate determination of the luminosity and acceptance and several tests will be done to achieve this objective.

The most demanding GPD measurement is the DVCS $\mu p \to \mu p \gamma$ which requires to select events with one (and only one) muon in the very forward direction, one (-id-) photon at moderate forward angle and one (-id-) slow recoiling nucleon. Many competing reactions can generate background:

- Deep π^0 production $\mu p \to \mu p \pi^0$ where the high energy γ from π^0 decay mimics the DVCS photon,
- Dissociation of the target $\mu p \to \mu (p\pi^0) \gamma$ where the extra π^0 is accompanying the slow proton,
- DIS with many outgoing particles such as π^0 which have to be identified.

The resolution in missing mass required to reject an extra pion is $(m_p + m_\pi)^2 - m_p^2 = 0.25$ GeV^2. The experimental resolution which can be achieved at COMPASS energy is larger than 1 GeV^2, therefore the missing mass energy selection using the energy balance of the scattered muon and photon is not accurate enough. The background from π^0 decay has to be removed directly by rejecting the associated low energy photon. The COMPASS spectrometer comprises two forward stages (see Fig. 7), one for angles up to 2^o (after SM2) and one for angles up to 10^o (after SM1). The photon detection has to be performed with excellent energy resolution and with high efficiency in a harsh environment of high flux and background. This puts strong constraints on the existing calorimetry and justifies the construction of a new calorimeter ECAL0 [35] to access larger angles of up to about 20^o. In addition a 4m long recoil detector has to be built, surrounding the 2.5 m long H_2

(or D_2) target to measure precisely the type, number and momenta of charge particles, in order to ensure exclusivity of the selected reaction.

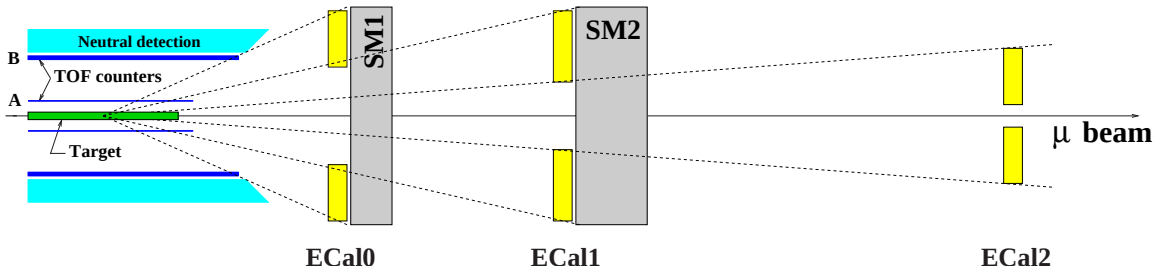

Figure 7. General principle of the COMPASS layout. At present COMPASS is a two stage spectrometer comprising many tracking and particle identification detectors grouped around the 2 dipole magnets SM1 and SM2. Only upgraded and new detectors (ECAL0, ECAL1, ECAL2, ToF, detector for neutral particles) discussed and specified in this report are shown.

6 Conclusion and Roadmap

For the GPD programme for 2010 and beyond, a 2.5 m long hydrogen target, a 4 m long recoil detector and a high-performance calorimetry are mandatory. Presently, a 40 cm long hydrogen target, and a 1 m long recoil detector are being designed for the hadron programme setup. The two existing calorimeters will be used to collect neutral particles such as π^0 and η in order to identify exotic mesons or glueballs. Since recoil proton detection and photon reconstruction are the two key experimental points of any DVCS experiment, the present hadron programme setup provides an excellent opportunity for a thorough preparation of the future DVCS setup. Although not optimized for a DVCS experiment, the available detectors can be used for preliminary studies and for quantitative evaluation of their performances. In addition, the versatility of the SPS M2 beam line makes it extremely easy to switch from a hadron beam to either positive or negative muon beam. Very preliminary tests will be requested during the 2008-9 COMPASS run. The goal is to demonstrate the feasibility of the DVCS experiments at COMPASS and to be ready for a complete GPD program after 2010 and before the outcome of other facilities as JLab 12 GeV around 2014. This gives an excellent opportunity for a unique program at COMPASS.

References

[1] D. Mueller *et al*, Fortsch. Phys. **42** (1994) 101.

[2] X. Ji, Phys. Rev. Lett. **78** (1997) 610; Phys. Rev. **D 55** (1997) 7114.

[3] A.V. Radyushkin, Phys. Lett. **B 385** (1996) 333; Phys. Rev. **D 56** (1997) 5524.

[4] K. Goeke, M.V. Polyakov, M. Vanderhaeghen, Prog. Part. in Nucl. Phys. 47 (2001) 401.

[5] M. Diehl, Generalized Parton Distributions, DESY-thesis-2003-018, hep-ph/0307382.

[6] A.V. Belitsky and A.V. Radyushkin, Phys. Rept. **418** (2005) 1.
[7] M. Burkardt, Int. J. Mod. Phys. **A 18** (2003) 173.
[8] "Exploring the 3D quark and gluon structure of the proton: Electron scattering with present and future facilities (JLab 12 GeV and EIC)" White Paper prepared for the discussion of the National Science Advisory Committee's Long Range Plan (2007).
[9] J.W. Negele *et al*, Nucl. Phys. Proc. Suppl. 128 (2004) 170.
[10] M. Goekeler *et al*, Nucl. Phys. Proc. Suppl. 140 (2005) 399.
[11] P. Haegler *et al*, hep-lat/0705.4295 (2007), JLAB-THY-07-651, TUM-T39-07-09.
[12] M. Strikman and C. Weiss, Phys. Rev. **D69** (2004) 054012.
[13] J.C. Collins, L. Frankfurt and M. Strikman, Phys. Rev. **D56**, 2982 (1997).
[14] H1 Collaboration, C. Adloff *et al.*, Phys. Lett. **B517** (2001) 47; A. Aktas *et al.*, Eur. Phys. J.C. **44** (2005) 1.
[15] H1 Collaboration, A. Aktas *et al.*, Eur. Phys. J.C. **46** (2006) 585.
[16] ZEUS Collaboration, S. Chekanov *et al.*, Phys. Lett. **B 573** (2003) 46.
[17] ZEUS Collaboration, S. Chekanov *et al.*, Nucl. Phys. **B 695** (2004) 3.
[18] CLAS Collaboration, S. Stepanyan *et al.*, Phys. Rev. Lett. **87** (2001) 182002.
[19] CLAS Collaboration, S. Chen *et al.*, Phys. Rev. Lett. **97** (2006) 072002.
[20] JLab Hall A Collaboration, C. Munoz Camacho *et al.*, Phys. Rev. Lett. **97** (2006) 262002.
[21] JLab Hall A Collaboration, M. Mazouz *et al.*, accepted for publication in Phys. Rev. Lett.
[22] HERMES Collaboration, A. Airapetian *et al.*, Phys. Rev. Lett. **87** (2001) 182001.
[23] HERMES Collaboration, A. Airapetian *et al.*, Phys. Rev. **D 75** (2007) 011103.
[24] HERMES Collaboration, F. Ellinghaus *et al.*, Nucl. Phys. **A 711** (2002) 171.
[25] M. Diehl, T. Gousset, B. Pire, J. Ralston, Phys. Lett. **B 411** (1997) 193.
[26] M. Diehl, contribution to the workshop "Future Physics @ COMPASS", 26-27 September 2002, CERN-2004-011.
[27] A.V. Belitsky, D. Müller, A. Kirchner, Nucl. Phys. **B 629** (2002) 323.
[28] M. Vanderhaeghen, P.A.M. Guichon, M. Guidal, Phys. Rev. Lett. **80** (1998) 5064; Phys. Rev. **D 60** (1999) 094017.
[29] VGG code [28, 4]; implementation by L. Mossé.
[30] M. Guidal, M.V. Polyakov, A.V. Radyushkin, M. Vanderhaeghen, Phys. Rev. **D 72** (2005) 054013
[31] M. Diehl, Th. Feldmann, R. Jakob, P. Kroll, Eur. Phys. J. **C 39** (2005) 1
[32] F. Ellinghaus, W.-D. Nowak, A.V. Vinnikov, and Z. Ye, Eur. Phys. J. **C46** (2006) 729, hep-ph/0506264.
[33] J. Bisplinghoff *et al.*, Extraction of Transverse Target Spin Asymmetry for Exclusive ρ^0 Production from COMPASS 2002-2004, COMPASS-note 2007-9.
[34] M. Diehl and S. Sapeta, Eur. Phys. J. **C41** (2005) 515, hep-ph/0503023;
M. Diehl, hep-ph/07041565v1.

[35] G.V. Mescheryakov, A.P. Nagaytsev, I.A. Savin, Preliminary MC studies for measurements of GPD with COMPASS, COMPASS-note 2006-11;
O.P. Gavrishchuk*et al.*, Continuation of the MC studies of the ECAL0 design parameters for the measurements of GPD with COMPASS, COMPASS-note 2007-7.

Discussion

Q. (X.Artru, IPN, Lion) 1) Did you show lattice result with quenched quarks?

Comm 2) The model which have no dependence on ξ imply that the nucleon has zero thickness in ξ.

A. 1) The first results were unquenched ($m_\pi = 870MeV$), the second ones (published at the end of May 07) are done at $m_\pi = 350MeV$ and take into account chiral consideration.

2) No, the models are always function of (x, ξ, t) it was just for simplicity that I have written $H(x, \xi, t) = q(x)F(t)$. I would have written $= q(x)R(x\xi)F(t)$.

SPIN PHYSICS WITH CLAS

G.E. Dodge[1†] for the CLAS Collaboration

(1) *Old Dominion University*
† *E-mail: gdodge@odu.edu*

Abstract

The CLAS collaboration at Jefferson Lab is pursuing a broad program of measurements with polarized electrons incident on polarized proton and deuteron targets. Our data include inclusive, semi-inclusive and exclusive inelastic scattering over a wide kinematical range in momentum transfer Q^2. These data will be reviewed, with an emphasis on new results. Experiments planned for the proposed 12 GeV upgrade to the CEBAF accelerator will also be discussed.

At Jefferson Lab a vigorous program of spin structure measurements has been underway in all three experimental halls over the past decade. These experiments have employed longitudinally polarized electron beams incident on polarized proton (NH_3), deuteron (ND_3) and ^{3}He targets. The primary goal of these experiments is the determination of the spin structure functions g_1 and g_2, along with their moments. As part of this program, the CLAS collaboration has collected a vast data set for g_1 over a wide kinematic range, which includes momentum transfer Q^2 from 0.05 to 5 GeV^2 and invariant mass W from the nucleon mass to 3 GeV. Recent results from this program and plans for the future are presented in this note.

In the EG1 experiment in Hall B, longitudinally polarized electrons with energies of 1.6, 2.4, 4.2 and 5.7 GeV were scattered from longitudinally polarized frozen amonia targets (NH_3 and ND_3) [1]. Data were also taken with ^{12}C, ^{4}He and frozen ^{15}N to determine the dilution from unpolarized material. The product of beam and target polarization was determined from the data through comparison with the known elastic scattering asymmetry and ranged from 0.50 to 0.60 for the NH_3 target and from 0.12 to 0.23 for the ND_3 target. Scattered electrons and other particles were detected in the CEBAF Large Acceptance Spectrometer (CLAS) [2], which covers a range in polar angles from 8° to 135°. The heart of the CLAS is a toroidal magnetic field produced by six superconducting coils which divide the 2π azimuthal phase space into six sectors, each consisting of three layers of drift chambers, time-of-flight scintillators, a gas Čerenkov counter and an electromagnetic calorimeter.

The raw inclusive double spin asymmetry was corrected for polarization, dilution, beam charge asymmetry, e^+e^- pair production, pion contamination and radiative effects to determine $A_{//} = D(A_1 + \eta A_2)$, where A_1 and A_2 are the virtual photon asymmetries and η and D are kinematic factors. Using a parametrization of the world data [3] to model F_1, A_2 and R, the ratio of transverse to longitudinal structure functions, we extracted $A_1(x, Q^2)$ as well as g_1:

$$g_1(x, Q^2) = \frac{F_1}{1+\gamma^2}(A_1 + \gamma A_2), \tag{1}$$

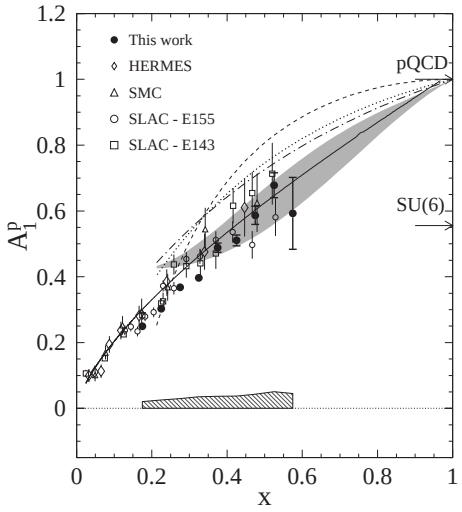

Figure 1. Results for A_1 on the proton. Filled circles show the CLAS data [3] while data from previous experiments are indicated with open symbols [4–7]. The solid line is our parametrization of the world data at $Q^2 = 10$ GeV^2. The calculations of SU(6) symmetry breaking by Isgur [8] using a hyperfine-interaction model is shown as the grey band. Three calculations by Close and Melnitchouk [9] are shown as the dashed, dotted and dash-dotted lines.

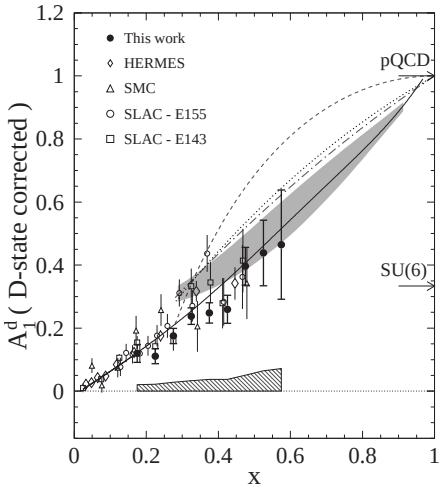

Figure 2. Results for A_1 for the deuteron. The symbols and calculations are the same as for Figure 1. The data are divided by 0.925 to correct for the deuteron D-state probability. The model calculations are derived from proton and neutron calculations assuming an isoscalar (proton plus neutron) target.

where $\gamma^2 = \frac{Q^2}{\nu^2}$ and ν is the difference in energy between the beam and scattered electron.

Figs. 1 and 2 show the EG1 result for A_1 on the proton and deuteron as a function of Bjorken x using only deep inelastic scattering (DIS) data, as defined by the requirements that $Q^2 > 1$ GeV^2 and $W > 2$ GeV [3]. Our data are consistent with the expectation that A_1 should approach 1 as $x \to 1$ and are in best agreement with the hyperfine-interaction model of Isgur [8]. Using these data in the naive quark model to estimate the quark polarizations, we find that $\Delta d/d$ remains negative up to $x = 0.6$, consistent with results from Hall A using a ^{3}He target [10]. Perturbative QCD requires that $\Delta d/d$ change sign and go to $+1$ at $x = 1$. However, according to a recent paper by Avakian et al., the inclusion of orbital angular momentum in the nucleon wavefunction may delay the zero crossing to at least $x = 0.7$ [11].

Our data have also been used to improve the Next-to-Leading Order (NLO) Parton Distribution Function (PDF) fit of Leader, Sidorov and Stamenov (LSS) as shown in Fig. 3. Inclusion of these data in the fit reduces the uncertainty on quark PDF's in the valence region by approximately one-third, while ΔG shows an even greater improvement. This reduction in uncertainty is attributable to the accuracy of the CLAS data at low Q^2, which decreases the uncertainty on higher twist corrections for g_1. The central values of the fits are not much affected by inclusion of the CLAS data, with the exception of ΔG, which decreases by approximately one-third [13].

We also studied the onset of quark-hadron duality in spin structure functions. Quark-hadron duality refers to the observation that the unpolarized structure function F_2, in the

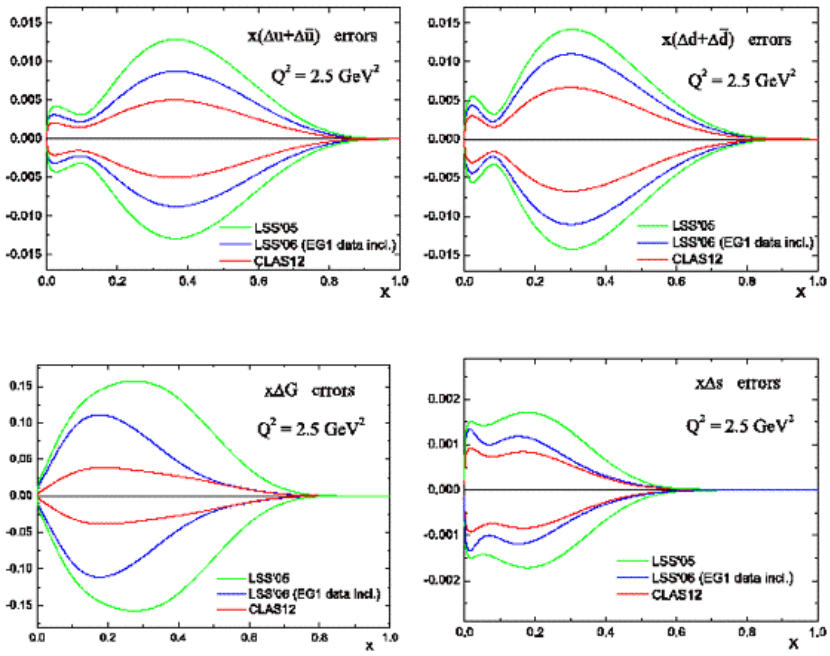

Figure 3. Expected uncertainties for polarized quark distributions Δu, Δd, ΔG and Δs from an NLO analysis of all world data. The outermost line (green) represents the fit by Leader, Sidorov and Stamenov [12] and the blue line is an updated fit [13] that includes the CLAS data [3]. The red line represents the projected uncertainties after taking data with CLAS12 for 80 days [23].

resonance region, averages to the smooth scaling curve for F_2 at high Q^2 [14]. This effect has been confirmed with high statistics data from Hall C [15].

In Fig. 4 we show xg_1 for the proton and deuteron as a function of x for various Q^2 bins [16]. The high Q^2 "scaling" curve is shown by the hatched area and indicates the range of xg_1 given by the PDF fits from the AAC [17] and GSRV [18] collaborations. At low Q^2 one can see that the data are negative in the region of the $\Delta(1232)$ resonance, as expected for a spin 3/2 excitation. Since the scaling curve is positive, one does not expect duality to hold under these circumstances. However, as Q^2 increases and the $\Delta(1232)$ loses strength, the resonances do indeed appear to oscillate about the scaling curve.

One can also examine "local" duality in which one averages g_1 over a particular region in the nucleon excitation spectrum. Fig. 5 shows g_1^p averaged over four different regions in invariant mass W. In the $\Delta(1232)$ region (top left) the data clearly fall below the scaling curve even at large Q^2. The elastic peak was included (open circles) to look for the possibility that duality holds when one sums over states of both spins, but in that case the data lie well above the scaling curve. In the second resonance region (top right) spin 1/2 resonances dominate and the data fall above the scaling curve. The other two regions include many overlapping resonances and show evidence of local duality, even for Q^2 below 1 GeV^2. We observe the onset of "global" duality (integrated over the whole resonance region) at approximately $Q^2 = 1.7$ GeV^2.

It is also interesting to study the first moment of g_1, $\Gamma_1(Q^2) = \int_0^{x_0} g_1(x, Q^2)dx$, where the upper limit excludes the elastic peak (which would otherwise dominate the behaviour

of the integral at low Q^2). $\Gamma_1(Q^2)$ is expected to be negative with a negative slope at very low Q^2, in order to be consistent with the predictions of the extended GDH Sum Rule [19]. However, at high Q^2, Γ_1 becomes positive as measured in previous DIS experiments [4–7]. Because of the large kinematic range of our data, we are able to compute Γ_1 without interpolation over a range in Q^2 from 0.05 to 3 GeV^2. For the extrapolation to the unmeasured region at low x we use our parameterization of world data. Our preliminary analysis of Γ_1 indicates, for the first time, the negative slope in the integral at low Q^2 for both the proton and the deuteron [20]. At very low Q^2 one expects Chiral Perturbation Calculations (χPT) to be valid, but their range of validity in Q^2 is not clear. We see that χPT calculations by Ji [21] and Bernard [22] are consistent with our data for Γ_1 up to a Q^2 of approximately 0.06 GeV^2 [20].

We have also examined one higher moment, the generalized forward spin polarizability of the proton [24]

$$\gamma_0^p(Q^2) = \frac{16\alpha M^2}{Q^6}\int_0^{x_0} x^2\left\{g_1(x,Q^2) - \frac{4M^2}{Q^2}x^2 g_2(x,Q^2)\right\}dx, \qquad (2)$$

where α is the fine structure constant and M is the mass of the nucleon (see Fig. 6). Here we find a large discrepancy between our preliminary analysis and the χPT calcuations even at our lowest Q^2. It is important to note that γ_0 is a more stringent test of χPT than Γ_1 because Γ_1 is constrained at low Q^2 by the extended GDH sum. Presently available χPT calculations do not seem to describe our data well. New experiments to investigate spin structure functions in more detail down to $Q^2 = 0.015$ GeV^2 have recently been completed at Jefferson Lab in Hall A with a ^{3}He target and in Hall B with NH_3 and ND_3 targets. These data are currently under analysis. At high Q^2 we expect g_2 to decrease significantly and g_1 to vary logarithmically with Q^2, so that γ_0 weighted by Q^6 should be largely independent of Q^2. In the right-hand panel of Fig. 6 we show γ_0^p weighted by Q^6, which shows evidence of the anticipated scaling at approximately $Q^2 = 1.5$ GeV^2.

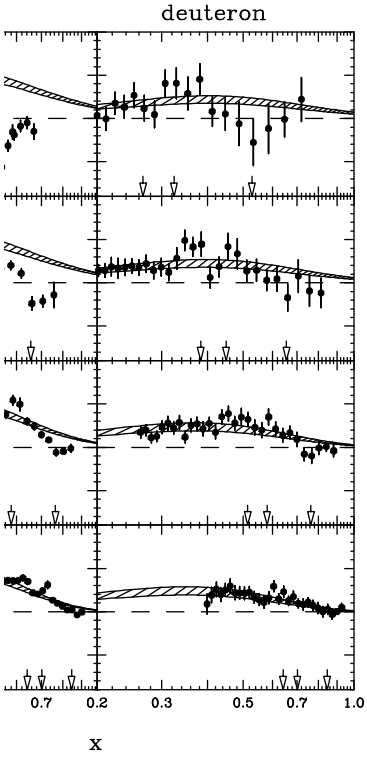

Figure 4. CLAS data for xg_1 [16] in several bins of Q^2 for the proton (left) and deuteron, per nucleon (right). The errors include statistical and systematic contributions added in quadrature. The hatched band represents the range of g_1 predicted by Next-to-Leading Order Parton Distribution Function fits [18,17], evolved to the Q^2 of our data and corrected for target-mass effects.

Because of the large acceptance of CLAS, our data include pions and other hadrons in addition to scattered electrons. Therefore, we are able to investigate single and double spin asymmetries for exclusive pion production from polarized protons and deuterons. There are three channels currently under investigation: (a) $p\pi^0$ from polarized protons,

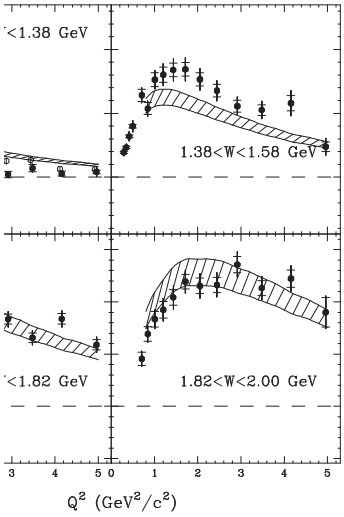

Figure 5. CLAS results for $Q^2 g_1(x, Q^2)$ for the proton, averaged over various regions of x, corresponding to the W range shown in the panels. The inner error bars are statistical and the outer error bars include both statistical and systematic contributions added in quadrature. The addition of the ep elastic contribution to the data is shown by the open circles.

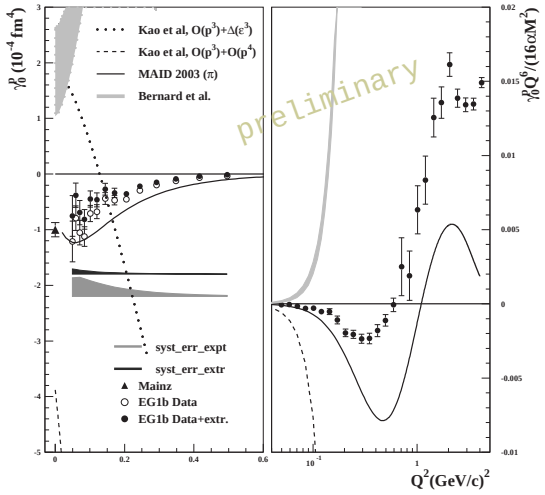

Figure 6. Preliminary result for γ_0^p as a function of Q^2. The full integral is shown as the filled circles and the measured portion of the integral is shown as the open circles. χPT calculations are shown [29, 22] along with MAID 2003 [30]. The data on the right are weighted by $Q^6/(16\alpha M^2)$.

(b) $n\pi^+$ from polarized protons, and (c) $pp\pi^-$ from polarized deuterons. These channels are identified using missing mass techniques and the asymmmetries are determined as a function of Q^2, W, θ^*, the polar angle of the emitted pion in the center-of-mass frame, and ϕ, the angle between the leptonic and hadronic planes. These asymetries will provide important constraints for phenomenological models of resonance transition amplitudes, especially since there are almost no data for the $n \to \pi^- p$ channel and only limited polarization data for the proton [25].

Another topic of high current interest is semi-inclusive pion production. One hopes to gain insight into the flavor and transverse momentum dependent distribution functions of the quarks in the nucleon by tagging the leading hadrons. Although the EG1 experiment was not optimized for such studies, we do have semi-inclusive data. For example, Fig. 7 shows preliminary results for the double-spin asymmetry with longitudinal beam and target A_{LL}^{π} for semi-inclusive π^+, π^- and π^0 production as a function of the transverse momentum of the detected hadron. Shown for comparison are calculations by Anselmino et al. [26] which reproduce the trend of the data for the π^+ and π^0 channels, but not as well for the π^- channel. New experiments are planned with CLAS at 6 GeV [27] and with CLAS12 at 11 GeV [28], which will hopefully shed some light on these results.

We look forward to continuing our investigation of nucleon spin structure at Jefferson Lab with the planned 11 GeV beam in Halls A, B and C. The energy upgrade project is on track with the recent approval by the Department of Energy of the project planning milestone known as CD-2. This project was named in the recent Nuclear Science Advi-

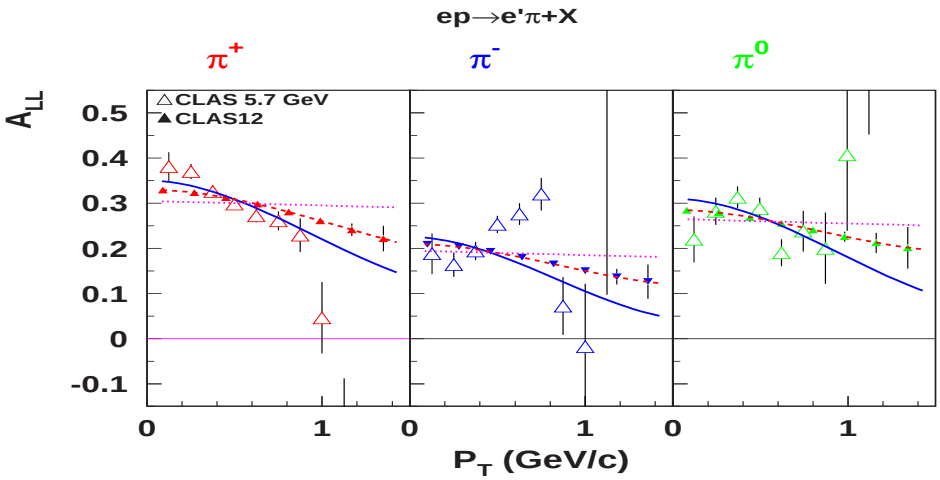

Figure 7. Preliminary CLAS result for A_{LL}^{π} as a function of the transverse momentum of the pion for semi-inclusive pion production (open triangles). Also shown are the projected uncertainties (closed triangles) for a future experiment with the 11 GeV beam at Jefferson Lab using CLAS12 [28].

sory Committee report as the highest priority for nuclear science in the United States. Construction is expected to start at the end of 2008 and the first high energy beam will be available in 2015. In Hall B, we plan to have longitudinally and transversely polarized proton and deuteron targets, along with an upgraded CLAS12 detector, designed for a luminsity of 10^{35} /cm^2/s. We will measure inclusive and semi-inclusive DIS up to $Q^2 = 10$ GeV^2 and $x = 0.8$. This will enable us to extend our measurements of A_1^p and A_1^d to larger x. Fig. 3 indicates the expected improvement in uncertainty on the PDF fits by Leader, Sidorov and Stamenov once CLAS12 data become available. Spin physics will continue to play an important and high profile role in the experimental program at Jefferson Lab in the next decade.

References

[1] C.D. Keith, et al., Nucl. Instrum. Methods A **501**, 327 (2003).

[2] B.A. Mecking, et al., CLAS Collaboration, Nucl. Instrum. Methods A **503**, 513 (2003).

[3] K.V. Dharmawardane et al., CLAS Collaboration, Phys. Lett. B **641**, 11 (2006).

[4] B. Adeva, et al., SMC Collaboration, Phys. Rev. D **58**, 112001 (1998).

[5] K. Abe, et al., E143 Collaboration, Phys. Rev. D **58**, 112003 (1998).

[6] P.L. Anthony, et al., E155 Collaboration, Phys. Lett. B **493**, 19 (2000).

[7] A. Airapetian, et al., HERMES Collaboration, Phys. Rev. D **71**, 012003 (2005).

[8] N. Isgur, Phys. Rev. D **59**, 034013 (1999).

[9] F.E. Close, W. Melnitchouk, Phys. Rev. C **68**, 035210 (2003).

[10] X. Zheng, et al., Jefferson Lab Hall A Collaboration, Phys. Rev. C **70**, 065207 (2004).

[11] H. Avakian, S.J. Brodsky, A. Deur, F. Yuan, hep-ph/0705.1553.

[12] E. Leader, A.V. Sidorov, D.B. Stamenov, Phys. Rev. D **73**, 034023 (2006).

[13] E. Leader, A.V. Sidorov, D.B. Stamenov, Phys. Rev. D **75**, 074027 (2007).

[14] E.D. Bloom and F.J. Gilman, Phys. Rev. Lett. **25**, 1140 (1970); Phys. Rev. D **4**, 2901 (1971).
[15] I. Niculescu et al., Phys. Rev. Lett. **85**, 1182 (2000); Phys. Rev. Lett. **85**, 1186 (2000).
[16] P.E. Bosted et al., CLAS Collaboration, Phys. Rev. C **75**, 035203 (2007).
[17] M. Hirai et al., Phys. Rev. D **69**, 054021 (2004).
[18] M. Gluck, E. Reya, M. Stratmann, W. Vogelsang, Phys. Rev. D **63**, 094005 (2001).
[19] X. Ji, J. Osborne, J. Phys. G **27**, 127 (2001).
[20] Y. Prok et al., CLAS Collaboration, in preparation for Phys. Rev. Lett.
[21] X. Ji et al., Phys. Lett. B **472**, 1 (2000).
[22] V. Bernard et al., Phys. Rev. D **67**, 076008 (2003).
[23] S.E. Kuhn, et al., CLAS Collaboration, "The Longitudinal Spin Structure of the Nucleon," Jefferson Lab Approved Experiment E12-06-109 (2006).
[24] D. Drechsel, B. Pasquini, M. Vanderhaeghen, Phys. Rept. **378**, 99 (2003).
[25] R. De Vita et al., CLAS Collaboration, Phys. Rev. Lett. **88**, 082001 (2002).
[26] M. Anselmino et al., Phys. Rev. D **74**, 074015 (2006).
[27] H. Avakian, et al., CLAS Collaboration, "Semi-Inclusive Pion Production with a Longitudinally Polarized Target at 6 GeV," Jefferson Lab Approved Experiment E-05-113 (2005).
[28] H. Avakian, et al., CLAS Collaboration, "Studies of Spin-Orbit Correlations with Longitudinally Polarized Target," Jefferson Lab Approved Experiment E12-07-107 (2007).
[29] C. Kao et al., Phys. Rev. D **67**, 016001 (2003).
[30] D. Drechsel, S. Kamalov, L. Tiator, Nucl. Phys. A **645**, 145 (1999).

Discussion

Q. (O.Tereaev, JINR, Dubna) Is it possible to test quality for the function $g_T = g_1 + g_2$ rather than g_1?

A. That is an interesting idea. Since g_T is smooth and positive duality may work down to lower Q^2. However, we cannot look at that with the EGI data since we do not have a transversely polarized target, which means that we do not extract g_2.

Q. (J.Nassalsky, SINS, Warsaw) What are uncertainties involved in the extrapolations of g_1 to the non measured region?

A. We estimate the uncertainties on the extrapolation to the unmeasured region by comparing the result for γ_0 or Γ_1 using different parameterizations of world data. For γ_0 the uncertainty on the extrapolation is very small, smaller than the systematic uncertainty on the measured data. Please note that the systematic error bands on the γ_0 plot were mislabeled.

RECENT RESULTS FROM STAR ON THE SPIN OF THE PROTON

J.C Dunlop[1†] for the STAR collaboration

(1) *Brookhaven National Laboratory, Upton, NY USA*
† *E-mail: dunlop@bnl.gov*

Abstract

The measurement of the origin of proton spin is a major program in the STAR experiment at the Relativistic Heavy Ion Collider (RHIC) at Brookhaven National Laboratory (BNL). RHIC is the first collider able to collide polarized protons. The current status of the use of these polarized beams to probe the polarization of the partons within the proton will be reviewed, along with prospects for future measurements of higher precision and differential analyzing power.

1 Introduction

The Relativistic Heavy Ion Collider (RHIC) can accelerate and collide beams of polarized protons at center of mass energies up to $\sqrt{s} = 500$ GeV. Two large-scale experiments, STAR and PHENIX, and one smaller experiment, BRAHMS, are capable of sampling and measuring the results of these collisions with high precision. There have been four major runs to date with these beams, mainly focusing on collisions at $\sqrt{s} = 200$ GeV, with with the most recent occuring in 2006. The stable polarization state in the collider has the protons polarized vertically, transverse to the direction in which they travel, but rotators outside the interaction regions of STAR and PHENIX allow the beams to be polarized both longitudinally and transversely at the collision vertex at the center of the experiment. Both types of polarization have been analyzed extensively.

2 Longitudinal Polarization

The focus of the longitudinal program to date has been on the measurement of the double longitudinal asymmetry, A_{LL}, in the production of jets at mid-rapidity. STAR reconstructs jets through a mid-point cone algorithm, using tracking in the STAR Time Projection Chamber (TPC) for the charged portion of the jet and signals in the Electromagnetic Calorimetry (EMC) for the neutral portion. The unpolarized differential cross-section for jet production has been measured up to approximately 50 GeV, and is in good agreement with calculations from perturbative QCD [1]. This agreement is critical to the interpretation of polarization of jets in the final state in terms of the polarization of the partons in the initially incoming protons.

At the time of the conference, the highest quality measurement from STAR of A_{LL} came from the 2005 run, which sampled an integrated luminosity of 2 pb^{-1} with average beam polarization of approximately 50%, and with a pseudorapidity coverage over $0.2 < \eta < 0.8$. Final results from this analysis were recently submitted for publication [3], and are reproduced in figure 1.

The utility of this type of measurement lays in its comparison to models, and its use in global fits. The kinematics of the incoming parton-parton collisions are not strongly resolved by simply measuring the transverse momentum (p_T) of a jet in the final state; instead, jets within a given p_T range sample a broad set of different kinematic conditions, as shown in Figure 2a. The precision of the data allows for strong constraints on model parameters, an example of which is shown in Figure 2b. In this model comparison, the dependence of the gluon polarization in the proton on momentum fraction and scale, $\Delta g(x)$, is constrained, while the integrated value of ΔG at one scale is allowed to vary. Strongly positive values for ΔG appear to be strongly excluded in this model framework. Stronger constraints will come from the 2006 dataset, in which the pseudorapidity coverage increased by more than a factor of 2, the polarization increased to more than 60% on average, and the integrated luminosity increased by a factor of 3.

While inclusive measurements provide a great amount of information towards constraining models, it is somewhat unsatisfying to depend so strongly on the models for the shape of the dependence of Δg on scale and momentum fraction. The way forward is to measure double spin asymmetries with more differential probes, such as dijets and photon-jet coincidences, across a broad range of pseudorapidity and momentum. These allow much tighter constraints on the momentum fraction of the parton probed, and will allow for high precision determination of $\Delta g(x)$ for momentum fraction x from approximately 10^{-3} to 0.3.

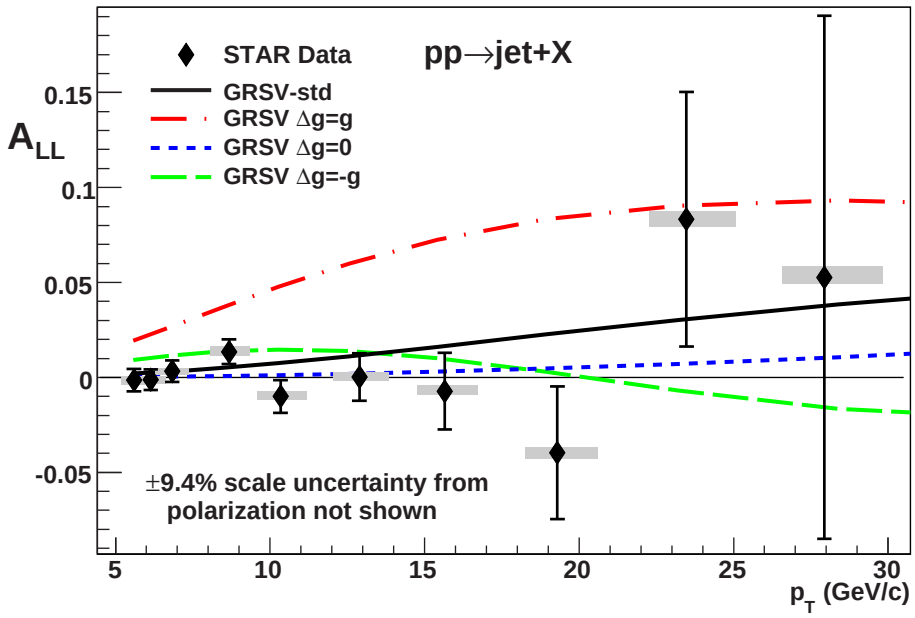

Figure 1. Longitudinal double-spin asymmetry A_{LL} for inclusive jet production at $\sqrt{s} = 200$ GeV versus jet p_T. The points show results for jets, with p_T corrected for detector effects but not hadronization effects, with statistical error bars, while the curves show predictions for NLO parton jets from one global analysis [2]. The gray boxes indicate the systematic uncertainties on the measured A_{LL} values (vertical) and in the corrections to the measured jet p_T (horizontal). Figure from [3]

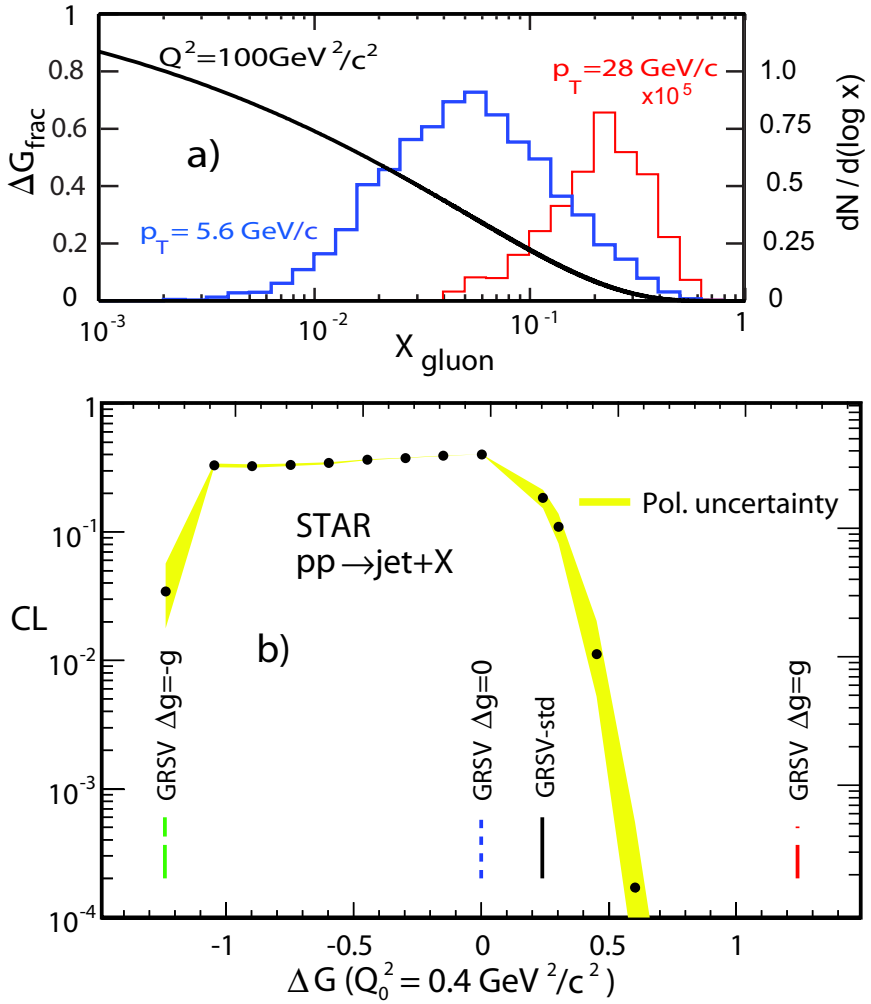

Figure 2. (a) The solid curve represents the fraction of ΔG for GRSV-std that has $x > x_{min}$ for scale $Q^2 = 100\,\mathrm{GeV}^2/\mathrm{c}^2$. The histograms show the x_{gluon} sampled in the lowest and highest jet p_T bins. (b) Confidence levels for several gluon polarization distributions, characterized by their ΔG at an input scale of $0.4\,\mathrm{GeV}^2/\mathrm{c}^2$ [4, 2]. Figure from [3]

3 Transverse Polarization

The first, and possibly the most unexpected, polarized measurement at RHIC came in the forward direction in STAR, in which it was found that the large single-spin asymmetries in pion production at high x_F seen at lower energies persisted to RHIC at $\sqrt{s} = 200$ GeV [5]. In run 6, the apparatus for measuring these asymmetries was extended, and the luminosity sampled dramatically increased. This allowed for simultaneous separation of the x_F and p_T dependence of the single spin asymmetry A_N, as shown in figure 3 [6]. The behavior of this single-spin asymmetry with p_T is quite surprising, since essentially any perturbative explanation will predict that A_N should fall with increasing p_T, while there is no sign for this decrease in the data measured to date. Future runs with the fully upgraded STAR Forward Meson Spectrometer, which covers the pseudorapidity range from 2.5 to 4 with full azimuthal coverage, should allow for exquisite precision in this

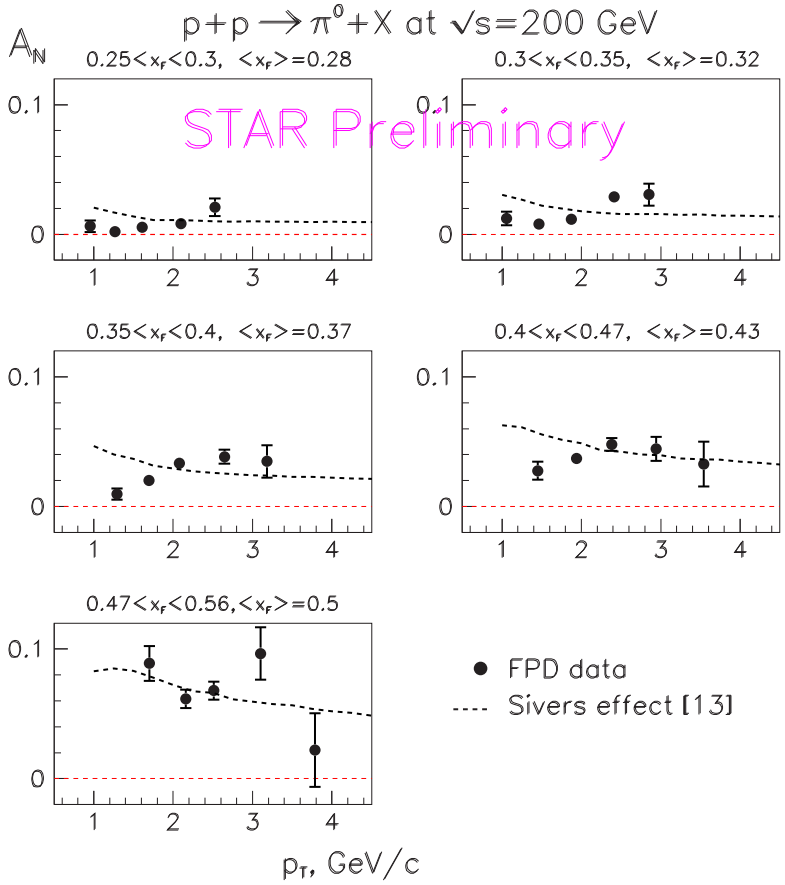

Figure 3. $\pi^0 A_N$ vs. p_t for different bins in x_F, at $\sqrt{s} = 200$ GeV. Figure from [6].

type of measurement, and distinguish between different scenarios (e.g. Collins vs. Sivers) for the production of these large single-spin asymmetries.

Another method was used to search for Sivers effects in run 6. These were predicted to create a strong and measurable correlation between the transverse momentum of a parton within the proton and the direction of transverse polarization. This can be measured by the azimuthal opening angle between dijet pairs, ζ, signed with respect to the polarization direction. Results have been published and are shown in figure 4 [7]. The measured value of ζ is consistent with zero in all kinematic regimes, counter to original calculations based on measurements of the Sivers effect in the HERMES experiment. This difference has led to a re-examination of the factorization assumptions underlying the application of perturbative QCD to this specific process in hadron-hadron collisions, with the conclusion that initial- and final-state effects are large

4 Summary and outlook

The spin program in STAR at RHIC is beginning to place world-class constraints on the spin of gluons in the proton with longitudinally polarized protons, and is making ground-breaking measurements with transversely polarized beams. The program is continually

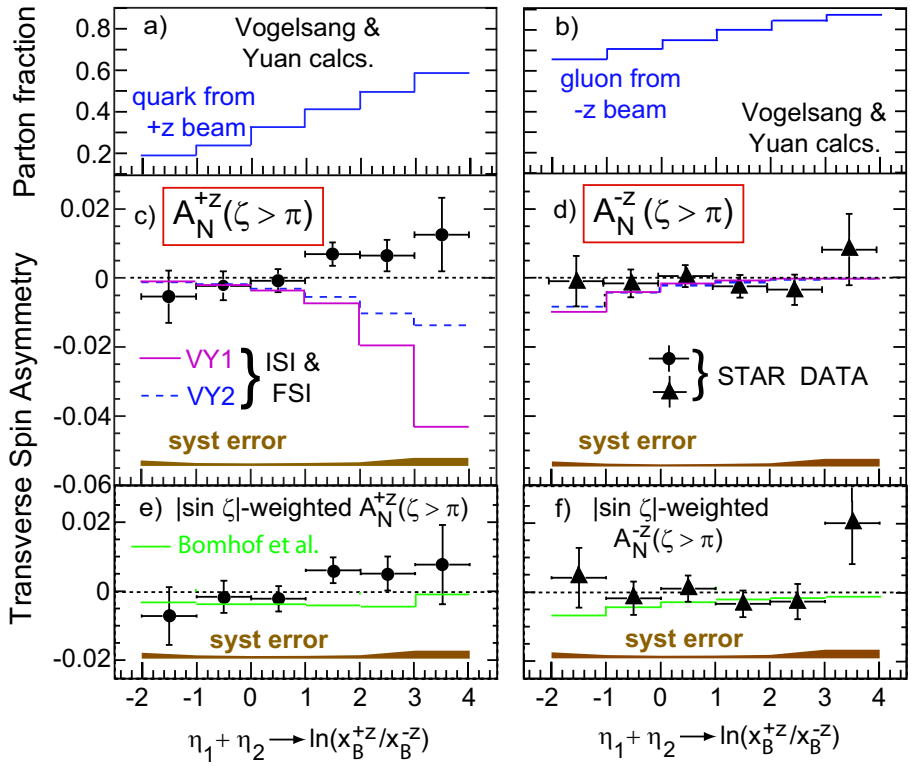

Figure 4. Top row: fractional contribution of quarks (left) or gluons (right) to the initial state parton-parton collisions as function of the sum of the dijet pseudorapidities, $\eta_1 + \eta_2$. Middle row: single spin asymmetry in signed azimuthal opening angle. Bottom row: —sin ζ—-weighted single-spin asymmetry. Figure from [7].

evolving, with luminosities and polarizations providing order-of-magnitude improvements in the figure of merit for polarization measurements from year to year. STAR's plan is to finish the program at $\sqrt{s} = 200$ GeV by 2010, with precision measurement of $\Delta g(x)$ via coincidence measurements, both with jet-jet correlations and photon-jet correlations. Beyond that, we plan to switch predominantly to $\sqrt{s} = 500$ GeV, which provides a lower momentum fraction x reach for $\Delta g(x)$ measurements, along with a critical test of the applicability of factorization in the region of kinematic overlap with the $\sqrt{s} = 200$ GeV beam. With this set of measurements, the contribution of the gluon spin to the proton spin will be precisely measured.

At 500 GeV, the cross section for W production is large enough that a new line of investigation becomes available. One can use parity violation in W decays to measure the flavor-separated polarization of quarks, $\Delta u/u$, $\Delta d/d$, and their respective antiquarks. Upgrades of reasonable scope are necessary to both STAR and PHENIX to facilitate these measurements.

The understanding of dffects from transversely polarized beams is still rapidly progressing. Measured effects are large, but much theoretical and experimental work remains to clarify the origin of these effects. An interesting possibility is that these effects may be related to orbital angular momentum of partons in the proton, which may become increasingly important if the gluon spin polarization ends up as a small contribution to

the spin of the proton. This will clearly be an active and fruitful region of inquiry in future years.

References

[1] B. I. Abelev *et al.* [STAR Collaboration], Phys. Rev. Lett. **97**, 252001 (2006).

[2] B. Jager, M. Stratmann, and W. Vogelsang, Phys. Rev. D **70**, 034010 (2004).

[3] B. I. Abelev *et al.* [STAR Collaboration], (2007), arXiv:0710.2048 [hep-ex].

[4] M. Gluck, E. Reya, S. M., and W. Vogelsang, Phys. Rev. D **70**, 09400 (2001).

[5] J. Adams *et al.* [STAR Collaboration], Phys. Rev. Lett. **92**, 171801 (2004).

[6] L. Nogach *et al.* [STAR Collaboration], (2007), hep-ex/0612030.

[7] B. I. Abelev *et al.* [STAR Collaboration], Phys. Rev. Lett. **99**, 142003 (2007).

Discussion

Q. (D.Sivers, Portland Phys. Inst.) Could you give a reference for the QCD prediction of exotic bound states?

A. The answer depends on what you mean by exotic bound states. If you are discussing glueballs, pentaquarks, etc. that occur at zero temperature that is outside my realm of expertise. If you are discussing bound states in the hot QGP, Shuryak first proposed this in E.V. Shuryak and I. Zahed, hep-ph/0307267, Phys. Rev. C 70, 021901(2004).

There is a bit of discussion and controversy on this subject, especially in the rebuttal from lattice data in V. Koch, A. Majumder and J. Randrup, Nucl. Phys. A **774** (2006) 841 and V. Koch, A. Majumder and J. Randrup, Phys. Rev. Lett. **95**, 182301 (2005) [arXiv:nucl-th/0505052] with the conclusion: "The analysis of present lattice results above the critical temperature severely limits the presence of $q\bar{q}$ bound states, thus supporting a picture of independent (quasi)quarks".

VECTOR AND TENSOR ANALYZING POWERS IN THE REACTION $^{12}C(\overrightarrow{d},p)^{13}C$ AT ENERGY T_d = 270 MeV.

A. S. Kiselev[1†], V. P. Ladygin[1], T. Uesaka[7], M. Janek[1,5], T. A. Vasiliev[1], M. Hatano[2], A. Yu. Isupov[1], H. Kato[2], N. B. Ladygina[1], Y. Maeda[7], A. I. Malakhov[1], S. Nedev[6], T. Saito[2], J. Nishikawa[4], H. Okamura[8], T. Ohnishi[3], S. G. Reznikov[1], H. Sakai[2], S. Sakoda[2], N. Sakomoto[3], Y. Satou[2], K. Sekiguchi[3], K. Suda[7], A. Tamii[9], N. Uchigashima[2] and K. Yako[2].

(1) *LHE-JINR, 141980 Dubna, Moscow region, Russia* (2) *Department of Physics, University of Tokyo, Bunkyo, Tokyo 113-0033, Japan* (3) *RIKEN, Wako 351-0198, Japan* (4) *Department of Physics, Saitama University, Urawa 338-8570, Japan* (5) *University of P.J. Safarik, 041-54 Kosice, Slovakia* (6) *University of Chemical Technology and Metallurgy, Sofia, Bulgaria* (7) *Center for Nuclear Study, University of Tokyo, Tokyo 113-0033, Japan* (8) *CYRIC, Tohoku University, Miyagi 980-8578, Japan* (9) *RCNP, Osaka University, Osaka 567-0047, Japan* † *E-mail: Antony@sunhe.jinr.ru*

Abstract

In this work the experimental results on analyzing powers at energy T_d = 140, 200 and 270 MeV for $^{12}C(\overrightarrow{d},p)^{13}C^*$ reaction with excitation of levels of a nucleus ^{13}C and $d(\overrightarrow{d},p)^3H$ reaction at emission angle Θ_{cm}=0° are presented. The data on the tensor A_{yy} and vector A_y analyzing powers for the $^{12}C(\overrightarrow{d},p)^{13}C^*$ reaction at energy T_d = 270 MeV in the angular range from 4° to 18° in laboratory system are also obtained. The experimental data for these reactions are sensitive to the spin structure of the deuteron.

Inrtoduction

The interest in the experimental and theoretical study of few nucleon transfer reactions has been renewed in the past years mainly due to the possibility to obtain the information of astrophysical relevance from these reactions [1-4]. Direct measurement of the capture reactions at energies of astrophysical interest is, in some cases, nearly impossible due to the low reaction yield, especially, if the capture involves exotic nuclei. Alternative indirect methods, such as the asymptotic normalization coefficient (ANC) method, based on the analysis of breakup or transfer reactions [1], have been used as a tool to obtain astrophysical S-factors. Single-nucleon transfer reactions that probe the degrees of freedom of single particles have been extensively used to study the structure of stable nuclei. The analysis of such reactions provides the angular momentum transfer, which gives information on the spin (j) and parity ($^{\pi}$) of the final state. The sensitivity of the cross sections to the single-nucleon components allows for the extraction of spectroscopic factors. The recent indications of reduced occupancies of single-particle states [5, 6] reveal that reliable measurements of spectroscopic factors in exotic nuclei are highly desirable. The $(\overrightarrow{d},p)$ stripping reaction has long been use as a means of probing the single particle structure of nuclei. In particular, through distorted wave Born approximation (DWBA) analyses it has been used to determine the orbital angular momentum and spectroscopic factors of specific states in the recoil nucleus [7]. The $d(\overrightarrow{d},p)^3H$ and $d(\overrightarrow{d},p)X$ processes concern

to single-nucleon transfer reactions too. These reactions are the simplest processes with a large momentum transfer, so they could be used as a tool to study the deuteron structure at short distances. The polarization observables of these reactions are sensitive to the D/S wave ratio in the deuteron within One-Nucleon Exchange (ONE) aproximation.

In this report we present the experimental results on the tensor A_{yy} and vector A_y analyzing powers for the $^{12}C(\overrightarrow{d},p)^{13}C^*$ reaction at energy $T_d = 270$ MeV in the angular range from 4° to 18° in laboratory system. The data on the tensor analyzing power T_{20} for $^{12}C(\overrightarrow{d},p)^{13}C^*$ and $d(\overrightarrow{d},p)X$ reactions at energy T_d = 140, 200 and 270 MeV and emission angle Θ_{cm}=0° are also obtained.

Experiment

The experiment was performed at RIKEN Accelerator Research Facility (RARF). The direction of symmetric axis of the beam polarization was controlled with a Wien filter located at the exit of polarized ion source (PIS). In this experiment, four spin modes were used: the mode 0 - unpolarized mode, mode 1 - pure tensor mode, mode 2 - pure vector mode and mode 3 is mixed mode. The obtained polarization values were $\sim 75\%$ of the ideal values. The polarized deuteron beam was accelerated up to 140, 200 and 270 MeV by the combination of the AVF cyclotron and Ring cyclotron. The beam polarizations were measured with D-room polarimeter (DroomPOL) located at D-room and Swinger polarimeter (SWPOL) just before the target. Both polarimeters utilize $d + p$ elastic scattering for polarimetry and value of polarization were derived using known analyzing powers A_y, A_{yy}, A_{xx} and A_{xz} [8, 9]. The scattering angle of the polarized deuteron beam were controlled by rotating the Swinger magnet. Scattered particles (^{3}H, ^{3}He or p) were momentum analyzed with quadrupole and dipole magnets (Q-Q-D-Q-D) and detected with MWDC followed by the three plastic scintillators at the second focal plane.

Criteria used for the identification of the scattered protons from the $^{12}C(\overrightarrow{d},p)^{13}C^*$ and $d(\overrightarrow{d},p)X$ reactions are the following: particle must be registered in the all three scintillation detectors and it was selected by the correlation of the energy losses in the 1st and the 2nd and the 1st and the 3rd scintillation detectors; radio frequency signal of the cyclotron was used as a reference for time-of-flight measurement. The number of useful events were obtained by the subtraction of the momenta spectra on C from CD_2 for $d(\overrightarrow{d},p)^3H$ reaction.

The events considered for the analysis were selected within polar angle acceptance $\leq 1.4°$. Typical momentum spectra for $^{12}C(\overrightarrow{d},p)^{13}C^*$ reaction are shown in fig. 1.

Results and discussion

Monte Carlo (MC) simulation was performed for the $d(\overrightarrow{d},p)X$ reaction at 270 MeV initial deuteron energy and small proton emission angles in accordance with 2 and 3 particle phase space. It is shown that MC simulation for 2 particle phase space ($p-dn$ in the final state) reproduces well the excitation energy spectra near threshold. The contribution of 3 particle phase space is quite small within the acceptance of the spectrometer.

A peak obliged to the Final State Interaction (FSI) near breakup threshold for the 3-nucleon unbounded state is not observed in contrast with np state. Thus, it gives the opportunity to conclude that FSI for the dn system is insignificant or much weaker than for the np one.[10]

The experimental results on the tensor analyzing power T_{20} for $d(\overrightarrow{d},p)X$ reaction are presented by the squares and triangles in figure 2. Squares are plotted for the events near breakup threshold with effective values of excitation energy of $\approx$ 7 MeV. Triangles correspond to the events with higher $E_x \approx 10$ MeV. Filled symbols correspond to the data for $d(\overrightarrow{d},p)^3H$ reaction.

Effective excitation energy for T_{20} of the $d(\overrightarrow{d},p)X$ reaction at the energy $T_d = 140$ and 200 MeV is close to $E_x \approx 4,7$ and $5,7$ MeV for np channel and $E_x \approx 6$ and 8 MeV for dn channel respectively.

The comparison of these polarization observables for the breakup reactions gives an opportunity to conclude that they are in an agreement within achieved experimental errors.

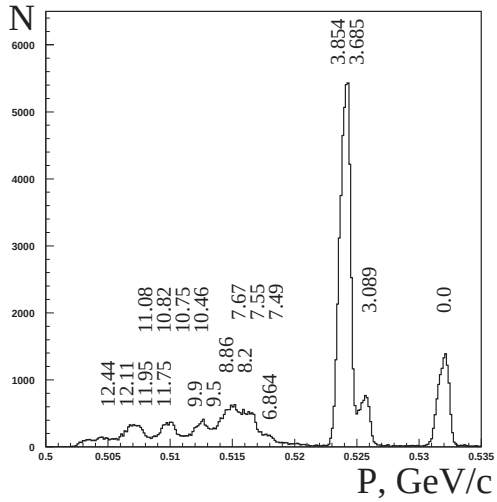

Figure 1: Typical momentum spectra for $^{12}C(\overrightarrow{d},p)^{13}C^*$ reaction and Θ_{cm}=0° (T_d=140 MeV). Peaks corresponding to the ^{13}C states are labeled by their excitation energies in MeV.

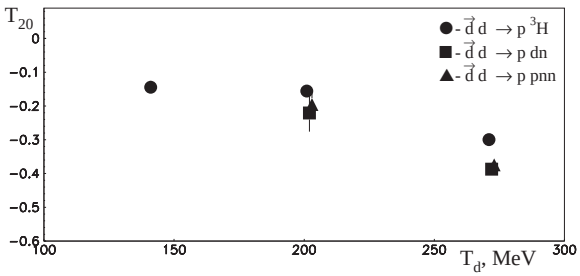

Figure 2: The experimental results on T_{20} analyzing power for $d(\overrightarrow{d},p)X$ reactions at energy $T_d = 140$, 200 and 270 MeV and emission angle Θ_{cm}=0°.

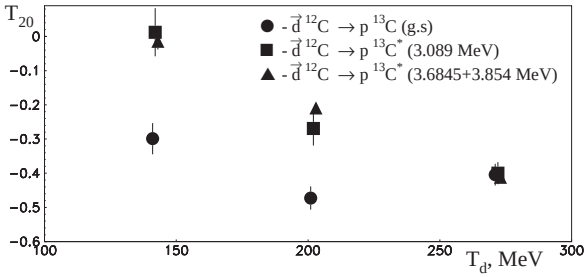

Figure 3: The experimental results on T_{20} in $^{12}C(\overrightarrow{d},p)^{13}C^*$ reactions at the energy T_d = 140, 200 and 270 MeV and emission angle Θ_{cm}=0°.

The results on the tensor analyzing power T_{20} for $^{12}C(\overrightarrow{d},p)^{13}C^*$ reaction are presented in figure 3. The circles, squares and triangles represent the data on T_{20} for $^{12}C(\overrightarrow{d},p)^{13}C(g.s.)$, $^{12}C(\overrightarrow{d},p)^{13}C(3,089MeV)$ and $^{12}C(\overrightarrow{d},p)^{13}C(3,6845+3,854MeV)$ reactions, respectively.

The experimental results on the vector A_y and tensor A_{yy} analyzing powers of the $^{12}C(\overrightarrow{d},p)^{13}C^*$ reaction at T_d = 270 MeV are presented by the filled symbols in figure 4. The sign of A_{yy} analyzing power is positive in accordance with the sign of the D/S wave ratio of deuteron. The experimental data on vector A_y analyzing power for $^{12}C(\overrightarrow{d},p)^{13}C(g.s.)$ and $^{12}C(\overrightarrow{d},p)^{13}C^*$ are negative and positive, respectively.

Summary

The results can be summarized as following. The results on the tensor analyzing power T_{20} in the $^{12}C(\overrightarrow{d},p)^{13}C^*$ and $d(\overrightarrow{d},p)X$ reactions at energy T_d = 140, 200 and 270 MeV and emission angle Θ_{cm}=0° are obtained. The experimental data on T_{20} for these reactions show the sensitivity to the spin structure of deuteron. The experimental results on the vector A_y and tensor A_{yy} analyzing powers of the $^{12}C(\overrightarrow{d},p)^{13}C^*$ reaction at energy T_d = 270 MeV in the angular range from 4° to 18° in laboratory system are also obtained. The negative sign of analyzing power T_{20} for $^{12}C(\overrightarrow{d},p)^{13}C^*$ and $d(\overrightarrow{d},p)X$ reactions and positive sign of A_{yy} for $^{12}C(\overrightarrow{d},p)^{13}C^*$ reflect the sign D/S ratio a components of wave function of deuteron.

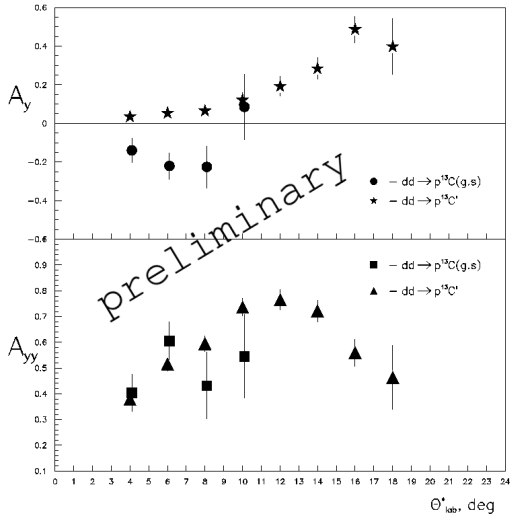

Figure 4. The experimental results on A_y and A_{yy} analyzing powers of the $^{12}C(\overrightarrow{d},p)^{13}C^*$ reaction at energy T_d = 270 MeV.

Acknowledgments

The work has been supported in part by the Russian Foundation for Fundamental Research (grant N^o 07-02-00102a)

References

[1] H.M. Xu, C.A. Gagliardi *et al.*, Phys. Rev. Lett. **73**, 2027 (1994).
[2] A.M. Mukhamedzhanov *et al.*, Phys. Rev. C **56**, 1302 (1997).
[3] C.A. Gagliardi *et al.*, Phys. Rev. C **59**, 1149 (1999).
[4] J.C. Fernandes, R. Crespo, *et al.*, Phys. Rev. C **61**, 064616 (2000).
[5] G.J. Kramer, H.P. Blok, and L. Lapikás, Nucl. Phys. **A679**, 267 (2001).
[6] A. Gade *et al.*, Phys. Rev. Lett. **93**, 042501 (2004).
[7] N. Keeley, N. Alamanos, and V. Lapoux Phys. Rev. C **69**, 064604 (2004).
[8] N. Sakamoto, Doctor Thesis, University of Tokyo (1996).
[9] T. Uesaka *et al.*, Riken Accel. Prog. Rep. **33**, 153 (2000).
[10] T.A. Vasiliev *et al.*, In Proc. of the VIII-th INTERNATIONAL WORKSHOP "RELATIVISTIC NUCLEAR PHYSICS:FROM HUNDREDS MeV to TeV", E1,2-2006-30, 106 (2006).

ΔG FROM HIGH p_T EVENTS AT COMPASS

On behalf of the COMPASS collaboration
Konrad Klimaszewski[1†]
(1) *The Andrzej Soltan Institute for Nuclear Studies, Warsaw*
† *E-mail: Konrad.Klimaszewski@fuw.edu.pl*

Abstract

One of the main goals of the COMPASS experiment is a precise determination of $\Delta G/G$. This will lead to better understanding of the nucleon spin structure. The polarization of the gluons in the nucleon is measured by tagging the Photon Gluon Fusion (PGF) process in scattering of polarized muons off a polarized deuteron target. One of the methods used to tag PGF events is a selection of a pair of high p_T hadrons in the final state. In the analysis presented here, the $Q^2 < 1$ (GeV/c)^2 region is considered. The preliminary value of $\Delta G/G$, $\frac{\Delta G}{G} = 0.016 \pm 0.058(stat.) \pm 0.055(syst.)$, is currently the most precise measurement available.

1 Introduction

In the frame of the Quark Parton Model the nucleon spin is described by a sum rule:

$$\frac{1}{2} = \frac{1}{2}\Delta\Sigma + \Delta G + L_q + L_g, \tag{1}$$

where $\Delta\Sigma$ is the contribution from quark helicities, ΔG the contribution from helicities of gluons and $L_{q,g}$ are the orbital momenta of quarks and gluons, respectively. A value of $\Delta\Sigma$ was first determined by the EMC [1]. That result was confirmed by several experiments [2–4]. All measurements indicate that $\Delta\Sigma$ cannot account for the whole spin of the nucleon. Recent results show that the value of $\Delta\Sigma$ is close to 30%, e.g. $\Delta\Sigma(Q^2 = 3(\mathrm{GeV/c})^2) = 0.30 \pm 0.01(\mathrm{stat.}) \pm 0.02(\mathrm{evol.})$ [4]. Therefore it is clear that the rest of the nucleon spin originates from polarised gluons and orbital motion of partons in the nucleon. The COMPASS experiment aims to further study the nucleon spin structure. A direct measurement of the gluon polarization is performed using cross-section asymmetries for PGF events in the scattering of polarized leptons on polarized nucleons which probes ΔG in the region of $x_g \simeq 0.1$.

In the COMPASS experiment we study interactions of a μ^+ beam of 160 GeV/c momentum and a polarization $P_B \simeq 80\%$ with a polarized deuteron target. The target material is ^{6}LiD which provides a good compromise between the dilution factor, $f \simeq 0.4$, and the achieved deuteron polarization of $P_T \simeq 50\%$. For more information about the COMPASS experimental setup see [5].

2 Experimental asymmetry

We measure a counting rate asymmetry as $A_{exp} = \frac{N^{\uparrow\Downarrow} - N^{\uparrow\Uparrow}}{N^{\uparrow\Downarrow} + N^{\uparrow\Uparrow}}$, where $N^{\uparrow\Downarrow(\uparrow\Uparrow)}$ are number of events with nucleons polarized anti-parallel (parallel) to muon spin direction. A two-cell target with cells polarized oppositely is used. This allows for a simultaneous measurement

of both spin configurations with the same beam flux. Due to that the flux as well as many other systematic effects will cancel out in the asymmetry calculation.

The raw counting asymmetry is related to cross-section asymmetry by

$$A_{||} = f P_T P_B A_{exp}. \tag{2}$$

To decrease statistical errors a weighting method of asymmetry extraction is used [6]. In this method a weight $w = fDP_B$, where D is the depolarization factor, is applied on an event by event basis instead of using average values.

3 $\Delta G/G$ measurement at COMPASS

A direct measurement of the gluon polarization in the nucleon can be performed using events originating from the PGF process. In this process a virtual photon emitted by an incoming lepton interacts with a gluon from a nucleon. The photon retains a part of the lepton polarization and thus provides a probe to sample the polarized gluons in the nucleon.

The PGF events have to be selected from a background originating from other processes. In LO QCD the following processes should be taken into account: the Leading Process (LP) where $\gamma*$ interacts with a quark from the nucleon, the QCD Compton (QCDC) process where an additional gluon is radiated and the PGF process. A hadron from LP obtains a transverse momentum with regards to the virtual gamma only from the fragmentation or from the intrinsic transverse momentum of the struck quark. This means that such hadrons will have a rather small p_T. Thus, by selecting high transverse momenta, a fraction of LP in the sample is greatly reduced.

The high p_T sample selection is based on a set of cuts. First, at least two hadron tracks are required to be reconstructed in a primary vertex. The p_T of two fastest hadrons should be above 0.7 GeV/c and their $\sum p_T^2$ exceed 2.5 $(\mathrm{GeV/c})^2$ to suppress the contribution from the LP. To remove regions with low sensitivity to ΔG and regions with large radiative corrections events with $0.35 < y < 0.9$ are selected. Finally, to ensure that mainly events from the current fragmentation region are selected and to remove the ρ resonance three additional cuts are imposed: $x_F,\ z > 0$ and $M_{inv} > 1.5\ \mathrm{GeV/c^2}$.

In the region of $Q^2 < 1\ (\mathrm{GeV/c})^2$ there is an additional contribution from the resolved photon processes. In Fig. 1 the fractions of the contributing processes are presented. They were estimated from a MC simulation based on the PYTHIA generator [7]. Apparatus behaviour is simulated by the GEANT3 [8]. Although Q^2 is small we can treat our sample as being in the perturbative region as the hard scale is set by p_T cuts. The PGF and two resolved photon processes that probe gluons from the nucleon - gq, gg are treated as signal. LP and so called "low p_T" sample, which consists of nonperturbative processes are neglected as they contribute only a small fraction of events. Finally we obtain:

$$\begin{aligned}\frac{A_{||}}{D} = {} & R_{PGF}\left\langle \frac{a_{LL}^{PGF}}{D}\right\rangle \frac{\Delta G}{G} + R_{QCDC}\left\langle \frac{a_{LL}^{QCDC}}{D}\right\rangle \frac{\Delta q}{q} + R_{qq}\left\langle \frac{a_{LL}^{qq}}{D}\right\rangle \frac{\Delta q}{q}\frac{\Delta q^\gamma}{q^\gamma} \\ & + R_{qg}\left\langle \frac{a_{LL}^{qg}}{D}\right\rangle \frac{\Delta q}{q}\frac{\Delta G^\gamma}{G^\gamma} + R_{gq}\left\langle \frac{q}{D}\right\rangle \frac{\Delta G}{G}\frac{\Delta q^\gamma}{q^\gamma} + R_{gg}\left\langle \frac{a_{LL}^{gg}}{D}\right\rangle \frac{\Delta G}{G}\frac{\Delta G^\gamma}{G^\gamma}\end{aligned} \tag{3}$$

where R_i is the fraction of the process i, a^i_{LL} is the partonic level asymmetry [9], q and Δq are the Parton Distribution Functions (PDFs) in the nucleon, q^γ, G^γ are unpolarized PDFs in the photon and Δq^γ, ΔG^γ are polarized PDFs in the photon.

In the expression (3) $\Delta G/G$ is the quantity we would like to extract, and $A_{||}$ is the measured asymmetry (2). The fractions of processes R_i and the average values of a_{LL} are taken from the MC simulation. The parton distributions in the nucleon are obtained from parameterizations to world data [10]: GRV98 and GRSV2000. Also unpolarized PDFs are taken from parameterization [11]. For polarized PDFs in the photon there are no measurements available. From theory we know that these PDFs are sums of a nonperturbative (VMD) term, and of a perturbative (point-like) term. The point-like PDFs are calculable in QCD but the VMD part is not. To cope with that we use the minimal $\Delta f^\gamma_{VMD} = -f^\gamma_{VMD}$ and the maximal $\Delta f^\gamma_{VMD} = f^\gamma_{VMD}$ scenarios [12]. This model uncertainty is taken into account in the systematic error.

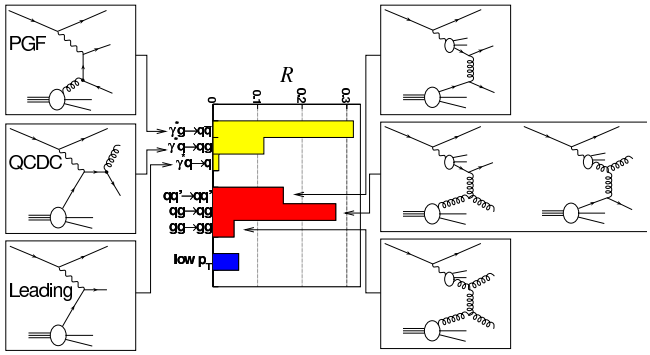

Figure 1: Relative contributions of the dominant high p_T processes at $Q^2 < 1$ (GeV/c)^2 as obtained by the PYTHIA MonteCarlo. Left: direct processes, right: resolved photon processes.

The main contribution to the experimental systematic error originates from false asymmetries. It is estimated on a sample of low p_T events with much larger statistics. Other sources of systematic errors, including the error on the beam and target polarizations, are proportional to the (small) measured asymmetry and as such were neglected.

As the $\Delta G/G$ extraction is based on quantities obtained from MC simulations, a good agreement between data and MC is crucial. It is presented in Fig. 2. In order to estimate the systematic error originating from MC simulations, the $\Delta G/G$ was determined for different values of most important parameters: parameters of the parton fragmentation model, the primordial transverse momentum of partons within the nucleon and the photon, the renormalization and factorization scales and switching on and off the parton showers.

From the data collected in years 2002-2003 the following value of the gluon polarisation is measured $\Delta G/G = 0.024 \pm 0.089(stat.) \pm 0.057(syst.)$ at $x_g \approx 0.095^{+0.08}_{-0.04}$ [10]. The scale at which measurement is made was estimated to be 3(GeV/c)^2. Analysis of combined data from years 2002-2004 provides us with a more precise preliminary result:

$$\frac{\Delta G}{G} = 0.016 \pm 0.058(stat.) \pm 0.055(syst.)$$

4 Conclusions and outlook

The method for extracting $\Delta G/G$ from high p_T hadron pairs for the $Q^2 < 1$ (GeV/c)^2 was presented. The result indicates that the gluon polarisation is small, compatible with zero, in the region of $x_g \simeq 0.1$.

During a technical stop of the SPS accelerator in 2005 our spectrometer has undergone a major upgrade. The most important one for the considered channel is the installation of a new target solenoid magnet with larger aperture. Data taking was restarted in 2006 and provided a considerable gain in the collected statistics. Analysis of 2006 data is ongoing. Other means of increasing available statistics are also considered e.g using Neural Networks as a tool for selecting PGF events.

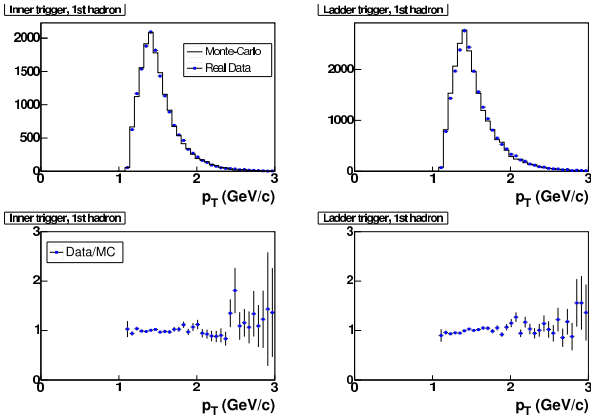

Figure 2: Comparison of data and MC for the high p_T $Q^2 < 1$ (GeV/c)^2 sample. The upper plots present the p_T distribution of a leading hadron for two selected triggers. On the bottom plots the ratio data/MC is presented.

If the gluon polarization is indeed small it would be very interesting to measure the contribution of the parton orbital angular momentum to the nucleon spin. Such a measurement using the Deeply Virtual Compton Scattering to access the Generalized Parton Distributions is considered for the COMPASS successor.

References

[1] **European Muon** Collaboration, J. Ashman *et. al. Phys. Lett.* **B206** (1988) 364.

[2] **Spin Muon** Collaboration, B. Adeva *et. al. Phys. Rev.* **D58** (1998) 112002.

[3] **E155** Collaboration, P. L. Anthony *et. al. Phys. Lett.* **B493** (2000) 19–28.

[4] **COMPASS** Collaboration, V. Y. Alexakhin *et. al. Phys. Lett.* **B647** (2007) 8–17.

[5] **COMPASS** Collaboration, P. Abbon *et. al. Nucl. Instrum. Meth.* **A577** (2007) 455–518.

[6] **COMPASS** Collaboration, E. S. Ageev *et. al. Phys. Lett.* **B647** (2007) 330–340.

[7] T. Sjostrand, S. Mrenna and P. Skands *JHEP* **05** (2006) 026.

[8] R. Brun *et. al. CERN-W5013* (1994).

[9] C. Bourrely, J. Soffer, F. M. Renard and P. Taxil *Phys. Rept.* **177** (1989) 319.

[10] **COMPASS** Collaboration, E. S. Ageev *et. al. Phys. Lett.* **B633** (2006) 25–32.

[11] M. Gluck, E. Reya and I. Schienbein *Phys. Rev.* **D60** (1999) 054019.

[12] M. Gluck, E. Reya and C. Sieg *Eur. Phys. J.* **C20** (2001) 271–281.

TRANSVERSE SPIN PHYSICS AT HERMES

V.A. Korotkov†
(on behalf of the HERMES Collaboration)

Institite for High Energy Physics, Protvino, Russia
† *E-mail: Vladislav.Korotkov@ihep.ru*

Abstract

The HERMES experiment at DESY collected data with a transversely polarized hydrogen target from 2002 to 2005. Azimuthal asymmetries were measured in the semi-inclusive production of pions and kaons. These asymmetries provide information on the quark transversity and the Sivers distribution functions. A two-hadron azimuthal asymmetry provides additional information on the quark transversity and on the interference fragmentation function. A study of the transverse target-spin asymmetries (TTSA) in hard exclusive electroproduction of real photons and vector mesons allows to set a model-dependent constraint on the total angular momentum of quarks in the nucleon.

1 Introduction

A description of the nucleon quark structure at leading twist requires three quark distribution functions: the unpolarized $f_1^q(x)$, the helicity $g_1^q(x)$, and the transversity $h_1^q(x)$ distribution. In contrast to its chiral-even partners, $f_1^q(x)$ and $g_1^q(x)$, the transversity distribution is chiral-odd, and can therefore not be probed in inclusive deep-inelastic scattering. However, it may be probed in a semi-inclusive deep-inelastic process involving an additional chiral-odd structure, i.e., a chiral-odd fragmentation function. Two examples of such processes were investigated at HERMES. Semi-inclusive hadron production which involves the Collins fragmentation function [1] and semi-inclusive two-hadron production which involves an interference fragmentation function [2].

An important piece in understanding the spin structure of the nucleon is the total angular momentum of partons, J_a, an elusive quantity up to now. Ji noted [3] that generalized parton distributions (GPDs) can be utilized to determine the total angular momentum of partons through the relation $J_a = \lim_{t\to 0} \frac{1}{2} \int_{-1}^{+1} dx\, x\, [H^a(x,\xi,t) + E^a(x,\xi,t)]$. Here, $H(x,\xi,t)$ and $E(x,\xi,t)$ are parton spin non-flip and spin flip GPDs, respectively. The ordinary parton distributions represent the probability to find a parton with specific longitudinal momentum fraction x in the fast moving hadron. GPDs, in contrast, represent the interference of different wave functions, one with a parton having momentum fraction $x+\xi$ and one with a parton having momentum fraction $x-\xi$. In addition, GPDs depend on a third variable, the momentum transfer $-t = (p-p')^2$ between two hadron states with momenta p and p', respectively. The GPDs combine the characteristics of both the ordinary parton distributions and of nucleon form factors. GPDs can be measured in hard exclusive processes, such as deeply virtual Compton scattering (DVCS) ($ep \longrightarrow ep\gamma$).

The results presented here are based on data obtained by the HERMES experiment in 2002–2005 running period using a transversely polarized hydrogen gas target internal

to the 27.6 GeV lepton (e^+ and e^-) beam of the HERA storage ring. The HERMES dual-radiator ring-imaging Čerenkov detector allows full $\pi^\pm$, $K^\pm$, p separation in the momentum region $2 \div 15$ GeV. Further details of the experiment might be found in Ref. [4]. The average value of the proton polarization $S_\perp$ was 0.74±0.06. The data was summed over both lepton beam helicity states, corresponding to a study of single target-spin asymmetries with an unpolarized lepton beam.

2 Semi-Inclusive Single Hadron Production

Results on the transverse target-spin asymmetry based on data collected by HERMES in 2002 were published in Ref. [5]. Below, results based on the full statistics are presented.

The Collins mechanism [1] produces a correlation in the fragmentation process of the transverse target spin vector $\boldsymbol{S}_\perp$ with the vector $\boldsymbol{P}_h \times \boldsymbol{q}$ (see Fig. 1). The corresponding Collins fragmentation function $H_1^\perp$ describes the influence of the transverse polarization of the struck quark on the transverse momentum $\boldsymbol{P}_{h\perp}$ of the produced hadron. Another source of azimuthal asymmetries is the chiral-even Sivers distribution function $f_{1T}^\perp(x)$, which describes the correlation of the transverse polarization of the target nucleon with the transverse momentum of the struck quark [6]. The polarized part of the semi-inclusive cross section for unpolarized beam (U) and a transversely polarized target (T) with contributions from both mechanisms is proportional to a sum of two terms [7]:

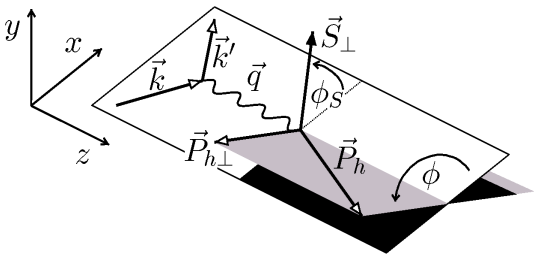

Figure 1: Definitions of azimuthal angles of the hadron production plane ϕ and the target spin ϕ_S relative to the lepton scattering plane.

$$d\sigma_{UT} \propto \sin(\phi+\phi_S)\cdot\sum_q e_q^2\cdot\mathcal{I}\left[\frac{\boldsymbol{P}_{h\perp}\cdot\boldsymbol{k}_T}{M_h}\cdot h_1^q(x,p_T^2)\cdot H_1^{\perp,q}(z,k_T^2)\right]$$
$$+\sin(\phi-\phi_S)\cdot\sum_q e_q^2\cdot\mathcal{I}\left[\frac{\boldsymbol{P}_{h\perp}\cdot\boldsymbol{p}_T}{M}\cdot f_{1T}^{\perp,q}(x,p_T^2)\cdot D_1^q(z,k_T^2)\right], \qquad (1)$$

where the azimuthal angles ϕ and ϕ_S are depicted in Fig. 1, while $h_1^q(x,p_T^2)$, $f_{1T}^{\perp,q}(x,p_T^2)$ and $H_1^{\perp,q}(z,k_T^2)$, $D_1^q(z,k_T^2)$ are transverse-momentum dependent quark distribution and fragmentation functions, respectively. $\mathcal{I}[...]$ denotes a convolution integral over transverse momentum of the initial quark, $\boldsymbol{p}_T$, and transverse momentum of fragmented hadron, $\boldsymbol{k}_T$. The Collins and the Sivers mechanisms produce a different dependence of the azimuthal asymmetry on the two angles ϕ and ϕ_S. This permits one to use the variation of ϕ and ϕ_S to disentangle the two contributions experimentally.

Semi-inclusive DIS events were selected subject to the kinematic requirements $Q^2 > 1$ GeV^2, $y < 0.95$, $W^2 > 10$ GeV^2, $2 < P_h < 15$ GeV, $0.2 < z < 0.7$ and $\theta_{\gamma^* h} > 0.02$ rad, where $\theta_{\gamma^* h}$ is the angle between the direction of the virtual photon and the hadron. The selected range in x is $0.023 < x < 0.4$.

The Collins $2\langle\sin(\phi+\phi_S)\rangle_{UT}^h$ and the Sivers $2\langle\sin(\phi-\phi_S)\rangle_{UT}^h$ azimuthal amplitudes were extracted simultaneously using maximum likelihood fits. To allow for contribution

from all theoretically possible Fourier modulations [7] the terms for $\sin\phi_S$, $\sin(2\phi-\phi_S)$ and $\sin(3\phi-\phi_S)$ were added in the probability density function.

The extracted Collins and Sivers amplitudes for charged pions and kaons, and neutral pions are presented in Fig. 2 as a function of x, z, and $P_{h\perp}$. The error bands represent the systematic uncertainties due to acceptance and detector smearing effects and due to a possible contribution from the $\langle\cos\phi\rangle_{UU}$ moment in the unpolarized cross section. In addition, there is a common overall 8.1% scaling uncertainty due to the target polarization uncertainty. The present results are based on nearly ten times larger statistics than the previously published results for charged pions [5], and are consistent with them.

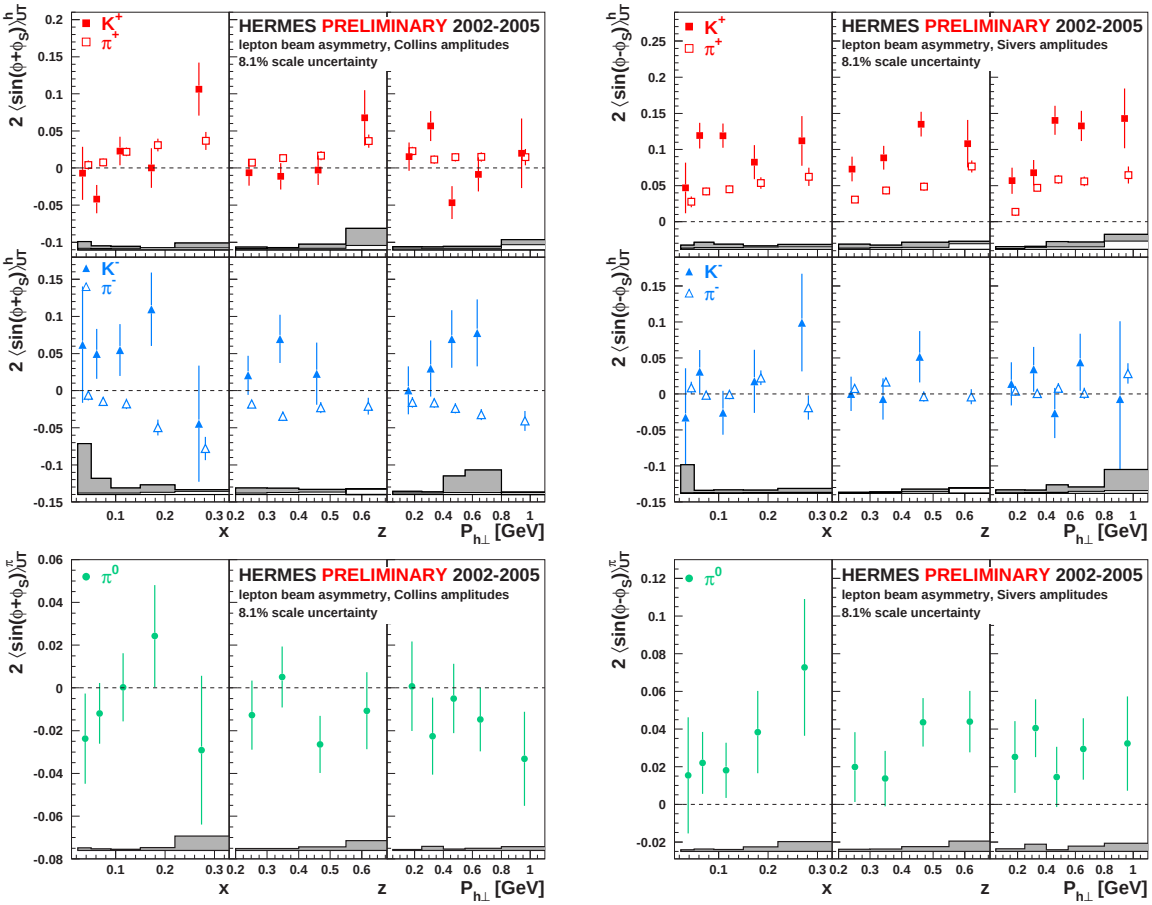

Figure 2: Collins (left panel) and Sivers (right panel) amplitudes for charged pions and kaons, and neutral pions (as labelled) as a function of x, z, and $P_{h\perp}$. The bands represent the systematic uncertainties.

The average Collins amplitude is positive for π^+, compatible with zero for π^0, and negative for π^-. This is expected if the transversity distribution h_1^u is positive and h_1^d is negative, the latter being analogous to the relation between the helicity distributions. However, the magnitude of the π^- amplitude appears to be as large as the π^+ amplitude, which was unexpected. This could be explained by a substantial unfavored (e.g., $u \to \pi^-$) Collins fragmentation function with the opposite sign to that of the favored function, i.e., $H_1^{\perp,unf} \approx -H_1^{\perp,fav}$. For charged kaons the Collins amplitudes are compatible with zero. At the same time, the Collins amplitudes for K^+ are consistent to the π^+ amplitudes within the statistical accuracy.

The results for the Collins amplitudes have been analyzed [33, 9] simultaneously with data from the BELLE experiment [10] on azimuthal asymmetries between two hadrons produced in a fragmentation of a quark and antiquark, $e^+e^- \to q\bar{q} \to h_1h_2 + X$. The analysis demonstrated a compatibility of results on the Collins fragmentation function between HERMES and BELLE experiments. Using this Collins function the first extraction of the transversity distributions $h_1^u(x)$ and $h_1^d(x)$ was achieved.

The average Sivers amplitude are significantly positive for π^+, π^0, and K^+. This result implies a non-zero Sivers distribution function $f_{1T}^{\perp}(x)$ and non-vanishing orbital angular momentum of the quarks inside the nucleon. The average Sivers amplitude for K^+ is by a factor 2.3 ± 0.3 higher in magnitude than the amplitude for π^+. This suggests that sea quarks provide an important contribution to the Sivers function. Such conclusion was confirmed by a direct fit to all available data on the Sivers amplitudes [9]. The first extraction of the Sivers distribution functions for $u-$, $d-$, and sea quarks was performed [33, 9].

3 Semi-Inclusive Two-Pion Production

A measurement of the single spin asymmetry in semi-inclusive two-hadron production provides an independent method to access the quark transversity distributions. The method has an advantage with respect to that presented in the previous section as it doesn't require a deconvolution procedure because the asymmetry is a product of the transversity distribution and corresponding fragmentation function. An extraction of the $h_1^q(x)$ distribution, however, requires the knowledge of the involved two-hadron interference fragmentation function. Although it is unknown at present, it can be measured, in principle, in e^+e^- experiment.

The polarized part of the differential cross section $d\sigma_{UT}$ can be written as [11]

$$d\sigma_{UT} = -|\boldsymbol{S}_\perp| \sum_q e_q^2 \frac{\alpha^2}{4\pi Q^2 y} (1-y) \sqrt{1 - 4m_\pi^2/M_{\pi\pi}^2} \tag{2}$$
$$\times \sin(\phi_{R\perp} + \phi_S) \cdot \sin\theta \cdot h_1^q(x) \cdot \left[H_{1,q}^{\sphericalangle,sp}(z, M_{\pi\pi}^2) + H_{1,q}^{\sphericalangle,pp}(z, M_{\pi\pi}^2) \cdot \cos\theta \right],$$

where z is the fraction of available energy carried by the two pions, $M_{\pi\pi}$ the invariant mass of the pion pair, and m_π the pion mass. The angle ϕ_S is defined in Fig. 1 while the angle $\phi_{R\perp}$ is explicitly defined by

$$\phi_{R\perp} = \frac{(\boldsymbol{q} \times \boldsymbol{k}) \cdot \boldsymbol{R}_T}{|(\boldsymbol{q} \times \boldsymbol{k}) \cdot \boldsymbol{R}_T|} \arccos \frac{(\boldsymbol{q} \times \boldsymbol{k}) \cdot (\boldsymbol{q} \times \boldsymbol{R}_T)}{|\boldsymbol{q} \times \boldsymbol{k}| \cdot |\boldsymbol{q} \times \boldsymbol{R}_T|}, \tag{3}$$

where $\boldsymbol{q} = \boldsymbol{k} - \boldsymbol{k'}$, $\boldsymbol{k}$ and $\boldsymbol{k'}$ are the initial and scattered lepton momenta, respectively. Vector $\boldsymbol{R}_T$ is the component of $\boldsymbol{R} = (\boldsymbol{P}_1 - \boldsymbol{P}_2)/2$ perpendicular to $\boldsymbol{P}_h = \boldsymbol{P}_1 + \boldsymbol{P}_2$ and $\boldsymbol{P}_1$, $\boldsymbol{P}_2$ are the pions momenta. The angle θ is defined as the polar angle of the pion pair in their center of mass system with respect to their direction in the target rest frame. The cross section depends on the product of the transversity distribution $h_1^q(x)$ and a combination of the two-pion interference fragmentation functions, $H_{1,q}^{\sphericalangle,sp}$ and $H_{1,q}^{\sphericalangle,pp}$. These functions describe the interference between different production channels of the pion pair, the interference between s and p wave states, and the interference between two p wave states, respectively.

Experimentally, the single target-spin asymmetry is defined as

$$A_{UT}(\phi_{R\perp},\phi_S,\theta) = \frac{1}{|S_\perp|}\frac{N^{\uparrow}(\phi_{R\perp},\phi_S,\theta) \; - \; N^{\downarrow}(\phi_{R\perp},\phi_S,\theta)}{N^{\uparrow}(\phi_{R\perp},\phi_S,\theta) \; + \; N^{\downarrow}(\phi_{R\perp},\phi_S,\theta)}, \tag{4}$$

where $N^{\uparrow(\downarrow)}(\phi_{R\perp},\phi_S,\theta)$ is the semi-inclusive luminosity-normalized yield of $\pi^+\pi^-$ pairs in the corresponding target spin state.

The asymmetry amplitude coupled to $H_{1,q}^{\sphericalangle,sp}$, $A_{UT}^{\sin(\phi_{R\perp}+\phi_S)\sin\theta}$, is presented in Fig. 3 as a function of the pion pair invariant mass $M_{\pi\pi}$. The amplitude is positive over the entire mass region and does not show a sign change at the ρ^0 mass as predicted in Ref. [12]. In contrast, the model predictions of Ref. [13] are qualitatively compatible with the data.

Bottom panel of Fig. 3 also shows the average values of $\sin\theta$ and z for each invariant mass bin. The data collected by HERMES corresponds to large values of $\sin\theta$, i.e., to angles around $\theta = \frac{\pi}{2}$. This currently prevents the extraction of the part of the asymmetry amplitude that is coupled to $H_{1,q}^{\sphericalangle,pp}$.

The results presented in this section are based on 2002-2004 data only.

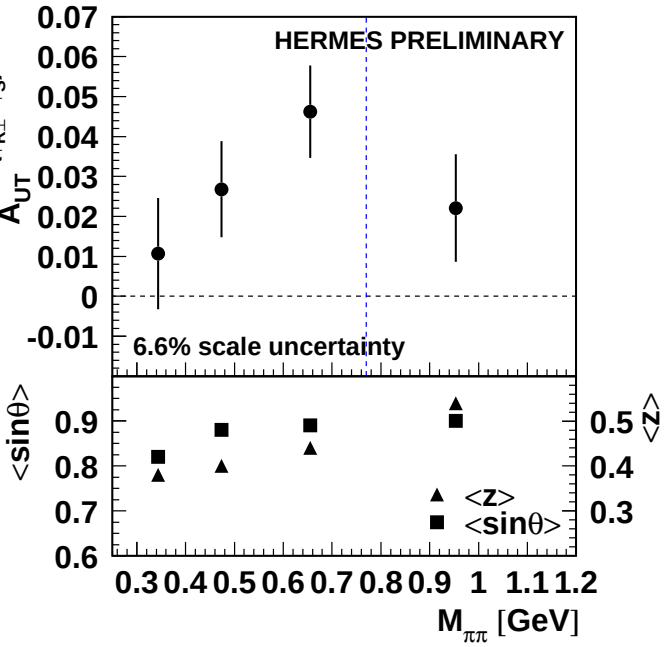

Figure 3: Asymmetry amplitude $A_{UT}^{\sin(\phi_{R\perp}+\phi_S)\sin\theta}$ as a function of the $\pi^+\pi^-$ pair invariant mass. The lower panel shows the average $\langle\sin\theta\rangle$ and the average $\langle z\rangle$ for each invariant mass bin.

4 Total Angular Momentum of Quarks

An evaluation of the total angular momentum of quarks in the nucleon requires, according to Ji's relation, a knowledge of GPDs H and E. The GPD H is accessible through many observables coupled to DVCS or to meson electroproduction. In contrast, a contribution of GPD E is usually suppressed. The two most promising observables to access GPD E are transverse target-spin asymmetries in DVCS and vector meson electroproduction.

The possibility to access the total angular momentum of u- and d-quarks in the nucleon with a study of the TTSA in DVCS and exclusive ρ^0 production at the HERMES experiment was considered in Ref. [14]. The authors use a parametrization [15] of GPD $E_q(x,\xi,t)$ based on chiral quark soliton model. In such a parametrization the total angular momenta carried by u and d quarks enter directly as free parameters. The TTSA associated with DVCS on the proton represents an observable that is particulary sensitive to GPD $E_q(x,\xi,t)$. The azimuthal amplitude of the TTSA can be approximated as

$$A_{UT}^{\sin(\phi-\phi_S)\cos\phi} \propto Im[F_2\mathcal{H} - F_1\mathcal{E}]. \tag{5}$$

Here, $\mathcal{H}$ and $\mathcal{E}$ are convolutions of the corresponding GPDs H and E with hard scattering kernels, F_1 and F_2 are the Dirac and Pauli nucleon form factors, and the angles ϕ and ϕ_S are defined in Fig. 1 where $\boldsymbol{P}_h$ is the real photon momentum now.

The recoil proton in the DVCS process escapes the HERMES acceptance and the missing-mass technique was applied to select a sample of events containing the scattered positron and a real photon. Exclusive events are identified by the requirement that the missing mass of the reaction $ep \longrightarrow e\gamma X$ corresponds to the proton mass.

The TTSA amplitude $A_{UT}^{\sin(\phi-\phi_S)\cos\phi}$ is presented in Fig. 4 as a function of $-t$, x_B, and Q^2. The main contributions to the systematic uncertainty come from the background correction, the target polarization measurement uncertainties and acceptance effects. The curves in Fig. 4 represent the TTSA amplitudes evaluated for a set of u-quark total angular momentum values, J_u, as a model parameter and a fixed value of the d-quark total angular momentum $J_d = 0$ [14]. The average value of the TTSA amplitude was found to be $\langle A_{UT}^{\sin(\phi-\phi_S)\cos\phi}\rangle = -0.149 \pm 0.058(stat) \pm 0.033(syst)$. The measurement corresponds to the average kinematics $\langle -t\rangle = 0.12$ GeV^2, $\langle x_B\rangle = 0.095$, $\langle Q^2\rangle = 2.5$ GeV^2.

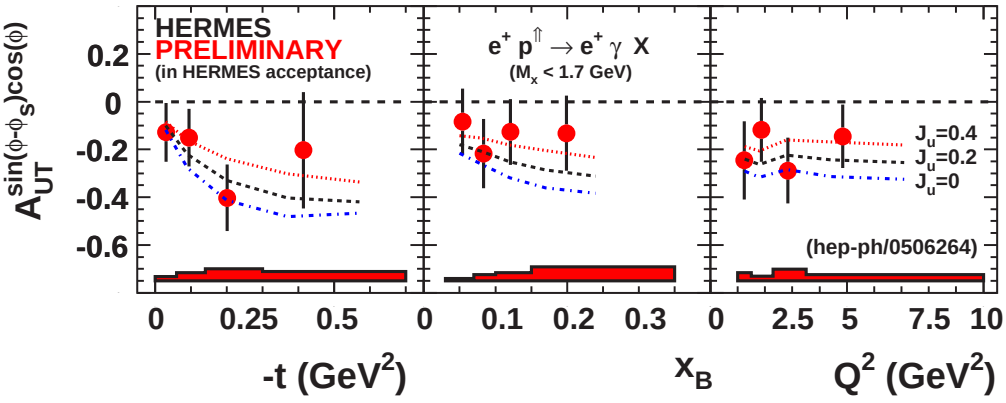

Figure 4: The TTSA amplitude $A_{UT}^{\sin(\phi-\phi_S)\cos\phi}$ as a function of $-t$, x_B, and Q^2. The bands represent the systematic uncertainties of the measurement. The curves represent the predictions from a GPD model with various u-quark total angular momentum values, J_u, while fixing the d-quark total angular momentum $J_d = 0$.

The sensitivity of the amplitude to the total angular momenta of quarks, demonstrated in Fig. 4, allows to set a model-dependent constraint on the total angular momenta of u- and d-quarks in the nucleon (see Fig. 5). This was achieved by a comparison of the measured TTSA amplitude to the theoretical calculation based on the GPD model [15] containing the values of the u- and d-quark total angular momenta as free parameters. The resulting one-standard-deviation constraint is $J_u + J_d/2.9 = 0.42 \pm 0.21 \pm 0.06$. The first uncertainty originates from the experimental uncertainty of the measured TTSA amplitude. The second uncertainty is a model uncertainty obtained by varying the parameter that controls the skewness dependence of GPDs [15].

The leading-order amplitude for hard exclusive electroproduction of longitudinally polarized vector mesons, V_L, by longitudinally polarized virtual photons, $\gamma_L^* + N \longrightarrow V_L + N$, depends on the unpolarized GPDs H and E only [15]. Even more interestingly, the transverse target spin asymmetry for such processes depends linearly on GPD E. Thus, this TTSA provides an additional with respect to that from DVCS method to

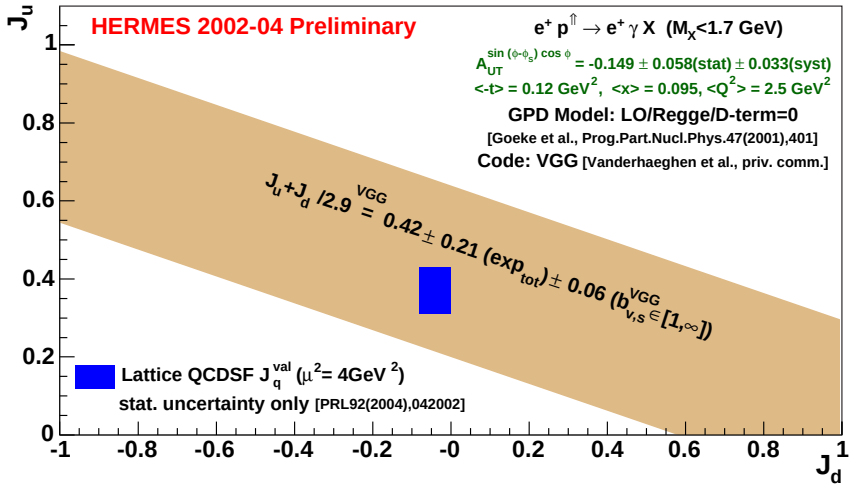

Figure 5: Model-dependent constraint on the u- and d-quark total angular momentum J_u and J_d. A lattice calculation result (valence contributions only) from the QCDSF collaboration is shown also.

extract J_q. One should also note that because the transverse target spin asymmetry involves a ratio of cross sections, it is expected to be a useful observable even at Q^2 values accessible at HERMES, as the precise form of the t-dependence of the GPDs, the NLO corrections and higher twist effects cancel to a large extent [15].

For the selection of exclusive events, $ep \longrightarrow ep\rho^0$ ($\rho^0 \rightarrow \pi^+\pi^-$), the following cuts were applied to a sample of $\pi^+\pi^-$ pairs produced in coincidence with the scattered lepton: $0.6 < M_{\pi\pi} < 1.0$ GeV, $\Delta E = \frac{M_x^2 - M_p^2}{2M_p} < 0.6$ GeV, and $-t' = t_0 - t < 0.4$ GeV^2. Here, M_x is the missing mass, and t_0 is the maximum kinematically allowed value of t.

The transverse target-spin asymmetry is defined as

$$A_{UT}(\phi - \phi_S) = \frac{1}{|S_\perp|} \frac{N^\uparrow(\phi - \phi_S) \; - \; N^\downarrow(\phi - \phi_S)}{N^\uparrow(\phi - \phi_S) \; + \; N^\downarrow(\phi - \phi_S)}, \tag{6}$$

where $N^{\uparrow(\downarrow)}(\phi - \phi_S)$ is the luminosity normalized yield of the vector meson production events in the corresponding target polarization state. The angles ϕ and ϕ_S are defined as in Fig. 1 where $\boldsymbol{P}_h$ is the ρ^0 momentum now.

Since the factorization theorem for vector meson electroproduction holds for longitudinal photons only, the asymmetry of ρ^0 mesons induced from longitudinal photons is of theoretical interest. Under the assumption of s-channel helicity conservation (SCHC), which implies that a longitudinal vector meson originates from a longitudinal photon, the longitudinal component of the asymmetry is obtained experimentally through the decay angular distribution of ρ^0 ($\rho^0 \rightarrow \pi^+\pi^-$). Each ρ^0 helicity state (L, T) results in a characteristic dependence of the $\gamma^* p$ cross-section on the polar angle θ_π of π^+ in the ρ^0 rest frame. More details on the isolation of the asymmetry due to the longitudinal photons can be found in Ref. [16].

The dependence of the transverse target-spin asymmetry amplitude $A_{UT}^{\sin(\phi-\phi_S)}$ for longitudinal ρ^0 mesons on variables x_B and $-t'$ is presented in Fig. 6. Results of calculations [14] for different values of J_u at fixed value of $J_d = 0$ are shown also. One may conclude that in spite of quite low statistical accuracy the data favor positive values of

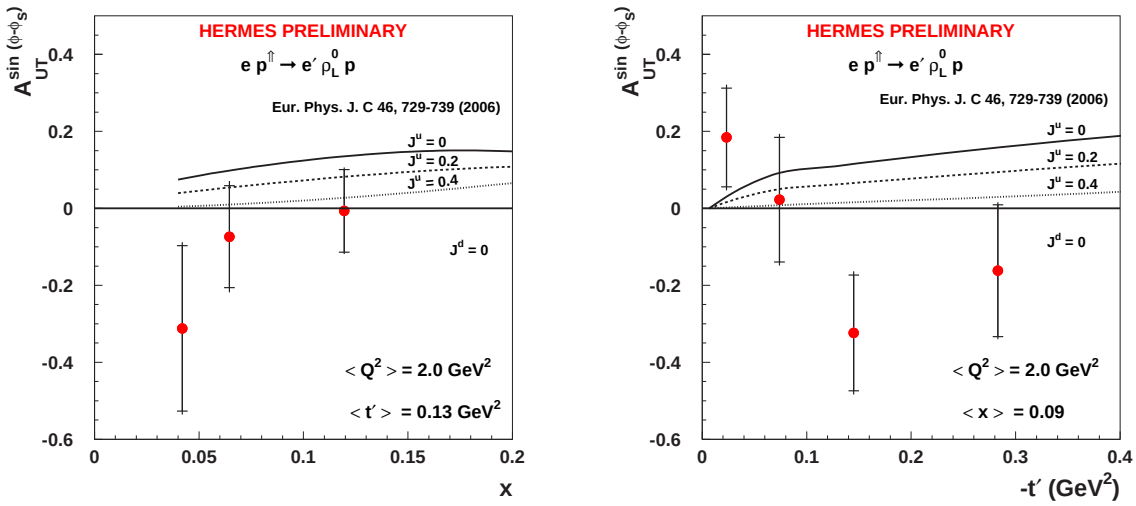

Figure 6: Transverse target spin asymmetry amplitude $A_{UT}^{\sin(\phi-\phi_S)}$ for exclusive production of ρ_L^0 mesons as a function of x_B (left panel) and $-t'$ (right panel). The error bars represent the total uncertainties.

J_u, compatible with the constraint on J_u and J_d obtained from the DVCS TTSA.

5 Summary

The measurement of the azimuthal asymmetry for pions and charged kaons, produced in semi-inclusive DIS, leads to a number of important conclusions: i) the Collins fragmentation function is non-zero – this allows a measurement of the transversity distribution $h_1^q(x)$; ii) unfavored Collins fragmentation function is about the same magnitude as favored one, but with an opposite sign: $H_1^{\perp,unf} \approx -H_1^{\perp,fav}$; iii) the Sivers distribution function $f_{1T}^{\perp u}(x)$ is non-zero – this implies that there is non-vanishing orbital angular momentum of the quarks inside the nucleon; iv) sea quarks play an important role in the Sivers distribution function. The HERMES data on these azimuthal asymmetries have been analyzed by two groups [33, 9] and first extractions of the quark transversity distribution, the Collins fragmentation function, and the Sivers distribution function were performed.

A first observation of the azimuthal asymmetry on a transversely polarized target due to an interference fragmentation function was presented. The data provide additional information about the quark transversity distribution and the interference fragmentation function.

A measurement of the transverse target-spin asymmetry in deeply virtual Compton scattering was performed for the first time. This asymmetry provides a unique observable to evaluate the total angular momentum of quarks in the nucleon. Although the experimentally available statistical accuracy of the present data is still not sufficient for an extraction of the GPD, an approach [14] based on a direct comparison of the measured asymmetries with theoretical predictions using a model [15] for $E(x, \xi, t)$ has been pursued. In this approach the total angular momenta of quarks can be considered as fit parameters, which led to a first, though model-dependent, constraint on the total angular momenta of u- and d-quarks in the nucleon.

A measurement of the TTSA in a process, $\gamma_L^* + p \to \rho_L^0 + p$, was performed for the first time. A validity of the SCHC hypothesis for an isolation of the process was assumed. The data favor positive values of J_u and are compatible with the constraint on J_u and J_d obtained from the DVCS TTSA.

In 2003–2005 running period the lepton beam was longitudinally polarized. The average value of the product of the longitudinal beam polarization, P_B, and the transverse target polarization, P_T, was $\langle P_B \cdot P_T \rangle \approx 0.30$. This allows an extraction of the polarized structure function $g_2(x)$ and new types of azimuthal asymmetries in semi-inclusive DIS. These studies are underway.

Acknowledgments. I wish to thank my colleagues in the HERMES collaboration. I acknowledge G. Schnell for critical reading of the manuscript, and I thank the organizers of DSPIN-2007 for their financial support.

References

[1] J. C. Collins, *Nucl. Phys.* **B396**, 161 (1993).

[2] J.C. Collins, S.F. Heppelmann, G.A. Ladinsky, *Nucl.Phys* **B420**, 565 (1994), J.C. Collins, G.A. Ladinsky, e-Print: hep-ph/9411444.

[3] X. Ji, *Phys. Rev. Lett.* **78**, 610 (1997).

[4] K. Ackerstaff *et al.*, *NIM* **A417**, 230 (1998).

[5] A. Airapetian *et al.*, *Phys. Rev. Lett.* **94**, 012002 (2005).

[6] D.W. Sivers, *Phys. Rev.* **D41**, 83 (1990).

[7] A. Bacchetta *et al.*, *JHEP* **0702**, 093 (2007), and references therein.

[8] A.V. Efremov, these proceedings.

[9] A. Prokudin, these proceedings.

[10] R. Seidl *et al.*, *Phys. Rev. Lett.* **96**, 232002 (2006), A. Ogawa *et al*, *AIP Conf.Proc.* **915**, 575 (2007).

[11] A. Bacchetta, M. Radici, *Phys. Rev.* **D67**, 094002 (2003).

[12] R.L. Jaffe, X. Jin, J. Tang, *Phys. Rev. Lett.* **80**, 1166 (1998).

[13] A. Bacchetta, M. Radici, *Phys. Rev.* **D74**, 114007 (2006).

[14] F. Ellinghaus *et al.*, *Eur.Phys.J* **C46**, 729 (2006).

[15] K. Goeke, M.V. Polyakov, and M. Vanderhaeghen, *Prog. Nucl. Part. Phys.* **47**, 401 (2001), and referencies therein.

[16] A Rostomyan and J Dreschler for the HERMES Collaboration, e-Print: arXiv:0707.2486

Discussion

Q. (A.Efremov, JINR, Dubna) To what extent the data on Sivers K^+ asymmetry are finite?

A. The analysis is based on the full statistics collected by HERMES with the transversely polarized hydrogen target. The result is under preparation for a publication.

Q. (J.Nassalski, SINS, Warsaw) What improvements do you expect for the analysis of data taken with the RPD in 2006 and 2007?

A. HERMES run in 2006 and 2007 years with an unpolarized target.

Q. (A.Prokudin, Univ. Torino) In your analysis of Collins and Sivers asymmetries you include also other harmonics that may appear in a general formulae for polarized cross section. Do you have results on those new asymmetries?

A. A study of the systematic uncertainties on extraction of other harmonics has not been finished yet.

Q. (N.d'Hose, CEA Saclay) Statistics for TTSA and DVCS will be increased by a factor 2.5. Statistics for TTSA and ϱ will not be increased.

A. Yes.

DEEPLY VIRTUAL PSEUDOSCALAR MESON PRODUCTION WITH CLAS

V. Kubarovsky[1,2,†], P. Stoler[2] and I. Bedlinsky[3]

(1) *Jefferson Lab, USA*
(2) *Rensselaer Polytechnic Institute, USA*
(3) *Institute for Theoretical and Experimental physics, Russia*
† *E-mail: vpk@jlab.org*

Abstract

Deeply virtual Compton scattering, cross sections and asymmetries for the π^0 and η exclusive electroproduction in a very wide kinematic range of Q^2, t and x_B have been measured with CLAS (JLab). Initial analyses are already showing remarkable results. These data will help us to better understand the transition from soft to hard mechanisms.

Deeply virtual exclusive reactions offer a unique opportunity to study the structure of the nucleon at the parton level as one varies both the size of the probe, i.e. the photon virtuality Q^2, and the momentum transfer to the nucleon t. Such processes can reveal much more information about the structure of the nucleon than either inclusive electroproduction (Q^2 only) or elastic form factors ($t = -Q^2$). The characterization of deeply virtual exclusive reactions in terms of their common nucleon structure is one of the major objectives of the Jefferson Lab 12 GeV upgrade.

There have been two commonly used theoretical tools which relate exclusive reactions to the structure of the nucleon. At lower Q^2, where the probe is on the order of the size of hadrons and the interactions are strong, Regge phenomena have proved effective. At high Q^2 the probe interacts with individual quarks, and in the limit $Q^2 \to \infty$ and $-t/Q^2 \to 0$ the QCD factorization theorem [3] unifies all exclusive reactions in terms of their common nucleon structure encoded by generalized parton distributions (GPDs). In this article we consider deeply virtual meson production (DVMP), specifically the reaction $\gamma^* p \to pM$, where M is a meson ($\pi, \eta, \rho, \omega, \phi, etc$). In the GPD approach, which is schematically shown in Fig. 1, the ingredients involve a hard interaction between a virtual photon and quark which produces a meson whose internal structure is given by the distribution amplitude $\Phi(z)$, and the remaining nucleon whose structure is represented by GPDs. A caveat is that the proof for factorization applies only to the case when the virtual photon has longitudinal polarization. In that case, in the limit $Q^2 \to \infty$ the cross section scales as $\sigma_L \sim 1/Q^6$ and the ratio as $\sigma_T/\sigma_L \sim 1/Q^2$.

While most theoretical work on the GPD approach has focused on the high Q^2 and low $|t|$ kinematic region, exclusive production of photons and mesons at large $|t|$ can also be described in terms the nucleon GPDs. Theory also predicts σ_L and σ_T in the high $-t$ low Q^2 region. For example for the pseudoscalar meson electroproduction we have:

$$\frac{d\sigma}{dt} \propto \left(R(t) \int dz \Phi(z) f(z, s, Q^2, t) \right)^2 \tag{1}$$

$$R(t) \propto (e_u R^u(t) - e_d R^d(t)^d) \qquad R^q(t) = \int \frac{dx}{x} e^{\alpha t((1-x)/2x} \left[\Delta q(x) - \Delta \bar{q}(x)\right]$$

where $\Phi(z)$ is the meson distribution amplitude, $f(z, s, Q^2, t)$ is parton level amplitude and the $R(t)$s describe new form factors which are the $1/x$ moments of the GPDs. Δq and $\Delta\bar{q}$ are the polarized parton and antiparton distributions for u, d and s quarks. The constant in the exponent α is approximately 1 GeV^{-2}. The Fourier transforms with respect to $\overrightarrow{\Delta}_\perp$ ($\Delta^2 = -t$) describe the correlation between the transverse spatial distribution of quark impact and x_B in the proton.

Deeply virtual Compton scattering (DVCS) is the cleanest way of accessing GPDs. However, DVCS does not access the helicity dependent GPDs and it is difficult to perform a flavor separation. In the case of pseudoscalar meson production the amplitude involves the axial vector-type GPDs $\tilde{H}$ and $\tilde{E}$. These GPDs are closely related to the distribution of quark spin in the proton, and $\tilde{H}$ reduces to the polarized quark/antiquark densities in the limit of zero momentum transfer. Vector and pseudoscalar meson production allows one to separate flavor and isolate the helicity-dependent GPDs. This is summarized in Table 1.

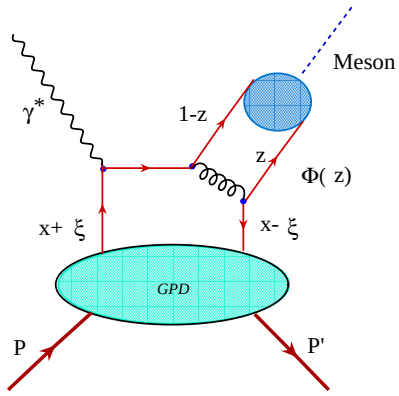

Figure 1. Schematic illustration of the GPD approach to meson electroproduction.

$\tilde{H}$, $\tilde{E}$	π^+	$\Delta u - \Delta d$
	π^0	$2\Delta u + \Delta d$
	η	$2\Delta u - \Delta d$
H, E	ρ^+	$u - d$
	ρ^0	$2u + d$
	ω	$2u - d$

Table 1: GPDs and quark flavor selectivity of pseudoscalar and vector meson electroproduction.

The extraction of GPDs from electroproduction data is a challenging problem. A detailed understanding of the reaction mechanism is essential before one can compare with theoretical calculations. It is not yet clear at what values of Q^2 the application of GPDs to meson electroproduction becomes valid. However, detailed measurements of observables may test model-independent features of the reaction mechanism, such as t-slopes, flavor ratios, and generally by studying the variation of observables over a wide range of Q^2 and t. Even though current experiments are limited in Q^2 and t, it has been argued [4] that *precocious factorization* ratios of cross sections as a function of x_B could be valid at relatively lower Q^2

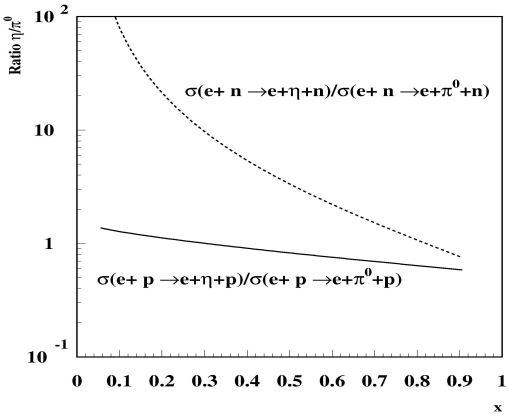

Figure 2. Predictions of the ratio of cross sections for π^0 to η electroproduction from protons and neutrons [4] utilizing the concept of *precocious factorization.*

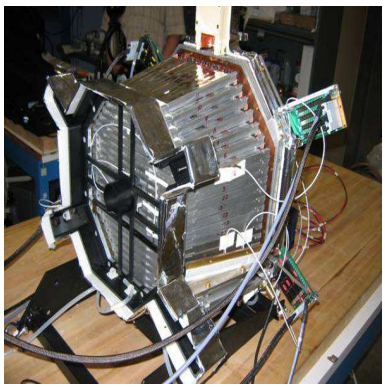

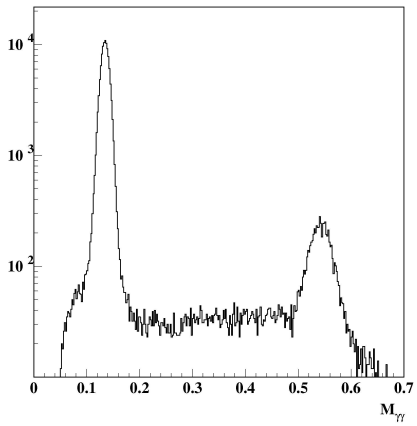

(a) **(b)**

Figure 3a. Photograph of the new CLAS lead-tungsten electromagnetic calorimeter.
Figure 3b. 2γ invariant mass spectrum in which the π^0's and η's are clearly observed (note log scale).

than for cross sections themselves. For example, the ratio of cross sections for π^0 and η electroproduction from a proton is related to the helicity structure of the quark flavors as

$$\pi^0/\eta = \frac{1}{2}\left[\frac{2}{3}\Delta u + \frac{1}{3}\Delta d\right]^2 / \frac{1}{6}\left[\frac{2}{3}\Delta u - \frac{1}{3}\Delta d + \frac{1}{3}\Delta s\right]^2 \qquad (2)$$

The results of a calculation of this ratio as a function of x_B is shown in Fig. 2.

Recent CLAS measurements of π^0 and η production.

Cross section data for DVCS [1] and DVMP [2] have recently been obtained at Jefferson Lab with the CLAS spectrometer, up to a $Q^2 \sim 5$ GeV^2. This has been made possible by constructing a high quality electromagnetic calorimeter consisting of 424 lead-tungsten glass crystals covering an angular range from 4.5° to 15°, which was positioned into the existing CLAS large acceptance detector. The pions and etas are identified through their 2γ decays. A photograph of the new detector and the 2γ invariant mass distribution is shown in Fig. 3. One can see that the pions and etas are clearly observed, even before all final data selection cuts are performed. The kinematic coverage in the variables Q^2, x_B, t and W is shown in Fig. 4. The virtual photon cross section can be written in well known notation as

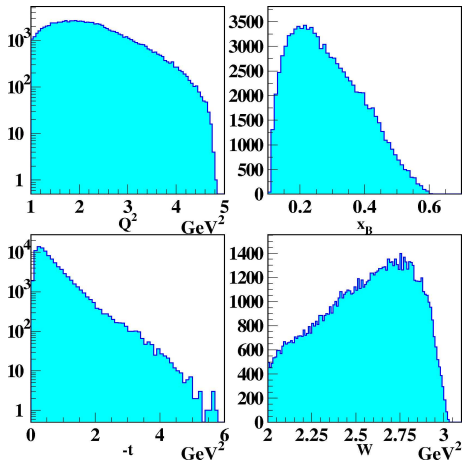

Figure 4. The kinematic coverage in Q^2, t, x_B and W for neutral pions of the CLAS DVMP experiment.

$$\frac{d\sigma}{d\Omega_\pi} = \sigma_T + \epsilon\sigma_L + \epsilon\sigma_{TT}cos2\phi + \sqrt{2\epsilon(1+\epsilon)/2}\sigma_{LT}cos\phi_\pi + h\sqrt{\epsilon(\epsilon-1)}\sigma'_{LT}sin\phi \qquad (3)$$

where ϕ denotes the azimuthal angle between the hadronic and leptonic scattering planes and h is the electron beam polarization.

The large acceptance of CLAS enabled the data to be grouped into intervals in Q^2, t x_B and ϕ. For unpolarized electrons ($h = 0$) the separation of the ϕ dependence in moments of a *constant*, $cos\phi$, and $cos2\phi$ allows us to obtain $\sigma_T + \epsilon\sigma_L$, σ_{TT} and σ_{LT}. An example of a ϕ distribution for $t = 0.3$ GeV^2 integrated over Q^2 are shown in Fig. 5.

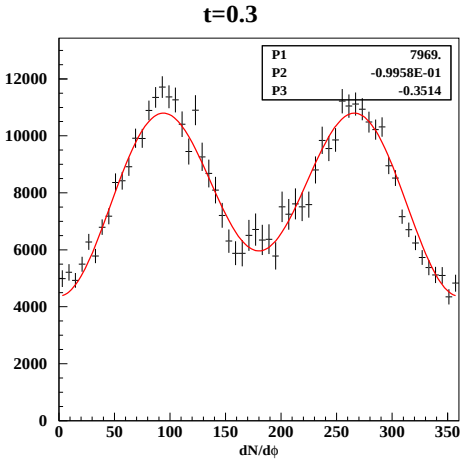

Figure 5. The angular distribution for $t = 0.3$ GeV^2 integrated over $Q^2 > 1$ GeV^2 and $W > 2$ GeV.

The separated structure functions versus t for Q^2 = 2.3 GeV^2 is shown in Fig. 6. The cross sections are in arbitrary units and radiative corrections have not been applied. It is observed that all the structure functions have significant non-zero values. σ_{LT} is comparable to $\sigma_T + \epsilon\sigma_L$ which implies that there are significant contributions of transverse amplitudes at these relatively low values of Q^2, so the factorization cannot be applied. However, one may analyze these data in terms of a hadron based models such as Regge phenomenology [5]. Fig. 6 shows the results of such a calculation, which qualitatively follows the sign of the separated structure functions, but not always the shape.

The Fourier transformation of the GPDs gives information about the impact parameter $\boldsymbol{b}_\perp$ dependence of parton distributions. The Fourier transformations are given by

$$F(x, \boldsymbol{b}_\perp) \propto \int \frac{d^2\boldsymbol{\Delta}_\perp}{2\pi} e^{i\boldsymbol{\Delta}_\perp \boldsymbol{b}_\perp} \tilde{H}(x, 0, \Delta_\perp^2) \tag{4}$$

Due to the significant contribution of transverse amplitudes at the current kinematics we

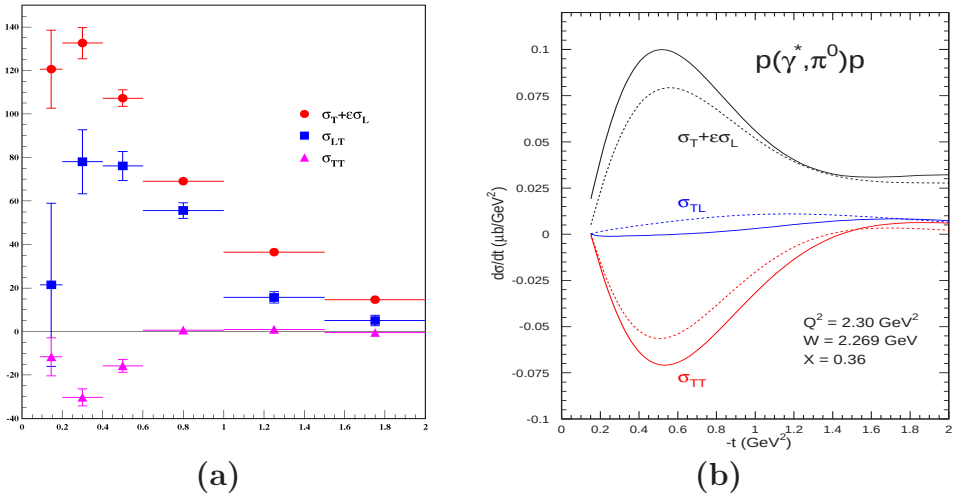

(a) (b)

Figure 6a. The separated structure functions $\sigma_T + \epsilon\sigma_L$, σ_{TT} and σ_{LT} as a function of $-t$ at $Q^2 = 2.3$ GeV^2 obtained with the CLAS spectrometer (very preliminary, arbitrary units).
Figure 6b. The results of a Regge model calculation [5].

do not have access to GPDs.

However, we can apply a Fourier transformation to the cross sections to get impact parameter information. Slope parameters B have been extracted by fitting the t distributions using the parametrization $d\sigma/dt \propto exp\,(B(x_B, Q^2)t)$. The result is shown in Fig. 7. Note that B does not appear to significantly depend on Q^2.

In a Regge inspired GPD model, the x_B dependence of the slope parameter is given by $B(x_B) = 2\alpha ln(1/x_B)$, with $\alpha \sim 1$. The curve in Fig. 7 is a plot of this parametrization for B. Remarkably, this curve appears to accurately account for the data with no further parameters or normalization applied.

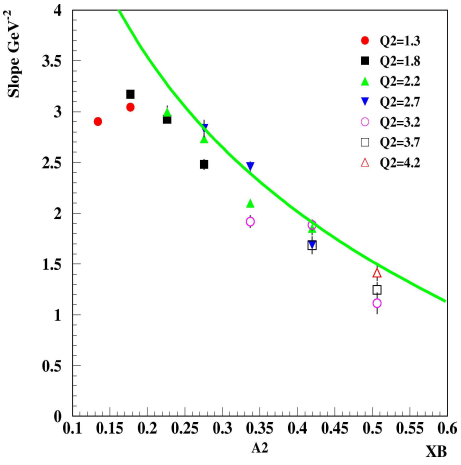

Figure 7. The experimental slope parameters B (very preliminary) obtained from fits to the data for various values of Q^2 and x_B with the function $d\sigma/dt \propto exp\,(B(x_B, Q^2)t)$. The solid curve is the Regge inspired parametrization $B(x_B) = 2\alpha ln(1/x_B)$ with $\alpha = 1.1$.

For the interpretation in terms of the impact parameter, the $\Delta_\perp^2$ slope is relevant, where $\Delta_\perp^2$ is the transverse component of the momentum transfer ($\Delta^2 = t$), and the slope parameter is $B_\perp = \frac{B}{1-x_b}$ [6]. The fact that the t-slope goes to zero for large x_B may be purely kinematical. However, even taking into account this factor, we note that $B_\perp$ falls with x_B in the region x_B from 0.1 to 0.5 where we have experimental data. This implies that the impact parameter distribution is broadest at lowest x_B and becomes narrower at increasing x_B.

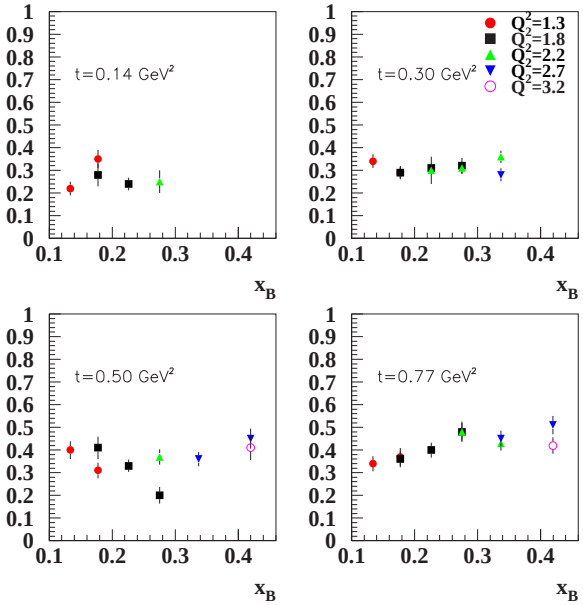

Figure 8. η to π^0 cross sections ratio as a function of x_B for different values of Q^2 and t (very preliminary).

The ratio of cross sections for η and π^0.

As it was noted in the introduction the ratio of cross sections may play an important role due to the *precocious factorization*. This ratio is presented in Fig. 8 for the different values of t and Q^2 as a function of x_B. Note that this ratio is almost independent of x_B and varies from 0.3 to 0.4 with increasing t. This is in contrast with the prediction [4] (see Fig. 2), where this ratio is equal to 1. However, we can not compare directly with [4] since σ_L and σ_T were not separated.

Beam spin asymmetry.

The beam spin asymmetry (BSA) is defined by

$$A = \frac{\vec{\sigma} - \overleftarrow{\sigma}}{\vec{\sigma} + \overleftarrow{\sigma}} \sim \alpha sin\phi. \tag{5}$$

From Eq. 3 the beam spin asymmetry directly yields the $L-T$ interference structure function σ'_{LT}. Any observation of a non-zero BSA would be indicative of an L-T interference. If σ_L dominates, then σ_{LT}, σ_{TT}, and σ'_{LT} should be small. An example of a ϕ distribution of the BSA for π^0 and η production at a particular kinematic bin is shown in Fig. 9.

Sizable beam-spin asymmetries for exclusive π^0 and η mesons electroproduction have been measured above the resonance region for the first time. These non-zero asymmetries imply that both transverse and longitudinal amplitudes participate in the process. However, the results of a Regge model calculation qualitatively describe the experimental data too.

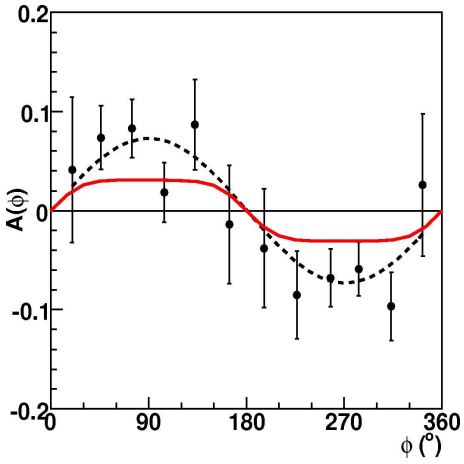

Figure 9. The angular distribution of the BSA for π^0 at $Q^2 = 2$ GeV^2, $t = -0.3$ GeV^2, and $x_B = 0.25$. The dashed curve is a fit to the function $A = \alpha \sin\phi$ and the solid curve is the result of a Regge model [5] calculation.

Conclusion.

Cross sections and asymmetries for the π^0 and η exclusive electroproduction in a very wide kinematic range of Q^2, t and x_B have been measured and initial analyses already are showing remarkable results. These data will help us to better understand the transition from soft to hard mechanisms. Initial results show that both transverse and longitudinal amplitudes participate in the exclusive processes at currently accessible kinematics. The π^0/η cross section ratio will check the hypothesis of precocious scaling.

We view the work presented here as leading into the program of the Jefferson Lab 12 GeV upgrade. The increased energy and luminosity will allow us to make the analysis presented here at much higher Q^2 and x_B as well as to perform Rosenbluth L/T separations. In parallel, we pose the following theoretical questions. What does the t-slope $B(Q^2, x_B)$ tell us? What can we learn from the Q^2 evolution of the cross sections? Can

the measurement of σ_L, σ_T,σ_{LT}, σ_{TT} and $R \equiv \sigma_L/\sigma_T$ constrain GPDs within the approximations and corrections which have to be made due to non-asymptotic kinematics? How big are the corrections?

References

[1] CLAS collaboration, F.X. Girod et al., arXiv:0711.4805 [hep-ph], 29 Nov. 2007.

[2] CLAS collaboration, R. De Masi et al., arXiv:0711.4736 [hep-ex], 4 Dec. 2007.

[3] J. C. Collins, L. Frankfurt and M. Strikman, Phys. Rev. D **56**, 2982 (1997) [arXiv:hep-ph/9611433].

[4] M. I. Eides, L. L. Frankfurt and M. I. Strikman, Phys. Rev. D **59**, 114025 (1999).

[5] J-M. Laget, private communication.

[6] Mattias Burkardt, arXiv:0711.1881 [hep-ph], 13 Nov. 2007.

THE ANGULAR DISTRIBUTIONS OF THE VECTOR A_y AND TENSOR A_{yy}, A_{xx}, A_{xz} ANALYZING POWERS IN THE $dd \rightarrow {}^3H\ p$ REACTION AT 200 MeV

A.K. Kurilkin[1†], T. Saito[2], V.P. Ladygin[1], T. Uesaka[3], T.A. Vasiliev[1], M. Janek[1,5], M. Hatano[2], A.Yu. Isupov[1], H. Kato[2], N.B. Ladygina[1], Y. Maeda[3], A.I. Malakhov[1], J. Nishikawa[4], T. Ohnishi[6] H. Okamura[8], S.G. Reznikov[1], H. Sakai[2,3], N. Sakamoto[6], S. Sakoda[2], Y. Satou[7], K. Sekiguchi[6], K. Suda[3], A. Tamii[7] N. Uchigashima[2], K. Yako[2]

(1) *LHE-JINR, 141-980 Dubna, Moscow region, Russia* (2) *Department of Physics, University of Tokyo, Bunkyo, Tokyo 113-0033, Japan* (3) *Center for Nuclear Study, University of Tokyo, Bunkyo, Tokyo 113-0033, Japan* (4) *Department of Physics, Saitama University, UraWa 338-8570, Japan* (5) *University of P.J. Safarik, 041-54 Kosice, Slovakia* (6) *RIKEN, Wako, Saitama 351-0198, Japan* (7) *Research Center for Nuclear Physics, Osaka University, Ibaraki 567-0047, Japan* (8) *CYRIC, Tohoku University, Sendai, Miyagi 980-8578, Japan* † *E-mail: akuril@sunhe.jinr.ru*

Abstract

The behavior of the vector A_y and tensor A_{yy}, A_{xx}, A_{xz} analyzing powers in the $\overrightarrow{d}\,d \rightarrow {}^3Hp$ reactions at 200 MeV has been investigated. The data on polarization observables in the angular range of 0 - 95 degrees in the c.m.s have been obtained. These polarization observables are sensitive to the momentum distribution of the proton spin in ${}^3H$ at the small internucleonic distances in the framework of one-nucleon exchange approximation. The experimental data are compared with theoretical calculations in the framework ONE with the use of Urbana, Paris and RSC wave functions of three-nucleon bound state.

Introduction. The $dd \rightarrow {}^3H\ p$ and $dd \rightarrow {}^3He\ n$ processes with large momentum transfer are the simplest ONE reactions where the three nucleon structure is relevant and, therefore, can be used as an effective tool to investigate the structure ${}^3H$ and ${}^3He$ at short distances.

These reactions can be described within the framework of the ONE model. Analysis of the polarization effects have shown that the tensor analyzing powers for these reactions at the forward angles are connected to D/S ratio of wave functions ${}^3He$ and ${}^3H$ [1].

Three-nucleon bound states are of interest, because even such constant as a binding energy of system is not reproduced by the calculations, which use modern pairwise NN potentials. Calculations with the use of local potentials such as Nijm-2, Reid'93, AV18 predict result of approximately 7.62 MeV while the experimental value is 8.48 MeV.

The spin structure of light nuclei has been extensively investigated during the last decades [2]- [9]. There are only few data, which sensitive to the spin structure of the three-nucleon bound state, especially, in the connection with the polarization studies. The large part of these data is dedicated to the spin structure of ${}^3He$ [10]- [11]. An experimental study of tritium is difficult because of its radioactivity.

In spite of the sensitivity of the polarization observables to the spin structure of light nuclei, difference from the predictions of the ONE is observed already of the relatively small internal momentum $\approx$ 200 MeV/c. This difference can be connected both with the

inadequate description of the spin structure of light nuclei at short distances and with the contribution of the mechanisms additional to ONE. In this respect new experimental data sensitive to the spin structure of light nuclei is the great importance.

In this report the data on the tensor A_{yy}, A_{xx}, A_{xz} and vector A_y analyzing powers for the $\overrightarrow{d}\,d \to {}^3Hp$ reactions obtained in R308n experiment at RIKEN are presented.

Experiment. Experiment was performed at the acceleration complex at RIKEN. The polarized beam of deuterons was ensured by the polarized ion source(PIS) and accelerated by AVF and Ring Cyclotrons up to the energy of 200 MeV. The measurement of the polarization of beam was carried out with the help of Swinger polarimeter (SwingerPOL) and Droom polarimeter (DroomPOL). Two kinds of deuterized polyethylene(CD_2) sheets were used as the target. The carbon target were used for evaluating the background events.

The scattered particles (^3He, ^3H and p) were registered by spectrometer SMART. The identification of particles was based on the time-of-light and the value of ionization losses in the plastic of scintillation detectors. Scattering angle and momentum of the particle were determined by the information of multiwire drift cambers (MWDC) and optical characteristics of the spectrometer. Further details on the experiment can be found in [12]- [13].

The criteria used for the identification of the scattered particle ^3H from the $\overrightarrow{d}\,d \to {}^3Hp$ reactions are the following. Particle must be registered in the all three scintillation detectors. The amplitudes must be correlated. The Radio Frequency signal of the cyclotron (TDRF) must be synchronized with the signals from the plastic scintillators.

The energy spectrum was measured on carbon target to take account for the contribution of CD_2 target carbon content. The quality of the $CD_2 - C$ subtraction procedure for the $\overrightarrow{d}\,d \to {}^3Hp$ reactions at 200 MeV is demonstrated in Fig.1. The spectra are plotted versus excitation energy E_x. The quality of subtraction is represented in Fig.1 a, b, c and d for the angles $12°, 36°, 56°$ and $87°$ in the center of mass system, respectively.

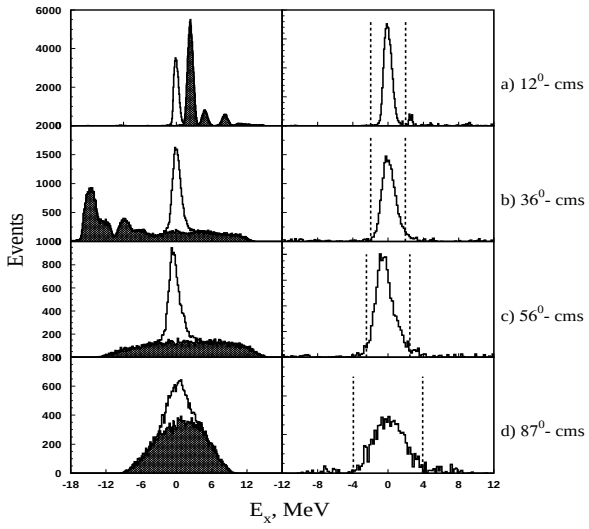

Figure 1. The quality of the CD2-C subtraction procedure for the $\overrightarrow{d}\,d \to {}^3Hp$ reaction at 200 MeV for several angles in the c.m.s.

To obtain the analyzing powers A_{yy}, A_{xx}, A_{xz} and A_y for the $\overrightarrow{d}\,d \to {}^3Hp$ reaction the asymmetries and beam polarization values for the three different spin modes of PIS was used.

Results. The experimental results on the vector A_y and tensor A_{yy}, A_{xx}, A_{xz} analyzing powers $\overrightarrow{d}\,d \to {}^3Hp$ reactions at 200 MeV are presented in Fig.2. The errors of the experimental values shown in these figures include both the statistical and the systematic

errors. The systematic errors were derived from the errors of the beam polarizations measurements.

The solid, long-dashed, and dotted curves are the results of ONE calculations [13] using Urbana [14], Paris [15] and Reid soft core [16] ^3He wave functions. All calculations have been performed with the use of Paris deuteron wave function [17]. One can see the strong sensitivity to the ^3H spin structure when ^3H is emitted in the forward angle in the centre of mass system and strong variation of analyzing powers versus an angle.

ONE calculation predicts that the tensor analyzing powers at the forward scattering are sensitive to the spin structure ^3H. For the angles near 90 degrees in the center of mass system analyzing powers are sensitive to the both deuterons and ^3H wave functions.

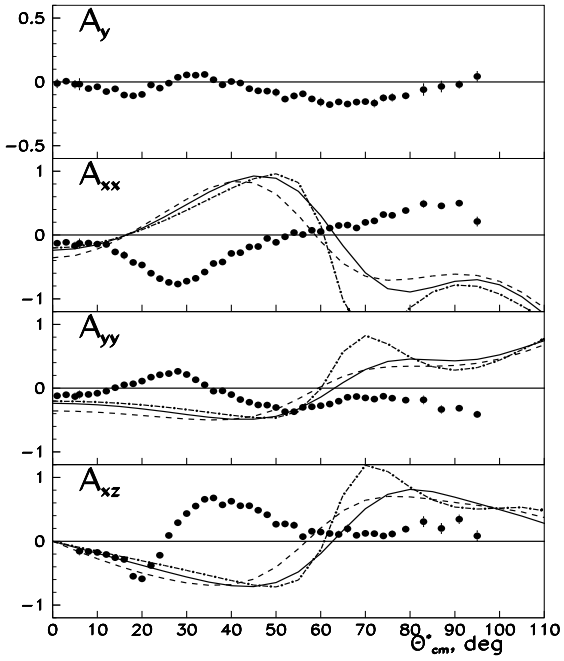

Figure 2. The results of the vector A_y and tensor A_{yy}, A_{xx}, A_{xz} analyzing powers in the center of mass system. The curves are explained in the text.

As can be seen, the experimental data for A_{yy}, A_{xx}, A_{xz} analyzing powers strongly disagree with the predictions of ONE model calculations. The predictions of ONE model calculations qualitatively reproduce the angular distributions of the tensor analyzing powers at small angles only. These results imply that there might be some problems in the descriptions of the realistic $^3He(^3H)$ wave functions used in ONE calculations.

ONE calculation predicts a zero value of the vector analyzing power, but some structure in the angular distribution of the vector analyzing power is observed. Since ONE calculations does not produce non-zero vector analyzing powers, this result will be a clue to investigate of the reaction mechanism beyond the ONE model.

Conclusion. The results of the vector A_y and tensor A_{yy}, A_{xx}, A_{xz} analyzing powers in the $\overrightarrow{d}\,d \rightarrow {}^3Hp$ reactions at the energy of deuterons 200 MeV in the angular range of 0 - 95 degrees in the center of mass system have been obtained. The data demonstrate large values of the analyzing powers.

The experimental data were compared with theoretical predictions of ONE calculations based on Urbana, Paris and RSC ^3He wave functions. The predictions of ONE model calculations qualitatively reproduce the angular distributions of the tensor analyzing powers at small angles only. However, the ONE calculations cannot reproduce the data in the whole angular range of the measurements.

The obtained experimental data require further development of the theoretical approaches either for adequate description of the structure of light nuclei at short distances or taking into account mechanisms in addition to ONE.

Acknowledgments

The work has been supported in part by the Russian Foundation for Basis Research (grant $No.07-02-00102a$)

References

[1] V. P. Ladygin and N. B. Ladygina, Yad. Fiz. **65**, 188 (2002) [Phys. Atom. Nucl. **65**, 182 (2002)].

[2] T. Uesaka et al. Phys. Lett., **B533**, 1 (2002).

[3] V. Punjabi et al., Phys. Lett. **B350**, 178 (1995).

[4] T. Uesaka., et al., Phys. Lett.**B467**, 199 (1999).

[5] L. S. Azhgirey et al., Phys. Lett. **B391**, 22 (1997).

[6] N. Sakamoto et al., Phys. Lett. **B367**, 60 (1996).

[7] H. Sakai et al., Phys. Lett. **84**, 5288 (2000).

[8] R. Bieber et al., Phys. Lett. **84**, 606 (2000).

[9] T. Uesaka, H. Sakai, H. Okamura, et al.,FewBody Systems Suppl. **12**, 497 (2000).

[10] M. Tanifuji, et al., Phys. Rev. **C61**, 024602 (2000).

[11] A. M. Eiro and F. D. Santos., J.Phys.G:Nucl.Phys.**16**, 1139 (1990).

[12] T. Ichihara et al.. Nucl. Phys., **A569**, 287 (1994).

[13] V. P. Ladygin et al. Part. Nucl. Lett., **3[100]**, 74 (2000).

[14] R. Schiavilla, V. R. Pandharipande, R. B. Wiringa Nucl.Phys., **A449**, 219 (1986).

[15] J. M. Laget, J. F. Lecolley, F. Lefebvres Nucl.Phys., **A370**, 479 (1981).

[16] F. D. Santos, A. M. Eiro, A. Barosso Phys.Rev., **C19**, 238 (1979).

[17] M. Lacombe et al. Phys.Lett. **B101**, 139 (1981).

Discussion

Comm. (N.Piskunov, JINR, Dubna) The data strongly disagree with different model calculation. Models reproduce the angular differential cross section for unpolarized deuteron beam?

A. We did not calculate the cross section. However, the similar model by Laget reproduce the cross section in the $dd \to Hp$ reaction measured in Saclay. In this model apart from ONE, the Δ-isobar excitation is taken into account. At our energy, ONE dominates.

Q. (N.Piskunov, JINR, Dubna) Experimental values strongly disagree with theoretical curves. Are the cross-section of this reaction with the calculations will agree?

A. The cross-section was not measured in this experiment.

THE ANGULAR DISTRIBUTIONS 0F THE VECTOR AND TENSOR ANALYZING POWERS IN dp ELASTIC SCATTERING AT THE ENERGY OF 880 MeV.

P.K. Kurilkin[1†], K. Suda[2], T. Uesaka[2], V.P. Ladygin[1], Yu.V. Gurchin[1], A.Yu. Isupov[1], K. Itoh[3], M. Janek[1,4], J.-T. Karachuk[1,5], T. Kawabata[2], A.N. Khrenov[1], A.S. Kiselev[1], V.A. Kizka[1], J. Kliman[1,6], V.A. Krasnov[1], N.B. Ladygina[1], A.N. Livanov[1], Y. Maeda[2], A.I. Malakhov[1], V. Matoucek[6], M. Morhac[6], S.G. Reznikov[1], S. Sakaguchi[2], H. Sakai[2,7], Y. Sasamoto[2], K. Sekiguchi[8], M.A. Shikhalev[1], I. Turzo[6], T.A. Vasiliev[1]

(1) *JINR, Dubna, Russia* (2) *Center for Nuclear Study, University of Tokyo, Tokyo, Japan* (3) *Saitama University, Saitama, Japan* (4) *P.J.Safarik University, Kosice, Slovakia* (5) *Advanced Research Institute for Electrical Engineering, Bucharest, Romania* (6) *Institute of Physics Slovak Academy of Sciences, Bratislava, Slovakia* (7) *Department of Physics, University of Tokyo* (8) *Institute for Physical and Chemical Research (RIKEN), Saitama, Japan* † *E-mail: pkuril@sunhe.jinr.ru*

Abstract

The results on the angular dependence of the vector A_y and tensor A_{yy}, A_{xx} analyzing powers in dp elastic scattering at $T_d = 880\ MeV$ are presented. A region of center-of-mass system angles from 60° to 140° is covered. The obtained data are compared with the preliminary calculations obtained within framework of multiple scattering models. These data are necessary for receiving the information of three-nucleon forces structure and the relativistic effects. The obtained data are also important for the development of the efficient deuteron beam polarimetry at high energies.

1 Introduction

A hot topic today in the nuclear physics is the study of the three nucleon forces properties through the investigation of the few-nucleon system. 3NF are relatively weak in comparison with NN forces. Therefore, it is hard to reveal them and find the confirmation for them experimentally.

The modern nucleon-nucleon (NN) potentials (AV18[1], CD-Bonn[2], Nijmegen[3] et al.) cannot describe experimental binding energy of the few-nucleon systems as well as the data on the deuteron proton ($d-p$) interaction. The 3NF inclusion makes it possible to reproduce the data on the nonpolarized $d-p$ interaction and the binding energy of the few-nucleon systems. However, the polarization data are not described even with the 3NF inclusion, that indicates the defects in spin parts of the 3NF. On the other hand, the NN interaction (2NF) itself has also several problems which are connected with relativistic and off-shell effects, non-locality etc. Therefore, the investigation of the polarization observables sensible to the 2NF and 3NF structure in different kinematic conditions for different reaction is very important.

Another goal is to find a suitable reaction to provide efficient polarimetry of high energy deuteron. We suggested to use the $d-p$ elastic scattering at backward angles ($\theta_{c.m.} > 60°$)

for the polarimetry at the energies of $0.88 - 2.0$ GeV. The data at higher energy are necessary for PHe3 project[4] at the LHE(JINR). The experiment has been performed at the Internal Target Station at Nuclotron within the framework of the program on the study of light nuclei spin structure proposed at JINR(Russia) and RIBF(Japan)[5]. The details of the experiment can be found in ref.[6].

2 Results and discussion

The experiment included two groups of the measurements of $d-p$ elastic scattering.
1) Measurement of deuteron beam polarizations at 270 MeV.
2) Measurements at 880-2000 MeV.

Polarization measurement at 270 MeV. The polarization of the deuteron beam was measured at 270 MeV, where high-precision data of the analyzing powers from RIKEN exist [7]. Two particles from the $d-p$ elastic scattering were clearly distinguished by their time-of-flight differences from the target and their energy losses in the plastic scintillators. The background from carbon content of CH_2 target was less than 1% and it was not taken into account.

Obtained values on the vector and tensor polarizations of the deuteron beam are presented in the table1. The values are in good agreement with the results obtained by low energy polarimeter based on $^3He(d,p(0^\circ))^4He$ reactions[8].

	Pol.	Mode 2-6	Mode 3-5
ITS	T	0.557± 0.026	-0.555± 0.022
ITS	V	0.215± 0.012	0.221± 0.015
LEP	T	0.69±0.13	-0.67± 0.16

Table 1: The preliminary values of the deuteron beam polarization at 270 MeV

The measurements at $\mathbf{T_d}$ = 880MeV. To obtain the true number of the deuteron-proton elastic events from all triggers, cut on two-dimensional plot on the correlations ADC signals from deuterons and protons detectors was imposed. Also the graphical cuts were applied on the time-of-flight difference between deuterons and protons from the target. The contribution of the carbon depends on the detection angle.

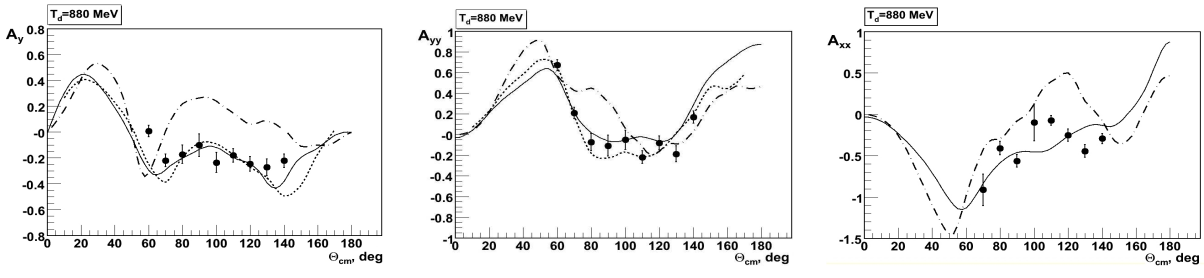

(a) (b) (c)

Figure 1 Vector A_y(a) and tensor A_{yy}(b), A_{xx}(c) analyzing powers for the $d-p$ elastic scattering at 880 MeV. The curves are described in the text.

The obtained values of the vector and tensor analyzing powers in $d-p$ elastic scattering at the energy 880 MeV are presented in Fig1. A_y has relatively large values (-0.25) in the wide angular range $\theta_{c.m.} = 70 - 140^\circ$. A_{yy} has moderately large values at the

angles $\leq 70°$. A_{xx} has a small values at the backward angles. This indicates that the vector and tensor polarizations of the beam can be measured at different angles.

Experimental data obtained at 880 MeV are compared with theoretical predictions in Fig1. Solid curve corresponds to Faddeev calculation using the CD-Bonn NN potential[9]. One can see that the Faddeev calculation reproduces all the analyzing powers.

Dotted curve corresponds to the calculations in optical potential framework with the use of deuteron wave function(DWF), derived from the dressed bag model of Moscow-Tuebingen group[10]. Dash-dotted curve conforms to the calculation in the multiple scattering expansion formalism with the use of CD-Bonn DWF[11]. The parametrization of the NN t-matrix has been used to take the off-shell effects into account.

The amplitude of the dp elastic scattering in these two calculations was presented as a sum of the following three contributions: one nucleon exchange, single scattering and double scattering terms. The relativism was also taken into account.

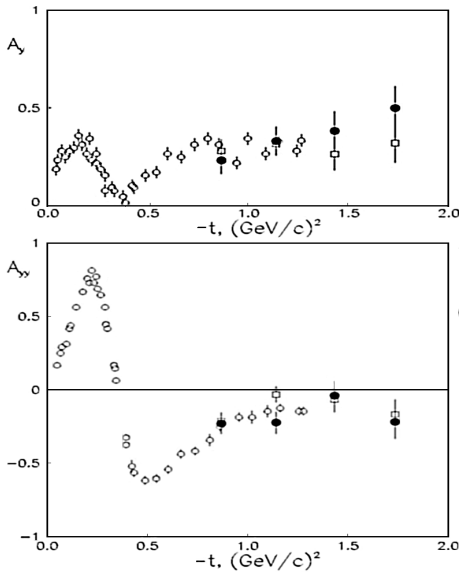

Figure 2. Vector A_y and tensor A_{yy} analyzing power at 2000 MeV. The data shown by the ∘ and •(□) are obtained at ANL[12] and Dubna, respectively.

The calculation[11] describe well the data on the vector A_y and tensor A_{yy} analyzing powers. The calculation[10] reproduces behaviour of the A_y and A_{yy} is described only at the backward angles, while the tensor analyzing power A_{xx} is reproduced in the whole angular range.

The measurements at $\mathbf{T_d = 2000MeV}$. The preliminary results on the measurement of the vector A_y and tensor A_{yy} at the energy 2000 MeV are presented in Fig2. Open circles are the data obtained at Argone National Laboratory[12]. The data obtained at Nuclotron are shown by the black circles and open squares. The points marked by the squares are obtained on the CH_2 target. The black points are obtained as a result of the subtraction of the carbon background. Relatively large values of the analyzing powers show a possibility to provide the polarimetry at this energy.

3 Conclusion.

The experiment on the measurements of the analyzing powers in $d-p$ elastic scattering was performed at the Internal Target Station at Nuclotron in June 2005.

The data on the deuteron analyzing powers A_y, A_{yy} and A_{xx} at the energy of 880 MeV covered angular region of $60-140°$ in the center-of-mass system are obtained.

The obtained data at 880 MeV are compared with different theoretical predictions without inclusion of the 3NF. These calculations describe the obtained data quite good.

Large values of the analyzing powers in some angular region are suitable for conducting the polarimetry at the energy of 880 MeV. These data will be useful to construct a new polarimeter at RIBF.

The preliminary results on the measurements of the vector A_y and tensor A_{yy} analyzing powers at $T_d = 2000$ MeV are presented.

Acknowledgments. The authors are grateful to H.Witala for this calculation. They also would like to express their gratitude to the Nuclotron accelerator staff. We thank Yu. S. Anisimov, A. F. Elishev, Z. P. Kuznezova, A. P. Laricheva, A. G. Litvinenko, V. G. Perevozchikov and V. N. Zhmyrov for the help during the preparation and performance of the experiment. This work was supported in part by the Russian Foundation for Basic Research (grant N^o 07-02-00102a) and by the Grant Agency for Science at the Ministry of Education of the Slovak Republic (grant N^o 1/4010/07).

References

[1] R.B. Wiringa, V.G.J. Stoks, and R. Schiavilla, Rhys. Rev. **C51**, 38 (1995)

[2] R. Machleidt, Phys.Rev. **C63**, 024001 (2001)

[3] V.G.J. Stoks, R.A.M. Klomp, C.P.F. Terheggen, and J.J. de Swart, Rhys. Rev. **C49**, 2950 (1994)

[4] T. Uesaka et al. PHe3 Project (unpublished).

[5] V.P. Ladygin et al. Proc. of the Intern. Workshop "Relativistic Nuclear Physics: from Hunders of MeV to TeV" Varna, Bulgaria, Sept. 10-16, 2001. Dubna, 2001. V.1.P.131.

[6] T. Uesaka, V.P. Ladygin et al. Phys.Part.Nucl.Lett. **3**, 305 (2006)

[7] K. Sekiguchi et al. Phys. Rev. **C65** 034003 (2002)

[8] Yu.K. Pilipenko et al. AIP Conf. Proc. **570**, 801 (2001)

[9] H. Witala et al. private communication

[10] M.A. Shikhalev arXiV:Nucl-th/0612108v1 (2006)

[11] N.B. Ladygina arXiV:Nucl-th/0705.3149v1 (2007)

[12] M. Haji-Saied et al. Phys. Rev. **C36** 2010 (1987)

Discussion

Q. (X.Artru, Inst. de Phys. Nucl. de Lyon) Is there a relation between A_{yy} and A_{zz} and why not measure also A_{zz}?

A. (by V.Ladygin, JINR, Dubna) Yes, there is the relation $A_{xx} + A_{yy} + A_{zz} = 0$. In one set up (for large angle scattering), it is difficult to measure A_{zz}

Q. (N.Piskunov, JINR, Dubna) Are you going to continue the measurements in future?

A. Yes, we are plan to continue the measurement in future, with a new PIS.

SPIN PHYSICS AT NUCLOTRON-M

V.P. Ladygin[1†] on behalf of LHE SPIN group

(1) *Joint Institute for Nuclear Research, Dubna, Moscow region, Russia*
† *E-mail: ladygin@sunhe.jinr.ru*

Abstract

The review of the current status of the polarization experiments at Nuclotron will be reported. New high intensity polarized deuterons ion source as well as the upgade of Nuclotron will extend significantly the spin program at LHE.

The main goal of the polarization program at Nuclotron is to investigate the spin effects in the region of transition regime from nucleon-meson degrees of freedom to the fundamental ones: quarks and gluons, where non-perturbative QCD effects are playing a main role.

The main topics of the research program at Nuclotron are the studies of manifestation of the effective degrees of freedom like $\Delta\Delta$, NN^*, N^*N^* configurations connected with the problem of hidden color in the light nuclei; threshold effects in neutral meson-production in polarized nucleon-nucleon interaction; relativistic effects in the composite systems; medium effects for the polarization observables connected with the problem χ-symmetry restoration.

The availability of the relativistic polarized deuterons from POLARIS source [1] and consequently polarized nucleons from deuteron breakup provides the uniqness of the spin program at LHE.

On of the traditinal topics of these studies is the deuteron short range spin structure. Such static properties of the deuteron as a binding energy ϵ, quadrupole, Q_d, and magnetic, μ_d, momenta, electromagnetic radius r_d are very well measured and are reproduced by the non-relativistic calculations using standard nucleon-nucleon potentials based on one-bosons exchange.

The non-relativistic deuteron wave function (DWF), obtained by the solving of the Schrödinger equation, depends on the relative nucleon momentum $\mathbf{q}$ only: $\Psi = \Psi(\mathbf{q})$. However, as the deuteron and its nucleons energies increase, the relativistic effects play more important role at short internucleonic distances, as well as in the dynamics of the interaction.

The principal feature of the relativistic quantum mechanics is the impossibility to separate the relative motion of the constituents and motion of the composite system as a whole. This leads to the dependence of the relativistic wave function not only on the relative momenta of the nucleons $\mathbf{q}$ inside the composite system, but also on the total momentum $\mathbf{p}$ of this system: $\Psi = \Psi(\mathbf{q}, \mathbf{p})$. Therefore, relativistic wave function is the function of the relative momentum $\mathbf{q}$ in each new reference system. However, it is enough to know wave function in the infinite momentum frame, $\mathbf{p} \to \inf$, where the structure of the wave function simplifies. Namely, the dependence on $|\mathbf{p}|$ disappears, wave function depends on the direction of the vector $\mathbf{n} = \mathbf{p}/|\mathbf{p}|$ only: $\Psi = \Psi(\mathbf{q}, \mathbf{n})$.

For instance, relativistic deuteron wave function on light cone is defined by 6 invariant functions $f_1, ..., f_6$ (instead of 2 in the non-relativistic case), each of them depends on 2 scalar variables $\mathbf{k}$ and $z = cos(\widehat{\mathbf{kn}})$ [2]:

$$\psi(\mathbf{k},\,\mathbf{n}) = \frac{1}{\sqrt{2}}\sigma f_1 + \frac{1}{2}\left[\frac{3}{k^2}\mathbf{k}(\mathbf{k}\cdot\sigma) - \sigma\right] f_2 + \frac{1}{2}\left[3\mathbf{n}(\mathbf{n}\cdot\sigma) - \sigma\right] f_3 + \frac{1}{2k}[3\mathbf{k}(\mathbf{n}\cdot\sigma) + 3\mathbf{n}(\mathbf{k}\cdot\sigma) - 2\sigma(\mathbf{k}\cdot\mathbf{n})] f_4 + \sqrt{\frac{3}{2}}\frac{i}{k}[\mathbf{k}\times\mathbf{n}] f_5 + \frac{\sqrt{3}}{2k}[[\mathbf{k}\times\mathbf{n}]\times\sigma] f_6, \quad (1)$$

$$k = \sqrt{\frac{m_p^2 + \mathbf{p}_T^2}{4\alpha(1-\alpha)} - m_p^2}, \qquad (\mathbf{n}\cdot\mathbf{k}) = (\frac{1}{2} - \alpha)\cdot\sqrt{\frac{m_p^2 + \mathbf{p}_T^2}{\alpha(1-\alpha)}}. \quad (2)$$

Here α is the longitudinal momentum fraction taken away by the proton in the infinite momentum frame and p_T is the proton transverse momentum.

Therefore, to study the relativistic effects in light nuclei one needs to measure the polarization observables as the functions of α and p_T (or as the functions of the initial energy and scattering angle for the binary reactions). When the distances between the nucleons are comparable with the size of the nucleon, the nucleon-nucleon interaction is non-local. The modern NN potentials like CD-Bonn [3] take into account this property of NN interaction at short distances.

However, fundamental degrees of freedom in the frame of QCD are the quarks and gluons. These degrees (effective ones as $\Delta\Delta$, N^*N, N^*N^* or $6q$ and $9q$ components) begin to play a role at the internucleonic distances comparable with the size of the nucleon. At high energies s and large transverse momenta p_T the constituent counting rules (CCR) [4, 5] are working. These rules predict the dependence of the cross section of the binary reactions at the fixed scattering angle in the cms as a power-law of s.

The analysis of the experimental data on the cross sections of the $dp \to pd$ and $dd \to {}^3\mathrm{He}n$ reactions [17] has shown that the regime corresponding to CCR can occur already at $T_d \sim$500 MeV. During last several years a new generation of NN potentials are built (Nijmegen, CD-Bonn, AV-18 etc.). These potentials reproduced the NN scattering data up to 350 MeV with very good accuracy. But these potentials cannot reproduce triton binding energy (underbinding is 0.8 MeV for CD-Bonn), deuteron-proton scattering and breakup data.

Incorporation of three nucleon forces (3NF), when the interaction depends on the quantum numbers of the all three nucleons, allows to reproduce triton binding energy and unpolarized deuteron-proton scattering and breakup data (see [7] and references therein). However, the use of different 3NF models in Faddeev calculations cannot reproduce polarization data intensively accumulated during last decade at different facilities. New data sensitive to the spin structure of ^{3}He(^{3}H) and 3NF are necessary to build adequate model of 3NF.

Two selected results on the deuteron and NN spin structure obtained in the recent years at Synchrophasotron demonstrate the importance of a GeV range studies.

First experiment has been performed with a polarized deuteron beam at the SPHERE setup [20]. A slowly extracted polarized deuteron beam with a typical intensity of $\sim 5\cdot10^8 \div 10^9$ $\boldsymbol{d}$/spill provided by POLARIS [1] was directed onto a liquid hydrogen target 30 cm long or onto nuclear (carbon and beryllium) targets with a varying length. Separation

of the protons and inelastically scattered deuterons was achieved by the measurements of their time-of-flight (TOF) over a base line of ~ 34 or ~ 28 m.

The data on the tensor analyzing power A_{yy} in deuteron inclusive breakup obtained at different energies can be compared in terms of internal variables describing the internal structure of the deuteron. The A_{yy} data plotted versus the transverse momentum of the proton at values of the longitudinal momentum fraction $\alpha \sim 0.61$, ~ 0.67, ~ 0.72 and ~ 0.78 are shown in Fig.1. a), b), c) and d) , respectively. The data obtained on hydrogen and carbon targets are shown by the filled and open circles, respectively. The values of A_{yy} are positive at small p_T and monotonously decrease while transverse momentum increasing for all α values changing the sign at $p_T \sim 600$ MeV/c independently on the value of α. This behavior definitely contradicts the predictions of the relativistic hard scattering (RHS) model using either standard DWFs depending on one variable only shown in Fig.1. by the dashed and dash-dotted lines, or relativistic DWF [2] depending on two variables (solid lines).

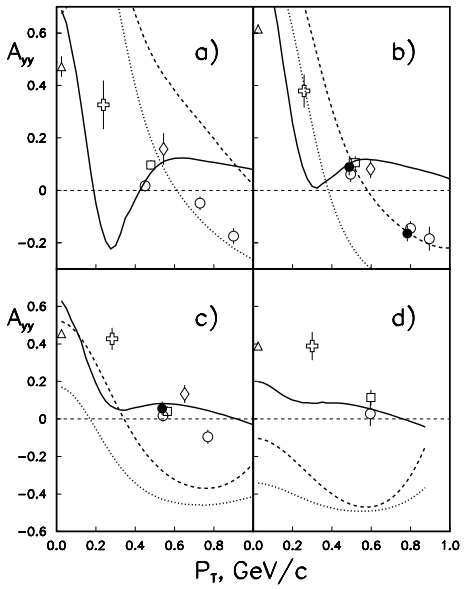

Figure 1. A_{yy} in $A(d,p)X$ reaction as a function of p_T at the fixed values of α: a) $\alpha \sim$0.61, b) $\alpha \sim$0.67, c) $\alpha \sim$0.72 and d) $\alpha \sim$0.78. The figure is taken from the paper [20].

The observed features of the A_{yy} data, namely, the marked dependence of A_{yy} plotted at fixed values of the longitudinal momentum fraction α on the transverse momentum p_T, clearly demonstrate that an adequate description of the data may be achieved by using a deuteron structure function that depends on more than one variable for $\alpha \geq$0.6. The precision of the data put the serious constraints on the theoretical approaches in the description of the deuteron short range spin structure.

The second advantage of the Synchrophasotron-Nuclotron due to deuteron is the possibility to form the relativistic quasi-monochromatic neutron beam because the data on np interaction at the energies higher than 1.1 GeV are practically absent.

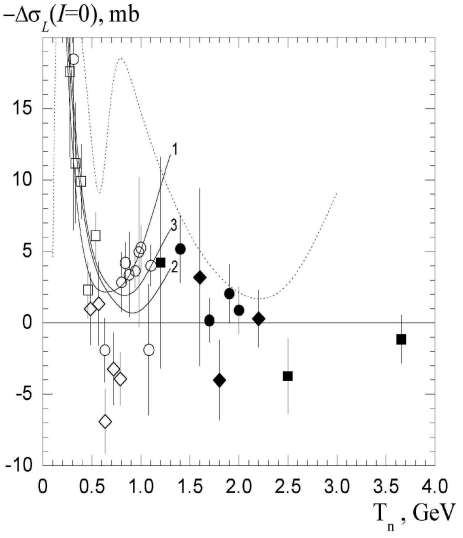

Figure 2. The cross section difference $\Delta\sigma_L$ for an isospin $I = 0$ plotted versus the neutron energy. Black points are the results obtained in Dubna. Figure is taken from the paper [9].

Such neutron beam channel for the energies 0.55-3.7 GeV equipped by the polarized proton, liquid and nuclear targets has been created. Neutrons are obtained from deuteron breakup on the nuclear target. The momentum spread of neutrons is about 3% only with the typical intensity of $3{\cdot}10^5$– $\cdot 10^6$ depending on energy.

The importance of the use of neutrons is the possibility to extract the amplitudes of nucleon-nucleon scattering with an isospin $I = 0$. The results on the cross section differ-

ence $\Delta\sigma_L(I=0)$ due to longitudinal polarization of the colliding nucleons is presented in Fig.2.

The black points are obtained in Dubna by $\Delta\sigma$-collaboration [9]. One can see the significant variation of $\Delta\sigma_L(I=0)$ versus the initial energy and some structure around T_n ~0.5–1.0 GeV. The authors claim that the obtained results are sensitive to the dibaryon production predicted in bag models.

To summarize the introduction: LHE spin complex is the unique facility to study relativistic effects, non-nucleonic degrees of freedom, three-nucleon forces energy dependence via the measurements of spin observables in a GeV range.

The current LHE spin program is focused on the study of the spin structure of few-nucleon systems, on the spin structure of nucleon-nucleon interaction, on the spin effects in meson production and development of the polarization techniques. Also there are several postponed experiments which can be done with high intensity polarized beam in future.

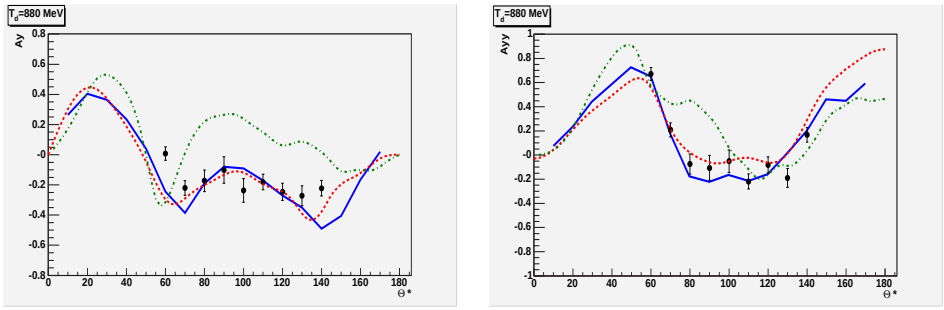

(a) (b)

Figure 3. Vector A_y (a) and tensor A_{yy} (b) analyzing powers in *dp*- elastic scattering at 880 MeV versus angle in the cms. Curves are explained in the text. Figures are taken from the talk of P.K.Kurilkin at this conference [11].

Due to relatively low intensity of the deuteron polarized beam at Nuclotron (~2–3·10^7 ppp) spin physics at the moment is limited. On the one hand, the use of the internal target allows to use the full available intensity. On the other hand, new internal target station is very well suited for the measurements of *dp*- elastic scattering at large angles in the cms. The experiment on the study of the energy dependence of the $3NF$ spin structure via the measurements of the analyzing powers in *dp*-elastic scattering has been proposed [10].

The results on the vector A_y and tensor A_{yy} analyzing powers in *dp*- elastic scattering obtained at 880 MeV [11] are shown in Figs.3a and 3b, respectively. The solid, dashed and dotted lines are the results of the relativistic multiple scattering calculations [12] using CD-Bonn DWF, of the Faddeev calculations [21] using CD-Bonn nucleon-nucleon potential and the optical potential calculation with the dibaryon DWF [14], respectively. One can see that Faddeev and multiple scattering models give good description of the data. However, the Faddeev calculations [21] fail to reproduce the cross section at the angles larger than 90°, while relativistic multiple scattering calculations [12] are in a reasonable agreement with the data at the angles between 30° and 130°.

The dependence of the tensor analyzing power A_{yy} in dp- elastic scattering obtained at 60°, 70°, 80° and 90° in cms versus transverse momentum p_T is shown in Fig.4. The open points are the world data [15], while the black ones represent the results obtained at Nuclotron [11, 16]. The values of A_{yy} are positive at small p_T and changes the sign at p_T ∼600–650 MeV/c as in the case of deuteron inclusive breakup [20]. The negative sign of A_{yy} is observed at large p_T. It would be interesting to extend the range of the measurements to larger p_T, where the manifestation of non-nucleonic degrees of freedom is expected.

Other experiments at Nuclotron at the moment use unpolarized beams.

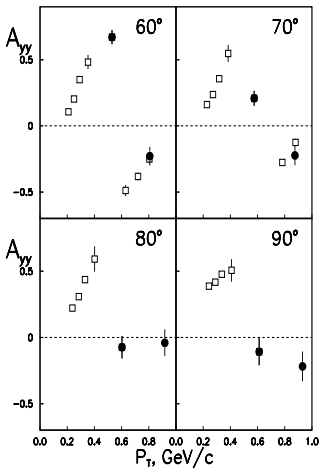

Figure 4. A_{yy} in dp- elastic scattering obtained at the fixed angles in the cms: 60°, 70°, 80° and 90°.

TPD project is devoted to the tensor polarizability of the deuteron passing through the matter. The value of the induced tensor polarization should depend on the thickness of the target. The first data have been obtained using unpolarized 5.5 GeV/c deuteron beam in March 2007 [17]. The induced tensor polarization has been measured by the beam-line tensor polarimeter described elsewhere [18].

The preliminary results [17] demonstrate the increase of the value of the tensor polarization of the secondary deuteron beam as the target length increase. One of the explanation of this effect is the multiple scattering and the effect of the D- state in the deuteron. The experiment is planned to be continue in 2007-2008.

The results on the ratio of the cross sections of neutron-proton charge-exchange reaction, (n, p), on deuteron and proton R_{dp} as a function of neutron kinetic energy is shown in Fig.5. The full points are the results obtained by $\Delta\sigma$ collaboration at Nuclotron [19, 20]. In the framework of plane wave impulse approximation this ratio is defined by the ratio of spin-dependent to spin-independent parts of np- backward elastic scattering amplitude. In this respect, R_{dp} is an additional observable to the total cross section σ_{tot}, total cross section differences $\Delta\sigma_L$ and $\Delta\sigma_T$ in np- forward elastic scattering and spin correlations A_{oonn} and A_{ookk} in np- backward elastic scattering necessary for the full determination of the np- forward elastic scattering matrix element.

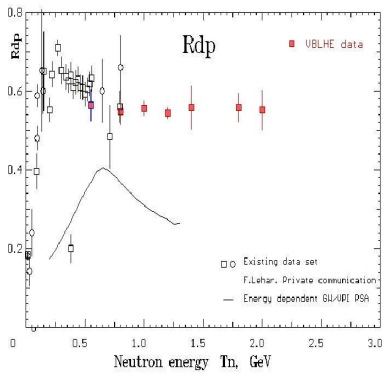

Figure 5. R_{dp} ratio of the (n, p) charge-exchange reactions on deuteron and proton. Figure is taken from the talk of V.I.Sharov at this conference [20].

The data obtained at Nuclotron [19, 20] demonstrate the large value of R_{dp} close to $\sim 2/3$. This reflects the significance of the spin-dependent part of the np- elastic scattering amplitude at the energies 0.5-2.0 GeV. On the other hand, such a behavior at the energies 0.5–1.3 GeV contradicts to the results of current partial wave analysis given in Fig.5 by the solid line. The additional considering of the final state interaction (FSI) in the system of two undetected neutrons does not improve the agreement with the data [21].

The same process in the exclusive mode is planned for the studies by the $STRELA$ collaboration [22]. The dp- charge exchange reaction will be investigated via the detection of two outgoing protons emitted at the angles less than 3° with relative momentum less than 100 MeV/c in the lab. The detected protons have a momentum close to the half of the incoming deuteron momentum. The detection system is almost ready. The achieved position resolution provided by the set of drift chambers is better tham 100μm. The collaboration is planning to measure both cross section and tensor analyzing power T_{20} in 2008-2009. The results on T_{20} are sensitive to the ratio of the spin-dependent to spin-independent parts of the np- backward elastic scattering amplitude in spite of large FSI effects [23].

All the above experiments are devoted to the study of the spin structure of $2N$ and $3N$ forces at the nucleon energies 0.5–1.0 GeV, where some years ago a signature in the T_{20} behavior in dp- backward elastic scattering have been observed [24].

The measurements of the η- meson yield in polarized NN collisions using transversally polarized neutron beam and proton target is planned within $DELTA-2$ experiment [25]. Due to $s\bar{s}$ component in η- meson wave function, the spin correlation $C_{y,y}$ in the $\boldsymbol{np}$ reaction is expected to be sensitive to the polarized strange content of the proton. The detection of π°- and η- mesons will be done by 300 channel lead-glass spectrometer via 2γ decay modes. The collaboration is now in the state of the setup preparation.

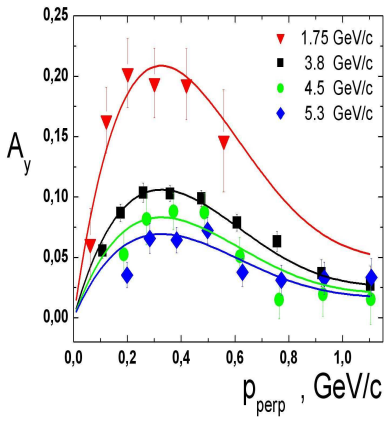

Figure 6. Analyzing power for inclusive $\boldsymbol{p}CH_2 \to pX$ at the proton momenta between 1.75 and 5.3 GeV/c. Figure is taken from the paper [26].

The main goal of $ALPOM$ project [26] is to obtain the analyzing powers for inclusive $\boldsymbol{p}CH_2 \to pX$ reaction at high momenta. These data are very important to construct the efficient focal-plane proton polarimeter at JLAB for the measurements of elastic electromagnetic form-factor ratio G_{E_p}/G_{M_p} at large Q^2 [27] and at hadronic facilities too. The data on the analyzing power in inclusive $\boldsymbol{p}CH_2 \to pX$ reaction at the momenta between 1.75 and 5.3 GeV/c [26] obtained at Synchrophasotron using polarized protons from deuteron breakup are shown in Fig.6. The continuation of the experiment is planned at Nuclotron in 2009-2010.

The development of new polarized source is necessary to fulfill the current experimental program. This source on the base of IUCF source will provide the intensity up to 10^{10} ppp and larger values of polarization than POLARIS. The first operation of this source is scheduled in 2010 [28]. At the same time it is necessary to make an upgrade of the existing polarized proton target in order to have the proton polarization normal to the beam direction. Upgraded PPT will put into operation also in 2010 [28]. Unpolarized beams and polarized deuterons from POLARIS [1] will be used in 2007-2009 for realization of short-term program. The main items of the long-term studies (after 2009) at Nuclotron-M with new PIS and PPT are the following: spin structure of $2N$ and $3N$ forces (relativity, transition regime to non-nucleonic degrees of freedom etc.); polarization effects in meson production related with the spin crisis; medium effects for polarization observables, development of polarization techniques for other facilities including NICA.

According to JINR topical researh plan [29] it is planned to construct new heavy ion and polarized particles collider NICA for the energies $\sqrt{s_{NN}}$=4–9 GeV. The serious advantage of NICA compared to AGS, J-PARC and U-70 will be the possibility to have the collisions of polarized deuterons (neutrons). The main topics of the spin studies at NICA can be spin content of nucleon, nuclear and color transparency in spin observables, polarization effects in hyperon production, single and double asymmetries in meson production, NN and deuteron short-range spin structure.

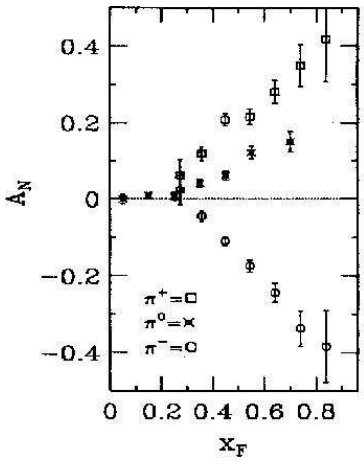

Figure 7. Single spin asymmetry A_N for inclusive pion production in pp- collisions at 200 GeV. Figure is taken from the paper [30].

Fig.7 demonstrates the single spin asymmetries (SSA) A_N obtained in proton-proton collision for π^+, π° and π^- inclusive production at 200 GeV [30]. The signs of SSA follow to the polarization of the valence quarks in the pions. The perturbative QCD regime occurs already at 22 GeV [31], where SSA is found to be sensitive to the quark content of projectile. In this case SSA has to change the sign for neutron-proton collision at large x_F. Single and double spin asymmetries for charged mesons production in neutron-proton collisions can be measured at NICA using polarized deuterons. Neutrons will be produced from deuteron breakup with spectator proton identification. The same motivation and method of measurements are also valid for studies polarization, A_N and D_{NN} for Λ° and Ξ^- production [5]. Unfortunately, the main detector of NICA - MPD will be able to detect the charged particles only and will have poor identification at large x_F, where spin effects are large.

Another topic is the study of the nucleon spin content in Drell-Yan process [33]. Sivers effect having an opposite sign in SIDIS can be studied in by the measurement of SSA. Transversity measurements can be done in the collisions of both transversally polarized nucleons A_{TT}. The double longitudinal asymmetry A_{LL} at NICA energies is related mostly to the quark polarization. Polarized $\boldsymbol{Nd}$ Drell-Yan process can provide the information on the tensor structure of the deuteron [34].

The short-range deuteron spin structure in (d,p) reactions [20], charmonium production in polarized nucleons collisions [35], nuclear and color transparencies [36,37] also can be studied at NICA energies.

For these purposes it is necessary to build the double-arms wide apperture spectrometer at the second interaction point at NICA. This spectrometer has to detect and identify both leptons and hadrons.

-The current spin program at Nuclotron-M brings new insight on the spin effects in the region of nonperturbative QCD, where the transition from nucleon-meson degrees of freedom to the quark-gluon ones occurs.

-The putting into operation new PIS and upgrade of the existing PPT will significantly increase the potentialities of Nuclotron-M as a spin facility in a GeV range. These developments are also the key point for NICA.

-The development of the setup with the possibility to detect both hadrons and leptons at the NICA is necessary to have rich spin physics complimentary to the studies proposed at U-70, J-PARC and FAIR.

Author thanks the members of LHE SPIN-group L.S.Azhgirey, V.V.Glagolev, V.V.Fimushkin, V.A.Krasnov, P.K.Kurilkin, A.N.Livanov, A.A.Morozov, N.M.Piskunov, E.B.Plekhanov, V.I.Sharov, S.S.Shimansky, L.S.Strunov, R.A.Shindin and L.S.Zolin for support and providing of the matherials for this talk. The discussions with N.B.Ladygina, M.A.Shikhalev and H.Witala were helpful for the preparation of this report. This work has been supported in part by the Russian Foundation for Fundamental Research (under grant N^o07-02-00102a).

References

[1] N.G. Anishchenko et al., AIP Conf.Proc. **95**, 445 (1983).

[2] V.A. Karmanov, A.V. Smirnov, Nucl.Phys.A **546**, 691 (1992); Nucl.Phys.A **575**, 520 (1994); J. Carbonell, V.A. Karmanov, Nucl.Phys.A **581**, 625 (1995); Nucl.Phys.A **589**, 713 (1995); J. Carbonell, B. Desplanques, V.A. Karmanov, J.F. Mathiot, Phys.Rep. **300**, 125 (1998).

[3] R. Machleidt, Phys. Rev.C **63**, 024001 (2001).

[4] S.J. Brodsky, G.R. Farrar, Phys.Rev.Lett. **31**, 1153 (1973); Phys.Rev.D **11**, 1309 (1975); G.P. Lepage, S.J. Brodsky, Phys.Rev.D **22**, 2157 (1980).

[5] V.A. Matveev, R.M. Muradyan, A.N. Tavkhelidze, Lett. Nuovo Cim. **7**, 719 (1973).

[6] Yu.N. Uzikov, JETP. Lett. **81**, 3031 (2005).

[7] W. Glöckle, H. Witala, D. Hüber, H. Kamada, J. Golak, Phys.Rep. **274**, 107 (1996).

[8] S.V. Afanasiev et al., Phys.Lett.B **434**, 21 (1998); L.S.Azhgirey et al., Yad.Fiz. **62**, 1796 (1999); Yad.Fiz.**66**, 719 (2003); Yad.Fiz. **68**, 2191 (2005); Phys.Lett.B **595**, 151 (2004); V.P.Ladygin et al., Few-Body Systems **32**, 127 (2002); Phys.Lett.B **629**, 60 (2005). L.S.Azhgirey et al., Yad. Fiz. **66** (2003) 719.

[9] B.P.Adiasevich et al., Z.Phys.C **71**, 65 (1996); V.I.Sharov et al., Eur.Phys.J.C **13**, 255 (2000); Eur.Phys.J.C **37**, 79 (2004); Yad.Fiz.**68**, 1858 (2005).

[10] T. Uesaka et al., Phys.Part.Nucl.Lett.**3**, 305 (2006).

[11] P.K.Kurilkin et al., talk at this conference.

[12] N.B.Ladygina, arXiv:0705.3149 [nucl-th], submitted to Yad.Fiz.

[13] H.Witala, private communication.

[14] M.A.Shikhalev, arXiv:0710.4040 [nucl-th], submitted to Yad.Fiz.

[15] K.Sekiguchi et al., Phys.Rev.C **70**, 014001 (2004); M.Bleszynski et al., Phys.Lett.B **87**, 178 (1979); Phys.Lett.B **106**, 42 (1981); M. Haji-Saied et al., Phys.Rev.C **36** 2010 (1987); M.Garson et al., Nucl.Phys.A **458**, 287 (1986).

[16] V.P.Ladygin et al., Czech.J.Phys.**56**, F135 (2006).

[17] L.S.Azhgirey et al., talk at this conference.

[18] L.S.Zolin et al., JINR Rapid Comm. **2[88]-98**, 27 (1998).

[19] V.I.Sharov et al., Czech.J.Phys.**56**, F117 (2006).

[20] V.I.Sharov et al., talk at this conference.

[21] N.B.Ladygina, arXiv:0704.2653 [nucl-th], Yad.Fiz. (2007) in press.

[22] V.V.Glagolev, G.Martinsky, N.M.Piskunov et al., STRELA experiment, unpublished.

[23] N.B.Ladygina, A.V.Shebeko, Eur.Phys.J.A **22**, 29 (2004).

[24] V.Punjabi et al., Phys.Lett.B **350**, 178 (1995).
[25] V.A.Krasnov et al., DELTA-2 experiment, unpublished.
[26] L.S.Azhgirey et al., Nucl.Instrum.Meth.A **538**, 431 (2005).
[27] M.K.Jones et al., Phys.Rev.Lett.**84**, 1398 (2000); O.Gayou et al., Phys.Rev.C **64**,038202 (2001); Phys.Rev.Lett. **88**, 092301 (2002).
[28] V.D.Kekelidze, talk at JINR-PAC Meeting, 28-29 June (2007), Dubna.
[29] A.N.Sisakian, A.S.Sorin, A.D.Kovalenko, Topical plan for JINR research and international cooperation in 2007, 02-0-1065-2007/2009.
[30] D.L.Adams et al., Phys.Lett.B **261**, 201 (1991); Phys.Lett.B **264**, 462 (1991).
[31] C.E.Allgower et al., Phys.Rev.D **65**, 092008 (2002).
[32] A.Bravar et al., Phys.Rev.Lett.**75**, 3073 (1995); Phys.Rev.Lett.**78**, 4003 (1997).
[33] A.V.Efremov et al., Czech.J.Phys.**56**, F181 (2006) and references therein.
[34] M.Hino, S.Kumano, Phys.Rev.D **59**, 094026 (1999); Phys.Rev.D **60**, 054018 (1999); S.Kumano, M.Miyama, Phys. Lett.B **497**, 149 (2000).
[35] A.N.Vasiliev et al., talk at this conference.
[36] A.S.Carroll et al., Phys.Rev.Lett.**61**, 1698 (1988).
[37] S.S.Shimansky, talk at this conference.

Discussion

Comm. (S.Belostotsky, PNPI, S.Petersburg) The idea to build this new NICA machine looks promising. It is clear, however that in addition to efforts and enthusiasm of Dubna people a wide support from the spin-physics community with be highly required. Such contributions from the leading physicists would be thus so much welcome.

Comm. (G.Bunce, BNL) It is very interesting to study A_N for π and K production with both polarized proton and neutron beams. Although the cross section are described by peace at RHLC, they are not described well at lower energy (see Soffer talk). However, the spin asymmetries look very similar at lower energies to the results at RHIC. If the A_N for π^+ and π^- show minor asymmetry for polarized p and n, with the signs of A_N reversing for p and n beams, this is strong evidence that the physics is due to valence quarks, even at lower energy.

Q. (J.Nassalski, SINS, Warsaw) What is the main physics justification for NICA, in view of already approved new projects (FAIR, J-PARC)?

A. Certainly, the advantage of NICA in the sense of spin physics is the availability of polarized deuterons and, therefore, polarized neutrons. The second advantage is that in the collider mode, the momenta of the secondary particles can be measured with good momentum resolution, as well as focal plane polarimetry is possible. The last items, are very important to study spin structure of deuteron and color nuclear transparency.

RESULTS OF THE MEASUREMENT OF THE CROSS-SECTION RATIO $R_{\rm dp}(0)$ IN CHARGE-EXCHANGE (np) REACTIONS ON H_2/D_2 at 0° AND $T_n = 1; 1.2$ GeV

A.A. Morozov[1†], V. G. Antonenko[2], S. B. Borzakov[6], Yu. T. Borzunov[1], E. V. Chernykh[1], V. F. Chumakov[1], S. A. Dolgii[1], M. Finger[3,7], M. Finger, Jr.[3], L. B. Golovanov[1], A. Janata[3], A. D. Kirillov[1], A. D. Kovalenko[1], V. A. Krasnov[1,8], N. A. Kuzmin[11], F. Lehar[9], A. N. Livanov[1,8], P. K. Maniakov[1], E. A. Matyushevsky[1], G. P. Nikolaevsky[1], A. A. Nomofilov[1], Tz. Panteleev[6,10], I. L. Pisarev[3], Yu. P. Polunin[2], A. N. Prokofiev[4], V. Yu. Prytkov[1], P. A. Rukoyatkin[1], V. I. Sharov[1], R. A. Shindin[1], M. Slunečka[3,7], V. Slunečková[3], A. Yu. Starikov[1], L. N. Strunov[1], E. I. Vorobiev[1], I. P. Yudin[11], I. V. Zaitsev[1], A. A. Zhdanov[4], V. N. Zhmyrov[3]

(1) *JINR, Veksler and Baldin Laboratory of High Energies, 141980 Dubna, Russia.* (2) *Russian Scientific Center "Kurchatov Institute", 123182 Moscow, Russia.* (3) *JINR, Dzhelepov Laboratory of Nuclear Problems, 141980 Dubna, Russia.* (4) *St.Petersburg Nuclear Physics Institute, High Energy Physics Division, 188350 Gatchina, Russia.* (5) *Kharkov Institute of Physics and Technology, 310108 Kharkov, Ukraine.* (6) *JINR, Frank Laboratory of Neutron Physics, 141980 Dubna, Russia.* (7) *Charles University, Faculty of Mathematics and Physics, V Holešovičkách 2, 180 00 Praha 8, Czech Republic.* (8) *Institute for Nuclear Research, Russian Academy of Sciences, 117312 Moscow, Russia.* (9) *DAPNIA, CEA/Saclay, 91191 Gif-sur-Yvette Cedex, France.* (10) *Institute for Nuclear Research and Nuclear Energy, Bulgarian Academy of Sciences, Tsarigradsko shaussee boulevard 72, 1784 Sofia, Bulgaria.* (11) *JINR, Laboratory of Particle Physics, 141980 Dubna, Russia.*
† *E-mail: morozov@sunhe.jinr.ru*

Abstract

The results of the measurement at 0° of the cross-section ratio $R_{\rm dp}$ in charge-exchange (np) reaction on H_2/D_2 targets at the neutron beam kinetic energie 1.0 GeV and 1.2 GeV are presented.

The tasks of the Delta-sigma experiment investigation program [1] are the measurements of the **L**, **T** set of *np* spin observables $\Delta\sigma_{\rm L}$, $\Delta\sigma_{\rm T}$, A_{00kk}, A_{00nn} as well as the measurement of backward *np* scattering (elastic $np \to pn$ charge-exchange reaction using D_2 and H_2 targets at 0°) with the spin-flip (the data for D_2 target) and with the non spin-flip (measurement of the cross sections ratio $R_{\rm dp}(0) = \frac{d\sigma}{d\Omega}(nd \to pnn)/\frac{d\sigma}{d\Omega}(np \to pn)$). The results obtained in the course of the experiments [2, 3] allow to follow reliably $\Delta\sigma_{\rm L}$ energy dependence peculiarities in the new energy region. One can see here a fast decrease of $|\Delta\sigma_{\rm L}|$ while the energy increases beyond 1.1 GeV and the anomaly of energy dependence in the vicinity of 1.8 Gev with a suggested minimum, which is predicted by Lomon et al. [4] in "Cloudy bag model" as the lowest lying exotic six-quark configuration in the isosinglet and the spin-triplet state $^3S_1$ with the mass M = 2.63 GeV.

For the exhaustive analysis of this structure using Argand diagrams for Re and Im parts of each of the three NN forward scattering amplitudes, it is required to measure not

only the complete set of np-spin observables at $0\,^\circ$ ($\Delta\sigma_{\rm L,T}$ and spin correlation coefficients A_{00kk} and A_{00nn} in $np \to pn$ charge exchange of L/T polarized neutrons), but also to measure at $0\,^\circ$ the ratio $R_{\rm dp}$ in the same energy region.

The ratio $R_{\rm dp} = \frac{d\sigma}{d\Omega}(nd \to pnn)/\frac{d\sigma}{d\Omega}(np \to pn)$ independently defines the ratio R^{ID} of non spin-flip to spin-flip contributions in $np \to pn$ charge-exchange process at $0\,^\circ$.

The $np \to pn$ differential cross section $(d\sigma/d\Omega)_{np}$ can be splitted in the "spin-independent" (SI) and "spin-dependent" (SD) parts [5,6]:

$$(d\sigma/d\Omega)_{np} = (d\sigma/d\Omega)^{SI}_{np} + (d\sigma/d\Omega)^{SD}_{np}. \qquad (1)$$

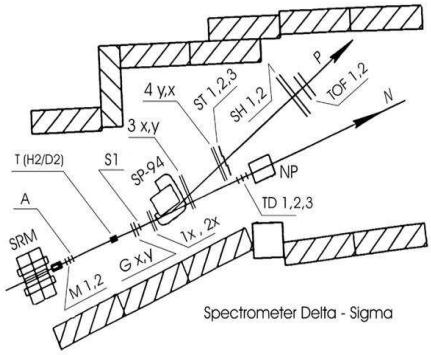

Figure 1. Spectrometer "Delta-Sigma"

The differential cross section for $nd \to p(nn)$ reaction in the frame of the impulse approximation can be written as:

$$(d\sigma/d\Omega)_{nd} = [1-F](d\sigma/d\Omega)^{SI}_{np} + [1-(1/3)F](d\sigma/d\Omega)^{SD}_{np}. \qquad (2)$$

Here F is the deuteron form-factor, which is equal to one in the backward direction. The first term on the right-hand side of (2) vanish and for the differential cross section at $\theta_{CM} = \pi$ the theory gives:

$$(d\sigma/d\Omega)_{nd} = (2/3)(d\sigma/d\Omega)^{SD}_{np}. \qquad (3)$$

Only if the impulse approximation holds, Eqs.(2) and (3) are valid. From (3) follows:

$$R_{dp} = \frac{(d\sigma/d\Omega)_{nd}}{(d\sigma/d\Omega)_{np}} = \frac{2}{3} \times \frac{(d\sigma/d\Omega)^{SD}_{np}}{(d\sigma/d\Omega)_{np}} = \frac{2}{3} \times \frac{1}{(1+R^{ID})}. \qquad (4)$$

where $R^{ID} = \frac{(d\sigma/d\Omega)^{SI}_{np}}{(d\sigma/d\Omega)^{SD}_{np}}$ — the ratio of the spin-independent contribution to the spin-dependent one in $np \to pn$ charge exchange reaction.

1. Investigation of elastic $np \to pn$ charge exchange process. To detect protons from charge-exchange reactions in our experiments magnetic spectrometer (Fig. 1) was created.The spectrometer is equipped with a system of tracking of charged particles emitted from the target at 0–$2\,^\circ$ angle range. This system provides a good momentum resolution of the spectrometer $\Delta p/p \approx 1.65\,\%$ (more than 2 times better compared with the momentum dispersion of the quasimonochromatic neutron beam produced by stripping of deuterons slow extracted from Nuclotron) and makes it possible to determine the angles of charge-exchange proton tracks with a good accuracy ($\approx 1\,$mrad). The system comprises a deflection magnet SP-94, 8 planes of X, Y coordinates detectors (multiwire proportional chambers Gx, Gy, 1x, 2x, 3x, 3y, 4x, 4y) placed in front of and behind the magnet, neutron monitors (M1,2), trigger scintillation counters: anticoincidence counter (A), S 1, ST 1, 2, 3; liquid H_2/D_2 targets, time-of-flight system counters separating protons and background deuterons from $np \to d\pi^0$ reaction (S1, TOF 1, 2).

To obtain the momentum spectra protons using H_2 and D_2 targets at the neutron beam energy 1 GeV (Fig. 2) and 1.2 GeV the charge particles deflection angles in spectrometer magnet SP-94 were measured.

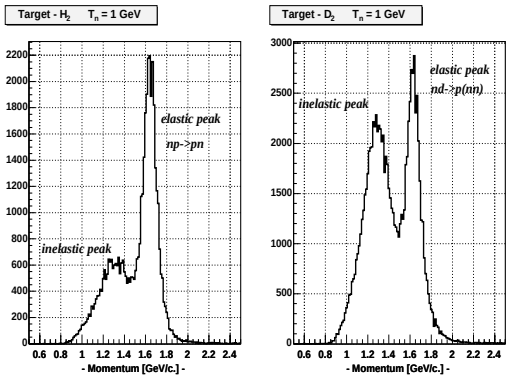

Figure 2. The momentum spectra of charged secondaries, detected by spectrometer using H_2 and D_2 liquid targets.

The inelastic peak grows fast when the energy T_n arises. This background 'hill' grows especially fast in np charge-exchange at deuteron. The main contribution to this background peak is due to the binary reaction with excitation of Δ^0-resonance. The $np \to pn$ charge-exchange process is accompanied by the background reaction $np \to d\pi^0$. Owing to this reaction kinematics the background deuterons are concentrated under the elastic proton peaks in the $np \to pn$ charge exchange reaction. The time-of-flight of the particles was measured to suppress this background. Fig. 3 show a good separation of particles d and p.

The reaction yield in the angular regions $0 < \theta < 0.012$ rad and $0 < \phi < 2\pi$ rad was analyzed to calculate the differential cross-section of $np \to pn$ elastic charge-exchange reactions at $0\,^\circ$. After the subtraction of the deuteron background in the reaction $np \to d\pi^0$ and the dummy target background the observed elastic peak was approximated by Gauss function, and the number of events in the peak was calculated.

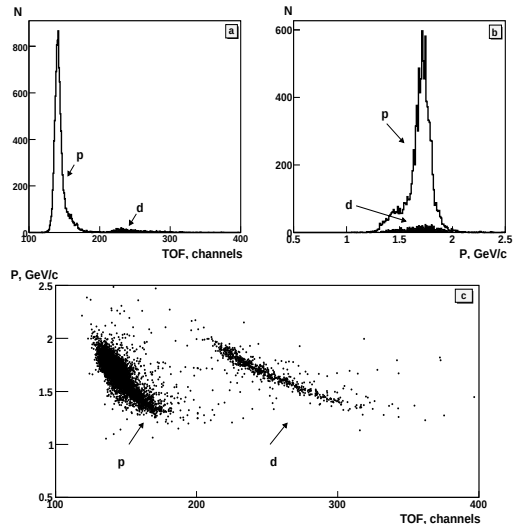

Figure 3. Demonstration of the particle identification, using both the magnetic analysis and time-of-flight spectra (Target - H_2, $T_n = 1.0$ GeV.).

The differential cross-section was calculated with the following formula:

$$\frac{d\sigma}{d\Omega} = \frac{N_{\text{events}}}{(M/\epsilon_M)\sin\theta\ \Delta\theta\ \Delta\phi\ \epsilon_{\text{spectr}}\ n_{\text{nucl}}}, \qquad (5)$$

where:

- N_{events} — number of events in the elastic peak
- M and ϵ_M — monitor counts and efficiency of neutron monitor
- ϵ_{spectr} — efficiency of the spectrometer
- n_{nucl} — number of H/D in the target.

Final values of differential cross-sections of $np \to pn$ elastic reaction on H_2 target at 1;1.2 GeV energy are shown in Fig. 5a. Obtained value of the ratio $R_{\text{dp}} = \frac{d\sigma}{d\Omega}(nd)/\frac{d\sigma}{d\Omega}(np)$ is submitted in Fig. 5b and Table 1. The ratio $R_{\text{dp}}(0)$ was obtained by the extrapolation of the direct line approximating of experimental $R_{\text{dp}}(\theta)$ data (Figs.4 a,b) with $\chi^2 \approx 0.5$.

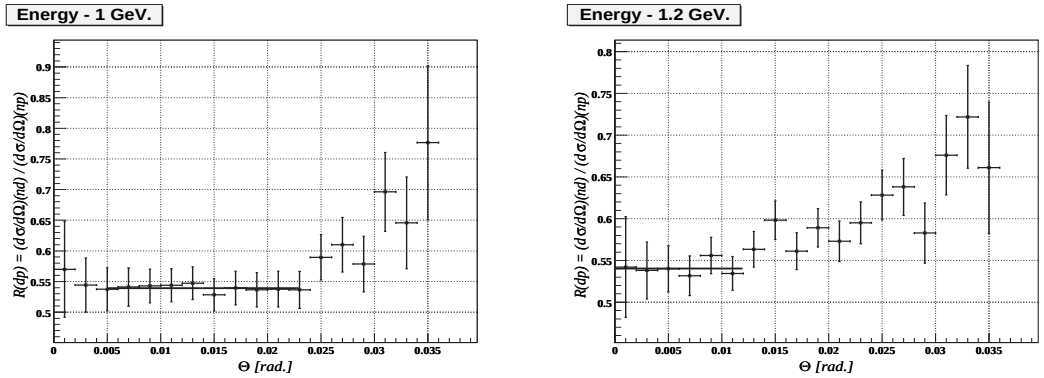

(a) (b)

Figure 4a. Angular dependence of ratio $R_{\rm dp}$ at neutron energy $T_n = 1.0\,\text{GeV}$.
Figure 4b. Angular dependence of ratio $R_{\rm dp}$ at neutron energy $T_n = 1.2\,\text{GeV}$.

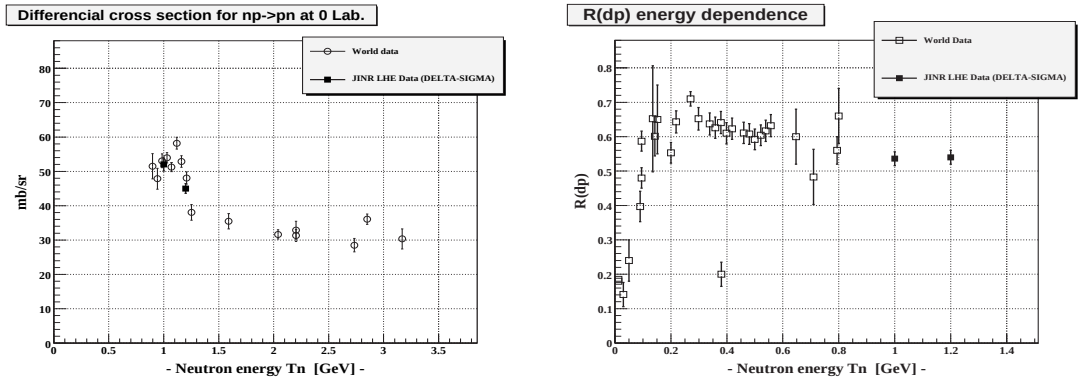

(a) (b)

Figure 5a. Differential cross section of the $np \to pn$ process at $0\,^\circ$.
Figure 5b. The ratio $R_{\rm dp}$.

Table 1: $R_{\rm dp}(0)$

Energy (GeV)	Value	Stat. Error	Syst.Error	Total Error
1.0	0.536	0.01	0.012	0.015
1.2	0.54	0.01	0.013	0.016

2. Conclusion. Our preliminary results on the momentum spectra of elastic charge exchange protons with H_2 target and corresponding $d\sigma/d\Omega(np)$ at 1.0 GeV are in agreement with the existing data [7, 8]. Our preliminary results of measurements of the ratio $R_{dp} = \frac{d\sigma/d\Omega(np)}{d\sigma/d\Omega(nd)}$ at 0° were obtained at the first time at $T_n \geq 1$ GeV. Changing over from $R_{\rm dp}(0)$ to $R^{ID}(0)$ by the formula (4)

$$R^{ID} = \frac{2}{3R_{\rm dp}(0)} - 1 \tag{6}$$

we obtained the value R^{ID} at the first time at $T_n \geq 1$ GeV:

$$R^{ID} = 0.23 \pm 0.03 \qquad \text{(energy 1.0 GeV)} \tag{7}$$

$$R^{ID} = 0.33 \pm 0.03 \qquad \text{(energy 1.2 GeV)} \tag{8}$$

We are grateful to the JINR, JINR VBLHE, DLNP and LPP Directorates for the investigations support. The investigations were supported in also by the Russian Foundation for Basic Research (Grant No 02-02-17129).

References

[1] V. I. Sharov, L. N. Strunov et all.: in book *Research Program of LHE JINR*, Ed. A. M. Baldin (Dubna 1999), "Delta-Sigma Experiment" p.p. 37-43

[2] V. I. Sharov et al.: Eur. Phys. J. **C 37** (2004) 79.

[3] V. I. Sharov et al.: *Preprint JINR* E1-2004-87, Dubna, 2004;

[4] E. L. Lomon et al. at the proper references in [2,3]

[5] N. W. Dean: Phys. Rev. D5 (1972) 1661

[6] N. W. Dean: Phys. Rev. D5 (1972) 2832

[7] G. Bizard, F. Bonthonneau, J. L. Laville et al.: Nucl.Phys. **B 85** (1975) 14.

[8] G. Bizard, F. Bonthonneau, J. L. Laville et al.: Nucl.Phys. **B 108** (1976) 189.

LONGITUDINAL POLARIZATION OF Λ AND $\bar{\Lambda}$ HYPERONS IN LEPTON-NUCLEON DEEP-INELASTIC SCATTERING

John Ellis[1], Aram Kotzinian[2,3,4], Dmitry Naumov[4†] and Mikhail Sapozhnikov[4]

(1) *CERN, Switzerland*
(2) *INFN, Torino, Italy*
(3) *Yerevan Physics Inst., Yerevan, Armenia*
(4) *JINR, Dubna, Russia*
† *E-mail: naumov@nusun.jinr.ru*

Abstract

We consider models for the spin transfers to Λ and $\bar{\Lambda}$ hyperons produced in lepton-nucleon deep-inelastic scattering. We make predictions for longitudinal Λ and $\bar{\Lambda}$ spin transfers for the COMPASS experiment and for HERA, and for the spin transfer to Λ hyperons produced at JLAB. We demonstrate that accurate measurements of the spin transfers to Λ and $\bar{\Lambda}$ hyperons with COMPASS kinematics have the potential to probe the intrinsic strangeness in the nucleon. We show that a measurement of $\bar{\Lambda}$ polarization could provide a clean probe of the spin transfer from $\bar{s}$ quarks and provides a new possibility to measure the antistrange quark distribution function. COMPASS data in a domain of x that has not been studied previously will provide valuable extra information to fix models for the nucleon spin structure. The spin transfer to $\bar{\Lambda}$ hyperons, which could be measured by the COMPASS experiment, would provide a new tool to distinguish between the SU(6) and Burkardt-Jaffe (BJ) models for baryon spin structure. In the case of the HERA electron-proton collider experiments with longitudinally-polarized electrons, the separation between the target and current fragmentation mechanisms is more clear. It provides a complementary probe of the strange quark distribution and helps distinguish between the SU(6) and BJ models for the Λ and $\bar{\Lambda}$ spin structure. Finally, we show that the spin transfer to Λ hyperons measured in a JLAB experiment would be dominated by the spin transfer of the intrinsic polarized strangeness in the remnant nucleon, providing an independent way to check our model predictions.

The negative net polarization of strange quarks in the nucleon found in experiments with polarized charged leptons scattering off polarized nucleon still remains an intriguing subject of both theoretical and experimental investigations. Burkardt and Jaffe first noticed [1] that a non-trivial spin structure of the nucleon implies also a non non-trivial spin structure of other octet baryons which can be studied experimentally investigating spin transfer to $\Lambda, \Sigma, \ldots$ and their anti-particles. Thus an accurate measurement of longitudinal polarization of these baryons could disentangle between a naive $SU(6)$ picture and BJ proposal. Unfortunately this elegant idea faces difficulties in realistic experiments due to overwhelming contribution from target nucleon remnants to a final polarization of strange baryons at low and medium energies.

In this work we show however that $\bar{\Lambda}$ hyperons (and other anti-particles) are much more cleaner instruments to study the spin structure of $\bar{\Lambda}$ hyperons due to a smaller contribution from the target nucleon end and large x_F. Also we show that spin transfers to Λ and $\bar{\Lambda}$ are sensitive to $s(x)$ and $\bar{s}(x)$ in thus can be considered as a *new additional method* to study the nucleon strangeness.

This article is a compact version of our more detailed paper [2] to which we refer for more details.

In what follows we use common definitions for the kinematic variables: x, y are the standard deep-inelastic scaling variables and x_F is the Feynman variable defined as $x_F = \frac{2P_L^\star}{W}$ where $P_L^\star$ is the particle longitudinal momentum in the hadronic centre-of-mass system, whose invariant mass is denoted by W. The negative range of x_F is often referred to as the target fragmentation region, and the positive range of x_F as the current fragmentation region.

We model the hadronization of quarks and target nucleon remnants into hadrons within the Lund string model, which has been used successfully to describe many unpolarized phenomena, albeit with many free parameters that need to be tuned. Here we use the Lund model as implemented in the JETSET 7.4 [3, 4] code, with the string fragmentation parameters tuned by the NOMAD experiment [5]. These parameters describe well the yields of the strange hadrons $\Lambda, \bar{\Lambda}, K_S^0$ and - what is important for our calculations - the relative contributions of Λ and $\bar{\Lambda}$ hyperons produced from decays of heavier states (Σ^*, Σ^0, Ξ and their antiparticles) [6–8]. Deep-inelastic lepton-nucleon scattering is simulated using the LEPTO 6.1 [9] package, with parton distributions provided by the PDFLIB package [10]. Please note that we implemented two important for polarization studies improvements to the LEPTO 6.1 package [2].

As preparation for the treatment of spin transfer to final-state Λ and $\bar{\Lambda}$ hyperons, we introduced in [11] two hadronization ranks R_q and R_{qq}. The ranks R_q and R_{qq} are integers equal to the numerical ordering of the hadron from the quark and the opposite end, which we call the nucleon target end. Some examples of the assignments of these two ranks are shown in Fig. 1.

We often use in the following the terms of quark (target remnant) fragmentation for the case $R_q < R_{qq}$ ($R_{qq} < R_q$). However, one must always bear in mind that one is dealing with string hadronization, and not with independent fragmentation.

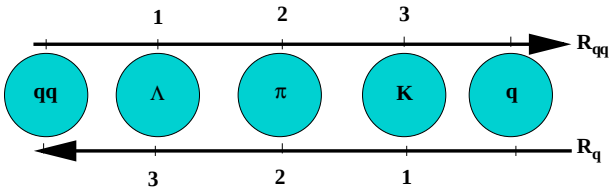

Figure 1: Λ hyperon has $R_{qq} = 1$ and $R_q = 3$, whereas the π has $R_{qq} = R_q = 2$.

The polarization of the interacting quark, denoted by P_q, is given by

$$P_q = P_B D(y), \tag{1}$$

where P_B is the charged-lepton longitudinal polarization, and D(y) is the depolarization depolarization factor, in the leading order taken to be $D(y) = \frac{1-(1-y)^2}{1+(1-y)^2}$. Corrections to $D(y)$ well parameterized for DIS are poorly known for SIDIS production of different hadrons.

We assume that there are two basic mechanisms for a baryon to be produced in a deep-inelastic process with longitudinal polarization, via spin transfer from the struck quark or from the target nucleon remnant. The Λ and $\bar{\Lambda}$ hyperons may be produced either promptly or via the decays of heavier resonances such as $\Sigma^\star, \Sigma^0, \Xi$ and their antiparticles, which also transfer partially their polarization to the Λ or $\bar{\Lambda}$. We take both possibilities into account.

The spin transfer from the nucleon target remnant to the Λ and $\bar{\Lambda}$ hyperons can be due to either polarization of the remnant diquark system (after the struck quark is removed

from the nucleon) or possible sea polarization of quarks (and antiquarks) produced via intermediate string breaking, which then fragment into the baryon considered.

Following [11], we consider in the following two extreme cases for spin transfer to hyperons.

- **Model A**: Restrict spin transfer in (di-)quark fragmentation to hyperons with $(R_{qq} = 1, R_q \neq 1)$ $R_{qq} \neq 1, R_q = 1$.
- **Model B**: Allow spin transfer in (di-)quark fragmentation to hyperons with $(R_{qq} < R_q)$ $R_{qq} > R_q$.

The spin transfer in quark and diquark fragmentation is then calculated as follows.

The polarization of Λ and $\bar{\Lambda}$ hyperons produced promptly or via the decay of a strange baryon Y in quark fragmentation is assumed to be related to the quark polarization P_q by:

$$\begin{aligned} P_{\Lambda}^{q}(Y) &= -C_q^{\Lambda}(Y) P_q, \\ P_{\bar{\Lambda}}^{\bar{q}}(\bar{Y}) &= -C_{\bar{q}}^{\bar{\Lambda}}(\bar{Y}) P_{\bar{q}}, \end{aligned} \tag{2}$$

where $C_q^{\Lambda}(Y) = C_{\bar{q}}^{\bar{\Lambda}}(\bar{Y})$ are the corresponding spin-transfer coefficients. For the sake of simplicity we use the notation $C_q^{\Lambda}(Y)$ for both Λ and $\bar{\Lambda}$.

We use two different models to calculate $C_q^{\Lambda}(Y)$: naive $SU(6)$ and BJ model by Burkardt and Jaffe (BJ) [1]. In Model A the Λ and $\bar{\Lambda}$ are polarized according to (2) if $R_q = 1$ and $R_{qq} \neq 1$. In Model B the corresponding condition is $R_q < R_{qq}$. We assume that no spin transfer occurs if $R_q = R_{qq}$.

We parameterize a possible sea-quark polarization as a *correlation* between the polarization of the sea quark and that of the struck quark, described by the spin-correlation coefficients C_{sq}:

$$P_s = C_{sq} P_q, \tag{3}$$

where P_q and P_s are the polarizations of the initial struck quark and the strange quark. The values of the C_{sq} parameters (one for scattering on a valence quark, the other for scattering on a sea quark) were found in a fit to NOMAD data [11].

In Figs. 3 we display the results of our calculations for the spin transfer to Λ (left) and $\bar{\Lambda}$ (right) hyperons as a function of x_F for $SU(6)$ and BJ models and CTEQ5L and GRV98 quark parameterizations for the COMPASS kinematics. One can see the spin transfer to Λ hyperons at $x_F < 0$ due to polarized nucleon strangeness. This region is not very much sensitive to details of Λ hyperon spin structure and to the strange quarks parameterization of the nucleon. Instead positive x_F region for both Λ and $\bar{\Lambda}$ displays a strong difference in the spin transfer for CTEQ5L and GRV98 parameterization and for $SU(6)$ and BJ models of Λ hyperon spin structure. Remarkably that an accurate measurement could disentangle both $s(x)$ in the nucleon and spin structure of the Λ (anti)hyperons in one experiment.

In [2] we provide also our predictions for different kinematics domains for fixed target experiments: COMPASS (160 GeV μ) and JLAB (12 GeV e^-), and HERA collider (27.5 GeV e^- and 820 GeVp) which do not fit to this short note.

In conclusion we have demonstrated that the accurate measurement of the spin transfers to Λ and $\bar{\Lambda}$ hyperons with COMPASS kinematics has the potential to probe the

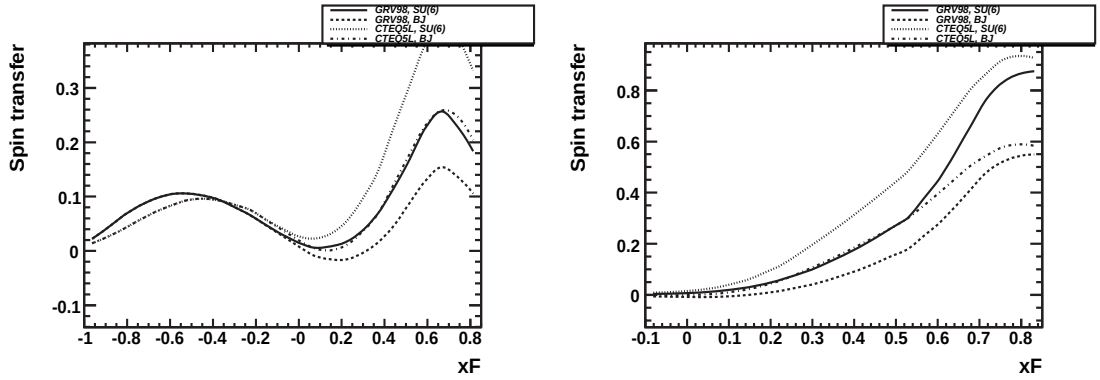

Figure 2: Spin transfer to Λ (left) and $\bar{\Lambda}$ (right) hyperons as a function of x_F for $SU(6)$ and BJ models and CTEQ5L and GRV98 quark parameterizations for COMPASS kinematics.

intrinsic strangeness in the nucleon. We have shown that a measurement of $\bar{\Lambda}$ polarization could provide a clean probe of the spin transfer from $\bar{s}$ antiquarks. It provides a new possibility to measure the antistrange quark distribution function.

References

[1] M. Burkardt and R. L. Jaffe, Phys. Rev. Lett. **70** (1993) 2537 [arXiv:hep-ph/9302232].

[2] J. R. Ellis, A. Kotzinian, D. Naumov and M. Sapozhnikov, Eur. Phys. J. C **52**, 283 (2007) [arXiv:hep-ph/0702222].

[3] T. Sjostrand, Comput. Phys. Commun. **39** (1986) 347.

[4] T. Sjostrand and M. Bengtsson, Comput. Phys. Commun. **43** (1987) 367.

[5] A.V. Chukanov, PhD thesis, in Russian, 2006

[6] P. Astier *et al.*, [NOMAD Collaboration], *Nucl.Phys.* **B588**, 3 (2000).

[7] P. Astier *et al.* [NOMAD Collaboration], *Nucl.Phys.* **B605**, 3 (2001), hep-ex/0103047.

[8] P. Astier *et al.* [NOMAD Collaboration], Nucl. Phys. B **621** (2002) 3 [arXiv:hep-ex/0111057].

[9] G. Ingelman, A. Edin and J. Rathsman, Comput. Phys. Commun. **101** (1997) 108 [arXiv:hep-ph/9605286].

[10] H. Plothow-Besch, Int. J. Mod. Phys. A **10** (1995) 2901.

[11] J.Ellis, A.Kotzinian, D.Naumov, *Eur.Phys.J.* **C25**, 603–613 (2002).

Discussion

Comm. (G.Bunce, BNL) Belle data may help constrain model for $s \to \Lambda$ and $u/d \to \Lambda$, polarized and unpolarized. $e^+e^- \to q\bar{q} \to 2$ jets, can compare correlation for $\Lambda, \bar{\Lambda}; \Lambda, \pi^+; \Lambda, \pi^-$, etc.

Q. (S.Gerasimov, JINR, Dubna) The relative percentage of scalar and pseudovector diquarks in the nucleon, and the flavour-spin structure of the Λ may be markedly different from those predicted by the 56-plet representation of $SU(6)$. Are you planning the calculations with mentioned symmetry breaking effects taken into account?

A. This effect is included into the JETSET package. There is a special parameter which controls relative contributions of scalar and vector di-quarks states. We in NOMAD used various available data in order to tune the JETSET generator. The mentioned parameter was also tuned and it is really quite important for a proper data description. The found value is different from a naive $SU(6)$ picture, you are completely right.

Q. (S.Belostotsky, PNPI, St.Petersburg) How much u-quark contributes to $\bar{\Lambda}$ production as compared to $\bar{s}$-quark? Does large contribution from u-quark (u-dominance) would make the analysis strongly model dependent?

A. $\bar{u}$ quarks contribute to $\bar{\Lambda}$ production, however their contribution to $\bar{\Lambda}$ polarization is really modest, thus we do not observe large dependence on Monte Carlo model. Also the model we use is tuned on a large amount of unpolarized data which adds us a credibility to it.

Q. (S.Nurushev, IHEP, Protvino) You made calculations for Λ-spin transfer parameter. There are many of them. Which component of the spin parameter (N, S or L) was calculated?

A. We considered longitudinal polarization of $\Lambda, \bar{\Lambda}$ hyperons.

THE COMPARATIVE STUDY OF THE INCLUSIVE π^0 ANALYZING POWER IN REACTIONS $p + p_\uparrow \to \pi^0 + X$ AND $\pi^- + p_\uparrow \to \pi^0 + X$ AT 50 AND 40 GEV/C RESPECTIVELY

V.V. Mochalov[1†], S.B. Nurushev[1], A.N. Vasiliev[1], N.A. Bazhanov[2], N.S. Borisov[2], Y.M. Goncharenko[1], A.M. Davidenko[1], A.A. Derevschikov[1], V.G. Kolomiets[2], V.A. Kormilitsin[1], V.I. Kravtsov[1], A.B. Lazarev[2], Yu.A. Matulenko[1], Yu.M. Melnick[1], A.P. Meschanin[1], N.G. Minaev[1], D.A. Morozov[1], A.B. Neganov[2], L.V. Nogach[1], Yu.A. Plis[2], A.F. Prudkoglyad[1], A.V. Ryazantsev[1], P.A. Semenov[1], O.N. Shchevelev[2], L.F. Soloviev[1], Yu.A. Usov[2], A.E. Yakutin[1]

(1) *Institute for High Energy Physics, Protvino, Russia*
(2) *Joint Institute for Nuclear Research, Dubna, Russia*
† *E-mail: mochalov@ihep.ru*

Abstract

Single-spin asymmetries A_N in reactions $p + p_\uparrow \to \pi^0 + X$ and $\pi^- + p_\uparrow \to \pi^0 + X$ at 50 and 40 GeV/c respectively behave in drastically different ways in function of transverse momentum in the central region. At the same time A_N in the polarized proton fragmentation region of these reactions are practically coinciding. Our new data on the analyzing power at 50 GeV/c in the polarized proton fragmentation region in reaction $p + p_\uparrow \to \pi^0 + X$ confirm this conclusion with better statistics and coincide with our previous data at 70 GeV/c for the same reaction.

Our previous measurements (see Fig. 1) of the single spin asymmetries in reactions $\pi^- + p_\uparrow \to \pi^0 + X(1)$ at 40 GeV/c [1] and $p + p_\uparrow \to \pi^0 + X(2)$ at 70 GeV/c [2] showed that they behave in drastically different ways in function of transverse momentum in the central region.

The analyzing power of reaction (1) is close to zero around the momentum transfer p_T=1 GeV/c and then increases with growth of p_T up to 40% for p_T >2.2 GeV/c. The same behavior was found in reaction $\pi^- + d_\uparrow \to \pi^0 + X$ at the same kinematical region [3]. At the same time A_N for reaction (2) at 70 GeV/c is compatible with zero in the central region for the same domain of the transverse momentum. We may think about the following sources of the discrepancy. First one is related to the difference in the initial

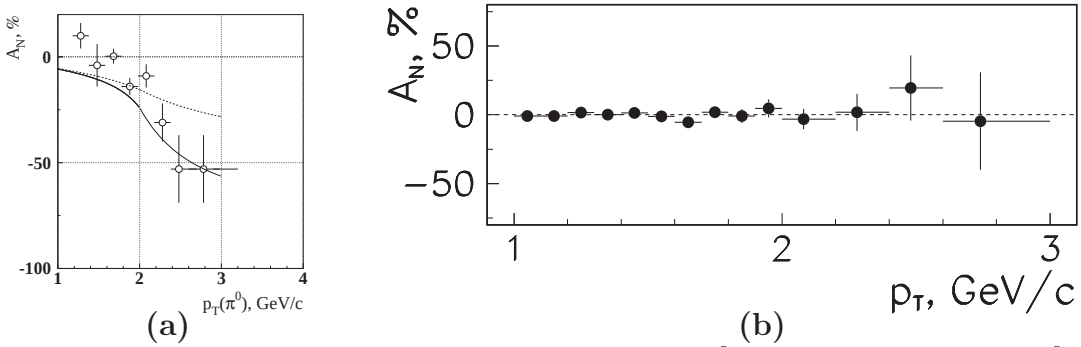

(a) **(b)**

Figure 1. Analyzing power of the reactions $\pi^- + N_\uparrow \to \pi^0 + X$ **(a)** and $p + p_\uparrow \to \pi^0 + X$ **(b)** at the central region at 40 and 70 GeV/c respectively.

momentum of the incident particles, namely, 40 and 70 GeV/c. This argument does not work for the following reason. As it's well known, one half of the incident hadron energy is carried by quarks and another one half is carried by gluons. Therefore the momentum of the interacting incident quark is 10 GeV/c in the case of pion beam and around 12 GeV/c in the case of proton beam. Assuming that the incident quark interacts with the constituent quark of the mass around 0.3 GeV we estimate the initial energy of the quark interaction in the center of mass system as 2.4 GeV for reaction (1) and 2.7 GeV for reaction (2). Such a small difference in the interaction energy should exclude the big difference in the spin effects in the reactions under discussion. As we show later our new result on A_N for reaction (2) at 50 GeV/c experimentally confirms such conclusion for the beam fragmentation region. The second possibility for difference in analyzing power might be the existence of the antiquark in pion and the possible role of the annihilation process. We are not aware of any theoretical judgments about this subject.

The next discovery of the PROZA Collaboration, presented in Fig.2, is relevant to the single spin asymmetries in reactions (1) and (2) in the polarized proton fragmentation region. The asymmetry in the reaction (1) is close to zero in the interval $0 < -x_F < 0.4$, then increases with growth of the $|x_F|$ reaching the value around 30% at $|x_F|$=0.7 [4]. Similar behavior is illustrated by the reaction (2) [5]. So we do not see the flavor dependence of the asymmetry in contrast to the data for those reactions at the central region.

The goal of this article is to present our new data for reaction (2) with better statistics, but at the initial proton momentum 50 GeV/c, which corresponds to the quark energy in c.m.s around 2.2 GeV.

The layout of the experiment PROZA-M is presented in Fig.3. The proton beam of momentum 50 GeV/c extracted by curved mono-crystal [6] comes from the left side, passes through the scintillation counters S1-S3, hodoscopes H1, H2 and strikes the polarized proton propane-diol target (PPT). Specific features of the PPT are the fairly high target polarization (90%), the long polarization life time and sufficiently large target length which was used in the frozen spin mode. [7]. The photons emitted from target are detected by the electromagnetic calorimeter EMC-720, consisting of 720 lead glass counters packed as 30×24 matrix. Cell sizes are 38.1×38.1×450 mm^3 (18 X_0). It is installed under angle 30° to the beam direction at the distance l =2.16 m from the center of the PPT. The dashed box around the PPT denotes the unique magnet carrying two functions: building up the target polarization and holding it during the data taking. The PROZA setup is described in detail somewhere [8].

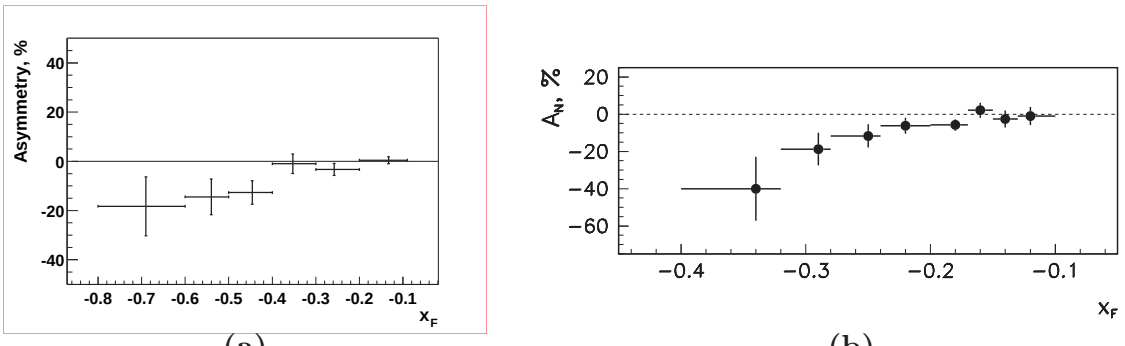

(a) **(b)**

Figure 2. Analyzing power of the reactions $\pi^- + p_\uparrow \to \pi^0 + X$ **(a)** and $p + p_\uparrow \to \pi^0 + X$ **(b)** at the polarized target fragmentation region at 40 and 70 GeV/c respectively.

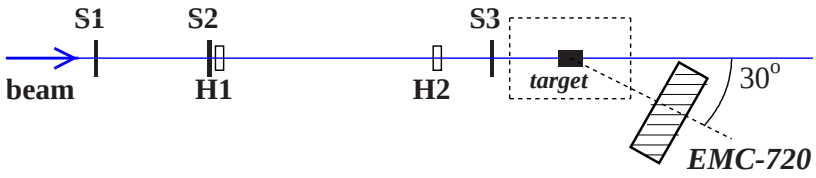

Figure 3. Experimental Setup PROZA-M. S1-S3 – trigger scintillation counters; H1-H2 – hodoscopes; $EMC-720$ – electromagnetic calorimeter; *target* – polarized target.

EMC was calibrated by wide electron beam of 5 GeV/c using inverse matrix method. Sensitivity of the ADC channels is about 2.2 MeV/channel. Additional calibration using π^0-mass during data taking was used to monitor EMC energy stability in time with accuracy 0.1%.

Trigger requires the coincidence of signals from three scintillation counters, at least one hit in each plane of hodoscopes and total deposited energy in EMC $\Sigma E > 2$ GeV. The DAQ system includes the registers for hodoscopes, 12 bits ADC for EMC, scalers, the read-out processor on the base of processor MC68030. In average 700 events per spill were registered. During 10 days data taking $5 \cdot 10^7$ events were accumulated.

For shower reconstruction it is required that at least 5 cells among 9 central (3×3) were activated; energy deposit in the central counter should be at least 100 MeV. For reconstruction of the π^0 the photons in the energy region 0.5-5 GeV were used. Additional procedures were implemented to reconstruct actual photon energy and coordinate:

1. The dependence of the reconstructed photon energy on the real initial photon energy [2]. This correction was of order of 10%.
2. The dependence of the reconstructed photon energy and coordinate on its inclination angle [9, 10]. The energy correction was of order 5%. The coordinate correction is 2-3 cm for 15° gamma inclination angle.

After corrections the reconstructed π^0 mass was consistent with its table mass within precision less than 1% in whole kinematical range.

The raw asymmetry was calculated by usual way normalizing the counting rate to the events outside of the π^0-mass region. In order to check that the false asymmetry is zero for the fixed target polarization the vents were divided in two groups with almost equivalent statistics. Using these two groups we calculated the false asymmetry. Such procedure was applied to both sign of the polarization target independently. The results for such false asymmetries are presented in Fig.4a.

New results for the reaction $p + p_\uparrow \to \pi^0 + X$ in the polarized target fragmentation region at 50 GeV are shown in Fig.4b. A_N in the inclusive π^0 production at polarized

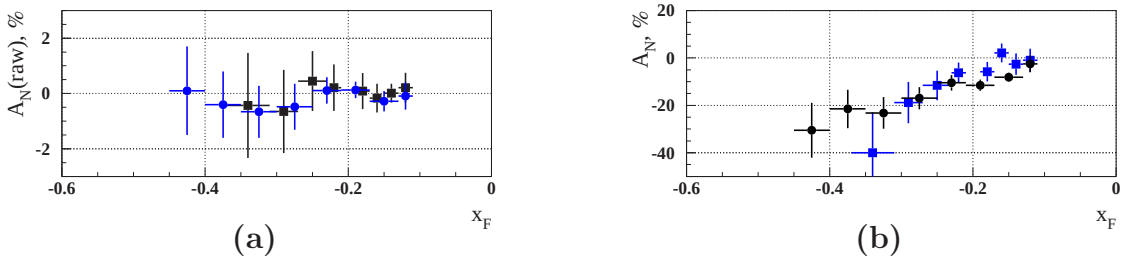

Figure 4a. False raw asymmetry for different sets of data

Figure 4b. A_N in the reactions $p + p_\uparrow \to \pi^0 + X$ at the polarized target fragmentation region at 50 GeV/c (circles) and 70 GeV/c (squares).

target fragmentation region increases by magnitude with growth of $|x_F|$ and achieves $-(20.4 \pm 3.3)\%$ at $-0.45 < x_F < -0.25$. These data are consistent with our previous measurement of the analyzing power for the same reaction and at the same kinematical region at 70 GeV/c presented in the same figure. It supports our conclusion that asymmetry in quark scattering is not sensitive to the small energy difference in the initial state.

We can conclude that the analyzing power in the inclusive π^0 production at high energies appears to illustrate the following features:

- In the central region it is zero for reaction (2) [PROZA, E704, PHENIX] in the energy range $\sqrt{s} = 10 - 200$ GeV and non zero for reaction (1) [PROZA only];
- In the polarized particle fragmentation region for reactions (2) [PROZA, STAR] and (1) [PROZA] it is non zero and A_N does not depend on the energy in the range $\sqrt{s} = 10 - 200$ GeV for reaction (2).

Current activity was partially supported by RFBR grant 06-02-16119.

References

[1] V.D. Apokin et al, Phys. Lett. **B243**, 461 (1990).
[2] A.N. Vasilev et al, Phys. Atom. Nucl. **67**, 1487 (2004) [Yad. Phys. **67**, 1512 (2004)].
[3] N.S. Amaglobeli et al, Sov.J.Nucl.Phys. **50**, 432 (1989), [Yad. Phys. **50**, 695 (1989)].
[4] A.N. Vasilev et al, Phys. Atom. Nucl. **67**, 1495 (2004), [Yad. Phys. **67**, 1520 (2004).
[5] A.N. Vasilev et al, Phys. Atom. Nucl. **68**, 1790 (2005) [Yad. Phys. **68**, 1852 (2005)].
[6] A.P. Bugorsky et al, Instrum.Exp.Tech. **44**, 1 (2001).
[7] N.S. Borisov et al, JINR Preprint 1-80-98, Dubna, 1980.
[8] V.D. Apokin et al,Instrum.Exp.Tech. **41**, 464 (1998).
[9] A.N. Vasilev et al, Instrum.Exp.Tech. **49**, 468 (2006) [Prib.Tekh.Eksp **49**, 24 (2006)].
[10] A. Vasilev, V. Mochalov and L. Solovev, Instrum.Exp.Tech. **50**, 458 (2007).

Discussion

Q. (S.Belostotsky, PNPI, St.Petersburg) Is there any QCD based explanation of this asymmetry, which is a very large spectacular effect?

A. Our kinematic domain ($\sqrt{s} \simeq 10GeV$, $p_T \leq 2GeV/c$) seems not suitable for perturbative QCD calculation (see J.Soffer's recent paper). But the theoretician participating in this workshop may be ready to add some comments.

Comm. (G.Bunce, BNL) Saroff et al., AGS experiment at 13, 18 GeV, also saw very large A_N at mid-rapidity for $p \uparrow p \to \pi^+ X$. I note that paper suggested possible scaling for $x_R = \sqrt{x_F^2 + x_T^2}$. This is as the approach to kinematic limit.

THE ANALYSIS OF ELASTIC $\overline{P}P$ SCATTERING IN THE FORWARD DIRECTION FOR PAX EXPERIMENT ENERGY RANGE

S.B. Nurushev, M.F. Runtso

Moscow Engineering Physics Institute (State University), Russia
† *E-mail: mfruntso@email.mephi.ru*

Abstract

The study is made of discrepancy between the dispersion relation prediction for the ratio of real to imaginary part of forward scattering amplitude ρ and its experimental values for $\overline{p}p$ elastic scattering in the Coulomb-nuclear interference (CNI) region for future PAX experiment energy interval (3 – 10) GeV.

The measurement of the differential cross-section in the CNI region allows to extract simultaneously two observables, namely, the total cross section σ_T, related through the optical theorem to the imaginary part of the forward spin non flip scattering amplitude $f_n(0)$

$$\mathrm{Im}f_n\left(0\right) = k_{cm}\sigma_T/4\pi \tag{1}$$

and parameter ρ, defined as the ratio of real to imaginary part of the amplitude $f_n(0)$

$$\rho \equiv \mathrm{Re}f_n\left(0\right)/\mathrm{Im}f_n\left(0\right) \tag{2}$$

In fig. 1 we show the momentum dependence of ρ from E760 paper [1] with world data (black symbols), E760 data in the range 3.7 – 6.2 GeV/c (white circles) and the curve representing dispersion relation calculation of Kroll and Schweiger [2].

We see the drastic discrepancy between theoretical prediction and very precise data of E760 in the momentum region 3 – 6 (GeV/c).

Below we analyze the method of derivation of ρ from experimental data in [1].

Antiproton-proton elastic scattering can be expressed throw Coulomb and nuclear amplitudes, f_c and f_n. Taking into account usual parameterization of the nuclear amplitude at small t, we can get:

$$\frac{d\sigma}{dt} = \frac{\pi}{k^2} \mid f_c e^{i\delta} + f_n \mid^2 = \frac{d\sigma_c}{dt} + \frac{d\sigma_{int}}{dt} + \frac{d\sigma_n}{dt}, \tag{3}$$

where

$$\frac{d\sigma_c}{dt} = \frac{4\pi\alpha_{EM}^2 G^4\left(t\right)\left(\hbar c\right)^2}{\beta^2 t^2}, \tag{4}$$

$$\frac{d\sigma_{int}}{dt} = \frac{\alpha_{EM}\sigma_T}{\beta\left|t\right|} G^2\left(t\right) e^{-\frac{1}{2}b|t|}\left(\rho\cos\delta + \sin\delta\right), \tag{5}$$

and

$$\frac{d\sigma_n}{dt} = \frac{\sigma_T^2\left(1+\rho^2\right)e^{-b|t|}}{16\pi\left(\hbar c\right)^2}. \tag{6}$$

Here α_{EM} is the fine structure constant, the proton dipole form factor $G(t) = (1+\Delta)^{-2}$, with $\Delta \equiv |t| / \left[0.71(\mathrm{GeV/c})^2\right]$. The Coulomb phase was borrowed from [3]:

$$\delta(t) = \alpha_{EM}\left[0.577 + \ln\left(\frac{b|t|}{2} + 4\Delta\right) + 4\Delta\ln(4\Delta) + 2\Delta\right] \tag{7}$$

The E760 experimental data on $d\sigma/dt$ vs t are shown in fig. 2. These data were parameterized according the equations (3 – 6) with free parameters σ_T, ρ and b. In the above expression for $d\sigma/dt$ the spin effects are not taken into account. But in the paper [4] was suggested the modification of nuclear part of differential proton-proton cross section with spin corrections:

$$\frac{d\sigma_n}{dt} = \frac{\sigma_T^2(1+\rho^2)\left(e^{-b_1|t|} + \beta^2 e^{-b_2|t|}\right)}{16\pi(\hbar c)^2} \tag{8}$$

New parameters b_1, b_2 and β are obtained as follows.

Let us consider the nucleon-nucleon scattering in the c.m. system where $\overrightarrow{k}$ and $\overrightarrow{k'}$ are the momentum before and after the collision $\left(|\overrightarrow{k}| = |\overrightarrow{k'}| = k\right)$. In the Pauli formalism the scattering amplitude may be written as following 4×4 matrix [5]:

$$M = a + b\sigma^{(1)}\overrightarrow{n}\sigma^{(2)}\overrightarrow{n} + ic\left(\sigma^{(1)}\overrightarrow{n} + \sigma^{(2)}\overrightarrow{n}\right) + e\sigma^{(1)}\overrightarrow{m}\sigma^{(2)}\overrightarrow{m} + f\sigma^{(1)}\overrightarrow{l}\,\sigma^{(2)}\overrightarrow{l} \tag{9}$$

where $\sigma^{(1)}$ and $\sigma^{(2)}$ are the spin operators for the two nucleons and $\overrightarrow{l}$, $\overrightarrow{m}$, $\overrightarrow{n}$ are the unit vectors in the directions $\overrightarrow{k} + \overrightarrow{k'}$, $\overrightarrow{k} - \overrightarrow{k'}$ and $\overrightarrow{k} \times \overrightarrow{k'}$ respectively. From kinematics only, as a consequence of angular momentum conservation, at t=0 we have:

$$c(0) = 0,\ b(0) = c(0). \tag{10}$$

From the usual expression of differential cross section throw Coulomb and nuclear amplitudes we have:

$$\frac{d\sigma}{dt} = \frac{\pi}{k^2}\left[|a_n + a_c|^2 + |b_n + b_c|^2 + 2|c_n + c_c|^2 + |e_n + e_c|^2 + |f_n + f_c|^2\right] = \frac{d\sigma_n}{dt} + \frac{d\sigma_c}{dt} + \frac{d\sigma_{int}}{dt}. \tag{11}$$

In the case of antiproton-proton collision we must only change the sign of interference term to negative one.

In the CNI region, t varies approximately between 10^{-3} and 10^{-2} (Gev/c)^2 so by using eqs. (10) and assuming the exponential fall off with t for the amplitudes we can write for fixed energy:

$$\frac{d\sigma_n}{dt} = \frac{\pi}{k^2}\left[|a_n(0)|^2 e^{-b_1|t|} + \left(2|e_n(0)|^2 + |f_n(0)|^2\right)e^{-b_2|t|}\right], \tag{12}$$

where b_2 is the slope of the spin-dependent part, which is in principle different from b_2 for spin-independent part.

In the paper [4] is introduced the denomination:

$$\beta = \sqrt{\frac{2|e_n(0)|^2 + |f_n(0)|^2}{|a_n(0)|^2}}, \tag{13}$$

where β is called the *spin parameter*. So using the optical theorem we can get expression (8). In this paper were analyzed world data on proton-proton elastic scattering and was found, that in the momentum region 8 – 10 (GeV/c) β values equal 0.15 – 0.26 and ρ values equal –0.3 – 0..

We decided to check if including the spin parameter into the expression for differential antiproton-proton cross-section can allow another fit with β parameter which will make ρ value lower and so remove the discrepancy between dispersion theory and experiment, shown in fig. 1. As we didn't find E760 experimental numerical data for fig. 2, we took the values from this figure. We understood, that these values are not precise and correspondingly have got bad χ^2 /d.o.f. values (40 – 60) for fitting of these points by expressions (3 – 6).

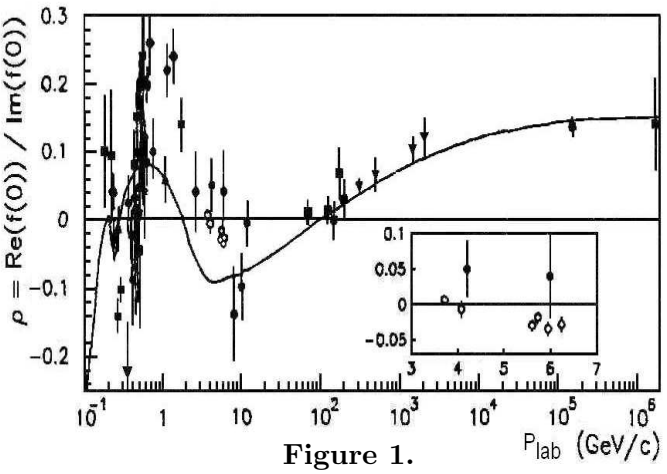

Figure 1.

So we took expressions (3 – 6) and calculated their values for experimental points at each momentum. After that we scattered the values of $d\sigma/dt$ randomly according normal distribution, increasing the dispersion of distribution function until we have got approximately the same value of χ^2/d.o.f. (near 1), as in the paper [1].

Using scattered fit values as experimental points we tried to fit these values by expressions (3 – 6), and the second time by the same expressions (3 – 6) where nuclear term was replaced by expression (8) in which in one case we supposed $b_1 = b_2$, as in [4] and in the other case we tried to vary b_1 as well as b_2 independently.

In the table 1 are shown the results for spin independent and spin dependent (the case when we suppose $b_1 = b_2$) forms of differential cross-section compared with E760 results (σ_T here is fixed according world data).

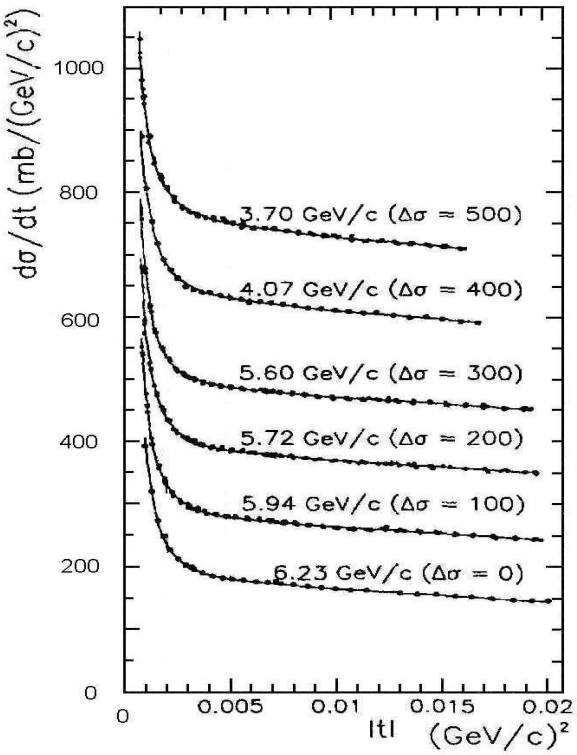

Figure 2.

When we tried to vary the slope b_2 independently from b_1 it appears that parameters b_2 and β tend to make the term $\beta e^{-b_2|t|}$ negligible.

So we can say, that our investigation doesn't show the spin contribution into the differential cross-section of $\overline{p}p$ elastic scattering and therefore no any change of the ρ parameter.

Next steps, which can be done in these investigations are:

- comparison with original data of E760 experiment
- analysis of spin contribution to the dispersion relations.

p_{lab}, GeV/c	fit	σ_T, mb	b, (Gev/c)$^{-2}$	ρ	β	χ^2 /d.o.f.
5.60	E760	61.3	12.5(3)	–0.030(7)	–	1.04
5.60	No spin	61.30±0.09	12.4±0.2	–0.033±0.002	–	0.80
5.60	With spin	61.3±69	12.4±0.5	–0.03±0.07	0.01±100	0.82
5.72	E760	60.9	12.2(4)	–0.018(8)	–	1.20
5.72	No spin	60.8±0.1	12.1±0.3	–0.022±0.002	–	1.00
5.72	With spin	60.6±77	12.1±0.5	–0.02±0.07	0.08±15	1.02
5.94	E760	60.2	12.6(3)	–0.035(8)	–	1.26
5.94	No spin	60.2±0.1	12.7±0.3	–0.040±0.002	–	0.97
5.94	With spin	60.0±76	12.7±0.6	–0.040±0.09	0.0004±3385	1.00
6.23	E760	59.4	12.2(6)	–0.029(10)	–	0.50
6.23	No spin	59.32±0.08	2.3±0.2	–0.032±0.002	–	0.65
6.23	With spin	59.3±63	12.3±0.5	–0.03±0.07	0.01±83	0.67

References

[1] Armstrong T.A. et al., Physics Letters **B385**, 479 (1996).
[2] Kroll P. and Schweiger W., Nucl. Phys. **A503**, 865 (1989) .
[3] Cahn R., Z. Phys. **C15**, 253 (1982) .
[4] Bourrely C., Soffer J. and Wray D., Nucl. Phys. **B77,** 386 (1974) .
[5] Wolfenstein L., Ann. Rev. Nucl. Sci. **6**, 43(1956).

Discussion

Comm. (J.Soffer, Temple Univ., Philadelphia) I believe that if you get the numerical values of E760, you could repair the fit of β^2 with the ρ values of DR by P.Kroll.

COMPASS RESULTS ON INCLUSIVE AND SEMI-INCLUSIVE POLARISED DIS

Helena Santos[1], on behalf of the COMPASS Collaboration

(1) *LIP - Laboratório de Instrumentação e Física Experimental de Partículas*
Av. Elias Garcia, 14, 1000-149, Lisboa, Portugal

Abstract

The COMPASS experiment at the CERN SPS has an extensive experimental program focused on the nucleon structure and on hadron spectroscopy. A main topic of investigation is the spin structure of the nucleon via deep-inelastic scattering of 160 GeV polarised muons on polarised nucleons. Results obtained in the kinematic ranges $Q^2 < 1$ (GeV/c)^2 and $0.0005 < x < 0.02$, as well as $1 < Q^2 < 100$ GeV^2 and $0.004 < x < 0.7$ are shown. The results of a global QCD fit at NLO to the world g_1 data are discussed. Then, the evaluation of the polarised valence quark distributions $\Delta u_v(x) + \Delta d_v(x)$ is presented. The analysis is based on the difference asymmetry, $A^{(h^+ - h^-)}$, for hadrons of opposite charges. This approach gives direct access to the valence quark helicity distributions, as the fragmentation functions do cancel out in LO QCD. The results derived provide information about the contribution of the sea quarks to the nucleon spin. Comparison with SMC and HERMES results is also shown.

1 Introduction

The investigation of the spin structure of the nucleon begun more than 30 years ago with polarised deep inelastic scattering measurements at SLAC [1]. At that time the quark-parton model and the analyses on weak baryon decays have predicted that 60% of the nucleon spin was entirely given by the u and d quarks [2]. The first experimental results supported this prediction but were obtained at a poor x range ($x > 0.1$). The EMC Collaboration extended the measurements to $x > 0.01$ and came out with the unexpected value of $0.12 \pm 0.09 \pm 0.14$ [3]. Such a result motivated a series of experiments covering different x ranges at CERN [4], SLAC [5–8], DESY [9] and JLAB [10]. All these experiments confirmed the small contribution of the quarks (about 20–30%) to the nucleon spin, and thus more contributions are necessary. For a nucleon with $+1/2$ helicity one has the sum rule:

$$S_n = \frac{1}{2} = \frac{1}{2}\Delta\Sigma + \Delta G + L_q + L_G \tag{1}$$

where $\Delta\Sigma$ stands for the contribution from the quarks ($\Delta\Sigma = \Delta u + \Delta d + \Delta s$), ΔG is the contribution of the gluons and $L_{q,G}$ are their angular orbital momenta.

2 Experimental Procedure

COMPASS makes use of the SPS facilities, impinging a high intensity 160 GeV muon beam on a ^{6}LiD polarised target. Besides the scattered muon, other particles produced

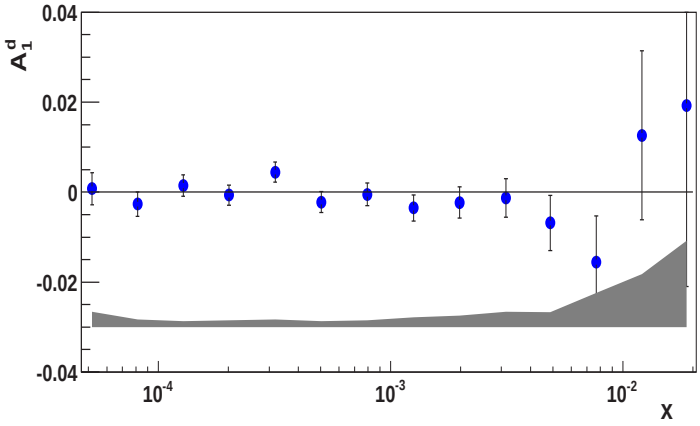

Figure 1: The asymmetry $A_1^d(x)$ for quasi-real photons ($Q^2 < 1\,(\mathrm{GeV}/c)^2$) as a function of x. The errors bars are the statistical ones. The grey band shows the systematic errors.

in deep inelastic scattering are detected in a two-stage spectrometer. Data presented in this article have been collected in the years 2002, 2003 and 2004, corresponding to an integrated luminosity of about 2 fb^{-1}. The detailed description of the spectrometer can be found at Ref. [11].

3 The A_1^d Asymmetries

In order to access the spin-dependent structure function, g_1^d, the longitudinal photon-deuteron asymmetry, A_1^d, has to be evaluated. In the framework of the quark parton model this quantity can be directly related to the quark polarisation, Δq, via

$$A_1 = \frac{(\sigma_{\gamma\mu}^{\uparrow\downarrow} - \sigma_{\gamma\mu}^{\uparrow\uparrow})}{(\sigma_{\gamma\mu}^{\uparrow\downarrow} + \sigma_{\gamma\mu}^{\uparrow\uparrow})} \simeq \frac{\sum_q e_q^2(\Delta q + \Delta\bar{q})}{\sum_q e_q^2(q + \bar{q})} \tag{2}$$

where the arrows indicate the relative beam and target spin orientations. Figure 1 shows A_1^d as a function of x for quasi-real photon interactions for the data collected in the years 2002 and 2003. Events are selected by cuts on the four-momentum transfer squared ($Q^2 < 1\,(\mathrm{GeV}/c)^2$) and the fractional energy of the virtual photon ($0.1 < y < 0.9$). Such a kinematic window allows a wide Bjorken scaling variable interval, $0.0005 < x < 0.02$ and provides more than 300 million events. The asymmetry is compatible with 0 over the whole x range. The error bars are the statistical ones and the grey band corresponds to systematic errors, which are due to false asymmetries mainly. Details on this analysis can be found in [12]. Figure 2 shows A_1^d as a function of x for DIS events ($Q^2 > 1\,(\mathrm{GeV}/c)^2$), as measured by COMPASS using 2002, 2003 and 2004 data [13]. After data selection, $89{\times}10^6$ events are available for analysis. The results of the SMC [4], E143 [6], E155 [8] and HERMES [14] experiments are also shown. The asymmetry is 0 for $x < 0.05$ and gets larger as x increases, reaching 60% at $x \simeq 0.7$. The agreement is very good between the different data sets. It should be noted that only COMPASS and SMC were able to measure this asymmetry at very low x, the COMPASS results being essential

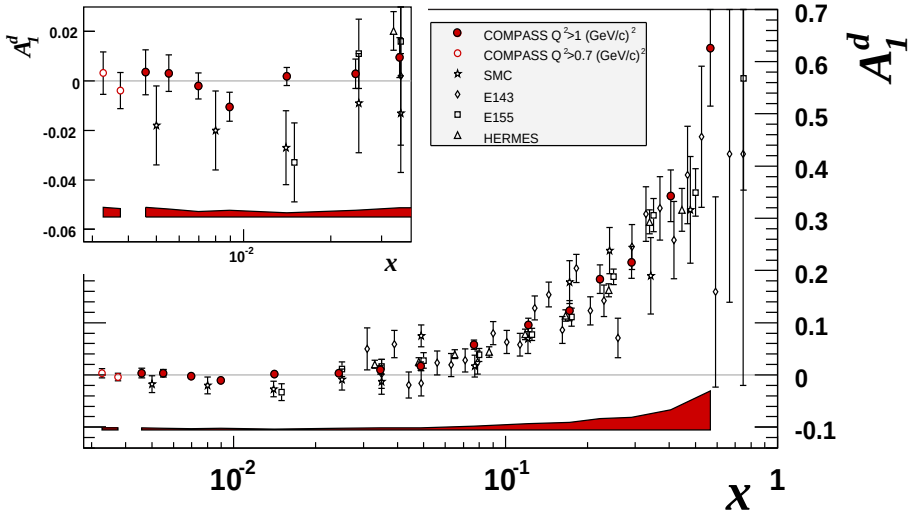

Figure 2: The asymmetry $A_1^d(x)$ as measured by the world spin experiments. The error bars are the statistical ones. The bands show the COMPASS systematic errors.

to disentangle the A_1^d behaviour at $x < 0.03$. Error bars are the statistical ones and the grey band corresponds to systematic errors of the COMPASS measurements, whose sources come from the uncertainty on beam and target polarisations (5% each), dilution factor (6%) and depolarisation factor (4-5%). Radiative corrections and the neglect of the transverse asymmetry A_2 are found to have a small effect. The upper limit for the systematic error due to false asymmetries is half of the statistical one.

4 The g_1^N Structure Function

The spin-dependent structure function of the nucleon, $g_1(x)$, is obtained from $A_1(x)$ and the spin-independent structure function $F_2(x)$ through

$$g_1(x) = A_1(x)\frac{F_2(x)}{2x(1+R)} \ , \tag{3}$$

where R is the ratio of the longitudinal to transverse photon absorption cross-sections. Figure 3 shows g_1^d as a function of x for DIS events [13]. The SMC results [4] have been evolved to the Q^2 of the corresponding COMPASS points. The two curves are the results of two QCD fits at the Q^2 of each data point. They are performed at NLO in the $\overline{\text{MS}}$ renormalisation and factorisation scheme. These fits require input parameterisations of the quark singlet spin distribution $\Delta\Sigma(x)$, non-singlet distributions $\Delta q_3(x)$ and $\Delta q_8(x)$, and the gluon spin distribution $\Delta G(x)$, which evolve according to the DGLAP equations. Data are well described by two solutions of DGLAP, with $\Delta G > 0$ and with $\Delta G < 0$. Figure 4 shows the QCD fit to proton, deuteron and neutron targets with positive ΔG solution (an indistinguishable curve is obtained for the solution with $\Delta G < 0$). All data have been evolved to a common $Q_0^2 = 3\,(\text{GeV}/c)^2$, which corresponds to the average Q^2 of the COMPASS DIS data. The deuteron data are taken from Refs [4, 6, 8, 14], the proton data from Refs [4, 6, 14–16] and the ^{3}He data from Refs [10, 5, 17, 18]. For this analysis

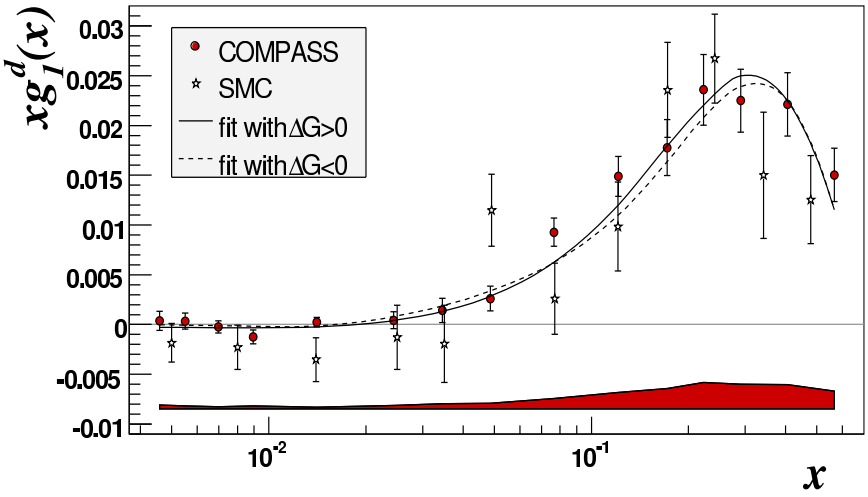

Figure 3: The spin-dependent structure function of the deuteron, g_1^d, as a function of x ($Q^2 > 1\,(\mathrm{GeV}/c)^2$). The errors bars are the statistical ones. The band shows the COMPASS systematic errors. The curves show the results of QCD fits with $\Delta G > 0$ and $\Delta G < 0$.

all bins, except the last one, have been subdivided into three Q^2 intervals. The number of COMPASS data points used in the fit to deuteron data is 43, out of a total of 230. Two different programs have been used to fit the data – one uses the DGLAP evolution equations for the spin structure functions in x and Q^2 phase space [20], the other uses the DGLAP evolution equations in the space of moments [21]. Both programs give consistent values of the fitted PDF parameters and similar χ^2-probabilities. Although the shapes of the gluon distributions obtained with the two ΔG solutions differ over the whole x range, the fitted values of the first moment, η_G, are small and similar in absolute value $|\eta_G| \approx 0.2 - 0.3$. Similarly η_Σ reveals weak dependence on the shape of ΔG, being slightly larger in the fit with $\Delta G < 0$. The results from the two fits have been averaged and give:

$$\eta_\Sigma(Q^2{=}3\,(\mathrm{GeV}/c)^2) \;=\; 0.30 \pm 0.01(stat.) \pm 0.02(evol.). \tag{4}$$

In the $\overline{MS}$ scheme η_Σ is identical to the matrix element a_0, detailed below. The direct measurements of $\Delta G/G$, obtained at leading order in QCD, is compared with the indirect approach provided by the NLO QCD fits in figure 5. The unpolarised gluon distribution is taken from the MRST parameterisation [19]. The large statistical uncertainties of the direct measurements do not allow to disentangle between the two solutions for ΔG. More details on our QCD analysis can be found at Ref. [13].

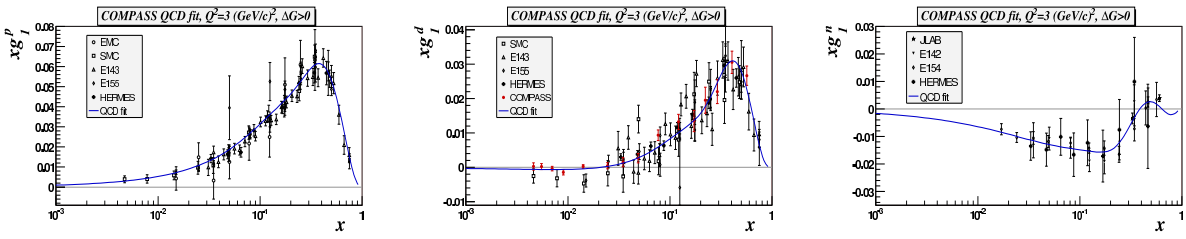

Figure 4: The world data and QCD fit at $Q^2 = 3\,\mathrm{GeV}^2$, obtained with the program of Ref. [20]. The curve corresponds to the solution with $\Delta G > 0$.

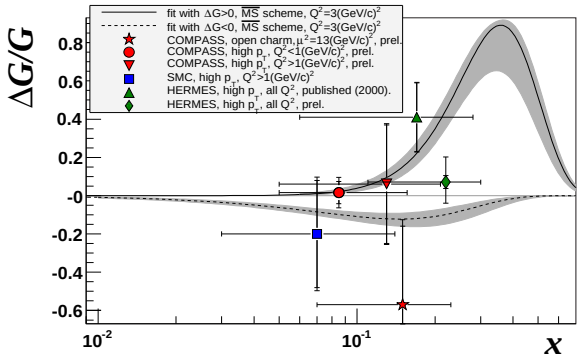

Figure 5: Distribution of the gluon polarisation $\Delta G(x)/G(x)$ at $\mathrm{Q}^2 = 3$ $(\mathrm{GeV}/c)^2$ for the fits with $\Delta G > 0$ and $\Delta G < 0$. Data points are taken from SMC [24], HERMES [22, 23] and COMPASS [25]. The error bars associated to the points are statistical. The error bands correspond to the statistical error on $\Delta G(x)$ at a given x.

We have calculated the integral of g_1^N using exclusively the experimental values of COMPASS evolved to $\mathrm{Q}_0^2 = 3$ GeV^2 and averaged over the two fits. Taking into account the contributions (2%, only) from the fits in the unmeasured regions of $x < 0.003$ and $x > 0.7$, we obtain:

$$\Gamma_1^N(Q^2{=}3\,(\mathrm{GeV}/c)^2) \;=\; 0.050 \pm 0.003(stat.) \pm 0.003(evol.) \pm 0.005(syst.). \qquad (5)$$

The second error accounts for the difference in Q^2 evolution between the two fits. The systematic error is the dominant one and mainly corresponds to the uncertainty on the beam and target polarisations and on the dilution factor. Γ_1^N is related to the matrix element of the singlet axial current a_0, which measures the quark spin contribution to the nucleon spin. The relation between Γ_1^N and a_0, now independent on Q^2 ($\hat{a}_0 = a_{0(Q^2\to\infty)}$) (Ref. [26]), is

$$\Gamma_1^N(Q^2)_{Q^2\to\infty} = \frac{1}{9}\,\hat{C}_1^S(Q^2)\;\hat{a}_0 \;+\; \frac{1}{36}\,C_1^{NS}(Q^2)\;a_8. \qquad (6)$$

The coefficients $\hat{C}_1^S$ and C_1^{NS} have been calculated in perturbative QCD up to the third order in $\alpha_s(Q^2)$ [26]. From the COMPASS result of Eq. 5 and taking the value of a_8 measured in hyperon β decay, assuming $SU(3)_f$ flavour symmetry ($a_8 = 0.585{\pm}0.025$ [27]), one obtains:

$$\hat{a}_0 = 0.33 \pm 0.03(stat.) \pm 0.05(syst.). \qquad (7)$$

with the value of α_s evolved from the PDG value $\alpha_s(\mathrm{M_z}^2) = 0.1187 \pm 0.005$. Combining this value with a_8, the first moment of the strange quark distribution is:

$$(\Delta s(x) + \Delta\overline{s}(x))_{Q^2\to\infty} = \frac{1}{3}(\hat{a}_0 - a_8) = -0.08 \pm 0.01(stat.) \pm 0.02(syst.). \qquad (8)$$

One should keep in mind that the data have been evolved to a common Q^2 through a NLO fit, whereas the coefficients $\hat{C}_1^S$ and C_1^{NS}, as well as $\alpha_s(Q^2)$, have been obtained beyond NLO. However, the choice of a value close to the average of Q^2 of the DIS data is expected to minimise the effect of the evolution in the results of $\hat{a}_0$ and $\Delta s(x) + \Delta\overline{s}(x)$ quoted above.

5 Valence Polarisations

In order to extract helicity distributions in LO QCD, unpolarised distributions and fragmentation functions for the hadron production from different quark flavours are needed:

$$A_1^h(x) = \frac{\sum_q e_q^2(\Delta q(x) D_q^h + \Delta\bar{q}(x) D_{\bar{q}}^h)}{\sum_q e_q^2(q(x) D_q^h + \bar{q}(x) D_{\bar{q}}^h)} \tag{9}$$

Figure 6 shows semi-inclusive asymmetries as a function of x for positive and negative unidentified charged hadrons. The kinematic range is basically the same as for inclusive analysis; in addition, the fraction of the photon energy carried out by the hadrons, z, is required to be between 0.2 and 0.85. COMPASS improves significantly the statistics with respect to SMC. A suitable way to get valence quark polarisations is to measure difference asymmetries [29,30]. In LO QCD, under the assumption of isospin and charge conjugation symmetries, fragmentation functions do cancel out. Furthermore, for a deuteron target, no hadron identification is required, as difference asymmetries have the same expression both for pions and kaons:

$$A_N^{h^+-h^-} = A_N^{\pi^+-\pi^-} = A_N^{K^+-K^-} = \frac{\Delta u_v + \Delta d_v}{u_v + d_v}\,, \tag{10}$$

The measured single hadron asymmetries combined with the ratio of the charged hadron cross-sections are used to define difference asymmetries:

$$A^{h^+-h^-} = \frac{1}{1-r}(A^{h^+} - rA^{h^-})\,, \text{ with } r = \frac{\sigma_{\uparrow\downarrow}^{h-} + \sigma_{\uparrow\uparrow}^{h-}}{\sigma_{\uparrow\downarrow}^{h+} + \sigma_{\uparrow\uparrow}^{h+}} = \frac{\sigma^{h-}}{\sigma^{h+}}. \tag{11}$$

The measured x range is slightly smaller as the r factor becomes 1 for $x < 0.006$. In order to determine the hadron acceptances a full chain Monte Carlo simulation is performed, in which the generated events face the same experimental conditions as real data do. Once the difference asymmetries are determined and knowing the unpolarised valence distributions the valence spin distributions are obtained from

$$\Delta u_v + \Delta d_v = \frac{(u_v + d_v)_{\mathrm{MRST}}}{(1+R)(1-1.5\omega_D)} A_d^{h^+-h^-}\,. \tag{12}$$

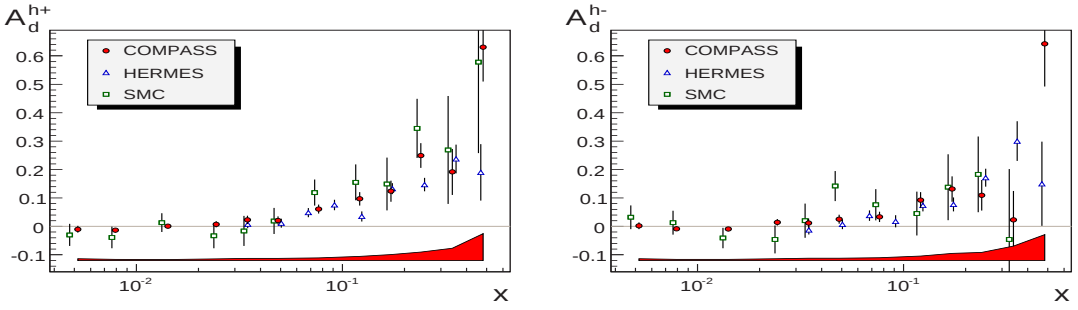

Figure 6: Hadron asymmetries A_d^{h+} (left) and A_d^{h-} (right) measured by COMPASS, SMC [28] and HERMES [14] experiments. The errors bars are the statistical ones. The band shows the COMPASS systematic errors.

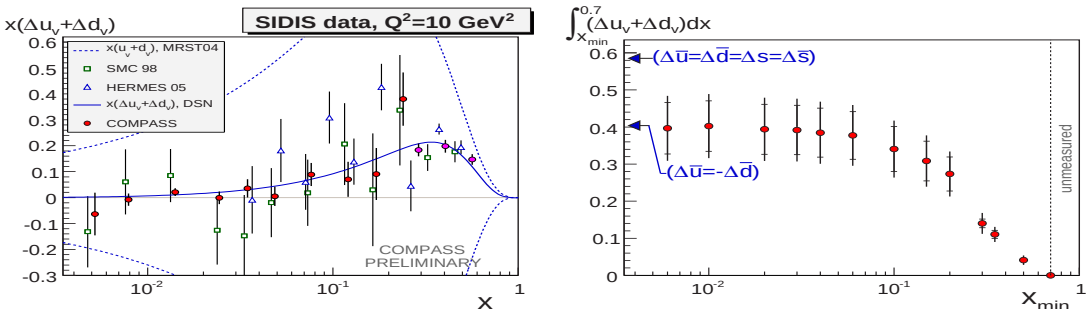

Figure 7: (Left) Polarised valence quark distribution $x(\Delta u_v(x) + \Delta d_v(x))$ for COMPASS, SMC [28] and HERMES [14]. The line shows the DNS fit which does not include the present COMPASS data. Three additional points at high x are obtained from g_1^d [13]. (Right) The integral of $\Delta u_v(x)+\Delta d_v(x)$ over the range $0.006 < x < 0.7$ as the function of x minimum, evaluated at $Q^2 = 10$ (GeV/c)^2.

For x >0.3 the unpolarised sea contribution to F_2 vanishes and thanks to the positivity condition, $|\Delta q + \Delta\overline{q}| \leq |q + \overline{q}|$, the polarised sea contribution to the nucleon spin also becomes negligible in this region. These features allow the use of three points from the inclusive $g_1(x)$ COMPASS result [13] to define the valence polarisation. The advantage of this procedure is the gain in precision. A LO DNS analysis using KKP [31] fragmentations functions has been performed [32]. It includes all DIS g_1 results prior to COMPASS data, the partial COMPASS data on g_1 from Ref. [33] and all SIDIS results from SMC [28] and HERMES [14], where a symmetric sea in the valence range has been considered. Unpolarised MRST2004 [34] LO PDFs have been used. Figure 7(left) shows the comparison between COMPASS results and previous analyses from SMC and HERMES. All data points are evolved to a common Q_0^2=10 (GeV/c)^2 accordingly to DNS. The line stands for the DNS fit to SMC and HERMES data, only. Indeed, the COMPASS data agree very well with the other experiments and DNS parameterisation predicts successfully our result. Figure 7(right) shows the integral of the valence polarisation as a function of x minimum, evaluated at Q_0^2=10 (GeV/c)^2. Its value over the measured x range (0.006 – 0.7) is 0.41 $\pm$ 0.07(stat.) $\pm$ 0.05(syst.). The contribution from the upper unmeasured region is estimated to be 0.004. Also the contribution from lower x values are expected to be small as the integral almost does not change for low x values.
The contribution of sea quarks to the nucleon spin can be obtained by combining the matrix elements a_0 and a_8 and the first moment of the valence polarisation:

$$\Delta\overline{u} + \Delta\overline{d} = (\Delta s + \Delta\overline{s}) + \frac{1}{2}(a_8 - \Gamma_v) = 3\,\Gamma_1^N - \frac{1}{2}\Gamma_v + \frac{1}{12}a_8 \qquad (13)$$

The result shown in figure 7(right) favours an asymmetric scenario for the sea polarisation, $\Delta\overline{u} = -\Delta\overline{d}$, at a confidence level of two standard deviations, in contrast to the usual assumed symmetric scenario, $\Delta\overline{u} = \Delta\overline{d} = \Delta\overline{s} = \Delta s$. However, the statistical errors are still large and do not allow to draw firm conclusions. More details on this analysis can be found in [35].

6 Conclusions

COMPASS has measured the deuteron spin asymmetry A_1^d and its longitudinal spin-dependent structure function g_1^d with improved precision at $Q^2 < 1$ (GeV/c)^2 and $0.0005 < x < 0.02$, as well as $1 < Q^2 < 100$ (GeV/c)^2 and $0.004 < x < 0.7$. The measured DIS results have been evolved to a common Q^2 by a NLO QCD fit of the world g_1 data. The fit yields two solutions, one corresponding to $\Delta G(x) > 0$ and other to $\Delta G(x) < 0$, which describe the data equally well. The absolute values of the first moment of $\Delta G(x)$ are similar and not larger than 0.3. From the first moment Γ_1^N the matrix element of the singlet axial current $\hat{a}_0$, in the limit $Q^2 \to \infty$, is found to be $0.33 \pm 0.03(stat.) \pm 0.05(syst.)$. The polarised valence quark distribution has been determined using the difference asymmetry approach in LO QCD. The integral at Q_0^2=10 (GeV/c)^2 over the measured x range, and including the extrapolation to the full x range, disfavours a symmetric sea at 2σ level and appoints to a opposite sign of $\Delta\overline{u}$ and $\Delta\overline{d}$.

References

[1] M.J. Alguard *et al.* (E80 Coll.), Phys. Rev. Lett. **37**, 1261 (1976).
[2] J.R. Ellis and R.L. Jaffe, Phys. Rev. D **9**, 1444 (1974).
[3] J. Ashman *et al.* (EMC Coll.), Phys. Lett. B **206**, 364 (1988).
[4] B. Adeva *et al.* (SMC Coll.), Phys. Rev. D **58**, 112001 (1998).
[5] P.L. Anthony *et al.* (E142 Coll.), Phys. Rev. D **54**, 6620(1996).
[6] K. Abe *et al.* (E143 Coll.) Phys. Rev. D **58**, 112003 (1998).
[7] K. Abe *et al.* (E154 Coll.), Phys. Lett. B **405**, 180 (1997).
[8] P. L. Anthony *et al.,* (E155 Coll.) Phys. Lett. B **463**, 339 (1999).
[9] A. Airapetian *et al.* (HERMES Coll.), Phys. Lett. B **442**, 484 (1998).
[10] X. Zheng *et al.* (JLAB/Hall A Coll.), Phys. Rev. Lett. **92** 012004 (2004).
[11] P. Abbon *et al.,* (COMPASS Coll.), Nucl. Inst. Meth. A **577** (2007) 455.
[12] V.Yu. Alexakhin *et al.* (COMPASS Coll.), Phys. Lett. B **647**, 330 (2007).
[13] V.Yu. Alexakhin *et al.* (COMPASS Coll.), Phys. Lett. B **647**, 8 (2007).
[14] A. Airapetian *et al.* (HERMES Coll.), Phys. Rev. D **75**, 012003 (2005)
[15] P. L. Anthony *et al.* (E155 Coll.), Phys. Lett. B **493**, 19 (2000).
[16] J. Ashman *et al.* (EMC Coll.), Nucl. Phys. B **328** (1989).
[17] K. Abe *et al.* (E154 Coll.), Phys. Rev. Lett. **79**, 26 (1997).
[18] K. Ackerstaff *et al.* (HERMES Coll.), Phys. Lett. B **404**, 383 (1997).
[19] A. D. Martin, R. G. Roberts, W. J. Stirling and R. S. Thorne, Eur. Phys. J. C **4**, 463 (1998).
[20] B. Adeva *et al.* (SMC Coll.), Phys. Rev. D **58** 112002 (1998).
[21] A. N. Sissakian, O. Yu. Shevchenko and O. N. Ivanov, Phys. Rev. D **70**, 074032 (2004).
[22] A. Airapetian *et al.,* (HERMES Coll.), Phys. Rev. Lett. **84**, 2584 (2000).
[23] D. Hasch (HERMES Coll.), AIP Conf. Proc. **915**, 307 (2006).
[24] B. Adeva *et al.,* (SMC Coll.), Phys. Rev. D **70**, 012002 (2004).
[25] E. S. Ageev *et al.,* (COMPASS Coll.), Phys. Lett. B **633**, 25 (2006).

[26] S. A. Larin *et al.*, Phys. Lett. B **404**, 153 (1997).
[27] Y. Goto *et al.*, Phys. Rev. D **62**, 037503 (2003).
[28] SMC Collaboration, B. Adeva *et al.,* Phys. Lett. B **420** (1998) 180.
[29] L.L. Frankfurt *et al.,* Phys. Lett. B **230** (1989) 141.
[30] E. Christova, E. Leader, Nucl. Phys. B **607** (2001) 369. Also these Proceedings.
[31] B.A. Kniehl, G. Kramer, B. Potter, Nucl. Phys. B **582** (2000) 514.
[32] D. de Florian, G.A. Navarro, R. Sassot, Phys. Rev. D **71** (2005) 094018.
[33] E.S. Ageev *et al.,* (COMPASS Coll.) Phys. Lett. B **612** (2005) 154.
[34] A.D. Martin, W.J. Stirling, R.S. Thorne, Phys.Lett. B **636** (2006) 259.
[35] M. Alekseev *et al.* (COMPASS Coll.), CERN-PH-EP/2007-024, hep-ex/0707.4077, *subm. to Phys. Lett. B.*

Discussion

Q. (S.Belostotsky, PNPI, St.Petersburg) Quark contribution to nucleon spin from COMPASS is now 0.33, while COMPASS stated negative strange quark contribution. HERMES give also 0.33 but zero for strange quark. How to explain such a discord?

A. A possible explanation can be the different x-range of the measurements in the two experiments. The limited x-range of HERMES implies large extrapolation to $x = 0$. Another explanation (standard) is the systematics on the approaches. Have both experiments much the same assumptions.

Q. (S.Nurushev, IHEP, Protvino) You may know that the preliminary data on ΔG from RHIC is close to zero or negative. May you exclude from new COMPASS data the negative values of ΔG? If yes, on which confidence level?

A. We cannot exclude at all negative ΔG from COMPASS data, either from direct measurements (open charm channel and high-$p_\perp$ pairs) or from indirect estimations from QCD fits. Statistical errors are still very large and the systematic uncertainty on ΔG from QCD fits is 100%. On the other hand, in my opinion, the present x_g range of the measurements (SMC, COMPASS and HERMES) is too narrow to take definite conclusions, even if the statistical errors become drastically reduced. For sure, that RHIC results on ΔG as a function of x_g will help to disentangle the sign of ΔG as its x_g range is larger.

POLARIZED MEASUREMENT OF ENERGY DEPENDENCE OF THE COMPLETE SET np - OBSERVABLES AT $1-6$ GeV MONOCHROMATIC NEUTRON BEAMS AND DIRECT RECONSTRUCTION OF THE ISOSINGLET NN - AMPLITUDES OF FORWARD SCATTERING – FOR SEARCH SIGNALS OF PHASE TRANSITION OF NN TO 6 - QUARKS.

L.N. Strunov and V.I. Sharov, R. A. Shindin amd A. A. Morozov

JINR, Veksler and Baldin Laboratory of High Energies, 141980 Dubna, Russia

E-mail: strunov@sunhe.jinr.ru

Abstract

To advance studies of the short range spin structure of NN interactions, there were (np) spin observables measured for the first time at 0° up to the highest nucleon internal momenta k in np-core. Both the bounded polarized (np)-couple (in deuteron) and a polarized free np-couple were probed up to $k \approx 5\,\mathrm{fm}^{-1}$ and $6\,\mathrm{fm}^{-1}$ respectively. The highest energy polarized deuteron (up to 9 GeV/c) and polarized monochromatic neutron beams (up to 4.5 GeV/c), provided now only by the JINR ACCELERATORS, were used [1, 2, 3] for energy dependence measurements $T_{20}(k)$ up to $k \approx 5\,\mathrm{fm}^{-1}$ [2a] in the $d \to p$ stripping up to kinematic limit of k, and $\Delta\sigma_{\mathrm{L}}(np)$ total np cross section differences in new energy range of 1.2–3.7 GeV [3].

1. These data [2, 3] are in agreement with the SATURNE II ones over the lower k-momentum common range of $2.5\,\mathrm{fm}^{-1}$. Several years ago Dubna (in collaboration with groups from 12 laboratories) began the transmission measurements using both a polarized neutron beam and a polarized proton target (PPT). For the first time we measured the energy dependence of the $\Delta\sigma_{\mathrm{L}}(np)$, neutron-proton total cross section difference for the pure longitudinal (**L**) spin states for parallel and antiparallel (np) spins, over a new kinetic energy range of 1.2–3.7 GeV for a quasi-monochromatic polarized neutron beam. The $-\Delta\sigma_{\mathrm{L}}(np)$ energy dependence [3, 4] shows an unexpected anomalous fast decrease to zero above 1.1 GeV and a structure with minimum $|\Delta\sigma_{\mathrm{L}}(I=0)|$ around 1.8 GeV predicted in Ref. [5a]. The authors [5a] used the Cloudy Bag Model and an R-matrix connection to long-range meson-exchange force region with the short-range region of asymptotically free quarks; this hybrid model gives the lowest exotic six-quark configurations in the isosinglet $^3\mathrm{S}_1$ state with the mass $\mathrm{M} = 2.63$ GeV ($\mathrm{T_{kin}} = 1.81$ GeV).

Since $-\Delta\sigma_{\mathrm{T}}$ contains no uncoupled spin-triplet contribution, a $^3\mathrm{S}_1$ resonance effect in this observable less will be diluted by other spin-states than in $-\Delta\sigma_{\mathrm{L}}$. The measurement $-\Delta\sigma_{\mathrm{T}}(np)$ and the determination of the $-\Delta\sigma_{\mathrm{T}}(\mathrm{I}=0)$ energy dependence provide a significant and sensitive check of the predicted resonance. For this reason, the accurate $-\Delta\sigma_{\mathrm{L,T}}(np)$ measurements near to $\mathrm{T_{kin}} = 1.8$ GeV are desirable [3b, 3c, 4]. The $\mathrm{I}=0$ spin dependent total cross section differences represent a considerable advantage for studies of the $^3\mathrm{S}_1$ state around 1.8 GeV, since this partial wave is expected to be dominant. This is in contrast with the $\mathrm{I}=1$ system. This state is not dominant and is strongly diluted in the forward direction. The obtained high momentum dependence of (np) spin observables [2, 3] are surprising for all traditional nuclear models. Their predictions are wrong for the highest momentum (asymptotic) behaviour of these observables related with almost fully

overlapping nucleons. In [3, 4] we discussed the QCD motivated model of a nonperturbative flavour-dependent interaction between quarks, induced by a strong fluctuation of vacuum gluon fields, i.e. instantons.

2. To exactly reveal a discovered structure at 1.8 GeV we are need in obtain the complete **L**,**T** data set [1] of np spin observables at 0° which is needed for the first direct reconstruction of all three isosinglet amplitudes of forward NN elastic scattering over a GeV energy range. With this very ambitious aim the following will be simultaneously measured for the first time at each chosen T_n: $\Delta\sigma_L$ and A_{00kk}, a spin correlation parameter for $np \to pn$ charge-exchange at zero angle with the **L** polarization of n beam and p target; $\Delta\sigma_T$ and A_{00nn} with the **T** - polarized beam and target. The proper equipment mounted in the last years was successfully tested (in the simultaneous $\sigma_{tot}(np)$ measurements of n beam transmission through D_2/H_2 targets and $d\sigma/dt$ of $n \to p$ charge-exchange at 0° on them). The Dubna group fulfilled first measurements under 0° of the ratios R_{dp} "elastic" np charge-exchange yields on D/H targets and defined the ratios $r^{nf/fl}_{np\to pn}(0)$ of "Non-Flip" to "Flip" contributions of $np \to pn$ process. In the region of $T_n \approx 1.8\,GeV$ one can expect an anomaly [3, 4] of $r^{nf/fl}_{np\to pn}$ - energy dependence (as in the case [3, 4] of the measurements of $\Delta\sigma_L$) if one follows the QCD-motivated reasoning (Lomon et al., Matsuda et al.) [5a, b] about a phase transition [5c] of the NN system into the exotic six-quark configuration in the isosinglet and the spin-triplet state $^3S_1$ with the mass $M \approx 2.63\,GeV$. For the exhaustive analysis of this structure [3, 4] using Argand diagrams for Re and Im parts of each of the three NN forward scattering amplitudes it is required to measure in Dubna not only the complete set [1] of np-spin observables at 0° but also to carry out pilot measurements in the same energy region of the ratio $R_{dp}(0) = d\sigma/d\Omega(nd)\ /\ d\sigma/d\Omega(np)$ for yields of "elastic" $n \to p$ charge-exchange non-polarized neutrons on D/H targets that independently defines [1b] the ratio $r^{nf/fl}_{np\to pn}$ for the charge exchange process at 0°: $r^{nf/fl}_{np\to pn} = 2/3R^{-1}_{dp} - 1$. Our preliminary results of R_{dp} at $T_n = 1.0$ and $1.2\,GeV$ were published in [6] and the later seven ones were given in [4]. Now we determinate new point at $T_n = 0.55\,GeV$ for more convention with other world experimental data at low energy and the final results (see item 6 and [7]) will be published in [8].

3. Accelerators and tools:

- The nuclotron of the JINR VBLHE. Relativistic beam $(1-6)\,GeV$ – polarized neutron beams with **L** or **T** orientation of the vector polarization (with the help of new [9] polarized d - source *CIPIOS* with intensity up to $5 * 10^{10}$ d/cycle), reversing of the polarization direction cycle by cycle, average polarization value ≈ 0.9 and unpolarized deuteron beam.
- Large polarized proton target (PPT) with volume of 140 cm^3 and $\pm$ **L/T** polarization value of $0.7 - 0.8$ and hydrogen H_2 and deuterium D_2 targets.
- Experimental set-up "DELTA–SIGMA" and same data processing [3c, 4, 7, 10].

4. The $\Delta\sigma_{L,T}(np)$ observables are expressed by the NN formalism (S. M. Bilenky and R. M. Ryndin, Phys. Lett. 6 (1963) 217, R. J. N. Phillips, Nucl. Phys. 43 (1963) 413). The general expression for the total cross section of a polarized nucleon beam transmitted through a polarized proton target, with the beam and target polarizations is:

$$\sigma_{tot} = \sigma_{0tot} + \sigma_{1tot}(P_B P_T) + \sigma_{2tot}(P_B k)(P_T k)\,, \qquad (1)$$

where P_B and P_T are the beam and target polarizations, and k is the unit vector in the incident beam direction. The term $\sigma_{0\mathrm{tot}}$ is the spin-independent total cross section, and $\sigma_{1\mathrm{tot}}$ and $\sigma_{2\mathrm{tot}}$ are the spin-dependent contributions which connect with the observables $\Delta\sigma_{\mathrm{T}}$ and $\Delta\sigma_{\mathrm{L}}$ by the relations:

$$-\Delta\sigma_{\mathrm{T}} = 2\sigma_{1\mathrm{tot}}\,, \tag{2}$$

$$-\Delta\sigma_{\mathrm{L}} = 2\,(\sigma_{1\mathrm{tot}} + \sigma_{2\mathrm{tot}})\,. \tag{3}$$

Values of $\sigma_{0\mathrm{tot}}$, $\Delta\sigma_{\mathrm{T}}$ and $\Delta\sigma_{\mathrm{L}}$ are connected with the imaginary parts of three invariant forward scattering amplitudes $a+b$, c and d via three optical theorems:

$$\sigma_{0\mathrm{tot}} = (2\pi/K)\,Im\,[a(0)+b(0)]\,, \tag{4}$$

$$-\Delta\sigma_{\mathrm{T}} = (4\pi/K)\,Im\,[c(0)+d(0)]\,, \tag{5}$$

$$-\Delta\sigma_{\mathrm{L}} = (4\pi/K)\,Im\,[c(0)-d(0)]\,. \tag{6}$$

where K is the c.m. momentum of the incident nucleon. Using the measured values of $\Delta\sigma_{\mathrm{L,T}}(np)$ and the existing very good $\Delta\sigma_{\mathrm{L,T}}(pp)$ data [11] at the same energies, one can deduce $\Delta\sigma_{\mathrm{L,T}}(\mathrm{I}=0)$ as:

$$\Delta\sigma_{\mathrm{L,T}}(\mathrm{I}=0) = 2\Delta\sigma_{\mathrm{L,T}}(\mathrm{np}) - \Delta\sigma_{\mathrm{L,T}}(\mathrm{pp})\,. \tag{7}$$

The $-\Delta\sigma_{\mathrm{L}}(np)$ data measured in Dubna, inclusive the new accurate latest data [3b, 3c] between 1.4 and 2 GeV, are plotted in Fig. 1. Their energy dependence (see darkened curve in Fig. 1) connect well with the also free-neutron $\Delta\sigma_{\mathrm{L}}$ data from Saclay. The *JINR* data show a fast unexpected decrease above 1.1 GeV, and suggest a minimum in the vicinity of 1.8 GeV. The solid curves $1-3$ represent the fits of $\Delta\sigma_{\mathrm{L}}$ from solution of the energy dependence (ED) phase shift analysis below 1.3 GeV. Above 0.6 GeV the PSA fits are only in qualitative agreement with the measured values. Moreover, above $1.0-1.3$ GeV the tendencies of the ED PSA (curves $1-3$) are in disagreement with the energy dependence of the Dubna data.

Below 2.0 GeV, a usual meson exchange theory gives the $-\Delta\sigma_{\mathrm{L}}(np)$ energy dependences [12] which disagree with data above 1 GeV (Fig. 1, the left panel). The presented values of isosinglet $\mathrm{I}=0$ part of $-\Delta\sigma_{\mathrm{L}}$ are calculated from np results and from pp data using Eq. 7 (see Fig. 1, the right panel). It show a plateau around 1.4 GeV, followed by a fast decrease and suggest a minimum in the vicinity 1.8 GeV. This structure is better pronounced in the $-\Delta\sigma_{\mathrm{L}}(\mathrm{I}=0)$ energy dependence than in the $-\Delta\sigma_{\mathrm{L}}(np)$ one. Above 0.5 GeV the PSA solutions are not in agreement with data.

The manifestation of exotic dibaryons in the energy $\Delta\sigma_{\mathrm{L}}$ dependence of np observables was predicted [5a] by the Cloudy Bag Model and R-matrix connection to long-range meson-exchange force region with the short-range region of asymptotically free quarks. This hybrid model gives the lowest lying exotic six-quark configurations in the isosinglet $^3\mathrm{S}_1$ state with the mass $\mathrm{M}=2.63$ GeV ($\mathrm{T_{kin}}=1.81$ GeV). It is close to the energy where the structure is suggested by our results.

A complete np data set at $0\,^\circ/180\,^\circ$ and DRSA for $(\mathrm{I}=0)$ would allow to discuss possible energy-dependent structures at the level of complex scattering amplitudes and not only at the level observables.

What can be deduced from the existing and planned $\Delta\sigma_{\mathrm{L,T}}(np)$ experiments? First of all $-\Delta\sigma_{\mathrm{T}}$ contains no uncoupled spin-triplet contribution, hence a $^3\mathrm{S}_1$ resonance effect in

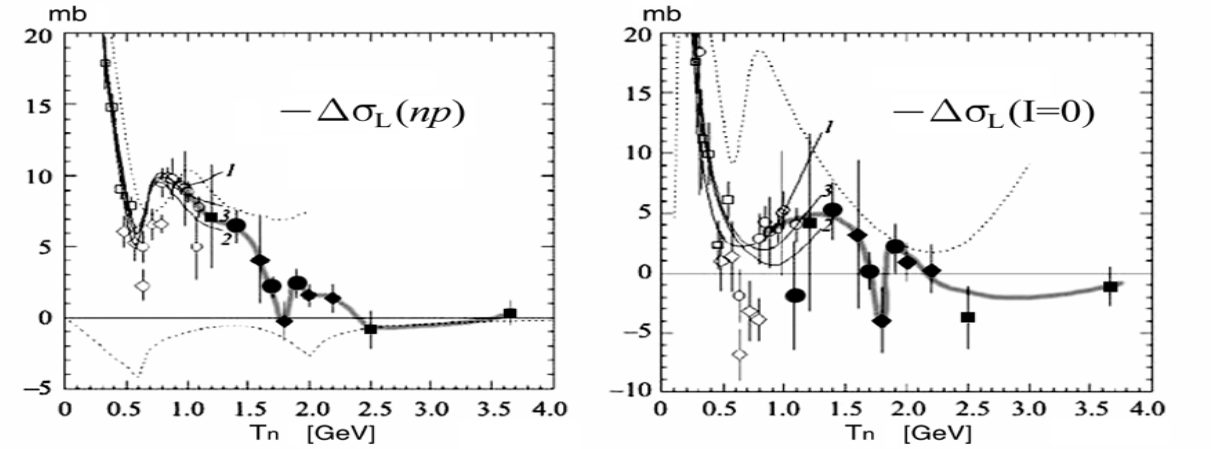

Figure 1: Energy dependence of the $-\Delta\sigma_{\rm L}(np)$ and $-\Delta\sigma_{\rm L}({\rm I}=0)$ respectively (black symbols – data of our experiment DELTA-SIGMA; open symbols – other world data; dotted curves at the left hist are the meson exchange model [12] (top curve) and the NPQCD (down curve); dotted curve at the right hist is the $-\Delta\sigma_{\rm L}({\rm I}=1)$ dependence from GW/VPI-PSA; full curves $1-3$ up to 1.3 GeV only at the both hists: 1) FA95 solution, 2) SP99 solution and 3) SP03 solution.

this observable may be less diluted by other spin-states than in $-\Delta\sigma_{\rm L}$. The measurement $-\Delta\sigma_{\rm T}(np)$ and the determination of the $-\Delta\sigma_{\rm T}({\rm I}=0)$ energy dependence provide a significant and sensitive check of the predicted resonance. Moreover, in difference $\Delta\sigma_{\rm L}-\Delta\sigma_{\rm T}$ the spin-singlet contribution vanishes. For this reason, the accurate $-\Delta\sigma_{\rm L,T}(np)$ measurements, in small energy steps, near to $T_{\rm kin}=1.8\,{\rm GeV}$ are desirable.

5. For the $A_{00kk}(np)$ and $A_{00nn}(np)$ coefficients according to [13] we have:

$$\begin{aligned}[d\sigma/d\Omega]_{\rm pol}(E,\Theta) = [d\sigma/d\Omega](E,\Theta)\Big[1 &+ A_{00n0}(E,\Theta)P_B^n + A_{000n}(E,\Theta)P_{\rm T}^n \\ &+ A_{00nn}(E,\Theta)P_B^nP_{\rm T}^n + A_{00ss}(E,\Theta)P_B^sP_{\rm T}^s \\ &+ A_{00kk}(E,\Theta)P_B^kP_{\rm T}^k + A_{00sk}(E,\Theta)(P_B^sP_{\rm T}^k) + P_B^kP_{\rm T}^s\Big]\,, \end{aligned} \tag{8}$$

where $d\sigma/d\Omega$ is a cross section for unpolarized nucleons. If the scattered particles are detected at 0° angle then analyzing powers $A_{00n0}(E,0)=A_{000n}(E,0)=0$ and parameters $A_{00sk}(E,0)=0$ and $A_{00ss}(E,0)=A_{00nn}(E,0)$. Thus, **only two** non-vanishing spin-dependent quantities of $A_{00nn}(E,0)$ and $A_{00kk}(E,0)$ **remain** in (8). Due to symmetries of amplitudes, which hold separately for isospins ${\rm I}=0$ and ${\rm I}=1$, the same relations are valid at $\Theta_{\rm c.m.}=\pi$. The measurements np observables at $\Theta_{\rm c.m.}=\pi$ are connected with the invariant amplitudes as follows:

$$d\sigma/d\Omega(\pi) = 1/2\left[|a|^2+|b|^2+|c|^2+|d|^2\right]\,, \tag{9}$$

$$d\sigma/d\Omega A_{00nn}(\pi) = 1/2\left[|a|^2-|b|^2-|c|^2+|d|^2\right]\,, \tag{10}$$

$$d\sigma/d\Omega A_{00kk}(\pi) = Re\;a^*d + Re\;b^*c\,, \tag{11}$$

where all experimental quantities and amplitudes are at $\Theta_{\rm c.m.} = \pi$. These equations can be transformed to:

$$d\sigma/d\Omega(1 + A_{00kk}) = |b + c|^2 = A + (Re\ b + Re\ c)^2\,, \tag{12}$$

$$d\sigma/d\Omega(1 - A_{00kk} - 2A_{00nn}) = |b - c|^2 = B + (Re\ b + Re\ c)^2\,, \tag{13}$$

$$d\sigma/d\Omega(1 - A_{00kk} + 2A_{00nn}) = |b + c - 2d|^2 = C + (Re\ b + Re\ c - 2Re\ d)^2\,, \tag{14}$$

where terms A, B, C contain the imaginary parts of amplitudes only. The **Re parts** of the amplitudes b, c and d **can be determined from Eqs. (12–14)** using known imaginary ones. A knowledge of I = 1 system is assumed in order to use the amplitude symmetries for the transformation of I = 0 amplitudes from $\Theta = 0$ to $\Theta = \pi$ and vice versa.

6. R_{dp} ratio for charge-exchange at $t = 0$ and ratio $r^{\rm nf/fl}_{np\to pn}$

Energy dependence of the ratio

$$R_{dp} = d\sigma/d\Omega(nd \to p(nn))\ /\ d\sigma/d\Omega(np \to pn) \tag{15}$$

for the charge exchange process at 0° in Lab. (quasi elastic $nd \to p(nn)$ and elastic $np \to pn$) was measured at high intensity non-polarized neutron beam from the Nuclotron using the magnetic spectrometer and hydrogen and deuterium targets. The differential cross section of $np \to pn$ reaction we separate to the "Flip" and "Non-Flip" parts:

$$d\sigma/d\Omega(np \to pn) = (d\sigma/d\Omega)^{\rm nfl}_{np\to pn} + (d\sigma/d\Omega)^{\rm fl}_{np\to pn}\ . \tag{16}$$

Using impulse approximation frame [14] the $nd \to p(nn)$ can be presented:

$$(d\sigma/d\Omega)(nd \to p(nn)) = (1 - F)\, d\sigma/d\Omega^{\rm nfl}_{np\to pn} + [1 - 1/3\, F]\, d\sigma/d\Omega^{\rm fl}_{np\to pn}\ ; \tag{17}$$

For zero angle the form-factor $F(t)$ equal to one, hence:

$$d\sigma/d\Omega(nd) = 2/3\, d\sigma/d\Omega^{\rm sfl}_{np\to pn} \tag{18}$$

This relation (18) demonstrates the using of a deuteron as a **filter for the "Non-Flip"** amplitudes at $t \approx 0$, i. e. the "Non-Flip" part, **due to the Pauli principle**, vanishes for $nd \to p\,(nn)$ quasi-elastic reaction with two slow neutrons with parallel spins. Using $R_{dp}(0)$ value we define the ratio $r^{\rm nf/fl}$ of "Non-Flip" to "Flip" parts of $np \to pn$ process:

$$r^{\rm nf/fl}_{np\to pn}(0) = 2/3\, R^{-1}_{dp} - 1\ \ , \quad \text{appiars from the (15) and (18).} \tag{19}$$

The Dubna $r^{\rm nf/fl}$ values obtained from the eight measurements of R_{dp} points (Table 1, Fig. 2) over the $0.5 \le {\rm T_n} \le 2\,{\rm GeV}$ energy region are in a good agreement with LAMPF [15] results at low energy (3 points below 1.0 GeV) and with JINR [16] point at ${\rm T}_n = 1.0\,{\rm GeV}$. In the formalism used in item $(4, 5)$ and Ref. [13] the ratio $r^{\rm nf/fl}$ can be expressed as:

$$r^{\rm nf/fl}_{np\to np}(\pi) = \frac{\mid a + b \mid^2}{\mid a - b \mid^2 + 2 \mid c \mid^2 + d^2}\ , \tag{20}$$

It has appeared that the $np \to pn$ forward and $np \to np$ backward scattering seem as absolutely identical but they have different separation to the "Flip" and "Non-Flip"

Table 1: Results of the R_{dp} and $r^{\mathrm{nf/fl}}$ values defined

T_n GeV	0.55	0.8	1.0	1.2	1.4	1.7	1.8	2.0
R_{dp}	0.589	0.554	0.553	0.551	0.576	0.565	0.568	0.564
ε	0.046	0.023	0.026	0.022	0.038	0.038	0.033	0.045
$r^{\mathrm{nf/fl}}$	0.133	0.204	0.206	0.209	0.158	0.179	0.174	0.183
ε	0.088	0.051	0.057	0.048	0.077	0.080	0.068	0.094

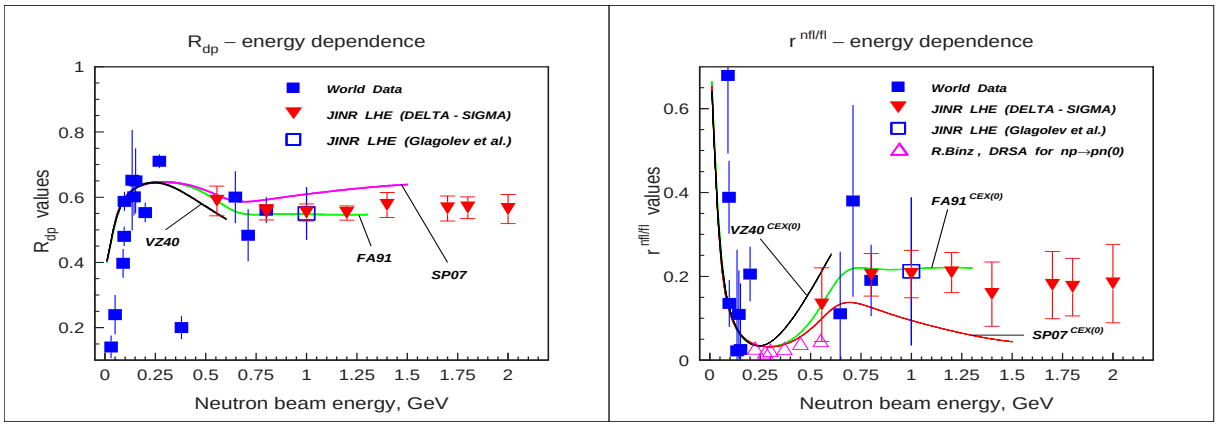

Figure 2: Energy dependence of $R_{dp}\,(\theta = 0)$ ratio of yields of $nd \to p\,(nn)$ quasi elastic to $np \to pn$ elastic charge exchange reactions (left) and energy dependence of $r^{nfl/fl}_{CEX(0)}$ ratio of "Non-Flip" to "Flip" contributions to the $np \to pn$ elastic one (right).

parts [7, 17] and for $r^{\mathrm{nf/fl}}_{np\to pn}(0)$ we should take the true c.ex. amplitudes at zero angle. Using PSA solutions [18] (FA 91 et al.) and the unitary transition [7] we transform the invariant amplitudes from np- backward to the c.ex. $np \to pn$ elastic one. As can be seen the experimental points and PSA curves resemble closely (see Fig. 2). Without a proper unitary transformation this agreement disappears (see PSA curve in Fig. 8 in [6b]).
For the first time the ratio $r^{nfl/fl}_{CEX(0)}$ is defined by us for the wide energy region using the R_{dp} measurements (our and the world data) and by the DRSA procedure (open triangles at the right panel – Binz points [4, item 6], [19] transformed now from the $np \to np$ backward to the charge exchange $np \to pn$ forward). The FA 91 solution agrees very closely with the data. Thus the **R_{dp}(0) is a well observable which allows as to define the spin characteristic** of np scattering even by non-polarized measurements **and will be used as an additional constraint for DRSA method**. The fast increase of ratio $r^{nfl/fl}_{CEX(0)}$ in the region around 0.5 GeV corresponds to the beginning of the meson and Δ production, i.e. this ratio is sensitive to the origin of the new degrees of freedom in the NN interaction. It allows to expect the similar change of energy dependence of $r^{nfl/fl}_{CEX(0)}$ at the GeV region where the **phase transitions NN→6q** will be appear [5].

7. Conclusion

1. New $-\Delta\sigma_{\mathrm{L}}(np)$ accurate results complete in the main the measurement of the $-\Delta\sigma_{\mathrm{L}}(np)$ and $-\Delta\sigma_{\mathrm{L}}(\mathrm{I}=0)$ energy dependence at the Dubna Synchrophasatron energy region. The comparison of the $\Delta\sigma_{\mathrm{L}}(\mathrm{I}=0)$ and $\Delta\sigma_{\mathrm{L}}(\mathrm{I}=1)$ energy dependence

shows that it is significantly different in the whole region of measured energies.

2. An unexpected anomalous rapid decrease of $-\Delta\sigma_{\rm L}(np)$, $-\Delta\sigma_{\rm L}({\rm I}=0)$ values above 1.1 GeV was confirmed in the latest run and a minimum around 1.8 GeV is observed. This minimum was predicted as a signal of NN system phase transition with excitation of lowest lying exotic 6q-configuration ${}^3{\rm S}_1({\rm I}=0)$ with mass 2.63 GeV [5].

3. The necessity of the complete np data set at $0\,^\circ/180\,^\circ$ for direct reconstruction of all three isosinglet amplitudes at $0\,^\circ$ in the kinetic energy region above 1.1 GeV (especially around 1.8 GeV) is emphasized.
4. The possibility of such measurements was demonstrated during the $\Delta\sigma_{\rm L}(np)$ and $np \to pn$ at $0\,^\circ$ investigations using Delta-Sigma set-up. A number of physical and methodical results on investigation of the quasielastic $nd \to p\,(nn)$ and the elastic $np \to pn$ charge exchange processes at $0\,^\circ$ over a few GeV region are also presented. The possibilities for R_{dp} measurements, using the prepared magnetic spectrometer, were demonstrated up to ${\rm T}_n = 2$ GeV. The $r^{\rm nf/fl}(0)$ ratio of "Non-Flip" to "Flip" parts in $np \to pn$ forward scattering was obtained for the first time by the $\mathbf{R}_{dp}$ **new observable** measurements, at ${\rm T}_n = 0.55$; 0.8; 1.0; 1.2; 1.4; 1.7; 1.8 and 2.0 GeV.
5. In $2007-2010$ years it needs to be done:
   - to continue our $r^{\rm nf/fl}_{np\to pn}(0)$ measurements by $R_{dp}(0)$ up to highest Dubna energies with small errors, especially around ${\rm T}_n = 1.8$ GeV;
   - to prepare T-mode of PPT-target polarization and to obtain **high intensity** and **high L/T-polarized** n **beam**, with new ***d*** source [9] at the Nuclotron;
   - to exactly reveal the observed structure in $-\Delta\sigma_{\rm L}({\rm I}=0)$ at 1.8 GeV, to obtain a complete np data set at $0\,^\circ/180\,^\circ$ in the Nuclotron energy region and to fulfill a Direct Reconstruction all of the three NN forward elastic Scattering Amplitudes and to reach the possible discovery of $NN \to 6q$ phase transitions [5] using Argand diagram exhaustive analysis of these amplitudes.
6. Our theme has been recently prolonged with the first priority; JINR management stipulates the finishing works for PPT (**L**/**T**-modes at high polarization of this large-sized target used earlier in FNAL), and to start a team work with INR RAS on the new source of vector polarized deuterons with the record intensity (CIPIOS from IUSF, USA) providing for the Nuclotron accelerated deuterons $\geq 10^{10}$ /cycle. That will give a chance to our big team of 80 high-skilled specialists from 13 laboratories world-wide to finish on time the specified in our project the ambitious precision investigations (with **potential discovery of** $NN \to 6q$ **phase transitions**) before assembling the NICA installation in VBLHE JINR building 205.

We are grateful to the JINR, JINR VBLHE, LPP, DLNP Directorates and all **our colleagues** and **friends** for these investigations support. The investigations were supported in part by the Russian Foundation for Basic Research, Grants N 02-02-17129 and N 07-02-01025

References

[1] **a.** In book Ed. A. M. Baldin Research Program of LHE JINR (Dubna 1999) 37–43, "Delta-Sigma Experiment", Spokesmen L. N. Strunov and V. I. Sharov;
b. L. Strunov: *In Proc. X Advanced Res. Workshop on H. En. Spin Phys. (Nato ARW Dubna Spin 03). Eds. A. V. Efremov, O. V. Terjaev, Dubna E1.2.-2004-800*

[2] **a.** A. A. Nomofilov et al.: Phys. Lett. B325 (1994) 327;
b. Phys. Rev. Lett. v.74, N25 (1995) 4997;
c. A. P. Kobushkin: *In Proc. of 10th Int. Symp. on High En. Phys. (Yamada Conf. XXXV)* Nov. 1992. Nagoya "Spin 92". Ed. T. Hasegawa et al. p.505;
d. L. N. Strunov: ibid. p.501.

[3] **a.** V. I. Sharov et al.: JINR Rapid Communication 3[77]-96 (1996) 13; 4[96]-99 (1999) 5; Z. Phys. C.71 N1 (1996) 65; Eur. Phys. J. C13 (2000) 255–265;
b. Eur. Phys. J. C37 (2004) 79; Yad. Phys. 68 N11 (2005) p. 1857;
c. V. I. Sharov et al.: Czech. J. Phys. 55 (2005) A289–A305.

[4] L. N. Strunov et al.: Czech. J. Phys **56** (2006) C343 C357

[5] **a.** E. L. Lomon et al.: at the proper references in [3];
b. M. Matsuda et al.: Few-Body Systems Suppl. 12 (2000) 457.
c. V. I. Kukulin, V. N. Pomerantsev, M. Kaskulov and A. Faessler: J. Phys. G: Nucl. Part. Phys. 30 (2004) 287 - 308.
d. V. G Boyko, L. L. Yenkovszky, V. M. Sysoev: Phys. El. Part. and Atom. Nucl. (1994), V. 22, p. 680-681.

[6] **a.** A. A. Morozov et al.: Czech. J. Phys. 55 (2005) A307–A314,
b. A. A. Morozov et al.: Czech. J. Phys. 56 (2006) C369–C377.

[7] R. A. Shindin et all.: in this *Proceeding*.

[8] V. I. Sharov, A. A. Morozov, R. A. Shindin et all.: to be submitted to "Yadernaya Fizika".

[9] A. I. Malakhov: Czech. J. Phys. 55 (2005) A65–A74.

[10] R. A. Shindin et al.: Czech. J. Phys. 55 (2005) A399–A405.

[11] C. Lechanoine-Leluc: *in Proc.of 10th Int. Symposium on High En. Phys. "Spin 92"* Nagoya. Ed. T. Hasegawa et al: p.125.
C. Lechanoine-Leluc, F. Lehar: Rev. Mod. Phys. (1993) v.65, p.47.

[12] T.-S. H. Lee.: Phys. Rev. 29 (1984) 59.

[13] F. Lehar: Private Comm. May 11, 2005.

[14] R. Lednicky, V. L. Lyuboshitz et al.: *in Proc. XVI Int. Seminar ISHEPP Dubna* June (2002), Dubna JINR (2004) v.1 p.199.

[15] **a.** B. E. Bonner et al.: Phys. Rev. C17 (1978) 664.
b. R. R. Larsen: Nuovo Cimento XVIII (1960) 1039.
c. C. W. Bjork et al.: Phys. Lett. B63 (1976) 31. We normalize the values R_{dp} of this reference by factor of 0,56/0,66 – ratio of R_{dp} values in the new and old measurements at LAMPF [15a] (78), according to the latest comment of Bonner [11] 1978 about mistakes in previous R_{dp} measurements, including [15c] (76) Bjork et al. used the same layout at "the Nucl. Phys. Lab at LAMPF" (Fig. 11 in [15c]).

[16] V. V. Glagolev et al.: Eur. Phys. J. A15 (2002) 471; *in Preprint JINR* P1-2006-112 (2006).

[17] V. L. Luboshitz, V. V. Luboshitz: in *Proceedengs of the XIV International Seminar on Interaction of Neuterons with Nuclei*, Dubna (2007) E3-2007-23, p.64-74.

[18] **a.** R. A. Arndt, W. J. Briscoe, I. I. Strakovsky and R. L. Workman: Phys. Rev. C 76 (2007);
b. R. A. Arndt, I. I. Strakovsky and R. L. Workman: Phys. Rev. C 62 (2000);
c. R. A. Arndt, C. H. Oh, I. I. Strakovsky, R. L. Workman and F. Dohrmann: Phys. Rev. C 56 (1997).

[19] R. Binz: Ph.D. Thesis. Freiburg University Germany (1991);
R. Binz et al.: Helvetica Phys. Acta 65 (1992) 880.

SEPARATION "FLIP" AND "NON-FLIP" PARTS of np→pn CHARGE-EXCHANGE AT ENERGIES T_n = 0.5 – 2.0 GeV AND COMPARISON WITH THE PSA SOLUTIONS

R.A. Shindin†, E.V. Chernykh, D.K. Guriev, A.A. Morozov,
A.A. Nomofilov, V.Yu. Prytkov, V.I. Sharov, L.N. Strunov

JINR, Veksler and Baldin Laboratory of High Energies, 141980 Dubna, Russia
† *E-mail: shindin@sunhe.jinr.ru*

Abstract

Using the new "Delta-Sigma" experimental data of the R_{dp} ratio and with the help of the "Dean" formula the "Flip" and "Non-Flip" parts of $np \to pn$ charge-exchange are separated. The PSA Solutions for the $np \to np$ elastic scattering are transformed to the charge-exchange process and good agreement have been obtain.

1 Introduction

The "Delta-Sigma" experiment research program [1] assumes to obtain a complete np data at 0°: the measurements of total cross section differences $\Delta\sigma_L(np)$ and $\Delta\sigma_T(np)$ for the longitudinal (L), or transverse (T) beam and target polarizations and spin-correlation parameters $A_{00kk}(np)$ and $A_{00nn}(np)$ [2]. The main task of these studies is to determine the Re and Im parts of np amplitudes over the energy region 1.2 – 3.7 GeV. The $\Delta\sigma_L(np)$ energy dependence [2] shows an anomalous fast decrease to zero above 1.1 GeV and structure in $-\Delta\sigma_L(\mathrm{I}=0)$ around 1.8 GeV [9] predicted in Ref. [3; 4]. For the exhaustive analysis of this structure it require to build the Argand diagrams for Re and Im parts of each of the three NN forward scattering amplitudes. To reduce the sign ambiguities the "Delta-Sigma" collaboration performed the measurements of the ratio $R_{dp} = [d\sigma/dt](nd)/[d\sigma/dt](np)$ for the charge-exchange quasi-elastic and elastic processes at 0° using the D_2 and H_2 targets. The knowledge of the R_{dp} could provide additional constraint and will allow to exclude one of some sign uncertainties for the direct reconstruction the Re parts of the scattering amplitudes. Also the R_{dp} value independently define the ratio $r^{nfl/fl}$ of "Non-Flip" to "Flip" contributions in the $np \to pn$ charge-exchange at 0°.

2 Theoretical approach for R_{dp} and $r^{nfl/fl}$

As mentioned above the observable R_{dp} is the ratio of a quasi-elastic $nd \to p\,(nn)$ differential cross section to the free $np \to pn$ charge-exchange (named CEX):

$$R_{dp} \;=\; \frac{d\sigma/dt\;{}_{nd\to p\,(nn)}}{d\sigma/dt\;{}_{CEX}} \tag{1}$$

Following the theory in [5; 6], when the duration of the nd collision is much smaller than the characteristic movement period of the deuteron nucleons, the $nd \to p\,(nn)$ reaction

in the frame of the impulse approximation can be expressed by "Dean" formula:

$$\frac{d\sigma}{dt}_{\,nd\to p\,(nn)} = (1 - F(t))\,\frac{d\sigma}{dt}^{\,Non-Flip}_{\,CEX} + (1 - \frac{1}{3}F(t))\,\frac{d\sigma}{dt}^{\,Flip}_{\,CEX} \tag{2}$$

Here $F(t)$ is the deuteron form-factor which equals one for the forward direction and when the scattering angle θ close to zero the first term on the right-hand of (2) vanish:

$$\frac{d\sigma}{dt}_{\,nd\to p\,(nn)\,(0)} = \frac{2}{3}\,\frac{d\sigma}{dt}^{\,Flip}_{\,CEX\,(0)} \tag{3}$$

Let's notice that similar simplification is not possible if we take the elastic backward reaction $np \to np$ instead of the charge-exchange forward, because neglecting the difference of the masses M_n and M_p the four-momentum transfer t will defined as $-4P_n^2$ and the deuteron form-factor $F(t)$ will not equal one. Such replacement could be justified if the both np - elastic scattering interpretation ($np \to np$ backward or $np \to pn$ forward) are absolutely identical together with their "Flip" and "Non-Flip" parts. However this hypothesis is not valid as it will be shown in the next item (see also [7]).

For the R_{dp} and $r^{nfl/fl}_{CEX\,(0)}$ ratios we have:

$$R_{dp} = \frac{2}{3}\,\frac{\frac{d\sigma}{dt}^{\,Flip}_{\,CEX\,(0)}}{\frac{d\sigma}{dt}_{\,CEX\,(0)}} = \frac{2}{3}\,\frac{1}{1 + r^{nfl/fl}_{CEX\,(0)}} \quad ; \quad r^{nfl/fl}_{CEX\,(0)} = \frac{2}{3}\,\frac{1}{R_{dp}} - 1 \tag{4}$$

Our preliminary experimental data of R_{dp} ratio at $\mathrm{T}_n = 1.0$ and $1.2\,\mathrm{GeV}$ were published in [8] and the seven later results were given in [9]. Now we determinate new point at $\mathrm{T}_n = 0.55\,\mathrm{GeV}$ for more convention with other world experimental data at low energy. Some doubts on a quality are caused with the point at $1.7\,\mathrm{GeV}$ but for another 7 values the presented results (see Tab. 1, Fig. 1) have a final status and will be published in [10]. Using formula (4) the respective ratios $r^{nfl/fl}_{CEX\,(0)}$ of "Non-Flip" to "Flip" contributions of the $np \to pn\,(0)$ charge exchange process are calculated (see Tab. 1 and Fig. 2).

3 Transition from the np backward to the charge-exchange forward

In the frame of isotopic invariance the nucleon-nucleon scattering matrix is:

$$M(k', k) = M_0(k', k)\,\frac{1 - \hat{\tau}_1\hat{\tau}_2}{4} + M_1(k', k)\,\frac{3 + \hat{\tau}_1\hat{\tau}_2}{4} \tag{5}$$

Here $\hat{\tau}_1$ and $\hat{\tau}_2$ are the isotopic Pauli operators of nucleons, k and k' are the unit vectors of initial and final relative momentums and the matrixes M_0 and M_1 describe the NN scattering for isotopic spin $T = 0$ and $T = 1$ respectively. For $np \to np$ and $np \to pn$ elastic reactions to the same angle θ it can be written:

$$< np|M|np > = \frac{1}{2}\,(M_1 + M_0) \qquad < np|M|pn > = \frac{1}{2}\,(M_1 - M_0) \tag{6}$$

Using the Pauli spin operators $\hat{\sigma}_1$ and $\hat{\sigma}_2$ the matrix $M(k', k)$ can be expressed in the *Goldberger-Watson* scattering amplitudes:

$$M_T(k', k) = a_T + b_T(\hat{\sigma}_1 n)(\hat{\sigma}_2 n) + c_T(\hat{\sigma}_1 n + \hat{\sigma}_2 n) + e_T(\hat{\sigma}_1 m)(\hat{\sigma}_2 m) + f_T(\hat{\sigma}_1 l)(\hat{\sigma}_2 l) \tag{7}$$

Here the (a, b, c, e, f) are the complex functions of the interacting particles energy and variable ($k\,k'$) $= \cos\theta$, the T index equals the value of isotopic spin and the basis vectors are defined as: $n = \frac{k*k'}{|k*k'|}$, $m = \frac{k-k'}{|k-k'|}$ and $l = \frac{k+k'}{|k+k'|}$. The *Goldberger-Watson* formalism very suitable for the separation elastic scattering to the "Flip" and "Non-Flip" parts because the a_T amplitude have not operator term and is "Non-Flip" in its definition:

$$\frac{d\sigma}{dt}^{Non-Flip} = |a|^2 \qquad \text{and} \qquad \frac{d\sigma}{dt} = |a|^2 + |b|^2 + 2|c|^2 + |e|^2 + |f|^2 \tag{8}$$

Another *Wolfenstein* representation allow to share the matrix $M(k',k)$ to the singlet and triplet parts using the spin projection operators $\hat{S} = \frac{1}{4}(1 - \hat{\sigma}_1\hat{\sigma}_2)$ and $\hat{T} = \frac{1}{4}(3 + \hat{\sigma}_1\hat{\sigma}_2)$:

$$M_T(k',k) = B_T\hat{S} + [\, C_T(\hat{\sigma}_1 n + \hat{\sigma}_2 n) + \frac{1}{2} G_T((\hat{\sigma}_1 m)(\hat{\sigma}_2 m) + (\hat{\sigma}_1 l)(\hat{\sigma}_2 l)) + \\ + \frac{1}{2} H_T((\hat{\sigma}_1 m)(\hat{\sigma}_2 m) - (\hat{\sigma}_1 l)(\hat{\sigma}_2 l)) + N_T(\hat{\sigma}_1 n)(\hat{\sigma}_2 n)\,]\,\hat{T} \tag{9}$$

These both matrix representations related by the linear transitions:

$$a_T = \frac{1}{4}(B_T + G_T + N_T) \qquad b_T = \frac{1}{4}(3N_T - B_T - G_T) \qquad c_T = C_T$$
$$e_T = \frac{1}{4}(G_T + 2H_T - B_T - N_T) \qquad f_T = \frac{1}{4}(G_T - 2H_T - B_T - N_T) \tag{10}$$

Let us to quote the work [11]: "The requirement of the antisymmetry of final wave function $M(k',k)\chi_S\chi_T$ (χ_S and χ_T – spin and isotopic function of initial state) relative to the total permutation, including permutation of scattering vector ($k' \to -k'$), permutation of spin and isotopic variables lead not to the change of sings of the amplitudes $B_1(\theta)$, $C_1(\theta)$, $H_1(\theta)$, $G_0(\theta)$ and $N_0(\theta)$ after the changing $\theta \to \pi - \theta$ but the amplitudes $B_0(\theta)$, $C_0(\theta)$, $H_0(\theta)$, $G_1(\theta)$ and $N_1(\theta)$ become inverse". According to this rule we perform the transition from the $np \to np\,(\pi - \theta)$ elastic to the charge-exchange $np \to pn\,(\theta)$. After the turn $k' \to -k'$ the vectors basis changed also: $n \to -n$, $m \to l$ and $l \to m$. Using symbolical changing $M_1^{CEX} = M_1$ and $M_0^{CEX} = -M_0$ and rewriting the n, m, l basic we define:

$$a_T^{CEX} = \frac{1}{4}(B_T - G_T - N_T) \qquad b_T^{CEX} = \frac{1}{4}(\,G_T - B_T - 3N_T) \qquad c_T^{CEX} = C_T$$
$$e_T^{CEX} = \frac{1}{4}(N_T + 2H_T - B_T - G_T) \qquad f_T^{CEX} = \frac{1}{4}(N_T - 2H_T - B_T - G_T) \tag{11}$$

It's possible to see in the (10) and (11) the "Non-Flip" amplitudes $a_T(\pi - \theta)$ and $a_T^{CEX}(\theta)$ are different among themselves due to the yield of spin-triplet amplitudes G_T and N_T. No difficult to define the direct amplitudes transition from the np elastic backward to the charge-exchange forward (12). Amplitudes c_T^{CEX} and c_T are equal and for other it is:

$$a_T^{CEX} = -\frac{1}{2}(a_T + b_T + e_T + f_T) \qquad b_T^{CEX} = -\frac{1}{2}(a_T + b_T - e_T - f_T)$$
$$e_T^{CEX} = -\frac{1}{2}(a_T - b_T - e_T + f_T) \qquad f_T^{CEX} = -\frac{1}{2}(a_T - b_T + e_T - f_T) \tag{12}$$

Inverse transition will be absolutely equivalent and have the unitary symmetry. Therefore the differential cross section of the np backward and charge-exchange forward are equivalent automatically (13) even if their "Non-Flip" or "Flip" parts are different.

$$\frac{d\sigma}{dt}\ np \to np\,(\pi - \theta) = \frac{d\sigma}{dt}\ np \to pn\,(\theta) \tag{13}$$

When the θ closes to zero the additional simplification appears: $b_T = f_T$, $b_T^{CEX} = e_T^{CEX}$ and $c_T^{CEX} = c_T = 0$. In this case we obtain the formulas which became known from [7]. Very interesting that the formalism for NN scattering was created more than 50 years ago but the essential distinction of the "Non-Flip" amplitudes a_T^{CEX} forward and a_T backward were reveal in 2005 year only. Before this time the both interpretation of np elastic were considered as an absolutely identical. We used the $np \to np$ backward amplitudes from the PSA solutions and agreement with our experimental data was very poor (see [8]). Now using the unitary transition (12) this problem goes away (see Fig. 1 and Fig. 2).

Table 1: Results of defining the R_{dp} and $r^{\mathrm{nf/fl}}$ values

T_n GeV	0.55	0.8	1.0	1.2	1.4	1.7	1.8	2.0
R_{dp}	0.589	0.554	0.553	0.551	0.576	0.565	0.568	0.564
ε	0.046	0.023	0.026	0.022	0.038	0.038	0.033	0.045
$r^{\mathrm{nf/fl}}$	0.133	0.204	0.206	0.209	0.158	0.179	0.174	0.183
ε	0.088	0.051	0.057	0.048	0.077	0.080	0.068	0.094

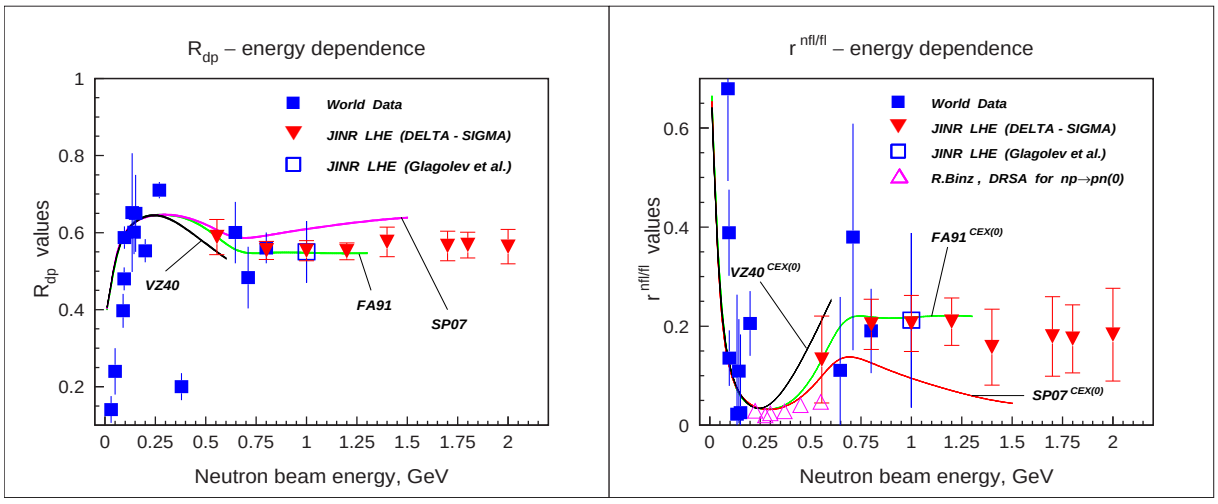

Figure 1: Energy dependence of $R_{dp}\,(\theta = 0)$ ratio of yields of $nd \to p\,(nn)$ quasi elastic to $np \to pn$ elastic charge exchange reactions. The PSA solutions FA 91, VZ 40 and SP 07 were taken from the SAID data base [13] as an amplitudes for np backward reaction, transformed to the charge-exchange by the (12) and the R_{dp} curves are calculated using "Dean" formulas (2, 3).

Figure 2: Energy dependence of $r_{CEX(0)}^{nfl/fl}$ ratio of "Non-Flip" to "Flip" parts in the $np \to pn$ charge exchange elastic process. These points have been obtain from the R_{dp} experimental data using "Dean" formulas (2, 3). The PSA solutions FA 91, VZ 40 and SP 07 were taken from the SAID data base [13] and transformed to the charge-exchange by the (12). The "Binz" points [12] were taken from the DRSA analysis for the np backward and again recalculated using (12).

4 Conclusion

The final [10] and preliminary at 1,7 GeV experimental results of defining the 8 points of R_{dp} ratio at zero angle at energies $T_n = 0.5 - 2.0$ GeV are presented (see Tab. 1, Fig. 1). The existed world experimental data at smaller energy consent with our points.

Using the "Dean" formula the respective values of $r^{nfl/fl}$ are calculated for the charge-exchange process $np \to pn\,(0)$ (see Tab. 1, Fig. 2). "Non-Flip" part is not zero and equals $\approx 17\,\%$ of the differential cross section.

The transition of the PSA solutions from the $np \to np$ elastic backward to the charge-exchange $np \to pn$ forward amplitudes has considered and the curves of R_{dp} and $r^{nfl/fl}$ calculated by this approach well describe the experimental points (see Fig. 1 and Fig. 2).

References

[1] V. I. Sharov, L. N. Strunov et al.: in *Research Program of LHE JINR*, Ed. D.M. Baldin (Dubna 1999), "Delta-Sigma" Experiment pp. 37-43.

[2] V. I. Sharov et al.: Eur. Phys. J. **C 37** (2004) 79; Yad. Phys. **68 N11** (2005) p. 185; Czech. J. Phys. **55** (2005) A289 A305

[3] E. L. Lomon, Colloq. Phys. (France) 51, C6-363 (1990);

[4] P. LaFrance and E. L. Lomon, in *Proceedings of the International Conference "Mesons and Nuclei at Intermediate Energies"*, Dubna, 1994, Ed. by M. Kh. Khankhasaev and Zh. B. Kurmanov (World Sci., Singapore, 1995), Vol. XV, p. 97.

[5] N. W. Dean: Phys. Rev. D bf 5 (1972) 1661.

[6] V. V. Glagolev, V.L. Luboshitz et all.: *Preprint JINR*, E1-99-280, Dubna (1999).

[7] V. L. Luboshitz, V. V. Luboshitz: in *Proceedengs of the XI International Workshop on Elastic and Diffractive Scattering. Towards High Enegy Frontiers* (Blois, France, May 15-20, 2005), Gioi Publishers, Vietnam (2006), p. 223-227. V. L. Luboshitz, V. V. Luboshitz: in *Proceedengs of the XIV International Seminar on Interaction of Neuterons with Nuclei*, Dubna (2007) E3-2007-23, p.64-74.

[8] A. A. Morozov et al.: Czech. J. Phys **55** (2005) A307 A314

[9] L. N. Strunov et al.: Czech. J. Phys **56** (2006) C343 C357

[10] V. I. Sharov, A. A. Morozov, R. A. Shindin et all.: to be submitted to "Yadernaya Fizika".

[11] S. M. Bilen'kii, L. I. Lapidus, R. M. Ryndin: Uspekhi Phys. Nauk (1964) LXXXIV (2), p. 243-301; Sov. Phys. Uspekhi (1965) 7 (5), p. 721-754.

[12] R. Binz: Ph.D. Thesis. Freiburg University Germany (1991). R. Binz et all.: Helvetica Phys Asta **65** (1992) 880.

[13] R. A. Arndt, W. J. Briscoe, I. I. Strakovsky and R. L. Workman: Phys. Rev. C 76, 025209 (2007), arXiv: 0706.2195 [nucl-th]. R. A. Arndt, I. I. Strakovsky and R. L. Workman: Phys. Rev. C 62, 034005 (2000), [nucl-th/0004039]. R. A. Arndt, C. H. Oh, I. I. Strakovsky, R. L. Workman and F. Dohrmann: Phys. Rev. C 56, 3005 (1997), [nucl-th/9706003].

ASYMMETRY MEASUREMENT IN THE ELASTIC π^+p SCATTERING AT 0.8 GEV/C

I.G. Alekseev[1], N.A. Bazhanov[2], Yu.A. Beloglazov[3], P.E. Budkovsky[1], E.I. Bunyatova[2], E.A. Filimonov[3], V.P. Kanavets[1], L.I. Koroleva[1], A.I. Kovalev[3], S.P. Kruglov[3], B.V. Morozov[1], V.M. Nesterov[1], D.V. Novinsky[3], V.V. Ryltsov[1], V.A. Shchedrov[3], V.V. Sumachev[3], D.N. Svirida[1†], A.D. Sulimov[1], V.Yu. Trautman[3], V.V. Zhurkin[1].

(1) *Institute for Theoretical and Experimental Physics, B. Cheremushkinskaya 25, Moscow, 117218, Russia.*
(2) *Joint Institute for Nuclear Research, Dubna, Moscow district, 141980, Russia.*
(3) *Petersburg Nuclear Physics Institute, Gatchina, Leningrad district, 188350, Russia.*
† *E-mail: Dmitry.Svirida@itep.ru*

Abstract

New experimental data on the asymmetry in the elastic π^+p scattering at 0.8 GeV/c are presented by the ITEP-PNPI collaboration. The kinematic region of the measurement corresponds to the very backward c.m. scattering angles, where no other experimental data are available due to low cross section values and the predictions of the partial wave analysis are most contradictory. The results are obtained in two geometrical configurations of the SPIN setup and cover the angular range of $137 - 173^o$ in the center of mass frame.

1 Introduction

We present the new experimental data on the asymmetry in the very backward π^+p elastic scattering ($137^o - 173^o$ c.m.) at 0.80 GeV/c. This experiment is the latest and the last one in the series of the polarization parameter measurements by the ITEP-PNPI collaboration. The aim of the whole set of our measurements was to provide necessary information for the *unambiguous reconstruction* of the pion-proton elastic scattering amplitude by partial-wave analyses (PWA).

The status of the modern experimental light baryon spectroscopy is far from satisfactory. The current PDG data on light resonances are still based mainly on the two PWAs: CMB80 [1] and KH80 [2], both performed more than two decades ago. However more recent analyses by VPI/GWU group [3] did not revealed 4 of 13 resonances in 1.7 and 1.9 GeV clusters. From the other hand the new data by ITEP-PNPI collaboration on the normal polarization [4] and spin rotation parameters [5] in the backward $\pi^{\pm}p$ scattering did not confirm the CMB80 and KH80 predictions.

The choice of the kinematic region for this experiment was based on the search for the areas, where the behavior of various PWA is most unstable. Zero trajectories of the transverse amplitudes ($F^+ = f + ig$, $F^- = f - ig$) reflect the global features of PWA. In fig. 1a one can see that in the region of backward scattering the trajectories closely approach or cross the real circle at energies around 0.8 GeV/c, leading to very small cross-section values (fig. 1b) since both amplitudes $F+$ and F^- are small. At the same time the scattering asymmetry is very sensitive to the relation between the two amplitudes, thus allowing to choose the correct solution branch.

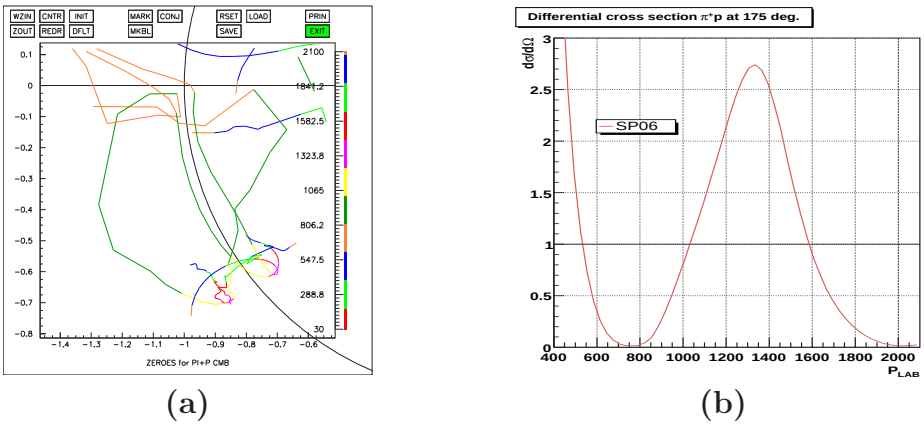

(a) (b)

Figure 1a. Transverse amplitude zero trajectories at backward c.m. angles from various PWA.

Figure 1b. Differential cross-section of the elastic π^+p scattering at 175^o as a function of incident momentum (from [3]).

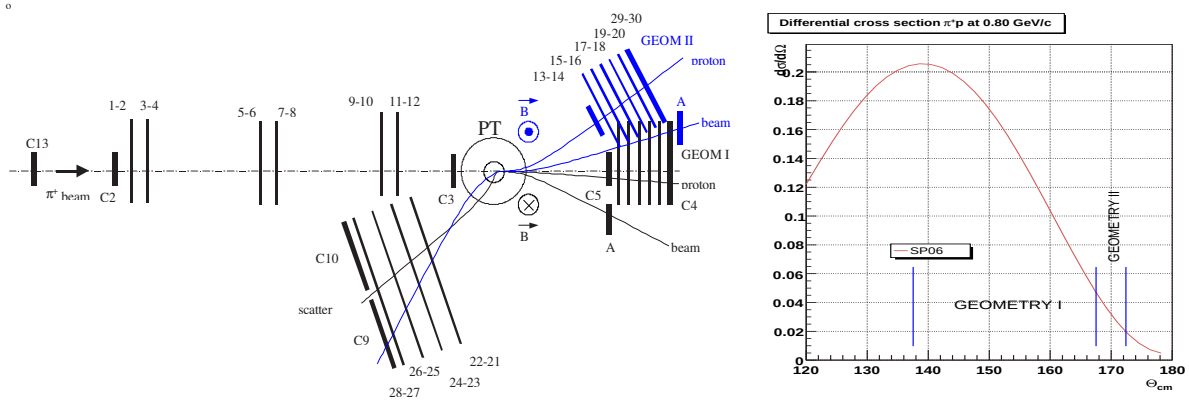

(a) (b)

Figure 2a. Experimental setup SPIN in two spatial configurations.

Figure 2b. Angular dependence of the differential cross-section of the elastic π^+p scattering at 0.8 GeV/c and the ranges covered by SPIN setup.

2 Experiment and Data Processing

The main elements of the experimental setup are [6]: a transversely polarized proton target inside a super-conductive solenoid, several sets of wire chambers for the tracking of the incident and scattered particles and a number of scintillation counters for triggering (see fig. 2a). To enlarge the angular coverage the data were taken in two spatial configurations of the setup ("geometry I" and "geometry II") with reversed direction of the target magnetic field resulting in different deflection angles of the recoil protons. "Geometry II" corresponds to the largest scattering angles, where the cross-section is extremely small (fig. 2b).

The procedure of the elastic event selection is illustrated by fig. 3. For each event the deviation from elastic kinematics was calculated in terms of two variables: $\Delta\theta$ – the difference in c.m. scattering angle for the pion and the proton and $\Delta\phi$ – sum of their

azimuthal deviations from the scattering plane, and two-dimensional distributions in these variables were filled. For the best background estimate the distributions were fit with a 2-dim 12-parameter polynomial excluding the area of the elastic peak. The number of the elastic events was calculated as the distribution excess over the background, interpolated to the area under the peak. The background level in the region of the low cross-section ("geometry II") is significantly larger than that at smaller scattering angles (compare fig. 3a and 3b), resulting in the error increase. The intensity normalization is done based on the quasi-elastic event counts which are believed to be unpolarized and give the main contribution to the background. Comparison of the results with various cuts around the elastic peak allowed to make additional systematic error tests. The normalization error of the data is defined by the accuracy of the target polarization measurement and does not exceed 3% which is well below the statistical accuracy.

3 Results and Conclusions

Figure 4 presents the results of the asymmetry measurement at 0.80 GeV/c. The data are in the best correspondence to the latest partial wave solution SP06 of VPI/GWU group [3], but significantly diverge from their earlier predictions SM95. The point at the smallest scattering angle is in agreement with older measurements, but the rest of the data definitely contradict to the measurements by Martin et al. [7].

More general conclusions can be drawn from the discussion of the whole set of the

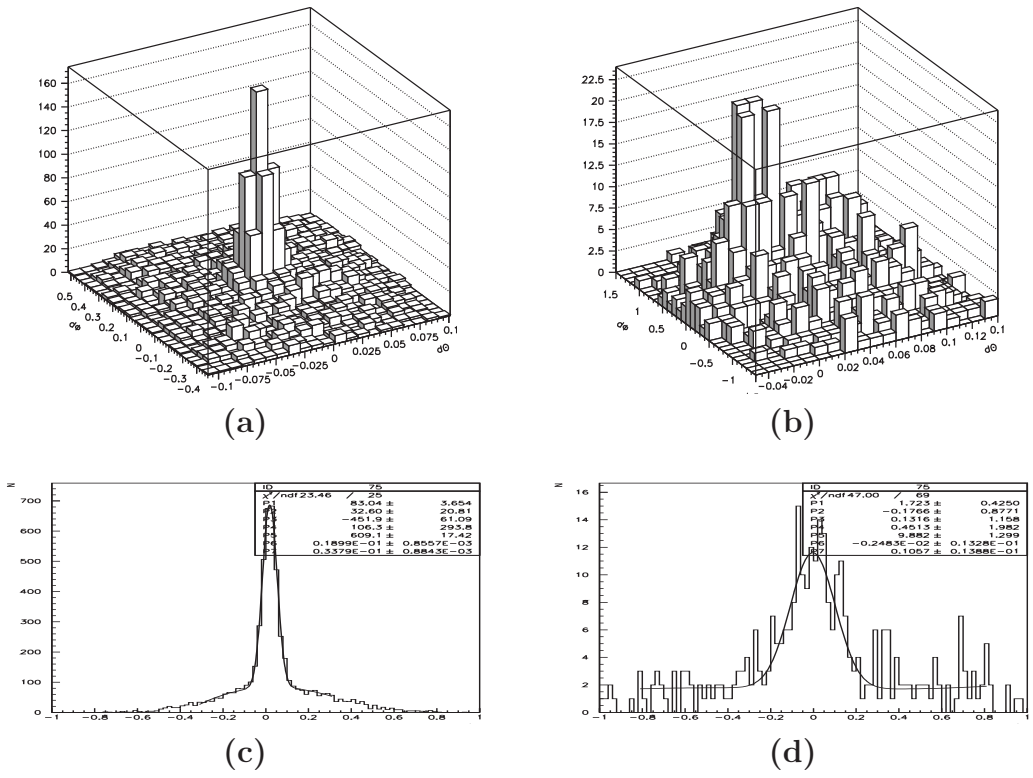

Figures 3a,b. Deviation from elastic kinematics in "geometry I" (a) and "geometry II" (b).
Figures 3c,d. Central slices of the above 2D histograms; background to signal ratio is about 0.1 in "geometry I" and close to 0.8 in "geometry II".

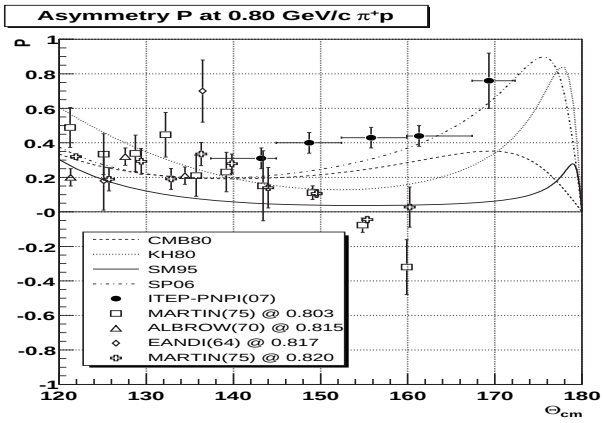

Figure 4. Results for the asymmetry in π^+p elastic scattering at 0.8 GeV/c (closed dots) compared to older data (open markers) and partial wave analyses predictions (lines).

latest experimental data on spin rotation parameters and asymmetry by ITEP-PNPI. It is clear that both old analyses (CMB80 and KH80) do not reconstruct properly the backward scattering amplitude. So one should be careful in comparison of the theory with the present day spectrum and parameters of the light quark baryon resonances, because it is based mainly on these two old analyses.

However one should mention the significant progress of the energy dependent partial wave analysis (DPWA) by VPI/GWU group. Approaches to the data selection and analysis technique were greatly improved. Growing activity of the Helsinki group on the strongly fixed-t dispersion relations constrained PWA [8] based on KH80 approach is very important, but the work is still in progress. Our results on the spin rotation parameters and new precise data on the asymmetry are important to resolve the remaining PWA uncertainties.

4 Acknowledgments

We are grateful to the ITEP accelerator team for providing us with excellent beam conditions. The work was partially supported by the Russian Fund for Basic Research grant 02-02-16111.

References

[1] R. E. Cutcosky, *Phys. Rev.* **D20**, 2839 (1979).
[2] G. Höehler, *Handbook of Pion-Nucleon Scattering, Physics Data* **12-1**, Fachinformationzentrum, Karlsruhe, 1979.
[3] R. A. Arndt et al., *Phys. Rev.* **C52**, 2120 (1995).
R. A. Arndt et al., *Phys. Rev.* **C74**, 045205 (2006).
[4] I. G. Alekseev et al., *Nucl. Phys.* **B348**, 257 (1991).
[5] I. G. Alekseev et al., *Phys. Lett.* **B351**, 585 (1995);
I. G. Alekseev et al., *Phys. Lett.* **B485**, 32 (2000);
I. G. Alekseev et al., *Eur. Phys. J.* **A12**, 117 (2001).
[6] Yu. A. Beloglazov et al., *Instr. and Exp. Tech.* **47**, 744 (2004)
[7] J. F. Martin et al., *Nucl. Phys.* **B89**, 253 (1975).
[8] P. Piirola and M. E. Sainio, *Int. J. Mod. Phys.* **A20**, 1810 (2005).

RECENT HERMES RESULTS ON THE QUARK HELICITY STRUCTURE OF THE NUCLEON

M. J. Varanda[1†] on behalf of the HERMES collaboration

(1) *Desy, 22603 Hamburg, Germany*
† *E-mail: mvaranda@mail.desy.de*

Abstract

During the period 1996 - 2000, the HERMES experiment measured inclusive and semi-inclusive deep inelastic scattering of 27.5 GeV positrons from longitudinally-polarized hydrogen and deuterium gas targets. Recent final HERMES results on the inclusive spin structure functions $g_1^{p,d,n}$ based on a refined analysis procedure are presented. The most precise determination to date of the neutron spin structure function is obtained combining the HERMES deuteron and proton data. Integrals of g_1 are calculated over the measured x-range. A preliminary result for the strange quark helicity obtained from semi-inclusive charged kaon production on a deuterium target is presented.

Introduction. Inclusive Deeply Inelastic Scattering (DIS) of polarized leptons by polarized spin-$\frac{1}{2}$ nucleons can be described by four structure functions (two spin-averaged ones, F_1 and F_2 and two spin-dependent ones, g_1 and g_2), while the description of scattering by spin-1 nuclei like deuterium needs additional structure functions (mainly the tensor structure function b_1).

The spin-dependent structure function $g_1(x, Q^2)$ has been measured at HERMES in inclusive DIS of longitudinally polarized positrons by longitudinally polarized atomic hydrogen or deuterium.

While absolute cross-sections are difficult to measure, asymmetries defined as the ratio between difference and sum of cross-sections of different relative polarization orientation, are the usual direct experimental observable. The measurable double longitudinal spin asymmetry is defined by:

$$A_{||} = \left[\frac{\sigma_{LL}}{\sigma_{UU}} - \frac{1}{2}P_{ZZ}A_{ZZ}\right] = \frac{1}{P_T P_B}.\frac{N^{\Rightarrow}L^{\leftrightarrows} - N^{\leftrightarrows}L^{\Rightarrow}}{N^{\Rightarrow}L^{\leftrightarrows} + N^{\leftrightarrows}L^{\Rightarrow}} \tag{1}$$

where the term $\frac{1}{2}P_{ZZ}A_{ZZ}$ is only present for deuterium. For the tensor polarization an average value of $P_{ZZ} = 0.83 \pm 0.03$ was used in the present analysis. The tensor spin asymmetry defined as $-\frac{3}{2}A_{ZZ} = \frac{b_1(x,Q^2)}{F_1(x,Q^2)}$, measured at HERMES for deuterium, was found to have an average amplitude [1] $A_{ZZ} \sim 0.01$. In equation 1 $\sigma_{UU} = \frac{1}{2}(\sigma^{\leftarrow}_{\Rightarrow} + \sigma^{\rightarrow}_{\Rightarrow})$ is the unpolarized cross-section, $\sigma_{LL} = \frac{1}{2}(\sigma^{\leftrightarrows} - \sigma^{\rightrightarrows})$ is the double longitudinal polarized cross-section where LL indicates that both beam and target are longitudinally polarized. The arrows denote the relative orientations of beam ($\rightarrow$) and target ($\Rightarrow$) polarizations, with P_B and P_T being their average values.

The proton and deuteron spin-dependent structure functions $g_1^{p,d}$ were extracted from HERMES data using the relation:

$$g_1^{p,d}(x,Q^2) = \frac{1}{1-\frac{y}{2}-\frac{y^2}{4}\gamma^2} \times \left[\frac{Q^4}{8\pi\alpha^2 y}\frac{d^2\sigma_{UU}}{dxdQ^2}(x,Q^2)A_{||}(x,Q^2) + \frac{y}{2}\gamma^2 g_2(x,Q^2)\right] \quad (2)$$

and are related with the neutron target structure function g_1^n by the relation:

$$g_1^n = (g_1^d - g_1^p)\frac{2}{(1-\frac{3}{2}\omega_D)} \quad (3)$$

where ω_D takes into account the D-state admixture to the deuteron wave function. A value of $\omega_D = 0.05 \pm 0.01$ was used to cover most of the available data [2].

The strange ($\Delta S(x)/S(x)$) and non-strange ($\Delta Q(x)/Q(x)$) quark polarizations are related with the inclusive and semi-inclusive charged kaon double spin asymmetries by the relation (assuming $g_2 \approx 0$):

$$\begin{bmatrix} A_1(x,Q^2) \\ \\ A_1^K(x,Q^2) \end{bmatrix} = \begin{bmatrix} P_Q & P_S \\ \\ P_Q^K & P_S^K \end{bmatrix} \begin{bmatrix} \frac{\Delta Q(x,Q^2)}{Q(x,Q^2)} \\ \\ \frac{\Delta S(x,Q^2)}{S(x,Q^2)} \end{bmatrix} \quad (4)$$

where the P's are the inclusive and semi-inclusive purities for the non-strange ($Q(x) = \sum_{q=u,d}(q(x)+\overline{q}(x))$) and strange ($S(x) = s(x)+\overline{s}(x)$) quarks as defined in ref [3]. This relation allows the extraction of the strange ($\Delta S = \Delta s + \Delta\overline{s}$) and non-strange ($\Delta Q = \sum_{q=u,d}(\Delta q + \Delta\overline{q})$) quark helicities if the Parton Distribution Functions (PDFs) are known.

Extraction of g_1 from inclusive data. The spin dependent structure function g_1 can be extracted for deuterium from the vector ($A_{||}$) and tensor (A_{ZZ}) asymmetries, using equations 1, 2. The tensor asymmetry measures the asymmetry between target spin states with $|m| = 1$ and $m = 0$ and was so far only measured at Hermes, using a deuterium polarized target, and, selecting states with different values of vector and tensor polarizations [1]. As shown in figure 2, the magnitude of the measured asymmetry does not exceed 0.02 over the measured range, and, it was estimated that the correction to g_1^d from the tensor asymmetry is less than 0.01.

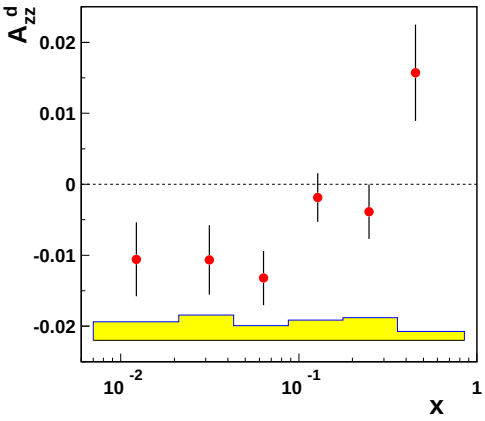

Figure 1: Deuteron tensor asymmetry.

For the extraction of A_1, the events were selected requiring $W^2 > 3.24$ GeV^2 to exclude the region of baryon resonances, and $0.1 < y < 0.91$ to discard data where the detector performance is worse. The A_1 asymmetry extracted for deuterium and proton is shown in figure 2, together with the results obtained in other experiments. As shown in the lower panel, the Q^2 values of the data points of the different experiments spread over one order of magnitude, for the same x bin. In the case of deuteron, the Hermes data provide the most precise measurement of A_1.

The results for xg_1^p and xg_1^d are shown in figure 3 together with the results obtained in other experiments.

For the proton, the central values of SMC are larger than those of HERMES in the low x region, reflecting the different Q^2 values between the two experiments, as expected from the Q^2 evolution of g_1. For the deuteron, HERMES data for $x < 0.04$ are compatible with zero while SMC data favors negative values. COMPASS results are also consistent with zero.

The neutron spin-dependent structure function g_1 extracted according to equation 3 is shown in figure 4. As seen from the figure, g_1^n is negative everywhere except in the very high x region. For decreasing low x values, g_1^n approaches zero. The behaviour is complementary to that of g_1^p.

The first partial moment of g_1 was calculated over the measured x range ($0.02 \leq x \leq 0.9$). The integral as a function of the lower cut value is shown in figure 5. It is observed that the deuteron integral saturates already at $x \sim 0.01$, while the other 3 partial integrals, for proton, neutron and non-singlet distribution, still increase when x reaches its minimum measured value.

The contribution to the deuteron and proton partial first moments from the non-measured high x region ($0.9 < x < 1$) was estimated and seen to be negligible.

The first moment of the deuteron spin dependent structure function $g_1^d(x, Q^2)$ is related with the singlet axial charge a_0 by the relation:

$$a_0 = \frac{1}{\Delta C_S^{\overline{MS}}} \left[\frac{9\Gamma_1^d}{(1 - \frac{3}{2}\omega_D)} - \frac{1}{4} a_8 \Delta C_{NS}^{\overline{MS}} \right] \quad (5)$$

where $\Delta C_S^{\overline{MS}}(\alpha_s(Q^2))$, $\Delta C_{NS}^{\overline{MS}}(\alpha_s(Q^2))$ are the singlet and non-singlet Wilson coefficients calculated in the Minimal Subtraction ($\overline{MS}$) scheme, respectively. In the $\overline{MS}$ scheme the axial charge a_0 is related with the quark helicity ($a_0 = \Delta\Sigma = \Delta u + \Delta\overline{u} + \Delta d + \Delta\overline{d} + \Delta s + \Delta\overline{s}$), and the strange helicity with the axial charges a_0 and a_8 by the relation $\Delta s + \Delta\overline{s} = \frac{1}{3}(a_0 - a_8)$.

Using the value for $a_0 = 0.330 \pm 0.010(theo) \pm 0.022(exp) \pm 0.025(evol)$ extracted in this analysis in NNLO according to equation 5 from deuterium data (table **??**), and, the values

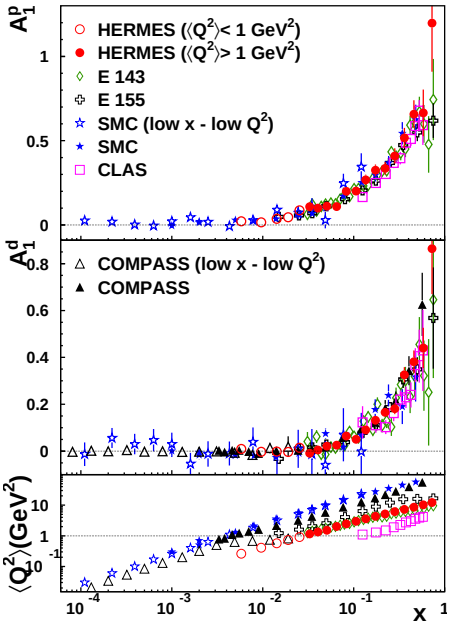

Figure 2: Measured proton and deuteron Born asymmetries.

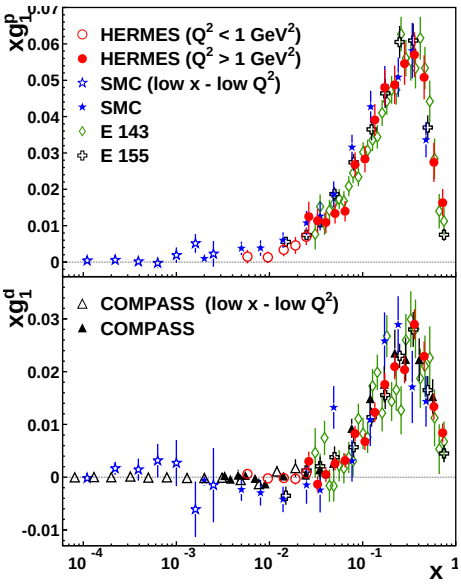

Figure 3: Structure functions xg_1^p and xg_1^d from HERMES data, compared with results from other experiments.

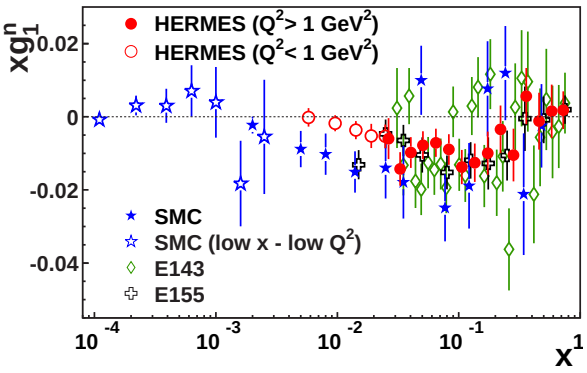

Figure 4: xg_1^n extracted from proton and deuteron data.

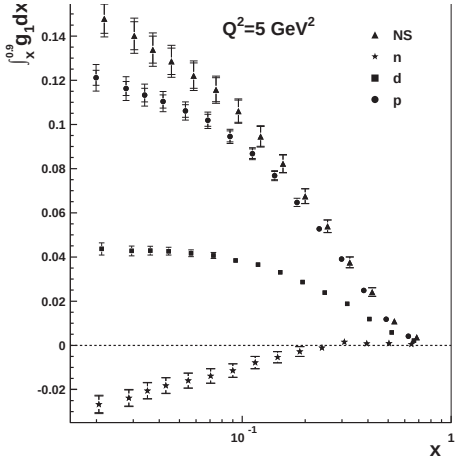

Figure 5: Integrals of $g_1^{p,d,n,NS}$ as a function of the low-x limit of integration, evaluated at $Q_0^2 = 5$ GeV^2.

extracted for a_8 from hyperon β-decay [4] under the assumption of SU(3) symmetry, the value $\Delta S = \Delta s + \Delta\bar{s} = -0.085 \pm 0.013(theo) \pm 0.008(exp) \pm 0.009(evol)$ at $Q_0^2 = 5$ GeV^2 was obtained for the strange helicity. This value is negative and different from zero by about 4.7σ.

Extraction of ΔS from a $K^{\pm}$ semi-inclusive analysis. The strange quark helicity was extracted from semi-inclusive DIS data where a charged kaon was detected in coincidence with the DIS lepton. The data was selected requiring $W^2 > 10$ GeV^2) and $y < 0.85$. Coincident charged kaons were accepted if $0.2 < z < 0.8$ and $x_F > 0.1$, where the upper z cut should suppress the contamination from exclusive events, the lower z and the x_F cuts are used to suppress events from the target fragmentation region. There is a constraint on the momentum of the detected kaon ($2 \leq p \leq 15$) which is due to the RICH constraints for $k^{\pm}/\pi^{\pm}$/proton separation.

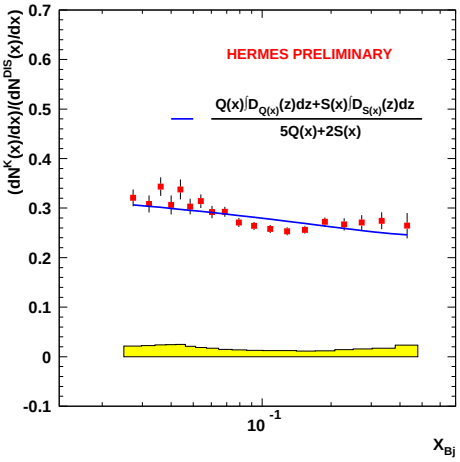

Figure 6: $K^{\pm}$ HERMES multiplicities, averaged over both kaon charges and spins.

The analysis has been performed in LO, without the assumption of SU(3) symmetry, and is based on the extraction of the Born inclusive and semi-inclusive double-spin asymmetries extracted from an isoscalar target (2000 deuteron data). The extraction of the non-strange and strange quark fragmentation functions was performed with a fit to the multiplicities calculated from the same data set averaging over both parallel and anti-parallel spin helicities and kaon charges, and leaving the integrated fragmentation functions as free parameters in the fit to the data (figure 6). Table 1 shows the values of the fragmentation functions extracted from the data, compared with those from Kretzer and KKP parame-

terizations. As shown in the table there is a significant difference between the HERMES values and the values given by the other two parameterizations.

	This analysis	Kretzer	KKP
$\int D^K_{nstrg}$	0.41±0.02	1.103	1.111
$\int D^K_{strg}$	1.41±0.29	0.783	0.296

Table 1: Strange and non-strange fragmentation functions extracted from charged kaon semi-inclusive data compared with Kretzer and KKP parameterizations.(Preliminary).

The A_1 and A_1^K asymmetries have been extracted assuming $g_2 \approx 0$ (equation 4). The values of the non-strange and strange quark helicities calculated over the measured range are shown in figure 7, after evolution of the data points to a common $Q_0^2 = 2.5$ GeV^2. The Q^2 evolution factors were taken from CTEQ6L.

As shown in figure 7, the preliminary result obtained for the strange helicity is compatible with zero over the measured range. The partial first moments (ΔQ and ΔS) are shown in table 2.

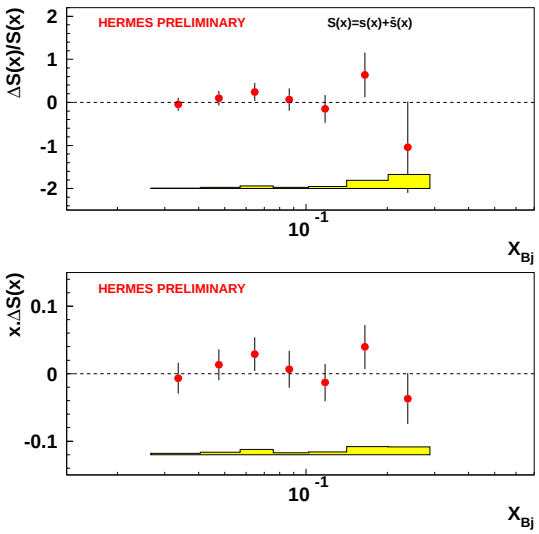

Figure 7: Strange and non-strange quark helicities.

The value obtained for the non-strange quark helicity ($\Delta Q(Q_0^2 = 2.5$ GeV$^2)$) is in agreement with the value extracted from a 5-flavour-decomposition analysis [3], and with the value of $\Delta\Sigma$ extracted from g_1 in the inclusive analysis presented in the previous section.

The partial first moment of the strange quark helicity at $Q_0^2 = 2.5$ GeV^2 in the measured x-range is compatible with zero, and agrees within the error bars with the value found in the inclusive analysis. The value extracted for the octet combination from the non-strange and strange quark helicities ($\Delta q_8(x) = \Delta Q(x) - 3\Delta S(x)$) is not in good agreement with the axial charge a_8 extracted from the hyperon β-decay constants assuming SU(3) symmetry, but as said before, the extraction was performed over a limited x-range and the analysis is not yet concluded.

Summary. HERMES measured the proton and deuteron structure functions $g_1^{p,d}(x)$ in the x-Bjorken range between 0.004 and 0.9 for 0.18 GeV$^2 < Q^2 <$ 20 GeV^2, or in the x range between 0.02 and 0.9 for Q^2 larger than 1 GeV^2. The precision of the proton data is comparable with that of the CERN and SLAC data. The deuteron data is the most precise so far. The deuteron integral is observed to saturate. The singlet axial charge extracted at $Q^2 = 5$ GeV^2 has the value $a_0 = 0.330 \pm 0.011(theor) \pm 0.025(exp) \pm 0.028(evol)$. The extracted strange helicity from the first moment of $g_1^d(x)$ over the measured DIS region and assuming SU(3) symmetry is negative (-0.085) by about 4.7σ.

ΔQ	0.286±0.026(stat)±0.011(sys)
ΔS	0.006±0.029(stat)±0.007(sys)
Δq_8	0.274±0.039(stat)±0.018(sys)

Table 2: Non-strange and strange helicities extracted from charged kaon semi-inclusive data. The value extracted for Δq_8 is also shown. The partial integrals were calculated over the x-range $0.02 - 0.6$. (Preliminary).

The HERMES semi-inclusive charged kaon preliminary analysis of the deuteron data gives a non-strange helicity ($\Delta Q = 0.286 \pm 0.026(stat) \pm 0.011(sys)$) consistent with the value of $\Delta\Sigma$ extracted from the inclusive analysis. The extracted strange helicity is consistent with zero over the measured x-range, with strange and non-strange fragmentation functions extracted from a fit to the same data.

Acknowledgements. I would like to express my gratitude to the DESY management and to the HERMES collaboration for their support and for the opportunity to present their results at the DSPIN 2007 workshop.

References

[1] A. Airapetian et al., Phys. Rev. Lett. 95 (2005) 242001.
[2] A. Airapetian et al., Phys. Rev. D 75 (2007) 012007.
[3] A. Airapetian et al., Phys. Rev. D 71 (2005) 012003.
[4] M. Anselmino et al., Phys. Rep. 261, (1995) 1.

Discussion

Q. (J.Nassalski, SINS, Warsaw) In semi-inclusive analysis you determine a_8 in a limited x_{Bj} range. Therefore it is not surprising that it is different from the "full" matrix element a_8.

A. Please see the two last sections of this note.

NEW POLARIZATION PROGRAM AT U70 (SPASCHARM PROJECT)

A.N. Vasiliev[1], V.V. Mochalov[1†], S.I. Alekhin[1], N.A. Bazhanov[2], N.I. Belikov[1], A.A. Belyaev[3], N.S. Borisov[2], B.V. Chujko[1], Y.M. Goncharenko[1], V.N. Grishin[1], A.M. Davidenko[1], A.A. Derevschikov[1], V.A. Kachanov[1], V.Y. Kharlov[1], A.S. Kozhin[1], D.A. Konstantinov[1], V.G. Kolomiets[2], V.A. Kormilitsin[1], V.I. Kravtsov[1], A.B. Lazarev[2], A.K. Likhoded[1], A.V. Luchinsky[1], A.A. Lukhanin[3],Yu.A. Matulenko[1], Yu.M. Melnick[1], A.P. Meschanin[1], N.G. Minaev[1], D.A. Morozov[1], A.B. Neganov[2], L.V. Nogach[1], S.B. Nurushev[1], Yu.A. Plis[2], A.F. Prudkoglyad[1], A.V. Ryazantsev[1], P.A. Semenov[1], O.N. Shchevelev[2], S.R. Slabospitsky[1], L.F. Soloviev[1], M.N.Ukhanov , Yu.A. Usov[2], A.V. Uzunian[1], A.S. Vovenko[1], A.E. Yakutin[1]

(1) *Institute for High Energy Physics, Protvino, Russia*
(2) *Joint Institute for Nuclear Research, Dubna, Russia*
(3) *Kharkov Institute of Physics and Technology, Ukraine*
† *E-mail: mochalov@ihep.ru*

Abstract

The new polarization program SPASCHARM is being prepared in Protvino. The program has two stages. The first stage is dedicated to single-spin asymmetries in the production of miscellaneous light resonances with the use of 34 GeV π^--beam. Inclusive and exclusive reactions will be studied simultaneously. The second stage is dedicated to single-spin and double-spin asymmetries in charmonium production with the use of 70 GeV polarized proton beam which will allow us to understand charmonium hadronic production mechanism and make gluon polarization $\Delta g(x)$ extraction at large x.

Introduction

A possibility to accelerate high-intensive polarized proton beam up to 70 GeV at the IHEP U70 accelerator, extract it from the main ring and deliver to several experimental setups was intensively studied last time in 2005 and Spring of 2006 in Protvino [1]- [4]. We proposed to study a wealth of single- and double-spin observables in various reactions using longitudinally and transversely polarized proton beams at U70. Unfortunately the proposal stuck in the Ministry of Education and Science in Summer 2006. But we believe that a possibility to push the proposal still exists.

The main goal of the SPASCHARM project is to study spin structure of the proton, starting with determination of gluon contribution into spin of the proton at large Bjorken x through study of spin effects in charmonium production. High sensibility to gluon content of the interacting particles is one of the main features of charmonia production in hadronic interactions. In case of collision of two longitudinally polarized protons it is used to define gluon polarization $\Delta G/G$ in the proton. A polarized proton beam is needed to make this study. We plan to have it at the second stage of the experiment after the measurements of single-spin asymmetries already in charmonia production have been carried out.

The project has a first stage when unpolarized beams will be used. The first stage is an experiment to study single-spin asymmetries A_N of light resonances consisting of u-, d- and s-valence quarks. Transverse single-spin asymmetries are very well known for a long time. In the Standard Model QCD at leading twist level all $A_N = 0$. But the experiments show very big A_N in the confinement region. Therefore A_N is very sensitive to the effects outside the SM. The known theoretical approaches (Sivers and Collins effects, twist-3 effect, etc.) try to reconcile theory and experiment. To discriminate the existing theoretical approaches and to stimulate to develop the new ones, a systematic study of A_N for a big number of miscellaneous inclusive and exclusive reactions is needed, especially in the confinement region, which is the most unclear for theory. To make this systematic study is the main goal of the first stage of the SPASCHARM project. The first stage will be finalized by the measurements of A_N in charmonia production. This will finally prepare the experimental setup to the second stage of the project where only one new thing will be needed - namely a polarized proton beam from U70.

This paper is organized as follows. First we will describe the second stage of the experiment dedicated to spin effects in charmonia production with the use of polarized proton beam from U70. After that we will describe the first stage dedicated to spin effects in light resonance production.

Charmonia production in polarized $p_{\rightarrow}p_{\rightarrow}$ interactions

At present only 30% of the longitudinally polarized proton spin is described by quark's spin. The other 70% of the proton spin may be explained by gluon and/or orbital momentum contributions. Experiments with polarized lepton beams at CERN, HERA, SLAC have been measuring mainly quark polarization over last twenty years. COMPASS and HERMES have tried to measure gluon polarization at small x, up to 0.1-0.15. The RHIC experiments STAR and PHENIX have begun to measure gluon polarization at very low x values (about 0.01) whereas gluon polarization has to be measured in the whole x range. So in spite of many years of experiments, a detailed decomposition of the spin of the proton remains elusive - new experimental data on $\Delta g(x, Q^2)$, especially at large x are badly needed. We propose to simultaneously measure the double-spin asymmetry A_{LL} for inclusive χ_{c2}, χ_{c1} and J/Ψ by utilizing the 70 GeV/c longitudinally polarized-proton beam on a longitudinally polarized target. Our goal is to obtain besides the quark-spin information also the gluon-spin information from these three processes in order to determine what portion of the proton spin is carried by gluons. Better understanding of charmonium production at U70 energies is needed – for this pion and proton beams will be used to produce charmonium. Gluon contribution into the proton spin as well as strange quarks and orbital momentum contributions – worldwide studies at HERMES, COMPASS, RHIC, JLAB and SLAC. We propose a new experiment in this field – it should be complimentary to the existing experiments. It will give new data at large x for Global analysis. One can see from Fig.1 that the biggest gluon polarization is anticipated near $x = 0.3$. SPASCHARM will measure

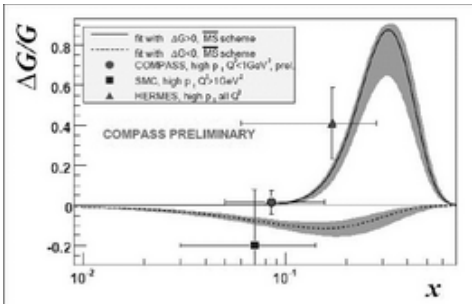

Figure 1. The solution of $\Delta G/G$ from experiment COMPASS [5].

gluon polarization in the region of x between 0.3 and 0.6.

Information about gluon polarization might be obtained through simultaneous measurements of A_{LL} in inclusive production of χ_{c2} and J/Ψ. This experiment was proposed at Fermilab (P838) at 200 GeV as a continuation of E704 [6]. The Fermilab's PAC pointed out that physics was very interesting, but an intensity of the polarized proton beam from Λ-hyperon decays was small – the statistics would not be enough. The experiment was not approved. In our new proposal for U70 we expect to have up to $4 \cdot 10^8$ p/min instead of $2.7 \cdot 10^7$ p/min in P838 which is a factor of 15 more.

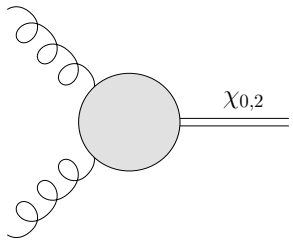

Figure 2. Gluon fusion ($\alpha_S^2, p_T = 0$).

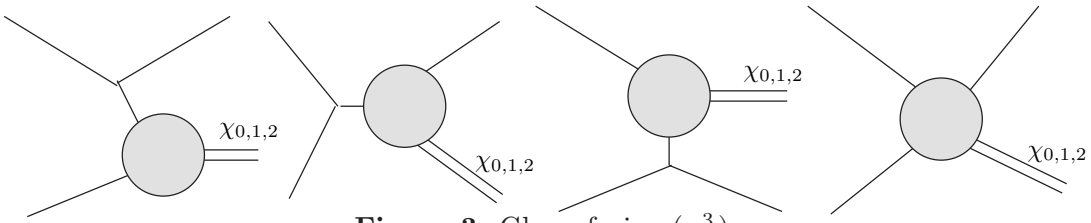

Figure 3. Gluon fusion (α_S^3).

The hadronic production of the χ states involves three parton fusion diagrams [7]:

1. gluon fusion (Fig.2-3);
2. quark-glion interaction (Fig.4);
3. quark-antiquark annihilation (Fig.5).

Estimate made by one of our authors (S.A.Alekhin) has shown that at 70 GeV the contributions of gluon-gluon fusion and quark-antiquark annihilation to produce charmonium with a mass of 3.5 GeV in *pp*-interactions are comparable.

The goal of the proposed experiment is to measure double-spin asymmetry A_{LL} with the use of longitudinally polarized beam and target in the process:

$$p_{\rightarrow} + p_{\rightarrow} \rightarrow \chi_{c2}(J/\Psi) + X, (\chi_{c2} \rightarrow J/\Psi + \gamma). \quad (1)$$

J/Ψ will be registered mainly via $\mu^+\mu^-$ decay due to bremmstrahlung in e^+e^- decay mode. The charmonia states under study are J/Ψ (3096, $J^{PC} = 1^{--}$), χ_{c1} (3510, $J^{PC} =$

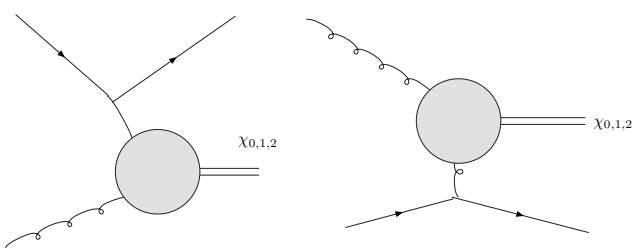

Figure 4. Quark-gluon interaction (α_S^3).

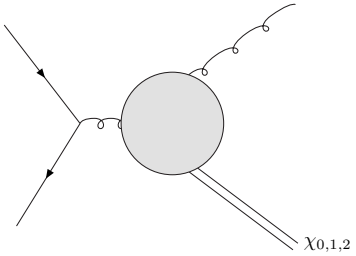

Figure 5. Quark-antiquark annihilation (α_S^3).

1^{++}) and χ_{c2} (3555, $J^{PC} = 2^{++}$). The measured experimental asymmetry is given by

$$A_{LL} = \frac{1}{P_B \cdot P_T^{eff}} \cdot \frac{I^{++} - I^{+-}}{I^{++} + I^{+-}}, \tag{2}$$

where P_B is the beam polarization, P_T^{eff} – effective target polarization, I^{++}, I^{+-} are the number of events normalized to the incident beam. The helicity states (++) and (+-) correspond to ($\leftarrow\rightarrow$) and ($\rightarrow\rightarrow$) states respectively, where arrows indicate the beam and target spin direction in the laboratory system.

Theoretical predictions of A_{LL} mainly depend on two assumptions:

- gluon polarization $\Delta G/G$ and
- charmonium production mechanism which defines $\hat{A}_{LL}$ at the parton level (in parton-parton interaction).

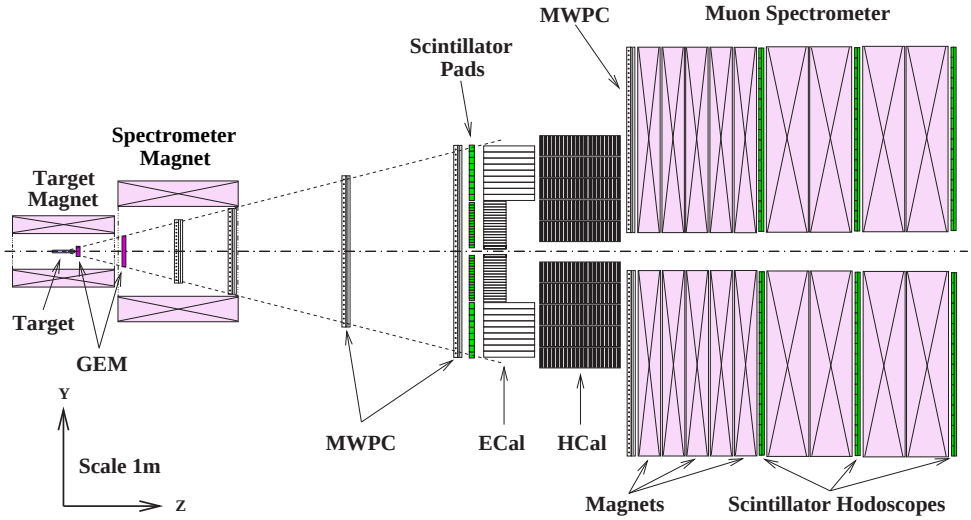

Figure 6. SPASCHARM Experimental Setup

The experimental setup SPASCHARM is presented in Fig.6. It is an open geometry experiment. The main parts of the setup are as follows:

- wide aperture spectrometer with GEM, drift chambers and proportional chambers;
- electromagnetic calorimeter and
- muon detector.

The central part of the calorimeter (1 m^2) will consist of lead tungstate blocks. It is critically needed to detect very precisely γ-quanta fro χ-decays to separate χ_{c1} and χ_{c2} through high precision energy resolution of the calorimeter. The x_F distribution of χ_{c2} (3555) detected by the setup at a beam energy of 70 GeV is presented in Fig. 7.

The principal point for this experiment is a separation of the two charmonia states with the spins equal to 1 and 2, namely χ_{c1} (3510) and χ_{c2} (3555). The Monte-Carlo simulations for 70 GeV have been made. The reconstructed masses of χ_{c0}(3410), χ_{c1} (3510) and χ_{c2} (3555) are presented in Fig.8. The J/Ψ (in $\mu\mu$-decay mode) 4-momentum is taken as a result of $1C$-fit. For charged particles $\Delta p/p$= 0.004 at 10 GeV/c. For γ-quanta $\sigma(E)/E$ was taken as $2.5\%/\sqrt{E}$. We can see that the two states of interest are well separated.

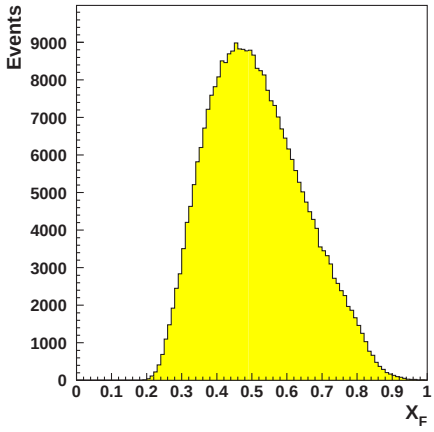

Figure 7. The x_F distribution of χ_{c2} (3555) detected by the setup at a beam energy of 70 GeV

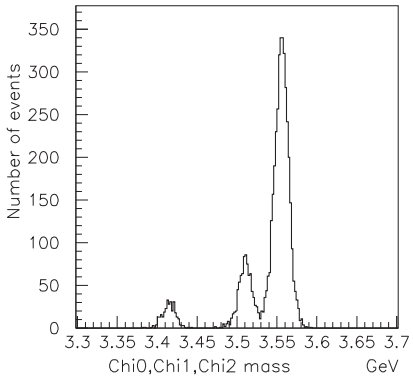

Figure 8. The reconstructed masses of χ_{c0} (3410), χ_{c1} (3510) and χ_{c2} (3555) as a result of Monte-Carlo simulations for the SPASCHARM experimental setup.

The SPASCHARM experiment plans to have 25000 electronic channels (7000 ADC, 2000 TDC and 16 000 registers). The trigger for interaction in the target will be the only hardware trigger. Information from the interaction will be digitized in each sub-detector, pre-processed and buffered for further processing. A high level trigger selection will occur in compute nodes which access the buffers via a high bandwidth network fabric. The experiment plans to operate at interaction rates of the order of 2 MHz. With pre-processing on the detector electronics for a substantial reduction of the data volume, typical event sizes are in the range of 2 to 4 kB. This amounts to total raw data rates in the order of 3 GB/s.

Our estimate has shown us that we expect to get a precision of $\sigma(A_{LL}) = 0.07$ for χ_{c2} and 0.025 for J/Ψ at $x = 0.3$ for 100 days of data taking.

With the use of polarized proton beam at SPASCHARM a precision measurement of single-spin asymmetry in inclusive production of miscellaneous resonances in the transverse polarized beam fragmentation region in a wide (x_F, p_T)-region will be worthwhile. Also it will be possible to measure transversity in Drell-Yan muon (electron) pairs.

Single-spin asymmetries in light resonance production

Before the polarized proton beam will be accelerated at U70 we can make single-spin measurements of miscellaneous inclusive and exclusive reactions with unpolarized beams, such as pions, kaons and protons, existing at the beam channel 14 of the Protvino accelerator. Why do we need to measure A_N in a big variety of inclusive and exclusive reactions? In the Standard Model QCD at leading twist level all A_N=0. But the experiments show very big A_N in the confinement region. Therefore A_N is very sensitive to the effects outside the SM. The known theoretical approaches (Sivers and Collins effects, twist-3 effect, etc.) try to reconcile theory and experiment. To discriminate the existing theoretical

approaches and to stimulate to develop the new ones, a systematic study of A_N for a big number of miscellaneous inclusive and exclusive reactions is needed, especially in the confinement region, which is the most unclear for theory. To make this systematic study is the main goal of the first stage of the SPASCHARM project.

It would be interesting to measure single-spin asymmetries in inclusive production of light resonances even in the unpolarized beam fragmentation region, but at big values of transverse momentum p_T, close to the boundary of phase space. In Fig.9 the single-spin asymmetry A_N in the inclusive reaction $\pi^- + d_\uparrow \to \pi^0 + X$ at 40 GeV/c at x_F >0.7 is presented [8]. We see that A_N is zero at small p_T and about 15% at p_T near 1 GeV/c and bigger. When x_F goes to 1, any inclusive reaction transfers into the proper exclusive reaction. In Fig.10 the single-spin asymmetry A_N in the exclusive reaction $\pi^- + p_\uparrow \to \pi^0 + n$ at 40 GeV/c is presented [9]. We see that A_N is also about 15% near $-t$ equal to 1 $(\mathrm{GeV/c})^2$, that is equivalent to p_T near 1 GeV/c. So asymmetries in the both inclusive and exclusive π^0-production at 40 GeV pion beam are equal each other (also it seems that asymmetries on polarized protons and neutrons are the same). It should be the case for other light resonances.

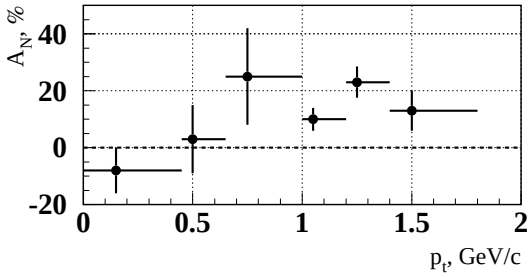

Figure 9. The p_T-dependence of single-spin asymmetry A_N in the inclusive reaction $\pi^- + d_\uparrow \to \pi^0 + X$ at 40 GeV/c at $x_F > 0.7$. The average value of A_N is (16±5)% near p_T equal to 1 GeV/c.

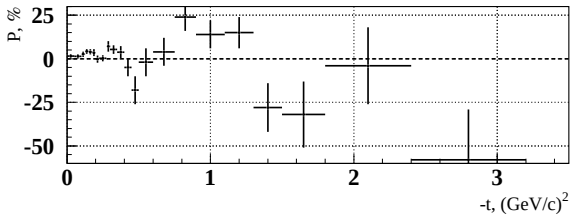

Figure 10. The t-dependence of A_N in the exclusive reaction $\pi^- + p_\uparrow \to \pi^0 + n$ at 40 GeV/c. The average value of A_N is (18±5)% near t equal to 1 $(\mathrm{GeV/c})^2$.

For the first stage of the experiment two multi-channel threshold Cherenkov counters will be added to the setup to distinguish between pions and kaons. They are of 1.5 m and 3 m long and will be placed between the end of the magnet and the calorimeter. They will be filled by freon and by air correspondingly, both at atmospheric pressure. Lead tungstate in the calorimeter is not needed for the first stage, lead glass with moderate energy resolution will be enough to detect light resonances. An acceptance of the whole setup will be decreased, however it will still be significant to detect light resonances. Due to very fast DAQ (practically without dead time) inclusive and exclusive reactions will be studied simultaneously.

There are some advantages of the new experiment. Exclusive and inclusive reactions were studied either in neutral decay modes or in charged decay modes in the previous experiments. We propose to measure the both modes simultaneously and therefore we expect a significant increase in statistics. Addition of new detectors (GEM, MDC, high quality EMC etc.) compare to the previous experiments might bring us to discovery of "new channels" (exotic glueballs, hybrids, etc). Extremely high-speed DAQ will allow to detect inclusive and exclusive reactions simultaneously. Partial wave analysis of a huge statistics on polarized target will raise a robustness of the results on rare resonances.

The setup has 2π-acceptance on azimuthal angle ϕ and therefore the systematic errors in single-spin asymmetries will be negligible.

One can see the advantage of proposed new measurements in sense of significant increase in statistics in a couple exclusive reactions in Fig.11 and Fig.12. The details are in the Figure captions.

For the MC simulations, two options of the setup were considered with two distances from the center of the polarized target to the beam downstream end of the last Cherenkov counter - "7 meters" and "4 meters". Variant "4 meters" has one Cherenkov counter in the setup. π-mesons will be identified in the momentum region of 3-23 GeV/c. Acceptance for "usual" (non-strange) resonances is huge (3 times bigger than for "7 m"). We request a beam time of 30 days. Variant "7 meters" has two Cherenkov counters in the setup and allows π/K-separation in the momentum region of 3-23 GeV/c. We request a beam time of 70 days. The expected accuracies of A_N in several inclusive reactions for the summing 100 days at beam in the kinematical region of $x_F = 0.5 - 1.0$ and $p_T = 0.5 - 2.5$ GeV/c are the following for different reactions:
$\sigma(A_N^{\pi^- + p_\uparrow \to \omega + X}) = 0.3\text{-}3$;
$\sigma(A_N^{\pi^- + p_\uparrow \to \rho + X}) = 0.2\text{-}2.5$;
$\sigma(A_N^{\pi^- + p_\uparrow \to \eta\prime + X}) = 0.3\text{-}4$;
$\sigma(A_N^{\pi^- + p_\uparrow \to f_2 + X}) = 0.1\text{-}1$; $\sigma(A_N^{\pi^- + p_\uparrow \to \phi + X}) = 3.\text{-}10.$; $\sigma(A_N^{\pi^- + p_\uparrow \to K^{*0} + X}) = 0.6\text{-}10.$

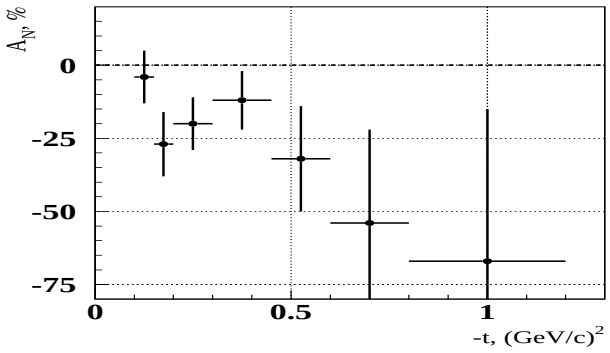

Figure 11. $A_N^{\pi^- + p_\uparrow \to \omega(782) + n}$ at 40 GeV [10]. The ω (782) has been detected in $\pi^0\gamma$ decay mode with 8% branching. 33,000 events on polarized target were collected. Solid angle was twice less than in the SPASCHARM setup for the first stage. By using two decay modes ($\pi^+\pi^-\pi^0$ with 89% branching and $\pi^0\gamma$), statistics can be increased in 20 times. Errors in the first four points would be 2% rather than 10% now.

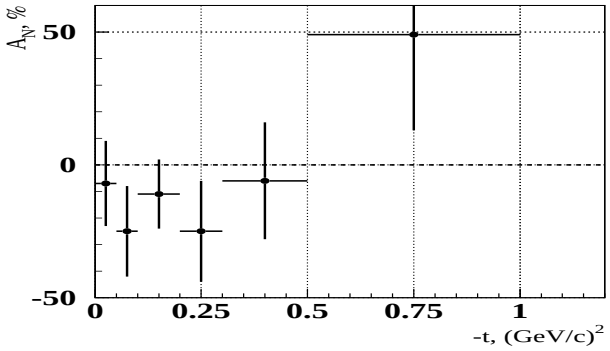

Figure 12. $A_N^{\pi^- + p_\uparrow \to \eta\prime(958) + n}$ at 40 GeV [11]. The $\eta\prime$ (958) has been detected in $\gamma\gamma$ decay mode with 2% branching. 11,000 events on polarized target were collected. Solid angle was about the same as in the SPASCHARM setup for the first stage. By using two additional decay modes ($\pi^+\pi^-\eta$ and $\pi^+\pi^-\gamma$ with branchings of 45% and 30%), statistics can be increased in 20 times. Errors in the first three points would be 3-4% rather than 13-17% now.

Conclusion

The new polarization program SPASCHARM is being prepared in Protvino. The program has two stages. The first stage (to be started in 2011) is dedicated to single-spin

asymmetries in the production of miscellaneous light resonances with the use of 34 GeV π^--beam. Inclusive and exclusive reactions will be studied simultaneously. The errors in the exclusive reactions with big asymmetries are expected to be several times less than now. The brand new data for inclusive reactions will be obtained. All the new data will much better help us to understand spin dependence of strong interaction in the most difficult from the theory point of view kinematical region, namely in the quark confinement region.

The second stage (to be started in 2015) is dedicated to single-spin and double-spin asymmetries in charmonium production with the use of 70 GeV polarized proton beam which will allow us to understand charmonium hadronic production mechanism and make $\Delta g(x)$ extraction at large x. The results on $\Delta g(x)$ at large x will be unique and will be complementary to those which exist and might be obtained at COMPASS, HERMES, RHIC and JLAB at smaller x. The global analysis with the use of the new large x data on $\Delta g(x)$ will significantly improve our knowledge of the gluon polarization integral ΔG.

This work has been partially supported by the RFBR grant 06-02-16119.

References

[1] V.V.Abramov et al, in *Proc. of XI Advanced Research Workshop on High Energy Spin Physics (Dubna-SPIN-05)*, 449 (2006); hep-ex/0511046.

[2] S.B. Nurushev et al - ibid, p.517.

[3] Y.M. Shatunov et al - ibid, p.531.

[4] V.V. Mochalov et al, Czech.J.Phys. **56**, : (F151)2006; hep-ex/0612038.

[5] E. Santos et al, et al, Czech.J.Phys. **56**, : (F71)2006.

[6] M.E. Beddo et al, Fermilab proposal P838, January 1991.

[7] A.K. Likhoded and A.V. Luchinsky, e-Print: hep-ph/0703091

[8] V.D. Apokin et al, in *Proc. of the IV Workshop on high energy spin physics, Protvino)*, 288 (1991).

[9] V.D. Apokin et al, Russ.Journal.Phys.Atom.Nucl. **45**, 840 (1987).

[10] I.A. Avvakumov et al Russ.Journal.Phys.Atom.Nucl. **42**, 725 (1985).

[11] V.D.Apokin et al Zeit.Phys. **C35**, 173 (1987).

Discussion

Q. (J.Nassalski, SINS, Warsaw) In SPASCHARM – what will be $x_{\rm gluon}$ range covered and what will be the precision on gluon polarization?

A. In SPASCHARM the x_{gluon} range from 0.3 to 0.7 might be covered with a reasonable statistics. At moment we do not know the precision on gluon polarization we might achieve. It depends on charmonium production mechanism in hadron interaction at our energies which we have to study first in SPASCHARM by using both proton and pion beams. But anyway we hope to get first estimate of the precision from our IHEP theoreticians sort of in an year or two.

MEASUREMENTS of A_{yy}, A_{xx} and A_y ANALYZING POWERS of TRITON FRAGMENTATION in $d(\overrightarrow{d},p)$ at 270 MeV

T.A.Vasiliev[1†], T.Saito[2], V.P.Ladygin[1], M.Hatano[2], A.Yu.Isupov[1], M.Janek[1,5], H.Kato[2], N.B.Ladygina[1], Y.Maeda[7], A.I.Malakhov[1], S.Nedev[6], J.Nishikawa[4], H.Okamura[8], T.Ohnishi[3], S.G.Reznikov[1], H.Sakai[2], S.Sakoda[2], N.Sakomoto[3], Y.Satou[2], K.Sekiguchi[3], K.Suda[7], A.Tamii[9], T.Uesaka[7], N.Uchigashima[2], K.Yako[2]

(1) *LHE JINR, Dubna, Moscow region, 141980 Russia* (2) *Department of Physics, University of Tokyo, Tokyo 113-0033, Japan* (3) *The Institute of Physical and Chemical Research (RIKEN), Wako 351-0198, Japan* (4) *Department of Physics, Saitama University, Saitama 338-8570, Japan* (5) *University of P.J.Safarik, 041-54 Kosice, Slovakia* (6) *University of Chemical Technology and Metallurgy, Sofia, Bulgaria* (7) *Center for Nuclear Study, University of Tokyo, Tokyo 113-0033, Japan* (8) *Cyclotron and Radioisotope Center, Tohoku University, Sendai, Miyagi 980-8578, Japan* (9) *Research Center for Nuclear Physics, Osaka University, Ibaraki, Osaka 567-0047, Japan*

† *E-mail: vasiliev@sunhe.jinr.ru*

Abstract

Final results on the polarization observables of the A_{yy}, A_{xx} and A_y analyzing powers of the $d(\boldsymbol{d},p)X$ breakup reaction at 270 MeV of deuteron kinetic energy are presented. The obtained angular distributions of these polarization observables compared with data of the $d(\boldsymbol{d},p)T$ binary reaction. The analyzed data refer to the triton breakup above threshold up to 10 MeV.

1. Introduction. Nowadays it is generally accepted that the NN force is a residual interaction of the underlying quark-gluon dynamics of quantum chromodynamics, similar to the intermolecular forces that stem from QED, and that it should be calculated from first principles, i.e. the Lagrange density of QCD. Since there is no theory at the moment that is able to give a qualitative as well as quantitative description of NN scattering based on these first principles, it is necessary to build an effective theory. Widely used are meson exchange pictures, dispersion relations or a phenomenologically supported operator ansatz. Examples for such interactions are the Bonn, Paris, Nijmegen or Argonne potentials.

In the 1970's and 80's, a field-theoretic model for the NN interaction was developed in Bonn potential. This model consists of single π, ω, and a_0/δ exchange, the field-theoretic 2π model, and $\pi\rho$ diagrams, as well as few more irreducible 3π and 4π diagrams (which are not very important, but indicate convergence of the diagrammatic expansion). This quasi-potential has become known as the 'Bonn full model' [1]. It has 12 parameters which are the coupling constants and cutoff masses of the meson-nucleon vertices involved. With a reasonable choice for these parameters, a very satisfactory description of the NN observables up to 300 MeV is achieved. Since the goal of the Bonn model was to put meson theory to a real test, no attempt was ever made ti minimize the χ^2 of the fit of the NN data.

In the 1990's, one focus has been on the quantitative aspect of the NN potentials. Even the best NN models of the 1980's [1] fit the NN data typically with a $\chi^2/datum \approx 2$

or more. This is still substantially above the perfect $\chi^2/dof \approx 1$. To put microscopic nuclear structure theory to a reliable test, one needs a prefect NN potential such that discrepancies in the predictions cannot be blamed on a bad fit of the NN data. Up to now the latest versions of the NN potentials have been obtained using meson-exchange or other more phenomenological approaches: AV18 [2], CD Bonn [3] and Nijm I,II, and 93 [4]. They describe the rich set of experimental NN data up to 350 MeV which is slightly higher than the pion threshold 290 MeV.

The CD Bonn [3] potential uses the full, original nonlocal Feynman amplitude for OPE, while all other potentials apply local approximations. The CD Bonn includes (besides the pion) the vector mesons $\rho(769)$ and $\omega(783)$, and two scalar-isoscalar bosons, σ, using the full, nonlocal Feynman amplitudes for their exchanges. Thus, all components of the CD Bonn are nonlocal and off-shell behavior is the original one as determined from relativistic field theory. As a consequence of this, the CD Bonn potential has a weaker tensor force as compared to all other potentials. This is reflected in the predicted D-state probabilities of the deuteron, P_D which is a measure of the strength of the nuclear tensor force. While CD Bonn predicts $P_D = 4.85\%$, the other potentials yield $P_D = 5.7(1)\%$. These differences in the strength of the tensor force lead to considerable differences in nuclear structure predictions.

The tensor analyzing T_{20} and polarization transfer coefficient k_0 in backward elastic scattering, $dp \to pd$, have been measured at Saclay and Dubna [5]. Later, the set of polarization observables was also obtained in dp-elastic scattering over wide angular range at intermediate energies at RIKEN [6, 7] and KVI [8]. Measurements of the polarization correlation coefficients $C_{//}$ in the $d\ ^3He \to\ p\ ^4He$ reaction have been performed at RIKEN [9].

All the data show the sensitivity to the deuteron spin structure at short distances. However, the remarkable deviation of the polarization observables from the One Nucleon Exchange (ONE) predictions using standard deuteron wave function occurs even at relatively small internal momenta of $q \sim 200\ MeV/c$. Such a discrepancy can be due to the non-adequate description of the light nuclei structure at short distances, as well as to the importance of the mechanisms in addition to ONE. For the $\overrightarrow{d}\,d \to\ p\ T$ all four nucleons are involved in the interaction, hence it would be useful to take into account 3NFs. Even binding energies for light nuclei cannot be reproduced with these realistic potentials. For instance, the underbinding amounts to 0.5-1 MeV in the case of triton and ^3He. One can achieve correct three-nucleon (3N) binding energy by including the Tucson-Melbourne (TM) [10] three-nucleon force which is refined version of Fujita-Miyazawa force [11].

The $\overrightarrow{d}\,d \to\ p\ T$ and $\overrightarrow{d}\,d \to\ p\ X$ process concern to ONE reactions. These reactions are the simplest processes with a large momentum transfer, so they could be used as a tool to study the deuteron structure at short distances. The polarization observables of these reactions are sensitive to the D/S wave ratio in the deuteron. The relative momentum of nucleons in deuteron achieves q $\sim$ 400 MeV/c at initial deuteron kinetic energy $E_d = 270\ MeV$.

2. Experiment. The experiment was performed at RIKEN accelerator Research Facility. A polarized deuteron beam extracted from polarized ion source was accelerated with the AVF and the Ring cyclotrons up to the energy of 270 MeV. The accelerated beam was transported to the spectrometer SMART which consist of 2 dipole magnets and 3

quadrupoles (arranged as QQDQD). Swinger magnet controlled the angle of deuteron injection onto a target thus it allowed to perform angular measurements with horizontally fixed detection system. The direction of the symmetry axis of the beam polarization was controlled with a Wien filter located at the exit window of Polarized Ion Source. Magnitude of the beam polarization determined by two beam line polarimeters. Each of them utilizes dp-elastic scattering with precisely obtained analyzing powers in the $^{12}C(\overrightarrow{d},\alpha)^{10}B^{*}2^{+}$ reaction [12]. Deuterated polyethylene was used as the deuteron target. Measurements with a carbon target was also performed to subtract the contribution of carbon nuclei in CD_2 target. For the $\overrightarrow{d}\,d \rightarrow\ p\,T$ reaction the detected protons scattered in the backward angles in the c.m.s. The MWDC was used for the reconstruction of the trajectory of the particles which went through the magnetic spectrograph. Information from MWDC was transformed to the scattering angles and the momenta of the particle using the optical matrix of the spectrometer.

3. Results and discussion. The experimental results on the vector A_y and tensor A_{yy}, A_{xx} and A_{xz} analyzing powers of the $\overrightarrow{d}\,d \rightarrow\ p\,T$ reaction at $E_d = 270\ MeV$ are presented by the filled symbols in Fig.1a. The solid, long-dashed and dotted curves are the results of ONE calculations using Paris [13], Bonn B [1], and Bonn C [1] deuteron wave functions, respectively. Urbana ^3He wave function [14] was used in the calculations to describe three-nucleon (3N) system. The dot-dashed curves are the calculations by Kamada [15] with a model of the reaction mechanism including the 3N-scattering amplitude. The structure of A_y is well reproduced by this calculations, whereas A_{yy}, A_{xx} and A_{xz} are not in agreement. In this respect, further development of theoretical studies are desirable to interpret the reaction mechanism.

ONE calculations predict that the tensor analyzing power at the backward angles is sensitive to the structure of the deuteron. At angles near 90° in the c.m.s. they are sensitive to both deuteron and ^3He wave functions. One can see from Fig.1a that the calculations reproduce the global feature of the experimental data at the backward angles, while they remarkably deviate from the experimental results near 90°. These results imply that there might be some problems in the description of the realistic ^3He wave functions used in ONE calculations. Fig.1a shows that there are some structures in the angular distribution of A_y in spite of zero predicted from ONE calculations. Since ONE calculation does not produce non-zero vector analyzing powers, this result will be a clue to investigate the reaction mechanism beyond the ONE model.

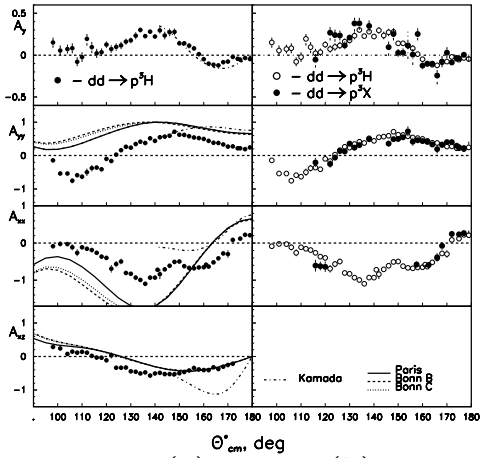

Figure 1. See the text for explanations.

Kamada calculated the analyzing powers for the $\overrightarrow{d}\,d \rightarrow\ ^3He\ n$ reaction [15] at $\Theta_{cm} = 140^0\ \sim\ 180^0$ with a model of the reaction mechanism using the 3N-scattering amplitude determined by a Faddeev calculations (this model is similar to that for the analysis of the $^3He(\overrightarrow{d},p)^4He$ reaction in [16]).

The signs of the tensor analyzing power A_{yy} and A_{xx} near 180° in the c.m.s. are

positive in accordance with the sign of the D/S wave ratio of deuteron. The experimental and predicted data for A_{yy} and A_{xx} have the same sign and qualitatively agree each other. However, the quantitative difference between them is observed. ONE predictions near 90° depend on both deuteron and ^3He functions simultaneously and the experimental data for A_{yy} and A_{xx} strongly disagree with the calculations in this region. The experimental A_{xz} data and the their predictions for backward angles are in agreement. The A_{xz} experimental data near 90° strongly differ from the predictions.

The experimental results on vector A_y and tensor A_{yy}, and A_{xx} analyzing powers for $\overrightarrow{d}\,d \rightarrow\ p\ X$ reaction at $E_d = 270\ MeV$ are presented by the filled symbols in Fig.1b. Events of breakup have effective values of excitation energy of $\approx\ 7\ MeV$. Open symbols correspond to the binary reaction.

The analysis of the experimental data on the cross sections of the $dp \rightarrow pd$ and $dd \rightarrow {}^3\mathrm{He}n$ reactions [17] has shown that non-nucleonic degrees of freedom can occur already at T_d ~500 MeV. The large angles in the c.m. in the present experiment correspond to the short internucleonic distances where the manifestation of non-nucleonic degrees of freedom is possible.

On the other hand, the discrepancy between the data on the tensor analyzing powers and ONE calculations [18] can be caused by the relativistic effects. In Fig.2 the tensor analyzing powers A_{yy}, A_{xx} and A_{xz} in the $dd \rightarrow\ pT$ reaction at 270 MeV is compared with the results of ONE calculations using the relativistic and non-relativistic Paris deuteron wave function [13] shown by the solid and dashed lines, respectively. Relativity in deuteron wave function is taken into account by the minimal relativization scheme [19].

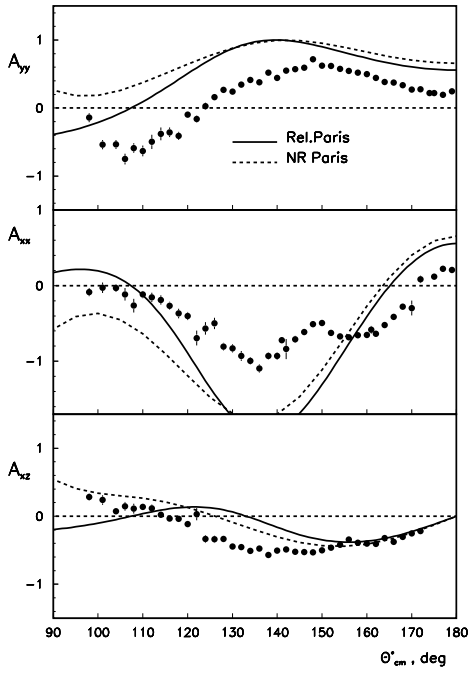

Figure 2. See the text for explanations.

One can see that the use of the relativistic deuteron wave function [19] does not allow one to reproduce A_{yy} data. The structure of deuteron can be more complicated and depends on more than one variable as in the case of the deuteron where the strong dependence of the spin structure on two variables was observed [20]. On the other hand, the relativistic effects for the both reaction mechanisms and deuteron structure should be treated in the consistent way. For instance, if one takes the relativistic kinematics, boost effects and Wigner spin rotations, it finally leads to rather small effects in the cross section and polarization observables in Nd- elastic scattering [21].

In summary, the experimental data on the tensor and vector analyzing powers A_{yy}, A_{xx}, A_{xz} and A_y for the $\overrightarrow{d}\,d \rightarrow\ p\ T$ are obtained at $E_d = 270\ MeV$ in the angular range $90° - 180°$ in the c.m.s. The experimental data on the tensor observables for this reaction show the sensitivity to the spin structure of the deuteron. The angular distribution of A_y indicates the necessity to take into account mechanisms beyond ONE.

The experimental data of the tensor and vector analyzing powers A_{yy}, A_{xx} and A_y for

the $\overrightarrow{d}\,d \to\ p\,X$ breakup reaction are obtained. The experimental data on A_{yy} and A_{xx} for this reaction also show the sensitivity to the spin structure of deuteron. The comparison of breakup data with the binary ones gives the opportunity to conclude that they are in agreement within achieved experimental errors.

The obtained experimental data require further development in theoretical approaches either for adequate description of the light nuclei structure at short distances and (or) taking into account mechanisms in addition to ONE.

Acknowledgments. This work was supported in part by the Russian Foundation for Basic Research (grant N^o 07-02-00102a) and by the Grant Agency for Science at the Ministry of Education of the Slovak Republic (grant N^o 1/4010/07).

References

[1] R.Machleidt, K.Holinde, C.Elster, *Phys.Rep.* **149**, 1 (1987).

[2] R.B.Wiringa et al.,*Phys.Rev.C***51**, 38 (1995).

[3] R.Machleidt et al.,*Phys.Rev.C* **53**, R1483 (1996).

[4] V.G.J.Stoks et al.*Phys.Rev.C* **49**, 2950 (1994).

[5] Punjabi V. et al., *Phys.Lett.* **B350**, 178 (1995).
L.S.Azhgirey et al.,*Phys.Lett.* **B391**, 22 (1997).

[6] N.Sakamoto et al., *Phys.Lett.* **B367**, 60 (1996).

[7] H.Sakai et al., *Phys.Lett.* **84**, 5288 (2000).

[8] R.Bieber et al.,*Phys.Lett.* **84**, 606 (2000).

[9] T.Uesaka et al.,*Phys.Lett.* **B533**, (2002).

[10] Coon and J.L.Friar,*Phys.Rev.C* **34**, 1060 (1996).

[11] J.Fujita and H.Miyazawa, *Prog.Theor.Phys.* **17**, 360 (1957).

[12] K.Suda et al.,*Annual report at CNS-REP-66 August 2005*

[13] M.Lacombe et al., *Phys.Lett.* **B101**, 139 (1981).

[14] R.Schiavilla, V.R.Pandharipande and R.B.Wiringa, *Nucl.Phys.* **A449**, 219 (1986).

[15] H.Kamada, private communication.

[16] H.Kamada et al., *Theor.Phys.* **104**, 703 (2000).

[17] Yu.N. Uzikov, JETP. Lett. **81**, 3031 (2005).

[18] V.P.Ladygin et al., *Phys.Atom.Nucl.* Vol.**65**, No. 9, 1609 (2002).

[19] P.A.M. Dirac, Rev.Mod.Phys. **21**, 392 (1949); S. Weinberg, Phys.Rev. **150**, 1313 (1966); L.L. Frankfurt, M.I. Strikman, Phys.Rep. **76**, 215 (1981).

[20] S.V. Afanasiev et al., Phys.Lett. B **434**, 21 (1998); V.P. Ladygin et al., Few-Body Systems **32**, 127 (2002); L.S. Azhgirey et al., Phys.Lett. B **595**, 151 (2004); V.P. Ladygin et al., Phys.Lett. B **629**, 60 (2005).

[21] H. Witala, J. Golak, W. Glöckle and H. Kamada, Phys.Rev. C **71**, 054001 (2005).

Λ AND $\bar{\Lambda}$ POLARIZATION AND SPIN TRANSFER IN PHOTOPRODUCTION AT HERMES

D. Veretennikov on behalf of the HERMES collaboration

Petersburg Nuclear Physics Institute
E-mail: denis.veretennikov@desy.de

Abstract

Transverse Λ and $\bar{\Lambda}$ polarization and spin transfer from longitudinally polarized target have been measured in the HERMES experiment. The data were accumulated in the years 1996-2000 using the 27.6 GeV polarized HERA positron beam incident on hydrogen, deuterium and heavier gaseous targets. The average transverse polarizations were found to be $P_n^{\Lambda} = 0.078 \pm 0.006_{stat} \pm 0.012_{syst}$ and $P_n^{\bar{\Lambda}} = -0.025 \pm 0.015_{stat} \pm 0.018_{syst}$ for Λ and $\bar{\Lambda}$ respectively. The longitudinal spin transfer coefficient is found to be $K_{LL}^{\Lambda} = 0.026 \pm 0.009_{stat} \pm 0.005_{syst}$ and $K_{LL}^{\bar{\Lambda}} = 0.002 \pm 0.022_{stat} \pm 0.008_{syst}$. The dependence of P_n^{Λ} and K_{LL}^{Λ} on the transverse and longitudinal momenta of the Λ hyperon were also studied.

1. Introduction. The transverse polarization of Λ particles has been observed and investigated in many high-energy scattering experiments, with a wide variety of hadron beams and kinematic settings [1, 2]. It is almost always found to be negative. A rather consistent kinematic behavior of the polarization has also been observed: its magnitude increases almost linearly with the transverse momentum p_T of the Λ hyperon up to $p_T \approx 1$ GeV, where a plateau is reached. In lepto/photoproduction, the data existing to date are not conclusive because of lack of statistics [3, 4].

Spin-transfer coefficient from the transversely or longitudinally polarized proton to the Λ has been measured by E704 [5], STAR [6] and PS185 [7]. In E665 [5] and COMPASS [8] experiments longitudinal spin transfer has been studied using polarized muon beams. The HERMES [9] experiment has measured D_{LL} using the polarized positron beam of the HERA accelerator [10, 11]. The data on spin transfer from the polarized *target,* reported here, have been obtained in photoproduction regime for the first time.

3. Transverse Λ and $\bar{\Lambda}$ polarization. The final-state hadron polarization in a reaction with unpolarized beam and target must point along a pseudo-vector direction, because of the parity-conserving nature of the strong interaction. In the case of inclusive hyperon production, the only available direction of this type is the normal $\overrightarrow{n}$ to the scattering plane formed by the cross-product of the vectors along the laboratory-frame momenta of the positron beam ($\overrightarrow{p}_e$) and the Λ ($\overrightarrow{p}_\Lambda$): $\overrightarrow{n} = \frac{\overrightarrow{p}_e \times \overrightarrow{p}_\Lambda}{|\overrightarrow{p}_e \times \overrightarrow{p}_\Lambda|}$. The extraction of the Λ polarization P_n from the data was accomplished using a moment method which exploits the top/bottom symmetry of the detector [12, 13].

In order to study possible effects of detector misalignment and inefficiency detailed Monte-Carlo simulations were performed. A contribution from the background under the Λ invariant mass peak to the extracted polarizations was taken into account using a sideband subtraction method.

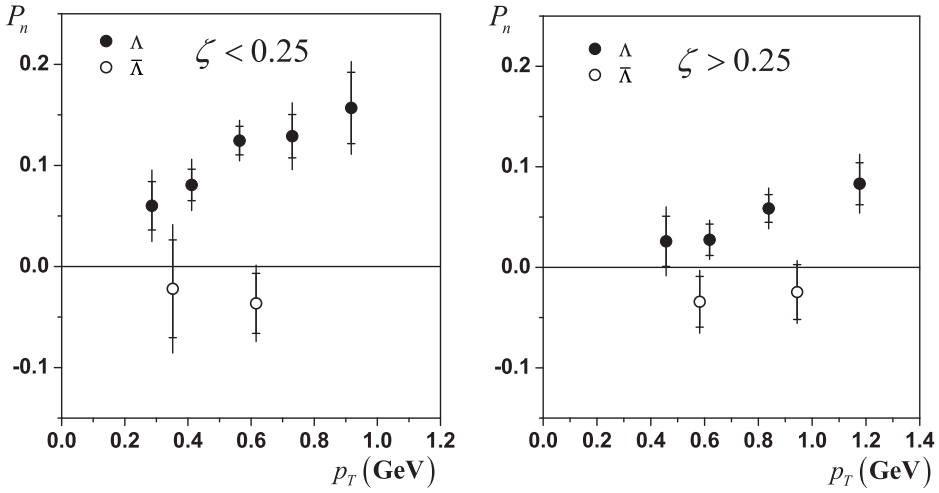

Figure 1. Transverse polarization P_n^{Λ} and $P_n^{\bar{\Lambda}}$ as function of p_T for the region $\zeta < 0.25$ (left panel) and $\zeta > 0.25$ (right panel).

In order to estimate the systematic uncertainty of the measurement an identical analysis was carried out for reconstructed h^+h^- hadron pairs, both with leading protons (Λ-like case) and with leading antiprotons ($\bar{\Lambda}$-like case).

Events within two mass windows above and below the Λ ($\bar{\Lambda}$) mass peak were selected under condition that the hadrons point of closest approach is found inside the target region. False polarization values of 0.012 ± 0.002 and 0.018 ± 0.002 were found in the Λ-like and $\bar{\Lambda}$-like cases respectively. These values were used as estimates of the systematic error on the Λ and $\bar{\Lambda}$ polarization. The decay $K_S^0 \to \pi^+\pi^-$ was studied as an additional check on a possible false polarization. The false polarization of the K_S^0 sample was found to be 0.012 ± 0.004.

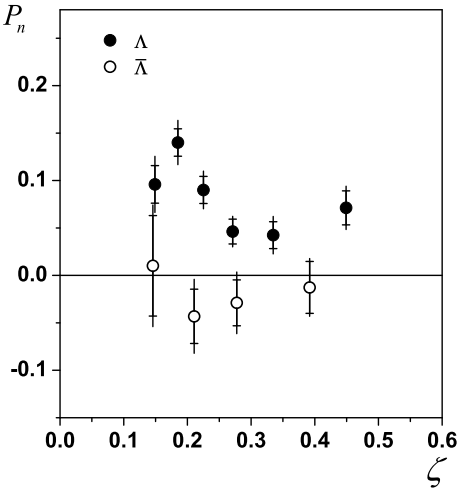

Figure 2. Transverse polarization P_n^{Λ} and $P_n^{\bar{\Lambda}}$ as function of ζ.

The net Λ polarization summing over events for all targets is found to be positive: $P_n^{\Lambda} = 0.078 \pm 0.006_{stat} \pm 0.012_{syst}$, while the net polarization is consistent with zero: $P_n^{\bar{\Lambda}} = -0.025 \pm 0.015_{stat} \pm 0.018_{syst}$. As information on the virtual photon kinematics was not available in this inclusive measurement, the kinematic dependence of the polarization could only be studied as a function of variables derived from the eN system. The selected variables were p_T and $\zeta \equiv (E_\Lambda + p_z^\Lambda)/(E_e + p_e)$, where p_T is the transverse momentum with respect to the (lepton) beam, E_Λ and p_z^Λ are the energy and z-component of the Λ momentum (where the z-axis is along the lepton beam direction), and E_e, p_e are the energy and momentum of the positron beam.

In Fig. 1, the transverse Λ and $\bar{\Lambda}$ polarizations are shown versus p_T for two kinematical domains $\zeta < 0.25$ and $\zeta > 0.25$. The Λ polarization rises linearly with p_T with higher slope at $\zeta < 0.25$. The Λ and $\bar{\Lambda}$ polarizations as functions of ζ are shown in Fig. 2. The Λ polarization appears to increase in the low-ζ region while the $\bar{\Lambda}$ polarization shows no visible dependence on either ζ or p_T.

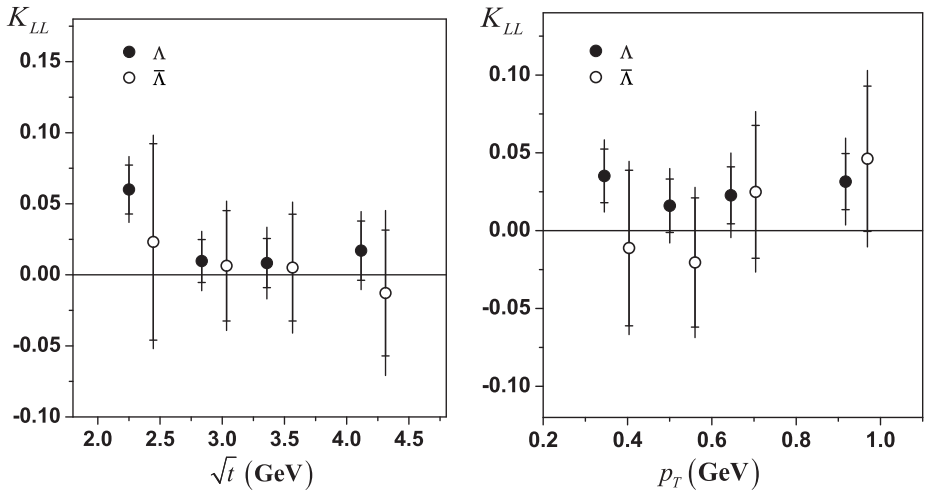

Figure 3. Spin transfer coefficient K_{LL} for Λ and $\bar{\Lambda}$ versus $\sqrt{t}$ (left panel) and p_T (right panel).

3. Spin transfer K_{LL}. In order to cancel the effect of the limited HERMES acceptance, the spin transfer to the Λ and $\bar{\Lambda}$ has been determined by combining the two data sets measured with opposite target polarizations into one helicity-balanced data sample, in which the luminosity-weighted average target polarization for the selected data is $\overline{P}_{Targ} \equiv \frac{1}{L}\int P_{Targ} dL = 0$. Here $L = \int dL$ is the integrated luminosity. A detailed derivation based on the method of maximum likelihood leads to the relation [14]. The analysis of false asymmetries for h^+h^- pairs and K^0_S decay was performed similar to the transverse polarization case. For h^+h^- pairs false spin transfer of -0.0005 ± 0.0028 and -0.002 ± 0.003 were found in the Λ-like and $\bar{\Lambda}$-like cases, respectively. For $K^0_S \to \pi^+\pi^-$ it was obtained 0.006 ± 0.008.

Averaged over the experimental kinematics, spin transfer to the Λ is found to be positive: $K^{\Lambda}_{LL} = 0.026 \pm 0.009_{stat} \pm 0.005_{syst}$ and spin transfer to the $\bar{\Lambda}$ is consistent with zero: $K^{\bar{\Lambda}}_{LL} = 0.002 \pm 0.022_{stat} \pm 0.008_{syst}$.

For spin transfer study in addition to ζ the Mandelstam variable $t \equiv -(p_\Lambda - p_p)^2$ was used. The variable ζ or t provides an approximate measure of whether a hyperon was produced in the forward or backward region in the center-of-mass frame of the $\gamma^* N$ reaction. The natural variable to use to separate these kinematic regimes would be $x_F \equiv p^{\Lambda}_{\parallel}/p^{\Lambda}_{max}$ evaluated in the $\gamma^* N$ system, but this variable is not available since primary photon energy is not measured in the experiment. Nevertheless, a simulation of the reaction using the PYTHIA program reveals a reasonable correlation between ζ and x_F variables.

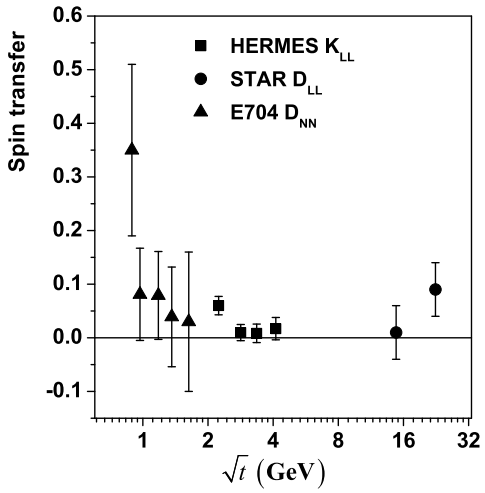

Figure 4. Compilation the world data of spin transfer.

In particular, all events at $\zeta \geq 0.25 (\sqrt{t} > 3.31$ GeV) are produced in the kinematic region $x_F > 0$, while for $\zeta < 0.25 (\sqrt{t} < 3.31$ GeV) there is a mixture of events originating from the kinematic regions $x_F > 0$ and $x_F < 0$.

Fig.3 shows p_T and $\sqrt{t}$ dependence of spin transfer coefficient K_{LL}. The spin transfer for Λ are p_T independent and increasing for $\sqrt{t} < 3.31$ GeV, while for $\sqrt{t} > 3.31$ GeV it compatible with zero. In $\bar{\Lambda}$ case both results are compatible with zero. In Fig.4 the HERMES data for spin transfer as function of $\sqrt{t}$ are presented together with data obtained by the E704 collaboration 200 GeV transversally polarized proton beam and the STAR collaboration with a longitudinally polarized proton beam and center of mass energy $\sqrt{s} \cong 200$ GeV. As seen from Fig.4 the E704 result confirms a trend to increase spin transfer in the region $\sqrt{t} < 3.31$ GeV.

References

[1] CERN-WA-004 Collaboration, D. Aston *et al.*, Nucl. Phys. **B195**, 189 (1982).

[2] SLAC-BC-072 Collaboration, K. Abe *et al.*, Phys. Rev. **D29**, 1877 (1984).

[3] J. Lach, Nucl. Phys. (Proc. Suppl.) 50 216 (1996).

[4] WA89 Collaboration, M.I. Adamovich, Eur. Phys. J. **C32** 221 (2004).

[5] Bravar *et al.*, Phys. Rev. Lett. 78:4003-4006, (1997).

[6] Qinghua Xu for the STAR collaboration., hep-ex/0612035.

[7] B. Bassalleck *et al.*, Nucl. Instr. and Meth. in Phys. Res. **B214** 167 (2004).

[8] M. G.Sapozhnikov, hep-ex/0602002.

[9] K. Ackerstaff *et al.*, Nucl. Instrum. Methods **A417** 230 (1998).

[10] A.Airapetian *et al.*, Phys. Rev. **D64**:112005, (2001).

[11] A.Airapetian *et al.*, Phys. Rev. **D74** (2006) 072004.

[12] S. Belostotski DESY-HERMES-06-57. Prepared for 58th Scottish Universities Summer School in Physics (SUSSP58), St. Andrews, Scotland, 22-29 Aug 2004.

[13] A. Airapetian *et al.*, arXiv:hep-ex/07043133 (2007).

[14] S. Belostotski in Proc. of the IX-Workshop on High Energy Spin Physics (SPIN-01), Dubna 2001, preprint JINR E1 2-2002-103 (2002) 192.

Discussion

Q. (X.Artru, Inst. de Phys. Nucl. de Lyon) Why do you reject leading pion?

A. We only reject leading π^+ in case of Λ production, not leading π^-.

Q. (G.Bunce, BNL) Since the production plane for Λ production cover almost 2π for the angle of the production plane relative to detector, what is the origin of the systematic error for the Λ polarization?

A. The acceptance does not completely cancels, so that leaves the systematic uncertainty that is presented.

TECHNICS
and
NEW DEVELOPMENTS

POLARIMETRY OF THE PROTON BEAMS AT RHIC

I.G. Alekseev[1†], A. Bazilevsky[2], K. Boyle[8], A. Bravar[2], G. Bunce[2,3], C. Camacho[13], S. Dhawan[4], A. Dion[8], K.O. Eyser[12], R. Gill[2], W. Haeberli[5], A. Hoffman[14], H. Huang[2], G. Igo[6], O. Jinnouchi[3], V.P. Kanavets[1], K. Kurita[7], A. Khodinov[8], H. Liu[13], W. Lozowski[9] Y. Makdisi[2], I. Nakagawa[11], A. Nass[2], H. Okada[10], N. Saito[10], M. Sivertz[2], E. Stephenson[9], D.N. Svirida[1], C. Whitten[6], T. Wise[5], J. Wood[6], and A. Zelenski[2]

(1) *Institute for Theoretical and Experimental Physics, Moscow, Russia*, (2) *Brookhaven National Laboratory, Upton, USA*, (3) *RIKEN BNL Research Center, Upton, USA*, (4) *Yale University, New Haven, USA*, (5) *University of Wisconsin, Madison, USA*, (6) *UCLA, Los Angeles, USA*, (7) *Rikkyo University, Tokyo, Japan*, (8) *SUNY, Stony Brook, USA*, (9) *IUCF, Bloomington, USA*, (10) *Kyoto University, Kyoto, Japan*, (11) *RIKEN, Saitama, Japan*, (12) *University of California, Riverside, USA*, (13) *Los Alamos National Laboratory, Los Alamos, USA*, (14) *MIT, Boston, USA*, † *E-mail: Igor.Alekseev@itep.ru*

Abstract

Spin physics program of RHIC (BNL, USA) requires good knowledge of the beam polarization for the experiments as well as the machine tuning. These data are provided by a set of two proton-carbon and one proton-hydrogen jet polarimeters. These polarimeters utilize a huge cross section of the small angle elastic scattering which despite of a small analyzing power provides an excellent figure of merit. Small energy dependence of the analyzing power together with energy independent geometry allows the same setup to cover the whole energy range $25 \div 250$ GeV.

This article covers the polarimeters progress and performance in the last proton run spring 2006.

Introduction. Elastic scattering in the region of very small momentum transfers is determined by two forces: nuclear and electro-magnetic. Interference between these forces results in nonzero phase between the amplitudes without spin flip and with single spin flip, which produces analyzing power A_N [1, 2]. The experimental test of this effect with carbon target was done at AGS in 1999 and turned out to be very successful [3]. The advantages of this process for the polarization measurement include:

- large cross section, which makes it easy to get large statistics;
- the fact that kinematics doesn't depend much on the beam momentum, which makes it possible to cover whole RHIC energy range from 25 to 250 GeV with a single setup;
- the fact that the event is completely defined by recoiled particle, so we can measure only it and avoid difficulties of registration of the scattered proton, which is deflected too slightly to leave the beam;
- weak dependence of the analyzing power on the energy, which also helps us to cover RHIC energy range.

But there are also some drawbacks, which include comparatively small (a few percents) analyzing power and the fact that it is not completely calculable theoretically. Due to the first drawback we need to collect large (about $2 \cdot 10^7$) statistics per one measurement. Due to the other we have to calibrate the polarimeter.

Polarimeters. RHIC design stated a goal to measure beam polarization to 5% [4]. Fast measurements for beam adjustments are also required. In order to achieve these goals two types of polarimeter were built. One is a fast polarimeter with carbon target [5] and the other is an absolute polarimeter with polarized hydrogen jet target [6]. Common features and differences of the two polarimeters are given in Tab. 1.

Table 1: The polarimeters

	Relative pC-polarimeter	Absolute H-jet polarimeter
Calibration	External	Self calibration
Process Kinematics	Elastic scattering in the CNI-region Fixed target, recoil at 90^o detected	
Detectors	Silicon detectors, measuring time and energy	
Recoil particle identification	Correlation between time-of-flight and kinematic energy	
Readout	DAQ is based on wave form digitizers(WFD)	
Target	Extremely thin carbon ribbon	Polarized hydrogen jet
Measurement	Two beams by independent polarimeters	One beam in a time by common polarimeter
$-t$ range T_R range	$0.007 \div 0.030$ (GeV/c)^2 $0.3 \div 1.3$ MeV	$0.0015 \div 0.01$ (GeV/c)^2 $0.8 \div 5.5$ MeV
Measurement of the recoil angle	Smashed by multiple scattering in the target	Used for elastic event selection
Flight distance Time-of-flight range	~ 15 cm $10 \div 50$ ns	~ 80 cm $20 \div 80$ ns
Counting rate Measurement time	Up to several MHz $20 \div 200$ s	~ 100 Hz Several fills
Radial polarization measurement	Yes, by 45^o detectors	No

Ran 2006. In run 2006 DAQ hardware and computers were set individually for each ring pC-polarimeter and H-jet polarimeter. This allowed us more flexibility in measurements and provide us with ability to upgrade H-jet DAQ without interference with pC-polarimeters. This upgrade included new firmware for WFD and new online monitoring program. The main new feature of the firmware was ability of saving long waveform which allowed better waveform analysis in the off-line. An example of the waveform is shown in fig. 1a together with the time and amplitude definitions used in the online. The performance of the polarimeter in the begin of the proton run is shown in the fig. 1b. The ratio of beam asymmetry to jet asymmetry is shown a function of fill number. Measurements of the blue beam are shown in the left and of the yellow beam in the right. An improved accelerator performance together with very high jet density allowed us to reach 10% absolute error just in one store.

High accelerator luminosity together with long run time in 2006 allow us also to make a study of the polarization profile. Significant profile was observed in both rings and in both

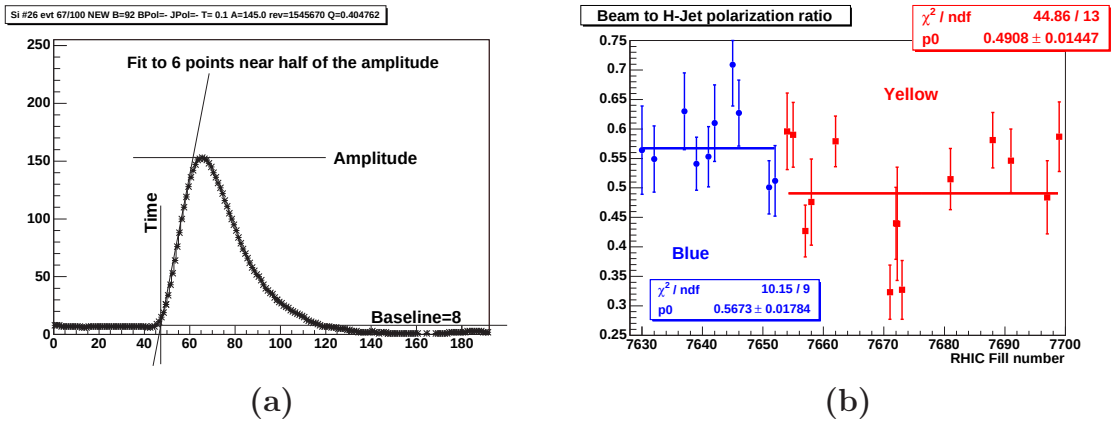

(a) (b)

Figure 1a. An example waveform and online parameters definition.
Figure 1b. Ratio of beam asymmetry to target asymmetry at the beginning of run 2006 as a function of fill number.

horizontal and vertical planes. The profile turned out to be also different from fill to fill and there were some fills where it was not observed. Both polarimeters (when pC is in the profile scan mode) measure the polarization averaged over beam intensity, while collider experiments average over luminosity, which is proportional to the product of the beam intensities. This introduces and additional correction to the polarimetry results. This correction varies in the range $+(0 \div 7)\%$ depending on the actual vertical and horizontal profiles in the given fill. Unfortunately only horizontal profile was measured regularly. So some additional systematics will contribute to run 2006 results.

The road to 5% measurement We will assume now that we are running both polarimeters:

- pC-polarimeter each 1-2 hours during fills, scanning both vertical and horizontal profiles;
- H-jet-polarimeter alternating beams each fill.

Our procedure of getting absolute polarization of the beams has following steps:

- Measure hydrogen jet polarization. This is performed by Breit-Rabi polarimeter. The error in jet polarization including uncertainty in the contamination by molecular hydrogen is about 2%.
- Measure ratio R of beam to jet asymmetries in the H-jet polarimeter. The data in the fig. 1b was collected in about two weeks and has statistical error in the asymmetry ratio about 3% for each beam. Small inelastic background contributes to both asymmetries and is canceled in the ratio with a good precision.
- Measure beam asymmetries with pC-polarimeter and normalize to the average beam polarization which we got in the two previous steps. The statistical precision of pC-polarimeter is very large and doesn't contribute to the total error. An estimation of the stability of pC-polarimeter analyzing power comes from observed change in our dead layer estimation. A safe limit to the systematics introduced by pC-polarimeter analyzing power drifts is 2%.

- Correct the polarization to the polarization profile. The correction is difficult to measure and it is in the range $+(0 \div 7)\%$. We hope that the error produced by profile will be corrected to the precision of 2%.

Total error in the polarization value is:

$$(\frac{\Delta P}{P})^2 = (\frac{\Delta P_{\rm jet}}{P_{\rm jet}}[2\%])^2 + (\frac{\Delta R}{R}[3\%])^2 + (\frac{\Delta P^{stat}_{pC}}{P^{stat}_{pC}}[0\%])^2 + (\frac{\Delta P^{sys}_{pC}}{P^{sys}_{pC}}[2\%])^2 + (\frac{\Delta P_{prof}}{P_{prof}}[2\%])^2$$

$$\sim (5\%)^2$$

So RHIC polarimeters can provide both fast and precise beam polarization measurements required for RHIC success as a polarized proton collider.

References

[1] B.Z. Kopeliovich and L.I. Lapidus, Sov. J. Nucl. Phys. **19** (1974) 114.

[2] N. H. Buttimore *et al.*, Phys. Rev. **D59** (1999) 114010.

[3] J. Tojo *et al.*, Phys. Rev. Lett. **89** (2002) 052302.

[4] T. Roser *et al.*, Polarized Proton Collider at RHIC, preliminary design report, 1997 (unpublished);
M. Bai *et al.*, Phys. Rev. Lett. **96** (2006) 174801.

[5] I. Nagava *et al.*, Proceedings of the 17th International Spin Physics Symposium, AIP Conference Proceedings, **vol 915**, Melville, New York, 2007, pp. 912-915

[6] A. Zelenski *et al.*, Nucl. Inst. and Meth. **A536** (2005) 248;
H. Okada *et al.*, Phys. Lett. **B638** (2006) 450-454;
H. Okada *et al.*, Proceedings of the 17th International Spin Physics Symposium, AIP Conference Proceedings, **vol 915**, Melville, New York, 2007, pp. 681-684;
K.O.. Eyser *et al.*, Proceedings of the 17th International Spin Physics Symposium, AIP Conference Proceedings, **vol 915**, Melville, New York, 2007, pp. 916-919;
Y. Makdisi *et al.*, Proceedings of the 17th International Spin Physics Symposium, AIP Conference Proceedings, **vol 915**, Melville, New York, 2007, pp. 975-978

Discussion

Comm. (G.Bunce, BNL) Due to the synchrotron motion, the protons in a bunch in RHIC mix longitudinally. Therefore it is not useful to try to measure the polarization in the longitudinal profile.

Q. (Y.Bedfer, CEA, Gif/Yvette) Don't you have to measure polarization as a function of the whole phase space of the beam rather then merely as a function of the transverse position?

A. With our target we can measure only transverse distribution. We don't know a way to measure longitudinal distribution. But according to accelerator people there should be no longitudinal distribution.

SOLID STATE POLARIZED TARGETS FOR PARTICLE PHYSICS EXPERIMENTS

D. G. Crabb

Physics Department, University of Virginia
Charlottesville VA 22903, USA

Abstract

Examples are given of dynamically polarized targets in use today and how the subsystems have changed to meet the needs of today's experiments. Particular emphasis is placed on target materials such as ammonia and lithium deuteride and their operation in an intense beam of charged particles. Recent polarization studies of irradiated materials such as butanol and polyethylene and their deuterated counterparts are presented. The operation of two non-DNP target systems as well as applications of traditional DNP targets are discussed briefly.

1 Introduction

Over more than forty years of use, solid polarized targets have seen many developments, innovations and improvements. Early on, ^{4}He evaporation refrigerators were used followed by ^{3}He evaporation refrigerators that allowed lower temperatures (˜0.5 K) to be reached. Later, dilution refrigerators were modified to operate efficiently in beams of charged particles, reaching even lower temperatures (˜50 mK) where the concept of frozen spin became a reality. In later years the ^{3}He refrigerators were displaced by dilution refrigerators for various practical reasons. Today it is a matter of scale: ^{4}He refrigerators typically operate in high intensity charged particle beams while dilution refrigerators operate with neutral or very low intensity particle beams, in both continuous or frozen spin mode.

In addition to the refrigerators, improvements in magnets, microwave sources and NMR and the use of many different materials have meant that through dynamic nuclear polarization (DNP), proton polarizations of close to 100% and deuteron polarizations of about 80% have been achieved. The range of operation for DNP of solid targets now goes from 100 mK to about 1 K and from 2 T to 7 T.

2 System Improvements

2.1 Refrigerators and Magnets

Examples of high power refrigerators are the UVA/SLAC/JLab ^{4}He refrigerator [1] and the SMC/Compass dilution refrigerator [2]. The UVA refrigerator operates in an electron beam of 100 nA with a small target (2.5 cm OD cylinder, 3 cm long) with 12000 m^3hr^{-1} pumping speed, while the SMC refrigerator can cool a very large target to a temperature of ˜50 mK, in the presence of a beam of $> 10^7$ μ s^{-1}.

The magnet for the UVA system is a superconducting split Helmholtz pair operating at 5 T. There is a large acceptance in the field direction, while normal to the field direction there is a split between coils of 8 cm and an opening with respect to the target center of ±

17°, horizontally and ± 25°,vertically. The current trend for transversity measurements is to open the access on the split as much as possible. Openings of about ± 22° are possible while maintaining the field uniformity requirement of ˜10^{-4} over a 2 -3 cm DSV, but at the expense of lowering the central field to about 4 T.

The magnet for the SMC target operates at 2.5 T and has a bore large enough to accommodate the large diameter refrigerator nose. The target size is 1600 mm long with a 70 mm diameter. The experiment detected muons at relatively small angles and therefore the bore was adequate. However in the COMPASS incarnation a new magnet has been installed; this allows detection of recoil particles at larger angles. Furthermore transverse measurements can be made with a saddle coil wound on the refrigerator which is operated in the frozen spin mode. As mentioned above, many experiments use dilution refrigerators operating in the frozen spin mode with the low magnetic field provided by an internally wound superconducting coil [3]

It is doubtful that much can be gained by going to larger systems than these. Thus one must look elsewhere for possible improvements for either increased polarization and the maintenance of that polarization or the better measurement of the polarization.

2.2 Microwaves and NMR

In general, the polarization of protons and deuterons increases with increasing magnetic field, as will be seen later in this talk. However the frequency of the microwaves necessary for the DNP process is linearly related to the value of the magnetic field. But as the frequency output of microwave devices increases the power available decreases. At the same time, the power required for DNP to proceed efficiently increases. Operation at 140 GHz and 5 T has been possible for some years because of EIO tubes, generating more than 15 watts at 140GHz. In the last few years EIO tubes have become available at around 200 GHz and which output a few watts and therefore allow operation with a magnetic field of ˜7 T. However the compromise is that there is a small tuning range of ˜200 MHz, compared to the 2 to 3 GHz available at 140 GHz, which is a consequence of removing the mechanical tuner. The span of frequency going from positive to negative enhancement for most materials is greater than 200 MHz so one operates at fixed frequency and adjusts the magnetic field into resonance.

The standard for NMR measurement continues to be the so-called Liverpool Q-meter [4]. Little has changed in more than 30 years of operation, except in the past few years the tunable resonant circuit has been removed from the room temperature Q-meter and placed in the refrigerator very near the target itself. This results in improved signal stability and noise reduction because of operation around 1 K [5]. Such a system is used on a polarized target running at PSI [6]. The target is thin, needing the noise reduction that is described above.

For the deuteron, sometimes it is not possible to use the standard method of calibration by measuring the area of a thermal equilibrium (TE) signal because the signal is too small for a reasonable measurement. However it has long been known that the characteristic shape of the deuteron signal can be used to estimate the polarization represented by that signal by measuring the ratio of the heights of the two peaks in the spectrum. Because of the dynamics of the polarizing, it is known that the method is not reliable below a polarization of about 20%. Using a method developed for the SMC polarized target [7], it has been shown [8] that this method for evaluating the polarization in deuterated

ammonia is valid above about 25%: the deuteron polarizations measured in the GeN and RSS experiments at JLab were obtained through careful area measurements of the TE signal and were compared to the ratio evaluation on the same data. The ratio method was used in the EG4 experiment at JLab and was used to obtain the calibration constant for the target(s) in the EG4 experiment in Hall B at JLab. The polarization history of the target is shown in Fig. 1 and discussed in Section 2.3.1

2.3 Materials

Several of the polarized target materials listed by Crabb and Meyer [9], still are in regular use; more is known about them, so there can be a better matching of target to the experiment under consideration.

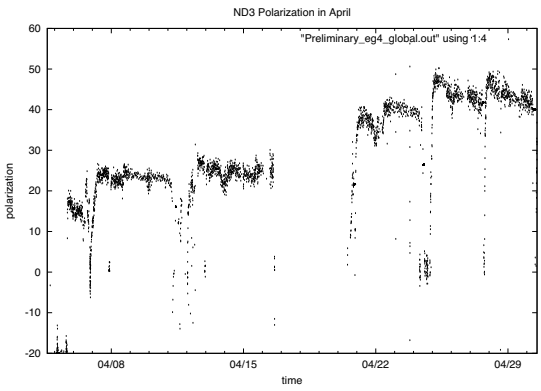

Figure 1: Deuteron polarization during experiment EG4. There are several sequences of irradiation followed by an anneal and repolarizing.

2.3.1 Ammonia

For many years ammonia ($^{14}NH_3$, $^{15}NH_3$) has been the material of choice for operation in high intensity beams; it has one of the best radiation resistances together with a rapid polarization rise to $> 90\%$. The material is prepared for DNP by irradiation doping by exposing it to a charged particle beam while under liquid argon. An exposure of about 10^{17} particles cm^{-2} gives the best initial performance. As shown in Fig. 2 the polarization decays under continuous exposure to the beam used in the experiment.

Annealing (warming the target ammonia to about 90 K) restores the polarization. Even with an electron beam of 100 nA, the target survives for many cycles of decay and anneal, though as can be seen the decay becomes faster after each successive anneal, and eventually the target material has to be changed. Obviously there is an advantage to using ammonia in lower intensity beams, giving slower decay and thus a higher average polarization. A sample of ammonia that was kept in liquid nitrogen for ten years and never used for an experiment, was polarized about once per year and shows a slow decay of the achievable polarization. The negative polarization fell from -95% to about -61%, while the positive still reached 82%.

Deuterated ammonia behaves in a different way: the initial doping irradiation under liquid argon yields a polarization of only about 15%. But then in a sequence of decay and anneal the polarization rises to about 45% [10] as shown in Fig. 3. The annealing procedure also changes over the dose history of the target; the temperature of the anneal increases from about 80 K to 110K, while the time spent at that temperature increases from 15 minutes to one hour. Deuterated ammonia has higher radiation resistance than normal ammonia, but shows the same trend of faster decay as a function of dose; so far a limit has not been reached.

The behaviour of the polarization in a beam is shown in Fig. 4; polarization builds up to about 45% without beam and after an anneal. The beam is turned on and there is an

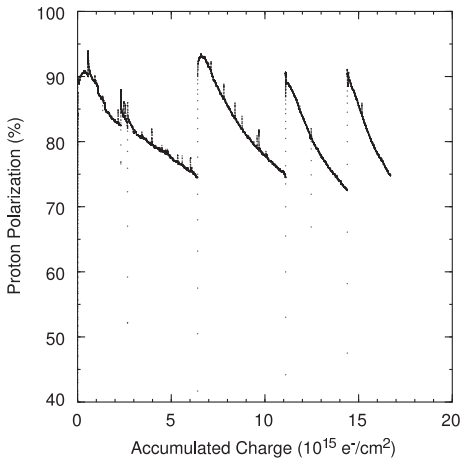

Figure 2: Proton polarization decay through radiation damage, as a function of incident charge.

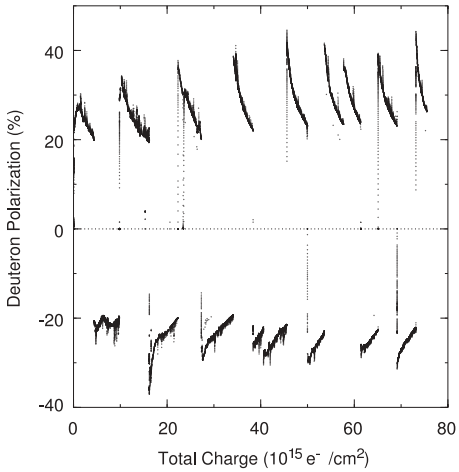

Figure 3: Deuteron polarization decay through radiation damage, as a function of incident charge.

immediate drop due to beam heating, after which there is a slower decay due to radiation damage. The spikes in the curve are due to beam trips; there is an immediate reponse as the target cools.

Because of the limited polarization available with ND_3 after the polarizing dose, it is not usually suitable for running in a low intensity beam because of the limitation of the substantial cold dose necessary to reach 40%. However in experiment EG4 in Hall B at JLab using the CLAS detector, it was possible to achieve a deuteron polarization of better than 45%. The luminosity limit for this experiment (to avoid high rates in the detector) meant that a beam intensity of about 2nA only could be used. However it was possible to turn off all the detectors and put 100nA through the target for about an hour and then anneal. This sequence was performed several times, raising the polarization from $< 20\%$ to about 45%. [11] This sequence of irradiating, annealing and polarizing is shown in Fig. 1.

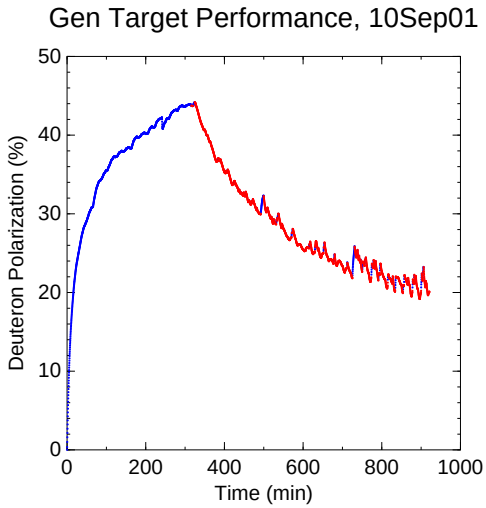

Figure 4: Deuteron polarization before and after beam is turned on.

2.3.2 ^{6}LiD

Abragam and co-workers [12] first showed that ^{6}LiD could be polarized after irradiation and under conditions of high magnetic field and low temperatures (in a dilution refrigerator). Deuteron and lithium polarizations of 70% were obtained. At SLAC it was first used as a deuteron target in experiment E155, operating with a 5 T magnet and at 1 K . Polarizations of up to 30% were obtained in the deuteron and in the ^{6}Li. The ^{6}Li can be considered in its simplest form, a combination of alpha particle and deuteron [13], thus providing a second deuteron for the interaction. In the case of E155, in comparison with E143 where the measurement of the A_1 asymmetry parameter was measured with

$^{15}ND_3$, the data agreed to within 5%. Fig. 5 shows the rise of the deuteron polarization, as a function of time, before and then also after the beam is turned on. It reaches a maximum and then turns over and starts falling due to radiation damage. Also shown is an indication of when beam is incident on the target. The structure in the polarization is due to beam stoppages. The radiation damage characteristic is two to three times better than deuterated ammonia.

2.3.3 Other DNP Materials

In the early days of polarized targets many experiments were carried out with alcohols such as butanol, propanediol, ethanediol etc. with paramagnetic radicals such as porphyrexide and Cr V. Typical proton polarizations were better than 80%, but the deuteron polarizations were typically less than 30%. depending on the radical-host combination. After the success of irradiated ammonia, the University of Virginia polarized target group thought it worthwhile to take another look at irradiating materials such as those mentioned above and others such as CH_2, CD_2 which could not be chemically doped very easily. Though earlier attempts had been made to irradiate and polarize, it was sporadic and not very high polarizations were obtained.

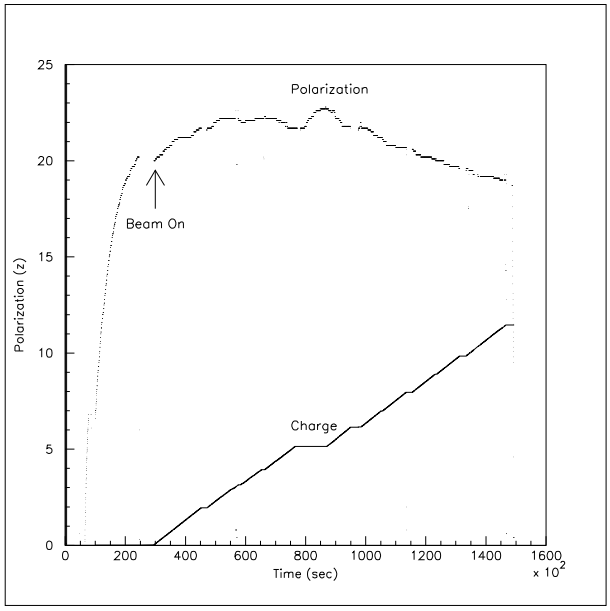

Figure 5: Deuteron polarization in ^{6}LiD before and after beam is turned on. Structure in polarization correlated with the beam being off or on as indicated by the charge line.

The group did a series of irradiations at the MIRF facility at NIST in Gaithersburg, MD with a 19 MeV electron beam at 10 or 15 μA. The results are shown in Fig. 7 and Fig. 6 at 5 T and 1 K.

The polarizations of various proton materials do not show much promise compared to chemically doped materials, though CH_2 cannot be doped in any other way and polarizations of > 20 % might be sufficient for some applications.

On the other hand, the deuterated materials have some possibilities with deuterated butanol reaching a deuteron polarization of $> 50\%$ and deuterated 1-pentanol showing a similar response. Some measurements were done at 6.55 T and 1K and, for deuterated butanol, deuteron polarizations of $> 60\%$ were obtained. This is the opposite effect to that measured at PSI where the polarization dropped to zero at 5 T, from about 50% at 2.5 T, with butanol doped with EDBA [14].

In a series of ESR studies by the Bochum target group, it was shown that the deuteron polarization, as a function of magnetic field, changes as the width of the ESR line changes. In this study, a standard X-band ESR spectrometer as well as one operating at around 70 GHz, (a typical polarized target operating frequency) allowed some measurements of how the line width changes with ESR frequency. Narrower lines lead to higher deuteron polarizations.

For example the line width of d-butanol doped with EDBA increases by a factor

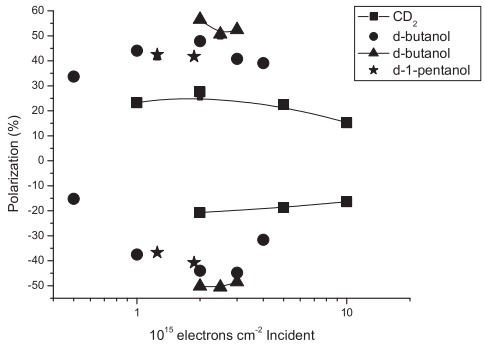

Figure 6: Deuteron polarizations for various materials as a function of incident charge.

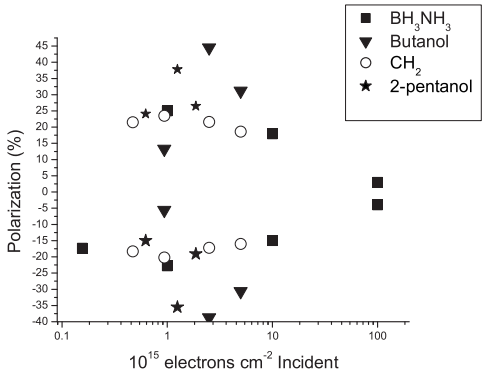

Figure 7: Proton polarizations for various materials as a function of incident charge.

of six from X-band to 70 GHz, while d-butanol doped with porphyrexide or TEMPO only increases by about a factor of two. Also irradiated d-butanol has a line width which is about half of that measured with TEMPO and porphyrexide. The polarizations obtained with these samples directly correlates with the ESR line width. The largest deuteron polarizations ever measured were achieved with the family of Trityl radicals [16]. At Bochum [15] deuteron polarizations of ±80% were achieved with Trityl doped d-butanol and d-propanediol. Unfortunately these radicals are difficult to obtain because of proprietary concerns.

2.4 Hydrogen Deuteride (HD)

This target, which uses the so called "brute force" method, has just finished a successful run at the LEGS facility at BNL. [17] The polarization is the H and D thermal equilibrium polarization obtained in a very high magnetic field (˜17 T) and very low temperatures (˜10 mK), with either ortho-hydrogen and/or para-deuterium as the dopant. The target is prepared over at least a month of curing, during which time the dopants decay to their magnetically inert state. The target has to be removed from the curing refrigerator and installed in the in-beam refrigerator without significant loss of polarization. The experiment can proceed as the polarization slowly relaxes; the relaxation time can be many weeks or months depending on the holding field and temperature. The deuteron polarization can be enhanced by transferring some of the protons' polarization through an adiabatic transition. At LEGS, the polarizations for the duration of the scattering experiment were about 58% for the proton and, after an adiabatic transition about 32% for the deuteron.

The LEGS facility has been closed and the HD target will be moved to JLab over the next year or so.

2.5 Solid Target with Aromatic Molecules

This target was developed for measurements in RI beams with very low magnetic fields (max =0.7 T) with operation at 0.09 T and at a temperature of about 100 K. A combination of several techniques are employed to polarize the aromatic molecules (napthalene

doped with pentacene) used in the target. The procedure and the results from an early run are described in [18].

2.6 Other Applications

Polarized targets are being used in areas other than in direct scattering measurements. Researchers in Malmo, Sweden [16] have used a ^{4}He refrigerator to polarize ^{13}C to about 45%. The idea is to use the polarized ^{13}C in high contrast MRI: ^{13}C enriched material, which must be a liquid at room temperature, is frozen and polarized and then extracted from the refrigerator, warmed to 300 K and injected into the patient (at this point, a mouse or rat) as fast as possible without losing too much polarization. The polarized ^{13}C is then detected in a MRI scanner in some parts of the body (e.g. heart) that are not covered so well by polarized ^{3}He gas. Some attempts have been made by the same group to polarize ^{129}Xe in a DNP apparatus to realize higher polarizations for Xe MRI measurements.

3 Conclusions

Two examples of dynamically polarized targets have been presented as representing the targets in use at various laboratories. A ^{4}He evaporation refrigerator for operation in intense particle beams and a dilution refrigerator for dynamic operation in low intensity or neutral beams and which can be used in a frozen spin mode. At the same time, subsystems have been improved to meet the demands of modern experiments. In an era where difficult and/or very precise experiments are being proposed, the traditional DNP style polarized targets have a significant rôle to play still. There have also been developments of non DNP targets to meet a specific experimental requirement. Indeed targets using DNP have been adapted as neutron spin filters, neutron spectroscopy and for MRI studies. Even without further developments of this mature technology, polarized targets will still be able to meet the future demands placed on them.

Acknowledgments

I wish to thank all the members of the U. of Virginia Polarized Target Group for their help and encouragement and those members of other groups who sent me information to include in this talk. I am indebted to the US Department of Energy for a grant which enabled this work to be carried out.

References

[1] D. G. Crabb & D. B. Day, Nucl. Instr. & Meth. in Phys. Res., A356, 9 (1995).
[2] J. Kyyäräinen et al., Nucl. Instr. & Meth. in Phys. Res., A356, 47 (1995).
[3] H. Dutz et al., Nucl. Instr. & Meth., in Phys. Res., A356, 111 (1995).
[4] G. R. Court et al., Nucl. Instr. & Meth., A324, 433 (1993)
[5] G. Court et al., Nucl. Instr. & Meth.in Phys. Res., A527, 253 (2004).

[6] F. Piegsa, Proc. of the Workshop on Polarized Sources,Targets and Polarimeters, Brookhaven National Laboratory, September 10 -14 2007, To be Published.
[7] C. M. Dulya, Nucl. Instr. & Meth. in Phys. Res., A356, 88 (2004).
[8] K. Kovacs, As in [6].
[9] D. G. Crabb and W. Meyer, Ann. Rev. Nucl. Part. Sci.,47, 67 (1997).
[10] P. M. McKee, Nucl. Instr. & Meth. in Phys. Res. A526, 60 (2004).
[11] K. Slifer, as in [6]
[12] V. Bouffard et al., Rev. Phys. Appl. 13, 304 (1978).
[13] O. A. Rondon, Phys. Rev., C60, 35201 (1999).
[14] S. Trentalange et al., Proc. 9th Int. Symp. on High Energy Spin Phys., Bonn 1990, Springer Verlag, 1991, eds Meyer, Steffens, Thiel, Vol. 2. p.325.
[15] S. T. Goertz et al., Nucl. Instr. & Meth. in Phys. Res., A526, 43 (2004).
[16] J. Wolber, et al., Nucl. Instr.& Meth. in Phys. Res., A526,173 (2004).
[17] X. Wei, As in [6].
[18] T. Wakui, Proc. 11th Int. Workshop on Polarized Sources and Targets (PST05), Tokyo 2005, World Scientific.
[19] J. Zhao, As in [6].

NONLINEAR MAGNETIC PHENOMENA IN HIGHLY POLARIZED TARGET MATERIALS

Yu.F. Kiselev[1†] and W. Meyer[2]

(1) *CERN CH-1211, Geneve 23, Suisse/Switzerland*
† *E-mail: Yury.kiselev@cern.ch*
(2) *Physics Department, University of Bochum, 44780 Bochum, Germany.*

(On behalf of COMPASS Collaboration)

Abstract

The report introduces and surveys nonlinear magnetic phenomena which have been observed at high nuclear polarizations in polarized targets of the SMC and of the COMPASS collaborations at CERN. Some of these phenomena, namely the frequency modulation effect and the distortion of the NMR line shape, promote the development of the polarized target technique. Others, as the spin-spin cross-relaxation between spin subsystems can be used for the development of quantum statistical physics. New findings bear on an electromagnetic noise and the spectrally resolved radiation from LiD with negatively polarized nuclei detected by low temperature bolometers. These nonlinear phenomena need to be taken into account for achieving the ultimate polarizations.

1. Frequency Modulation effect (FM).

A strong increase of polarization by a dramatic factor of 1.7 due to frequency modulation (FM) was discovered in D-butanol doped with paramagnetic Cr(V) complex which was the material used in the large 1.5 l target of the SMC-collaboration at CERN [1, 2]. FM is regularly used for the achievement of the highest polarizations. Dynamic nuclear polarization (DNP) is obtained by microwave (MW) saturation of the electron paramagnetic resonance (EPR) line of the dopant diluted in the target material. The efficiency of the method depends on intensity and spatial uniformity of MW field in a target cavity. At 2.5 T field the typical MW wavelength of $\lambda \approx 4$ mm is smaller than the target dimensions and the cavity field exhibits a standing wave structure. Polarization will be higher in the domains having larger paramagnetic absorptions in comparison to those in which there are the maxima of dielectric losses (so-called hot spots). To equalize a spatial saturation, the field maxima should be spread out over the material volume for a short enough time interval.

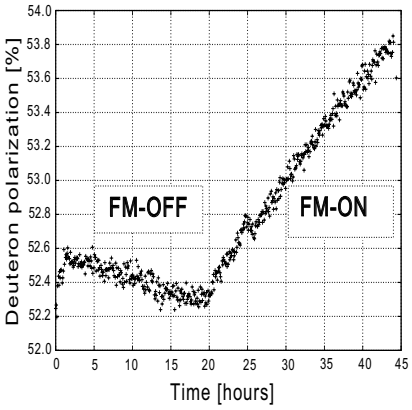

Figure 1. DNP-process in LiD over time with and without FM.

The novelty of FM-invention consists in the mechanism of MW field displacement by sweeping over the modes, in other words, by multi-mode excitation of the cavity [3]. For this, the carrier MW frequency is slightly modulated with an external modulation of about

20 MHz width. It was shown [3] that if the cavity design enables 3 to 4 non degenerate modes per 20 MHz frequency band, then FM provides a good spatial uniformity of the field as required for the highest polarizations. Following this way one can enlarge the fraction of the nonlinear (with respect to the input power) resonant magnetic losses in comparison with linear dielectric losses. Fig. 1 shows FM-action in case of the COMPASS LiD-target. Polarization went down when switching-off FM and it was growing up to ultimate values when restarting FM.

2. Line shape asymmetry.

The NMR line shape of polarized nuclei usually reveals an asymmetry which contains useful information about the status of the spin system. Fig. 2a shows the spectra of highly polarized deuterons ($S = 1$) in D-propanediol and D-butanol obtained at Bochum University [4]. Deuteron asymmetry of these spectra arises due to an interaction between the nuclear quadrupole moments and the electrical field gradient in the lattice. This interaction contributes to a quadratic term in the sublevel energies.

In an amorphous solid material, the energy of $S = 1$ spin system in a magnetic field can be introduced as [5]

$$E_m = E_0 - E_1 m + E_2(\theta) m^2 \,, \tag{1}$$

where m is magnetic quantum number, E_0 - doesn't depends on the spin, $E_1 = h\nu_D$ is the Zeeman energy and $E_2(\theta) = 3h\nu_q(3\cos^2\theta - 1)$ is the quadrupole energy, dependent on the angular distribution of the molecules about the magnetic field. In practice, the signal asymmetry R is handy to express in terms of relative populations p_m $(m = +1, 0, -1)$

$$R = \frac{p_+}{p_0} = \frac{p_0}{p_-} = \frac{p_+ - p_0}{p_0 - p_-} \,. \tag{2}$$

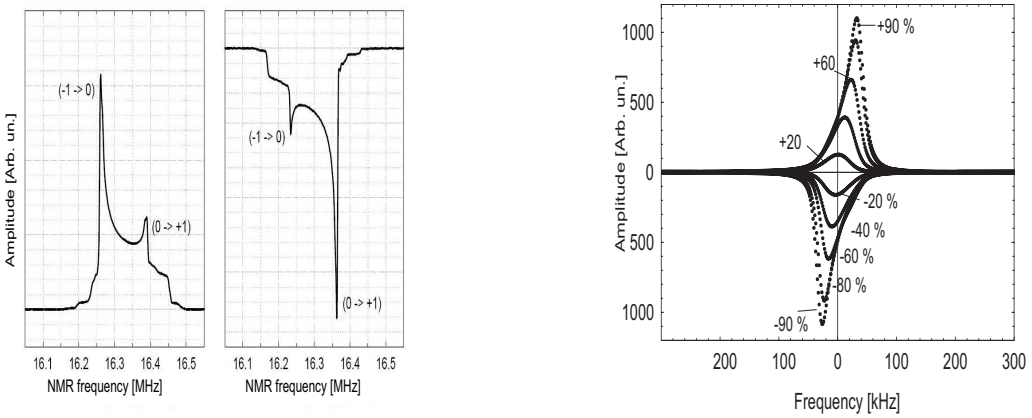

(a) **(b)**

Figure 2a. NMR-signals of D-propanediol (left) and D-butanol (right) with record polarizations of -81 % and +80 %, respectively [4]

Figure 2b. Proton spectra in NH_3 with different polarizations from -90 % to +90 % [8].

Using Eqs. 1, 2 and Boltzmann distribution for sublevels, we have [5]

$$R(\theta) = \frac{\exp(x-y)-1}{1-\exp-(x+y)}\ ,\quad x = \frac{E_1}{kT}\ ,\quad y = \frac{E_2(\theta)}{kT}\ . \tag{3}$$

where kT is the Boltzmann factor, E_2 gives nonequidistant splitting of sublevels. Let us estimate the quadrupole effects for spectra in Fig. 2a. Their maxima are situated at $\theta = \pi/2$, then Eqs. 1 yields $E_2(\theta = \pi/2)/E_1 = -3\nu_q/\nu_D$ and a signal asymmetry at low polarization ($T \to \infty$) equals to

$$\lim_{T\to\infty} R(\theta) = \frac{1 - E_2(\theta = \pi/2)/E_1}{1 + E_2(\theta = \pi/2)/E_1} = \frac{1 + 3\nu_q/\nu_D}{1 - 3\nu_q/\nu_D}\ . \tag{4}$$

The value of $3\nu_q/\nu_D$ is the relative shift of the deuteron peaks about the central Larmor frequency; from Figs. 2a this shift is equal to about 55 kHz/16300 $kHz \cong 3.4 \cdot 10^{-3}$ and Eq. 4 gives unity with accuracy of 0.7 %, therefore $E_2 \cong 0$ in Eq. 1 is a good approximation and a signal asymmetry vanishes at low polarizations. The asymmetry can be calculated by formula [6]

$$R(\theta) = \frac{S_{+1} - S_0/\sqrt{2}}{S_{-1} - S_0/\sqrt{2}}\ , \tag{5}$$

where S_{+1} is the right and S_{-1} is the left peak amplitude of the signals in Figs. 2a; S_0 is the amplitude of the medial point between these peaks. From Fig. 2a (left), they are $S_{+1}/S_0 \approx 1.3$, $S_{-1}/S_0 \approx 3.5$ and from Eq. 5 $R \approx 0.59/2.8 = 0.21$; also repeating the same calculations for the spectrum of Fig. 2a (right), we find $R \approx 5.5$. Since $E_2 \approx 0$, from Eqs. 2 it follows the well known formula for the polarization of $S = 1$ spin system [7]

$$P = p_+ - p_- = \frac{R^2 - 1}{R^2 + R + 1}\ , \tag{6}$$

which gives of -77 % and +78 % polarizations, as compared with more precise "area method" measurements of -81 % and +80 % in Figs. 2a (left) and 2b (right), respectively.

In contrast with the previous consideration, ^{14}N spins (S=1) in the ammonia exhibit a broadened NMR-spectra ($3\nu_q/\nu$=1.23 MHz/6.47 MHz=0.19) at 2.1 T, $S_0 \approx 0$ [8] and $R = 1.46$ for the limit in Eq. 4. In this case the quadrupole interaction will bring along a strong line shape asymmetry even at the lowest nitrogen polarizations .

Fig. 2b shows another example of asymmetry of the proton spectra in ammonia (NH_3) parametrized over polarization [8]. One can see again a strong line shape asymmetry increasing with polarization. Our preliminary analysis allows to conclude that the asymmetrical part of these spectra vary linearly with polarization. If further studies confirm this finding then the proton polarization in ammonia could also be determined by the signal asymmetry along with the routine "area method".

3. Spin-Spin Cross-Relaxation.

DNP in ammonia at 2.5 T and about 0.1 K allows to reach polarizations of about 14 % and 90 % of ^{14}N and ^{1}H spins, respectively. As stated above, the nitrogen spins ($S = 1$) have a strong quadrupole interaction with the lattice field. Unlike ^{14}N nuclei, the energy of the half-integral ^{1}H spins depends only on the magnetic field, so that, by ramping

down the field from 2.5 T to about 0.056 T [8], one can equalize resonant frequencies of both species. At such a field, flip-flop interactions conserve the total energy, allowing an effective cross-relaxation between subsystems. We estimate cross-relaxation time as $\tau = W^{-1}$, where W is an approximate rate of cross-polarization [9]

$$\tau = W^{-1} \approx T_2(\frac{\gamma_H}{\gamma_N})^2 \cosh(\xi \frac{\Delta_0}{\Delta_H}) \ . \tag{7}$$

Here $T_2 \approx 10^{-5}$ s is the transverse relaxation time of proton spins, $\Delta_H \approx 0.05$ MHz is the proton NMR line width, $\gamma_H/\gamma_N = 13.8$ is the ratio of gyromagnetic constants, $\xi \approx 1$ is a free parameter and Δ_0 is the frequency detuning between ^{14}N and ^1H spins. One can see from Eq. 7 that for small detuning of $\Delta_0 \approx \Delta_H$ τ is of the order of $T_2(\gamma_H/\gamma_N)^2 \approx 2 \cdot 10^{-3}$ s. In the case of broaden ^{14}N-spectral line, the detuning range is also broadened out within interval of $\Delta_H \approx 0.05$ MHz $< \Delta_0 < 3\nu_q \approx 1.23$ MHz. As a consequence, τ in Eq. 7 can vary from milliseconds to hundreds of seconds depending on the field setting. Studies done at CERN [8] confirm this conclusion. Different cross-relaxation tests allowed to gain the vector polarization of ^{14}N up to 40 % or they destroyed the equilibrium spin distribution. Cross-relaxation can be suppressed by replacing ^{14}N by the ^{15}N isotope. This isotope has spin $S = 1/2$ and $\gamma_H/\gamma_{15N} \approx 9.9$ with no quadrupole effects. In this case the cross coupling effects will vanish at a field larger than 0.05 T.

4. Self-induced spin spectroscopy.

NMR and EPR spectra are usually studying a response of a spin system to an external field excitation within their Larmor frequency [10]. Here, we consider the self-induced spectroscopy of negatively polarized, better saying, active spins without exciting field.

Fig. 3a shows an equivalent resonant circuit coupled with active spin media situated inside the coil which axis is perpendicularly directed about the field (B_0). In this circuit the coil resistance (r) is counterbalanced by the sample energy so that $r = -\eta\omega\chi'' L_0$ and the coil reactive impedance equals to

$$Z = r + j\omega L_0(1 + \eta(\chi' - j\chi'')) = j\omega L_0(1 + \eta\chi'(\omega)) \ , \tag{8}$$

where $j = \sqrt{-1}$, η, r, L_0, $\omega = 2\pi\nu$, $\chi' - j\chi''$ are the coil filling factor, resistance, inductance, the circuit resonant frequency and a sample susceptibility, respectively.

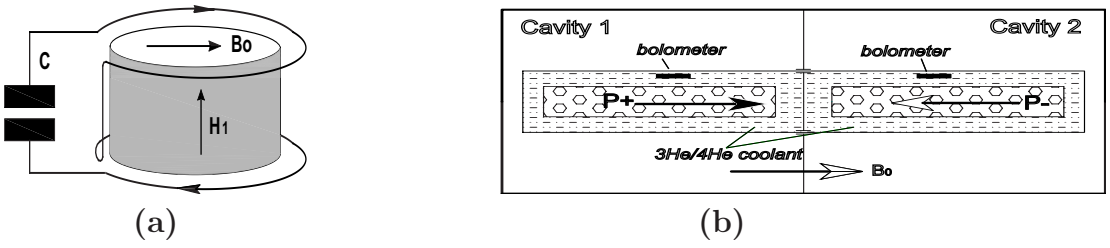

(a) (b)

Figure 3a. A circuit coupled with the active media looses a resistance and it acts as a transformer of any external flux deviations into ringing resonant current, generating H_1-field.
Figure 3b. Twin-cavity with opposite target polarizations. The electromagnetic radiation is detected by the temperature disbalance between bolometers (Speer-220).

For example, in the case of a sample made of frozen ammonia bits with a density of $N \approx 5.4 \cdot 10^{28}$ spin/m^3, the averaged value of $\overline{\chi''} = -\pi\chi_0\nu/2\Delta_H$, where χ_0 is the static magnetization. Eq. 8 holds when coil impedance is less than

$$r = -\eta\{\overline{\chi''}\}\omega L_0 = 0.5 \cdot \{\frac{\pi}{2}\frac{\nu_H}{\Delta_H}\frac{N\mu_0\mu_B}{B_0}\}\omega L_0 = 13\ Ohm\ . \tag{9}$$

Here $\mu_0 = 4\pi \cdot 10^{-7}$ H/m is the permeability of vacuum, $\mu_B = 5.0 \cdot 10^{-27}$ J/T is the nuclear magneton and we assume $\eta \approx 0.5$, $\nu \approx 10^8$ Hz at $B_0 = 2.5$ T, $\Delta_H = 5 \cdot 10^4$ Hz, $L_0 = 10^{-7}$ H and proton polarization of 100 %. Since typical coil resistance of $(1 \div 3)$ Ohm $\ll r$ the lossless (superconducting) circuit will transform any flux deviations through the coil into a ringing current generating H_1-field (see Fig. 3a). In turn, the H_1-flux feedback will change the sample susceptibility and the coil inductance (see Eq. 8), self-tuning of the circuit and the Larmor spin frequencies to a resonance; in full analogy with "pulling effect" in laser technique [12].

One can see that it should exist a particular "self-induced spectroscopy" which operates without an external excitation, with self-tuning to a circuit resonance, with direct indication of electromagnetic radiation using the extra low-noise cryo-bolometers; it is true, on the other hand, that the method can not be realized without an active media.

Our set-up [13] shown in Fig. 3b consists of the two electrically isolated MW cavities with oppositely polarized LiD-material in cells. The two resonance circuits enable radiation: NMR-circuits for polarization measurements and the MW cavity. The studies were performed with LiD at low fields of ≈ 0.1 T, where NMR circuits have not any resonance for Larmor frequencies for all nuclear species, therefore only electron spins can activate the radiation in the microwave cavity. This radiation will unbalance the bolometer temperatures which were measured by the low-frequency cryo-bridges.

The fast electromagnetic energy release, shown in Fig. 4a [11], with $\tau_f \approx 18$ min originated by electron spins coupled through the electron dipole-dipole reservoir [7] with Zeeman reservoir of negatively polarized nuclear species in LiD. It is most probable that

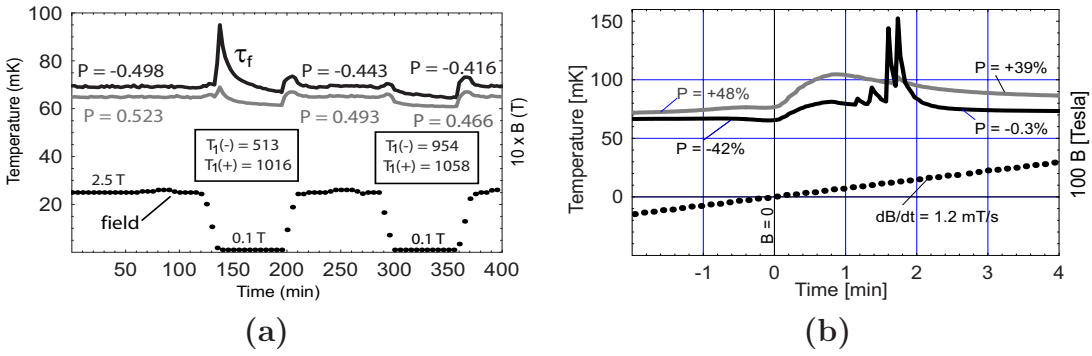

Figure 4a. Bolometer detects a fast release of spin energy with $\tau \approx 18$ min. After the exposure, NMR-reading confirms the different relaxation times $T_1(-) \ll T_1(+)$ (in hours) for opposite polarizations. This effect vanishes at the lower polarization in the second exposure [11].

Figure 4b. Specified spectrum from [11]; the specra-resolved spin-radiation (from the left to right): ^1H (90), ^7Li (101), D (121) and ^6Li (127) mT.

the generation goes in TM_{002} or TM_{022} modes of our cavity having a large radius of 10.5 cm with the low resonant frequencies in region of 2.5÷ 3.5 GHz and a large quality factor of the order of 10^4. Such radiation means that nuclear spins can relax their energy over a broad-band microwave noise due to their dipole-dipole contact with electron spins.

Figure 4b shows the first observation of the spectra-resolved radiation during reversal of B_0-magnetic field [11]. In this case, radiation discloses the individual contributions of nuclear species into the electron dipole-dipole reservoir.

In conclusion, we hope that our observations may provide useful information to a deeper understanding of self-induced processes in polarized spin systems.

Acknowledgment. Authors would like to thank all members of SMC and COMPASS collaborations at CERN who participated in the new studies of spin phenomena in polarized target materials.

References

[1] Yu. Kisselev (On behalf of SMC Collaboration), NIM in Phys. Res., A 356, 99, 1995;

[2] B. Adeva, A. Magnon et al., NIM in Phys. Res., A 372, 339, 1996;

[3] Yu. Kisselev et al., Proc. of the 11th International Workshop on Polarized Sources and Targets, Tokyo, Japan,14-17 Nov., 63, (2005);

[4] S. T. Goertz et al., NIM in Phys. Res., A 526, 43, 2004;

[5] L. I. Lapidus, JINR Preprint, Dubna, **P2-84-267**, 1984.

[6] Yu. Kisselev, S. A. Popov, A. N. Fedorov, Pys'ma Zh. Eksp. Teor. Fiz., **55**, 99 (1992).

[7] W. de Boer, Dynamic Orientation of Nuclei at Low Temperatures, Yellow Report, Geneva. **CERN 74-11**,(1974).

[8] B. Adeva and Ch. Dulya et al., NIM in Phys. Res., A 419, 60, 1998;

[9] F. S. Dzeparov, Zh. Eksp. Theor. Fiz., **99**, 982 (1991); Phys. Part. Nucl., **26**, 692 (1995).

[10] A. Abragam, Principles of Nuclear Magnetism (Clarendon Press. Oxford), **Ch. IV, IX**, (1989).

[11] Yu. Kisselev et al., SPIN-2004: proc. of the 16th Int. Spin Phys. Symp. and Workshop on Polar. Electron Sources and Polarimeters, Trieste, Italy, 10-16 Oct., 816, (2004).

[12] R. H. Pantell, H. E. Puthoff, Fundamentals of Quantum Electronics (Wiley, New York, etc), **Ch.3**, 90, (1969).

[13] J. Ball et al., NIM in Phys. Res., A 498, 101, 2003.

Discussion

Comm. (D.Crabb, Univ. of Virginia) In fact did see an improvement of deuteron polarization with f_n in the UVA target, but not so big an effect (target is much smaller than COMPASS).

A. Finally!

Crabb. It was reported about the same time as SMC.

Kiselev. We can discuss it later.

LAMB SHIFT POLARIMETER FOR A HELIUM-3 ION BEAM

Yu.A. Plis

Joint Institute for Nuclear Research, 141980 Dubna, Moscow region, Russia
E-mail: plis@nusun.jinr.ru

Abstract

The principle of the Lamb shift polarimeter intended for polarization measurement of $^3He^{++}$ ions emerging from the polarized ion source is described. The results of numeric calculations are presented. With use of level crossing at 0.75 T or 1.5 T it seems possible to develop a simple polarimeter of a low energy (10-20 keV) $^3He^{++}$ beam. Also, microwave irradiation at 2.5 T can be used for polarization measurement.

In first experiments with a polarized ^{3}He ion source, the nuclear scattering at rather a high energy was used to measure the polarization of the accelerated beam [1]. It would be very useful to measure the polarization at the ion source extraction energy of 10-20 keV, as it was made for protons or deuterons.

Heberle [2] first proposed to convert a portion of the protons (or deuterons) into metastable hydrogen atoms and to observe the intensity of the Lyman α-quanta after quenching the beam in suitable electric and magnetic fields. This idea was realized in [3,4].

By analogy, the polarization of slow $(10 - 20$ keV) $^3He^{++}$ ions can be measured by converting them into metastable ions $^3He^+(2S)$ in the electron capture process [6]. The method is based on the relation between the nuclear polarization of the primary $^3He^{++}$ ions and the populations of the hyperfine states of the $^3He^+(2S)$ ions, produced in the reaction

$$^3He^{++} + X \rightarrow {}^3He^{+} + X^{+}. \tag{1}$$

between the incident ions and target gas atoms or molecules X (for example, N_2). Subsequent radiative decays of the initial states lead to a mixture of the desired metastable $^3He^+(2S)$ ions and the ground state ions $^3He^+(1S)$.

The cross sections for the charge-transfer processes of this type in He, Ar, Kr, H_2, N_2 and O_2 were measured by Shah and Gilbogy [5] in an energy range of 10-60 keV. At impact energies of 20-30 keV the maximum fractional yield of $^3He^+(2S)$ ions was 2.5%

The populations of the states of the $^3He^+(2S)$, produced in a sudden process of the capture of unpolarized electrons by the $^3He^{++}$ ions with polarization P, are
(1) $\phi^+_{\rm He}\phi^+_{\rm e}$ population $\frac{1+P}{4}$, (2) $\phi^-_{\rm He}\phi^+_{\rm e}$ population $\frac{1-P}{4}$, (3) $\phi^+_{\rm He}\phi^-_{\rm e}$ population $\frac{1+P}{4}$,
(4) $\phi^-_{\rm He}\phi^-_{\rm e}$ population $\frac{1-P}{4}$. These states are not the eigenfunctions of a time-independent Hamiltonian:

$$\hat{H} = -\mu_J \boldsymbol{B}\boldsymbol{\sigma}_{\rm e} - \mu_{\rm He}\boldsymbol{B}\boldsymbol{\sigma}_{\rm He} + \frac{1}{4}\Delta W \boldsymbol{\sigma}_{\rm e}\boldsymbol{\sigma}_{\rm He}. \tag{2}$$

which are $\psi(\mathrm{F}=1,\mathrm{m}=1) = \phi^+_{\rm He}\phi^+_{\rm e}$, $\psi(1,0) = \cos\beta\phi^+_{\rm He}\phi^-_{\rm e} + \sin\beta\phi^-_{\rm He}\phi^+_{\rm e}$, $\psi(1,-1) = \phi^-_{\rm He}\phi^-_{\rm e}$, $\psi(0,0) = \sin\beta\phi^+_{\rm He}\Psi^-_{\rm e} - \cos\beta\phi^-_{\rm He}\phi^+_{\rm e}$. Where

$$\sin\beta = \frac{1}{\sqrt{2}}\left(1 - \frac{x}{\sqrt{1+x^2}}\right)^{1/2},\ \cos\beta = \frac{1}{\sqrt{2}}\left(1 + \frac{x}{\sqrt{1+x^2}}\right)^{1/2}, \tag{3}$$

$$x = \frac{B}{B_c}, \;\; B_c = \frac{|\Delta W|}{-2\mu_J + 2\mu_{\rm He}}. \tag{4}$$

For the ^{3}He($2S_{1/2}$) states $\Delta W = -1.083\,\mathrm{GHz}$, $B_c = 38.6\mathrm{mT}$.

The states (1)–(4) evolve in time:

$$\phi^+_{\rm He}\phi^+_{\rm e} \to \psi(1,1)\exp[-i\omega(1,1)t],$$

$$\phi^-_{\rm He}\phi^+_{\rm e} \to \sin\beta\psi(1,0)\exp[-i\omega(1,0)t] - \cos\beta\psi(0,0)\exp[-i\omega(0,0)t],$$

$$\phi^+_{\rm He}\phi^-_{\rm e} \to \cos\beta\psi(1,0)\exp[-i\omega(1,0)t] + \sin\beta\psi(0,0)\exp[-i\omega(0,0)t],$$

$$\phi^-_{\rm He}\phi^-_{\rm e} \to \psi(1,-1)\exp[-i\omega(1,-1)t],$$

Zeeman effect for $2S_{1/2}$ states gives the following energy values:

$$W(1,1) = -\frac{\Delta W}{4} - \mu_J B - \mu_{\rm He} B, \;\; W(1,0) = -\frac{\Delta W}{4} + \frac{\Delta W}{2}\sqrt{1+x^2},$$

$$W(1,-1) = -\frac{\Delta W}{4} + \mu_J B + \mu_{\rm He} B, \;\; W(0,0) = -\frac{\Delta W}{4} - \frac{\Delta W}{2}\sqrt{1+x^2}.$$

In usual consideration, correct only for high magnetic fields, the populations of the four $2S_{1/2}$ states are considered to be

$$N(1,1) = (1+P)/4, \;\; N(1,-1) = (1-P)/4,$$

$$N(1,0) = \cos^2\beta_0(1+P)/4 + \sin^2\beta_0(1-P)/4 = \frac{1}{4}\left(1 + P\frac{x}{\sqrt{1+x^2}}\right),$$

$$N(0,0) = \sin^2\beta_0(1+P)/4 + \cos^2\beta_0(1-P)/4 = \frac{1}{4}\left(1 - P\frac{x}{\sqrt{1+x^2}}\right).$$

The strict consideration will be given in APPENDIX.

In the absence of any fields $\tau_{2S} = 2 \times 10^{-3}$ sec. The presence of an electric field shortens the lifetime of the metastable state of the Stark effect, which produces a mixing of the $2S_{1/2}$ and $2P_{1/2}$ states and a fast decay of the 2S state to the ground 1S state, $\tau_{2P} = 10^{-10}$ sec.

According to Lamb and Skinner [7]:

$$\tau_{2S} = \tau_{2P}\left(\frac{\hbar^2(\omega^2 + \gamma^2/4)}{|V|^2}\right), \tag{5}$$

where $\hbar\omega$ is the energy difference between the levels involved in the transition, $\gamma = 1/\tau_{2P}$ ($\gamma/2\pi = 16$ GHz), $|V| = \int < \varphi_b|e\boldsymbol{E}\boldsymbol{r}|\varphi_a > \mathrm{d}\boldsymbol{r}$ is the electric dipole matrix element.

If an electric field is perpendicular to B, the allowed mixings: $\Delta m_J = \pm 1$, that is, $\alpha - f$ and $\beta - e$, if E parallel to B, $\Delta m_J = 0$, the allowed transitions are $\alpha - e$ and $\beta - f$. The labels for the levels follow the usage of Lamb and Retherford [8]: $\alpha - 2S_{1/2}(m_J = +1/2), \beta - 2S_{1/2}(m_J = -1/2), e - 2P_{1/2}(m_J = +1/2), f - 2P_{1/2}(m_J = -1/2)$. The matrix element equals

$$|V| = \frac{\sqrt{3}}{2}a_0\epsilon E\cos\omega t \approx 2.2 \times 10^{-18} E\cos\omega t, \tag{6}$$

where $a_0 = 0.529 \times 10^{-8}$ cm, $\epsilon \simeq 1$, ω – angular frequency of an oscillating electric field, equals zero for a static field, E (units of CGSE).

Populations of the α states:

$$N(\alpha) = N(1,1) + N(0,0) = \frac{1}{2}\left[1 + \frac{P}{2}\left(1 - \frac{x}{\sqrt{1+x^2}}\right)\right], \tag{7}$$

where I_0 is zero polarization, I_+ – polarized beam, I_- – reversed polarization.

$$P = \frac{2}{1 - x/\sqrt{1+x^2}}\left(\frac{I_+}{I_0} - 1\right). \tag{8}$$

$$P = \frac{2}{1 - x/\sqrt{1+x^2}}\left(\frac{I_+ - I_-}{I_+ + I_-}\right). \tag{9}$$

At the level crossing

$$\tau_{\rm S} = \tau_{\rm P}\frac{\hbar^2\gamma^2}{4|V|^2}. \tag{10}$$

First level crossing $(\beta - e)$ takes place at $B \approx 0.75$ T. In this case, the static electric field E should be perpendicular to the magnetic field B,

$\tau_\beta = 5.4 \times 10^{-5}/E^2$ s, E (V/cm), $\tau_\alpha = 6.8 \times 10^{-2}/E^2$ s, ratio equals 1380.

Let a beam of metastable helium ions pass through a magnetic field (length L) corresponding the level crossing and in a rather weak electric field, so chosen that only small quantity of the ions in the α state decays, while practically all the ions in the β state are quenched to the ground state.

In numeric calculations the magnetic field along the axis was accepted as linearly increasing up to maximum value at the length of 50 cm, hyperfine splitting of the states has been accounted. Electric dipole matrix elements have been taken from [9].

At $W = 20$ keV, $L = 3.4$ cm, $E = 90$ V/cm, 0.4% of the ions in the α state and 99% of the ions in the β state are quenched.

Second crossing $(\beta - f)$ is at $B \approx 1.5$ T. Here E should be parallel B,

At $W = 20$ keV, $L = 1.2$ cm, $E = 150$ V/cm, $U = EL = 180$ V, the result is approximately the same.

Another possibility is to detect the atoms in α state using microwave quenching ($\nu = 9.35$ GHz, $\lambda = 3.2$ cm) of β states at a relatively weak magnetic field 0.25 T [10].

In this case for $E_{\rm ampl.} = 300$ V/cm at $\nu = 9.35$ GHz at $L = 1.2$ cm, 3% of the ions in the α state and 97% of the ions in the β state are quenched.

For final quenching (and measurement) of the atoms in the α state with transverse electric field E with $B = 0$, accepting $W = 20$ keV, $L = 3.4$ cm, $E = 90$ V/cm, 99% of the atoms in the α state are quenched.

Detecting 40.8 eV photons, we can measure nuclear polarization [11].

APPENDIX

The exact wave function of the Schroedinger equation

$$i\hbar\frac{\partial\Psi}{\partial t} = (\hat{H} + \hat{H}')\Psi,$$

where $\hat{H}$ is a time-independent Hamiltonian ($\hat{H}u_n = E_n u_n$), is written in the form

$$\Psi = \sum a_n(t)u_n {\rm e}^{\frac{-iE_n t}{\hbar}}.$$

The coefficients a_n must satisfy to the equation: $i\hbar\dot{a}_k = \sum V_{kn}a_n e^{i\omega_{kn}t}$, where $\omega_{kn} = (E_k - E_n)/\hbar$, $V_{kn} = \int u_k^* H' u_n \, d\boldsymbol{r}$.

$\Psi(t) = c_1(t)\phi_{\rm He}^+\phi_{\rm e}^+ + c_2(t)\phi_{\rm He}^-\phi_{\rm e}^+ + c_3(t)\phi_{\rm He}^+\phi_{\rm e}^- + c_4(t)\phi_{\rm He}^-\phi_{\rm e}^-$.

Initial $\phi_{\rm He}^+\phi_{\rm e}^-$ evolves as $\cos\beta_0\psi(1,0)\exp[-i\omega(1,0)t] + \sin\beta_0\psi(0,0)\exp[-i\omega(0,0)t] \to [\cos\beta_0\cos\beta_1 + \sin\beta_0\sin\beta_1\exp(i\theta)]\phi_{\rm He}^+\phi_{\rm e}^- + [\cos\beta_0\sin\beta_1 - \sin\beta_0\cos\beta_1\exp(i\theta)]\phi_{\rm He}^-\phi_{\rm e}^+$.

After averaging: $|c_2(t)|^2 = \cos^2\beta_0\sin^2\beta_1(t) + \sin^2\beta_0\cos^2\beta_1(t)$,
$|c_3(t)|^2 = \cos^2\beta_0\cos^2\beta_1(t) + \sin^2\beta_0\sin^2\beta_1(t)$.

Initial $\phi_{\rm He}^-\phi_{\rm e}^+$ evolves as $\sin\beta_0\psi(1,0)\exp[-i\omega(1,0)t] - \cos\beta_0\psi(0,0)\exp[-i\omega(0,0)t] \to [\sin\beta_0\cos\beta_1 - \cos\beta_0\sin\beta_1\exp(i\vartheta)]\phi_{\rm He}^+\phi_{\rm e}^- + [\sin\beta_0\sin\beta_1 + \cos\beta_0\cos\beta_1\exp(i\vartheta)]\phi_{\rm He}^-\phi_{\rm e}^+$.

After averaging: $|c_2'|^2 = \cos^2\beta_0\cos^2\beta_1(t) + \sin^2\beta_0\sin^2\beta_1(t)$,
$|c_3'|^2 = \cos^2\beta_0\sin^2\beta_1(t) + (\sin^2\beta_0\cos^2\beta_1(t)$.

If $x \gg 1$, $\sin\beta_1 \to 0$, $\cos\beta_1 \to 1$,
$\phi_{\rm He}^+\phi_{\rm e}^- \to \cos\beta_0\phi_{\rm He}^+\phi_{\rm e}^- - \sin\beta_0\exp(i\theta)\phi_{\rm He}^-\phi_{\rm e}^+$
$\phi_{\rm He}^-\phi_{\rm e}^+ \to \sin\beta_0\phi_{\rm He}^+\phi_{\rm e}^- + \cos\beta_0\exp(i\vartheta)\phi_{\rm He}^-\phi_{\rm e}^+$.

$N(\alpha) = \frac{1+P}{4} + \frac{1+P}{4}|c_2|^2 + \frac{1-P}{4}|c_2'|^2 = \frac{1}{2} + \frac{P}{4}[1 + \cos^2\beta_0\sin^2\beta_1(t) + \sin^2\beta_0\cos^2\beta_1(t) - \cos^2\beta_0\cos^2\beta_1(t) - \sin^2\beta_0\sin^2\beta_1(t)] \to \frac{1}{2} + \frac{P}{4}(1 + \sin^2\beta_0 - \cos^2\beta_0) = \frac{1}{2}\left[1 + \frac{P}{2}\left(1 - \frac{x}{\sqrt{1+x^2}}\right)\right]$.

References

[1] S.D. Baker et al., Phys. Rev. Lett. **20** (1968) 738.

[2] J. Heberle, Helv. Phys. Acta Suppl. **6** (1960) 140.

[3] Yu.A. Plis and L.M. Soroko, Nucl. Instr. & Meth. **135** (1976) 497.

[4] A.S. Belov et al., Nucl. Instr. & Meth. **A 255** (1987) 442.

[5] M.B. Shah and H.B. Gilbody, J. Phys. B **7** (1974) 256.

[6] Yu.A. Plis, Proc. of the 13th International Symposium on High Energy Spin Physics, SPIN1998, World Scientific, 547.

[7] W.E. Lamb, Jr. and M. Skinner, Phys. Rev. **78** (1950) 539.

[8] W.E. Lamb, Jr. and R.C. Retherford, Phys. Rev. **79** (1950) 549.

[9] G.G. Ohlsen, J.L. McKibben, LA-3725, 1967.

[10] W.E. Burcham et al., Nucl. Instr. & Meth. **116** (1974) 1.

[11] M.F.A. Harrison et al., Rev. Sci. Instr. **36** (1965) 1443.

PHYSICAL PROGRAMM AND ACCELERATION OF POLARIZED LIGHT NUCLEI BEAMS AT JINR NUCLOTRON

S. Vokal[1],A.D. Kovalenko[1],A.M. Kondratenko[2],M.A. Kondratenko[2],V.A. Mikhailov[1], Yu.N. Filatov[1] and S.S. Shimanskiy[1†]

(1) *JINR, Dubna, Russia* , (2) *TPO "Zaryad", Novosibirsk, Russia*
† *E-mail: shimanskiy@jinr.ru*

Abstract

The physical spin program at high p_T region and energies $s_{NN}^{1/2} \sim 10\ GeV$ is discussed. It's shown that cumulative processes, color transparency problem and polarization phenomenons directly connect with properties new form of the nuclear matter as Color Quark Condensate(CQC). Studies of CQC one of the most important physical problem and can be realized using polarized ion beams at JINR nuclotron-M (and in future at NICA). The calculations of spin resonance strengthes in the linear approximation for p, d, t and ^3He beams in the JINR nuclotron are presented. The methods to preserve the degree of polarization during crossing the spin resonances are examined. The method of matching the direction of polarization vector during the beam injection in to the ring of the nuclotron is given. These methods of spin resonance crossing can be used to accelerate polarized beams in the other cyclic accelerators.

In the recent decades occurred the radical revision our understanding of forms of the nuclear matter which can be realized at different temperatures and densities [1]. Nowadays it is predicted that at low temperatures and high densities the nuclear matter is formed completely the new form, in which the dominant role play the constituent quarks. This state can be named as a Quark Color Condensate (QCC). The properties of this form of nuclear matter determine the physical properties of matter in the center of massive stars and, possibly, it is directly connected with the riddles of the explosions of supernovas. The discovered enormous magnetic fields in stars (up to $\sim\ 10^{17}$ T) can lead to the fact that the Quark Color Condensate (QCC) will be polarized. Therefore the polarization characteristics of super-dense nuclear matter not only are interesting by themselves, but they have important significance to developing the theory of evolution of massive stars.

Is it possible to obtain nuclear matter at the high densities and low temperatures in a laboratory? Studies of cumulative (subthreshold) processes have shown that we observe the processes, in which nuclear matter exist at low temperatures and densities which exceed the ordinary nuclear (hadron) density up to ten times [2]. The density three times greater then ordinary density was observed in the processes of the deep inelastic scattering (DIS) of electrons on the nuclei in JLAB [3]. Studies of cumulative processes and DIS processes have shown that the high density state with a certain probability exists in the ordinary nuclei (the fact that it is not the product of compression during the collision was shown by study of the special features of cumulative processes and lepton DIS processes at x up to 3, because lepton cannot compress the nuclear matter).

It means that in the nuclear matter exist nucleon clusters (Blokhintsev had named its as fluctons) with the density several times higher than usual and there is no energy gap for

the transition to the QCC phase. Most likely in the region at low temperature and high density for the nuclear matter there is not first-order transition. If we take additionally in to account the absence of the first-order transition in the region of high temperatures it can be considered as the indication for the nuclear matter generally there are not regions of the first-order transition. This is a picture of the phase transition of nuclear matter which was popular in the 90's years of the last century [1].

The high p_T processes (region of $x_T \sim 1$) deal with the high density of the nuclear (hadron) matter too. The color transparency (CT) (observed for the first time in 1988) [4] and elastic $p-p$ cross-sections in the singlet and triplet spin states at angles 90^o_{cm} (middle of 70th) [5] may be the most interesting phenomenons.

The cumulative processes and processes with high p_T in the range of energies up to $\sqrt{s_{NN}} \sim 10\ GeV$ is possible to describe well using phenomenological approaches based on the constituent picture only not polarization characteristics. However till now we can say that there are not complete understanding ("microscopic" models) of the nature of discovered effects. Especially difficultly to explain the nature of polarization effects. It means that there are very poor understanding of properties of the nuclear matter at high densities and low temperatures. Very important properties all these phenomenons that its not vanish at high energy region. Moreover some features very close to new phenomenons. Let us compare CT data [4] with data from RHIC for the so-called "jet quenching" effect (Figure 1). We can see very close shape of the CT data and the RHIC data. That's why we can say that the nature of high p_T suppression at RHIC directly connect with the nature of CT phenomena.

Before we have said that the cumulative effects and high p_T effects have been discovered in the energy range up to $\sqrt{s_{NN}} \sim 10\ GeV$. JINR nuclotron is the accelerator of relativistic nuclei which works and continues to be improved in the V.I. Veksler and A.M. Baldin Laboratory of high energies(LHE). The accelerator uses the magnets with superconductor coils developed in LHE and has been created to work with proton beams up to energy 12 GeV and nuclei up to 6 $AGeV$. In JINR is discussing plan to built new collider NICA with maximal energy $\sqrt{s_{NN}} = 9\ GeV$. The first stage to NICA project will be upgrade of the nuclotron to the nuclotron-M. Polarized light ion beams will be important part of this new project. With polarized ion beams we will have real possibility to resolve many problems connected with CQC properties there are:

- resolve the "spin crisis" of 70Ts using complete set polarized states $(p\uparrow - p\uparrow, p\uparrow - n\uparrow, n\uparrow - n\uparrow, ...)$;
- understand the nature of color transparency phenomenon $(p\uparrow - A, p\uparrow - {}^3He(d)\uparrow)$;
- understand the nature of cumulative(subthreshold) particle production;
- the first time study the properties of polarized nuclear matter $(d\uparrow - d\uparrow, {}^3He\uparrow - {}^3He\ \uparrow)$.

As the first step to realize this programm we will need to know details of the spin dynamic in the nuclotron-M.

Complete description of spin dynamic in circular accelerators can be realized using concept of a periodic precession axis $\boldsymbol{n}(\theta)$, which is periodical function of generalized azimuth θ: $\boldsymbol{n}(\theta) = \boldsymbol{n}(\theta + 2\pi)$ [6, 7].

Spin motion on the equilibrium orbit is a precession around the axis $\boldsymbol{n}$: the spin projection $J = \boldsymbol{s}\,\boldsymbol{n}$ on the axis $\boldsymbol{n}$ will be conserved and a transversal projection to $\boldsymbol{n}$ is turn to the angle $\Psi = 2\pi\nu$. Spin frequency ν is shown the turn number of the particle spin during one turn of particle in an accelerator. In traditional accelerator with the transverse master field (nuclotron is the accelerator this type) the precession axis $\boldsymbol{n}$ is parallel to the vertical axis. The spin frequency ν will changing in proportion to the particle energy: $\boldsymbol{n} = \boldsymbol{e}_z$, $\nu = G\gamma$, where γ — the relativistic factor, $G = (g-2)/2$ — anomalous part of the gyromagnetic ratio. Main characteristic to describe the collective spin motion of particle beam is a polarization vector $\boldsymbol{\Pi} = \langle \boldsymbol{s} \rangle = \langle J\boldsymbol{n} \rangle$ and a power of depolarization $D = D = 1 - |\boldsymbol{\Pi}|$. The angular brackets define that we take averaging over particle distribution in the beam.

The motion of particles on non-equilibrium orbits give deviation (spread) of precession axes $\Delta\boldsymbol{n}$ and spread spin frequencies $\Delta\nu$. If we inject beam of polarized particles in to the nuclotron with a spin perpendicular to the precession axis $\boldsymbol{n}$ during the "time" $\theta \sim 1/\Delta\nu$ (for the nuclotron it is a some hundreds tunes) will be full randomization spin directions related to the axis $\boldsymbol{n}$ and polarization will be lost fully. Therefore we need to match the polarization vector of the beam with the direction precession axis $\boldsymbol{n}$ (vector of polarization must be parallel to the axis $\boldsymbol{n}$). The existing channel of transportation have not this coordination. After the ion source the polarization vector is directed to the vertical direction. The vector polarization is not changing direction in the linac. During transportation to the nuclotron the rotation of polarization vector take place in vertical and in horizontal planes. As a result the direction of the vector of polarization will have the angle α_z with vertical axis (see Table 1). The power of depolarization for not correct matchings is

$$D_{inj} = 2\sin^2\frac{\alpha_z}{2}\,.$$

For eliminating this effect will be enough, for example, install the pair of the solenoids at the beginning and the end of the transport channel which do not influence the particle

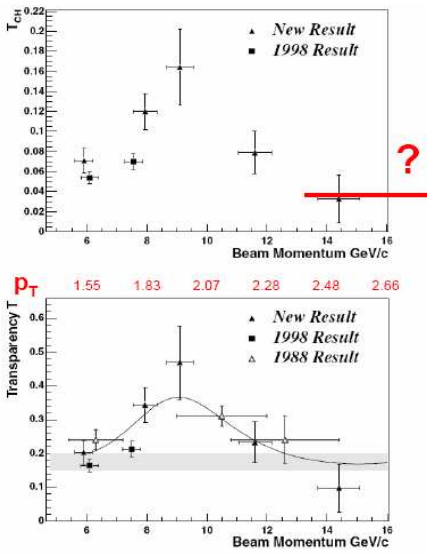

(a)

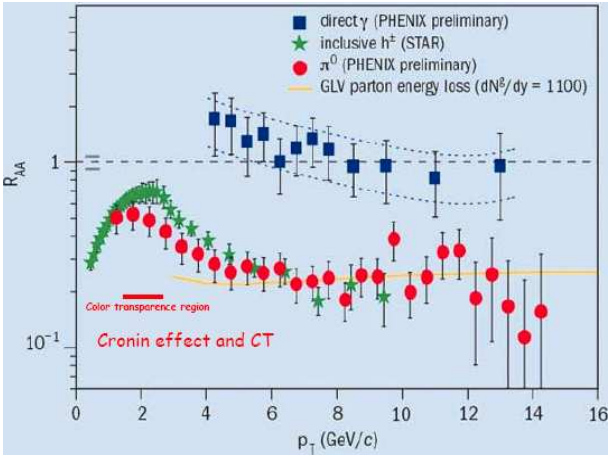

(b)

Figure 1a. The CT data from [4]. **Figure 1b.** RHIC data for "jet quenching" effect.

trajectory and same time will turn polarization vector to the vertical line.

	^1H	^2H	^3H	^3He
α_z, degree	67	9.8	116	79
$D_{\rm inj}$, %	62	1.5	55	81

Table 1: The power of the beam depolarization at some mismatching of polarization during injection in the nuclotron.

Degree of polarization in the process of acceleration can changes in region of the spin resonance, when spin frequency becomes equal to

$$\nu = \nu_k\,, \qquad \nu_k = k + k_z\,\nu_z + k_x\,\nu_x + k_\gamma\,\nu_\gamma\,. \tag{1}$$

where ν_x and ν_z are betatron frequencies, ν_γ is frequency of synchrotron motion. The values of betatron frequencies are equal $\nu_x = 6.8$, $\nu_z = 6.85$ for the Nuclotron.

The most strongest there are resonances of linear approximation, which include intrinsic resonances and resonances of structural imperfections: integer, nonsuperperiodical and the coupling resonances of x and z oscillations.

Intrinsic resonances appear when spin interact with the betatron motion. Remaining resonances are connected with the distortion of the magnetic structure of the rings which are caused by inaccuracies in production and misalignment of the structural elements, with the nonlinear effects of spin and orbital motions, with switching of corrective and functional elements(dipoles, quadrupoles, sextupoles and s.o.).

Table 2 shows the number of linear resonances for different particle beams ^1H, ^2H, ^3H, ^3He in the nuclotron (k and m — integer, $p = 8$ — number of superperiods).

Resonance type	Resonance condition	Number of resonances			
		^1H	^2H	^3H	^3He
Intrinsic resonances	$\nu = k\,p \pm \nu_z$	6	—	8	9
Integer resonances	$\nu = k$	25	1	32	37
Nonsuperperiodical resonances	$\nu = k \pm \nu_z\,(k \neq m\,p)$	44	2	55	64
Coupling resonances	$\nu = k \pm \nu_x$	49	2	63	73

Table 2: Linear resonances in the ring of the nuclotron.

The spin frequency grows proportionally to energy with acceleration of beam and the intersection of spin resonances becomes unavoidable. The basic parameters for crossing the spin resonance are the spin resonance strength w_k, detuning from the resonance $\varepsilon =$

$\nu - \nu_k$ and speed of detuning changing $\varepsilon' = d\varepsilon/d\theta$ (speed of crossing). The spin resonance strength w_k is the corresponding Fourier-harmonic of transverse spin disturbance $\boldsymbol{w}$ and determines the width of dangerous interval in region of the spin resonance.

We can distinguish three possibility to cross the resonance with constant speed there are fast, adiabatic and intermediate crossings. The beam practically completely will be depolarized with the intermediate crossing of resonance ($|w_k|^2 \sim \varepsilon'$).With the fast intersection ($|w_k|^2 \ll \varepsilon'$) the polarization vector $\mathbf{\Pi}$ hasn't time to considerably change and the degree of depolarization is equal to $D \simeq (\pi \langle |w_k|^2 \rangle)/\varepsilon'$. With the slow (adiabatic) crossing when ($|w_k|^2 \gg \varepsilon'$) take place overturn of the polarization vector relative to the vertical direction. In this case should be distinguished the case of "coherent" and "incoherent" crossing. "Coherent" crossing means that the resonance strength is identical for all particles (integer resonances). In this case the condition ($w_k^2 \gg \varepsilon'$) is satisfied for all particles of the beam and degree of polarization after crossing remains with exponential accuracy. With the "incoherent" crossing the resonance strength is different for different particles and, for example, it depends on the amplitude of betatron oscillations (intrinsic resonances). There are not only particles with adiabatic type crossing in the beam, but the intermediate and fast types of crossing, which leads to the partial depolarization of the beam. With the normal distribution of particle coordinates and momentums in the beam the degree of depolarization will be equal: $D \simeq \varepsilon'/(\pi \langle |w_k|^2 \rangle)$. With the adiabatic crossing it is necessary to consider the synchrotron oscillations of the particles, whose accounting can lead to the partial or even complete depolarization.

It is convenient for calculations to introduce new parameter as the characteristic resonance strength $w_d = \sqrt{\varepsilon'/\pi}$. Intersection of the spin resonance lead to practically the complete depolarization of the beam when the resonance strength is equal to w_d. Then the resonance strength, which corresponds to loss by 1% of polarization with the fast crossing, is equal to $0.1\, w_d$, and the resonance strength, which corresponds to loss by 1% of polarization with the adiabatic crossing, is equal to $10\, w_d$ ("incoherent" resonances), $3.26\, w_d$ ("coherent" resonances).

The results of calculation of main characteristics for crossing of the spin resonances and their strengthes are given in Table 3 [8, 9].

	^1H	^2H	^3H	^3He
G	1.793	-0.143	7.92	-4.184
$E_k^{\max}$, [GeV/u]	12.84	6.00	3.74	8.28
$\nu_{min} - \nu_{max}$	1.8 – 26.3	-1.05 – -0.144	7.92 – 39.5	-41.1 – -4.19
ε', ($\tau_{\text{accel}} = 0.5s$)	$7.0 \cdot 10^{-6}$	$2.8 \cdot 10^{-7}$	$1.0 \cdot 10^{-5}$	$1.1 \cdot 10^{-5}$
w_d, ($\tau_{\text{accel}} = 0.5s$)	$1.5 \cdot 10^{-3}$	$3.0 \cdot 10^{-4}$	$1.8 \cdot 10^{-3}$	$1.9 \cdot 10^{-3}$

Table 3: Crossing characteristics of the spin resonances in the nuclotron.

Figures 2-3 show the logarithmic graphs of the resonance strengthes of linear approximation in units of the characteristic strength w_d in the operating range of beam kinetic

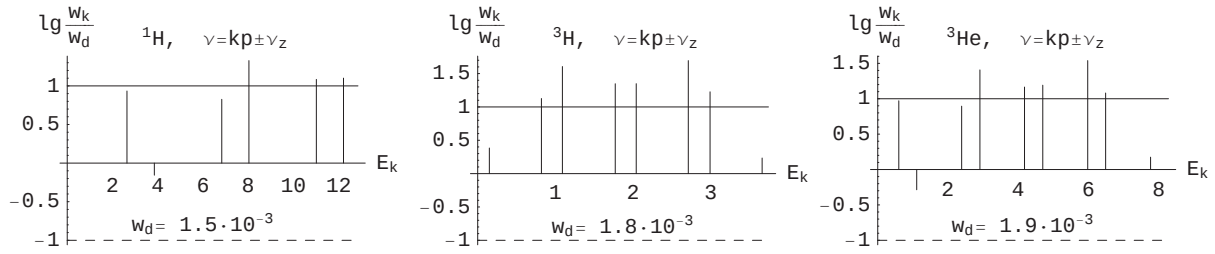

Figure 2: Intrinsic resonances.

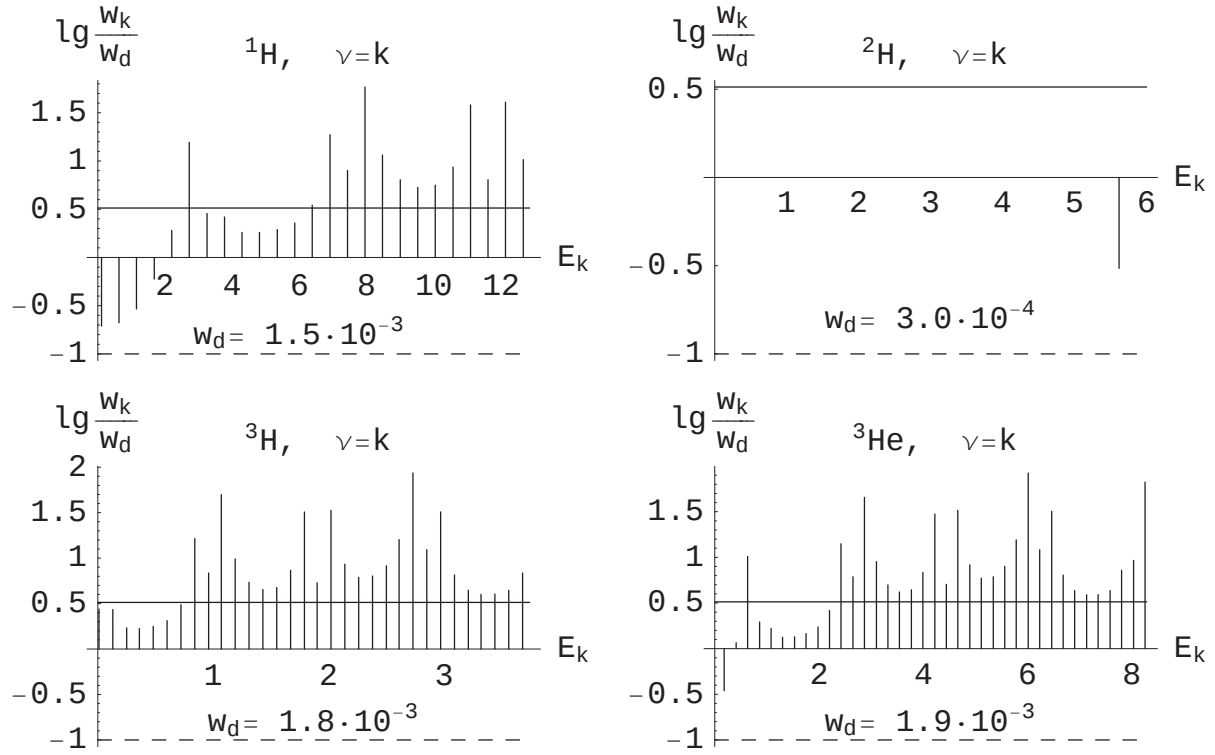

Figure 3: Integer resonances.

energy E_k. Each graph is split into three regions, which correspond to the intermediate crossing (region between the continuous and dotted lines), fast crossing (under the dotted line) and adiabatic crossing (above the solid line). It was assumed in calculation of the resonance strengthes that the emittances in the horizontal and vertical direction at the energy of injection there are equal 45π mm $\cdot$ mrad, adjustment errors of quadrupoles — 0.1 mm and adjustment errors of the turning for main magnets — 0.001 rad.

The resonances located in the zone of intermediate crossing lead to the depolarization of the beam. From the comparison of graphs it follows that almost in full of energy range the depolarization take place for intrinsic and integer resonances (Figure 2-3). The coupling resonances and nonsuperperiodical resonances also can lead to the depolarization of the beam in the same regions of energy where intrinsic resonances are located.

Let us consider methods of crossing of the spin resonances the most suitable for the nuclotron. In crossing of the integer resonances with the intermediate strength ($|w_k|^2 \sim \varepsilon'$) it is expedient to use a method of premeditated increasing of the resonance strength [7].

For this purpose it is enough to insert in free nuclotron gaps some longitudinal magnetic field. The resonance strength with this longitudinal field is determined by expression

$$w_k = \frac{\varphi_y}{2\pi} = \frac{(1+G)H_y L_y}{2\pi H R}$$

and must be correspond to the condition of the adiabatic crossing $|w_k|^2 \gg \varepsilon'$. Furthermore in order to avoid the effects of depolarization because of synchrotron modulation of energy necessary to satisfy also the condition: $|w_k|^2 \gg \sigma\,\nu_\gamma \sim 10^{-2}$, where $\sigma = \nu\sqrt{\langle(\Delta\gamma/\gamma)2\rangle}$ — the amplitude of synchrotron modulation of energy, and ν_γ — the frequency of synchrotron oscillations [9].

The maximal values of integrals of the longitudinal field (on the energy of extraction) which need to guarantee the adiabatic crossing of the integer resonances in full range of the energy are given in Table 4.

	^1H	^2H	^3H	^3He
$(H_y L_y)$, T · m	1	3.4	0.3	0.9

Table 4: The integrals of the longitudinal field for the adiabatic crossing.

When crossing the resonances with the betatron frequencies it is possible to use a method of compensation the degree of depolarization [10]. Conservation of the degree of polarization is ensured due to control of detuning $\varepsilon = \nu - \nu_k$ inside the resonance region. The control of detuning ε during crossing is possible due to changing the spin frequency ν. For this it is necessary to introduce into the ring of nuclotron an "insert" with an additional magnetic field which makes it possible to obtain the required dependence of the spin frequency on a magnetic field $\nu = \nu(\boldsymbol{H})$. There is possible to use the "insert" with the longitudinal and radial fields, depicted in Figure 4, where φ_x, φ_y — angles of spin turns around the radial and the longitudinal fields.

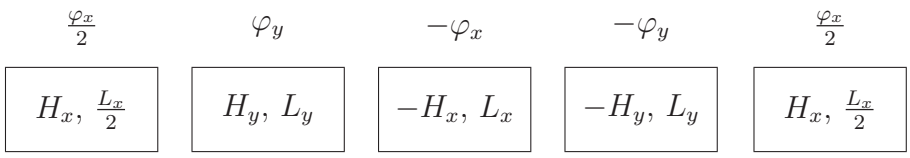

Figure 4: The "insert" to control the spin frequency.

In the approximation of a small spin angular turn ($\varphi_x, \varphi_y \ll 1$) the direction of the equilibrium polarization remains vertical and changing of the precession frequency of the spin is equal to $\Delta\nu = (\varphi_x\varphi_y)/(2\pi)$. The maximal vertical deviation of the equilibrium orbit caused by radial fields will be $\Delta z_{\max} = \varphi_x/(8\nu)(4L_y + 5L_x)$. The maximal length of the "insert" is limited by the length of free space in the accelerator which in the Nuclotron is about 350 cm.

The depolarization of beam is possible during the slow beam extraction from the Nuclotron when the energy of the beam close to energy of the spin resonances. The

degree of depolarization in this case depends on the spin resonance strength w_k and the detuning from the resonance ε. For the completely polarized beam at the beginning power of depolarization will be: $D \simeq \dfrac{\langle w_k^2 \rangle}{2\,\varepsilon^2}$. In this case to avoid depolarization one need move away from the resonance to the value $\Delta\varepsilon \sim 10 w_k\,(\Delta\gamma = \Delta\varepsilon/G)$. For example, for the beam of protons this value will be $\Delta\gamma \simeq 50$MeV for the detuning from the resonance with the strength $w = 10^{-2}$ (adiabatic crossing) and $\Delta\gamma \simeq 5$MeV for the detuning from the resonance with the strength $w = 10^{-3}$ (intermediate crossing).

References

[1] L. McLerran, 2006 European School of High-Energy Physics, Yellow Report CERN 2007-005, 75 (2007).

[2] , S. Shimanskiy, In: Proc. of the VIII International Workshop "Relativistic Nuclear Physics: from Hundreds of MeV to TeV", May 23-28 2005, Dubna, 297 (2006).

[3] K.S. Egiyan et al, Phys. Rev. Lett. **96**, 082501 (2006).

[4] J. Aclander et al, Phys.Rev. C **70**, 015208 (2004).

[5] A.D. Krisch, Eur. Phys. J. A **31**, 417 (2007).

[6] Ya.S. Derbenev, A.M. Kondratenko, A.N. Skrinsky, Sov.Phys.Dokl., **15**, 583 (1970).

[7] Ya.S. Derbenev, A.M. Kondratenko, A.N. Skrinskii, Zh.Eksp.Teor.Fiz.**60** 1216 (1971).

[8] I.B.Issinskii et al., Proc of VI Workshop on High Energy Spin Physics, Protvino, 207 (1996).

[9] N.I. Golubeva et al, Communication of the JINR P9-2002-289, Dubna, 2002

[10] A.M. Kondratenko, M.A. Kondratenko, Yu.N. Filatov, Phys.Part.Nucl.Lett.**1** 266 (2004).

FIRST RESULTS WITH THE HERMES RECOIL DETECTOR

Vilardi Ignazio (on behalf of the HERMES collaboration)[1†]

(1) *University of Bari, Department of Physics, Via Orabona 4, 70126 Bari, Italy*
† *E-mail: Ignazio.Vilardi@ba.infn.it*

Abstract

The HERMES experiment, installed in the 27.5 GeV HERA lepton ring at DESY/Hamburg, is used to study the spin structure of the nucleon. To get information about the orbital angular momentum L_q of quarks, exclusive DIS reactions are investigated. The HERMES Collaboration installed a new Recoil Detector to upgrade the existing spectrometer to improve the study of hard exclusive processes by detecting recoil protons with low momentum. Deeply Virtual Compton Scattering is the main processes to be studied. The HERMES Recoil Detector consists of three subcomponents inside a superconducting magnet that provides a longitudinal superconducting magnetic field of 1 Tesla. From the beam-line, surrounding the target cell inside the HERA e-beam vacuum, going outwards, the Silicon Detector is positioned, followed a by Scintillating Fibre Tracker and a Photon Detector with three tungsten/scintillator layers. The Recoil Detector was installed in January 2006 and commissioning started in February. First results from the detector are presented.

1 Introduction

Generalized Parton Distributions (GPD's) offer a way to unify the previously disjunct pictures of the nucleon given by Parton Distribution Functions on the one hand and nucleon Form Factors on the other. For the first time GPD's may provide detailed information on the localization of partons inside hadrons and access to their orbital angular momentum L_q [1]. GPD's can be accessed experimentally through the measurement of hard exclusive reactions, the cleanest of which is the Deeply Virtual Compton Scattering (DVCS) [2] (Figure 1, left panel). In the reaction $ep \rightarrow e'\gamma p$ at the beam energy of HERMES (27.5 GeV), the Bethe-Heitler process, Figure 1, right panel dominates over DVCS in most of the kinematic region. However, measurable asymmetries in beam spin and beam charge arise from the interference of both processes. The beam spin asymmetry is proportional to the imaginary part of the DVCS amplitude, while the beam charge asymmetry is proportional to the real part of the DVCS amplitude. Both can in turn be expressed in terms of GPD's.

2 The Recoil Detector

The HERMES Recoil Detector [3] has been designed to upgrade the HERMES spectrometer [4] for the measurement of hard exclusive reactions, in particular DVCS. Its objectives are the detection and identification of recoil protons and the rejection of background events, coming mainly from intermediate Δ-production and from semi-inclusive processes. The Recoil Detector is shown in Figure 2: it consists of three active components: a Silicon

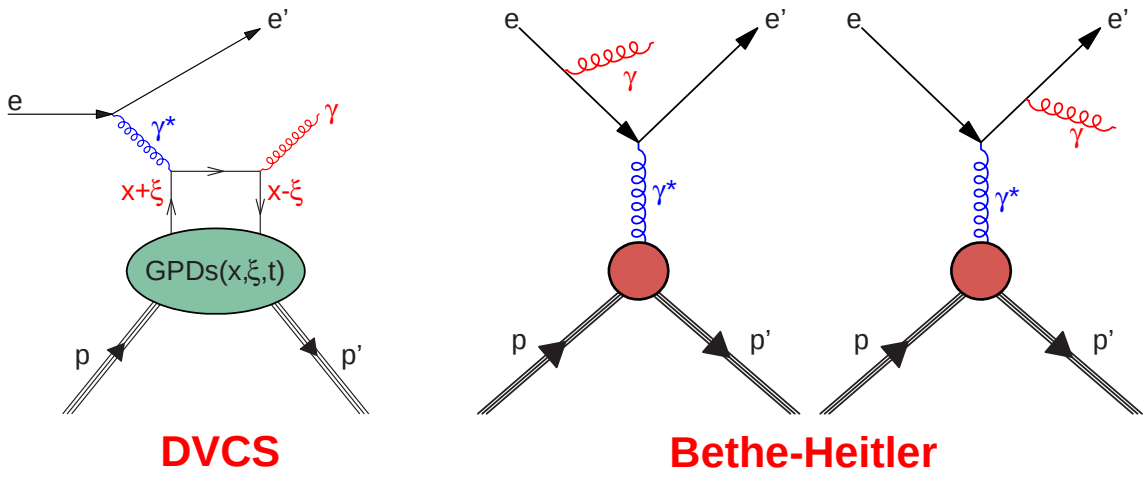

Figure 1: Feynman graphs of DVCS (left panel) and Bethe-Heitler (BH) processes (right panel). Both processes lead to the same final state, thus their amplitudes interfere.

Strip Detector surrounding the target cell inside the beam vacuum, a Scintillating Fibre Tracker and a Photon Detector consisting of three layers of tungsten/scintillator. All three detectors are located inside a superconducting solenoidal magnetic field of 1 Tesla. Together these detectors cover most of the kinematic region for DVCS/Bethe-Heitler events. The technical details of the different subsystems of the Recoil Detector will be described in the next subsections.

2.1 The Silicon Detector

The first sub-detector closest to the beam axis is the Silicon Strip Detector (SSD). The SSD is located inside the scattering chamber within the beam vacuum in order to detect recoil protons with momentum in the range of 135 - 400 MeV/c. The momentum and particle type of the detected particle are determined from the energy deposited in the silicon layers. Due to the very low energy of the recoil protons it is necessary to minimize the amount of material between the interaction point and the detector. Therefore the SSD is mounted inside the HERA ring vacuum in a scattering chamber. For this reason, all of the components and techniques used for the SSD must be vacuum compatible. The SSD consists of 8 modules mounted in two layers symmetrically around the target cell in roof-shaped structures. The main components of the SSD include two TIGRE (The Tracking and Imaging Gamma Ray Experiment) sensors and two readout hybrids with digital control and analog readout circuits. The double-sided silicon TIGRE sensors are from Micron Semiconductors Ltd with a size of 9.9×9.9 cm^2. The active thickness of the sensors is 300 μm. On each side of the sensor there are 128 strips with a 758 μm wide pitch. The necessary momentum dynamic range is established by splitting the signal into a high gain and a low gain path: each strip is read out by one HELIX chip connected directly to the sensor and by a second chip connected via a 10 pF capacitor [5]. The total surface area of the 16 silicon sensors constituting the SSD is 0.16 m^2, resulting in 4096 strips. The strip directions of the p-side and the n-side in one sensor are arranged perpendicularly to each other so that 2-dimensional position information is available.

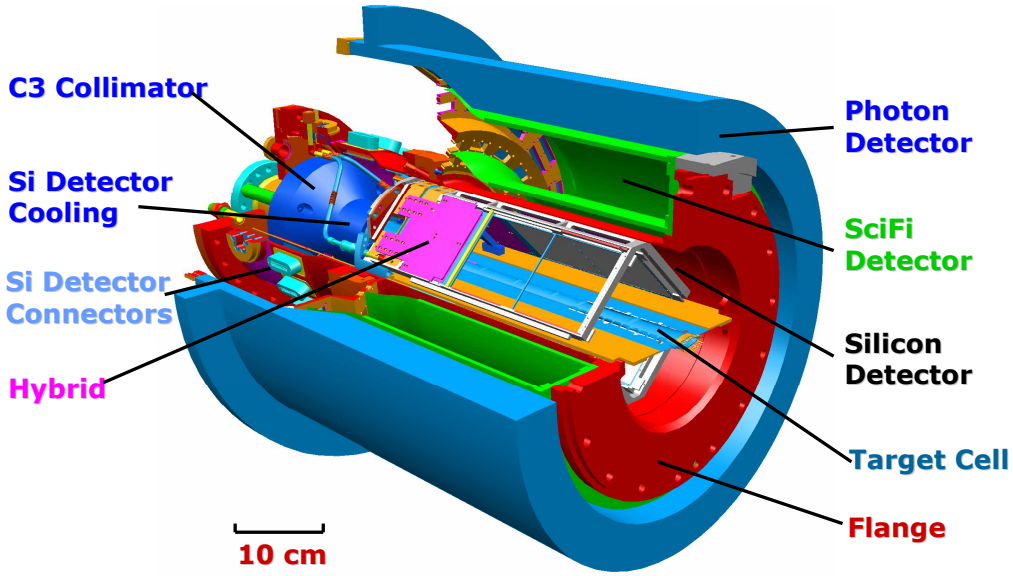

Figure 2: Schematic drawing of the Recoil Detector and its support structure. The electron beam enters from the left side, where an additional collimator protects the Recoil Detector from synchrotron radiation.

2.2 The Scintillating Fibre Tracker

The Scintillating Fibre Tracker (SFT) is the second detector located after the SSD, going from inside. Protons of higher momenta (above 250 MeV/c) which escape the 1.2 thick Aluminium scattering chamber are detected by the SFT. Their momentum is determined by the deflection of their track in the longitudinal magnetic field which also allows the identification of the sign of the charge. The radius of curvature ρ of a particle track in a magnetic field is given by

$$\rho = \frac{p_\perp}{eB} \tag{1}$$

with $p_\perp$ being the transverse momentum with respect to the magnetic field B and e being the particle charge. The SFT consists of two concentric barrels of scintillating fibres. Kuraray SCSF-78M with a diameter of 1 mm were chosen as active material for the SFT. Each SFT barrel in turn consists of two sub-barrels, resulting in 5120 channels in total, but, whereas the inner sub-barrel is oriented parallel to the beam axis, the outer sub-barrel is inclined by 10° in a stereo configuration. This configuration allows the determination of a space point of a particle track for each barrel. The scintillating fibres are connected via 4 m long light guides made of clear fibres to Multi-Anode Photo-Multiplier Tubes.

2.3 The Photo Detector

The outermost sub-detector of the Recoil Detector is the Photon Detector (PD). The PD improves the capability of the Recoil Detector to suppress background by rejecting semi-inclusive events in which a π^0 is produced and events in which an intermediate Δ-resonance is produced. This is achieved by detecting at least one of the photons into which a neutral pion emitted from a Δ-decay subsequently decays. Also, the first layer of the PD improves the pion/proton separation capability of the SFT: a pion rejection factor of ten is expected for momenta up to 800 MeV/c [3]. Finally, the PD provides

a method by which to align the subcomponents of the Recoil Detector by acting as a trigger for cosmic ray events. The PD is constructed from six layers, alternating between a tungsten converter layer from which incident photons and charged particles produce electromagnetic showers, and a scintillator layer which detects these showers. The inner layer is segmented into 60 trapezoidal blocks aligned parallel to the beam axis, the middle and outer layers are segmented into 44 blocks, aligned at +45 and -45 degrees to the beam.

2.4 The Magnet

The Recoil Detector is finally surrounded by a Superconducting (SC) 1 Tesla solenoid magnet. The primary purpose of the Recoil Detector SC magnet is to provide a means for the SFT to measure track momentum by bending charged particle tracks in a 1 T magnetic field. Additionally, the magnet protects the SSD from background electrons emitted from Møller scattering events by constraining these electrons to spiral forward in the magnetic field.

3 First Data

The Recoil Detector was installed in January 2006 and took first data in February. The tracking in the magnetic field using the SFT was possible with the recoil detector superconducting magnet. In March the target cell was damaged while it was being inspected which resulted in large radiation doses to the SSD when the beam was injected. This required rebuilding the SSD in March - June. End of June HERA switched the beam polarity from negative to positive. The data taking was continued with the fully installed Recoil Detector in July 2006 till the 30^{th} of June 2007, last day of HERA running.

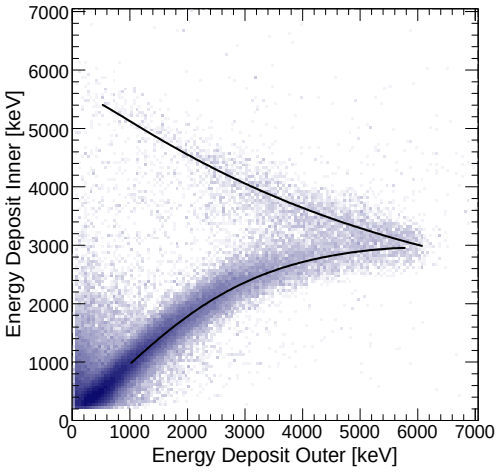

Figure 3: Energy loss in the inner silicon layer versus the energy loss in the outer silicon layer. The black line represents a Monte Carlo prediction.

As a demonstration of the performance of the SSD, Figure 3 shows the energy loss in the inner layer of the SSD versus the energy loss in the outer silicon layer. The black line in the Figure represents a Monte Carlo prediction. The upper line represents protons which punch through the first layer but get stuck in the second and the lower line represents protons which punch through both layers. Figure 4 shows the energy deposits in individual detection layers (SSD on the left and SFT on right) versus the reconstructed particle momentum: from the Figure a well defined proton/π^+ separation can be easily seen (π^- are recognized from their charge). Figure 5 shows a selection of events containing mainly e-p elastic scattering. It shows the azimuthal angle ϕ and the $\sin\theta$ (polar angle) measured by the Recoil Detector for the scattered proton versus the same quantities reconstructed by the spectrometer for the lepton track. An angular resolution of 8 mrad in ϕ is obtained. The gap in the azimuthal angle results from the spectrometer acceptance.

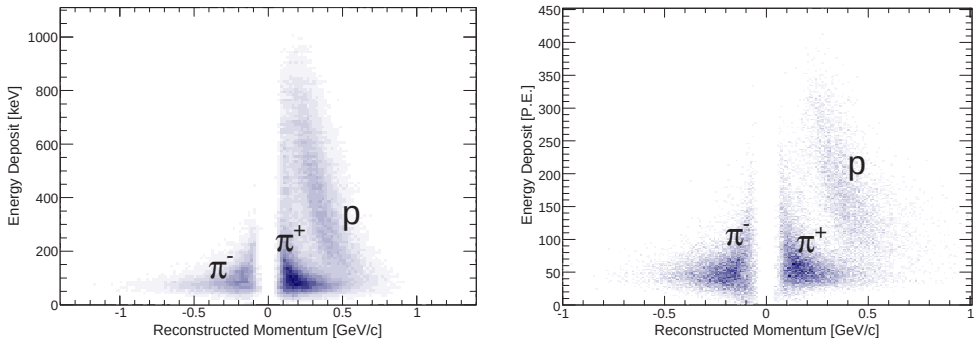

Figure 4: Energy deposits in individual detection layers (SSD on the left and SFT on right) versus the reconstructed particle momentum.

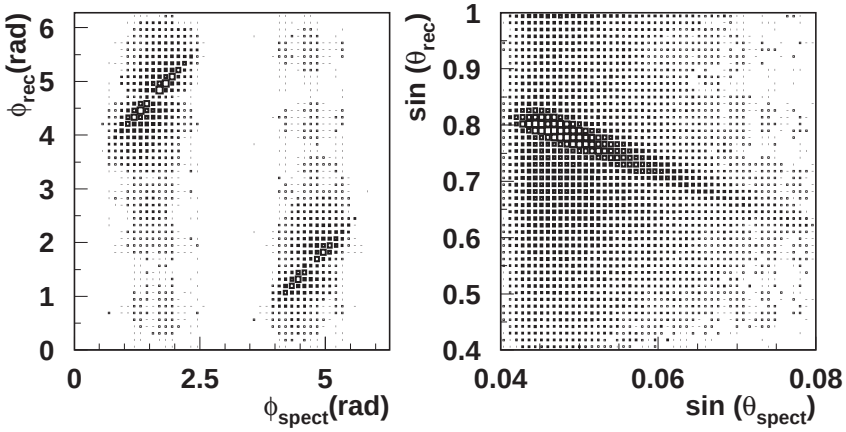

Figure 5: The azimuthal angle ϕ and the $\sin\theta$ (polar angle) measured by the Recoil Detector for the scattered proton versus the same quantities reconstructed by the spectrometer for the lepton track.

Figure 6 shows the sum of energy deposits in the SSD after a missing mass cut ($M_X < 1.7GeV$): it can be easily seen that only protons survive to this cut, as well as a small amount of π^+ coming from the Δ^+-decay. Therefore the Recoil Detector can also be used as a tool to measure background contribution to the previous Hermes DVCS analysis without the Recoil Detector.

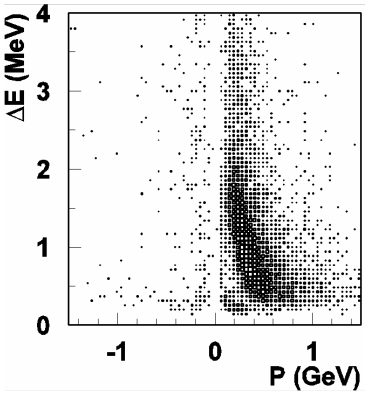

Figure 6: Sum of energy deposits in the SSD after a missing mass cut ($M_X < 1.7$ GeV).

References

[1] X.-D. Ji, Phys. Rev. Lett. **78** (1997) 610

[2] X.-D. Ji, Phys. Rev. **D55** (1997) 7114

[3] B. Seitz, Nucl. Instrum. and Meth. **A535** (2004) 538

[4] K. Ackerstaff et al. (HERMES Collaboration), Nucl. Instrum. and Meth. **A417** (1998) 230

[5] M. Reinecke et al., IEEE Trans. Nucl. Sci. **51** (2004) 1111

Discussion

Q. (N.d'Hose, CEA Saclay) 1. How large will be the statistics for BCA with the RPD?
2. What will be the effect of the absence of Si detector?

A. 1. The statistics collected for BCA with the RPD amount to an integrated luminosity of about $60pb^{-1}$ (electron data): a factor of 5 more data component to the BCA published by HERMES.
2. The absence of Si detector affects BCA (it will be extracted only with the SFT). Moreover the first proton momentum detectable in this period is 250 MeV/c (instead of 135 Mev/c with the full detector): effective measurements of small t.

Q. (J.Nassalski, SINS, Warsaw) 1) There is a systematic shift on your $(Z_{\mathrm{rec}} - 2_{\mathrm{spect}})$ plot. What is the reason?
2) Si was not reacting for part of data. What will be the impact of BCA measurements?

A. 1) The shift is due to the poor resolution of the spectrometer for elastic events and also to the beam position. A small shift equal to 1 mm in beam position can lead to a shift equal to 2 cm in Z calculation.
2) Recoil protons at small $-t$ are not detected as the SSD was not operating. The BCA measurements can be still extract using only SFT data, but it has to be demonstrated.

POLARIZATION BUILDUP BY SPIN FILTERING IN STORAGE RINGS

D. S. O'Brien

School of Mathematics, Trinity College Dublin, Ireland
E-mail: donie@maths.tcd.ie

Abstract

There has been much recent research into polarizing an antiproton beam, instigated by the recent proposal from the PAX (Polarized Antiproton eXperiment) project at GSI Darmstadt [1]. It plans to polarize an antiproton beam by repeated interaction with a polarized internal target in a storage ring. The method of polarization by spin filtering requires many of the beam particles to remain within the ring after scattering off the polarized internal target via electromagnetic and hadronic interactions. Sets of differential equations which describe the buildup of polarization by spin filtering in many different scenarios have recently been presented and solved [2 – 8]. In this paper we add to this literature by investigating a scenario where unpolarized particles are input into the beam at a linearly increasing rate, *i.e.* the input rate is ramped up.

The spin filtering method of polarization buildup [9–11] consists of a circulating beam repeatedly interacting with a polarized internal target in a storage ring. Many particles are scattered at small angles but remain in the beam. This introduces a characteristic acceptance angle $\theta_{\rm acc}$, scattering above which causes particles to be lost from the beam. There is also a minimum scattering angle $\theta_{\rm min}$, corresponding to the Bohr radius of the atoms in the target, below which scattering is prevented by Coulomb screening. The two physical processes that contribute to polarization buildup in spin filtering are: (a) spin selective scattering out of the ring, and (b) selective spin-flip, *i.e.* particles in one spin state may be scattered out of the beam (a), or have their spin flipped (b), at a higher rate than particles in the other spin state. Thus over time one spin state is depleted more than the other leading to a beam polarization. A problem with this method is that while there is an increase of beam polarization there is a significant decrease in beam intensity, since particles are continuously scattered out of the beam. We are investigating continuously inputing unpolarized particles into the beam, during spin filtering, to compensate this effect.

When circulating at frequency ν, for a time τ, in a ring with a polarized internal target of areal density n and polarization $\mathcal{P}_{\rm e}$ oriented normal to the ring plane, (or longitudinally with rotators)

$$\frac{\rm d}{{\rm d}\tau}\begin{bmatrix} N \\ \\ J \end{bmatrix} = -\,n\,\nu \begin{bmatrix} I_{\rm out} & \mathcal{P}_{\rm e}\,A_{\rm out} \\ \\ \mathcal{P}_{\rm e}\,A_{\rm all} - \mathcal{P}_{\rm e}\,K_{\rm in} & I_{\rm all} - D_{\rm in} \end{bmatrix} \begin{bmatrix} N \\ \\ J \end{bmatrix}, \qquad (1)$$

describes the rate of change of the number of beam particles $N(\tau) = N_{\uparrow}(\tau) + N_{\downarrow}(\tau)$ and their total spin $J(\tau) = N_{\uparrow}(\tau) - N_{\downarrow}(\tau)$ [3, 4]. The matrix entries are the spin observables integrated with respect to scattering angle θ over the following ranges. The **"in"** subscript

refers to particles that are scattered at small angles $\leq \theta_{\rm acc}$ remaining in the beam, and the **"out"** subscript refers to particles that are scattered out of the beam. Thus the integrals over scattering angle θ are labeled **"in"** where the range of integration is $\theta_{\rm min} \leq \theta \leq \theta_{\rm acc}$, **"out"** where the range of integration is $\theta_{\rm acc} < \theta \leq \pi$ and **"all"** = **"in"** + **"out"** where the range of integration is $\theta_{\rm min} \leq \theta \leq \pi$ as seen in table 1 of ref. [8]. $I = {\rm d}\sigma \,/\, {\rm d}\Omega$ is the spin averaged differential cross-section and A, K and D are the double spin asymmetry, polarization transfer and depolarization spin observables respectively as calculated in ref. [12]. The eigenvalues of the above matrix of coefficients are found to be

$$\lambda_1 \;=\; -\,n\,\nu\,(\,I_{\rm out} \,+\, L_{\rm in} \,+\, L_{\rm d}\,) \qquad \text{and} \qquad \lambda_2 \;=\; -\,n\,\nu\,(\,I_{\rm out} \,+\, L_{\rm in} \,-\, L_{\rm d}\,)\;, \quad (2)$$

where the discriminant $L_{\rm d}$ of the quadratic equation for the eigenvalues is

$$L_{\rm d} \;=\; \sqrt{\mathcal{P}_{\rm e}^{\,2}\,A_{\rm out}\,(A_{\rm all} \,-\, K_{\rm in}) \,+\, L_{\rm in}^{\,2}}\;, \quad (3)$$

and $L_{\rm in} = (\,I_{\rm in} \,-\, D_{\rm in})\,/\,2$ is a loss of polarization quantity. Note that $I_{\rm out}$, $L_{\rm in}$ and $L_{\rm d}$ are all positive. As a consequence the eigenvalues are negative and $\lambda_1 < \lambda_2 < 0$.

The system above and various alternative scenarios have been developed and solved recently in ref. [8]. These scenarios are: 1) spin filtering of a fully stored beam, 2) spin filtering while the beam is being accumulated, *i.e.* unpolarized particles are continuously being fed into the beam at a constant rate, 3) the particle input rate is equal to the rate at which particles are being lost due to scattering beyond ring acceptance angle, the beam intensity remaining constant, 4) increasing the initial polarization of a stored beam by spin filtering, 5) the input of particles into the beam is stopped after a certain amount of time, but spin filtering continues. In this paper we add to the literature by investigating a scenario where unpolarized particles are input into the beam at a linearly increasing rate, *i.e.* the input rate is ramped up. This is accounted for by the following system of spin evolution equations

$$\frac{d\,N(\tau)}{d\,\tau} \;=\; -\,n\,\nu\;[\,I_{\rm out}\;N(\tau) \;+\; \mathcal{P}_{\rm e}\,A_{\rm out}\;J(\tau)\,] \;+\; \beta\,\tau\,, \quad (4)$$

$$\frac{d\,J(\tau)}{d\,\tau} \;=\; -\,n\,\nu\;[\,\mathcal{P}_{\rm e}\;(\,A_{\rm all} - K_{\rm in}\,)\;\;N(\tau) \;+\; (\,I_{\rm all} - D_{\rm in}\,)\;\;J(\tau)\,]\;, \quad (5)$$

where $\beta\,\tau$ is the rate at which particles are fed in, the input ramped up at a rate proportional to the time elapsed. The initial conditions are $N(0) = N_0$ which we may later set to zero, and $J(0) = 0$. By differentiating eq.(5) with respect to τ and substituting in eq.(4) one obtains a second order linear inhomogeneous differential equation for $J(\tau)$:

$$\frac{d^2\,J(\tau)}{d\,\tau^2} \;-\; (\,\lambda_1 + \lambda_2\,)\;\frac{d\,J(\tau)}{d\,\tau} \;+\; \lambda_1\,\lambda_2\,J(\tau) \;=\; -\,n\,\nu\,\mathcal{P}_{\rm e}\;(\,A_{\rm all} - K_{\rm in}\,)\;\beta\,\tau\,, \quad (6)$$

the solution of which is

$$J(\tau) = F_{\lambda_2\,\lambda_1}\,e^{\,\lambda_1\,\tau} + F_{\lambda_1\,\lambda_2}\,e^{\,\lambda_2\,\tau} + \beta\;(\,A_1\,\tau + A_2\,)\;. \quad (7)$$

Where for convenience we have defined the constants

$$A_1 \;\equiv\; \frac{-\,n\,\nu\,\mathcal{P}_{\rm e}\;(\,A_{\rm all} - K_{\rm in}\,)}{\lambda_1\,\lambda_2} \quad \text{and} \quad A_2 \;\equiv\; \frac{2\,n^2\,\nu^2\,\mathcal{P}_{\rm e}\;(\,A_{\rm all} - K_{\rm in}\,)\,(\,L_{\rm in} + I_{\rm out}\,)}{\lambda_1^2\,\lambda_2^2}\,, \quad (8)$$

$$F_{\lambda_2\,\lambda_1} \;\equiv\; \frac{n\,\nu\,(\,A_{\rm all}-K_{\rm in}\,)\,N_0\,\mathcal{P}_{\rm e}+\beta\,(\,A_1-\lambda_2\,A_2\,)}{\lambda_2-\lambda_1}\,, \tag{9}$$

obtained by imposing the initial conditions $J(0)=0$ and $N(0)=N_0$ thus $d\,J(0)/d\,\tau = -\,n\,\nu\,\mathcal{P}_{\rm e}\,(\,A_{\rm all}-K_{\rm in}\,)\,N_0$. The function $F_{\lambda_1\,\lambda_2}$ is $F_{\lambda_2\,\lambda_1}$ with λ_1 and λ_2 interchanged. Differentiating eq.(7) with respect to τ and substituting into eq.(5) gives an expression for $N(\tau)$:

$$N(\tau) = \frac{-1}{(\,A_{\rm all}-K_{\rm in}\,)\,\mathcal{P}_{\rm e}}\,\Big\{\,F_{\lambda_2\,\lambda_1}\,e^{\,\lambda_1\,\tau}\,(\,L_{\rm in}-L_{\rm d}\,)+F_{\lambda_1\,\lambda_2}\,e^{\,\lambda_2\,\tau}\,(\,L_{\rm in}+L_{\rm d}\,) \tag{10}$$

$$+\,\beta\,\left[\,\frac{A_1}{n\,\nu}+(\,I_{\rm out}+2\,L_{\rm in}\,)\,(\,A_1\,\tau+A_2\,)\,\right]\Big\}\,. \tag{11}$$

As a consistency check it can be seen that the inhomogeneous solutions for $J(\tau)$ and $N(\tau)$ satisfy the initial conditions, and that when $\beta=0$ they reduce to the solutions of the homogeneous system eq.(1) presented in refs. [5,8].

Dividing $J(\tau)$ by $N(\tau)$ we obtain an expression for the polarization as a function of time (τ),

$$\mathcal{P}(\tau) \;=\; \frac{J(\tau)}{N(\tau)} \;=\; \frac{-\,\mathcal{P}_{\rm e}\,(\,A_{\rm all}-K_{\rm in}\,)}{L_{\rm in}+L_{\rm d}\left[\,\dfrac{2}{1-\frac{e^{\,\lambda_1\,\tau}\,F_{\lambda_2\,\lambda_1}\,(\,\lambda_2-\lambda_1\,)-\beta\,[\,A_1\,(\,1-\lambda_2\,\tau\,)-\lambda_2\,A_2\,]}{e^{\,\lambda_2\,\tau}\,F_{\lambda_1\,\lambda_2}\,(\,\lambda_1-\lambda_2\,)-\beta\,[\,A_1\,(\,1-\lambda_1\,\tau\,)-\lambda_1\,A_2\,]}}\;-\;1\,\right]}\,. \tag{12}$$

When $\beta=0$ the above equation simplifies to

$$\mathcal{P}(\tau) \;=\; \frac{-\,\mathcal{P}_{\rm e}\,(\,A_{\rm all}\,-\,K_{\rm in}\,)}{L_{\rm in}\,+\,L_{\rm d}\,\coth\,(L_{\rm d}\,n\,\nu\,\tau)}\,, \tag{13}$$

which is the solution of the homogeneous case eq.(1) presented in refs. [5,8].

Of interest is the case when $N(0)=N_0=0$, *i.e.* there are no particles in the beam initially. To obtain this result we set $N_0=0$ in the above equation to obtain

$$\mathcal{P}(\tau) = \frac{-\,\mathcal{P}_{\rm e}\,(\,A_{\rm all}-K_{\rm in}\,)}{L_{\rm in}+L_{\rm d}\left[\,\dfrac{2}{1-\frac{\left(\,e^{\,\lambda_1\,\tau}-1\,\right)\,\lambda_2\,A_2-A_1\left(\,e^{\,\lambda_1\,\tau}+\lambda_2\,\tau-1\,\right)}{\left(\,e^{\,\lambda_2\,\tau}-1\,\right)\,\lambda_1\,A_2-A_1\left(\,e^{\,\lambda_2\,\tau}+\lambda_1\,\tau-1\,\right)}}\;-\;1\,\right]}\,, \tag{14}$$

where for $\beta\neq 0$ the β dependence vanishes. We should note the obvious physical fact that if $N_0=0$ and $\beta=0$, *i.e.* there are no particles in the beam initially and no particles are fed into the beam, then there will never be any particles in the beam; so measuring the beam polarization is meaningless. Using a Taylor Series expansion we obtain the approximate initial rate of polarization buildup

$$\frac{\mathrm{d}\,\mathcal{P}}{\mathrm{d}\tau} \;\approx\; -\,n\,\nu\,\mathcal{P}_{\rm e}\,(A_{\rm all}\,-\,K_{\rm in})\,, \tag{15}$$

identical to that of the homogeneous case eq.(1) presented in refs. [5,8]. The maximum polarization achievable is the limit as time approaches infinity:

$$\mathcal{P}_{\rm max} = \lim_{\tau\to\infty}\mathcal{P}(\tau) = \frac{-\,\mathcal{P}_{\rm e}\,(\,A_{\rm all}-K_{\rm in}\,)}{I_{\rm all}-D_{\rm in}} = \frac{-\,\mathcal{P}_{\rm e}\,(\,A_{\rm all}-K_{\rm in}\,)}{I_{\rm out}+2\,L_{\rm in}}\,. \tag{16}$$

The above expression is only valid for $\beta \neq 0$, the $\beta = 0$ expression is presented in refs. [5,8].

The Figure Of Merit (FOM) provides a measure of the quality of the polarized beam, taking into account the trade-off between increasing beam polarization and decreasing beam intensity. For this inhomogeneous case the FOM is:

$$FOM(\tau) = \mathcal{P}^{\,2}(\tau)\, N(\tau) = \frac{J^{\,2}(\tau)}{N(\tau)} \;= \tag{17}$$

$$\frac{-\,\mathcal{P}_{\rm e}\,\left(\,A_{\rm all} - K_{\rm in}\,\right)\,\left[\,F_{\lambda_2\,\lambda_1}\,e^{\,\lambda_1\,\tau} + F_{\lambda_1\,\lambda_2}\,e^{\,\lambda_2\,\tau} + \beta\,\left(\,A_1\,\tau + A_2\,\right)\,\right]^{\,2}}{F_{\lambda_2\,\lambda_1}\,e^{\,\lambda_1\,\tau}\,\left(\,L_{\rm in} + L_{\rm d}\,\right) - F_{\lambda_1\,\lambda_2}\,e^{\,\lambda_2\,\tau}\,\left(\,L_{\rm in} + L_{\rm d}\,\right) + \beta\,\left[\,\frac{A_1}{n\,\nu} + \left(\,I_{\rm all} - D_{\rm in}\,\right)\,\left(\,A_1\,\tau + A_2\,\right)\,\right]}\,.$$

If the particle accumulation rate $\beta\,\tau$ is high enough to make the beam intensity constant or increase with time the FOM will be a monotonically increasing function of time, *i.e.* it will not have a finite maximum.

This research is funded by the Irish Research Council for Science, Engineering and Technology (IRCSET).

References

[1] PAX Collaboration [V. Barone *et al.*], arXiv:hep-ex/0505054.

[2] C. J. Horowitz, H. O. Meyer, Phys. Rev. Lett. **72**, 3981 (1994); H. O. Meyer, Phys. Rev. E **50**, 1485 (1994).

[3] A. I. Milstein, V. M. Strakhovenko, Phys. Rev. E **72**, 066503 (2005).

[4] N. N. Nikolaev, F. F. Pavlov, arXiv:hep-ph/0601184. Also Proc. of the 17th International Spin Physics Symposium, SPIN 2006, AIP Conference Proc. **V.915**, 932.

[5] D. S. O'Brien, N. H. Buttimore, Proc. of the 17th International Spin Physics Symposium, SPIN 2006, AIP Conference Proc. **V.915**, 936. [arXiv:hep-ph/0702088].

[6] W. W. MacKay, C. Montag, Phys. Rev. E **73**, 028501 (2006).

[7] Th. Walcher, H. Arenhövel, K. Aulenbacher, R. Barday, A. Jankowiak, arXiv:0706.3765 [physics.acc-ph].

[8] N. H. Buttimore and D. S. O'Brien, Submitted to Eur. Phys. J. A; arXiv:0707.2065 [hep-ph].

[9] P. L. Csonka, Nucl. Instrum. Meth. **63**, 247 (1968).

[10] F. Rathmann *et al.*, Phys. Rev. Lett. **71**, 1379 (1993).

[11] F. Rathmann *et al.*, Phys. Rev. Lett. **94**, 014801 (2005).

[12] D. S. O'Brien, N. H. Buttimore, Czech. J. Phys. **56**, F219 (2006) [arXiv:hep-ph/0609233].

RELATED PROBLEMS

KERR GEOMETRY PREDICTS THE COMPTON SIZE OF ELECTRON

A.Burinskii[1†],
(1) *NSI Russian Academy of Sciences*
E-mail: bur@ibrae.ac.ru

Abstract

The combined Dirac-Kerr model of electron is suggested, in which the Dirac equation plays the role of a master equation controlling the extended space-time structure of Kerr geometry. The extended Kerr source of this model contains a spinning disk bounded by a closed singular string of Compton size. It is conjectured that this Compton structure is formed by a coherent set virtual photons and it can be observed in the experiments with a very soft coherent scattering.

Introduction. The Kerr-Newman solution has gyromagnetic ratio $g = 2$, as that of the Dirac electron, which created series of works on the classical model of extended electron based on the Kerr geometry (see for references [1,2,3,4]). There appears a natural question, what is the relation between the Dirac equation and Kerr-Newman solution?

The related problem concerns the coordinate description of electron. In the Dirac theory electron is structureless and cannot be localized inside the Compton region. It does not allow one to incorporate gravity which demands clear coordinate description. Similar, in the multi-particle QED theory, the "naked" electron is point-like, however, the "dressed" one is to be smeared over the Compton region. However, coordinate description is again very obscure and central role is played by the momentum space. As a result, there appears the extreme point of view that the subsequent relativistic theory has to refuse from coordinate description at all [5].

One can ignore gravity, arguing that gravitational field of electron is negligibly weak. However, electron has the extremely large spin/mass ratio (about 10^{44} in the units $\hbar = c = G = 1$,) which shows that gravitational effects have to be estimated on the base of the Kerr-Newman solution. Corresponding analysis shows that the extremely high spin leads to the very strong polarization of space-time and to the corresponding very strong deformation of electromagnetic (em-) field which has to be aligned with the Kerr congruence. However, the *electromagnetic field of electron cannot be considered as small*, and the resulting influence turns out to be very essential! In particular, the em-field turns out to be singular at the Kerr ring which has the Compton size $a = J/m$. The space-time acquires two folds with a branch line along the Kerr ring, which gives a new background for the treatment of this problem.

In this work we obtain an exact correspondence between the spinor solutions of the Dirac equation and the spinor (twistorial) structure of the Kerr geometry. This relationship allows us to suggest a combined Dirac-Kerr model of an extended electron which acquires a natural coordinate description from the Kerr geometry displaying explicitly a peculiar role of the Compton region. The Dirac equation plays in this model the role of a *master equation* controlling twistorial polarization of the Kerr space-time and its dynamics in the external electromagnetic fields which turns out to be undisguised from the behavior of the Dirac electron.

Real structure of the Kerr geometry Angular momentum of electron $J = \hbar/2$ is extremely high with respect to the mass, and the black hole *horizons disappear* opening the naked Kerr singular ring which represents a closed string [3], excitations of which

generate spin and mass of the extended particle-like object - "microgeon" [1]. Singular ring may be regularized by Higgs field. If the Kerr string acquire tension T, $m = E = Ta$, the Kerr relation $J = ma$ yields the Regge behavior $J = \frac{1}{T}m^2$.

The Kerr principal null congruence is a twisted family of the lightlike rays – twistors. Frame of the Kerr geometry is formed by null vector field $k^\mu(x)$ which is tangent to the Kerr congruence. The Kerr-Schild form of metric is

$$g^{\mu\nu} = \eta^{\mu\nu} + 2Hk^\mu k^n, \tag{1}$$

where $\eta^{\mu\nu}$ is auxiliary Minkowski space-time with coordinates $x^\mu = (t, x, y, z)$.

Vector potential of the Kerr-Newman solution is aligned with this congruence

$$A_\mu = \mathcal{A}(x)k_\mu, \tag{2}$$

and the Kerr singular ring represents its caustic, see Fig. 1. **The Kerr theorem** determines the Kerr congruence via a holomorphic surface in the projective twistor space which has coordinates

$$Y, \quad \lambda_1 = \zeta - Yv, \quad \lambda_2 = u + Y\bar{\zeta}\,, \tag{3}$$

where $2^{\frac{1}{2}}\zeta = x + iy$, $\quad 2^{\frac{1}{2}}\bar{\zeta} = x - iy$, $\quad 2^{\frac{1}{2}}u = z - t$, $\quad 2^{\frac{1}{2}}v = z + t$ are the null Cartesian coordinates. Such congruences lead to solutions of the Einstein-Maxwell field equations with metric (1) and em-field in the form (2). Congruence of the Kerr solution is built of the straight null generators, twistors, which are (twisting) geodesic lines of photons. Therefore, for any holomorphic function F, the solution $Y(x^\mu)$ of the equation $F(Y, \lambda_1, \lambda_2) = 0$ determines congruence of null lines by the 1-form

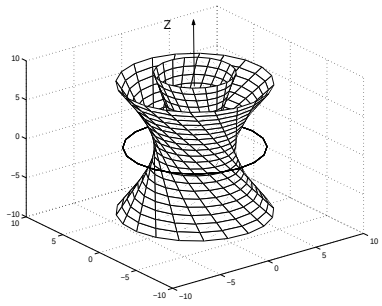

Figure 1. The Kerr singular ring and congruence.

$$e^3 = du + \bar{Y}d\zeta + Yd\bar{\zeta} - Y\bar{Y}dv\,. \tag{4}$$

The null vector field $k_\mu dx^\mu = P^{-1}e^3$ up to a normalizing factor P. Coordinate Y is a projective spinor $Y = \phi_2/\phi_1$, and in spinor form $k_\mu = \bar{\phi}_{\dot{\alpha}}\bar{\sigma}_\mu^{\dot{\alpha}\alpha}\phi_\alpha$.

Complex representation of Kerr geometry. Complex source of Kerr geometry is obtained as a result of complex shift of the 'point-like' source of the Schwarzschild solution written in the Kerr-Schild form. Applying the complex shift $(x, y, z) \to (x, y, z + ia)$ to the singular source $(x_0, y_0, z_0) = (0, 0, 0)$ of the Coulomb solution q/r, Appel (in 1887 !) obtained the solution $\phi(x, y, z) = \mathrm{Re}\, e\, q/\tilde{r}$, where $\tilde{r} = \sqrt{x^2 + y^2 + (z - ia)^2}$ turns out to be complex. On the real slice (x, y, z), this solution acquires a singular ring corresponding to $\tilde{r} = 0$. It has radius a and lies in the plane $z = 0$. The solution is conveniently described in the oblate spheroidal coordinate system $r,\ \theta$, where $\tilde{r} = r + ia\cos\theta$. The resulting real space is twofold having positive sheet $r > 0$, and negative one $r < 0$.

The Appel potential corresponds exactly to electromagnetic field of the Kerr-Newman solution written in the Kerr-Schild form [1]. The vector of complex shift $\boldsymbol{a}$ shows angular momentum of the Kerr solution $\boldsymbol{J} = m\boldsymbol{a}$. Newman and Lind suggested a description of the Kerr-Newman geometry in the form of a retarded-time construction, where its source is generated by a complex point-like source, propagating along a *complex world line* $X^\mu(\tau) \in CM^4$.

In the rest frame of the Kerr particle, one can form two null 4-vectors $k_L = (1,0,0,1)$ and $k_R = (1,0,0,-1)$, and represent the 3-vector of complex shift $i\boldsymbol{a} = i\Im m X^\mu$ as the difference $i\boldsymbol{a} = \frac{ia}{2}\{k_L - k_R\}$. The straight complex world line corresponding to a free particle may be decomposed to the form $X^\mu(\tau) = X^\mu(0) + \tau u^\mu + \frac{ia}{2}\{k_L - k_R\}$, where the time-like 4-vector of velocity $u^\mu = (1,0,0,0)$ can also be represented via vectors k_L and k_R $u^\mu = \partial_t \Re e X^\mu(\tau) = \frac{1}{2}\{k_L + k_R\}$. One can form two complex world lines related to the complex Kerr source,

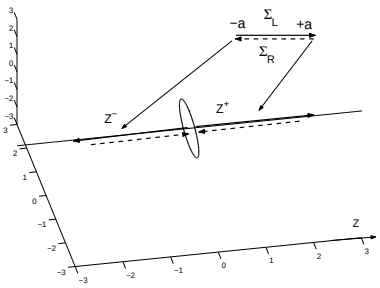

Figure 2. Singular ring and two singular half-strings.

$$X^\mu_+(t + ia) = \Re e X^\mu(\tau) + iak^\mu_L\,,$$
$$X^\mu_-(t - ia) = \Re e X^\mu(\tau) - iak^\mu_R\,, \qquad (5)$$

which allows us to match the Kerr geometry to the solutions of the Dirac equation. **Complex Kerr string.** The complex world line $X^\mu(\tau)$ is parameterized by complex time $\tau = t + i\sigma$ and represents the world sheet of a very specific string extended along imaginary time parameter $\sigma \in [-a, a]$. The Kerr congruence, gravitational and em- fields are obtained from this stringy source by a retarded-time construction which is based on the complex null cones, emanated from the worldsheet of this complex string [3,4]. The complex retarded time equation $\tau = t - r + ia\cos\theta$ sets the relation $\sigma = a\cos\theta$ between the complex points $X^\mu(t,\sigma)$ and angular directions θ of the real twistor lines. One sees that this string is open with the end points $\cos\theta = \pm 1$ which correspond to $X^\mu_\pm = X^\mu(t \pm ia)$. By analogue with the real strings, the end points may be attached to quarks. The complex light cones adjoined to the end points have a *real slice in the form of two especial twistors* having the discussed above null directions k^μ_L and k^μ_R which determine momentum and spin-polarization of the Kerr solution. These twistors form two half-strings of opposite chirality, see Fig. 2.

Chirons and excitations of the Kerr singular ring. The twistor coordinate Y is also the projective angular coordinate $Y = e^{i\phi}\tan\theta$ covering the celestial sphere, $Y \in CP^1 = S^2$. The exact Kerr-Schild solutions have em-field which is determined by arbitrary analytical function $\mathcal{A}(Y)$, in particular $\mathcal{A} = eY^{-n}$. The simplest case $n = 0$ gives the Kerr-Newman solution. The case $n = 1$ leads to an axial singular line along the positive semi-axis z. Due to factor $e^{i\phi}$, em-field of this solution has winding number n=1 around axial singularity. Since there is also pole at singular ring, $\sim (r + ia\cos\theta)^{-1}$, the em-field has also a winding of phase along the Kerr ring. Solution with $n = -1$ has opposite chirality and singular line along the negative semi-axis z. These elementary exact solutions ('chirons') have also the wave generalizations $\mathcal{A} = eY^{-n}e^{i\omega\tau}$ acquiring the extra dependence from the complex retarded time τ. The wave chirons are asymptotically exact in the low-frequency limit and describe the waves propagating along the Kerr circular string and induced waves along axial half-strings [3,4]. By lorentz boost the axial half-strings acquire modulation by de Broglie periodicity [3,4].

Dirac Equation in the Weyl Basis In the Weyl basis Dirac spinor has the form $\Psi = \begin{pmatrix} \phi_\alpha \\ \chi^{\dot\alpha} \end{pmatrix}$, and the Dirac equation splits into

$$\sigma^\mu_{\alpha\dot\alpha}(i\partial_\mu + eA_\mu)\chi^{\dot\alpha} = m\phi_\alpha, \quad \bar\sigma^{\mu\dot\alpha\alpha}(i\partial_\mu + eA_\mu)\phi_\alpha = m\chi^{\dot\alpha}. \qquad (6)$$

The Dirac current $J_\mu = e(\bar\Psi\gamma_\mu\Psi) = e(\bar\chi\sigma_\mu\chi + \bar\phi\bar\sigma_\mu\phi)$, can be represented as a sum of two lightlike components of opposite chirality $J^\mu_L = e\bar\chi\sigma^\mu\chi\ , \qquad J^\mu_R = e\bar\phi\bar\sigma^\mu\phi$. The corresponding null vectors

$$k^\mu_L = \bar\chi\sigma^\mu\chi\ , \quad k^\mu_R = \bar\phi\bar\sigma^\mu\phi, \tag{7}$$

determine the considered above directions of the lightlike half-strings. The momentum of the Dirac electron is $p^\mu = \frac{m}{2}(k^\mu_L + k^\mu_R)$, and the vector of polarization of electron in the state with a definite projection of spin on the axis of polarization is $n^\mu = \frac{1}{2}(k^\mu_L - k^\mu_R)$. In particular, in the rest frame and the axial z-symmetry, we have $k_L = (1, \boldsymbol{k}_L) = (1, 0, 0, 1)$ and $k_R = (1, \boldsymbol{k}_R) = (1, 0, 0, -1)$, which gives $p^\mu = m(1, 0, 0, 0)$, and $n^\mu = (0, 0, 0, 1)$, which corresponds to transverse polarization of electron, $\boldsymbol{np} = 0$. The Dirac wave wave function sets also synchronization of the null tetrad in the surrounding space-time, playing the role of an 'order parameter'.

Dirac Equation as a Master Equation Controlling Twistorial Polarization. Em-field of the Kerr-Schild solutions $F_{\mu\nu}$ is to be aligned with the Kerr congruence, obeying the constraint $F_{\mu\nu}k^\mu = 0$. Therefore, twistorial structure of the Kerr-Schild solutions determines strong polarization of the em field. In particular, the elementary em-excitations on the Kerr background lead to the waves propagating along the Kerr circular string. Virtual photons are also concentrated near this string, forming its excitation. There is exact correspondence between two null vectors (7) obtained from the Dirac wave function and similar vectors k_L and k_R related to the ends of the complex Kerr string, Fig. 2. It allows us to unify the Dirac and Kerr structures, considering the Dirac equation as a master equation controlling twistorial polarization of the Kerr space-time.

Scattering. Contradiction between the discussed Compton size of electron and the results obtained for the deep inelastic scattering has simple explanation. Relativistic boosts lead to asymmetry: $p_L << p_R$ or $p_L >> p_R$ which determines the sign of helicity. As a result one of the axial half-strings turns out to be strongly dominant. It allows one to use perturbative twistor-string model [6,7] which is based on a reduced description in terms of the lightlike momentum and helicity, and amplitude of scattering is determined *only by one* of the axial half-strings. One can conjecture that *the Compton size of the Dirac-Kerr electron may be observed for polarized electrons in the experiments with a very soft resonance scattering.*

References.

[1] A.Ya. Burinskii, Sov. Phys. JETP, **39** 193 (1974).

[2] A.Ya. Burinskii, Phys. Lett. **A 185** 441 (1994); gr-qc/9303003.

[3] A. Burinskii, Phys. Rev. D **70**, 086006 (2004), hep-th/0507109, 0710.4249 [hep-th].

[4] A. Burinskii, Grav.&Cosmology, **10**, 50 (2004), hep-th/0403212.

[5] V.B. Berestetsky, E.M. Lifshitz, L.P. Pitaevsky, "Quantum Electrodynamics, Oxford, UK: Pergamon (1982).

[6] V.P. Nair, Phys. Lett. **B 214** 215 (1988).

[7] E. Witten, Comm. Math. Phys. **252**, 189 (2004), hep-th/0312171.

ELECTROMAGNETIC WAVE-PARTICLE WITH SPIN AND MAGNETIC MOMENT

A.A. Chernitskii

A. Friedmann Laboratory for Theoretical Physics, St.-Petersburg, Russia;
State University of Engineering and Economics,
Marata str. 27, St.-Petersburg, Russia, 191002
E-mail: AAChernitskii@mail.ru, AAChernitskii@engec.ru

Abstract

An axisymmetric static solution of a nonlinear electrodynamics is considered as a massive charged particle with spin and magnetic moment. A linearization of the nonlinear electrodynamics around the static solution is investigated. The appropriate problem for linear waves around the static solution is considered. This wave part of the particle solution is considered to provide the appropriate wave properties for the particle. It has been found that the right (experimentally proved) formula for frequency of this wave appears theoretically for the static solution with ring singularity.

1. Introduction. The field electromagnetic particle concept in the framework of a unified nonlinear electrodynamics is considered here. In this approach a space-localized (soliton) solution of a nonlinear electrodynamics field model conforms to a physical elementary particle. The term "particle solution" will be used here. This theme was discussed in my articles (see, for example, [1–4]). The present work is concerned mainly with possible existence of a quick-oscillating part for a particle solution in intrinsic coordinate system. This quick-oscillating part in intrinsic coordinate system of the particle will be a wave part for arbitrary coordinates. This wave part must provide the appropriate wave properties for the particle.

2. Static electromagnetic particle with spin. Axisymmetric static electromagnetic field configuration can have the spin defined as the full angular momentum of the electromagnetic field:

$$\mathbf{s} = \int \boldsymbol{\mathcal{M}} \mathrm{dV} \ , \tag{1}$$

where $\boldsymbol{\mathcal{M}} \doteqdot \mathbf{r} \times \boldsymbol{\mathcal{P}}$ is an angular momentum density (spin density), $\mathbf{r}$ is a position vector, $\boldsymbol{\mathcal{P}} \doteqdot (\mathbf{D} \times \mathbf{B})/4\pi$ is a momentum density (Poynting vector), $\mathbf{D}$ and $\mathbf{B}$ are electric and magnetic inductions.

The origin of the spin density is discussed in my articles. In particular, it was considered three topologically different static field configuration with spin [4]. These are configurations with two dyon, with singular disk, and with singular ring.

Let us consider more closely the field configuration with singular ring.

3. Toroidally symmetrical configuration with singular ring. A consideration of the static linear electrodynamics equations in toroidal coordinates (ξ, η) gives the appropriate solution with toroidal symmetry. This solution can include an electric and a magnetic parts. They can be represented with the help of toroidal harmonics which are the spheroidal harmonics with half-integer index: $P^l_{n-\frac{1}{2}}(\cosh\xi)$, where n and l are integer. To obtain the right behaviour of the electromagnetic field at infinity for a charged particle with magnetic moment we must take the toroidal harmonics $P^0_{-\frac{1}{2}}(\cosh\xi)$, $P^0_{-\frac{3}{2}}(\cosh\xi)$ for the electric field and $P^1_{-\frac{1}{2}}(\cosh\xi)$, $P^1_{-\frac{3}{2}}(\cosh\xi)$ for the magnetic one. Because we intend to consider this solution as an initial approximation to a solution of a nonlinear electrodynamics model, it is reasonable to take the condition of vanishing of two electromagnetic invariants near the singular ring. This condition will be satisfied when the ratio between the electric and magnetic vector magnitudes tends to unit near the ring.

We have the following appropriate solution of the linear electrodynamics:

$$\begin{aligned}
D_\xi &= -\frac{e}{\sqrt{2}\,\pi\,\rho^2}\,\sqrt{\cosh\xi-\cos\eta}\;\mathrm{csch}\xi\,\Big[2\,(\cosh\xi-\cos\eta)\,\text{Ⱡ}\Big(-\sinh^2\frac{\xi}{2}\Big)\\
&\qquad -(1-\cos\eta)\,(1+\cosh\xi)\,\text{Ⱪ}\Big(-\sinh^2\frac{\xi}{2}\Big)\Big]\quad,\\
D_\eta &= -\frac{e}{\sqrt{2}\,\pi\,\rho^2}\,\sqrt{\cosh\xi-\cos\eta}\;\text{Ⱪ}\Big(-\sinh^2\frac{\xi}{2}\Big)\,\sin\eta\quad,\\
H_\xi &= -\frac{e}{\sqrt{2}\,\rho^2}\,i\,\sqrt{\cosh\xi-\cos\eta}\,P^1_{-\frac{1}{2}}(\cosh\xi)\,\sin\eta\quad,\\
H_\eta &= \frac{e}{\sqrt{2}\,\rho^2}\,i\,\sqrt{\cosh\xi-\cos\eta}\;\mathrm{csch}\xi\,\Big[(\cosh\xi-\cos\eta)\,P^1_{-\frac{3}{2}}(\cosh\xi)\\
&\qquad +(\cos\eta\,\cosh\xi-1)\,P^1_{-\frac{1}{2}}(\cosh\xi)\Big]\quad,
\end{aligned}\tag{2}$$

where D_ξ, D_η, H_ξ, H_η are the physical components of the electric induction and magnetic strength vectors in toroidal coordinates, Ⱪ(m) and Ⱡ(m) are complete elliptic integrals of the first and second kinds accordingly (can be expressed by means of $P^0_{-\frac{1}{2}}(\cosh\xi)$ and $P^0_{-\frac{3}{2}}(\cosh\xi)$), $P^l_{-\frac{1}{2}}(z)$ and $P^l_{-\frac{3}{2}}(z)$ are associated Legendre functions with half-integer negative index. Here ρ is the radius of the ring and e is a constant.

The field configuration (2) has the electric charge e and the magnetic moment

$$\mu = \frac{e\,\rho}{2}\quad.\tag{3}$$

About the definition of the electric charge and the magnetic moment see my article [3].

4. Wave part of the particle solution. In general case particle solution can include a time-periodic part. Having in view the wave properties of the physical particles this time-periodic part must be considered as quick-oscillating one. For the intrinsic coordinate system of the particle this quick-oscillating part can be a standing wave or a progressive wave around a closed singular line (ring, for example). A hyperbolic rotation of the particle solution with the quick-oscillating part gives the solution for moving particle having evident wave properties.

The appropriate time-periodic solutions well known for the linear electrodynamics. In particular, they exist for considered topologically different configurations of singularities: bidyon, disk, and ring.

For the nonlinear case we can investigate the time-periodic part by means of the linearization of the problem around the appropriate static field configuration (which may not be exact solution). The general method for the linearization is based on Frechet derivative for the nonlinear operator:

$$\begin{array}{ccc} \mathcal{N}\mathbf{Y}=\mathbf{0} & \rightarrow & \mathcal{N}'(\mathbf{Y_0})\tilde{\mathbf{Y}}=-\mathcal{N}\mathbf{Y_0} \\ \text{Nonlinear} & & \text{Linearized around } \mathbf{Y_0} \\ \text{system of equations} & \mathbf{Y}=\mathbf{Y_0}+\tilde{\mathbf{Y}} & \text{system of equations} \end{array} \quad .$$

This problem for point singularity was considered in my article [5].

5. About circular frequency of the time-periodic part of the particle solution. Let us consider that the circular frequency of the time-periodic part of the particle solution is given by the known formula: $m=\hbar\,\omega \;\; (c=1)$.

The magnetic moment of the Dirac spin one-half particle is $\mu=\dfrac{e\,\hbar}{2\,m}$.

Thus we have the important formula for the circular frequency:

$$\left.\begin{array}{l} \mu=\dfrac{e\,\hbar}{2\,m} \;\;\Rightarrow\;\; \dfrac{m}{\hbar}=\dfrac{e}{2\,\mu} \\ \\ m=\hbar\,\omega \;\;\Rightarrow\;\; \dfrac{m}{\hbar}=\omega \end{array}\right\} \;\Rightarrow\; \omega=\frac{e}{2\,\mu} \tag{4}$$

Here the initial formulas have the experimental confirmations. Thus the obtained formula must be considered as experimental one.

6. The advance for particle solution with ring singularity. The ring configuration gives birth to the appropriate periodic space boundary condition (on the ring). Thus it would appear reasonable that we will have the time-periodic part of the particle solution in the form of wave propagating along the ring. The wave-length of the appropriate fundamental mode is

$$\lambda=2\,\pi\,\rho \quad . \tag{5}$$

In general case the static part of the solution can modify the conditions of propagation for the wave part of the solution (see my article [6]). But for the special case of vanishing of the electromagnetic invariants for the static part of the solution we can have the changeless speed of light $c=1$ for the wave part.

In this case the fundamental circular frequency for the time-periodic part is

$$\omega=\frac{2\pi}{\lambda}=\frac{1}{\rho} \quad . \tag{6}$$

Combining the formulas (3) and (6) we have:

$$\left.\begin{array}{l} \mu=\dfrac{e\,\rho}{2} \\ \\ \omega=\dfrac{1}{\rho} \end{array}\right\} \;\Rightarrow\; \omega=\frac{e}{2\mu} \quad . \tag{7}$$

As we see this formula coincides with the experimental formula (4).

It should be noted that the appropriate field configuration with disk-shaped singularity (see, for example, [7]) has the magnetic moment described by formula $\mu = e\,\rho$ that is not leading in this approach to the right formula (4).

7. Conclusions. Thus we must call our attention to the particle solutions with ring singularity. Such particle solutions may represents the real physical elementary particles.

References

[1] A.A. Chernitskii, "Dyons and interactions in nonlinear (Born-Infeld) electrodynamics," *J. High Energy Phys.* **1999**, No 12, Paper 10, 1–34 (1999); [hep-th/9911093].

[2] A.A. Chernitskii, "Born-Infeld equations," in *Encyclopedia of Nonlinear Science*, edited by A. Scott, Routledge, New York and London, 2004, pp. 67–69; [hep-th/0509087].

[3] A.A. Chernitskii, "Mass, spin, charge, and magnetic moment for electromagnetic particle," in *XI Advanced Research Workshop on High Energy Spin Physics (DUBNA-SPIN-05) Proceedings*, edited by A. V. Efremov, and S. V. Goloskokov, JINR, Dubna, 2006, pp. 234–239; [hep-th/0603040].

[4] A.A. Chernitskii, "The field nature of spin for electromagnetic particle," in *Proceedings of the 17-th International Spin Physics Symposium (Kyoto, Japan, 2–7 Oktober 2006)*, edited by K. Imai, T. Murakami, N. Saito, and K. Tanida, AIP Conference Proceedings **915**, Melville, New York, 2007, pp. 264–267; [hep-th/0611342].

[5] A.A. Chernitskii, "Linear waves around static dyon solution of nonlinear (Born-Infeld) electrodynamics," *Hadronic Journal*, **29**, 497–528 (2006); [hep-th/0602079].

[6] A.A. Chernitskii, "Light beams distortion in nonlinear electrodynamics," *J. High Energy Phys.* **1998**, No 11, Paper 15, 1–5 (1998); [hep-th/9809175].

[7] A. Burinskii, "Microgeon with spin," *Sov. Phys. JETP* **39**, 193 (1974).

ASYMMETRY IN HEATING OF CHARGED LEPTONS AND ANTILEPTONS BY NEUTRINOS IN A STRONGLY MAGNETIZED THERMAL PLASMA

V. A. Guseinov[1,2†], R. E.Gasimova [1††] and B. T. Hajiyeva[1]

(1) *Department of General and Theoretical Physics, Nakhchivan State University, AZ 7000, Nakhchivan, Azerbaijan*
(2) *Laboratory of Physical Research, Nakhchivan Division of Azerbaijan National Academy of Sciences, AZ 7000, Nakhchivan, Azerbaijan*
† *E-mail: vgusseinov@yahoo.com*
††*E-mail: gasimovar@yahoo.co.uk*

Abstract

It is shown that the asymmetry in heating of charged leptons and charged antileptons by neutrinos in a strongly magnetized thermal plasma is sensitive to neutrino flavor and spin variables of initial charged leptons and charged antileptons and it also depends on the charged lepton (charged antilepton) energy and the medium characteristics. The obtained result is evidence for the asymmetry in heating of a matter and an antimatter by neutrinos in a strongly magnetized thermal plasma.

1 Introduction

We consider the neutrino-charged lepton scattering (NCLS) $\nu_i + l^- \to \nu_i + l^-$ and the neutrino-charged antilepton scattering (NCAS) $\nu_i + l^+ \to \nu_i + l^+$ in a magnetic field (MF). Neutrino-electron scattering (NES) in a magnetized thermal plasma has been considered in [1], where spin effects have not been investigated. One of the main purposes of this work is to present an analytic formula for the asymmetry in heating (AH) of a charged lepton (CL) gas and a charged antilepton (CA) gas in a strongly magnetized thermal plasma (SMTP) with allowance for longitudinal polarizations (LP) of CLs (CAs) in initial and final states and to demonstrate the AH of a matter and an antimatter by neutrinos in a SMTP in the model of CLs and CAs. When the momentum transferred is relatively small,$|q^2| \ll m_W^2, m_Z^2$ (m_W is the $W^{\pm}$-boson mass, m_Z is the Z-boson mass), the 4-fermion approximation of the Weinberg-Salam-Glashow standard model can be used. The gauge of a 4-potential is $A^\mu = (0, 0, xH, 0)$ and an external MF vector $\mathbf{H}$ is directed along the axis OZ. We deal with a massless neutrino.

2 The differential cross sections of the processes

The differential cross sections of the considered processes with allowance for the LP of CLs (CAs) are given by the following formulae (compare with [2])

$$\frac{d\sigma_{\mp}}{d\omega' d\Omega'} = \frac{G_F^2 eH\omega'^2}{32\pi^4} \sum_{n,n'=0}^{\infty} \sum_i \frac{E_i E_i'}{|E_i' p_{zi} - E_i p_{zi}'|} f_{\mp}(1 - f_{\mp}')Q_{\mp}, \tag{1}$$

where $Q_{\mp}$ is the function of a MF strength H, the spin variables ζ, ζ' and energies E,E' of CLs (CAs) in initial and final states, the polar angle of the incident (scattered) neutrino momentum (INM (SNM)) ϑ (ϑ'), the difference between the azimuthal angles of the INM and the SNM $\alpha - \alpha'$, the angle φ ($\tan\varphi = \frac{q_y}{q_x}$, $q = k - k'$, $k(k')$ is the INM (SNM)) and the parameter

$$x = (1/2eH)[\omega^2 \sin^2\vartheta + \omega'^2 \sin^2\vartheta' - 2\omega\omega' \sin\vartheta \sin\vartheta' \cos(\alpha - \alpha')]. \quad (2)$$

$\omega(\omega')$ is the incident (scattered) neutrino energy, G_F is the Fermi constant, e is the elementary electric charge, $d\Omega'$ is a solid angle element along the SNM, $f_{\mp} = f_{l^{\mp}}(E, T_{l^{\mp}}) = \{\exp[(E \mp \mu)/T_{l^{\mp}}] + 1\}^{-1}$ is the Fermi-Dirac distribution of CLs (CAs) in initial state, E is the energy of CLs (CAs) in initial state, μ is the CL (CA) chemical potential, $T_{l^{\mp}}$ is the temperature of the matter (CL (CA) gas) before scattering, $f'_{\mp} = f'_{l^{\mp}}(E', T'_{l^{\mp}})$ is the Fermi-Dirac distribution of CLs (CAs) in final state, E' is the energy of a CL (CA) in the final state, $T'_{l^{\mp}}$ is the temperature of the matter (CL (CA) gas) after scattering. Here the plus (minus) sign belongs to CAs (CLs). $p_z(p'_z)$ is the third component of the CL (CA) momentum and $p_{zi}(p'_{zi})$ satisfy the conservation law $p_z + k_z = p'_z + k'_z$.

3 AH of charged leptons and charged antileptons by neutrinos

The AH of CLs and CAs by neutrinos in a SMTP is determined by the expression

$$A = \frac{d\sigma_- - d\sigma_+}{d\sigma_- + d\sigma_+} = \frac{Q_- h_- - Q_+ h_+}{Q_- h_- + Q_+ h_+}, \quad (3)$$

where

$$h_- = f_{l^-}(1 - f'_{l^-}) = \exp[(E'_- - \mu)/T'_{l^-}]/\{\{\exp[(E'_- - \mu)/T'_{l^-}] + 1\}\{\exp[(E_- - \mu)/T_l] + 1\}\}, \quad (4)$$

$$h_+ = f_{l^+}(1 - f'_{l^+}) = \exp[(E'_+ + \mu)/T'_{l^+}]/\{\{\exp[(E'_+ + \mu)/T'_{l^+}] + 1\}\{\exp[(E_+ + \mu)/T_l] + 1\}\}, \quad (5)$$

$T_l = T_{l^{\mp}}$. When $E, E' \gg m_l$ and $\upsilon = p_z/\sqrt{E^2 - m_l^2} \ll 1$, $\upsilon' = p'_z/\sqrt{E'^2 - m_l^2} \ll 1$, in the kinematics $\vartheta' = \pi/2$, $\alpha' = \varphi$ we have for the AH

$$A = \frac{H_{1-}\zeta_-(I_4^2 - 2I_2I_3) + H_{2-}\zeta_+(I_3^2 - 2I_2I_4) - [G_-\zeta(1 + h_0) - G_+(1 - h_0)](1 + \zeta\zeta')I_2^2}{H_{1+}\zeta_-(I_4^2 - 2I_2I_3) + H_{2+}\zeta_+(I_3^2 - 2I_2I_4) - [G_-\zeta(1 - h_0) - G_+(1 + h_0)](1 + \zeta\zeta')I_2^2} \quad (6)$$

where $H_{1\pm} = g_L^2 \pm g_R^2 h_0$, $H_{2\pm} = g_R^2 \pm g_L^2 h_0$, $G_{\pm} = g_L^2 \pm g_R^2$, $g_L = 0.5 + \sin^2\theta_W$ and $g_R = \sin^2\theta_W$ for $\nu_l l$ -scatterings, $g_L = -0.5 + \sin^2\theta_W$, $g_R = \sin^2\theta_W$ for $\nu_i l$ - scatterings ($i \neq l$) $h_0 = h_+/h_-$, $\zeta_{\pm} = (1 \pm \zeta)(1 \pm \zeta')$ and $I_1 = I_{n,n'-1}$, $I_2 = I_{n-1,n'}$, $I_3 = I_{n-1,n'-1}$, $I_4 = I_{n,n'}$ are the Laguerre functions. In the considered kinematics $Q_{\mp}(\vartheta = 0)$ does not contain I_1.

When initial CLs (CAs) have a left-hand circular polarization (LHCP), we obtain for the AH

$$A_- = A(\zeta = -1) = \frac{g_L^2 - g_R^2 h_{0L}}{g_L^2 + g_R^2 h_{0L}} \quad (7)$$

where $h_{0L} = h_{+L}/h_{-L}$, $h_{+L} = h_+(T'_{l^+} = T'_{l^+_L})$, $h_{-L} = h_-(T'_{l^-} = T'_{l^-_L})$.

When initial CLs (CAs) have a right-hand circular polarization (RHCP)($\zeta = +1$) , we obtain for the AH

$$A_+ = A(\zeta = +1) = \frac{g_R^2 - g_L^2 h_{0R}}{g_R^2 + g_L^2 h_{0R}} \tag{8}$$

where $h_{0R} = h_{+R}/h_{-R}$, $h_{+R} = h_+(T'_{l^+} = T'_{l^+_R})$, $h_{-R} = h_-(T'_{l^-} = T'_{l^-_R})$.

4 Numerical estimations

For numerical estimations we consider the NES and the neutrino-positron scattering (NPS). For the transition $n = 1 \to n' = 2$ at the densities $n_0 \sim 10^{30} cm^{-3}$ we obtain $\mu \simeq 25.68 MeV\ (n_0/10^{33} cm^{-3})(10^{15} G/H) \simeq 0.026 MeV$ for the electron (positron) chemical potential. At characteristic temperatures of magnetars ($T \simeq 10^{11} K$) the characteristic energy for electrons (positrons) is $E_\pm \simeq 8.5 MeV$. So, $\mu \ll E_\pm$ and in the considered case the contribution of the electron (positron) number densities of the order of $n_0 \sim 10^{30} cm^{-3}$ can be neglected. However, at the densities $n_0 \sim 10^{33} cm^{-3}$ and $H \sim 10^{15} G$(e.g., $H \simeq 2.15 \times 10^{15} G$) we have $\mu \simeq E'_\pm \simeq 12 MeV$ and the contribution of the electron (positron) number densities of this order is essential. If we suppose $T'_{e^+_L} \simeq 1.4 \times 10^{11} K \simeq 12 MeV$ (for numerical estimations), in the last considered case we obtain $A_- \simeq 0.95$ for $\nu_e e^\pm$ - scatterings. If we suppose $T'_{e^+_R} \simeq 1.4 \times 10^{11} K \simeq 12 MeV$ and consider the same densities and magnetic field strength, we obtain $A_+ \simeq -0.42$ for $\nu_e e^\pm$ - scatterings. For $\nu_i e^\pm$ - scatterings ($\nu_i = \nu_\mu, \nu_\tau$) we obtain $A_- \simeq 0.70$ and $A_+ \simeq 0.50$. Analyses show that when electron neutrinos scatter on electrons and positrons having a LHCP, NES can contribute to the energy balance of the collapsing stellar core $d\sigma_- = 39 d\sigma_+$. When muon (tauon) neutrinos scatter on electrons and positrons having a RHCP, NPS can contribute to the energy balance of he collapsing stellar core more essentially than NES $d\sigma_+ = 2.5 d\sigma_-$. In case of $\nu_i e^\pm$ - scatterings NES can contribute to the energy balance of the collapsing stellar core more essentially than NPS. Within the considered kinematics and conditions and in the limiting case of very high temperature, $T \gg (eH)^{1/2}$, μ, an influence of a medium leads to the constant statistical factors of 1/2 both for CLs and CAs and the AH is determined as $A = (Q_- - Q_+)/(Q_- + Q_+)$. When initial CLs and CAs have a LHCP (RHCP), the AH is

$$A_\mp = \pm \frac{g_L^2 - g_R^2}{g_L^2 + g_R^2}. \tag{9}$$

In the limiting case of very high temperature we have $A_- = -A_+$. It means that the AH is sensitive to neutrino flavor and spin variables of initial CLs and CAs. For $\nu_l l^\pm$ -scatterings $A_{\nu_l l}(\zeta = \mp 1) \simeq \pm 0.82$ and for $\nu_i l^\pm$-scatterings $A_{\nu_i l}(\zeta = \mp 1) \simeq \pm 0.16$. Comparison of the AH for $\nu_l l^\pm$ - and $\nu_i l^\pm$ -scatterings gives $A_{\nu_l l}/A_{\nu_i l} \simeq 5.13$. In case of $\zeta = -1$ we obtain for $\nu_l l^\pm$-scatterings $d\sigma_- \simeq 10 d\sigma_+$. It means that when neutrinos scatter on their charged partners and charged antipartners having a LHCP, NCLS can contribute to the energy balance of the collapsing stellar core more essentially than NCAS. In case of $\zeta = +1$ we obtain for $\nu_l l^\pm$ -scatterings $d\sigma_+ \simeq 10 d\sigma_-$. It means that when neutrinos scatter on their charged partners and charged antipartners having a RHCP, NCAS can contribute to the energy balance of the collapsing stellar core more essentially than NCLS. All these effects

could contribute to the asymmetry of the subsequent explosion of the outer layers of the collapsing stellar core.

5 Conclusions

It is shown that the asymmetry in heating of CLs and CAs by neutrinos in a SMTP is sensitive to neutrino flavor and spin variables of initial CLs and CAs and it also depends on the CL (CA) energy and the medium characteristics. Analyses of the AH show that the dominant contribution to the asymmetry of the subsequent explosion of the outer layers of the collapsing stellar core is determined with the scattering of neutrinos at their charged partners having a LHCP and with the scattering of neutrinos at their charged antipartners having a RHCP. In principle, the formulae describing NCLS and NCAS can formally be applied to neutrino-quark (antiquark) scattering. The obtained result is evidence for the AH of a matter and an antimatter by neutrinos in a SMTP.

Acknowledgments

V. H. and R. G. express their gratitude to Professor A. Efremov for the kind invitation to DSPIN-07 Workshop. V. H. and R. G. are very grateful to the Organizing Committee of the Workshop and the Russian Foundation for Basic Research for supporting them to attend this workshop.

References

[1] V. G. Bezchastnov and P. Haensel, Phys. Rev. D 54, 3706 (1996).

[2] V. A. Guseinov, I. G. Jafarov, and R. E. Gasimova, Phys. Rev. D 75, 073021 (2007).

TENSOR MAGNETIC POLARIZABILITY OF THE DEUTERON IN STORAGE-RING EXPERIMENTS

A.J. Silenko[1†]

(1) *Institute of Nuclear Problems, Belarusian State University, Minsk, Belarus*
† *E-mail: silenko@inp.minsk.by*

Abstract

It was previously shown that the tensor magnetic polarizability of the deuteron causes the spin rotation with two frequencies and experiences beating for polarized deuteron beams in storage rings. We confirm an existence of this effect and derive general formulae describing deuteron spin dynamics. It is found that an initially tensor polarized deuteron beam can acquire a final horizontal vector polarization of order of 1%. This effect allows to measure the tensor magnetic polarizability of the deuteron in storage-ring experiments.

1 Introduction

Tensor electric and magnetic polarizabilities defined by spin interactions of nucleons are important parameters of deuteron and other nuclei. In particular, measurement of tensor polarizabilities of the deuteron gives an important information about spin-dependent nuclear forces. For polarized deuteron beams in storage rings, main effects caused by the tensor polarizabilities have been investigated by Baryshevsky *et al.* [1,2]. The tensor magnetic polarizability, β_T, conditions the spin rotation with two frequencies instead of one and therefore occasions beating with the frequency proportional to β_T [1,2]. We confirm the existence of this effect and carry out a detailed calculation of deuteron spin dynamics in storage rings. We use the matrix Hamiltonian obtained in Ref. [3] and derive general formulae describing an evolution of spin wave function. It is shown that an initially tensor polarized deuteron beam can acquire a final horizontal vector polarization of order of 1%. This effect makes it possible to measure the tensor magnetic polarizability of the deuteron in storage-ring experiments.

The system of units $\hbar = c = 1$ is used.

2 Hamiltonian approach in the method of spin amplitudes

The method of spin amplitudes uses quantum mechanics formalism to more easily describe spin dynamics. Vector and tensor polarization of particles/nuclei with spin $S \geq 1$ are specified by the unit polarization vector $\boldsymbol{P}$ and the polarization tensor P_{ij}.

The nontrivial spin dynamics predicted in Refs. [1, 2] and conditioned by the tensor electric and magnetic polarizabilities of the deuteron is a good example of importance of spin tensor interactions in the physics of polarized beams in storage rings. To describe tensor interactions of deuteron with the method of spin amplitudes, one should use

three-component spinors and 3×3 matrices. The method of spin amplitudes is mathematically advantageous because transporting the three-component spinor is much simpler than transporting the three-dimensional polarization vector $\boldsymbol{P}$ and five independent components of the polarization tensor P_{ij} together.

We follow the traditional quantum mechanical approach [4] and use the matrix Hamilton equation [3]. A determination of spin dynamics can be divided into several stages, namely, (i) a solution of the Hamilton equation and a determination of eigenvalues and eigenvectors of the Hamilton matrix H, (ii) a derivation of spin wave function consisting in a solution of a set of three linear algebraic equations, (iii) a calculation of time evolution of polarization vector and polarization tensor.

3 Dynamics of deuteron spin in storage rings

Correction to the Hamilton operator for the deuteron polarizabilities contains scalar and tensor parts. The scalar part is spin-independent and can be disregarded. The general form of the matrix Hamiltonian H has been found in Ref. [3]. The matrix Hamiltonian defining the deuteron spin dynamics in a uniform magnetic field takes the form

$$H = \begin{pmatrix} E_0 + \omega_0 + \mathcal{A} + \mathcal{B} & 0 & \mathcal{A} \\ 0 & E_0 + 2\mathcal{A} & 0 \\ \mathcal{A} & 0 & E_0 - \omega_0 + \mathcal{A} + \mathcal{B} \end{pmatrix}, \tag{1}$$

where [3]

$$\mathcal{A} = -\tfrac{1}{2}\alpha_T B_z^2 \gamma \beta^2, \quad \mathcal{B} = -\beta_T B_z^2 \gamma, \tag{2}$$

ω_0 is the angular frequency of spin rotation (g−2 frequency), E_0 is the zero energy level, α_T is the tensor electric polarizability, $\beta = v/c$ is the normalized velocity, B_z is the vertical magnetic field, and γ is the Lorentz factor. The nondiagonal components in Eq. (1) are nonresonant and can be disregarded because their average effect on the rotating spin is zero. Eq. (1) shows that not only does the tensor magnetic polarizability affect the deuteron spin in the horizontal plane but also the tensor electric polarizability.

The connection between spin amplitudes and components of polarization vector and polarization tensor is given by Eq. (44) in Ref. [3]. If the deuteron beam is vector polarized and the direction of its polarization is characterized by the spherical angles θ and ψ, the general equation defining the evolution of deuteron polarization has the form

$$P_\rho(t) = \sin\theta\cos\left(\omega_0 t + \psi\right)\cos\left(bt\right) - \sin\theta\cos\theta\sin\left(\omega_0 t + \psi\right)\sin\left(bt\right),$$
$$P_\phi(t) = \sin\theta\sin\left(\omega_0 t + \psi\right)\cos\left(bt\right) + \sin\theta\cos\theta\cos\left(\omega_0 t + \psi\right)\sin\left(bt\right),\ P_z(t) = P_z(0),$$

where

$$b = \mathcal{B} - \mathcal{A} = -\left(\beta_T - \frac{1}{2}\alpha_T\beta^2\right) B_z^2 \gamma. \tag{3}$$

Eqs. (3),(3) show the tensor polarizabilities of the deuteron cause the spin rotation with two frequencies $\omega_0 \pm b$ instead of ω_0 and therefore experience beating with the frequency $\Delta\omega = -2b$. Thus, these equations confirm the conclusion given by Baryshevsky *et al.* [1, 2]. However, Eq. (3) displays that the spin rotation is also affected by the tensor electric polarizability. While the effect predicted in Refs. [1, 2] is not negligible, its observation is a very difficult problem. There are three independent theoretical predictions

for the value of the tensor electric polarizability of deuteron, namely $\alpha_T = -6.2 \times 10^{-41}$ cm^3 [5], -6.8×10^{-41} cm^3 [6], and 3.2×10^{-41} cm^3 [7]. Two first values are very close to each other but they do not agree with the last result. The theoretical estimate for the tensor magnetic polarizability of deuteron is $\beta_T = 1.95 \times 10^{-40}$ cm^3 [5, 6]. Duration of measurement t is restricted by the spin coherence time τ. If we base our estimate on the values corresponding to the planned deuteron electric-dipole-moment experiment in storage rings [8] ($\gamma = 1.28,\ \beta = 0.625,\ \tau \sim 1000$ s, and $B_z = 3$ T), $b \sim 10^{-5}$ s^{-1} and $bt \lesssim 10^{-2}$. In this case, systematical errors caused by betatron oscillations, field defects and misalignments of magnets can appreciably exceed small perturbations of spin rotation conditioned by the deuteron tensor polarizabilities.

We propose the significant improvement of precision of a possible experiment. Measurement of the effect can be strongly simplified with the use of a *tensor-polarized* deuteron beam. If the initial vector polarization of such a beam in zero, any interactions of the magnetic moment of deuteron with external fields cannot lead to the appearance of vector polarization. Therefore, nonzero vector polarization of the beam can be conditioned by nothing but the tensor interactions. The initial tensor polarization can correspond to a zero projection of the deuteron spin onto the preferential direction. When this direction is defined by the spherical angles θ and ψ, the time dependence of the polarization vector has the form

$$P_\rho(t) = 2 \sin\theta \cos\theta \sin(\omega_0 t + \psi) \sin(bt),$$
$$P_\phi(t) = -2 \sin\theta \cos\theta \cos(\omega_0 t + \psi) \sin(bt), \quad P_z(t) = 0.$$

The final vector polarization is horizontal. Spin dynamics can be easily calculated for any other initial tensor polarization of the deuteron beam.

Eq. (4) shows the possibility of measurement of the quantity b in storage ring experiments. The final vector polarization of the beam is of order of 1%.

4 Discussion and summary

The presented analysis confirms the results obtained by Baryshevsky *at al.* [1, 2]. It is shown that the predicted rotation of the deuteron spin with two frequencies and beating in a uniform magnetic field are conditioned not only by the tensor magnetic polarizability but also by the tensor electric polarizability. Nevertheless, the latter quantity gives a minor contribution to the effect. If experimental conditions correspond to the planned deuteron electric-dipole-moment experiment in storage rings [8] ($\beta^2 = 0.4$) and theoretical estimates for the tensor polarizabilities of the deuteron given in Refs. [5–7] are used, the expected relative importance of β_T is one order of magnitude greater.

Unfortunately, the expected spin coherence time (about 1000 s [8]) is too short to register beating. In this case, systematical errors can prevent observation of small perturbations of spin rotation conditioned by the tensor polarizabilities of the deuteron. Possibly, the effect predicted in Refs. [1, 2] may be discovered with the use of a Penning trap being a mini-cyclotron. The Penning trap provides much longer duration of measurement.

The precision of a possible storage-ring experiment can be significantly improved, if the deuteron beam is tensor polarized. If the initial vector polarization of such a beam in zero, any interactions linear in the spin cannot lead to the appearance of vector polarization. The final vector polarization cannot also result from the betatron oscillations,

field defects, misalignments of magnets and other potential sources of systematical errors. Therefore, the tensor interaction of spin with the magnetic field defined by Eqs. (1),(2), and (3) is the only reason of nonzero vector polarization of the beam. Eq. (4) shows the beam can acquire the final horizontal vector polarization of order of 1%. The known experimental methods [9] permit safe measuring such a polarization and therefore determining the tensor magnetic polarizability of the deuteron. In addition, the observation of the predicted effect would prove an importance of taking into account spin-tensor interactions in storage ring physics. Since Eq. (3) contains both tensor polarizabilities, the tensor electric polarizability of the deuteron can also be measured in the proposed experiment. For this purpose, the obtained precision of polarization measurements should be significantly improved. The experiment should be performed with different values of the beam momentum (and the vertical magnetic field) on the same ring. In this case, both tensor polarizabilities of the deuteron can be determined. Another method of determination of the deuteron's tensor electric polarizability has been proposed in Ref. [3]. The use of the Penning trap in experiments with tensor-polarized deuterons can also be helpful for measuring the tensor polarizabilities.

Acknowledgements The author is grateful to V.G. Baryshevsky for bringing the considered problem to his attention, helpful discussions and comments. This work was supported by the Belarusian Republican Foundation for Fundamental Research.

References

[1] V. G. Baryshevsky, A. A. Gurinovich, hep-ph/0506135.

[2] V. G. Baryshevsky, hep-ph/0510158, hep-ph/0603191.

[3] A. J. Silenko, Phys. Rev. C **75**, 014003 (2007).

[4] R. P. Feynman, R. B. Leighton, M. Sands, *The Feynman Lectures on Physics. V. 2* (Addison-Wesley, Reading, MA, 1963).

[5] J.-W. Chen, H. W. Grießhammer, M. J. Savage, R. P. Springer, Nucl. Phys. A **644**, 221 (1998).

[6] X. Ji, Y. Li, Phys. Lett. B **591**, 76 (2004).

[7] J. L. Friar and G. L. Payne, Phys. Rev. C **72**, 014004 (2005).

[8] Y. F. Orlov, W. M. Morse, and Y. K. Semertzidis, Phys. Rev. Lett. **96**, 214802 (2006).

[9] L.S. Azhgirey *et al.*, Pisma Fiz. Elem. Chast. Atom. Yadra **2**, 91 (2005) [Phys. Part. Nucl. Lett. **2**,122 (2005)]; D. Chiladze *et al.*, Phys. Rev. ST Accel. Beams **9**, 050101 (2006).

WORKSHOP SUMMARY

Jacques Soffer

Department of Physics, Temple University,
Philadelphia, Pennsylvania 19122-6082, USA
E-mail: jsoffer@temple.edu

Abstract

During the five days of this workshop we had forty five hours of lectures, so a tremendous amount of new information was delivered. I will be able only to highlight some aspects of the numerous interesting topics, which were discussed, leaving out many of them.

5 Introduction

Let me first begin to say that, given the high density of the scientific program, I had to make a drastic selection and I apologize to the speakers, not or badly, mentioned in this summary. This is partly due to the lack of time and partly to my unability to "'digest"' quickly enough, all this new information. I will not touch technical talks because it is not my field. Fortunately, missing material can be found in these proceedings, collecting all the write-ups of the presentations.

From what we heard, it is amazing to realize that spin has some relevance all over the places, in a vast energy range from 100 MeV up to several TeV and in very many different collision processes, namely e^+e^-, $e^\pm p$, $\mu^\pm p$, νp, pp, etc...It is involved in numerous experiment facilities like, for example, RARF, CLAS, HERMES, HERA, COMPASS, BELLE, RHIC, etc....One notices also that significant advances have been achieved recently in polarized beams and targets, allowing to reach higher precision in the new measurements. New projects are under way, which I will just mention: in FAIR at GSI, the PANDA detector has a broad physics program to study QCD with antiprotons, at Protvino, U70 is preparing a new polarization program, as well as here in Dubna with the Nuclotron-M. On the theory side, the terminology used is also very rich since one has currently to decode the following sets of initials, PDF, GPD, TMD, DVCS, DIS, SIDIS, DGLAP, BFKL, NLO, NNLO, HT, SSA, etc...

Once more, it was clear at this meeting that substantial progress emerge whenever experiment and theory are "'talking to each other"'. I will try to find the right balence between new experimental results and recent theoretical developments, which have most impressed me, but it was a rather difficult exercise.

6 COMPASS Festival

The COMPASS experiment at the CERN SPS has undertaken a vast experimental program focused on the nucleon spin structure via deep-inelastic scattering (DIS) of 160 GeV polarized muons on polarized nucleons. They have obtained very precise results in two kinematic ranges, $Q^2 < 1$ GeV^2 and $0.0005 < x < 0.02$, as well as $1 < Q^2 < 100$ GeV^2 and

$0.004 < x < 0.7$, for the spin-dependent structure function g_1^d, by measuring the longitudinal photon-deuteron asymmetry A_1^d, with a polarized deuteron target. This asymmetry, shown in Fig. 1 (Left), is compatible with zero over the small x range and this indicates a strong cancellation between the polarization of the different sea quarks. For large x the asymmetry is large and positive, in agreement with earlier data from SMC and HERMES. They have also discussed the results of a global QCD fit at next-to-leading order (NLO), to the world data on g_1, which, unfortunately, does not lead to a unique determination of the gluon polarization ΔG.

Another interesting subject is the evaluation of the polarized valence quark distributions $\Delta u_v(x) + \Delta d_v(x)$. The analysis is based on the asymmetry difference $A^{(h^+ - h^-)}$, for hadrons of opposite charges and it gives direct access to the valence quark helicity distributions, as the fragmentation functions do cancel out. The results, shown in Fig. 1 (Right), provide information on the contribution of the sea quarks to the nucleon spin. They favour an asymmetric scenario for the sea polarization, $\Delta\overline{u} = -\Delta\overline{d}$, at a confidence level of two standard deviations, in contrast to the usual symmetric assumption, $\Delta\overline{u} = \Delta\overline{d} = \Delta\overline{s} = \Delta s$. However, the statistical errors are still large and do not allow yet a definite conclusion.

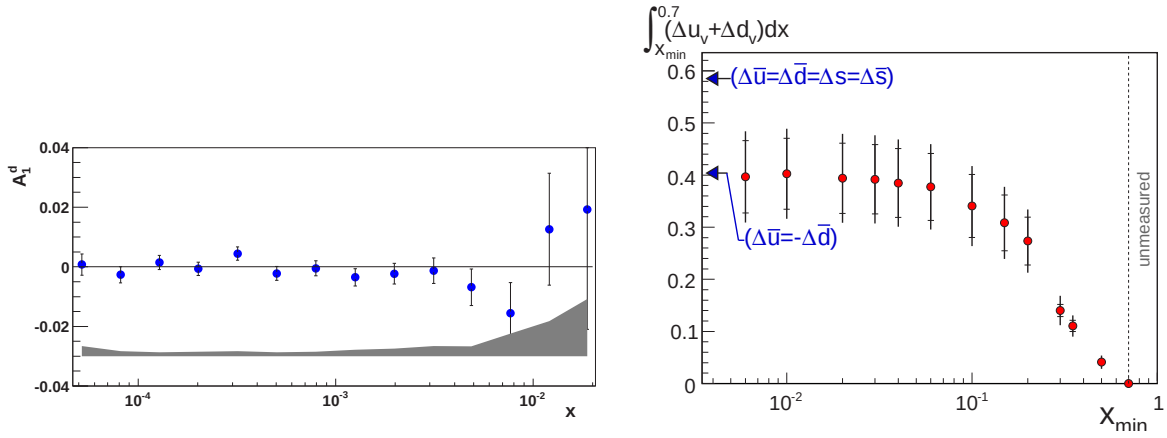

Figure 1: On the left the asymmetry $A_1^d(x)$ for quasi-real photons ($Q^2 < 1$ GeV^2), as a function of x. On the right the integral of $\Delta u_v(x)+\Delta d_v(x)$ over the range $0.006 < x < 0.7$, as the function of x minimum, evaluated at $Q^2 = 10$ GeV^2. (Taken from Santos's talk.)

The last relevant topic is the gluon polarization $\Delta G/G$, which is essential to clarify the spin structure of the nucleon. Since it is impossible to rely on an extraction based on the QCD evolution of the polarized structure functions, COMPASS has chosen to get a direct determination of this quantity, from the measurement of double spin asymmetries in the scattering of polarized muons off a polarized deuteron target.

Three different channels sensitive to the gluon distribution are being explored: open charm production and high transverse momentum (high-p_T) production, in either the quasi-real (virtuality $Q^2 < 1$ GeV^2) photoproduction or the DIS ($Q^2 > 1$ GeV^2) regimes. The first method was described by Y. Bedfer and a preliminary analysis, bearing 2002-2004 data, gives:

$$\Delta G/G = -0.57 \pm 0.41(stat.) \pm 0.17(syst.) \quad \text{at } x_g = 0.15 \pm 0.08 \quad \text{and } \mu^2 = 13\, GeV^2.$$

In his presentation K. Klimaszewski discussed the high-p_T events and reported that the analysis of combined data from years 2002-2004 leads to a more precise preliminary result: $\Delta G/G = 0.016 \pm 0.058(stat.) \pm 0.055(syst.)$. The results of COMPASS and from other experiments are shown on Fig. 2 and they definitely favor a low value of $\Delta G/G$.

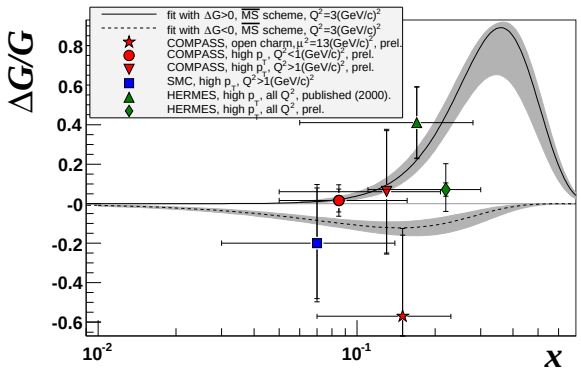

Figure 2: Comparison of the $\Delta G/G$ measurements from various experiments. (Taken from Bedfer's talk.)

7 HERMES Festival

The HERMES experiment at DESY has obtained new results in different area, which were introduced in the talk of S. Belostotski. From the analysis of high-p_T hadron production, they got the following estimate $\Delta G/G = 0.078 \pm 0.034(stat.) \pm 0.011(syst.)$, with a theoretical uncertainty of ~ 0.1. Polarized inclusive DIS is also used to determine $\Delta\Sigma$, the quark contribution to the nucleon spin, and under some reasonable assumptions, they reported $\Delta\Sigma = 0.330 \pm 0.025(exp.) \pm 0.011(theor.) \pm 0.028(evol.)$. Flavor separation for the quark helicity distributions has been achieved from semi-inclusive DIS data and, in particular, one gets $(\Delta s + \Delta\bar{s}) = -0.085 \pm 0.013(theor.) \pm 0.008(exp.)$, by means of $K^{\pm}$ production, which is a preliminary result.

Azimuthal asymmetries were measured in the semi-inclusive production of pions and kaons and HERMES has collected data with a transversely polarized hydrogen target from 2002 to 2005. The polarized part of the semi-inclusive cross section, for unpolarized beam (U) and a transversely polarized target (T), has contributions from both the Collins and Sivers mechanisms. These asymmetries provide information on the quark Collins fragmentation and Sivers distribution functions. These mechanisms produce a different dependence of the azimuthal asymmetry on the two angles ϕ and ϕ_S, so one can use the variation of ϕ and ϕ_S to disentangle the two contributions experimentally. The extracted Collins and Sivers asymmetries for charged pions and kaons, are presented in Fig. 3, as a function of x, z, and $P_{h\perp}$. The average Collins amplitude is positive for π^+ and negative for π^-. This is expected if the transversity distribution h_1^u is positive and h_1^d is negative, like for the helicity distributions. However, the magnitude of the π^- asymmetry appears to be as large as the π^+ one, which was unexpected. The average Sivers asymmetry are significantly positive for π^+ and K^+ and consistent with zero for π^- and K^-. Note that the Sivers asymmetry for K^+ is in the region of $x \approx 0.1$, by a factor 2.3 ± 0.3, higher in magnitude than the asymmetry for π^+.

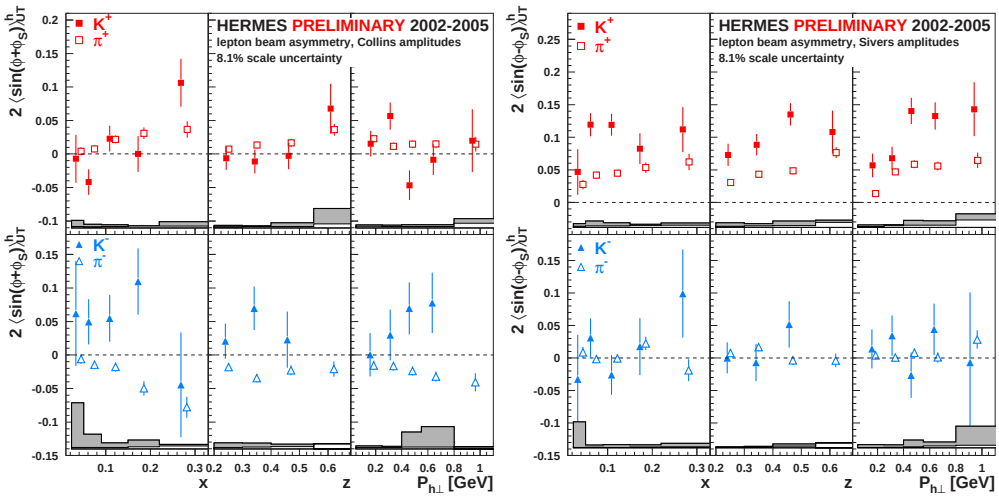

Figure 3: Collins (left) and Sivers (right) asymmetries for charged pions and kaons, (as labelled) as a function of x, z, and $P_{h\perp}$. (Taken from Korotkov's talk.)

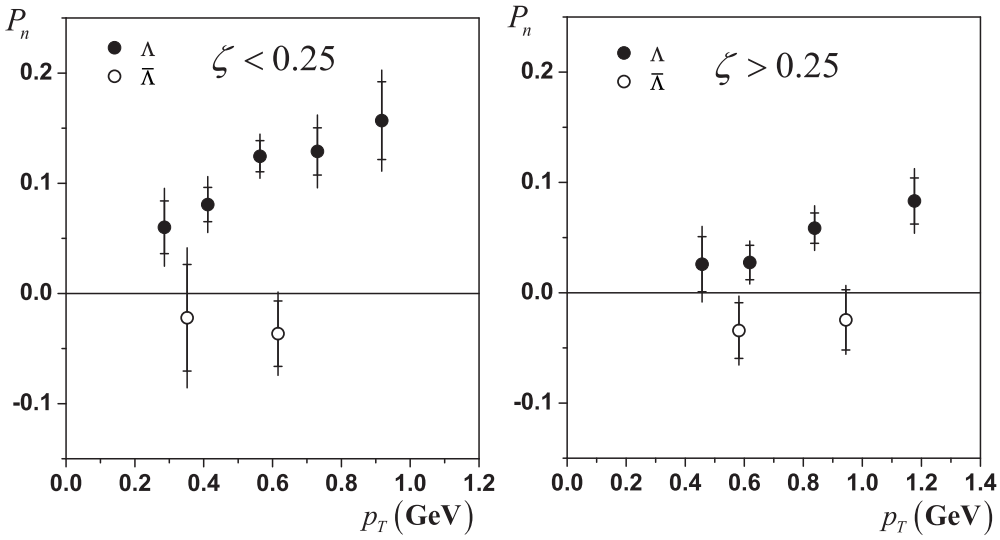

Figure 4: Transverse polarization P_n^{Λ} and $P_n^{\bar{\Lambda}}$ as function of p_T for the region $\zeta < 0.25$ (left) and $\zeta > 0.25$ (right). (Taken from Veretennikov's talk.)

Transverse Λ and $\bar{\Lambda}$ polarization and spin transfer from longitudinally polarized target have been measured in the HERMES experiment. The kinematic variables are p_T and $\zeta \equiv (E_\Lambda + p_z^\Lambda)/(E_e + p_e)$, where p_T is the transverse momentum with respect to the (lepton) beam, E_Λ and p_z^Λ are the energy and z-component of the Λ momentum (the z-axis is along the lepton beam direction) and E_e, p_e are the energy and momentum of the positron beam. In Fig. 4, the transverse Λ and $\bar{\Lambda}$ polarizations are shown versus p_T for two kinematical domains $\zeta < 0.25$ and $\zeta > 0.25$. The Λ polarization rises linearly with p_T with higher slope for $\zeta < 0.25$ and the $\bar{\Lambda}$ polarization is consistent with zero.

8 Belle, BNL and JLab Festival

We had a very instructive talk by M. Grosse Perdekamp on the analysis of hadronic events in e^+e^- annihilation at KEK by the Belle Collaboration. He presented the data on the azimuthal asymmetries between two hadrons produced in the fragmentation of a quark-antiquark pair, $e^+e^- \to q\bar{q} \to h_1h_2 + X$. The analyses demonstrated that the results on the Collins fragmentation functions from HERMES and Belle experiments are perfectly compatible. Using these Collins functions the first extraction of the transversity distributions $h_1^u(x)$ and $h_1^d(x)$ was achieved.

The RHIC spin program at BNL, underway since 2001, has been presented by G. Bunce. It consists of colliding polarized protons to study the spin structure of the proton. For 2006 they have achieved high luminosity collisions at $\sqrt{s}$=200 GeV, with 55 to 60% polarization and performed sensitive measurements on the gluon polarization. Lower p_T production of π^0 or jets is dominated by the gluon-gluon graph, and the double helicity asymmetry A_{LL} at mid-rapidity is essentially quadratic in the gluon polarization. At higher p_T, the quark-gluon graph dominates, and A_{LL} is linear in the gluon polarization. The data for A_{LL} for jet production, obtained by the STAR collaboration, was presented by J. Dunlop. It is displayed in Fig. 5 and indicates little or no gluon polarization in the measured region, which corresponds to a gluon momentum fraction of x_{gluon} from about 0.02 to 0.3. Fig. 5 shows also preliminary results from the BRAHMS experiment for charged pion transverse spin asymmetries, at $\sqrt{s}$=62 GeV. The asymmetries at 62 GeV are very large, and significantly larger than the asymmetries at 200 GeV. At this energy, STAR has also measured a remarkable asymmetry for π^0 production, which increases with x_F, for positive x_F and is consistent with zero for negative x_F. A very exciting direction for the transverse spin program is connecting semi-inclusive DIS and RHIC results. G. Bunce recalled that the final state interaction needed to generate the asymmetry of DIS and the corresponding initial state interaction of Drell-Yan, have different color interactions, giving in general an attractive force for DIS and a negative force for Drell-Yan, resulting in opposite sign transverse spin asymmetries. This unique prediction of gauge theory

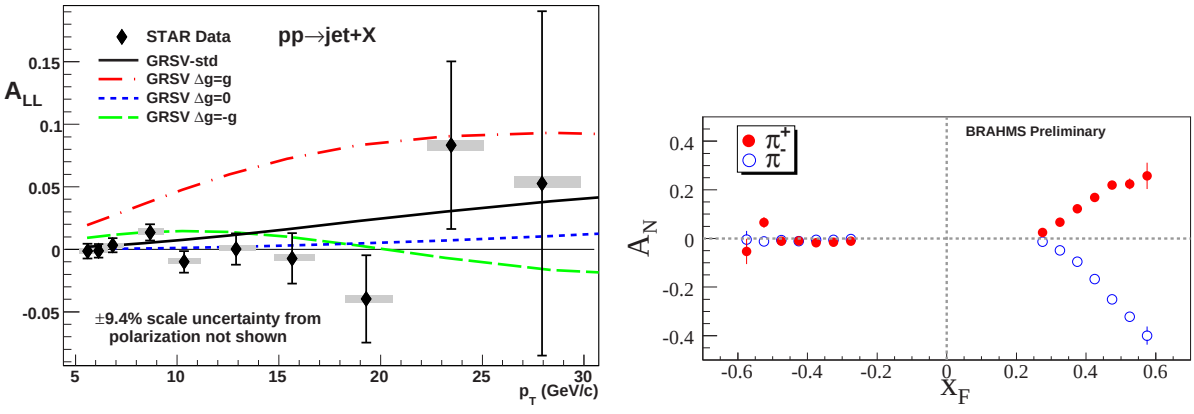

Figure 5: Left: Double helicity asymmetry A_{LL} for inclusive jet production at $\sqrt{s}$ = 200 GeV versus p_T of the jet from the STAR experiment. (Taken from Dunlop's talk.) Right: A_N versus x_F for inclusive production of charged pions, at $\sqrt{s}$=62 GeV, preliminary data from 2006, from the BRAHMS experiment. (Taken from Bunce's talk.)

must be checked and this will be done at RHIC.

The CLAS collaboration at Jefferson Lab is pursuing a wide program of measurements with polarized electrons incident on polarized proton and deuteron targets, which was partially covered in the talk of G. Dodge. It involves inclusive, semi-inclusive and exclusive inelastic scattering over a wide kinematical range in momentum transfer Q^2. The data are consistent with the expectation that the A_1 asymmetry should approach 1 as $x \to 1$ and they find that $\Delta d/d$ remains negative up to $x = 0.6$, consistent with results from Hall A using a ^{3}He target. They also studied the onset of quark-hadron duality in spin structure functions. Quark-hadron duality refers to the observation that the unpolarized structure function F_2, in the resonance region, averages to the smooth scaling curve for F_2 at high Q^2. In Fig. 6 one displays xg_1 for the proton and deuteron as a function of x for various Q^2 bins. The high Q^2 "scaling" curve is shown by the hatched area and indicates the range of xg_1 given by PDF fits. At low Q^2 one can see that the data are negative in the region of the $\Delta(1232)$ resonance, as expected for a spin 3/2 excitation. However, as Q^2 increases and the $\Delta(1232)$ loses strength, the resonances do indeed appear to oscillate about the scaling curve.

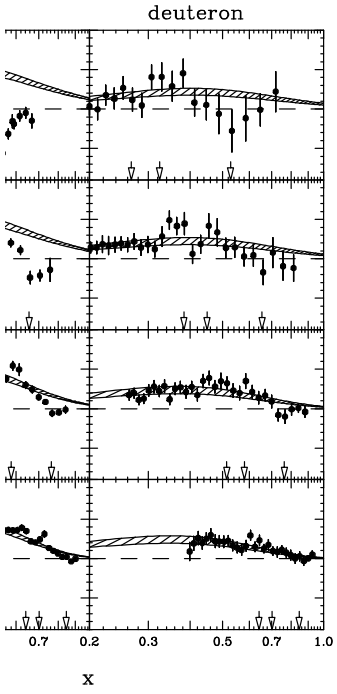

Figure 6: CLAS data for xg_1 in several bins of Q^2 for the proton (left) and deuteron, per nucleon (right). (Taken from Dodge's talk.)

9 GPD Festival

Generalized Parton Distributions (GPD), introduced 10 years ago, is a powerful tool which offers a way to unify two pictures of the nucleon, disconnected so far, on the one hand the PDF's $f(x, Q^2)$, obtained from DIS, and on the other hand the nucleon form factors $F(t)$, obtained from ep elastic scattering. The GPD's provide a three-dimensional picture of the nucleon and therefore a more detailed information on its partonic structure, designated "'nucleon tomography"' by N. d'Hose. One hopes to gain some insight on the localization of partons inside the nucleon and to access to their orbital angular momentum L_q, as first suggested by X. D. Ji. GPD's can be extracted experimentally through the measurement of hard exclusive reactions, the cleanest one is the Deeply Virtual Compton Scattering (DVCS)(or meson production), shown on the left of Fig. 7. In the reaction $ep \to e'\gamma p$, the Bethe-Heitler (BH) process on the right of Fig. 7, dominates over DVCS in most of the kinematic region. However, measurable asymmetries in beam spin and beam charge arise from the interference of both processes. The beam spin asymmetry is proportional to the imaginary part of the DVCS amplitude, while the beam charge asymmetry is proportional to the real part of the DVCS amplitude and both asymmetries can be expressed in terms of GPD's. Several models are emerging and predictions made

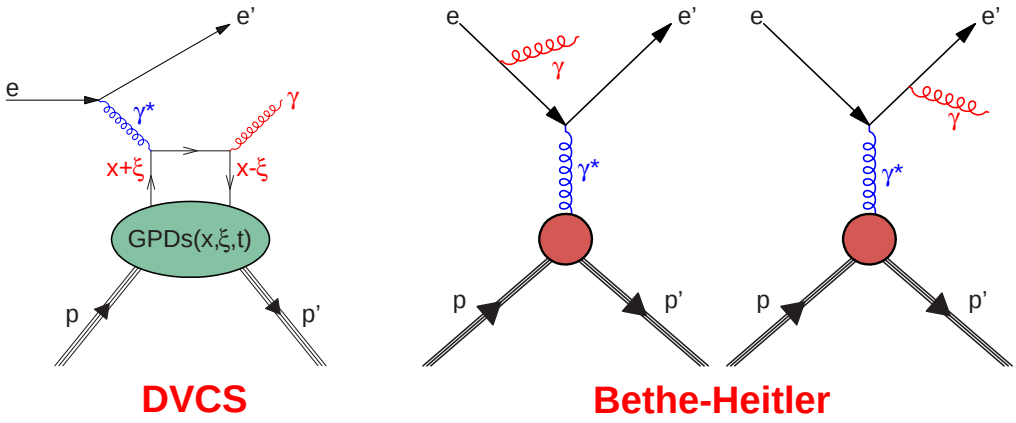

Figure 7: Feynman graphs of DVCS (left) and Bethe-Heitler (right) processes. Both processes lead to the same final state, therefore their amplitudes can interfere. (Taken from Vilardi's talk.)

from lattice QCD for the first moments of the nucleon GPD's confirm that the transverse size of the nucleon depends significantly on the momentum fraction x. The kinematical domain accessible in COMPASS and its availability of positive and negative polarized muons gives it a major opportunity to measure the different configurations of charge and spin of the beam, as explained by N. d'Hose.

Finally, let us mention the results presented by A. Borissov on exclusive diffractive production of light vector mesons (ρ^0 and ϕ) on Hydrogen and Deuterium targets, measured by HERMES in the kinematic region $0.5 < Q^2 < 7$ GeV^2 and $3.0 < W < 6.3$ GeV. Data for the Q^2 and W dependences of longitudinal cross sections and spin density matrix elements are in fair agreement with GPD calculations based on the 'handbag factorization'. This model was presented by S. Goloskokov and it seems to work well up to HERA energies.

10 Theory Festival

Several talks were devoted to single spin asymmetries and their connection to the Sivers and Collins effects, which generate the most sizeable single spin asymmetries (SSA) in semi-inclusive deep-inelastic scattering (SIDIS) with transverse target polarization, as already mentioned above. In his talk A. Efremov gave our present understanding of these phenomena. Within some uncertainties it was found that the SIDIS data from HERMES and COMPASS, on the Sivers and Collins SSA from different targets, are in agreement with each other and with Belle data on azimuthal correlations in e^+e^--annihilations. At the present stage of the art, large-N_c predictions for the flavour dependence of the Sivers function are compatible with data, and provide useful constraints.

The global analysis of HERMES, COMPASS and Belle data reported by A. Prokudin is leading to the extraction of favoured and unfavoured Collins fragmentation functions and the unknown transversity distributions for u and d quarks, $h_1^u(x)$ and $h_1^d(x)$. They turn out to be opposite in sign, with $|h_1^d(x)|$ smaller than $|h_1^u(x)|$, and both are smaller than their corresponding Soffer bound. This is just a first step for extracting transversities, as noticed by M. Wakamatsu, who carried out a comparative analysis of the transversities and the longitudinally polarized PDF's. He concluded that a complete understanding

of the spin dependent fragmentation mechanism is mandatory for getting more definite knowledge of the transversities and that some independent determination of transversities is highly desirable, for example, through double transverse spin asymmetry in Drell-Yan processes.

O. Teryaev recalled that twist-three quark-gluon correlators were proposed long ago to explain non-zero SSA and he presented some arguments to establish a relation between the Sivers function and these twist-three matrix elements. As a result, the Sivers mechanism may be applied at large momentum transfer. It is also possible to find some connection between Sivers function and GPD.

D. Sivers discussed chiral dynamics and introduced the concept of spin-directed momentum transfer from the measurement of a parity-conserving SSA.

In his talk, A. Sidorov studied the impact of the CLAS and latest COMPASS data on the polarized parton densities and higher twist (HT) contributions. It was demonstrated that the inclusion of the low Q^2 CLAS data in the NLO QCD analysis of the world DIS data improves essentially our knowledge of HT corrections to g_1 and does not affect the central values of PDF's. However the large Q^2 COMPASS data influence mainly the strange quark and gluon polarizations, but practically do not change the HT corrections. The uncertainties in the determination of polarized parton densities is significantly reduced due to both data sets and he concluded that it is impossible to describe the very precise CLAS data, if the HT corrections are not taken into account.

B. Ermolaev presented a description of spin structure function g_1 at arbitrary x and Q^2. It is known that the extrapolation of DGLAP to the very small-x involves necessarily the singular fits for the initial parton densities without any theoretical basis. On the contrary, according to B. Ermolaev, the resummation of the leading logarithms of x is the straightforward and most natural way to describe g_1 at small x. Combining this resummation with the DGLAP results leads to the expressions for g_1 which can be used at large Q^2 and arbitrary x, leaving the initial parton densities non-singular.

The talk presented by X. Artru contains two parts. In the first one, he recalls that positivity restrains the allowed domains for pairs or triples of spin observables in polarized reactions, some of which having non-trivial shapes. Various domain shapes in reactions of the type $1/2 + 1/2 \to 1/2 + 1/2$ are displayed and some methods to determine these domains are mentioned. The second part deals with classical and quantum constraints in spin physics, from both discrete symmetries and positivity.

Finally, A. A. Pankov considered the e^+e^- International Linear Collider (ILC) to study four-fermion contact interactions in fermion pair production process $e^+e^- \to \bar{f}f$ and he stressed the role played by the initial state polarization, to increase the potentiality of this future machine to discover new phenomena.

Acknowledgements. I would like to thank Konrad Klimaszewski for a serious technical help to prepare this talk. I am grateful to the organizers of DSPIN07, for their invitation to this conference dedicated to L.I. Lapidus, I had the great privilege to meet several times. My special thanks go also to Prof. A.V. Efremov for providing a full financial support and for making, once more, this meeting so successful.

List of participants of DSPIN-07

Name (Institution, Town, Country)	E-mail address
1. **Abramov Victor** (IHEP, Protvino, Russia)	Victor.AbramovATihep.ru
2. **Alekseev Igor** (ITEP, Moscow, Rus.)	igor.alekseevATitep.ru
3. **Alexakhin Vadim** (JINR, LPP, Dubna, Russia)	alexATsunse.jinr.ru
4. **Alikhanov Ibragim** (St. Petersburg State Univ., Russia)	ialspbuATyandex.ru
5. **Artru Xavier** (Inst.Phys.Nucl.&Univ. Lyon -1, France)	x.artruATipnl.in2p3.fr
6. **Azhgirey Leonid** (JINR, LPP, Dubna, Russia)	azhgireyATjinr.ru
7. **Bedfer Yann** (CEA, Gif/Yvette, France)	Yann.BedferATcern.ch
8. **Belostotski Stanislav** (PNPI, Gatchina, Russia)	belostotATmail.desy.de
9. **Bogdanov Aleksei** (MEPI, Moscow Russia)	Asp9702ATnm.ru
10. **Borissov Alexander** (DESY, Hamburg, Germany)	borissovATifh.de
11. **Brona Grzegorz** (Univ. of Warsaw, Poland)	Grzegorz.BronaATfuw.edu.pl
12. **Bunce, Gerry** (BNL, Brookhaven, USA)	bunceATbnl.gov
13. **Burinskii Alexander** (NSI, Moscow, Russia)	burATibrae.ac.ru
14. **Chen Ye**(Shandong Univ. China)	yerchenATmail.sdu.edu.cn
15. **Cherednikov Igor** (JINR, Dubna, Russia)	igor.cherednikovATjinr.ru
16. **Chernitskii Alexander** (Uni.Eng.&Econ., S.Petersburg, Russia)	Alexandr.chernitskiiATengec.ru
17. **ChetvertkovaVera** (MSU, Moscow, Russia)	tcheATrambler.ru
18. **Christova Ekaterina** (Inst.Nucl.Res.&Nucl.En., Sofia, Bulgaria)	echristoATinrne.bas.bg
19. **Crabb Donald G.** (Univ. of Virginia, Charlottesville, USA)	dgc3qATgalileo.phys.virginia.edu
20. **d'Hose Nicole** (CEA Saclay, France)	nicole.dhoseATcea.fr
21. **Dodge Gail** (Old Dominion Univ. Norfolk, USA)	dodgeATphysics.odu.edu
22. **Dorokhov Alexander** (JINR, Dubna, Russia)	DorokhovATtheor.jinr.ru
23. **Dunlop James** (BNL, Brookhaven, USA)	dunlopATbnl.gov
24. **Efremov Anatoly** (JINR, Dubna, Russia)	efremovATtheor.jinr.ru
25. **Ermolaev Boris** (Ioffe PTI, St. Petersburg, Russia)	boris.ermolaevATcern.ch
26. **Filatov Yury** (JINR, Dubna, Russia)	yuriifilatoffATmail.ru
27. **Finger Miroslav** (JINR, Dubna, Russia)	fingerATnusun.jinr.ru
28. **Finger Michael** (JINR, Dubna, Russia)	michael.fingerATcern.ch
29. **Gasimova Rasmiyya** (Nakhchivan Univ Azerbaijan)	GasimovarATyahoo.co.uk
30. **GerasimovSergo** (JINR, Dubna, Russia)	gerasbATtheor.jinr.ru
31. **Ginzburg Ilja** (IMSBRAN Novosibirsk, Russia)	ginzburgATmath.nsc.ru
32. **Glagolev Victor** (JINR, LHE, Dubna, Russia)	glagolevATsunhe.jinr.ru
33. **Goloskokov Sergey** (JINR, Dubna, Russia)	goloskkvAT jinr.ru
34. **Grigoriev Alexander** (MSU Moscow, Russia)	ax.grigorievATmail.ru
35. **GrossePerdekamp Matthias** (Univ. of Illinois, Upton, USA)	matthiasATbnl.gov
36. **Hoek Matthias**(Univ. of Glasgow,UK)	m.hoekATphysics.gla.ac.uk
37. **Huseynov Vali** (Nakhchivan Univ Azerbaijan)	VgusseinovATyahoo.com
38. **Isayev Alexander** (Kharkov IPhT, Ukrain)	isayevATmail15.com
39. **Ivanov Dmitry** (IMSBRAN Novosibirsk, Russia)	d-ivanovATmath.nsc.ru
40. **Ivanov Igor** (Univ. de Liege, Belge)	Igor.IvanovATulg.ac.be
41. **Ivanov Oleg** (JINR, Dubna, Russia)	ivonATjinr.ru
42. **Jenkovszky Laszlo** (IthP, Kiev, Ukrain)	jenkATbitp.kiev.ua
43. **Kiselev Anton** (JINR, LHE, Dubna, Russia)	antonyAThe.jinr.ru
44. **Kiselev Yury**(CERN, Geneve, Switzerland)	yury.kiselevATcern.ch
45. **Kivel Nikolai** (Ruhr Uni. Bochum, Germany)	Nikolai.KivelATtp2.ruhr-uni-bochum.de
46. **Klimaszewski Konrad** (Inst.Nucl.Stud., Warsaw, Poland)	Konrad.KlimaszewskiATfuw.edu.pl
47. **Koerner Jurgen** (Univ. of Mainz, Germany)	koernerATthep.physik.uni-mainz.de
48. **Kolganova Elena** (JINR, Dubna, Russia)	keaATtheor.jinr.ru
49. **Korotkov Vladislav** (IHEP, Protvino, Russia)	Vladislav.KorotkovATihep.ru
50. **Kotikov Anatoly** (JINR, Dubna, Russia)	KotikovATtheor.jinr.ru
51. **Kubarovsky Valery** (Jlab, Newport News, USA)	vpkATjlab.org
52. **Kurilkin Aleksey** (JINR LHE, Dubna, Russia)	akurilATsunhe.jinr.ru
53. **Kurilkin Pavel** (JINR LHE, Dubna, Russia)	pkurilATsunhe.jinr.ru
54. **Ladygin Vladimir** (JINR, Dubna, Russia)	ladyginATsunhe.jinr.ru
55. **Lykasov Gennadi** (JINR, Dubna, Russia)	lykasovATjinr.ru
56. **Lyuboshitz Valery** (JINR, LHE, Dubna, Russia)	Valery.LyuboshitzATjinr.ru
57. **Lyuboshitz Vladimir** (JINR, LHE Dubna, Russia)	LyuboshATsunhe.jinr.ru
58. **Meissner Stephan** (Ruhr-Univ. Bochum, Germany)	stephan.meissnerATtp2.ruhr-uni-bochum.de
59. **Mochalov Vasily** (IHEP, Protvino, Russia)	mochalovATihep.ru
60. **Morozov Alexey** (JINR, LHE, Dubna, Russia)	morozovATsunhe.jinr.ru
61. **Mueller Dieter** (Ruhr-University Bochum, Germany)	dieter.muellerATphysik.uni-regensburg.de
62. **Musulmanbekov Genis** (JINR, Dubna, Russia)	genisATjinr.ru

Name (Institution, Town, Country)	E-mail address
63. **Nassalski Jan** (Inst. for Nucl. Studies, Warsaw, Poland)	jan.nassalskiATfuw.edu.pl
64. **Naumov Dmitry** (JINR, Dubna, Russia)	naumovATnusun.jinr.ru
65. **Neznamov Vasily** (RFNC, Sarov, Russia)	NeznamovATvniief.ru
66. **Nikolenko Dmitri** (Inst. for Nucl. Phys. Novosibirsk, Russia)	nikolenkoATinp.nsk.su
67. **Novikova Valentina** (JINR, Dubna, Russia)	valentinaATjinr.ru
68. **Nurushev Sandibek** (IHEP, Protvino, Russia)	nurushevATihep.ru
69. **O'Brien Donie** (Trinity Coll. Dublin, Ireland)	donieATmaths.tcd.ie
70. **Okorokov Vitaly** (MEPhI, Moscow, Russia)	OkorokovATbnl.gov
71. **Panebrattsev Yuri** (JINR, Dubna, Russia)	panebratATsunhe.jinr.ru
72. **Pankov Alexander** (Gomel Techn. Univ. Belarus.)	pankovATictp.it
73. **Pasechnik Roman** (JINR, Dubna,Russia)	rpasechATtheor.jinr.ru
74. **Perevalova Ekaterina** (JINR LPP, Dubna, Russia)	perevalATsunse.jinr.ru
75. **Pilipenko Yuri** (JINR, Dubna, Russia)	pilipenATsunhe.jinr.ru
76. **Piskunov Nikolay** (JINR, Dubna, Russia)	piskunovATsunhe.jinr.ru
77. **Plis Yuri** (JINR, Dubna, Russia)	plisATnusun.jinr.ru
78. **Prokudin Alexei** (Univ. Torino, Italy)	prokudinATto.infn.it
79. **Ramilli Marco** (Univ. Insubria, Como, Italy)	marco.ramilliATgmail.com
80. **Ramsey Gordon** (Loyola Univer. Chicago, USA)	gprAThep.anl.gov
81. **Runtso Mikhail Fedorovich** (MEPhI, Moscow, Russia)	mfruntsoATemail.mephi.ru
82. **Sandacz Andrzej** (Inst. for Nucl. Studies, Warsaw, Poland)	sandaczATfuw.edu.pl
83. **Santos Helena** (Lab. de Instr.&Fis. Exper. de Parti. Lisboa, Portugal)	helenaATlip.pt
84. **Samoylov Oleg** (JINR LNP, Dubna, Russia)	samoylovATnusun.jinr.ru
85. **Sapozhnikov Mikhail** (JINR, Dubna, Russia)	sapozhATsunse.jinr.ru
86. **Savin Igor** (JINR, Dubna, Russia)	savinATsunse.jinr.ru
87. **Selyugin Oleg** (JINR,Dubna,Russia)	seluginATtheor.jinr.ru
88. **Sharov Vasiliy** (JINR, Dubna, Russia)	sharovATsunhe.jinr.ru
89. **Shikhalev Maxim** (JINR LHE, Dubna, Russia)	max.shikhalevATgmail.com
90. **Shimanskiy Stepan** (JINR, LHE, Dubna, Russia)	shimanskATsunhe.jinr.ru
91. **Shindin Roman** (JINR, LHE, Dubna, Russia)	shindinATsunhe.jinr.ru
92. **Sidorov Alexander** (JINR, Dubna, Russia)	sidorovATtheor.jinr.ru
93. **Silenko Alexander** (INP, Belarusian State Univ, Minsk)	silenkoATinp.minsk.by
94. **Sitnik Igor** (JINR, LHE, Dubna, Russia)	sitnikATsunhe.jinr.ru
95. **Sivers Dennis** (Portland Phys. Inst. USA)	densiversATsivers.com
96. **Soffer Jacques** (TempleUniv. Philadelphia, USA)	jacques.sofferATGmail.com
97. **Strokovsky Eugene** (JINR, LPP, Dubna, Russia)	strokATsunse.jinr.ru
98. **Strunov Leonid** (JINR, LHE, Dubna, Russia)	strunovATsunhe.jinr.ru
99. **Studenikin Alexander Iv.** (MSU, Moscow, Russia)	studenikATsrd.sinp.msu.ru
100. **Svirida Dmitry** (ITEP, Moscow, Russia)	Dmitry.SviridaATitep.ru
101. **Teryaev Oleg** (JINR, Dubna, Russia)	teryaevATtheor.jinr.ru
102. **Tikhonin Feodor** (IHEP, Protvino, Russia)	feodor.tikhoninATmail.ihep.ru
103. **Tkatchev Leonid** (JINR, Dubna, Russia)	tkatchevATnusun.jinr.ru
104. **Troshin Sergey** (IHEP, Protvino, Russia)	troshinATihep.ru
105. **Varanda Maria** (DESY, Hamburg, Germany)	mvarandaATmail.desy.de
106. **Vasiliev Alexander** (IHEP, Protvino, Russia)	vasilievATmx.ihep.su
107. **Vasiliev Taras**(JINR, LHE, Dubna, Russia)	tavasilievATjinr.ru
108. **Veretennikov Denis** (DESY, Zeuthen, Germany)	denis_vATmail.desy.de
109. **Vilardi Ignazio** (Univ. of Bari, Italy)	Ignazio.VilardiATba.infn.it
110. **Wakamatsu Masashi** (Osaka Univ. Japan)	wakamatuATphys.sci.osaka-u.ac.jp
111. **Zemlyanichkina Elena** (JINR, Dubna, Russia)	elenazemATsunse.jinr.ru
112. **Zolin Leonid** (JINR, LHE, Dubna, Russia)	zolinATsunhe.jinr.ru
113. **Zulkarneev Rafail** (JINR, Dubna, Russia)	Rafail.ZulkarneevATsunse.jinr.ru